Copy No.

MSC-A-R-66-4

POSTLAUNCH REPORT FOR MISSION AS-201

(Apollo Spacecraft 009)

FACILITY FORM 602

X67-17342 (ACCESSION NUMBER) (THRU)

439 (PAGES) 28 (CODE)

TMX-59649 (NASA CR OR TMX OR AD NUMBER) 3 (CATEGORY)

NATIONAL AERONAUTICS AND SPACE ADMINISTRATION

MANNED SPACECRAFT CENTER

HOUSTON, TEXAS

May 6, 1966

Restriction/Classification Cancelled

U

Contract

RQ7-44687

APOLLO SPACECRAFT FLIGHT HISTORY

Mission	Spacecraft	Description	Launch date	Launch site
PA-1	BP-6	First pad abort	Nov. 7, 1963	White Sands Missile Range, N. Mex.
A-001	BP-12	Transonic abort	May 13, 1964	White Sands Missile Range, N. Mex.
AS-101	BP-13	Nominal launch and exit environment	May 28, 1964	Cape Kennedy, Fla.
AS-102	BP-15	Nominal launch and exit environment	Sept. 18, 1964	Cape Kennedy, Fla.
A-002	BP-23	Maximum dynamic pressure abort	Dec. 8, 1964	White Sands Missile Range, N. Mex.
AS-103	BP-16	Micrometeoroid experiment	Feb. 16, 1965	Cape Kennedy, Fla.
A-003	BP-22	Low-altitude abort (planned high-altitude abort)	May 19, 1965	White Sands Missile Range, N. Mex.
AS-104	BP-26	Micrometeoroid experiment and service module RCS launch environment	May 25, 1965	Cape Kennedy, Fla.
PA-2	BP-23A	Second pad abort	June 29, 1965	White Sands Missile Range, N. Mex
AS-105	BP-9A	Micrometeoroid experiment and service module RCS launch environment	July 30, 1965	Cape Kennedy, Fla.
A-004	SC-002	Power-on tumbling boundary abort	Jan. 20, 1966	White Sands Missile Range, N. Mex.
AS-201	SC-009	Supercircular re-entry with high heat rate	Feb. 26, 1966	Cape Kennedy, Fla.

MSC-A-R-66-4

POSTLAUNCH REPORT FOR MISSION AS-201 (APOLLO SPACECRAFT 009)

Comment Sheet

In keeping with the President's policy on cost reduction and in order to update the distribution of this document please detach, fill in and return to MSC-PM4. If this document is no longer needed please destroy, or if at MSC return to PM4.

To: PM4
National Aeronautics and Space Administration
Manned Spacecraft Center
Houston, Texas 77058

Subject: Comments - AS-201 Distribution - Postlaunch Report for Mission AS-201, Apollo Spacecraft 009 - MSC-A-R-66-4.

1. This office has received _____copies of the AS-201 Postlaunch Report (MSC-A-R-66-4).

2. This office _____(does or does not) have need of this document and _____(does or does not) wish to receive future Postlaunch Reports on Apollo flights.

3. Distribution changes (please show present recipient and address according to current distribution list).

   a. Change quantity from _____copies to _____copies.

      Name_____
      (present recipient)

      Mailing Information_____

      _____

      _____

   b. Add_____copies for:

      Name_____
      (additional distribution)

      Complete mailing address_____

      _____

      _____

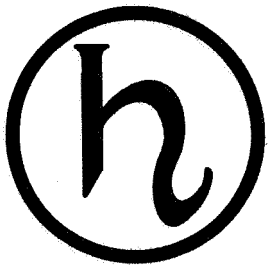
_____ _____
Signed Date

U. S. Government Agencies and Contractors Only

MSC-A-R-66-4

POSTLAUNCH REPORT FOR MISSION AS-201

(APOLLO SPACECRAFT 009)



Owen E. Maynard, Chief
Mission Operations Division

NATIONAL AERONAUTICS AND SPACE ADMINISTRATION

MANNED SPACECRAFT CENTER

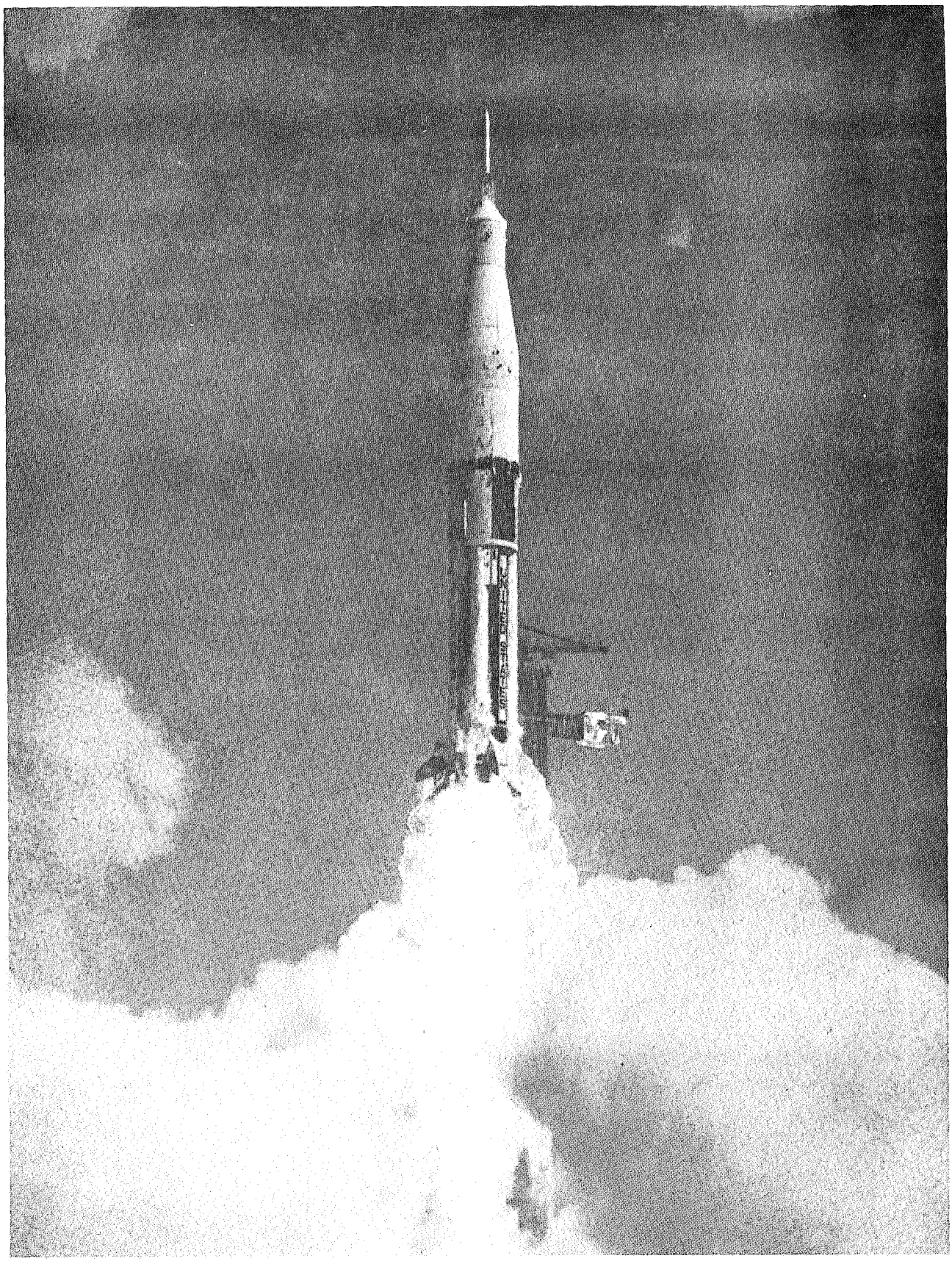
HOUSTON, TEXAS

May 6, 1966

NOTICE

Unless otherwise specified, zero time (T-0) for all data in this report is referenced to "Range zero" which is the first integral second of Range time prior to "lift-off." Lift-off is the instant of Saturn Instrument Unit umbilical disconnect,

NASA-S-66-6155 MAY 6



Lift-off, **Mission AS-201.**

CONTENTS

Section		Page
	TABLES	vii
	FIGURES	xi
	ABBREVIATIONS AND SYMBOLS	xxiii
	Abbreviations	xxiii
	Symbols	xxvii
1.0	MISSION SUMMARY	1-1
2.0	INTRODUCTION	2-1
3.0	TEST OBJECTIVES AND PERFORMANCE CRITERIA	3-1
3.1	Test Objectives	3-1
3.2	Performance Criteria	3-4
4.0	SPACE VEHICLE DESCRIPTION	4-1
4.1	Spacecraft Description	4-3
4.2	Launch Vehicle Description	4-8
5.0	FLIGHT TRAJECTORIES	5-1
6.0	AERODYNAMICS AND AEROTHERMODYNAMICS	6-1
6.1	Aerodynamics	6-1
6.2	Aerothermodynamics	6-8
7.0	SPACECRAFT SUBSYSTEMS	7-1
7.1	Structural Loads	7-1
7.2	Structural Dynamics	7-28
7.3	Heat Transfer	7-56
7.4	Heat Protection	7-65
7.5	Mechanical Subsystems	7-88
7.6	Earth Landing and Impact Attenuation Subsystems	7-98
7.7	Service Propulsion Subsystem	7-104
7.8	Launch-Escape Subsystem	7-145
7.9	Reaction Control Subsystems	7-147
7.10	Pyrotechnic Devices	7-175

Section		Page
	7.11 Stabilization and Control Subsystem and Control Programmer	7-184
	7.12 Electrical Power Subsystem	7-210
	7.13 Sequential Subsystem	7-228
	7.14 Emergency Detection Subsystem	7-231
	7.15 Instrumentation	7-236
	7.16 Communications Subsystem	7-248
	7.17 Environmental Control Subsystem	7-256
	7.18 Crew Station Acoustics	7-265
	7.19 Spacecraft Windows	7-268
	7.20 Crew Related Dynamics	7-274
8.0	LAUNCH VEHICLE PERFORMANCE	8-1
9.0	FLIGHT OPERATIONS	9-1
	9.1 Flight Control	9-1
	9.2 Network Instrumentation and Communication	9-4
	9.3 Recovery Operations	9-7
10.0	POSTFLIGHT TESTING AND ANOMALY SUMMARY	10-1
	10.1 Postflight Testing	10-1
	10.2 Summary of Failures, Malfunctions, and Deviations	10-3
11.0	11.0 CONCLUDING REMARKS	11-1
12.0	APPENDIX A	12-1
	12.1 Spacecraft History	12-1
	12.2 Launch Operations	12-4
13.0	APPENDIX B	13-1
	13.1 Photographic Coverage	13-1
	13.2 Metric Data Review	13-6
14.0	REFERENCES	14-1

TABLES

Table		Page
2.0-I	MISSION EVENTS	2-2
4.1-I	MASS PROPERTIES AT LAUNCH FOR MISSION AS-201	4-5
5.0-I	COMPARISON OF PLANNED AND ACTUAL TRAJECTORY PARAMETERS, MISSION AS-201	5-3
5.0-II	IMPACT AND TOUCHDOWN POINTS FOR MISSION AS-201	5-8
7.1-I	EVENTS AND CONDITIONS SIGNIFICANT TO STRUCTURAL ANALYSIS	7-7
7.1-II	CM FORWARD LONGERON AND AFT HEAT SHIELD STRESSES FOR MISSIONAS-201	7-10
7.1-III	SM RADIAL BEAM TRUSS STRESSES FOR MISSION AS-201	7-12
7.1-IV	SM RADIALBEAM CAP AND CM/SM TENSION-TIE STRESSES FOR MISSION AS-201	7-13
7.1-v	SLA SKIN AND STABILIZING MEMBER STRESSES FOR MISSIONAS-201	7-14
7.1-VI	SLA STABILIZING CABLE LOADS FOR MISSION AS-201	7-16
7.1-VII	STRUCTURAL LOAD COMPARISON FOR MISSION AS-201	7-17
7.2-1	STRUCTURAL DYNAMIC MEASUREMENTS, MISSION AS-201	7-33
7.4-I	COMPARISON OF MEASURED AND PREDICTED HEAT SHIELD PERFORMANCE DATA	7-69
7.7-I	SPS PERFORMANCE FOR MISSION AS-201	7-112
7.7-II	CRITICAL SPS PROBLEMS DURING KSC CHECKOUT OF SPACE-CRAFT 009	7-113
7.7-III	PROPELLANT AND PRESSURANT SERVICING OF SPS FOR MIS-SION AS-201	7-115
7.7-IV	RESULTS OF CLEANLINESS ANALYSES OF PROPELLANTS AND PRESSURANT FOR MISSION AS-201	7-116
7.7-V	ON-PAD MONITORING OF SPS SERVICE SUBSYSTEMS FOR MIS-SION AS-201	7-117

Table		Page
7.7-VI	CRITICAL LIFE COMPONENTS, MISSION AS-201	7-118
7.7-VII	PRE-IGNITION SPS MEASUREMENTS, MISSION AS-201	7-119
7.7-VIII	FIRST SPS BURN, MISSION AS-201	7-120
7.7-IX	COAST CONDITIONS (Ti-1395.2 to Ti-1310.7 SECONDS)	7-121
7.7-X	MALFUNCTION MODE EVALUATION MATRIX, MISSION AS-201 . .	7-122
7.9-I	RCS EVENT TIMELINE, MISSION AS-201	7-156
7.9-II	SM RCS PROPELLANT SERVICING, MISSION AS-203.	7-158
7.9-III	RCS PROPELLANT ANALYSIS, MISSION AS-201	7-159
7.9-IV	SM RCS HELIUM SERVICING, MISSION AS-201	7-160
7.9-V	SM RCS INITIAL OPERATION PARAMETERS, MISSION AS-201 . .	7-161
7.9-VI	CM RCS PREPARATION, MISSION AS-201	7-162
7.11-1	CONTROL PROGRAMMER COMMANDS SEQUENCE	7-191
7.15-I	FLIGHT MEASUREMENT SUMMARY	7-243
7.19-I	EMISSION SPECTROGRAPHIC ANALYSIS OF WINDOW CONTAMINATES FOR MISSIONS A-004, AS-201, AND AEDC ENGINE TESTS . .	7-270
7.20-1	SUMMARY OF POWER SPECTRAL DENSITIES	7-276
9.2-I	RADAR AND TELEMETRY TIMES FOR MISSION AS-201	3-6
9.3-I	RECOVERY SUPPORT FOR MISSION AS-201	9-11
13.1-I	ACTUAL PHOTOGRAPHIC COVERAGE, MISSION AS-201	13-2
13.2-I	DATA PROCESSING.	13-8
13.2-II	SOURCES OF MISSION AS-201 EVENT TIME USED IN EVALUATION	13-9

FIGURES

Figure		Page
2.0-1	Sequence of major events, Mission AS-201.	2-3
4.0-1	Space vehicle, Mission AS-201	4-2
4.1-1	Apollo spacecraft 009, Mission AS-201	4-6
4.1-2	ApoUo spacecraft body axis system	4-7
5.0-1	Ground track for Mission AS-201	5-9
5.0-2	Time histories of trajectory parameters for Mission AS-201 launch phase	
	(a) Inertial velocity and inertial flight-path angle	5-10
	(b) Relative velocity and relative flight-path angle	5-11
	(c) Altitude, longitude and geodetic latitude	5-12
	(d) Mach number and dynamic pressure	5-13
	(e) Longitudinal acceleration	5-14
5.0-3	Time histories of trajectory parameters for Mission AS-201 midcourse phase	
	(a) Inertial velocity and inertial flight-path angle	5-15
	(b) Relative velocity and relative flight-path angle	5-16
	(c) Altitude, longitude and geodetic latitude	5-17
5.0-4	Time histories of trajectory parameters for Mission AS-201 reentry phase	
	(a) Inertial velocity and inertial flight-path angle..	5-18
	(b) Relative velocity and relative flight-path angle.	5-19
	(c) Altitude, longitude and geodetic latitude	5-20
	(d) Mach number, maximum g load and dynamic pressure	5-21
5.0-5	Time history of altitude and downrange, Mission AS-201	5-22

Figure		Page
5.0-6	Altitude plotted against downrange, Mission AS-201 . . .	5-23
6.1-1	Variation of peak deceleration load during reentry with lift-to-drag ratio for several density deviations from the 1962 Standard Atmosphere, Mission AS-201 . .	6-4
6.1-2	Correlation of flight data with preflight data in the high Mach number region, Mission AS-201	6-5
6.1-3	Angle of attack as determined from flight rate data with corresponding Mach number, Mission AS-201	6-6
6.1-4	Flight roll coefficient determination, Mission AS-201	
	(a) Averaged roll rate buildup from postflight simulations compared with flight measured data	6-7
	(b) Averaged roll coefficient from postflight simulations and estimated flight roll coefficient . . .	6-7
6.2-1	Time histories of measured pressures on the blunt face of the CM, Mission AS-201	
	(a) CA1141P, Y0, 275, S/R 1.0	6-10
	(b) CA1142P, Y0, Z-71, S/R .947	6-11
	(c) CA1143P, Y0, Z71, S/R .947	6-12
	(d) CA1145P, Y71, Z0, S/R .947	6-13
	(e) CA1146P, Y0, Z61, S/R .81	6-14
	(f) CA1147P, Y0, Z55, S/R .73	6-15
	(g) CA1148P, Y0, Z39, S/R .51	6-16
	(h) CA1150P, Y39, Z0, S/R .51	6-17
	(i) CA1151P, Y-39, Z0, S/R .51	6-18
	(j) CA1152P, Y0, Z0, S/R 0	6-19
6.2-2	Comparison of measured pressure distribution with wind-tunnel data and flow field program, Mission AS-201 . .	6-20
6.2-3	Time histories of actual heating rates on the CM conical surface of Mission AS-201	
	(a) CA1253R, X_C44, 90°, S/R 1.42	6-21
	(b) CA1256R, X_C60, 90°, S/R 1.67	6-22
	(c) CA1259R, X_C81, 90°, S/R 1.99	6-23
	(d) CA1262R, X_C112.25, 90°, S/R 2.47	6-24
	(e) CA1341R, apex	6-25

Figure		Page
6.2-3 (Continued)		
	(f) CA1265R, X_C23.2, 135°, S/R 1.1	6-26
	(g) CA1323R, X_C44, 180" S/R 1.42	6-27
	(h) CA1168R, X_C81, 188°, S/R 1.99	6-28
	(i) CA1274R, X_C88, 185°, S/R 2.1	6-29
	(j) CA1280R, X_C23.2, 225°, S/R 1.1	6-30
	(k) CA1286R, X_C40, 214°, S/R 1.36	6-31
	(l) CA1298R, X_C50, 228°, S/R 1.51	6-32
	(m) CA1332R, X_C67, 270°, S/R 1.77	6-33
	(n) CA1295R, X_C112.25, 270°, S/R 2.47	6-34
	(o) CA1277R, X_C23.2, 180°, S/R 1.1	6-35
	(p) CA1283R, X_C21.5, 270°, S/R 1.09	6-36
6.2-4	Instrumentation locations on the conical surface of the CM, showing actual maximum heating rates, Mission AS-201.	6-37
6.2-5	Time histories of high range calorimeter temperatures, Mission AS-201	
	(a) CA1228R and CA1234R	6-38
	(b) CA1213R and CA1382R	6-39
7.1-1	CM heat shield, Mission AS-201	7-18
7.1-2	Boost protective cover, Mission AS-201	7-19
7.1-3	Service module structure, Mission AS-201	7-20
7.1-4	Spacecraft – LEM adapter, Mission AS-201	7-21
7.1-5	Wind velocity obtained at 60 ft level during launch of Mission AS-201 at Complex 34	7-22
7.1-6	Tower and CM lift-off accelerations, Mission AS-201	7-23
7.1-7	Launch winds, Mission AS-201	
	(a) hunch wind magnitude	7-24
	(b) Launch wind direction	7-25

Figure		Page
7.1.8	Longitudinal acceleration time history, Mission AS-201	
	(a) S-IB inboard and outboard engine cutoff	7-26
	(b) S-IVB engine buildup	7-26
7.1-9	Longitudinal acceleration time history, S-IVB engine cutoff, Mission AS-201	7-27
7.2-1	Acceleration spectral density of Z-axis tower acceleration at lift-off, Mission AS-201	7-35
7.2-2	S-IB engine thrust buildup, Mission AS-201	7-36
7.2-3	Command module inner structure accelerometer locations, Mission AS-201	7-37
7.2-4	Acceleration rms time history, Mission AS-201	
	(a) Inner structure forward bulkhead X-axis acceleration	7-38
	(b) Inner structure aft sidewall radial acceleration	7-38
	(c) Inner structure aft bulkhead X-axis acceleration	7-39
	(d) Lower equipment bay cable tray Z-axis acceleration	7-39
7.2-5	Acceleration spectral density of CM inner structure forward maximum vibration, Mission AS-201	7-40
7.2-6	Acceleration spectral density of CM inner structure of sidewall maximum vibration, Mission AS-201	7-41
7.2-7	Acceleration spectral density of CM inner structure aft bulkhead maximum vibration, Mission AS-201	7-42
7.2-8	Acceleration spectral density of lower equipment bay cable tray maximum vibration, Mission AS-201	7-43
7.2-9	Acceleration spectral density of CM inner structure aft sidewall vibration during transonic flight, Mission AS-201	7-44
7.2-10	Comparison of CM inner structure maximum vibration with criteria, Mission AS-201	7-45

Figure		Page
7.2-11	SM accelerometer locations, Mission AS-201. (SPS engine dome location not shown.)	7-46
7.2-12	Acceleration spectral density of SM helium pressurization panel radial vibration during transonic flight, Mission AS-201	7-47
7.2-13	Acceleration spectral density of SM helium pressurization panel tangential vibration during transonic flight, Mission AS-201.	7-48
7.2-14	Acceleration spectral density of maximum SPS engine dome, radial vibration, during supersonic flight, Mission AS-201	7-49
7.2-15	Acceleration spectral density of SPS engine dome radial vibration during SPS burn, Mission AS-201	7-50
7.2-16	Acceleration spectral density of maximum SPS engine dome longitudinal vibration during supersonic flight, Mission AS-201	7-51
7.2-17	SLA skin panel accelerometer locations, Mission As-201..	7-52
7.2-18	Comparison of SLA shell panel vibration with criteria, Mission AS-201	
	(a) Lift-off	7-53
	(b) Transonic flight	7-54
	(c) Supersonic flight	7-55
7.3-1	Peak temperatures measured on service module outer surface during launch on Mission AS-201. (Sensors in cork insulated area are under the cork.)	7-59
7.3-2	Longitudinal variation of peak temperatures measured on the service module surface during launch on Mission AS-201	7-60
7.3-3	Circumferential variation of peak temperatures measured on service module surface during launch on Mission AS-201	7-61
7.3-4	Temperature time histories for service module sensors SA7911T and SA7912T, Mission AS-201	7-62

Figure		Page
7.3-5	Peak temperatures measured on spacecraft – LEM adapter outer surface during launch on spacecraft 009, Mission AS-201	7-63
7.3-6	Temperature time histories for SLA sensors AA7931T and AA7932T, Mission AS-201	7-64
7.4-1	Command module three-part heat shield, Mission AS-201.	7-70
7.4-2	CM/SM shear compression pad and tension tie - Block I type, Mission AS-201.	7-71
7.4-3	CM ablator thickness distribution, Mission AS-201	7-72
7.4-4	Aft heat shield ablator measurement locations, Mission AS-201	7-73
7.4-5	Temperature measurement locations on CM forward and crew compartment, Mission AS-201	7-74
7.4-6	Char condition of aft heat shield, Mission AS-201	
	(a) General view from -Z-axis to -Y-axis	7-75
	(b) View from center toward +Z-axis	7-76
7.4-7	Aft heat shield measurements, Mission AS-201	
	(a) Station Z71, YO	7-77
	(b) Station ZO, YO	7-78
	(c) Station Z-71, YO	7-79
	(d) Station ZO, Y39	7-80
	(e) Station ZO, Y71	7-81
7.4-8	Typical aft heat shield core (Z-71), Mission AS-201	7-82
7.4-9	Aft heat shield core measurements, Mission AS-201.	7-83
7.4-10	Char and erosion around CM RCS system A roll engines after propellant depletion burn, Mission AS-201	7-84
7.4-11	Char condition of conical section, Mission AS-201	
	(a) General view, +Z axis	7-85
	(b) General view, -Y axis	7-86
	(c) General view, -Z axis	7-87

Figure		Page
7.5-1	CM uprighting subsystem, Block I, Mission AS-201	
	(a) CM stable flotation attitudes	7-92
	(b) Location of air bags, stowed and deployed	7-92
7.5-2	Uprighting subsystem and recovery aid components, Mission AS-201	7-93
7.5-3	Uprighting subsystem canister and valve location, Mission AS-201	7-94
7.5-4	Uprighting subsystem compressor location, Mission AS-201	7-95
7.5-5	Sea dye marker canister and mechanism, Mission AS-201.	7-96
7.5-6	Original pressure hatch pinion gear which was replaced with ground-handling unit for Mission AS-201	7-97
7.6-1	Strut impact load mechanism, Mission AS-201	7-101
7.6-2	Impact attenuation strut design load - stroke curves for unmanned mission, Mission AS-201	
	a) X-X foot strut	7-102
	b) X-Xhead strut	7-102
	c) Y - Y strut	7-103
	d) Z-Z strut	7-103
7.7-1	Chamber pressure during first burn, Apollo Mission AS-201	7-124
7.7-2	Second SPS burn, Mission AS-201	7-125
7.7-3	Service propulsion subsystem, Mission AS-201	7-126
7.7-4	SPS critical measurements during launch and exit, Mission As-201	
	(a) S-YB booster effects	7-127
	(b) S-IVB booster effects	7-128
	(c) Various g effects	7-129
7.7-5	Oxidizer retention reservoir (zero g can), Mission AS-201	7-130

Figure Page

7.7-6 Propellant tank and interface pressures during first burn, Mission AS-201

(a) Oxidizer tank pressure 7-131
(b) Oxidizer engine interface pressure 7-131
(c) Fuel tank pressure 7-131
(d) Fuel engine interface pressure 7-131

7.7-7 SPS helium consumption during first burn, Mission AS-201.. 7-132

7.7-8 Oxidizer tank and interface pressure plotted against time, (second SPS burn), Mission AS-201 7-133

7.7-9 Fuel tank and interface pressures plotted against time, (second SPS burn), Mission AS-201 7-134

7.7-10 Engine feed line temperatures (SP0005T and SP0008T) plotted against time, Mission AS-201 7-135

7.7-11 First SPS ignition chamber pressure transient (SPS on at 1211.2 sec), Mission AS-201 7-136

7.7-12 Second SPS ignition chamber pressure transient, Mission AS-201 7-137

7.7-13 Propellant valve opening times, Mission AS-201

(a) First SPS ignition 7-138
(b) Second SPS ignition 7-139

7.7-14 First SPS shutdown chamber pressure transient, Mission AS-201 7-140

7.7-15 Second SPS shutdown chamber pressure transient, Mission AS-201 7-141

7.7-16 Propellant valve closing times, Mission AS-201

(a) First SPS shutdown 7-142
(b) Second SPS shutdown 7-143

7.7-17 Comparison of calculated chamber pressure and observed chamber pressure during first SPS burn, Mission AS-201.. 7-144

Figure		Page
7.8-1	Launch escape subsystem, Block I configuration, Mission AS-201	7-146
7.9-1	Service module reaction control subsystem, Mission AS-201	7-163
7.9-2	Schematic of typical SM RCS quad, Mission AS-201	7-164
7.9-3	SM RCS quad engine package temperatures, Mission AS-201	
	(a) Engine package quad A (SR5065T)	7-165
	(b) Engine package quad B (SR5066T)	7-165
	(c) Engine package quad C (SR5067T)	7-165
	(d) Engine package quad D (SR5068T)	7-165
7.9-4	SM RCS quad A fuel valve and injector head temperatures, Mission AS-201	
	(a) -Pitch engine injector head temp (SR7125T)	7-166
	(b) -Pitch engine fuel valve temp (SR7145T)	7-166
	(c) CCW roll engine injector head temp (SR7134T)	7-166
	(d) CCW roll engine fuel valve temp (SR7148T)	7-166
7.9-5	SM RCS helium source pressures, Mission AS-201	
	(a) He press quad A (SR5001P)	7-167
	(b) He press quad B (SR5002P)	7-167
	(c) He press quad C (SR5003P)	7-167
	(d) He press quad D (SR5004P)	7-167
7.9-6	SM RCS quad B forward firing engine injector head temperature, Mission AS-201	7-168
7.9-7	CM RCS component location, Mission AS-201	
	(a) +Y axis	7-169
	(b) -Y axis	7-170
7.9-8	Schematic of CM RCS propellant distribution, Mission AS-201	7-171
7.9-9	Schematic of CMRCS engines, Mission AS-201	7-172
7.9-10	CMRCS propellant tank pressures, Mission AS-201	7-173
7.9-11	CM RCS helium source tank pressures, Mission AS-201	7-174

Figure		Page
7.10-1	Spacecraft – LEM adapter separation system, Mission AS-201	7-177
7.10-2	Spacecraft – LEM adapter separation system, explosive train schematic, Mission AS-201	7-178
7.10-3	Spacecraft – LEM adapter panel attenuation and retention, Mission AS-201	7-179
7.10-4	Charge, explosive train, Mission AS-201	7-180
7.10-5	Confined detonating cord assembly, Mission AS-201 . .	7-181
7.10-6	Umbilical disconnect, service module to SLA, Mission As-201	7-182
7.10-7	Pressure cartridge, explosive train initiated, Mission As-201	7-183
7.11-1	Stabilization and control subsystem, Mission AS-201. .	7-193
7.11-2	Pitch rate and attitude transients during S-IVB/CSM separation, Mission AS-201	7-194
7.11-3	CSM coast phase limit cycles, Mission AS-201	7-195
7.11-4	Thrust vector control operation, second +X translation, 1st gimbal position set, Mission AS-201	7-196
7.11-5	Thrust vector control operation, +X translation, 2nd gimbal position set, 2nd SPS ΔV maneuver, Mission AS-201..	7-197
7.11-6	Thrust vector control operation, 1st SPS ΔV maneuver, Mission As-201.	7-198
7.11-7	fie-separation pitch maneuver, SC rate and attitude errors, Mission AS-201.	7-199
7.11-8	Pitch ARS gimbal angle, Mission AS-201	7-200
7.11-9	Spacecraft rates and attitude errors at CM/SM separation, Mission AS-201	7-201
7.11-10	CM pitch and roll maneuvers, SC rates and attitude errors, Mission AS-201	7-202

Figure		Page
7.11-11	Roll ARS gimbal angle, Mission AS-201	7-203
7.11-12	CM coast phase limit cycles, Mission AS-201	7-204
7.11-13	CM reentry rate time histories, Mission AS-201	
	(a) 1580 to 1650 seconds	7-205
	(b) 1650 to 1720 seconds	7-206
	(c) 1720 to 1790 seconds	7-207
	(d) 1790 to 1860 seconds	7-208
7.11-14	Yaw ARS gimbal angle, Mission AS-201	7-209
7.12-1	Electrical power subsystem, Mission AS-201	7-214
7.12-2	Battery bus A and main bus A during CM/SM separation, Mission AS-201	7-215
7.12-3	Pyro bus B voltage from T+1300 to 1650 seconds, Mission AS-201	7-216
7.12-4	Three battery currents during the period from T+1631.64 to 1636.44 seconds, Mission AS-201	
	(a) Current battery A	7-217
	(b) Current battery B	7-218
	(c) Current postlanding battery	7-219
7.12-5	Effects of circuit breaker 18 opening, Mission AS-201.	7-220
7.12-6	Main EPS failure sequence of events, Mission AS-201	7-221
7.12-7	Main bus A and main bus B voltage, Mission AS-201	
	(a) 1300 to 1650 seconds	7-222
	(b) 1650 to 2000 seconds	7-223
	(c) 2000 to 2350 seconds	7-224
7.12-8	Batteries A and B dc currents from T+1300 seconds to impact, Mission AS-201	
	(a) 1300 to 1650 seconds	7-225
	(b) 1650 to 2000 seconds	7-226
	(c) 2000 to 2350 seconds	7-227

Figure		Page
7.13-1	Sequential events control system block diagram, Mission AS-201	7-230
7.14-1	EDS launch vehicle and Q-ball interface, Mission AS-201	7-232
7.14-2	Emergency detection subsystem automatic abort circuit, showing open-loop configuration, Mission AS-201	7-233
7.14-3	Spacecraft automatic abort and LV engine cutoff, Mission AS-201	7-234
7.14-4	Q-ball vector sum output, Mission AS-201	7-235
7.15-1	R & D instrumentation subsystem for command module, Mission AS-201	7-244
7.15-2	Instrumentation system block diagram for Mission AS-201..	7-245
7.15-3	GFE instrumentation CM PAM/FM/FM telemetry package and 90 x 10 commutators, Mission AS-201	7-246
7.15-4	GFE instrumentation SM PAM/FM/FM telemetry package, Mission AS-201.	7-247
7.16-1	Communication subsystem, Mission AS-201	7-255
7.17-1	Flow diagram of ECS water/glycol coolant circuit, Mission AS-201.	7-260
7.17-2	ECS cabin pressure relief valve, Mission AS-201	7-261
7.17-3	Coolant circuit evaporator outlet liquid temperature, Mission AS-201	7-262
7.17-4	Command module cabin environment, Mission AS-201	7-263
7.17-5	Power and control diagram for ECS back pressure control, Mission AS-201	7-264
7.18-1	Overall sound pressure level time histories of crew station acoustics, Mission AS-201	7-267
7.19-1	Window contaminate smear locations, Mission AS-201	7-271

Figure		Page
7.19-2	Spectral transmission and reflection characteristics of left side window, Mission AS-201	7-272
7.19-3	Integrity sphere spectral transmission and light scattering characteristics, Mission AS-201	
	(a) Left side window	7-273
	(b) Left rendezvous window	7-273
7.20-1	Determination of accelerometer resultant for CM forward bulkhead conditions, Mission AS-201	7-278
7.20-2	Lift-off X-axis vibration, Mission AS-201	7-279
7.20-3	Resultant acceleration (CK0004A, CK0005A, and CK0006A), Mission AS-201	7-280
7.20-4	Resultant acceleration amplitude spectral density, g (mas), Mission AS-201	7-281
7.20-5	X-axis vibration amplitude spectral density, g (rms), Mission AS-201	7-282
7.20-6	Y-axis vibration amplitude spectral density, g (rms), Mission AS-201	7-283
9.1-1	Mission AS-201 operation and support plan	9-3
9.3-1	Recovery force deployment, Mission AS-201	9-12
9.3-2	Spacecraft in water, collar attached, Mission AS-201	9-13
9.3-3	Forward heat shield, Mission AS-201	9-14
9.3-4	Spacecraft being hoisted aboard U.S.S. Boxer, Mission AS-201	9-15
12.1-1	Apollo spacecraft 009 at Dmey, preflight	12-2
12.1-2	Apollo spacecraft 009 at Cape Kennedy, preflight	12-3
12.2-1	Countdown, Mission AS-201	
	(a) February 20th through 23rd	12-7
	(b) February 25th through 26th	12-8

Figure		Page
13.1-1	Camera locations, Mission AS-201	13-4
13.1-2	Long range camera locations, fission AS-201	13-5
13.2-1	Data coverage of flight time, **Mission** AS-201	13-11

ABBREVIATIONS AND SYMBOLS

Abbreviations

AEDC-VKF	Arnold Engineering Development Center - Von Karman Facility
AFETR	Air Force Eastern Test Range
ANT	Antigua Island
APS	auxiliary propulsion system
ARS	attitude reference system
ASC	Ascension Island
BDA	Bermuda
BPC	boost protective cover
CADD	Computation and Data Division
CADFISS	computation and data flow integrated subsystem
CDC	confined detonating charge
CM	command module
CNV	Carnarvon
CP	control programmer
CSM	command and service module
CTE	central timing equipment
DOD	Department of Defense
DPDM	differential pulse duration modulation
DSE	data storage equipment
ECS	environmental control subsystem
EDS	emergency detection subsystem

ELS	earth landing subsystem
ELSC	earth Landing sequence controller
EPS	electrical power subsystem
FM	frequency modulation
FQR	flight qualification recorder
G&N	guidance and navigation
GBI	Grand Bahama Island
g.e.t.	ground elapsed time
GFE	government furnished equipment
G.m.t.	Greenwich mean time
GRTS	Goddard real-time subsystem
GSE	ground support equipment
GSFC	Goddard Space Flight Center
GTK	Grand Turk Island
IECO	inboard engine cutoff
IP	impact predictor
IRIG	interrange instrumentation group
IU	instrument unit
KSC	Kennedy Space Center
LARC	lighter, amphibious, resupply, carrier
LCU	landing craft, utility
L/D	lift-to-drag ratio
LES	launch-escape subsystem
LET	launch-escape tower

LOX	liquid oxygen
LPH	landing platform, helicopter
LVTR	landing vehicle, tracked, reconnaisance
MCC-H	Mission Control Center, Houston
MCC-K	Mission Control Center, Kennedy
MDF	mild detonating fuse
MESC	master events sequence controller
MILA	Merritt Island Launch Area
MSFC	Marshall Space Flight Center
m.s.l.	mean sea level
MSO	minesweeper, ocean
MSOB	Manned Spacecraft Operations Building
NRZ-C	non-return-to-zero change
OCP	operational checkout procedures
OECO	outboard engine cutoff
PAT	Patrick Air Force Base
PCM	pulse code modulation
PCVB	pyro continuity verification box
PLSC	postlanding sequence controller
RCC	radio command control
RCE	radio command equipment
RCS	reaction control subsystem
RCSC	reaction control subsystem controller
RF	radio frequency

RKV	Rose Knot Victor
rms	root mean square
RSDP	remote site data processor
RTCC	real-time computer facility
RTC	room temperature vulcanizing
SCE	signal conditioning equipment
SCO	spacecraft operations office
SCS	stabilization and control subsystem
SECS	sequential events control subsystem
SEP	spacecraft electronic package
SLA	spacecraft - LEM adapter
SM	service module
SMJC	service module jettison controller
SM RCS	service module reaction control subsystem
SOC	Satellite Operations Control Center
SPL	sound pressure level
SPS	service propulsion subsystem
SSB	single side band
SSR	system support room
TEL 2	Telemetry 2
TEL 3	Telemetry 3
TJM	tower-jettison motor
UV-IR	ultra violet-infrared
WMS	waste management system

Symbols

g	gravitational constant
I_{sp}	resolution of specific impulse
I_{xy}	product of inertia, X-Y axis
I_{xz}	product of inertia, X-Z axis
I_{yz}	product of inertia, Y-Z axis
M	Mach number
q	dynamic pressure, lb/sq ft
$q\alpha$	product of dynamic pressure and angle of attack (lb/sq ft) (deg)
T	launch time
X	longitudinal axis of the spacecraft and launch vehicle
X_A	longitudinal location, referenced to the spacecraft (fig. 4.1-2)
X_C	longitudinal location, referenced to the command module (fig. 4.1-2)
X_L	longitudinal location, referenced to the launch-escape subsystem (fig. 4.1-2)
X_S	longitudinal location, referenced to the service module (fig. 4.1-2)
Z	lateral axis of the spacecraft, passing through the center of the main hatch and normal to the X axis
Y	lateral axis of the spacecraft, normal to the X-Z plane
α	angle of attack, deg
ΔV	pressure differential
ΔV	velocity differential
	Flight test symbols, Saturn-Apollo: Saturn symbol within ApoVo symbol. Basic symbols: Greek and Roman.

1.0 MISSION SUMMARY

Mission AS-201 was accomplished using Apollo spacecraft 009 and a Saturn IB launch vehicle. The unmanned spacecraft was launched from Cape Kennedy, Florida, on February 26, 1966 at 11:12 a.m. e.s.t. after several holds in the countdown due to adverse weather and launch vehicle technical difficulties.

Apollo spacecraft 009 was essentially of the Block I type configuration, consisting of a launch-escape subsystem, a command module, a service module, and a spacecraft - LEM adapter. The major differences between spacecraft 009 and the Block I configuration were the omission of fuel cells, crew equipment, suit loop, cabin postlanding ventilation, cryogenics subsystem, guidance and navigation subsystem; and the inclusion of the mission control programer, battery power only, open-loop emergency detection subsystem, and inoperative radiators for the environmental control subsystem and the electrical power subsystem.

The Saturn IB two-stage launch vehicle, consisting of stages S-IB and S-IVB and an instrument unit, performed satisfactorily. First-stage ignition, lift-off, programmed roll and pitch, and cutoff were executed as planned. Separation and second-stage ignition occurred as planned, with S-IVB cutoff and command and service module/spacecraft - LEM adapter/S-IVB separation 10 seconds later than predicted. At separation the trajectory was near nominal, with the greatest deviation being a range of 22.2 nautical miles.

Tower and boost protective cover jettison occurred on time at T+172 seconds. As a result of the delay in S-TVB cutoff the spacecraft control programer was activated 10 seconds later than planned. Consequently, subsequent event times reflected this initial delay.

The spacecraft structural behavior during the launch phase was generally as expected with no serious structural responses occurring.

The service module reaction control subsystem provided adequate +X translation for the S-IVB/command and service module separation and ullage for the two service propulsion subsystem burns. However, the +X translations produced a velocity increment that was less than nominal because the quad A oxidizer isolation valve failed to open. Preflight test experience had indicated a tendency toward valve seizure because of incompatible materials. The service module reaction control subsystem successfully provided spacecraft attitude and rate control even though quad A was inactive and a negative yaw engine in quad B or quad D was inoperative.

Mission AS-201 was the first flight test of the service propulsion subsystem. Although the reaction control subsystem +X translation resulted in 25 to 45 percent of the ullage velocity increment expected, the ignition for the first service propulsion subsystem burn occurred successfully at Ti-12ll.2 seconds. Performance was near nominal for the first 80 seconds of the 184-second burn. At engine cutoff the chamber pressure had decayed to approximately 70 percent of nominal. The second burn, initiated at Ti-1410.7 seconds and planned for a LO-second duration, was very erratic with chamber pressure oscillations ranging from 12 to 70 percent of nominal. The below-nominal performance of the service propulsion subsystem has been attributed to helium ingestion.

Orientation of the spacecraft for command module/service module separation was initiated at T+1424.1 seconds and accomplished as planned, and at Ti-1453.0 seconds satisfactory separation occurred. The pitch and roll maneuvers required to orient the command module to the reentry inertial attitude were completed at T+1515.1 seconds.

The partial environmental control subsystem, as installed in spacecraft 009, performed satisfactorily throughout the flight except that water-glycol evaporator liquid outlet temperatures were lower than planned.

Spacecraft communications blackout began at T+1580 seconds and lasted until T+1695 seconds. Reentry was initiated with a space-fixed velocity of 26 481 ft/sec. The command module was subjected to a maximum reentry heating rate of 164 $Btu/ft^2/sec$ at T+1631.7 seconds, and a maximum deceleration of 14.3g at T+1639.7 seconds. The command module structure and heat shields adequately performed in the reentry environment with no adverse effects.

At Ti-1635 seconds, circuit breaker CB18 opened, resulting in a loss of power to logic bus B and pyro bus B. This event removed power from certain command module reaction control subsystem functions and from the earth landing subsystem system B.

At T+1641 seconds, power to system A of the reaction control subsystem was lost, followed by a loss of power to system B at Ti-1649 seconds. Postflight analysis and testing revealed that two wires in the reaction control subsystem propellant isolation main bus A and B lines had shorted to the ground support equipment reset line.

The loss of power to the command module reaction control subsystems systems A and B resulted in an uncontrolled rolling (excess of 26 deg/sec) reentry instead of the planned lifting reentry. The vehicle roll was attributed to the effects of spacecraft protuberances (scimitar antennas) coupled with the offset center of gravity.

With the return of power to reaction control subsystem system A at T+2121 seconds, the required depletion burning of the command module reaction control subsystem propellants was accomplished through the system B roll engines,

Apex cover jettison, drogue parachute deployment, and main parachute deployment occurred as planned. The command module landed undamaged, upright in the stable I attitude at T+2239.7 seconds, 30.8 seconds earlier than the preflight prediction.

Upon landing, the recovery aids deployed, including the HF antenna; however, signals fromthe HF transceiver were not received. The main parachute disconnect on system A was accomplished but the system B leg remained attached because of the electrical power subsystem malfunction.

The point of touchdown was 8.18° S. latitude and 11.15° W, longitude, 45 miles uprange northwest of the recovery ship. The main parachutes were cut loose fromthe command module by the recovery forces and the spacecraft was aboard the recovery ship at 2:20 p.m. e.s.t. (3 hr 8 min after lift-off).

Postflight tests were conducted for the evaluation of subsystem performance and for the resolution of anomalies.

2.0 INTRODUCTION

Mission AS-201 (Apollo spacecraft 009) was the first flight test of a production Apollo Block I type spacecraft utilizing the Saturn IB launch vehicle. Lift-off of the unmanned suborbital flight from Launch Complex 34, Cape Kennedy, Florida, occurred at 11:12 a.m. e.s.t. (16:12 G.m.t.) February 26, 1966. The spacecraft command module landed safely in the primary landing area near Ascension Island, approximately 37 minutes later (16:49 G.m.t.), and was recovered as planned.

The major spacecraft mission objectives were to demonstrate the compatibility and structural integrity of the spacecraft/Saturn IB configuration and to evaluate the spacecraft heat-shield performance during a high heat rate reentry. The complete test objectives are presented in section 3.1 of this report. The mission profile is presented in figure 2.0-1 and the times of mission events are given in table 2.0-1.

This report includes an evaluation of the mission, a brief summary of the launch vehicle performance, and an analysis of the spacecraft, performance on the basis of flight-test data and results of completed postflight tests.

In addition to the analysis and pertinent data included in this report, the complete plotted flight data are contained in a companion volume, "Flight Data Report for Mission AS-201 (Apollo spacecraft 009)" (ref. 1).

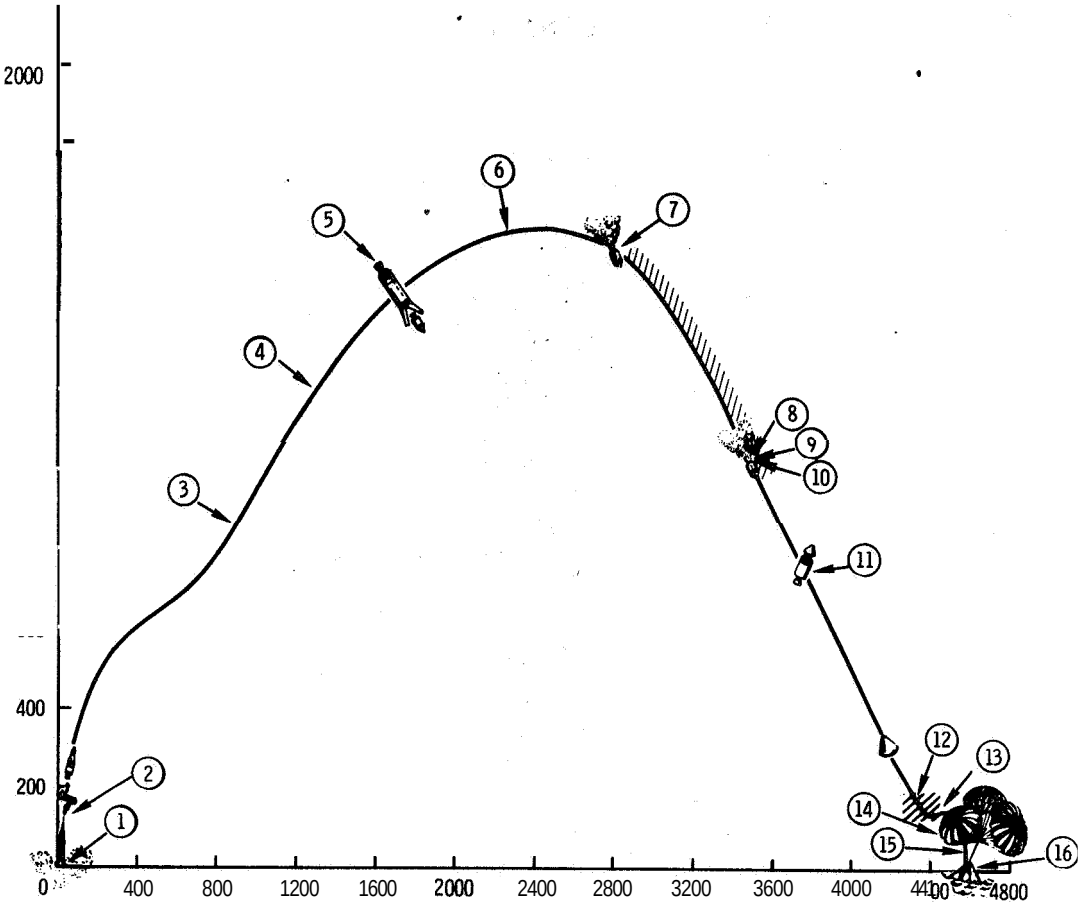
Prior to Mission AS-201, one other production type spacecraft and ten boilerplate type spacecraft had been flight tested (see inside front cover). All were unmanned. The results of the missions, which included functioning spacecraft subsystems, have been presented in mission or postlaunch reports (refs. 2 to 9).

Unless otherwise specified, zero time (T-0) for all data in this report is referenced to range zero, which is the first integral second before lift-off. (Lift-off is the instant of umbilical disconnect of the launch vehicle instrument unit.)

TABLE 2.0-I.- MISSION EVENTS

Event	Range time, sec		Difference, sec
	Predicted	Actual	
Lift-off	0.31	0.37	0.06
LET jettison	172.3	172.6	.3
Control programmer start	652.7	663.1	10.4
Onboard recorders off	654.7	665.2	10.5
S-IVB/CSM separation command	832.7	843.2	10.5
S-IVB/CSM separation	834.4	844.9	10.5
RCS +X translation 1 on	836.2	846.7	10.5
RCS +X translation 1 off	854.2	864.6	10.4
RCS +X translation 2 on	1170.7	1181.2	10.5
SPS thrust on burn 1	1200.7	1211.2	10.5
RCS +X translation 2 off	1201.7	1212.2	10.5
Tape recorders on	1311.2	1321.9	10.7
SPS thrust off burn 1	1384.7	1395.2	10.5
RCS +X translation 3 on	1385.2	1395.7	10.5
SPS thrust on burn 2	1400.2	1410.7	10.5
RCS +X translation 3 off	1401.2	1411.7	10.5
SPS thrust off burn 2	1410.2	1420.7	10.5
Pitch rate (-5 deg/sec) initiate	1413.7	1424.2	10.5
Pitch rate (-5 deg/sec) terminate	1431.7		10.4
CM/SM separation command	1443.7		11.0
CM/SM separation physical (0.25 ft)	1444.2	1455.0	10.8
CM pitch rate (-5 deg/sec) initiate	1452.2	1462.6	10.4
CM pitch rate (-5 deg/sec) terminate	1468.7	1479.1	10.4
CM roll rate (5 deg/sec) initiate	1468.7	1479.2	10.5
CM roll rate (5 deg/sec) terminate	1504.7	1515.1	10.4
Drogue parachute deployment	1954.1	1855.4	-98.7
Main parachute deployment	1994.9	1908.4	-86.5
Touchdown	2360.6	2239.7	-120.9

NASA-S-66-6156 MAY 6



		Actual time from lift-off, sec
1	Lift-off (11:12:01 a. m. e. s. t.)	
2	OECO	146.9
3	S-IVB cutoff	602.9
4	Separation attitude achieved	728.3
5	S-IVB/CSM separation	844. 9
6	Apogee	1020. 0
7	1st SPS burn on	1211.2
8	1st SPS burn off	1395.2
9	2nd SPS burn on	1410.7
10	2nd SPS burn off	1420.7
11	CM/SM separation	1455.0
12	Blackout	1580.0
13	End of blackout	1695.0
14	Drogue parachute deployment	1855.4
15	Main parachute deployment	1908. 4
16	Touchdown	2239.7

Figure 2.0-1. - Sequence of major events, Mission AS-201.

3.0 TEST OBJECTIVES AND PERFORMANCE CRITERIA

3.1 Test Objectives

The spacecraft test objectives for Mission AS-201 were accomplished to the degree indicated in the following listing:

General test objectives.-

Primary test objectives:

(a) Demonstrate the structural integrity and compatibility of the launch vehicle and spacecraft, and confirm launch loads. Satisfactorily demonstrated and confirmed, objective accomplished.

(b) Demonstrate separation of the S-IVB from the S-IB, the launch escape subsystem (US) and boost protective cover (BPC) from the command and service module (CSM), the CSM from the S-IVB/instrument unit (IU)/ spacecraft - LEM adapter (SLA), and the command module (CM) from the service module (SM). Satisfactorily demonstrated, objective accomplished.

(c) Verify operations of the launch vehicle propulsion, guidance and control, and electrical subsystems. Launch vehicle objective, see reference 13.

(d) Verify operation of the following spacecraft subsystems:

1. CM heat shield adequacy for entry from low earth orbit. Verified, objective accomplished.

2. Service propulsion subsystem, including restart. Verified initial start capability in space, nominal performance during first 80 seconds of initial bum, and satisfactory operation of subsystem excluding standpipe in retention reservoir. Output performance after first 80 seconds below nominal. Restart erratic. Objective partially accomplished.

3. Environmental control subsystem pressure and temperature control. Freezing of evaporator coolant circuit and back-pressure control problems were known before flight and corrected for Mission AS-204. Objective accomplished.

4. Communication (partial). No signals received from HF transceiver; all other communications were satisfactory. Objective partially accomplished.

5. CM reaction control subsystem. Operation verified for maneuvering CM to proper reentry attitude and for CM attitude control through reentry maximum q and first part of blackout. Loss of electrical power to systems A and B prevented use of CM RCS during balance of reentry. Depletion burn operation, after return of power to system A, verified. Objective partially accomplished.

6. SM reaction control subsystem. Quad A did not operate and the equivalent of one negative yaw engine on quad B or quad D did not operate; however, the subsystem completed operational functions required. Objective partially accomplished.

7. Stabilization and control subsystem. Operation verified, objective accomplished.

8. Earth landing subsystem. Operation verified, objective accomplished.

9. Electrical power subsystem. The shorting of nondeadfaced 28 volt wires after CM/SM umbilical disconnect prevented normal operation of the subsystem. Proper operation of the protective circuit breakers made it possible to return power to some circuits in time to satisfactorily recover the spacecraft. Objective not accomplished.

(e) Evaluate the space vehicle emergency detection subsystem (EDS) in the open-loop configuration. Subsystem evaluated, objective accomplished. (Also see ref. 13.)

(f) Evaluate the CM heat shield ablator at a high heating rate of approximately 200 Btu/ft^2/sec during reentry at approximately 28 000 ft/sec. Maximum reentry heating rate was above the 160 Btu/ft^2/sec minimum; however, complete evaluation of the ablator was not possible because of loss of temperature data during the time of maximum reentry heating. Objective not accomplished.

(g) Demonstrate the mission support facilities required for launch, mission operations, and CM recovery. Satisfactorily demonstrated, objective accomplished.

Secondary test objectives: The secondary test objective for Mission AS-201 was to determine subsystem performance other than the minimum required to demonstrate manned orbital capability.

Detailed spacecraft test objectives.-

Primary test objectives:

(a) Demonstrate structural integrity and compatibility of the launch vehicle and spacecraft, and confirm launch loads, including:

1. Demonstrate compatibility and structural integrity of CSM/Saturn IB. Satisfactorily demonstrated, objective accomplished.

2. Determine structural loading of the spacecraft adapter when subjected to the Saturn IB launch environment. Loading determined, objective accomplished.

(b) Demonstrate separation of the S-IVB from the S-IB, the LES and boost protective cover from the CSM, the CSM from the S-IVB/IU/SLA, and the CM from the SM. Satisfactorily demonstrated, objective accomplished.

(c) Determine CM adequacy for manned entry from low earth orbit. Adequacy determined, objective accomplished.

(d) Verify SPS operation for a minimum of 20 seconds after at least 2 minutes in a space environment and verify restart capability. Verified satisfactory operation for more than 20 seconds and satisfactory start after more than 2 minutes in space environment. Restart was erratic and below specifications. Objective partially accomplished.

(e) Determine performance of the SCS, CM RCS, SM RCS, ECS (pressure and temperature control), EPS (partial) and communication (partial), and determine their adequacy for manned orbital flight. Satisfactory performance and adequacy for manned orbital flight were determined for the SCS, for the CM RCS except for the inoperative period after reentry maximum q until main parachute deployment, and for communications except for the HF transceiver and antenna. Prior to Mission AS-201, the equipment and system associated with the problems encountered with the SM RCS and the ECS pressure and temperature control were superseded by newer designs for Mission AS-204. Performance of the EPS was below specifications due to the shorting of nondeadfaced 28 volt wires in the CM after umbilical disconnect. Objective partially accomplished.

(f) Demonstrate operation of the parachute recovery subsystem and recovery aids following reentry. Satisfactorily demonstrated, objective accomplished.

(g) Evaluate the space vehicle emergency detection subsystem (EDS) in the open-loop 'configuration. Subsystem evaluated, objective accomplished. (Also see ref. 13.)

(h) Evaluate the CM heat shield ablator at a high heating rate of approximately 200 $Btu/ft^2/sec$ during entry at approximately 28 000 ft/sec. Complete evaluation of the ablator was not possible because of the loss

of temperature data during the time of reentry heating. Objective not nccomplished.

(i) Demonstrate the mission support facilities required for launch, mission operations, and CM recovery. Satisfactorily demonstrated, objective accomplished.

Secondary test objectives:

(a) Determine long duration (approximately 200 sec) SPS performance including shutdown characteristics. Performance and shutdown characteristics determined for below specification levels after first 80 seconds. Objective partially accomplished.

(b) Obtain data on SPS engine firing stability. Data obtained for 80 seconds of stable operation and for a helium ingestion condition for the balance of the time. Objective partially accomplished.

3.2 Performance Criteria

In addition to the analysis relative to the accomplishment of the test objectives, the mission evaluation was required to present information in this report which could be used to establish whether or not the following performance criteria were fulfilled on Mission **AS-201.**

(a) Establish that launch environment did not stress CSM beyond structural design limits requiring redesign of CSM structure.

(b) Establish that launch environment did not stress SLA beyond structural limits requiring redesign of **SLA** structure.

(c) Establish that the LES did separate from CSM/SLA/S-IVB combination at time specified and in a manner which did not compromise completion of the planned mission.

(d) Establish that the CSM did separate from the S-IVB at the time specified and in a manner which did not prevent completion of the planned mission.

(e) Establish that the CM did separate from the SM at the time specified **and** in a manner which did not prevent completion of the planned mission.

(f) Establish that the SPS did operate for a minimum of 20 seconds within specified limits, having started after at least 2 minutes in space environment.

(g) Establish that the SPS did restart and burn after a coast period, and that the restart and burn were within specified limits.

(h) Establish that the SPS did burn for a minim total of 200 seconds, and that thrust, stability, shutdown characteristics, and thrust tailoff during the burn were within specified limits.

(i) Establish that each of the following subsystems performed within specified limits: SCS, CM RCS, SM RCS, ECS pressure control, EPS, Communications, and Instrumentation.

(j) Establish that no false abort signal. was generated by the spacecraft EDS.

(k) Establish a high heating rate of approximately 200 Btu/ft^2/sec during reentry at approximtely 28 000 ft/sec.

(1) Establish that heat shield data were within specified limits to the extent that no redesign requirement is indicated for completion prior to Saturn V mission heat-shield certification.

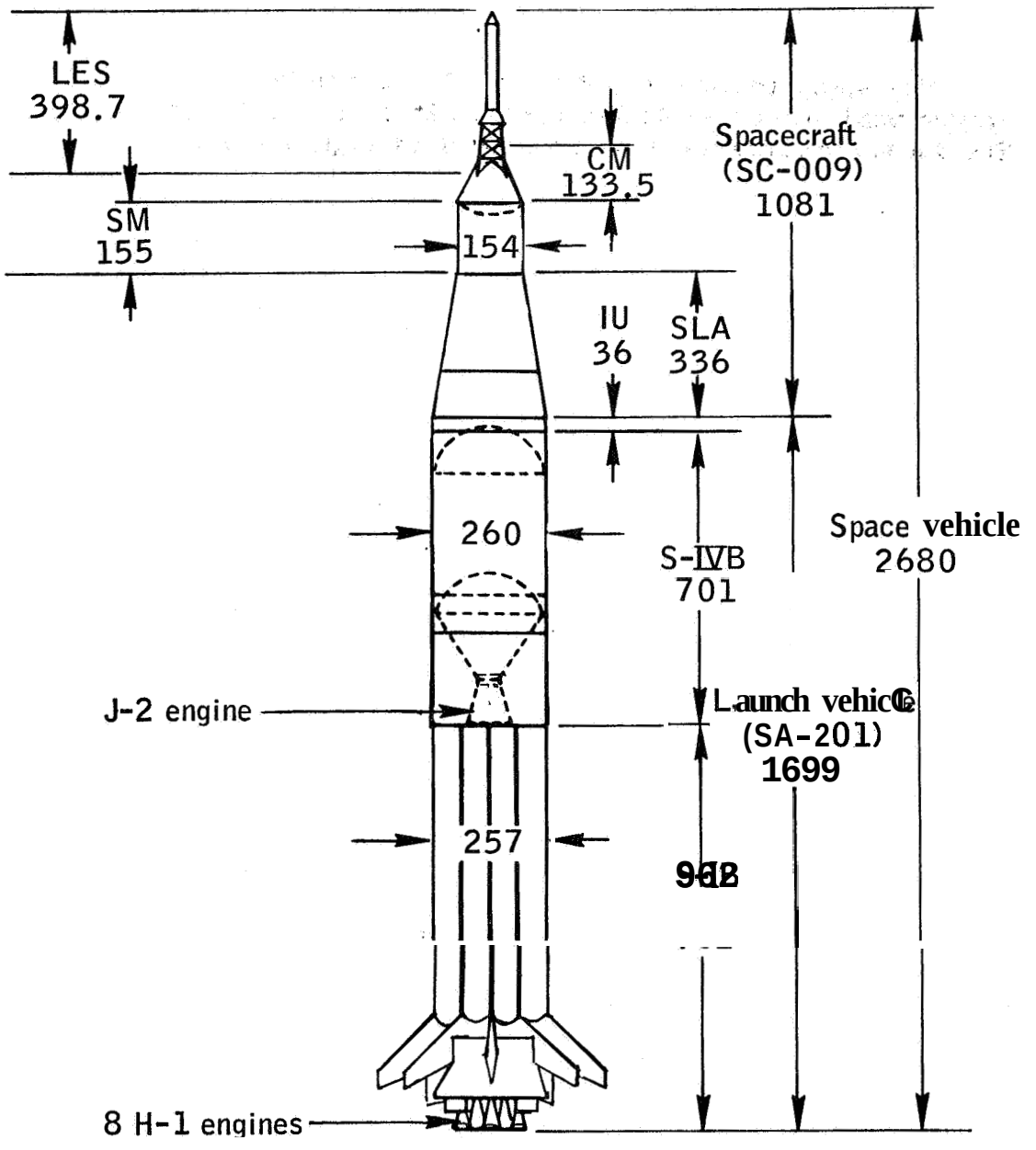
(m) Establish that the ELS did operate at the specified altitude and that deceleration and descent velocities were within specified limits.

(n) Establish that the recovery aids did operate at the specified times and within the specified limits.

4.0 SPACE VEHICLE DESCRIPTION

The space vehicle for Mission AS-201 consisted of a Saturn IB launch vehicle and an Apollo spacecraft of Block I type configuration. The launch configuration is indicated in figure 4.0-1.

NASA -S-66-6157 MAY 6



Notes: All dimensions are in inches
All dimensions are approximate
Drawing not to scale

Figure 4.0-1.- Space vehicle, Mission AS-201.

4.1 Spacecraft Description

Apollo spacecraft 009 consisted of a Block I type configuration for the launch escape subsystem (LES), command module (CM), service module (SM), and spacecraft - LEM adapter (SLA) as indicated in figure 4.1-1. Reference 10 describes the typical Apollo Block I spacecraft, and the differences between the configuration of spacecraft 009 and Block I are presented in reference 11. The differences included:

(a) Omission of the guidance and navigation subsystem

(b) Omission of couches, space suits, and crew provisions

(c) Omission of S-band communications equipment

(d) Omission of biomedical instrumentation

(e) Omission of crew station displays

(f) Use of batteries in place of fuel cells

(g) Use of CM control programmer

(h) Use of open-loop emergency detection subsystem

For Mission AS-201 the following operational subsystems and major components were included on a flight test for the first time:

(a) Service propulsion subsystem

(b) CM and SM reaction control subsystems

(c) **Aft,** crew compartment, and forward heat-shield assemblies

(d) Spacecraft - LEM adapter structure

In addition, partial operational subsystems being flight tested for the first time included portions of the environmental control subsystem, communications subsystem, and instrumentation subsystem.

Mass properties for spacecraft 009 for the mission are summarized in table 4.1-I. Weights and centers of gravity for each module were measured prior to stacking. Changes accomplished prior to launch were monitored, and measured data revised as required. Inertial values are calculated for the actual weights shown. The mass properties of the ring retained with the service module following separation from the adapter were calculated, but total weight and centers of gravity of the adapter were measured.

Spacecraft launch weights shown in table 4.1-I did not vary significantly from the predicted values used in operational trajectory calculations. Propellant loading difficulties resulted in a deficiency of approximately 311 pounds of fuel and an excess of approximately 336 pounds of oxidizer. Propellant tanks were X-rayed to verify propellant quantities. Loading accuracy cannot be accurately established; however, actual uncertainty of propellant loading will exceed predicted values based on loading equipment accuracies. Other expendable loading did not vary from predicted values.

Spacecraft body axes are indicated in figure 4.1-2. (Also see ref. 12.)

TABLE 4.1-I.- MASS PROPERTIES AT LAUNCH FOR MISSION AS-201

	Control weight, lb (a)	Launch weight, lb	Center of gravity, in. (b)			Moment of inertia, slug-ft^2 (c)			Product of inertia, slug-ft^2 (c)		
			X	Y	Z	I_{xx} Roll	I_{yy} Pitch	I_{zz} Yaw	I_{xy}	I_{xz}	I_{yz}
Command module	11 090	11 002	1 039.0	0.7	5.5	5 757	5 205	4 553	-35	-304	28
Service module[d]	8 250	8 055	910.4	1.0	0.2	5 132	9 018	8 889	-42	-96	-87
SLA attachment ring	62	87	837.1	0.0	-1.8	108	56	53	0	0	0
Total, less propellant[d]	19 402	19 144	984.0	0.8	3.2	11 027	31 315	30 502	-113	298	-61
[illegible] pellant, [illegible]	14 465	14 661	889.5	28.7	-10.5	4 703	4 830	5 527	194	148	336
Total, with propellant	33 867	33 805	943.0	12.9	-2.7	17 455	52 476	53 413	-4 634	2 764	592
[illegible]apter, less ring	3 533	3 691	639.6	1.1	-2.6	9 390	11 926	11 657	-33	-73	-70
Total injected	37 400	37 496	913.1	11.7	-2.7	26 945	130 518	131 286	-2 096	2 669	1 521
Launch escape subsystem	8 360	8 334	1 297.6	-0.2	1.2	658	23 169	23 156	4	482	0
Total launch	45 760	45 830	983.0	9.6	-2.0	27 835	371 251	372 193	-8 847	5 352	1 453

[a]Used for operational trajectory calculations.

[b] Centers of gravity are in the NASA reference system except that the longitudinal axis has an origin 1000 inches below the tangency point of the command module substructure mold line.

[c]Measured about the center of gravity.

[d]Includes unusable SPS residuals but excludes the usable SPS propellant.

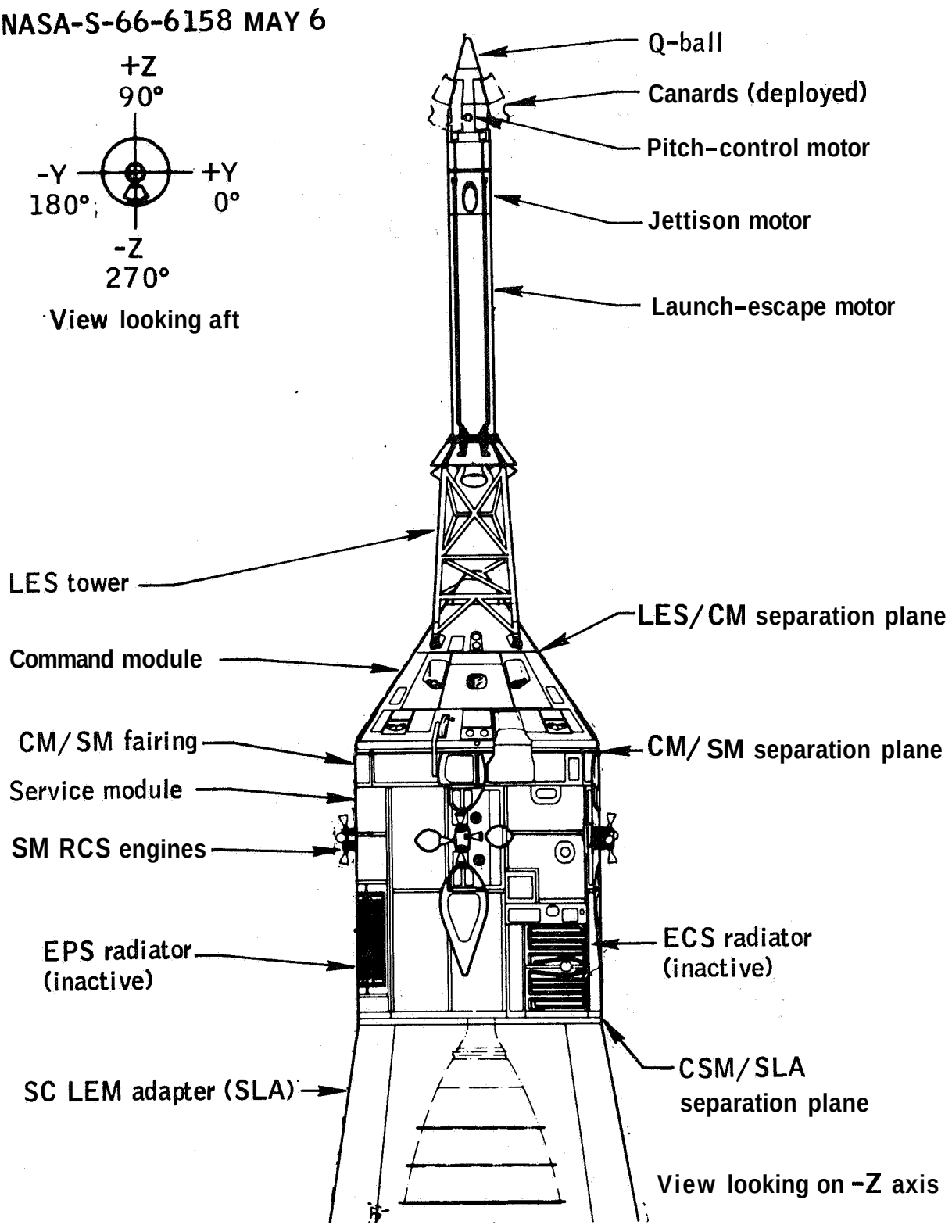
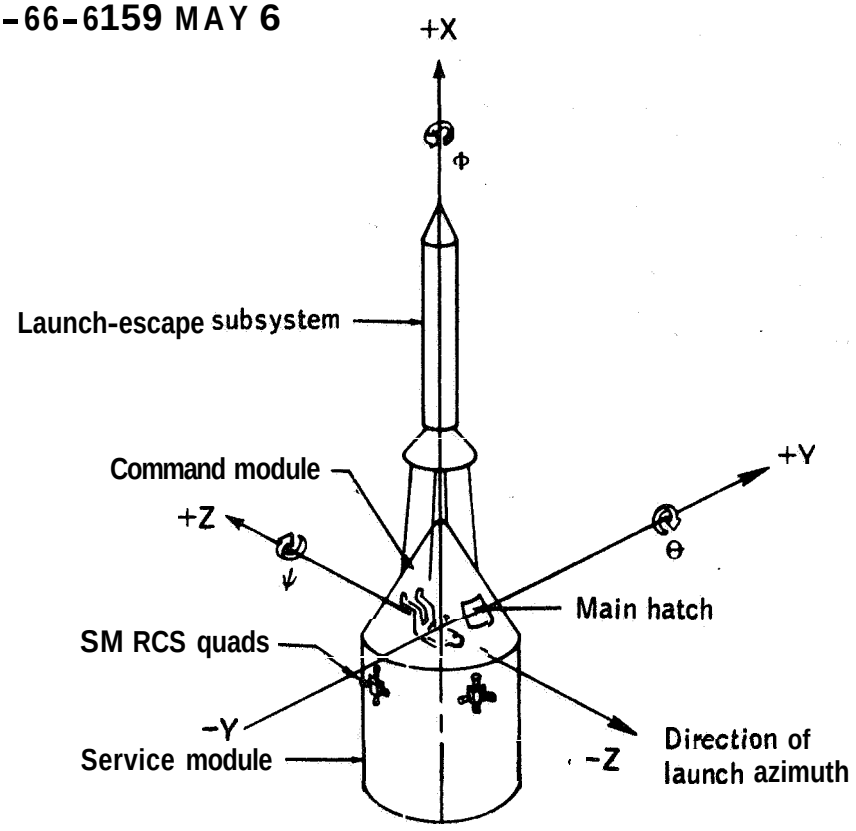


Figure 4.1-1.- Apollo spacecraft *009*, Mission AS-201.

NASA-S-66-6159 MAY 6



Direction	Axis	Moment	Positive direction	Spacecraft maneuver & symbol	Linear velocity	Angular velocity
Longitudinal	X	L	Y to Z	Roll Φ	u	p
Lateral	Y	M	Z to X	Pitch Θ	v	q
Vertical	Z	N	X to Y	Yaw Ψ	w	r

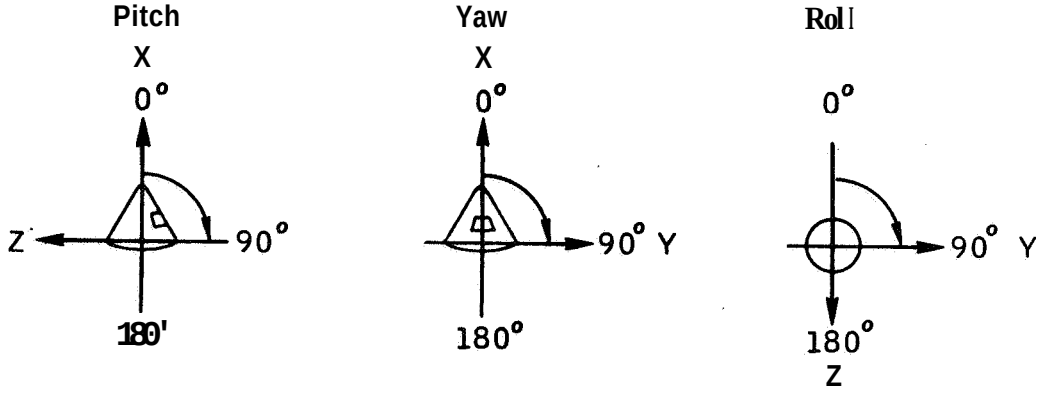


Figure 4.1-2.- Apollo spacecraft body axis system.

4.2 Launch Vehicle Description

The two-stage Saturn IB launch vehicle consisted of stages S-IB and S-IVB, an instrument unit (IU), and various fairings and adapters, The general arrangement of the launch vehicle is shown in figure 4.0-1.

The S-IB stage *dry* weight was 92 500 pounds with a propellant capacity of approximately 880 500 pounds (LOX and RP-1). Eight H-1 engines mounted in two clusters, four inboard and four outboard, produced a total sea-level thrust of 1.6 million pounds.

The S-IVB stage *dry* weight was 23 400 pounds with a propellant capacity of approximately 228 500 pounds (LH_2 and LOX). The single J-2 engine of the S-IVB stage produces a thrust of 200 000 pounds at vacuum conditions.

The instrument unit contained most of the flight control equipment, including the vehicle inertial guidance and control system and the airborne hardware of two tracking systems and four telemetry links. The IU also had an integral power supply and distribution system, cooling systems, and a gaseous nitrogen supply system. The IU began to function prior to lift-off in order to command S-IB start sequencing and to maintain programming, sequencing, and flight control through S-IB and S-IVB stage operation and coast.

Vehicle telemetry systems were provided for each stage and the IU. These telemetry systems included four airborne links in the S-IB stage (two FM/FM, one PCM, and one single side band (SSB)), five in the S-IVB stage (three FM/FM, one PCM, and one SSB), and four links in the IU (two FM/FM, one PCM, and one SSB). One tracking system was located in the S-IB stage and two in the IU.

A detailed description and the performance of the Saturn IB launch vehicle, SA-201, is presented in reference 13.

5.0 FLIGHT TRAJECTORIES

The trajectories referred to as "planned" are preflight-calculated nominal trajectories (ref. 14), and the trajectories referred to as "actual" are based on the Manned Space Flight Network tracking data. The "actual" launch trajectory presented in this report was calculated by the Marshall Space Flight Center. The "actual" midcourse and reentry trajectory phases were calculated by the Manned Spacecraft Center. A ground track for this mission is presented in figure 5.0-1.

The actual trajectory parameters are compared with the planned significant event times during the launch phase, midcourse phase, and reentry phase in table 5.0-I.

Launch phase.- The trajectory parameters for the actual and planned launch phase are shown in figure 5.0-2. The actual data in general show good agreement with the planned trajectory for the first 300 seconds; however, the actual parameters are slightly lower than the planned trajectory from T+300 seconds until S-IVB cutoff, which occurred 10 seconds later than the nominal time.

Midcourse phase.- The trajectory parameters for the actual and planned midcourse phase are presented in figure 5.0-3. This phase is from S-IVB cutoff +10 seconds to the time when the command module (CM) reaches an altitude of 400 000 feet. The actual data up to the ullage prior to the first service propulsion subsystem (SPS) burn were calculated from Antigua radar data, and the actual data fromthe end of the second SPS burn down to an altitude of 400 000 feet were calculated from Ascension radar data. Since radar tracking was not obtained during the SPS burns, the actual trajectory data were simulated during this phase, based on the thrust conditions that had been observed. At the end of the second SPS burn (see table 5.0-1) the velocity was 850 ft/sec lower and the flight-path angle was 0.83° higher than the planned conditions. These differences indicated that the SPS performance was somewhat less than planned, and resulted in the separation of the command module at a higher altitude than planned (see table 5.0-1).

Reentry phase.- The low performance of the SPS resulted in a degradation of the reentry (400 000 ft altitude) conditions. The inertial velocity at reentry was 778 ft/sec lower and the flight-path angle was 0.44° shallower than the planned conditions. (See table 5.0-I and fig. 5.0-4.) As a result, the total maxim heating rate and maximum structural loading produced was less than expected (188 $Btu/ft^2/sec$ and 16.0g respectively, expected). The calculated total maxim heat rate

achieved was 164 Btu/ft^2/sec (total convective, 151.3; total radiative, 12.8) and surpasses the minimum heat-rate test requirements of 160 Btu/ft^2/sec. The structural loads during reentry reached a maxim of 14.3g.

During reentry at Ti-1649 seconds, the control system ceased to function and a positive roll rate developed instead of the planned lifting reentry. The reentry trajectory was calculated by using the position and velocity vector at 400 000 feet based on the Ascension radar tracking data. This position velocity vector was integrated through reentry by using a lift-to-drag (L/D) ratio of 0.33, a density profile defined in "Arcasonde Ascension Data" (dated Feb. 26, 1966, measured at 1850 G.m.t.), and a -10° bank-angle orientation for the spacecraft into blackout until Ti-1649 seconds. Actual. roll-rate data were employed to simulate the trajectory to drogue parachute deployment at T+1855.4 seconds (24 552 ft altitude). Main parachutes were deployed at T+1908.4 seconds corresponding to an estimated altitude of 10 016 feet which is 734 feet lower than the planned deployment at 10 750 feet. The simulated reentry trajectory agrees closely with maximum g and the time of drogue parachute deployment recorded onboard the spacecraft, and matches the actual impact point (8.18" S. latitude, 11.15° W. longitude) as reported by the recovery ship. If the roll rates had not occurred, the command module would have landed at latitude 9.40° S. and longitude 9.18" W. which is 58 nautical miles downrange of the planned landing point. The actual landing point was 40.6 nautical miles uprange of the planned landing point (latitude 8.77° S. and longitude 10.72° W.) as can be seen in figure 5.0-5. Table 5.0-II presents the calculated actual impact and touchdown points for the S-IB, launch-escape tower, the S-IVB, service module, and command module.

The actual. range plotted against altitude in figure 5.0-6 was close to planned during the launch phase and the midcourse phase up to the first SPS burn. During the burn, the range versus altitude was above the planned until blackout. After blackout, the actual range was less than planned.

TABLE 5.0-I.- COMPARISON OF PLANNED AND ACTUAL TRAJECTORY PARAMETERS, MISSION AS-201

Condition	Planned	Actual
S-IB cutoff		
Time from range zero, sec	146.6	146.9
Time from range zero, min:sec	2:26.6	2:26.9
Geodetic latitude, deg North	28.38	28.37
Longitude, deg West	79.95	79.94
Altitude, ft	193 035	190 521
Altitude, n. mi.	31.8	31.4
Range, n. mi.	33.5	33.9
Space-fixed velocity, ft/sec	7 471.43	7 499.66
Space-fixed flight-path angle, deg	24.77	24.52
Space-fixed heading angle, deg East of North	102.32	102.46
S-IVB cutoff		
Time from range zero, sec	592.7	602.9
Time from range zero, min:sec	09:52.7	10:02.9
Geodetic latitude, deg North	23.66	23.55
Longitude, deg West	65.56	65.30
Altitude, ft	854 793	857 672
Altitude, n. mi.	140.7	141.2
Range, n. mi.	859.8	857.9
Space-fixed velocity, ft/sec	22 768.98	22 769.23
Space-fixed flight-path angle, deg	7.93	7.94
Space-fixed heading angle, deg East of North	112.00	112.12

TABLE 5.0-I.- COMPARISON OF PLANNED AND ACTUAL TRAJECTORY PARAMETERS, MISSION AS-201 - Continued

Condition	Planned	Actual
S-IVB cutoff +10 sec (insertion)		
Time from range zero, sec	602.7	612.9
Time from range zero, min:sec	10:02.7	10:12.9
Geodetic latitude, deg North	23.44	23.33
Longitude, deg West	65.01	64.74
Altitude, ft.	885 780	887 706
Altitude, n. mi.	145.8	146.1
Range, n. mi.	894	909
Space-fixed velocity, ft/sec	22 747	22 750
Space-fixed flight-path angle, deg	7.80	7.81
Space-fixed heading angle, deg East of North	112.24	112.37
CSM/S-IVB separation		
Time from range zero, sec	834.4	844.9
Time from range zero, min:sec	12:54.4	14:04.9
Geodetic latitude, deg North	17.84	17.70
Longitude, deg West	53.00	52.74
Altitude, ft.	1423 640	1 427 377
Altitude, n. mi.	234.3	235.1
Range, n. mi.	1 647	1 664
Space-fixed velocity, ft/sec	22 049	22 050
Space-fixed flight-path angle, deg	4.12	4.13
Space-fixed heading angle, deg East of North	116.83	116.92

TABLE 5.0-I.- COMPARISON OF PLANNED AND ACTUAL TRAJECTORY PARAMETERS, MISSION AS-201 - Continued

Condition	Planned	Actual
Beginning of +X translation prior to first SPS thrust period		
Time from range zero, sec	1 170.7	1 181.2
Tim from range zero, min:sec	19:30.7	19:41.2
Geodetic latitude, deg North	8.70	8.53
Longitude, deg West	37.56	37.34
Altitude, ft	1 575 924	1 586 803
Altitude, n. mi.	259.4	261.2
Range, n. mi.	2 702	2 724
Space-fixed velocity, ft/sec	21 853	21 851
Space-fixed flight-path angle, deg	-1.70	-1.64
Space-fixed heading angle, deg East of North	120.72	120.80
Second SPS cutoff (+3 sec for tailoff)		
Tim from range zero, sec	1 413.2	1 423.7
Time from range zero, min:sec	23:33.2	23:43.7
Geodetic latitude, deg North	1.07	.99
Longitude, deg West	25.81	25.72
Altitude, ft	920 024	969 858
Altitude, n. mi.	151.4	159.6
Range, n. mi.	3 540	2 553
Space-fixed velocity, ft/sec	26 674	25 824
Space-fixed flight-path angle, deg	-9.88	-9.05
Space-fixed heading angle, deg East of North	120.68	120.69

TABLE 5.0-I.- COMPARISON OF PLANNED AND ACTUAL TRAJECTORY PARAMETERS, MISSION AS-201 - Continued

Condition	Planned	Actual
CM/SM separation		
Time from range zero, sec	1 444.2	1 455.0
Time from range zero, min:sec	24:04.2	24:15.0
Geodetic latitude, deg South	.03	.09
Longitude, deg West	24.09	24.04
Altitude, ft	779 115	844 244
Altitude, n. mi.	128.4	138.9
Range, n. mi.	3 663	3 660
Space-fixed velocity, ft/sec	26 831	25 968
Space-fixed flight-path angle, deg	-9.68	-8.90
Space-fixed heading angle, deg East of North	120.70	120.69
Reentry conditions (400 000 ft altitude)		
Time from range zero, sec	1 530.3	1 565.6
Time from range zero, min:sec	25:30.3	26:05.6
Geodetic latitude, deg South	3.18	3.99
Longitude, deg West	19.18	17.94
Altitude, ft	400 000	400 000
Altitude, n. mi.	65.8	65.8
Range, n. mi.	4 012	4 107
Space-fixed velocity, ft/sec	27 260	26 481
Space-fixed flight-path angle, deg	-9.04	-8.60
Space-fixed heading angle, deg East of North	120.55	120.47

TABLE 5.0-I.- COMPARISON OF PLANNED AND ACTUAL TRAJECTORY PARAMETERS, MISSION AS-201 - Concluded

Condition	Planned	Actual
Maximum conditione		
Exit acceleration, g	4.1	4.1
Exit dynamic pressure, lb/sq ft	626	617
Altitude, a. mi	264.8	265.7
Space-fixed velocity, ft/sec	27 393	26 620
Earth-fixed velocity, ft/sec	26 092	25 318
Reentry acceleration, g	16.0	14.3
Reentry dynamic pressure, lb/sq ft	1 043	930
Maximum heat rate, $Btu/ft^2/sec$	188.4	164.1

TABLE 5.0-II.- IMPACT AND TOUCHDOWN POINTS FOR MISSION AS-201:

System	Elapsed time, sec	Latitude, deg	Longitude, deg	Range, n.mi.
S-IB	533.3	27.30	-76.04	251
Tower	687.5	27.09	-75.26	295
S-IVB	1916.6	-9.66	-10.08	4677
SM	1725.7	-6.93	-13.3	4437
CM	2239.7	-8.18	-11.15	4577

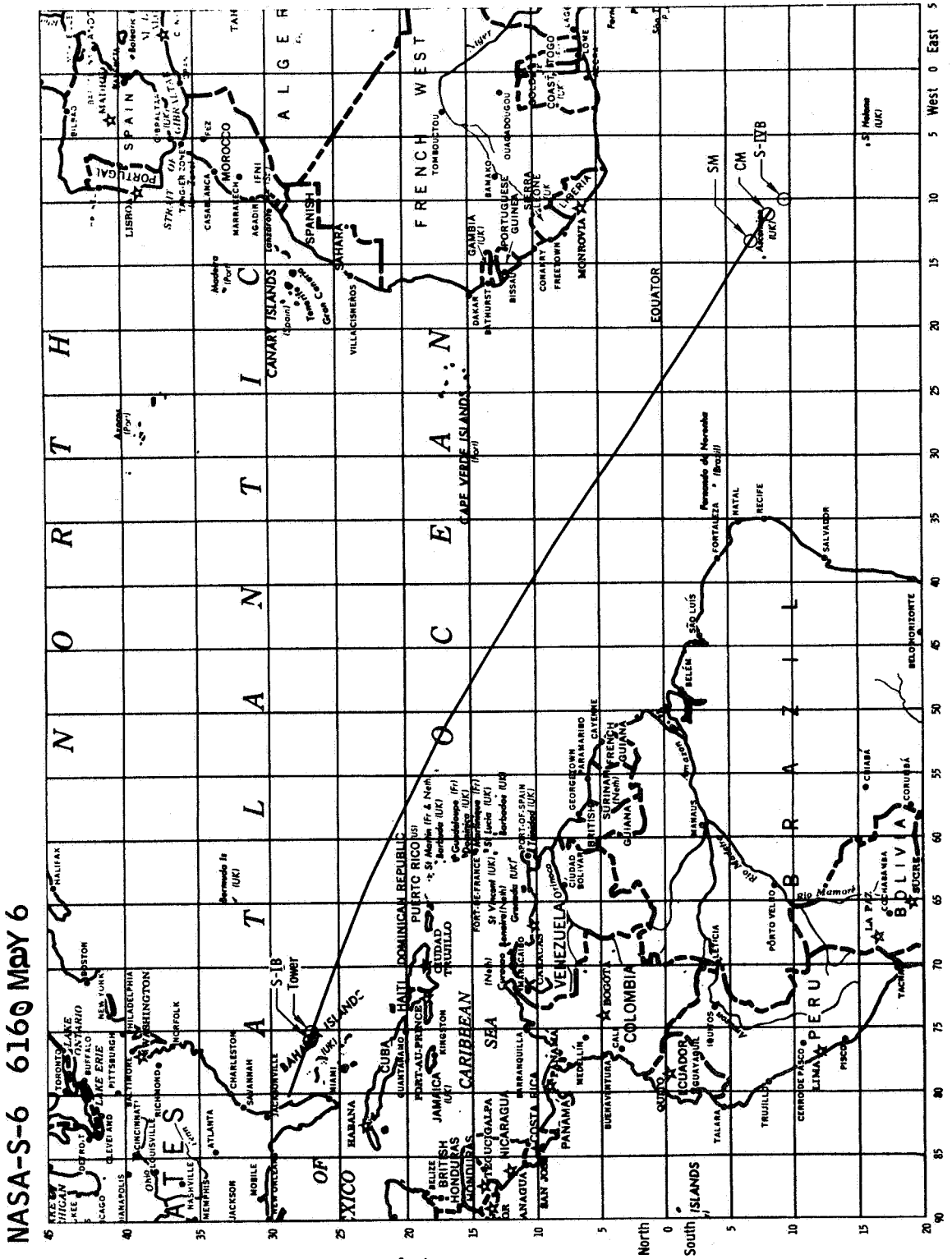
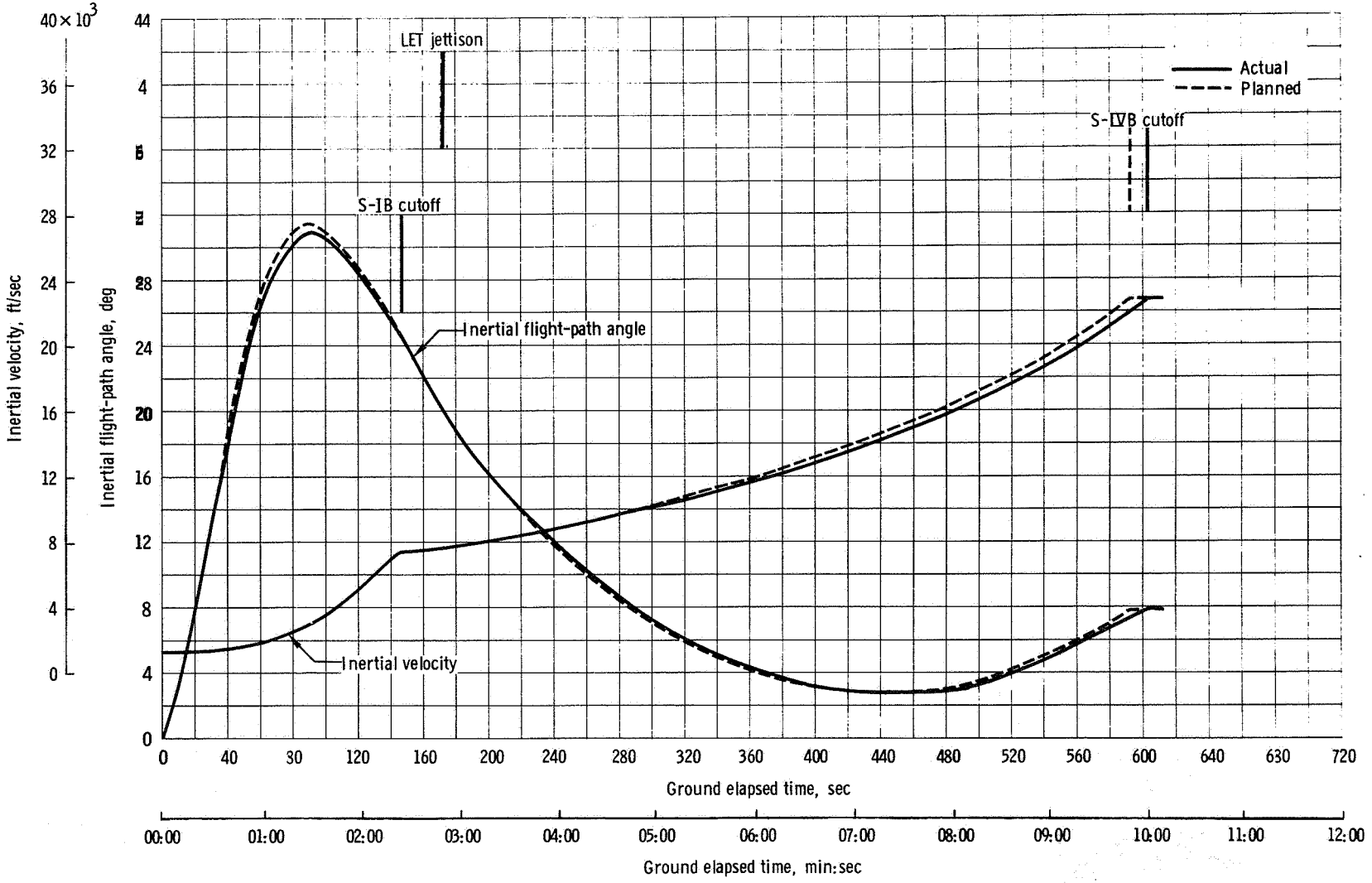
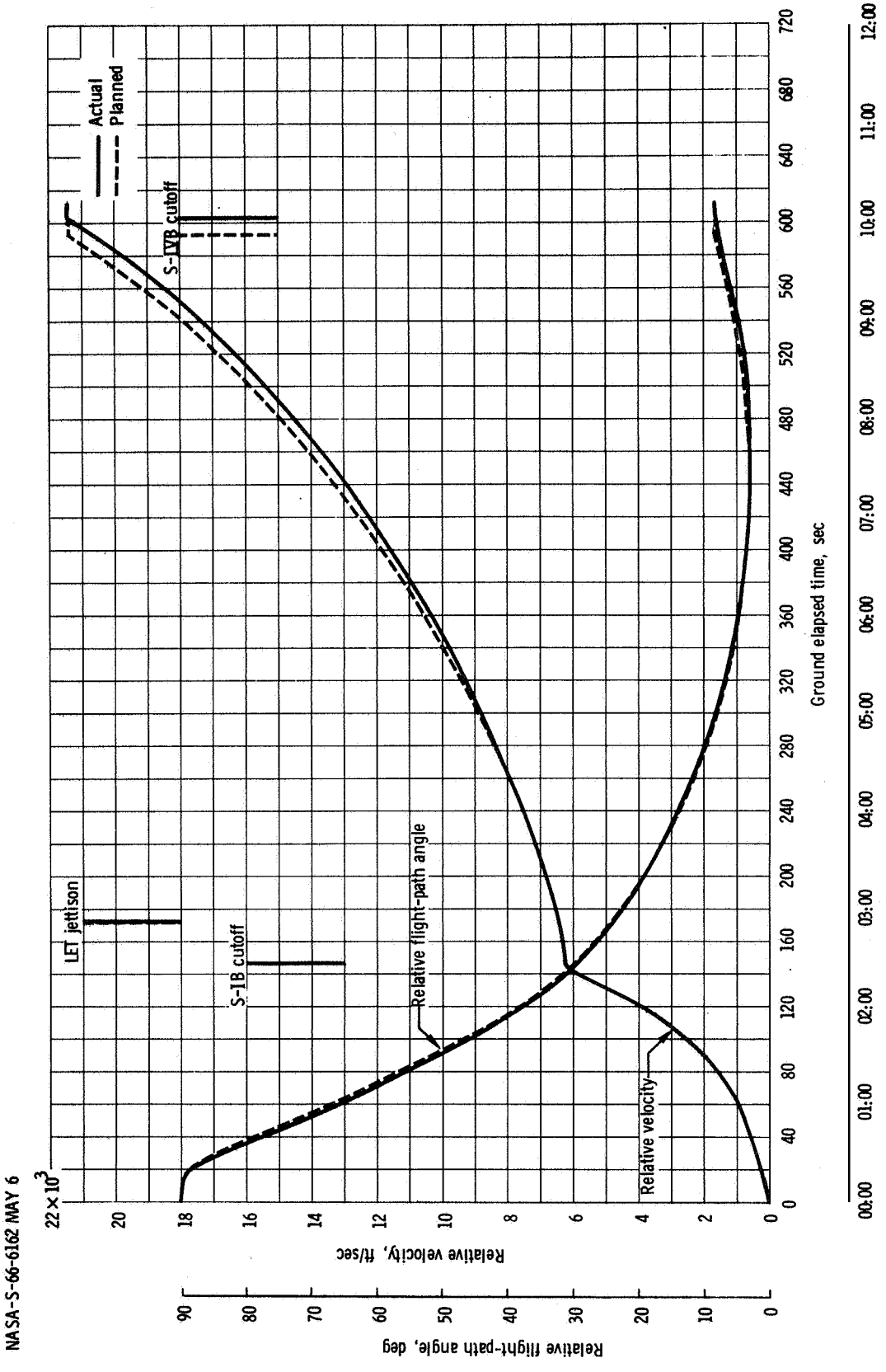


Figure 5.0-1.- Ground track for Mission AS-201.



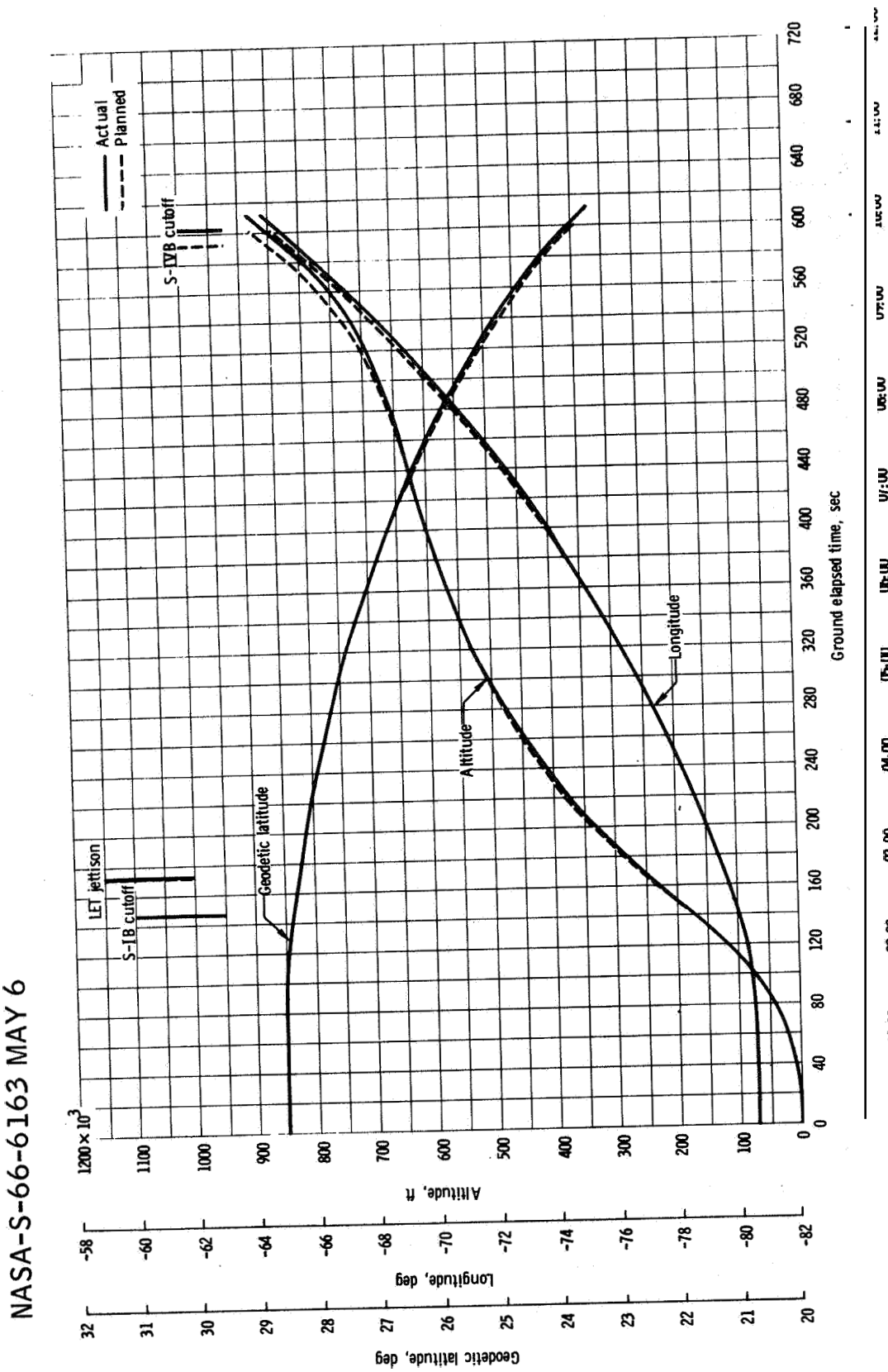
(a) Inertial velocity and inertial flight-path angle.

Figure 5.0-2.- Time histories of trajectory parameters for Mission AS-201 launch phase.



(b) Relative velocity and relative flight-path angle.

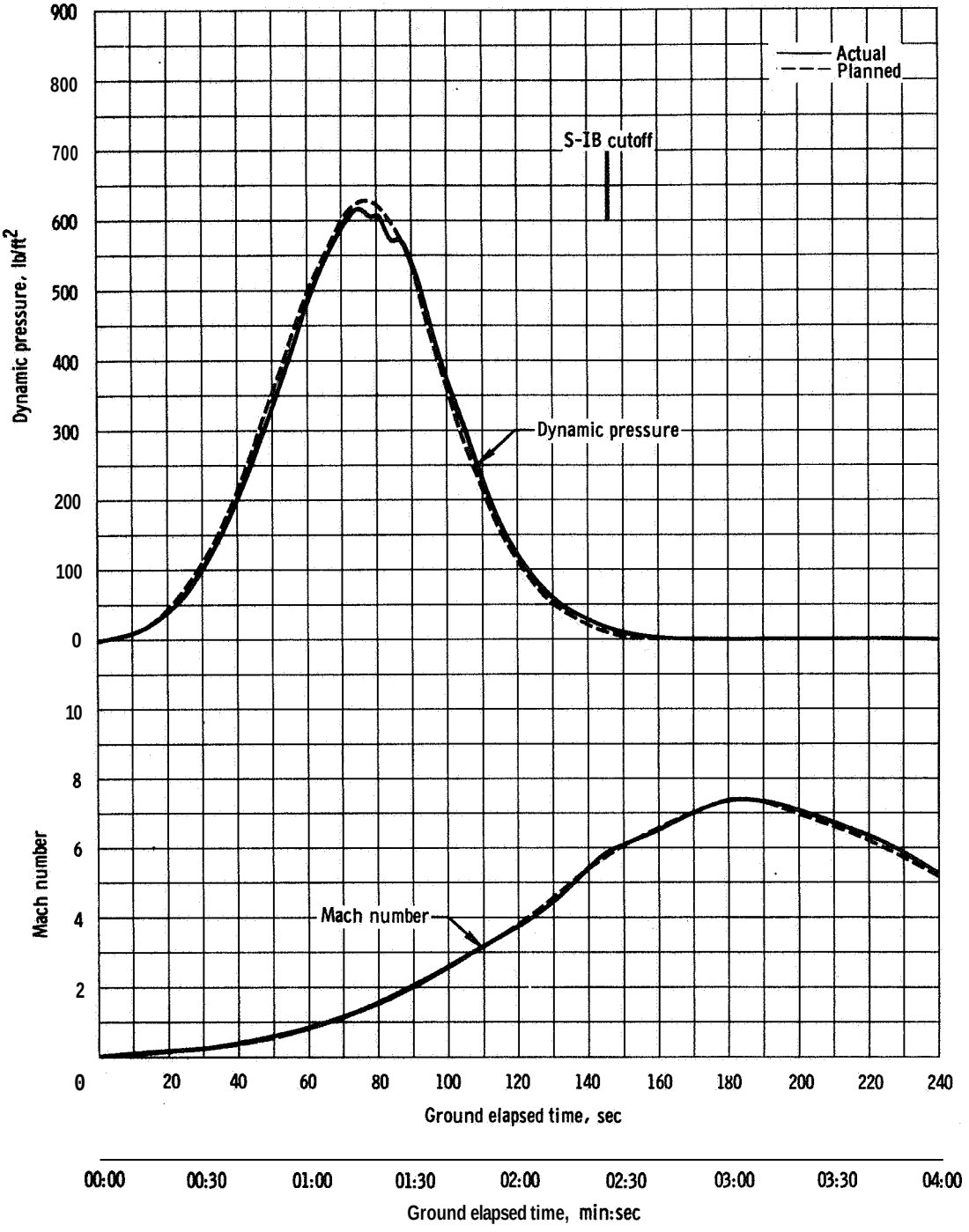
Figure 5.0-2. - Continued.



(c) Altitude, longitude and geodetic latitude.

Figure 5.0-2.- Continued.

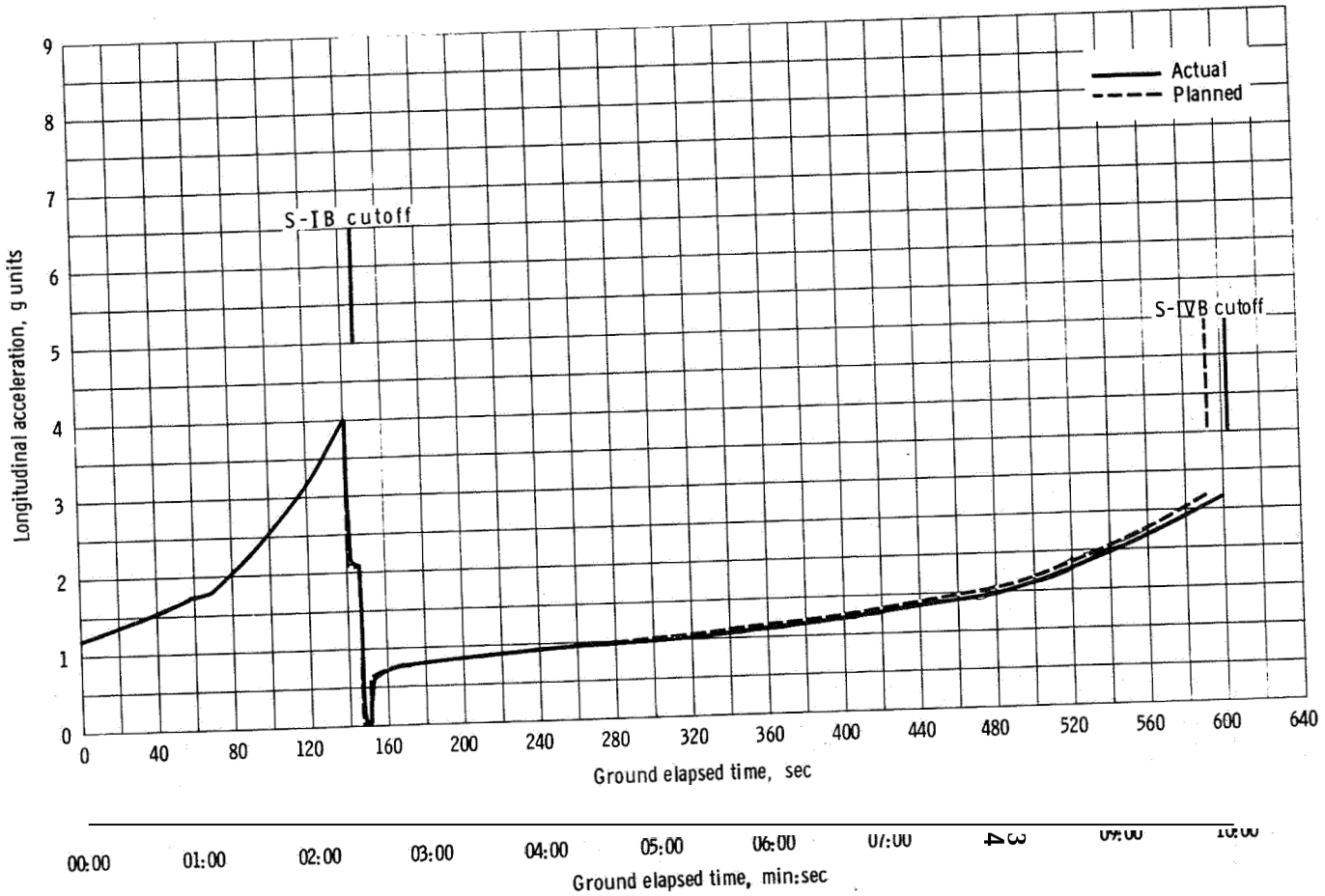
NASA-S-66-6161 MAY 6



(d) Mach number and dynamic pressure.

Figures 5.0-2. - Continued.

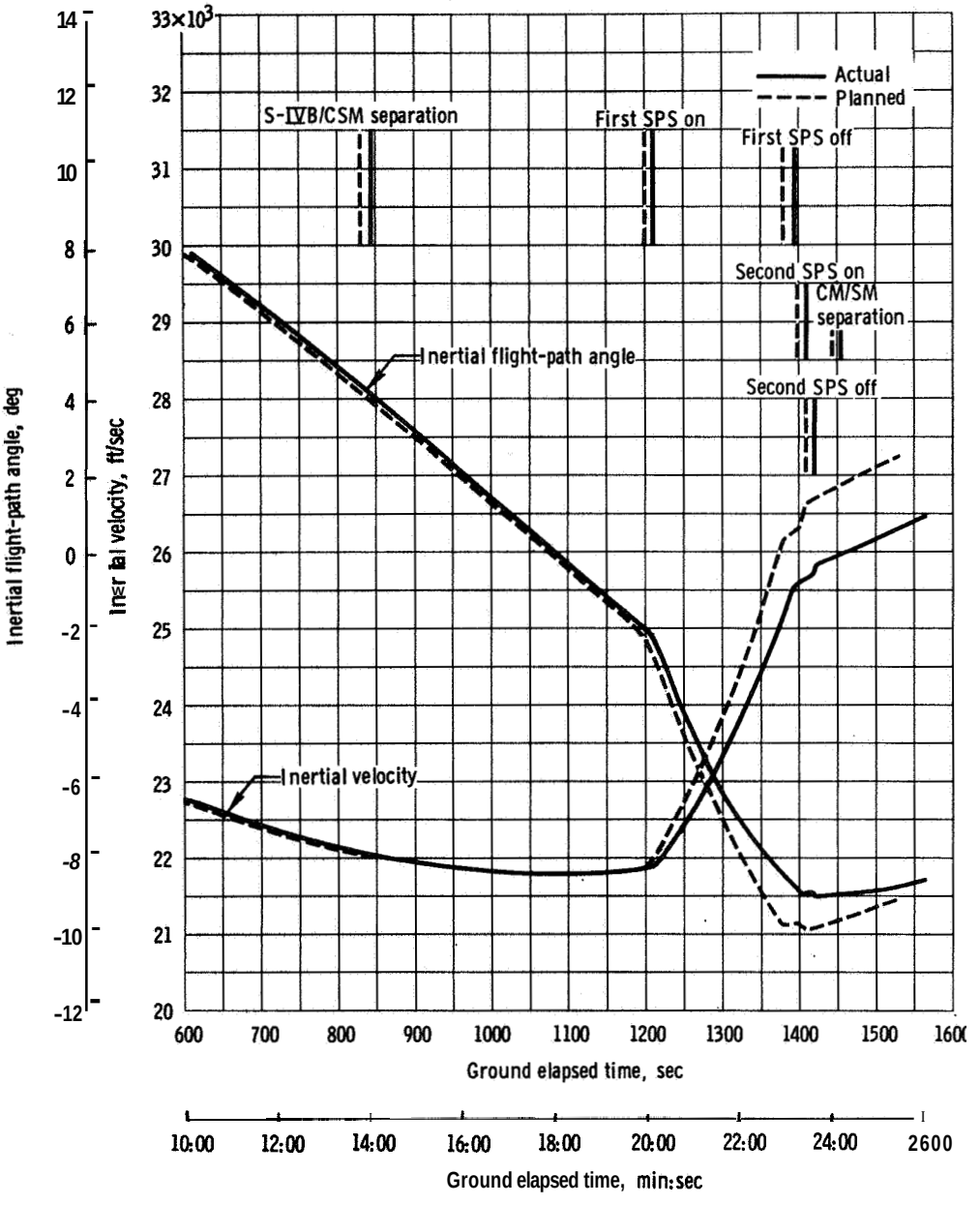
NASA-S-66-6165 MAY 6



(e) Longitudinal acceleration.

Figure 5.0-2.- Concluded.

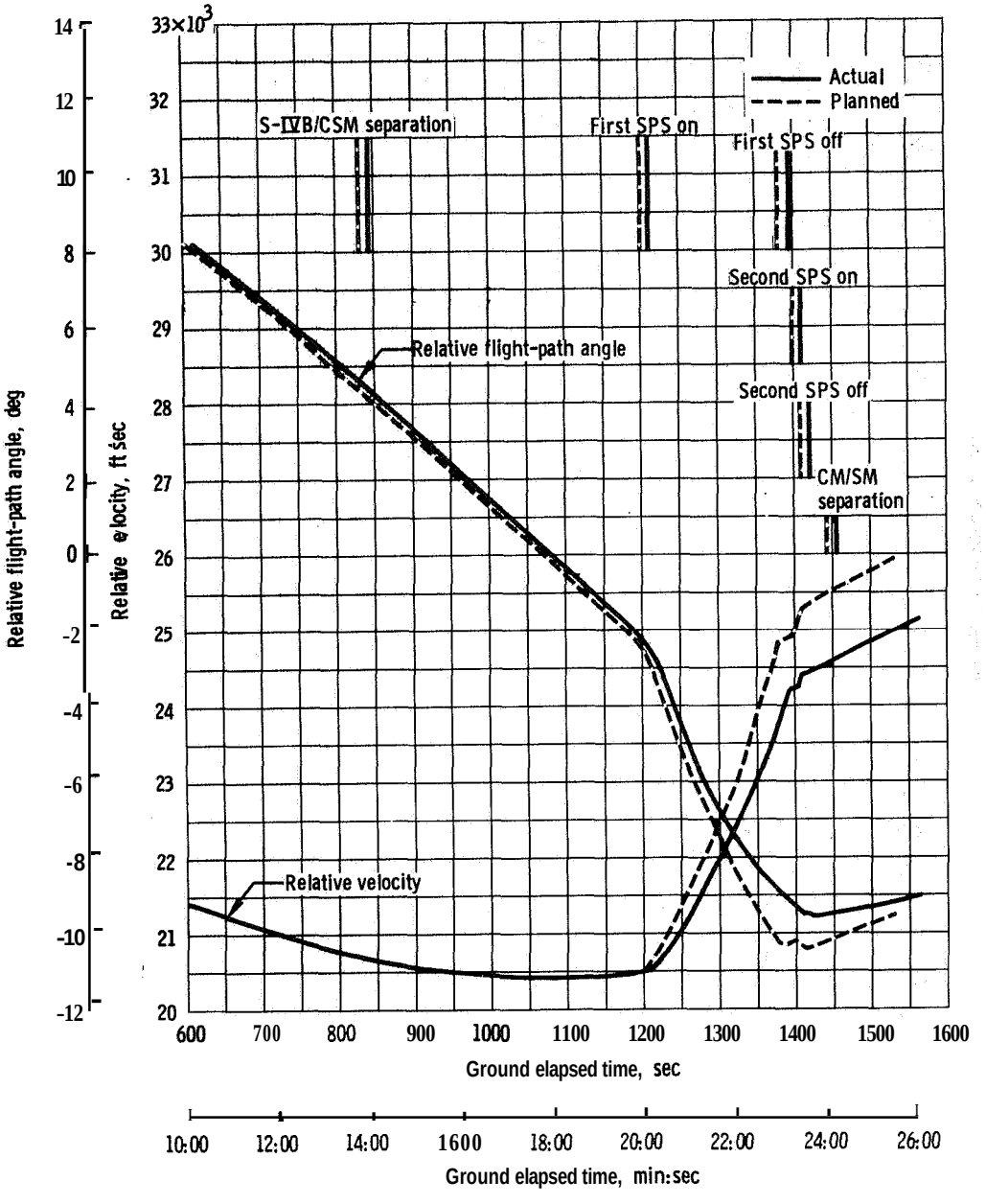
NASA-566-6166MAY 6



(a) Inertial velocity and inertial flight-path angle.

Figure 5.0-3. - Time histories of trajectory parameters for Mission AS-201 midcourse phase.

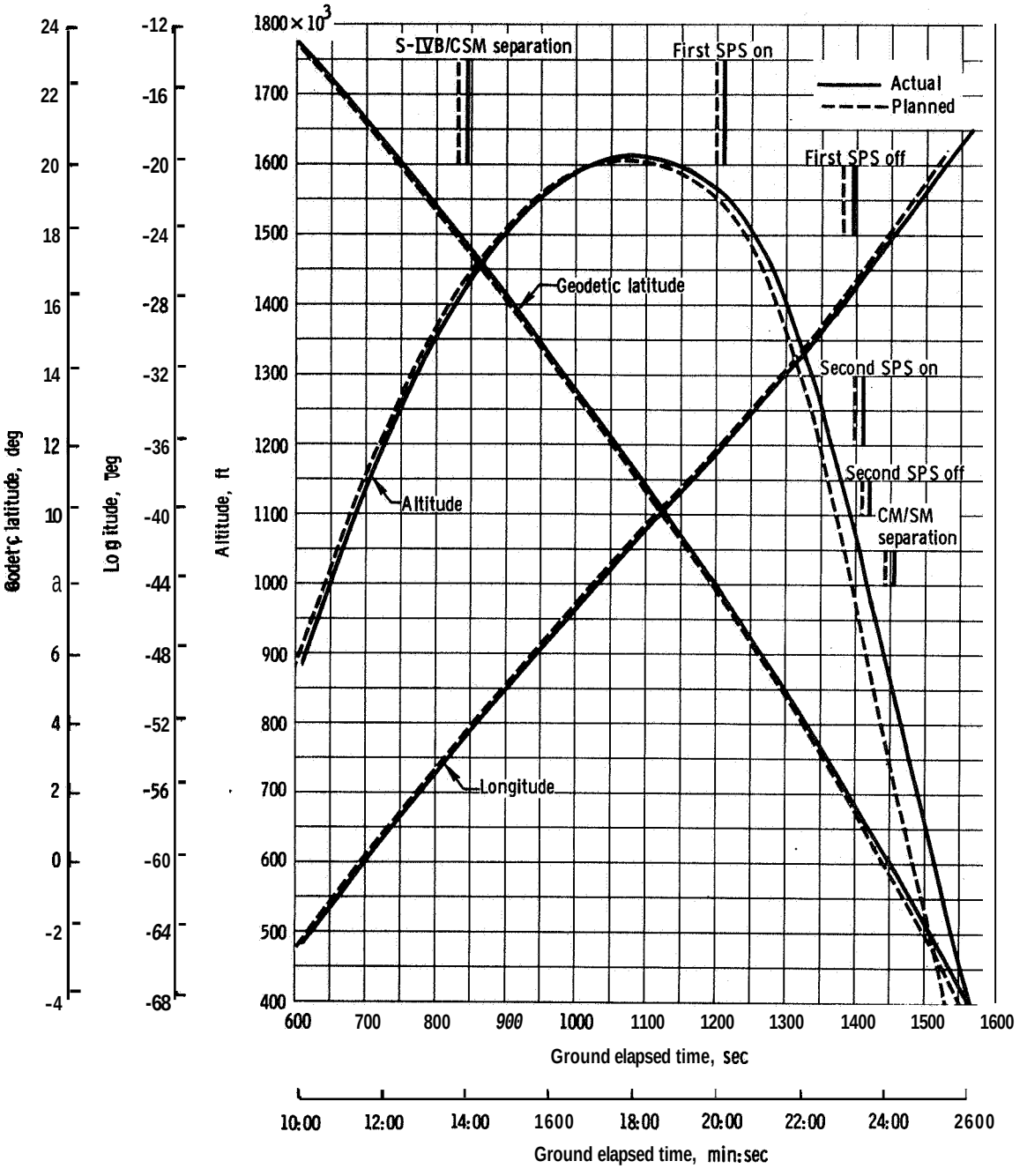
NASA-S-66-6167 MAY 6



(b) Relative velocity and relative flight-path angle.

Figure 5.0-3. - Continued.

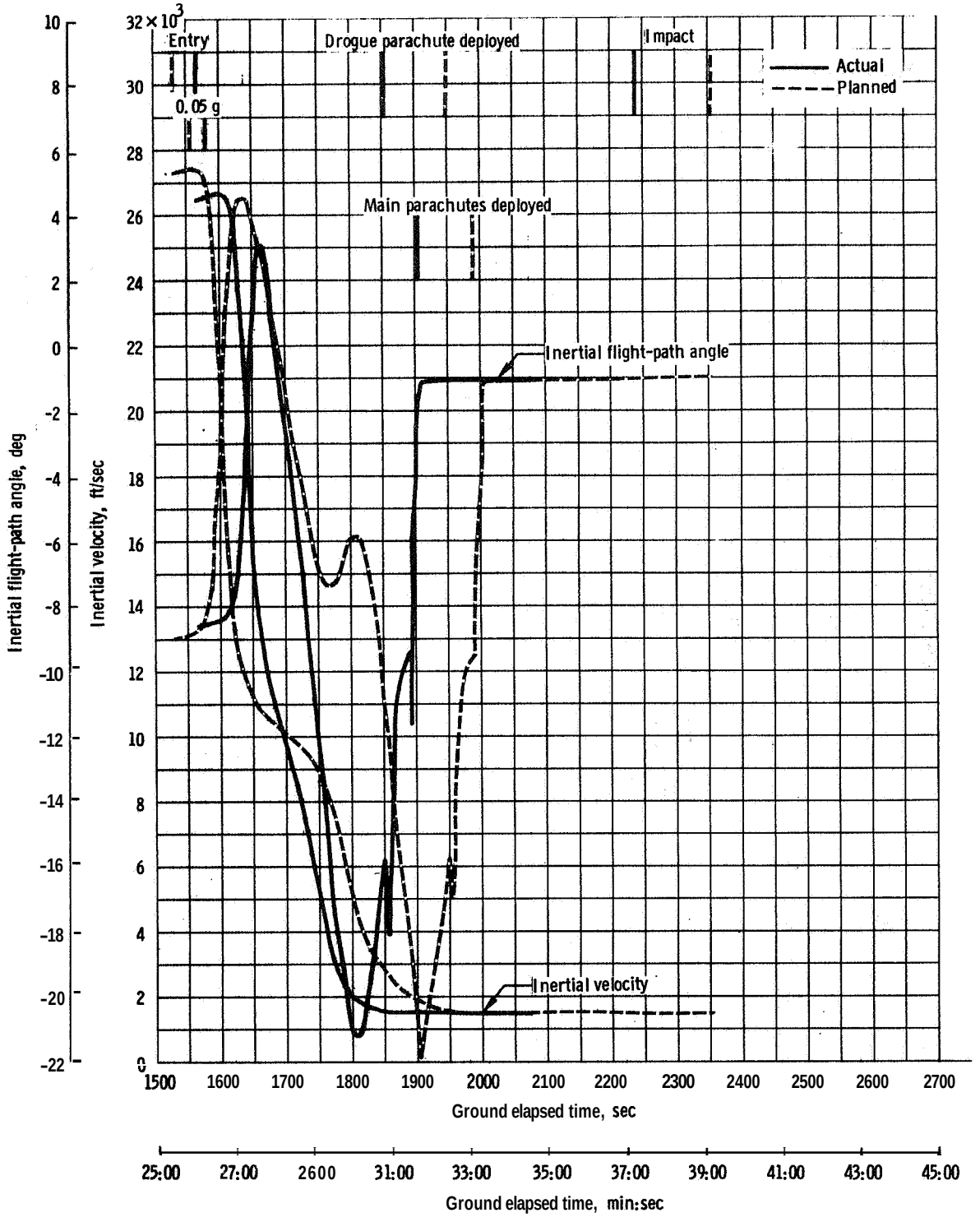
NASA-S-66-6168MAY 6



(c) Altitude, longitude and geodetic latitude.

Figure 5.0-3. - Concluded.

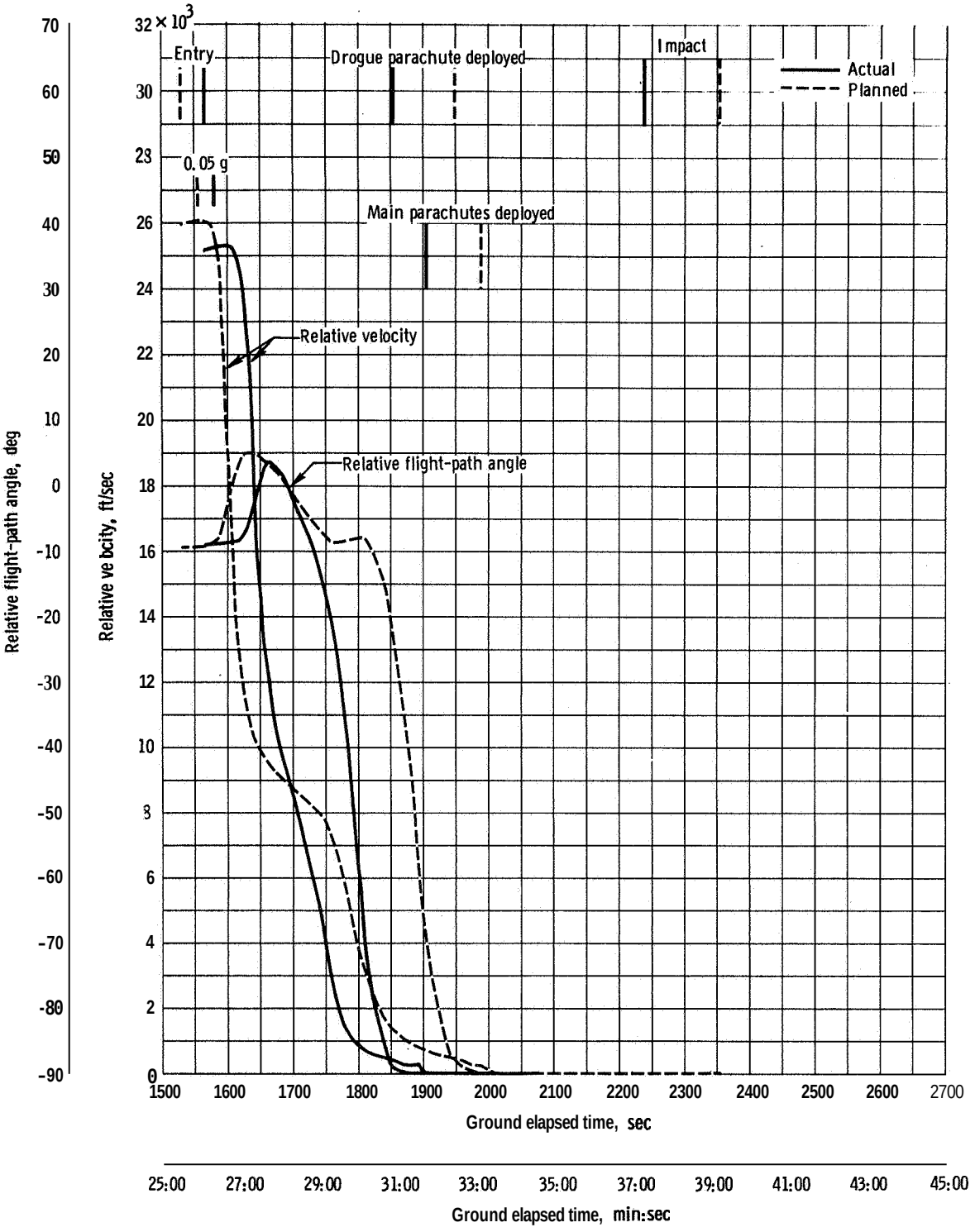
NASA-S-66-6169 MAY 6



(a) Inertial velocity and inertial flight-path angle.

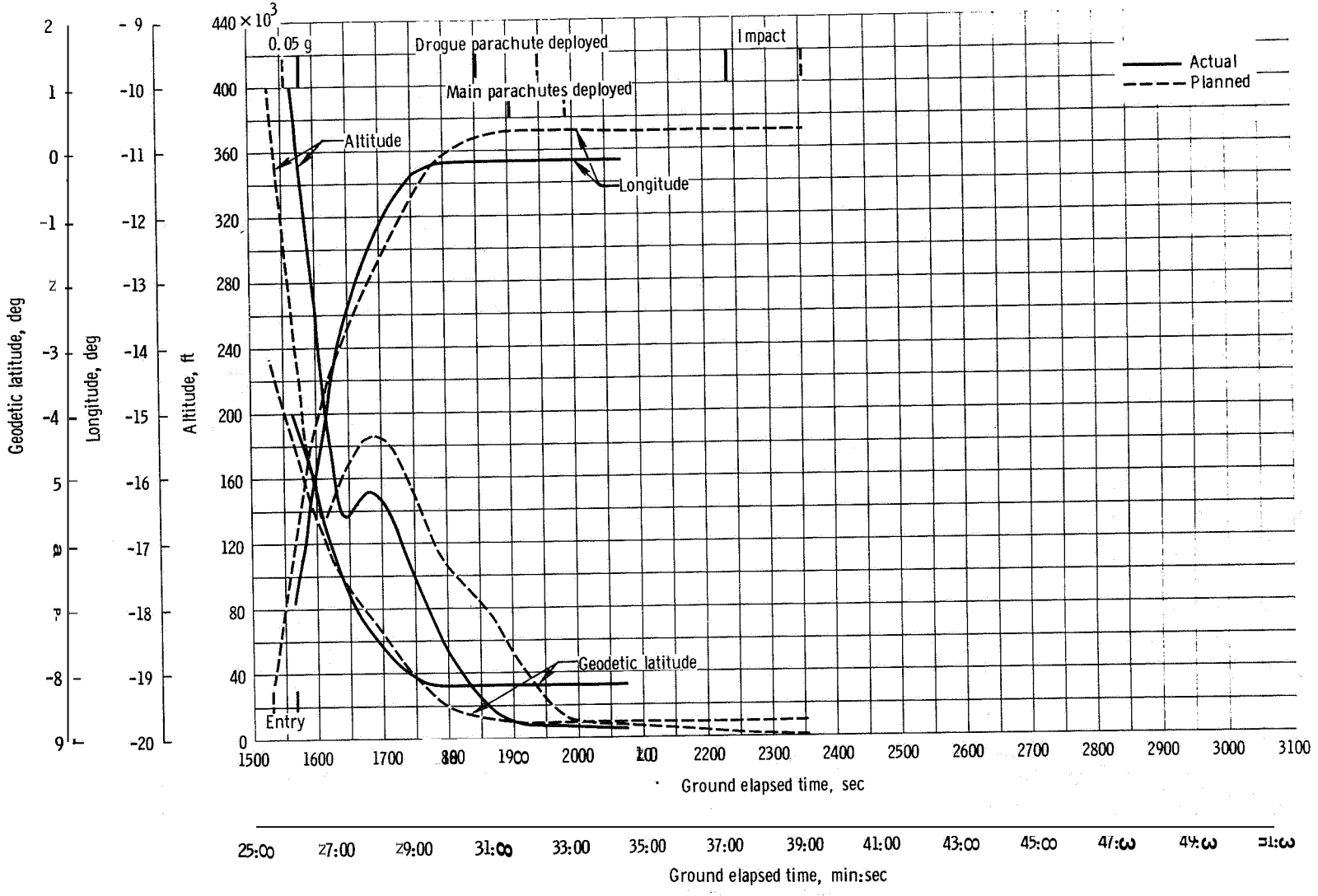
Figure 5.0-4. - Time histories of trajectory parameters for Mission AS-201 reentry phase.

NASA-S-66-6170 MAY 6



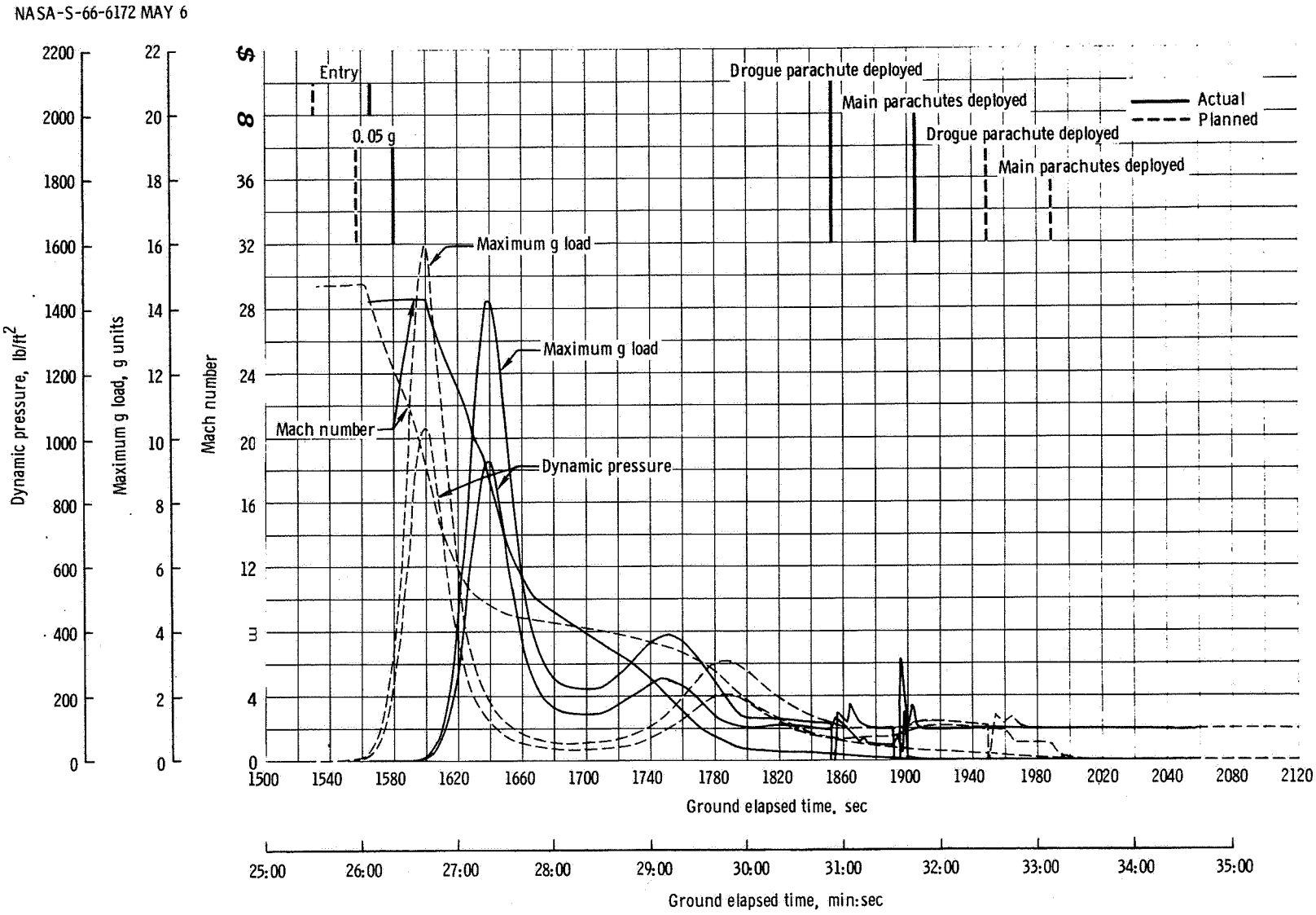
(b) Relative velocity and relative flight-path angle.

Figure 5.0-4. - Continued.



(c) Altitude, longitude and geodetic latitude.

Figure 5.0-4. - Continued.



(d) Mach number maximum g load and dynamic pressure.

Figure 5.0-4.- Concluded.

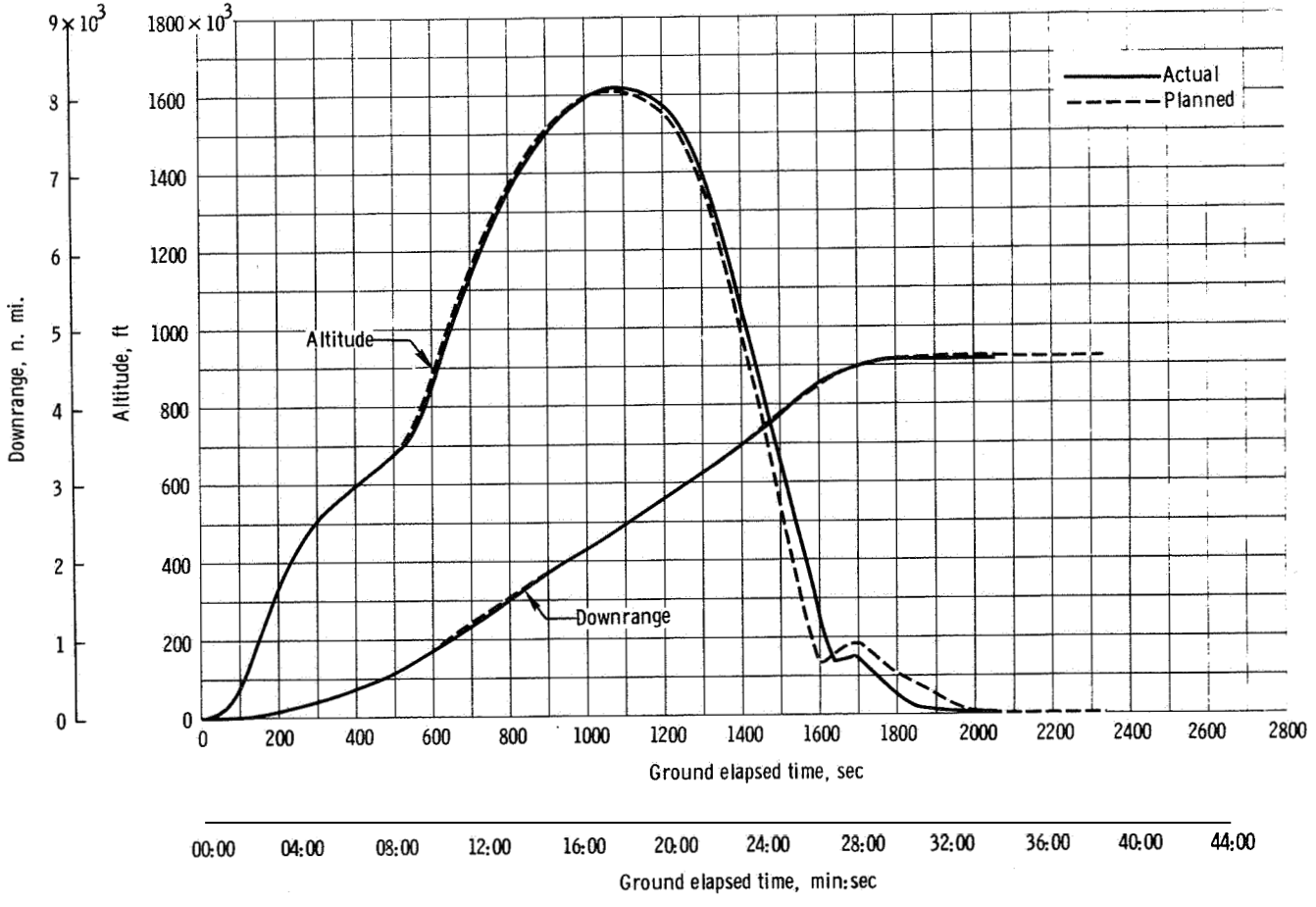
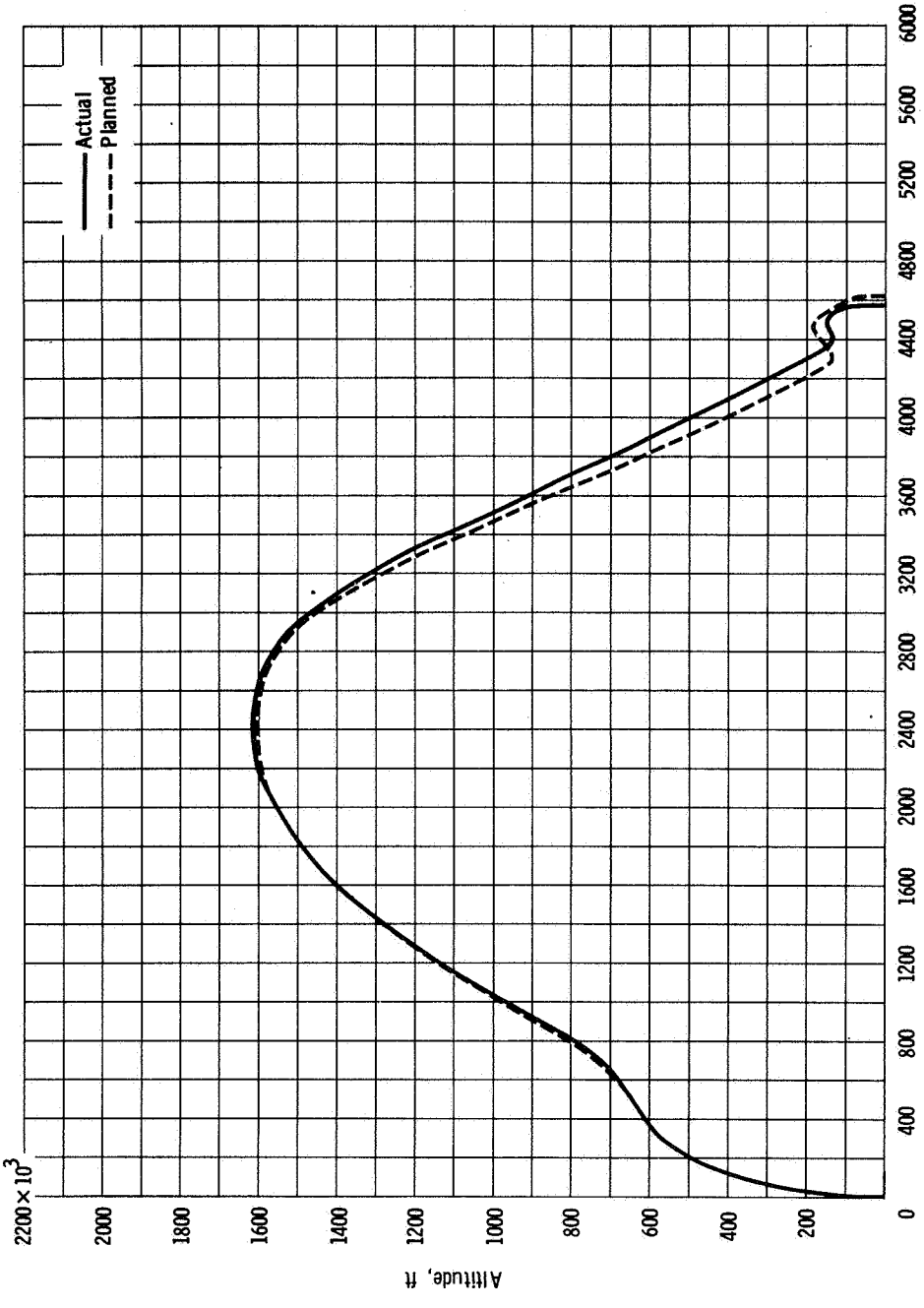


Figure 5.0-5. - Time history of altitude and downrange, Mission AS-201.



NASA-S-66-6174 MAY 6

Figure 5.0-6. - Altitude plotted against downrange, Mission AS-201.

6.0 AERODYNAMICS AND AEROTHERMODYNAMICS

6.1 Aerodynamics

Summary.- Analysis of the preflight wind-tunnel aerodynamic data for the reentry configuration of Apollo spacecraft 009 resulted in a hypersonic lift-to-drag ratio (L/D) of 0.34 ± 0.04. The hypersonic trim angle of attack (α) was correspondingly 157° ± 3°. On the basis of a preliminary analysis of limited flight data and postflight simulation, both the L/D ratio and the trim angle of attack during the mission were within the preflight estimates even though the command module (CM) was not attitude-controlled during reentry from T+1649 seconds until drogue parachute deployment at T+1853.9 seconds (see section 7.9). The control that was exercised during the initial portion of the reentry adequately maintained the proper spacecraft trim attitude in the full lift-vector-up position. During the uncontrolled portion of the flight, postflight simulations indicate that, while rolling about the velocity vector, the CM was also oscillating approximately ±5° in the pitch and yaw planes about the nominal aerodynamic trim angle. The CM roll was attributed to the effects of protuberances coupled with the Y and Z offset of the center of gravity.

Instrumentation.- The analysis of the aerodynamic characteristics of spacecraft 009 during reentry was based on two types of data from the flight instrumentation: accelerometer data and angular rate data. Because of unforeseen difficulties during the flight these data must be qualified. The lift- and drag-axis linear accelerometer readings were on the flight qualification tape recorder only and therefore are considered unusable where the data from this recorder becomes erratic at about T+1653 seconds. These data were the sole source for the flight-measured peak deceleration load during reentry and although they disagree somewhat with the calculated value of section 5, it was thought that the measured values were more pertinent to the analysis of this section. Structural X-, Y-, and Z-axes linear accelerometer data were available throughout reentry; however, the X-axis accelerometer had an upper limit of +10g and therefore did not measure the peak g load. Rate gyro data about the spacecraft body axes were available during reentry with one exception: the roll rate instrumentation reached its saturation point (26 deg/sec) at approximately T+1778 seconds and remained saturated until the drogue parachutes were deployed at T+1855.4 seconds.

Performance, attitude-controlled phase.- The reaction control subsystem (RCS) positioned the CM in a blunt-end-forward attitude prior to reentry. During the portion of the flight that the vehicle was-controlled (considered to be until T+1649 sec) it was stable in an aerodynamically trimmed attitude. The predominant control observed during this time was

both negative roll (-R) engines firing frequently, indicating the presence of a positive aerodynamic roll force.

To determine the lift-to-drag ratio during the controlled phase of the reentry, a parametric study was made varying L/D and the atmospheric density. Figure 6.1-1 shows the family of curves resulting from this study. An extension of the curve representing a nominal 1962 Standard Atmosphere to the line of the flight-measured maxim deceleration load gives a L/D of 0.326. Arcasonde atmosphere data were extrapolated above 200 000 feet and showed a density deviation from -2 percent to almost +9 percent in the altitude region to peak g. Extension of the curve representing an average deviation of +10 percent indicates an L/D approximately equal to 0.32. These values so obtained are for a high Mach number region and agree well with the preflight estimates as shown on figure 6.1-1.

By using flight data from the body-axis accelerometers, values of the ratio of aerodynamic normal-force coefficient to axial-force coefficient, C_N/C_A, were calculated and are presented in the top half of figure 6.1-2 as a function of Mach nmber. The ratio is presented rather than the individual aerodynamic coefficients to eliminate the effects of atmospheric density. In the lower half of the figure the same ratio, C_N/C_A, is shown as obtained from the preflight wind-tunnel data (Mach numbers from 6 to 25). For the same C_N/C_A dues, the flight data indicate an angle of attack of approximately 159°. This corresponds to an L/D = 0.32 from preflight data and supports the previous determination of L/D from the trajectory study, although these accelerometer data show a large band of uncertainty due to data scatter.

Performance, attitude-uncontrolled phase. - At T+1649 seconds the CM lost all rate and attitude control. Due to its inherent aerodynamic characteristics, the vehicle began rolling quite rapidly to rates above the instrumentation limit of 26 deg/sec. During this time the yaw rate was also increasing negatively indicating a coordinated roll about the velocity vector. This condition allowed the determination of the angle of attack, a. A time history of calculated a is shown in figure 6.1-3 compared with preflight data. The flight data show an oscillatory characteristic about an averaged trim angle of attack as shown by the dashed line. The data agree to within 3° of preflight data at the higher Mach numbers where this type of analysis is questionable due to the law roll rates. Agreement is better at lower Mach numbers where the roll rates were considerable. From the flight data and from postflight simulations the indication is that the vehicle was oscillating in the aerodynamic pitch - yaw plane approximately ±5° about the aerodynamic trim angle while rolling about the velocity vector;

Preflight prediction evaluation.- Preflight wind-tunnel measurements (from tests conducted at the AEDC-VKF on July 16, 1965) of the aerodynamic roll coefficient due to protuberances $\left(C_{l_A}\right)$, where offset terms are negligible, indicated that the CM would roll negatively, whereas the flight-measured data show a positive roll rate. Subsequent wind-tunnel tests have been conducted (AEDC-VKF, April 15, 1966), and the combined results were used in postflight simulations. Figure 6.1-4 presents the time histories of the averaged roll rate $(p)_{avg}$ and the averaged roll coefficient $\left(C_{l_A}\right)_{avg}$ with effects of a roll coefficient uncertainty of +0.00002 included. Comparing the rates so generated with the actual flight-measured rates in figure 6.1-4(a) indicated that when the +0.00002 uncertainty was included the results of the latest tests would predict flight comparable roll rates in the positive direction. The variation of the average roll coefficient from additional postflight simulations that bracketed the flight-measured roll rate was interpolated to give an estimate of the actual flight roll coefficient time history which is shown as a dashed line in figure 6.1-4(b). In view of these results, a revision to the roll coefficient uncertainties in the Apollo Mission Data Specifications will be made for all affected subsequent mission spacecraft.

The absence of tumbling during the uncontrolled portion of the reentry indicated that the actual flight damping characteristics were better in the low Mach number regime than the preflight data would predict. Using preflight wind-tunnel damping coefficient data $\left(C_{m_q} + C_{m_{\dot{\alpha}}}\right)$ and comparable flight roll rates in a simulation of the CM reentry dynamics will cause a tumbling motion just prior to drogue parachute deployment, It should be noted, however, that the damping data used represents the "worst case," the philosophy being that the control system should be adequate to contain this possible destabilizing energy input. This would indicate that the dynamic trim angle of the spacecraft during the reentry phase was other than that for the "worst case."

NASA-S-66-6175 MAY 6

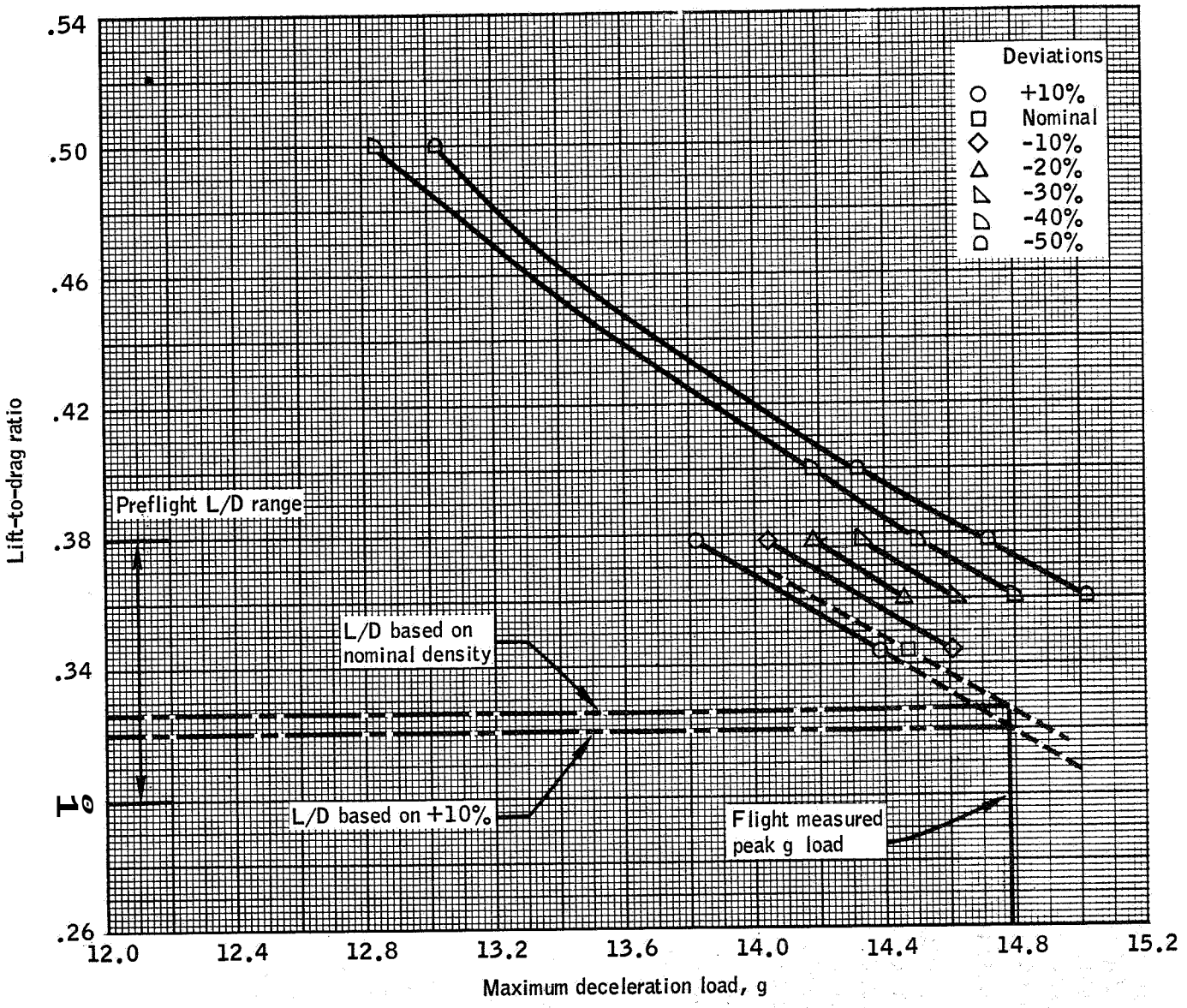


Figure 6.1-1.- Variation of peak deceleration load during reentry with lift-to-drag ratio for several density deviations from the 1962 Standard Atmosphere, Mission AS-201.

NASA-S-66-6176 MAY 6

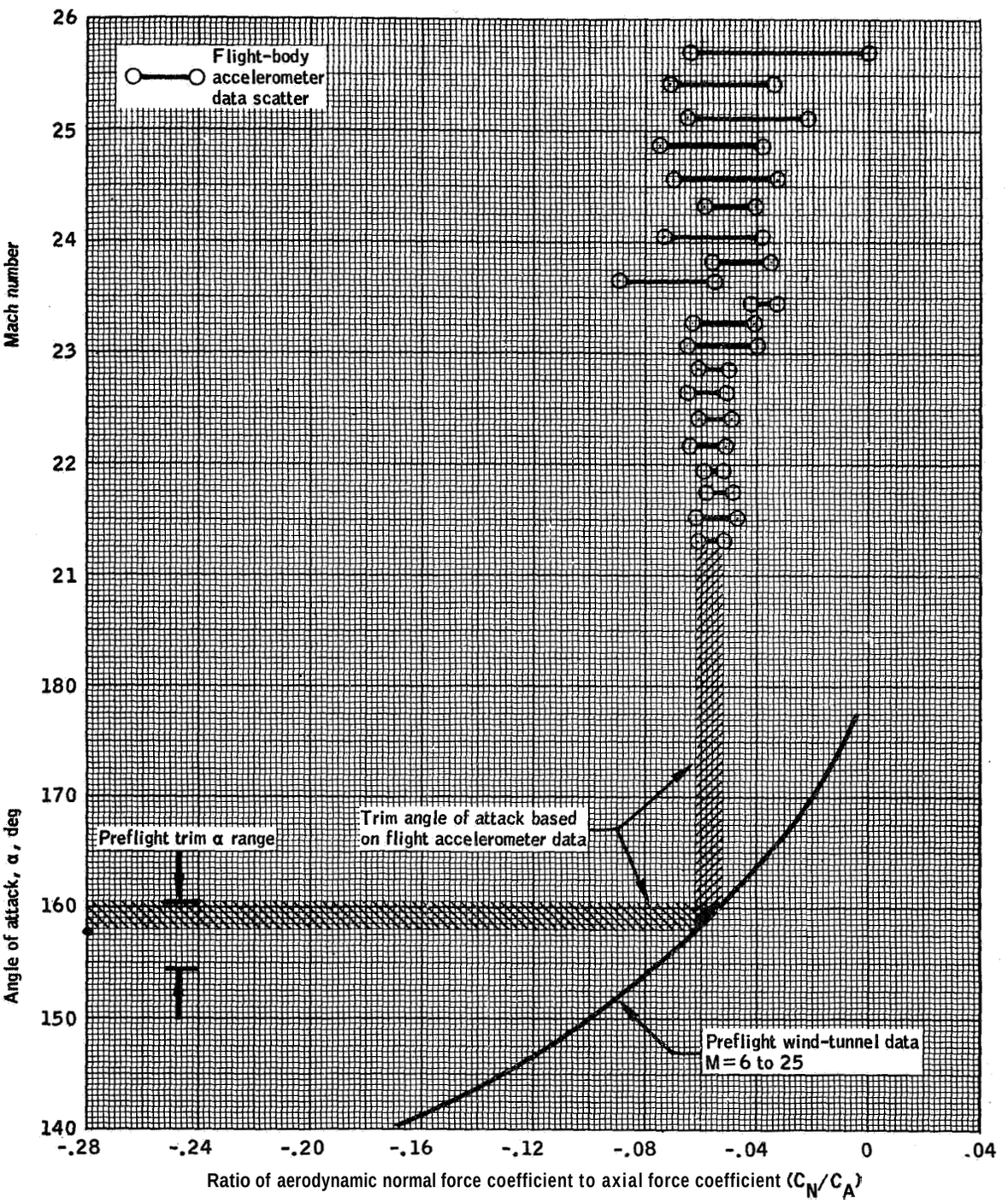


Figure 6.1-2.- Correlation of flight data with preflight *data* in the high Mach number region, Mission AS-201.

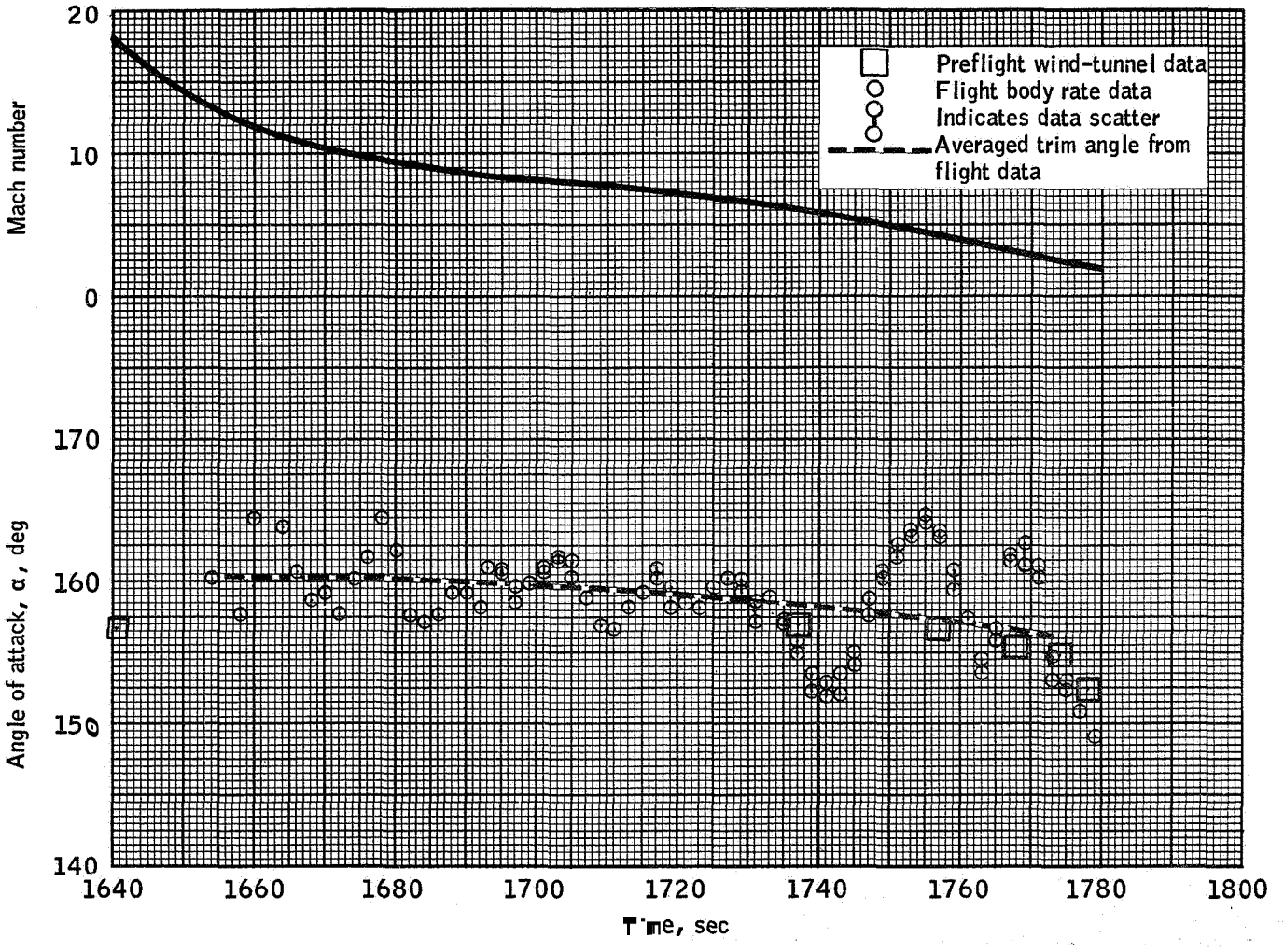
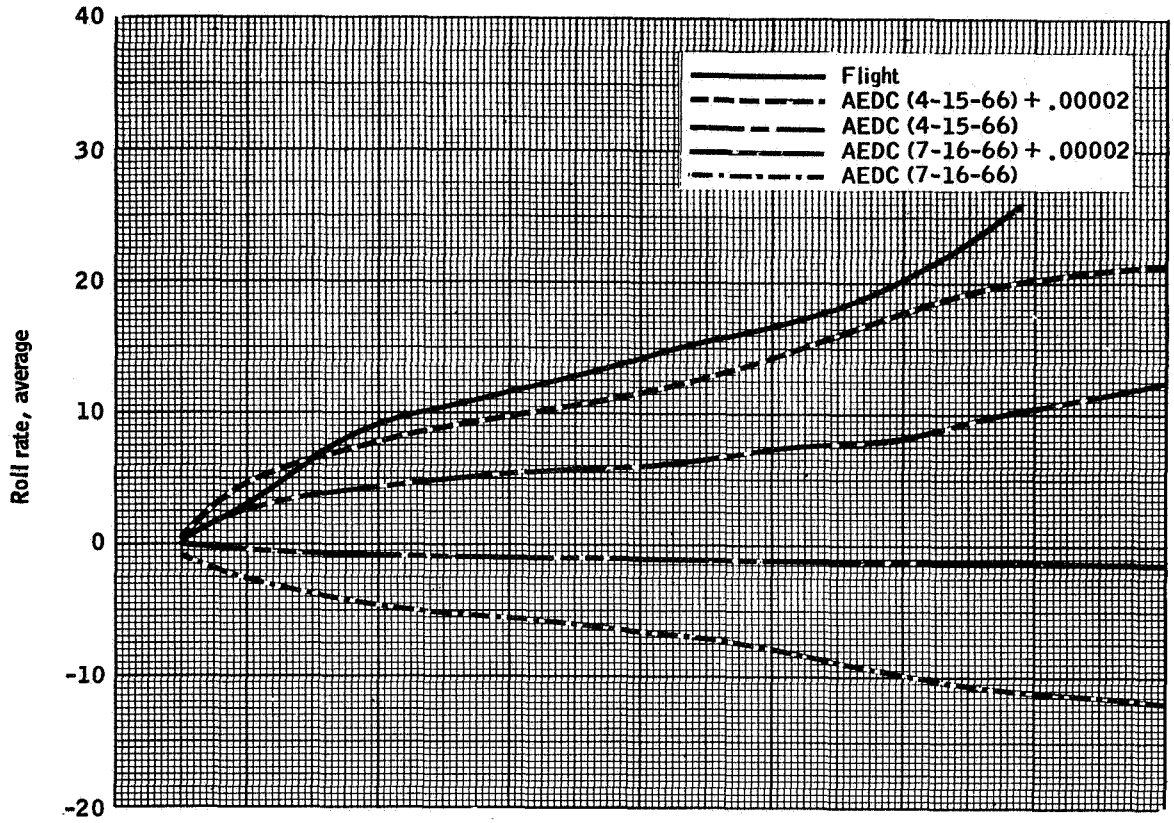
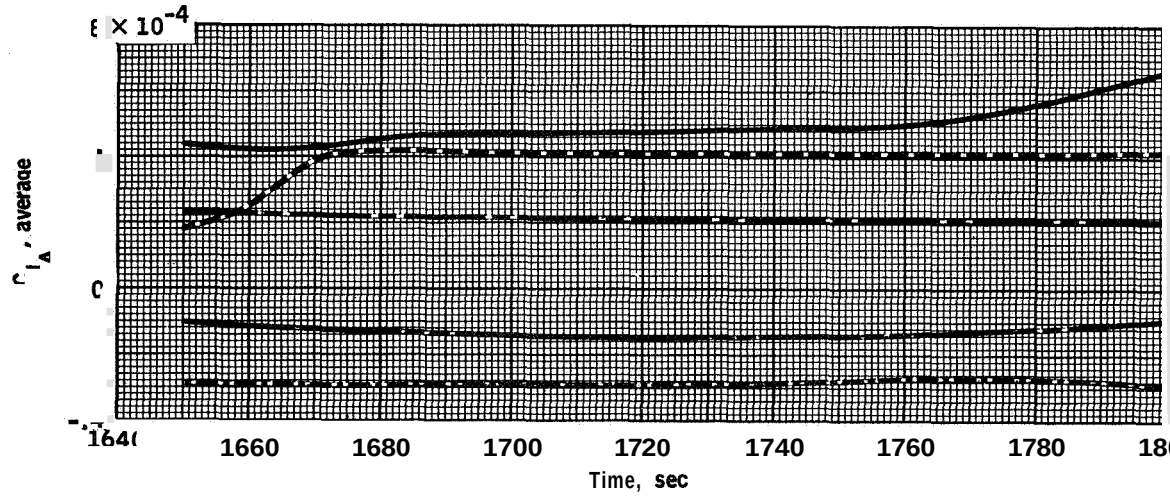


Figure 6.1-3.- Angle of attack as determined from flight rate data with corresponding Mach number, Mission AS-201.

NASA-S-66-6178 MAY 6



(a) Averaged roll rate buildup from postflight simulations compared with flight measured data.



(b) Averaged roll coefficient from postflight simulations and estimated flight roll coefficient.

Figure 6.1-4.- Flight roll coefficient determination, Mission AS-201.

6.2 Aerothermodynamics

The evaluation of the performance of the Apollo heat-shield material requires knowledge of the thermal environment. In order to determine the environment, pressure transducers and surface-mounted calorimeters were installed on spacecraft 009.

Pressure measurements.- A total of 36 pressure transducers were installed around the command module: 12 on the aft heat shield, and 24 on the conical section. Of the 36 transducers, 3 did not operate, 17 gave no usable data, 6 (on the conical section) exhibited erratic histories, and 10 (on the aft heat shield) provided usable data.

Histories of the pressures measured on the aft heat shield are shown in figure 6.2-1. The data appear smooth until T+1635 seconds when a drop in the data can be observed. Examination of oscillograph records reveals a significant loss of data at this time and a return 1 second later. Recorded data were not usable after approximately T+1665 seconds, which was 25 seconds after peak pressure was measured.

The measurements shown in figure 6.2-1 are raw data corrected for the deviation from zero that existed for each transducer prior to reentry.

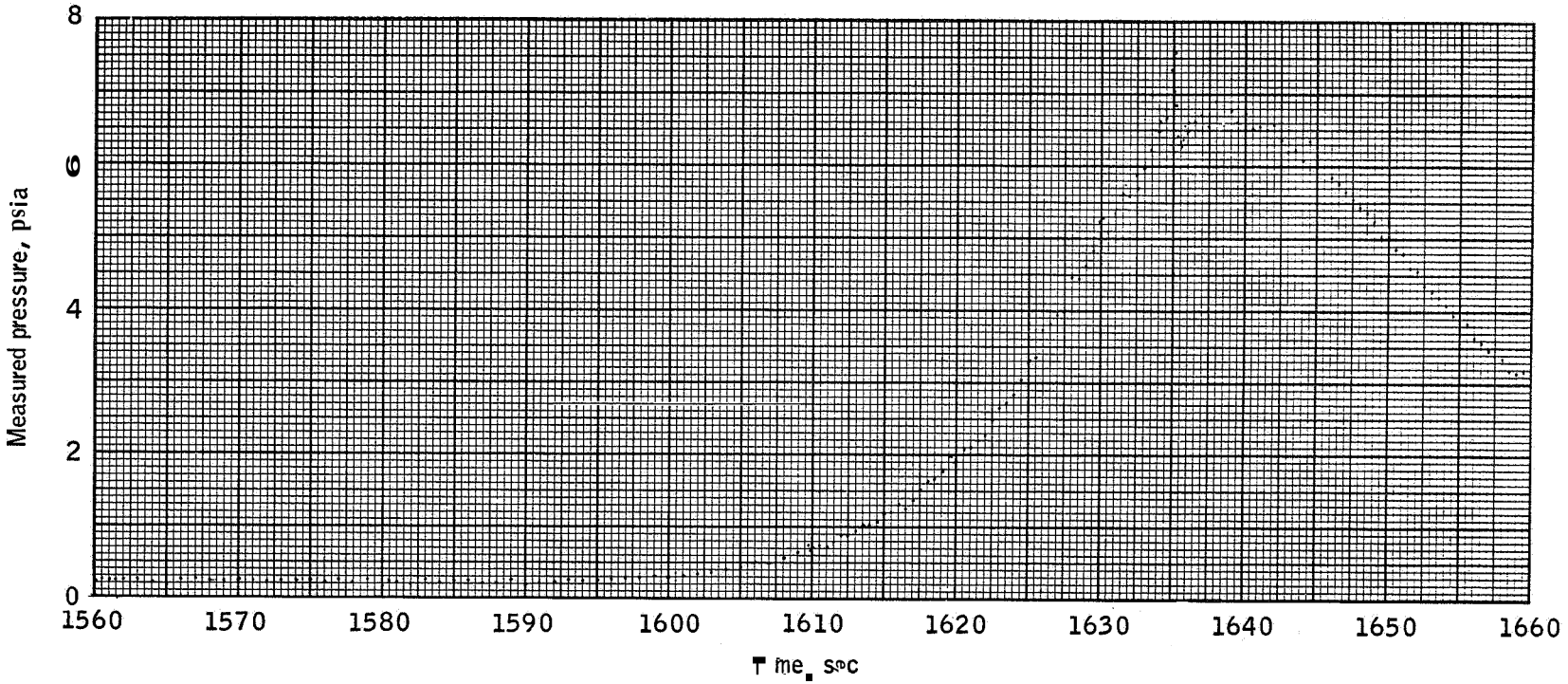
In order to correlate the flight data with results obtained in wind-tunnel tests, distributions of measured pressure divided by a calculated stagnation pressure were obtained and are shown in figure 6.2-2. The theoretical stagnation pressure was computed using the relation for equilibrium real air behind a normal shock. The calculations were made for the time interval from T+1610 to T+1630 seconds (M = 25 to 21) when the data are of relatively good quality. The flight measurements are compared with wind-tunnel data measured at a Mach number of 10 and an angle of attack of 22°, and with a flaw-field solution calculated for a Mach number of 20.7 and an angle of attack of 2P. Close agreement can be observed for times T+1625 and T+1630 seconds. The earlier measurements are approximately 10 percent lower, which m y be due to the lower magnitudes of the absolute pressures at the earliest times. The reasonable agreement shown indicates that aft heat-shield pressures used in Apollo aerothermodynamic analyses are on a sound basis.

Calorimeters.- Two types of calorimeters were used to measure heating rates around the command module. One was an asymptotic calorimeter for low range measurements (below 50 Btu/ft^2/sec) and the other a high range sensor which consisted of several graphite wafers stacked one above the other to allow removal of single wafers by aerodynamic forces when the surrounding heat-shield material ablates away.

There were 22 asymptotic calorimeters on the conical section, 12 high-range calorimeters on the aft heat shield, and 1 high-range calorimeter on the conical section. Only 19 of the asymptotic calorimeters operated with 3 of these not functioning properly. The remaining 16 heating-rate histories are shown in figure 6.2-3 along with rates calculated for the entry trajectory based on wind-tunnel data for 22° angle of attack and the hemispherical stagnation-point theory of Detra, Kemp, and Riddell for laminar theory. Turbulent calculations are based on the flat-plate theory of Van Driest. Most of the asymptotic calorimeters experienced an apparent burst of irregular heating between T+1580 and T+1595 seconds which is unexplained. Since some of the calorimeter outputs went to zero after the irregular burst, no attempt was made to correct the data for possible zero shift even though they may have recorded as much as 4 $Btu/ft^2/sec$ prior to initial entry time. While the scatter of the data prevents precise comparisons, the measurements appear to be in reasonable agreement with the estimates. The apex and the conical-toroid tangency point for $\theta = 135°$ and 225° (figs. 6.2-3(e), 6.2-3(f), and 6.2-3(j)) are unexplainably lower than would be predicted with wind-tunnel measurements. Examination of figure 6.2-3 shows a slight time lag between the measured peak heating and the estimated laminar peak heating. The lag, however, never exceeds 10 seconds. This may be partly due to turbulent effects which would introduce delays of the peaks on the order of 5 seconds. A sketch of the command module is shown in figure 6.2-4 with the measured peak heating rate noted above each sensor location.

Only 6 of the 13 high-range calorimeters were operative. These 6 calorimeters produced usable data only between T+1560 and T+1622 seconds. These sensors measured temperature with tungsten-rhenium thermocouples imbedded in each thin graphite wafer. Figure 6.2-5 shows the rapid temperature rise of 4 of these sensors to values as high as 1400° F. Heating rates can be calculated in principle from the temperature time history and knowledge of the sensor material properties. Because of anomalous experimental results of ground test data from prototypes of the high-range sensor, further study will be required before heating rates can be determined from the flight data.

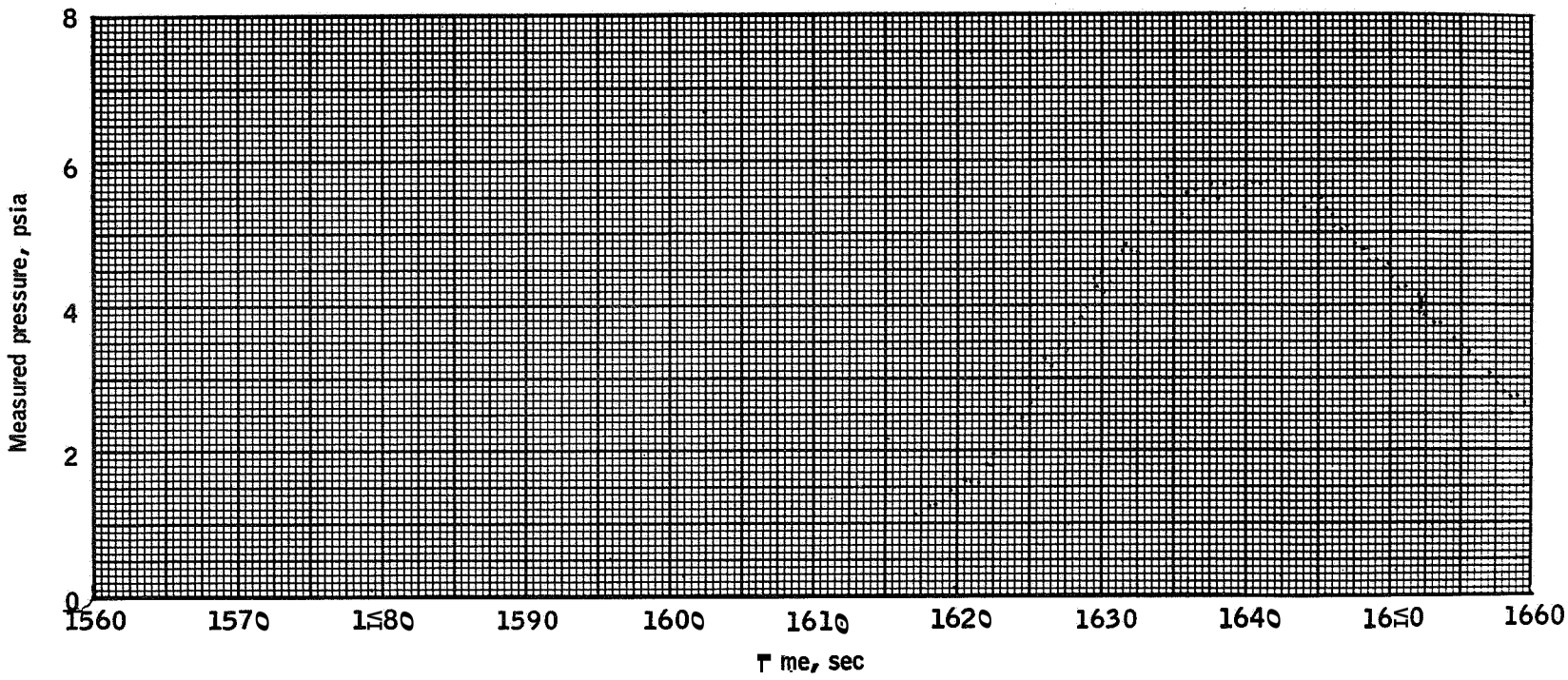
Analysis of the spacecraft 009 flight data will continue. The pressure and calorimeter measurements presented herein are in reasonable agreement with wind tunnel and theoretical estimates. Since the results from the flight data are substantially based on the measured heating rates for the crew and forward heat shield and the interpretation of pressure data for the aft heat shield as expected, the environment for orbital entry conditions may be regarded as well established.



(a) CA1141, Y0, Z75, S/R 1.0.

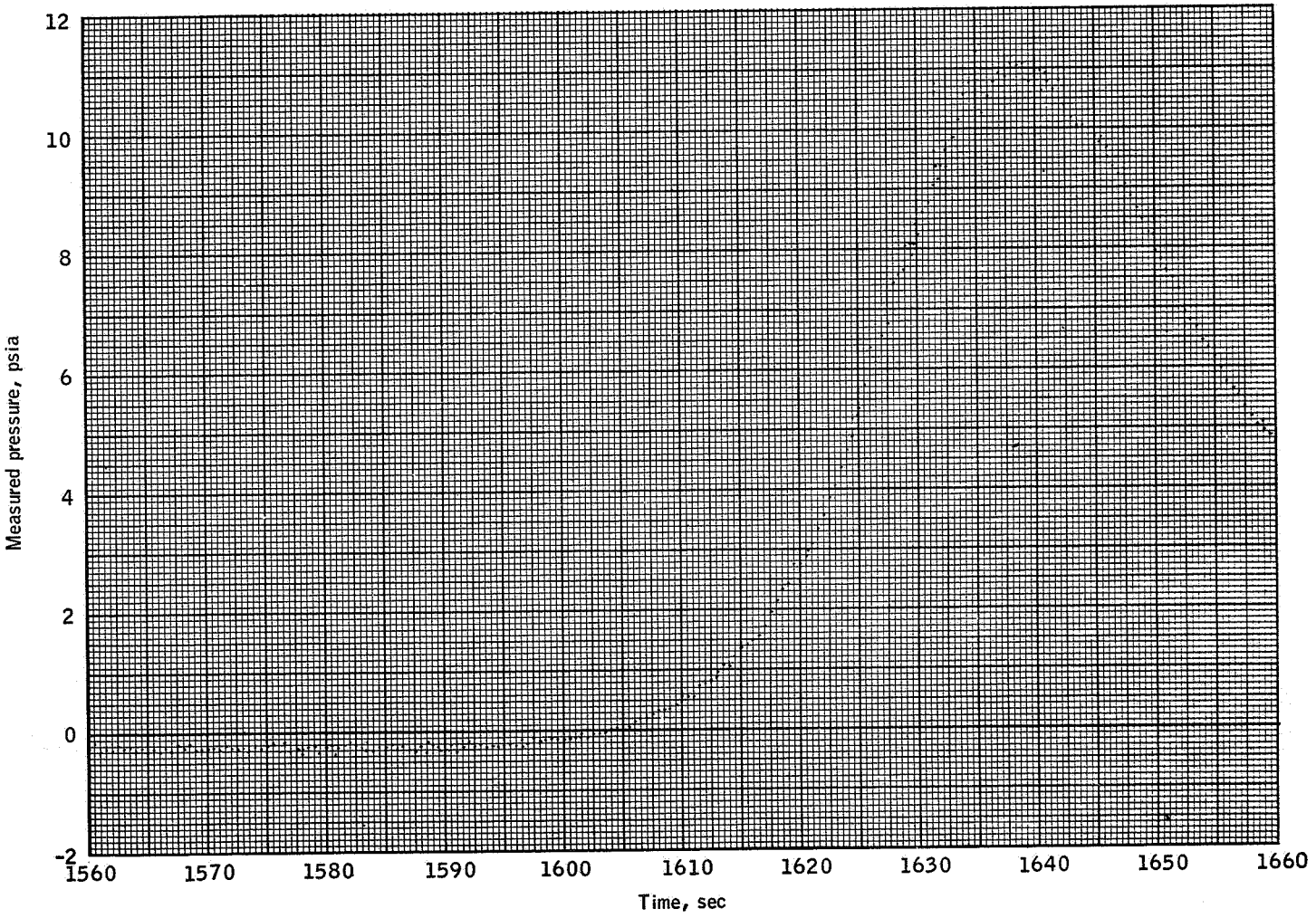
Figure 6.2-1.- Time histories of measured pressures on the blunt face of the CM, Mission AS-201

NASA-S-66-6180 MAY 6



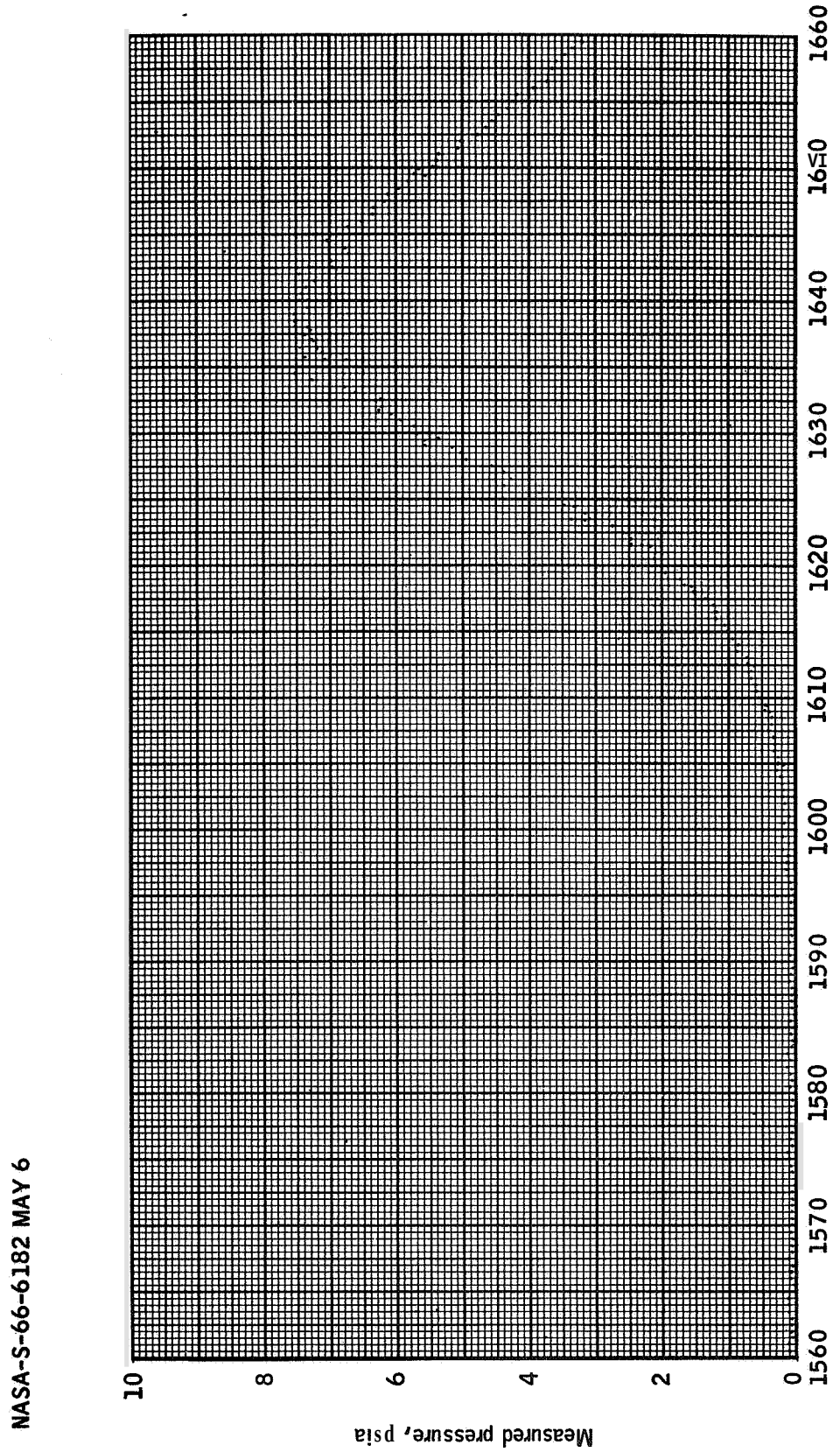
(b) CA1142P, Y0, Z-71, S/R .947.

Figure 6.2-1.- Continued.



(c) CA1143P, Y0, Z71, S/R .947.

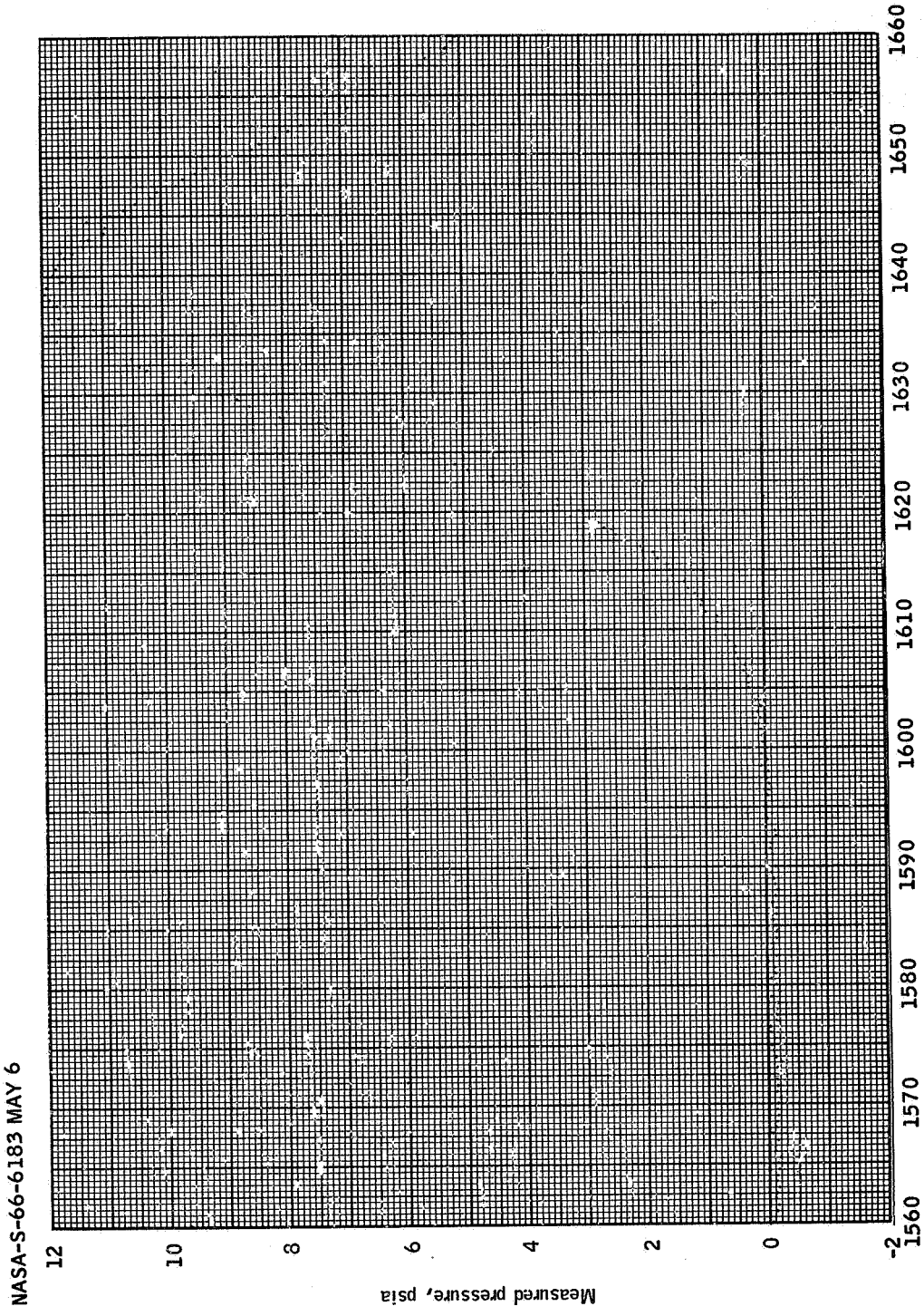
Figure 6.2-1.- Continued.



NASA-S-66-6182 MAY 6

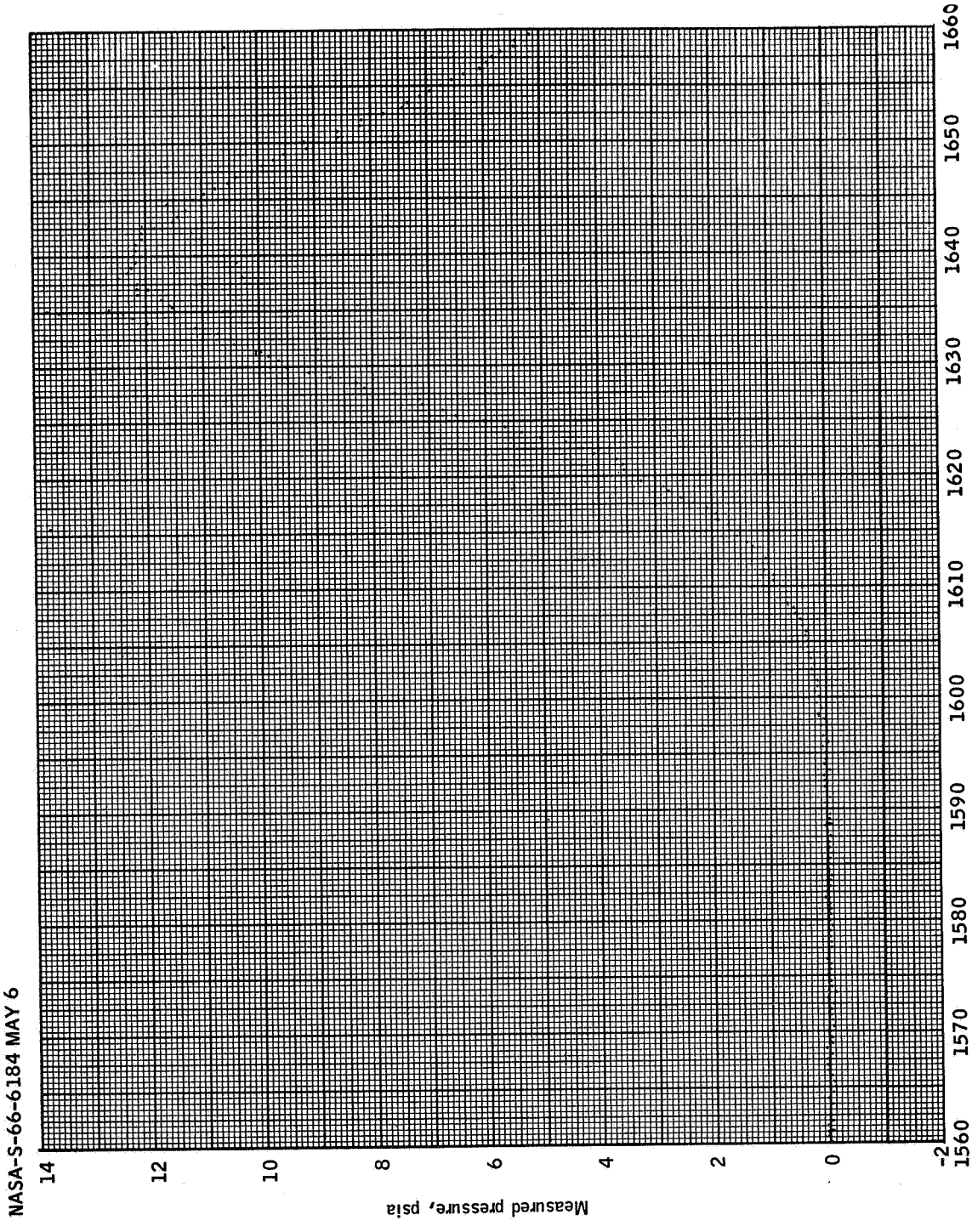
(d) CA1145P, Y71, Z0, S/R .947.

Figure 6.2-1.- Continued.



(e) CA1146P, Y0, Z61, S/R .81.

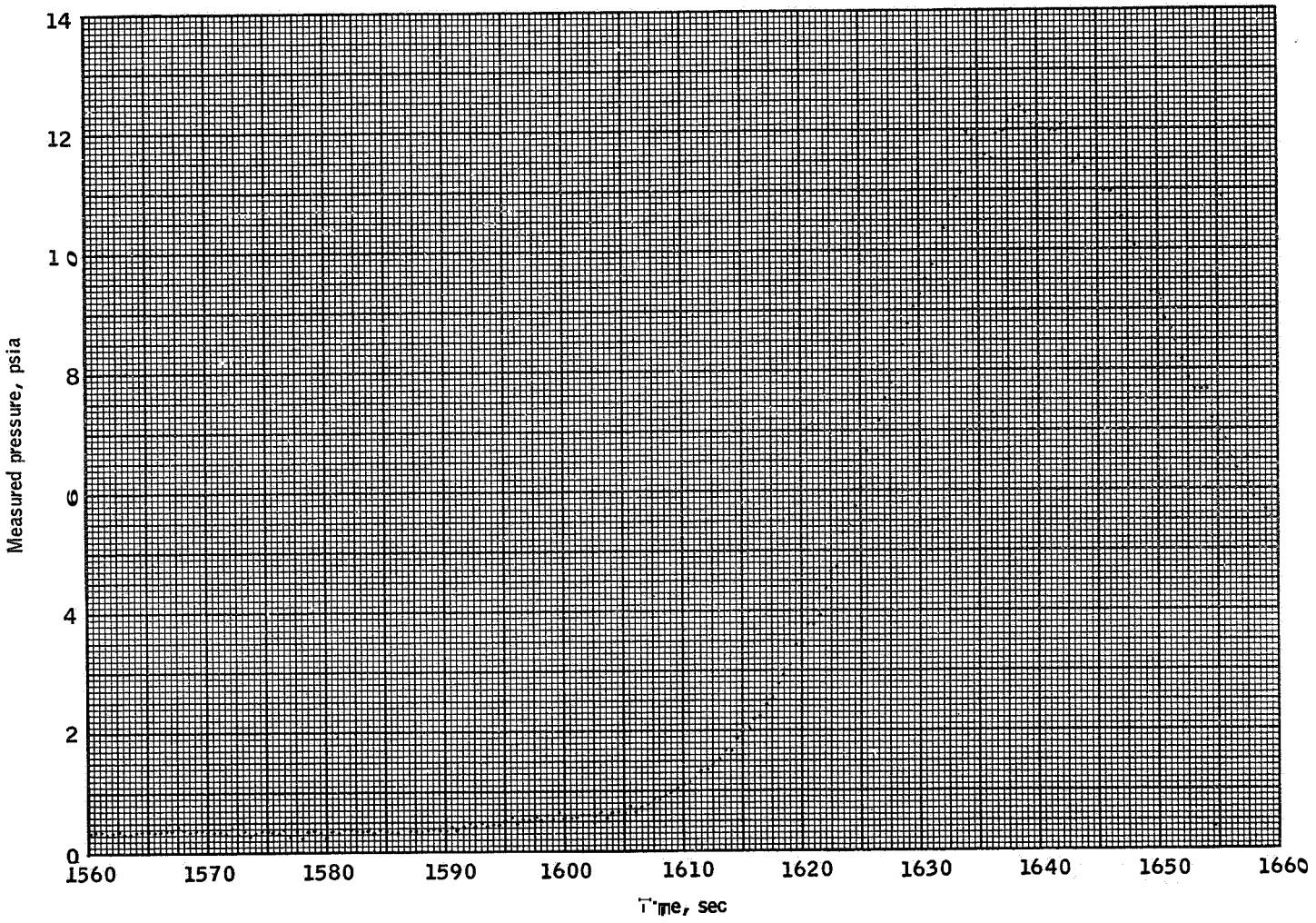
Figure 6.2-1.- Continued.



(f) CA1147P, Y0, Z55, S/R .73.

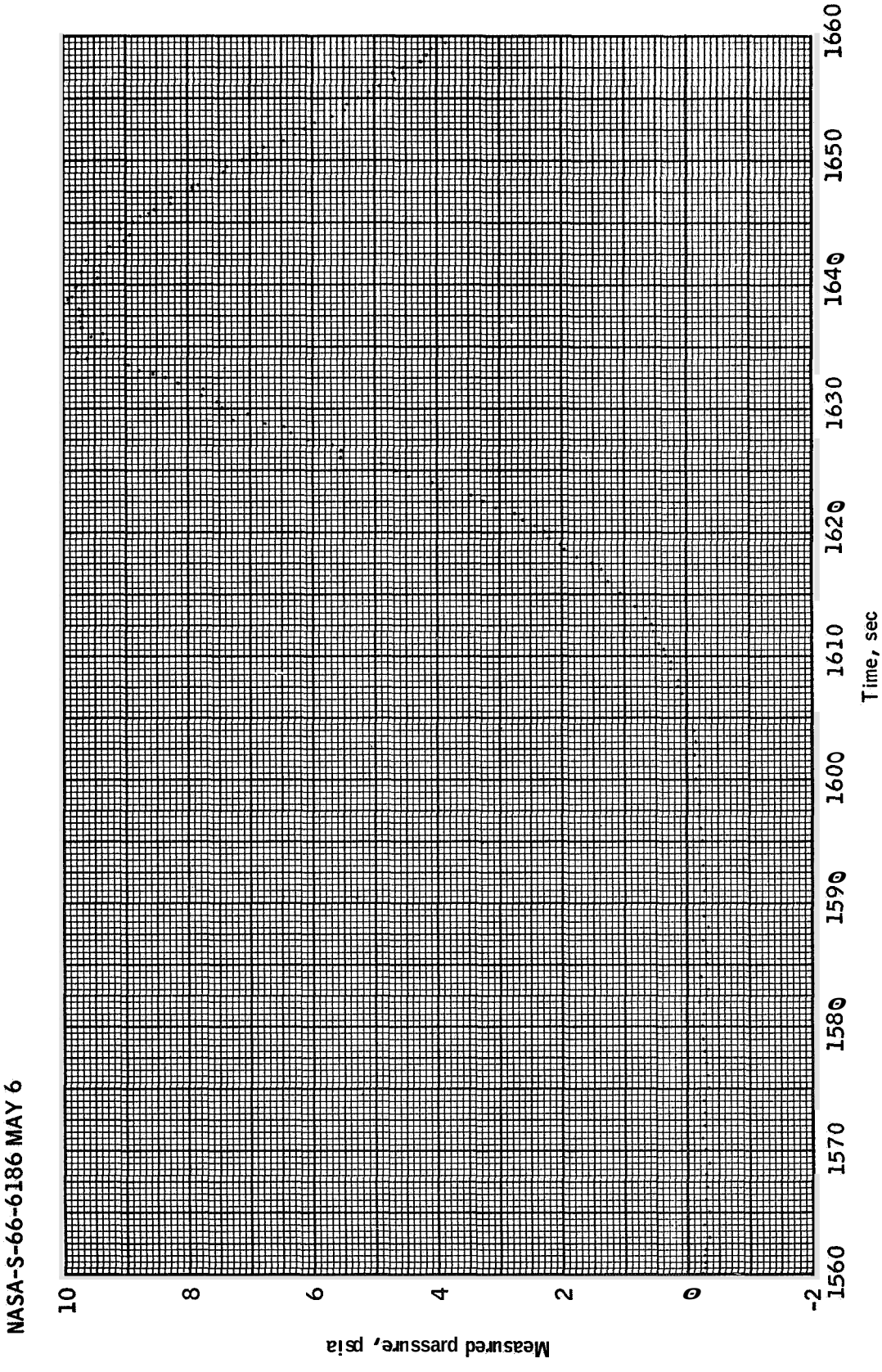
Figure 6.2-1.- Continued.

NASA-S-66-6185 MAY 6



(g) CA1148P, Y0, Z39, S/R .51.

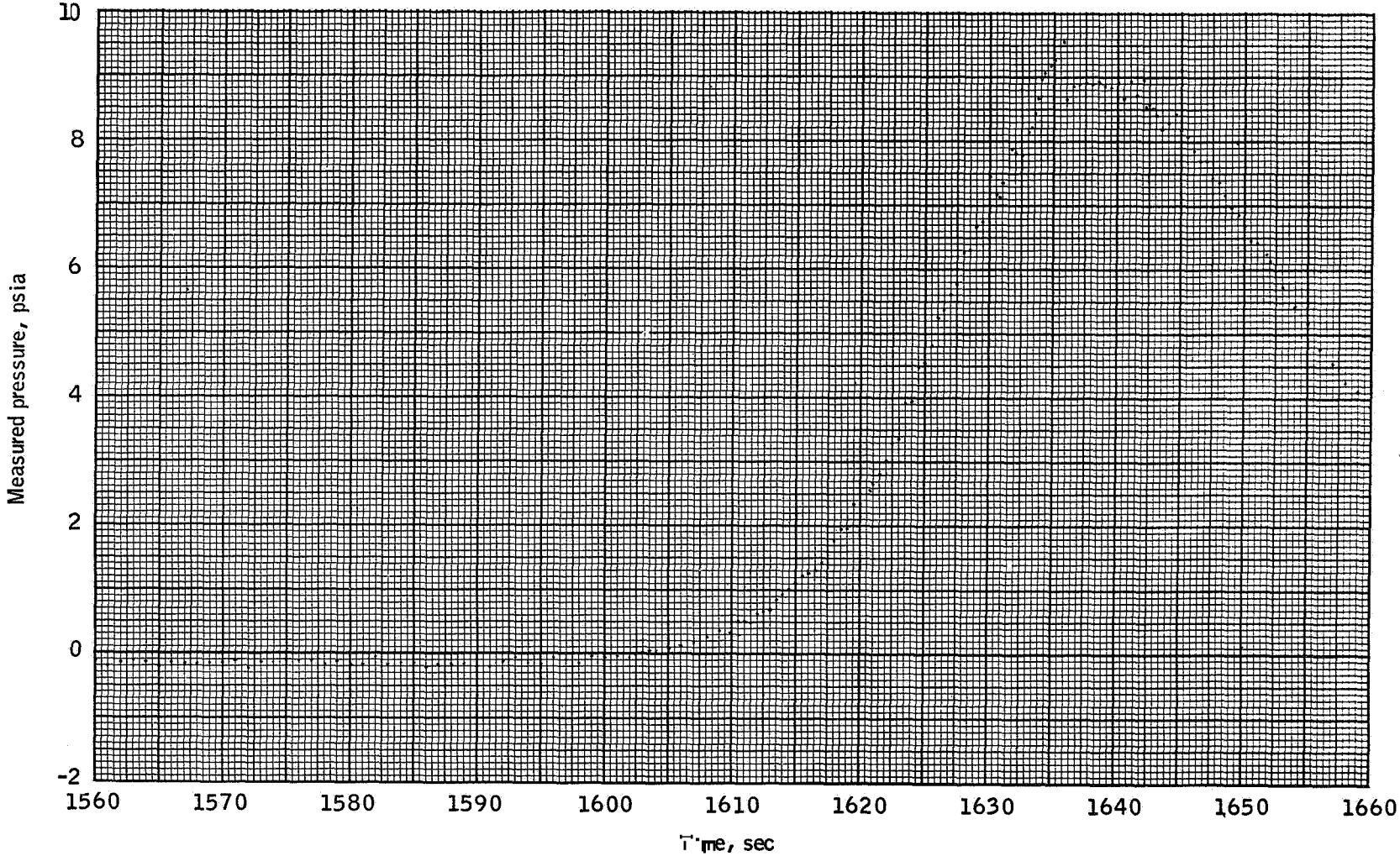
Figure 0.2-1.- Continued.



(h) CA1150P, Y39, Z0, S/R .51.

Figure 6.2-1 - Continued

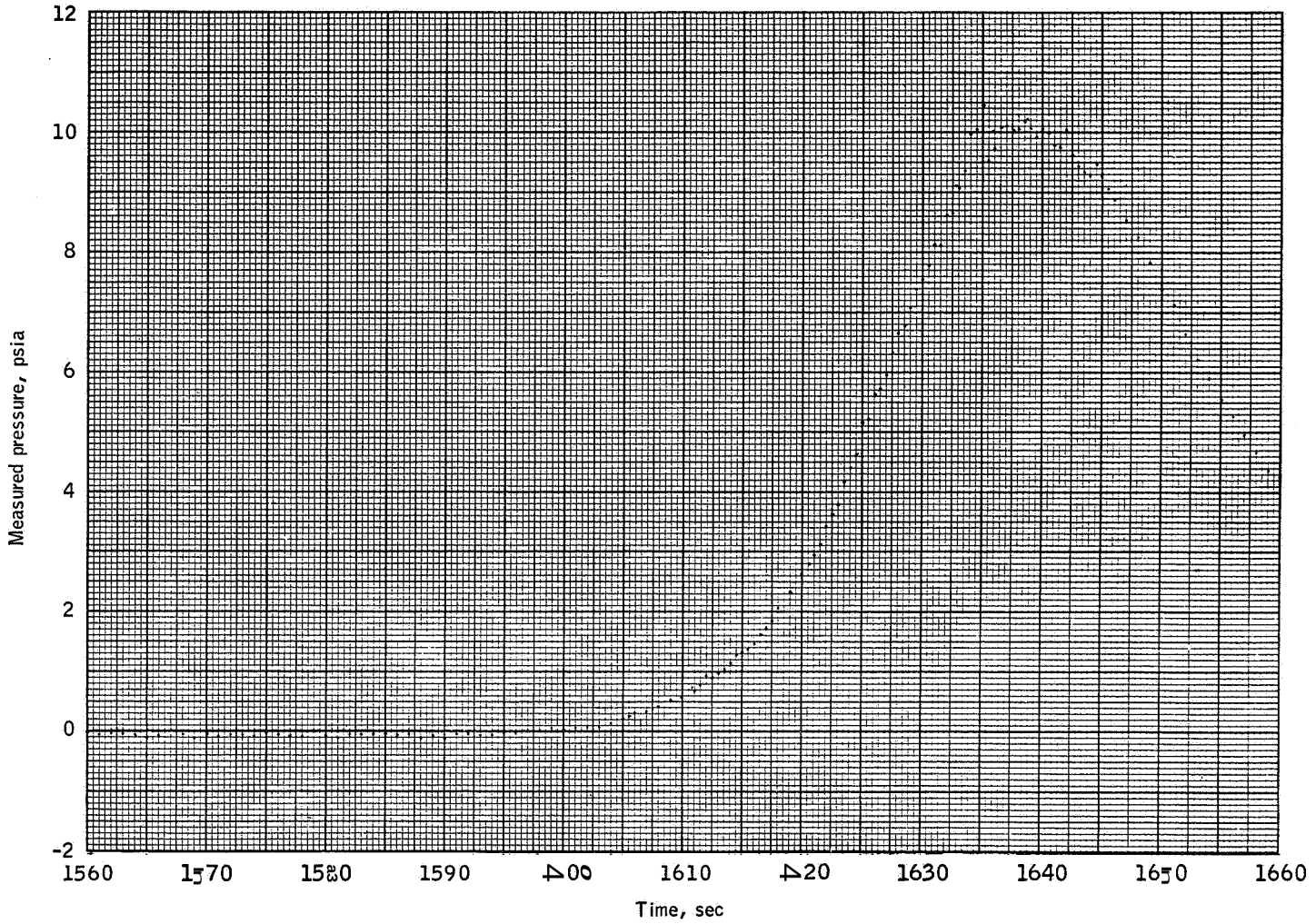
NASA-S-66-6187 MAY 6



(i) CA1151P, Y-39, Z0, S/R .51.

Figure 6.2-1.- Continued.

NASA-S-66-6188 MAY 6



(j) CA1152P, Y0, Z0, S/R 0.

Figure C nc l ed

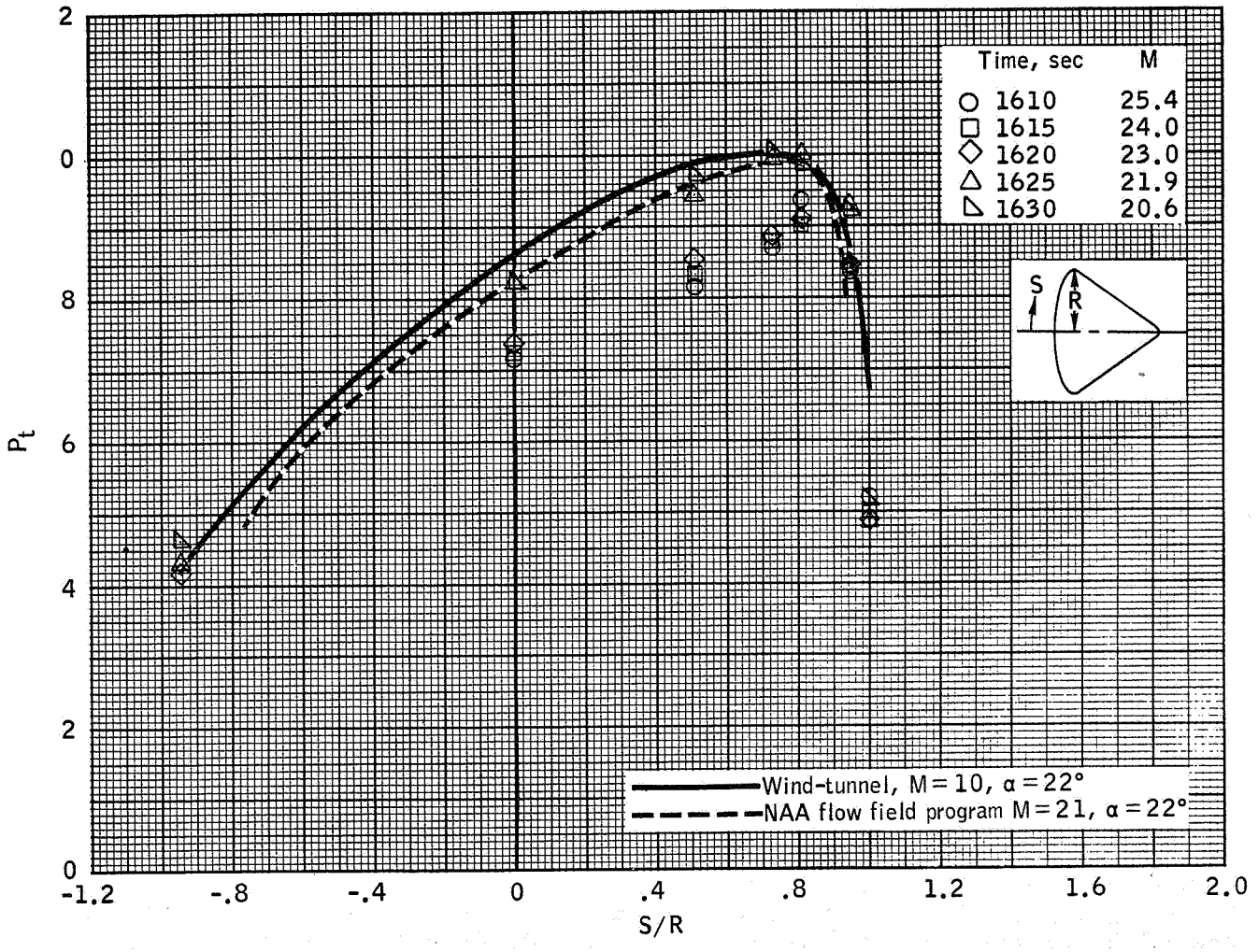
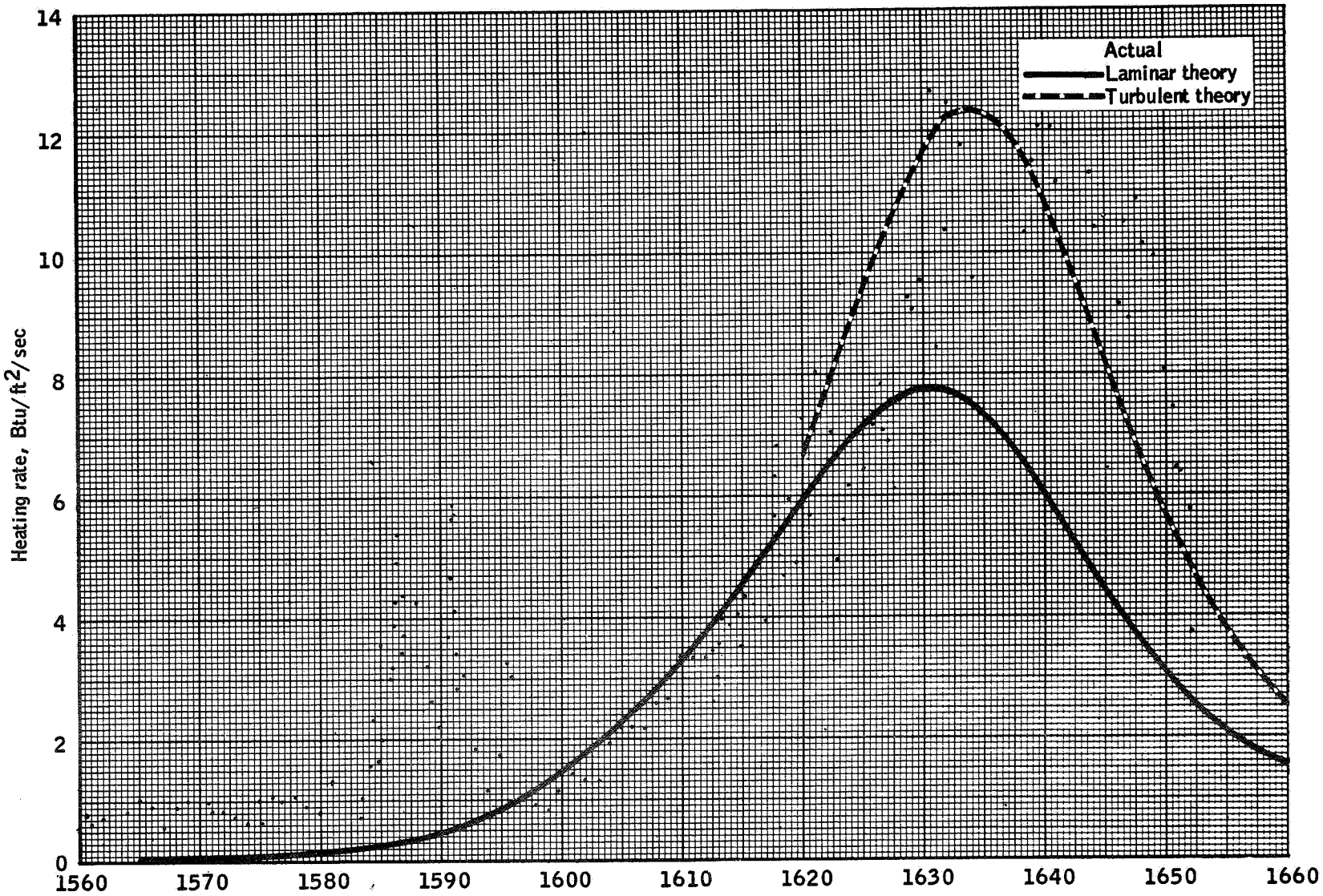


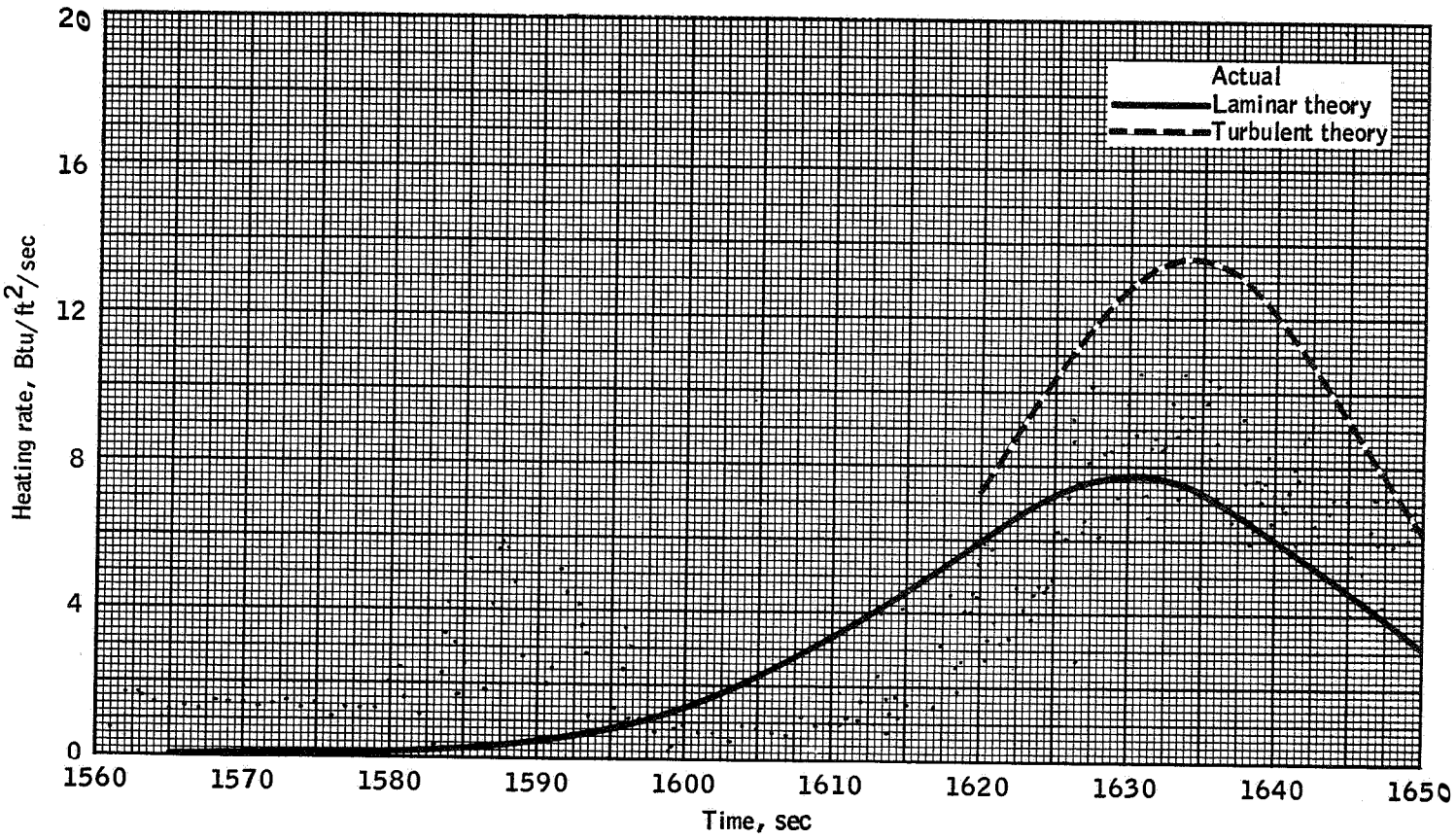
Figure 6.2-2.- Comparison of measured pressure distribution with wind-tunnel data and flow field program, Mission AS-201.

NASA-S-66-6190 MAY 6



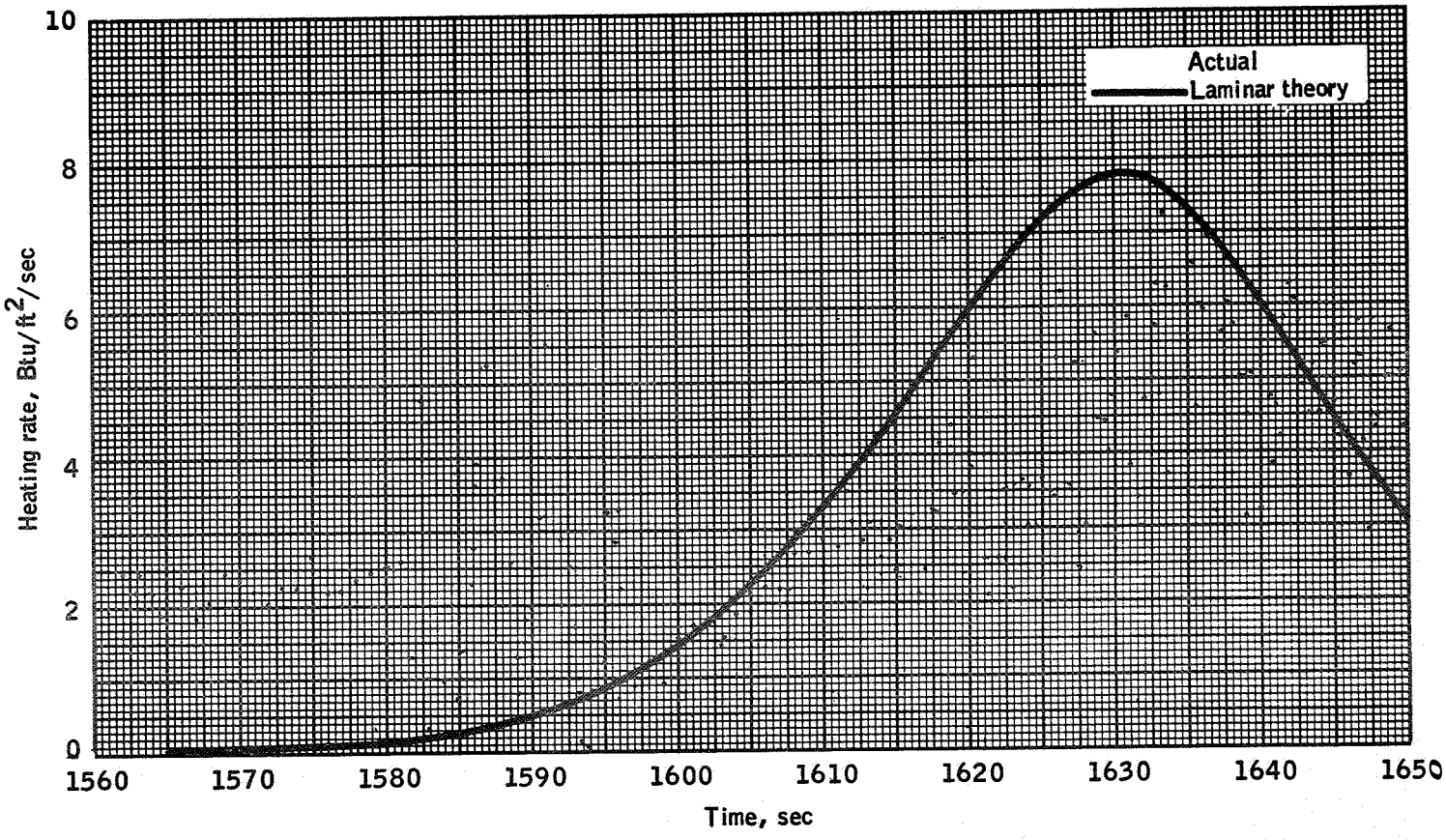
(a) CA1253R, X_C44, 90°, S/R 1.42.

Figure 0.2ω.- Time histories of actual heating rates on the CM conical surface of Mission AS-201.



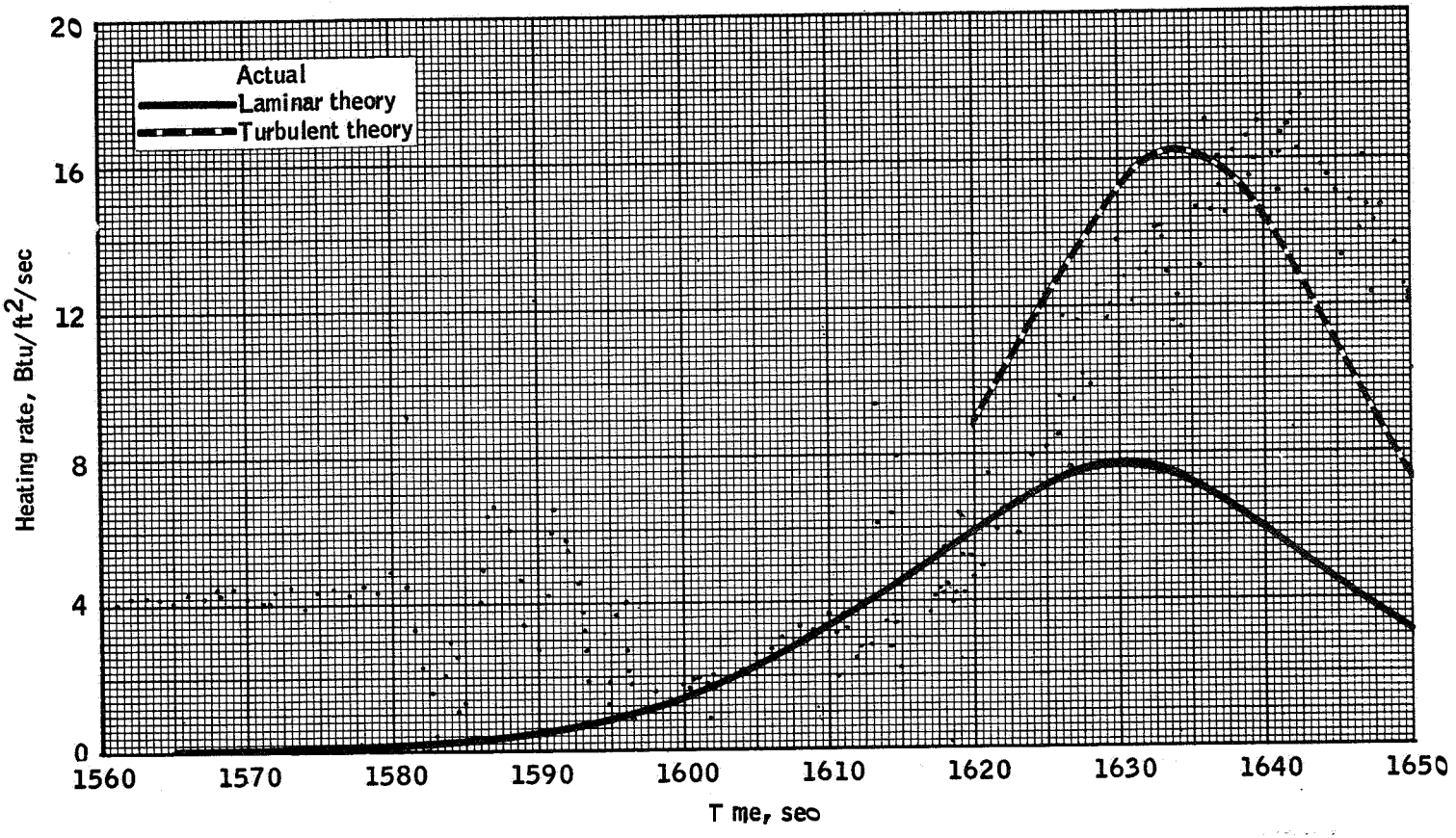
(b) CA1256R, X_C60, 90°, S/R 1.67.

Figure 6.2-3.- Continued.



(c) CA1259R, X_C81, 90°, S/R 1.99

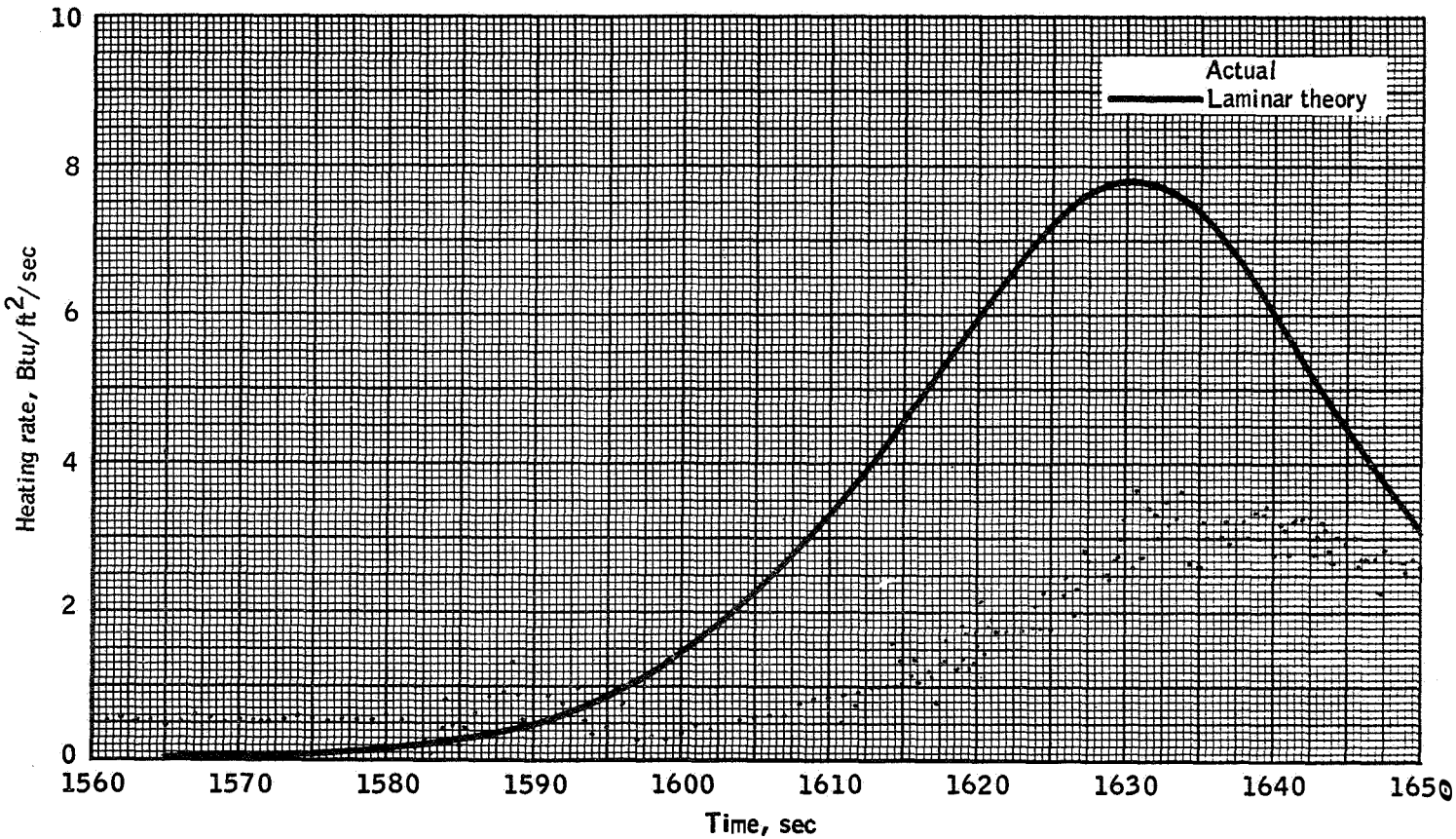
Figure 6.2-3.- Continued.



ω) Cω1262R, X_C112.25, 90°, S/R 2.47.

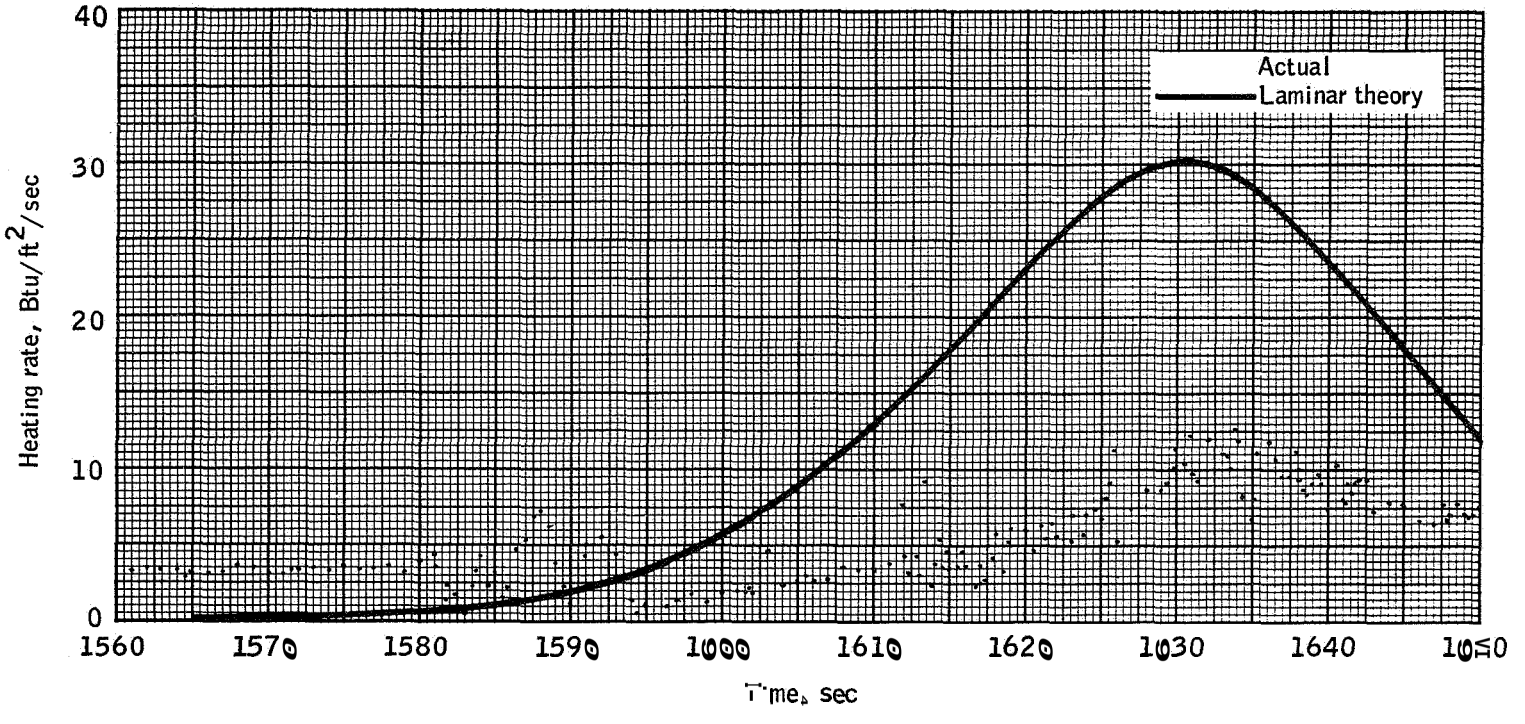
Figure 6.2-3.- Continued.

NASA-S-66-6194 MAY 6



(e) CA1341R, apex.

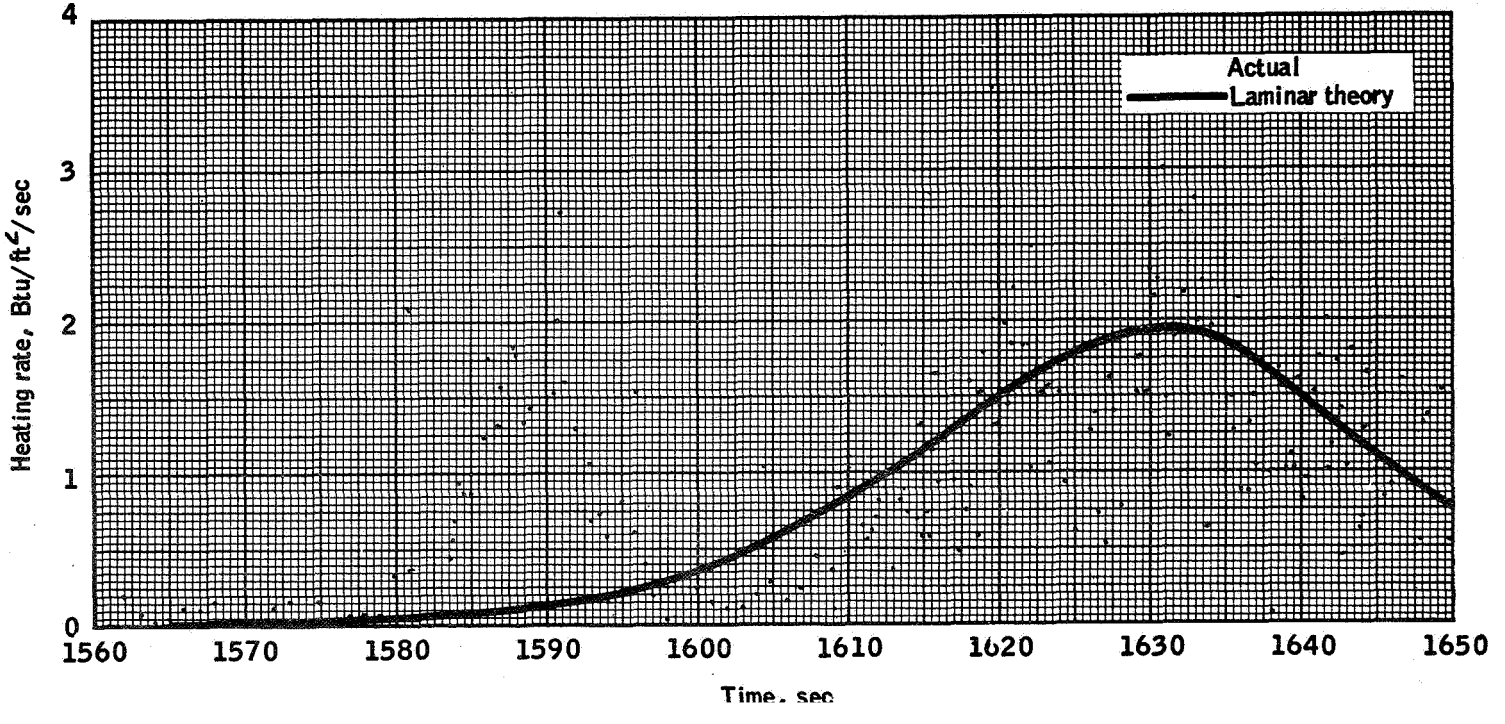
Figure 6.2-3.- Continued.



(f) Cᘓ126≦R, ×C23.2, 13≦°, S/R 1 1

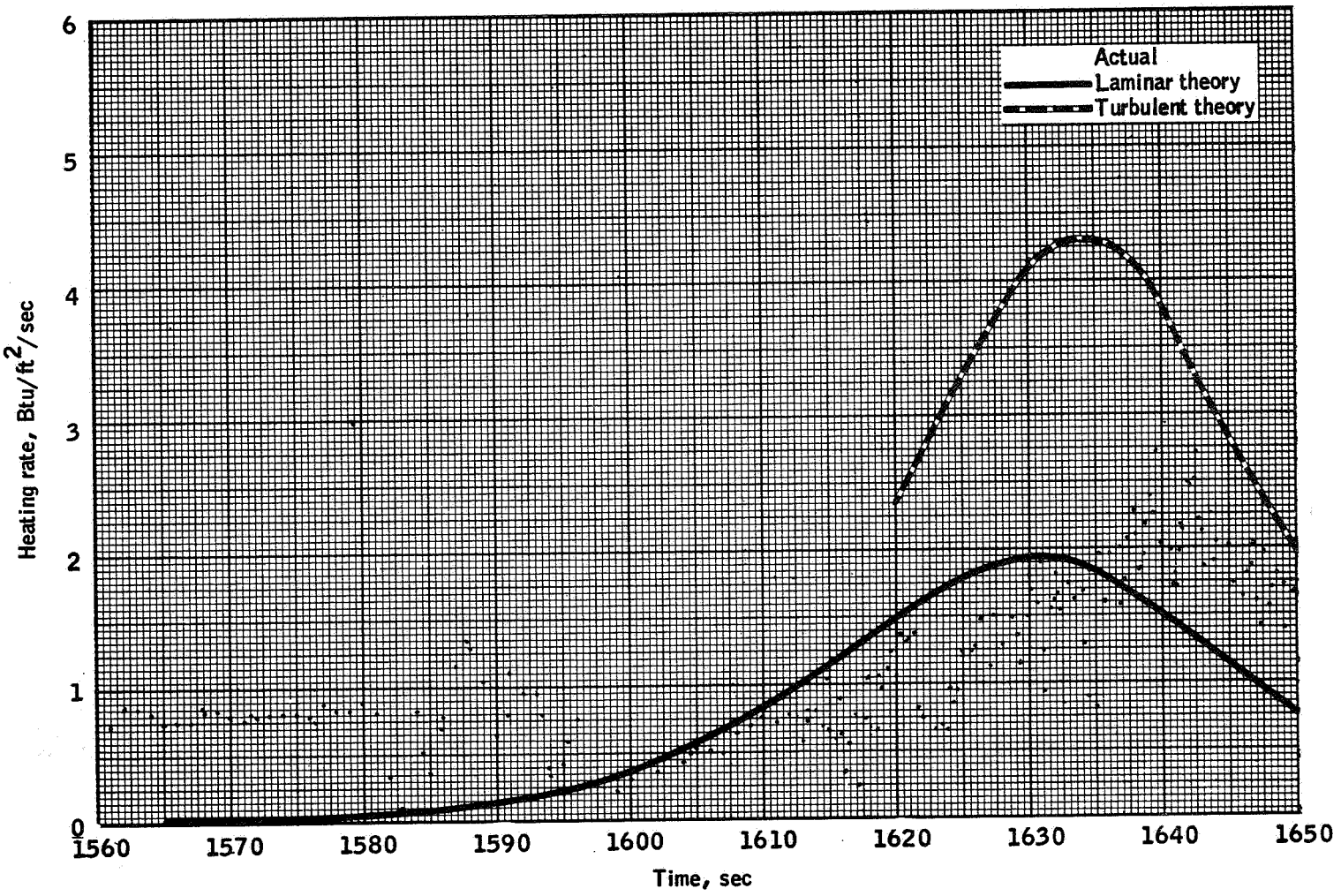
Figure 6.2ᘐ.- Continued.

NASA-S-66-6196 MAY 6



(g) CA1323R, X_C44, 180°, S/R 1.42.

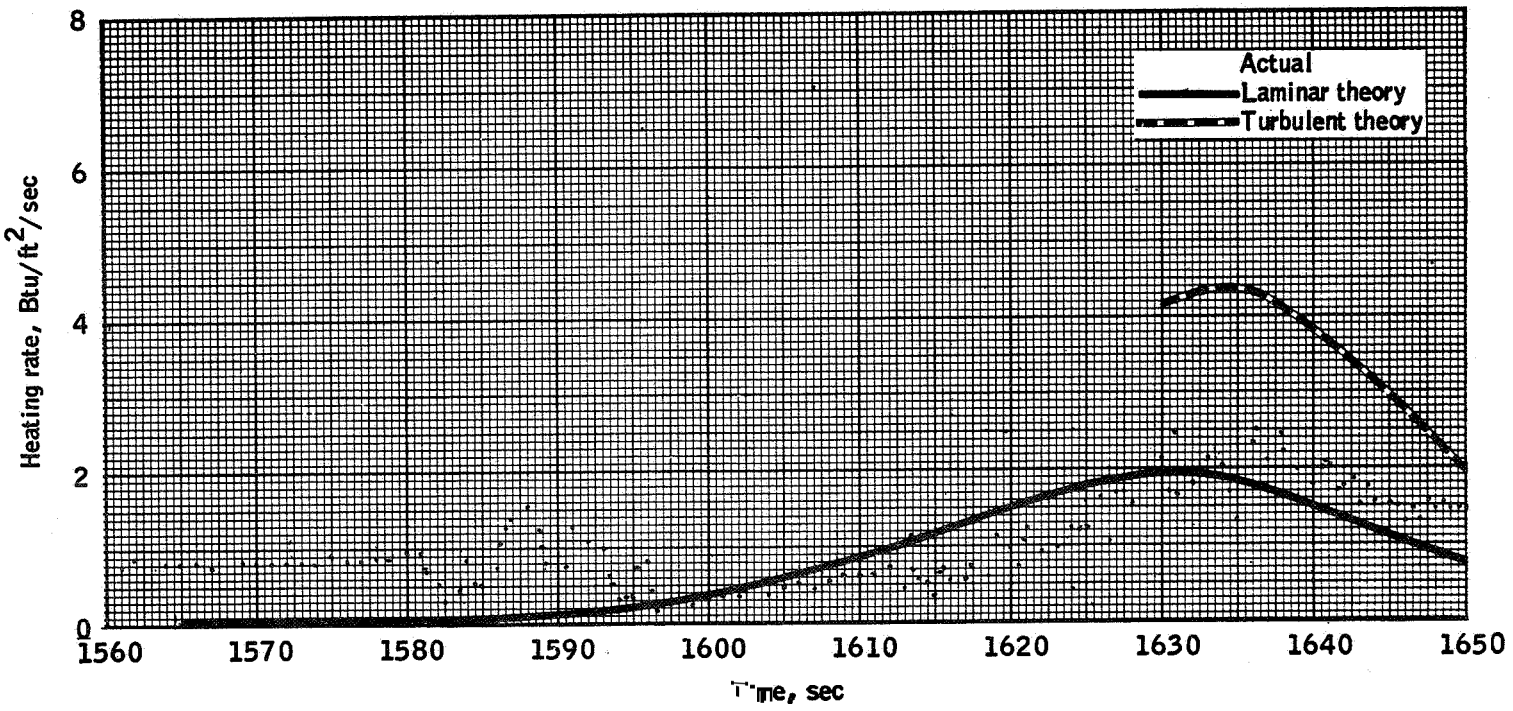
Figure 6.2ω.- Continued.



(h) CA1168R, X_C81, 188°, S/R 1.99

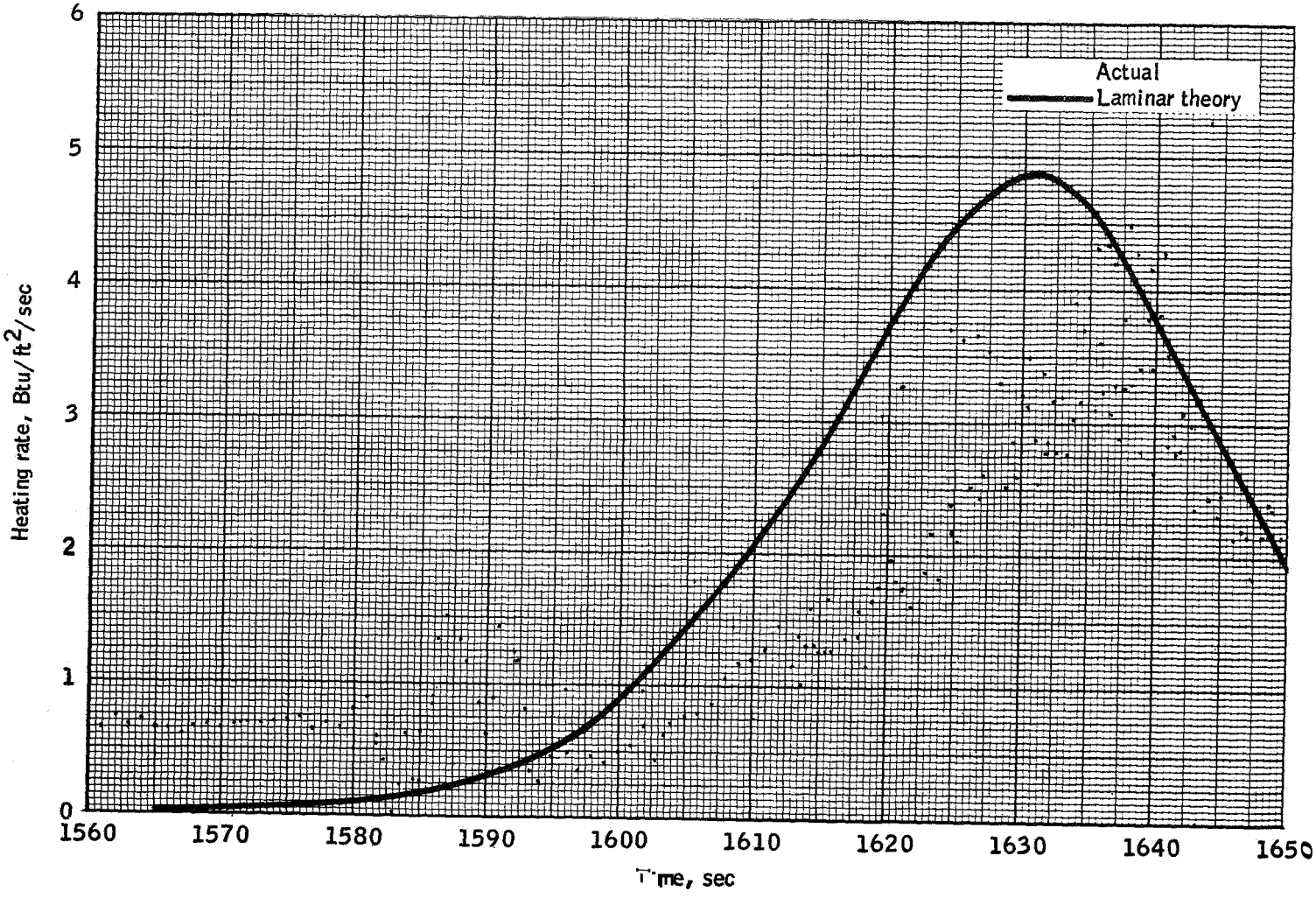
Figure 6.2-3.- Continued.

NASA-S-66-6198 MAY 6



(i) CA1274R, X_c88, 185°, S/R 2.1

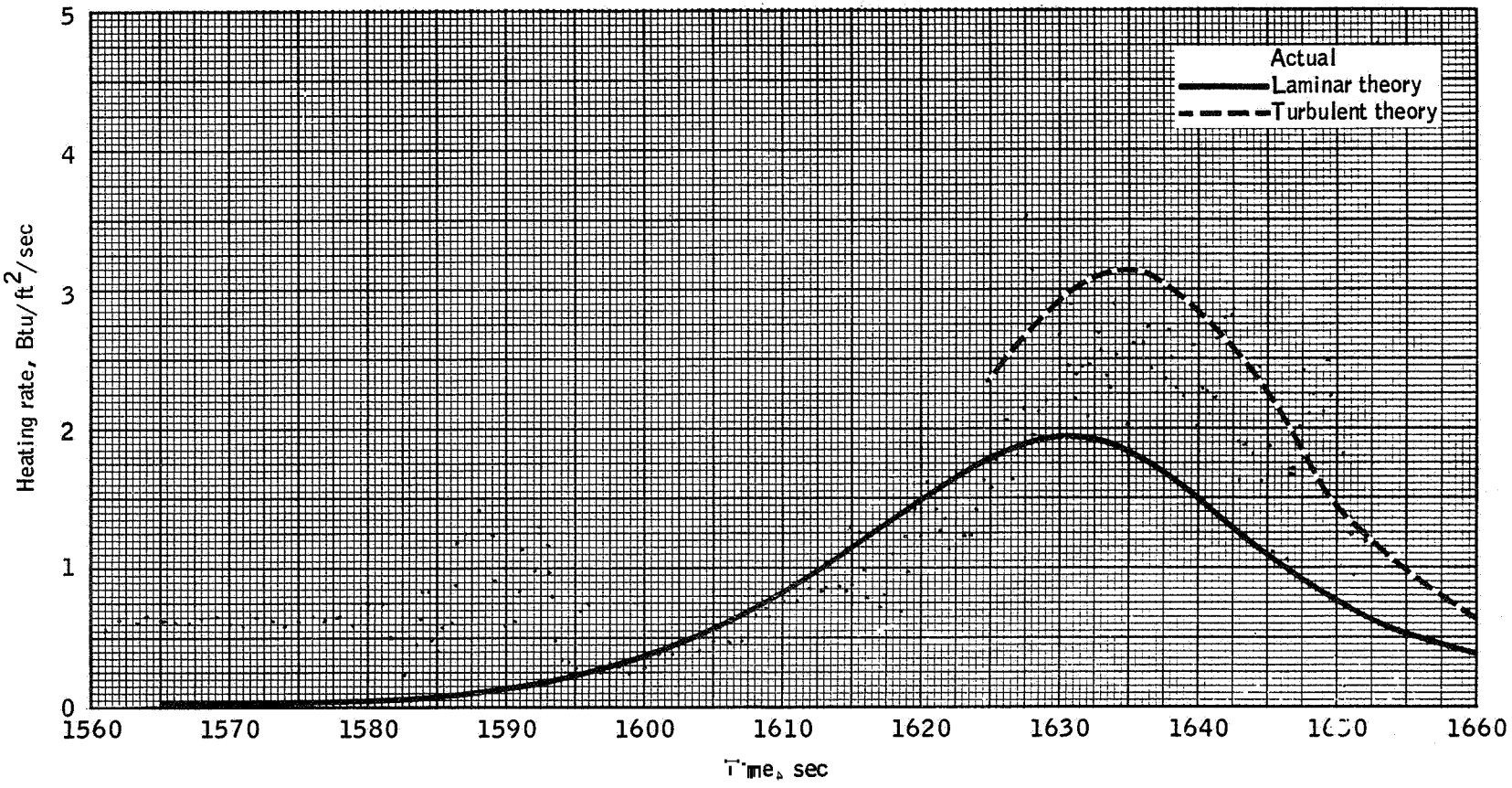
Figure 6.20.- Continued.



(j) CA1280R, X_C 23.2, 225°, S/R 1.1.

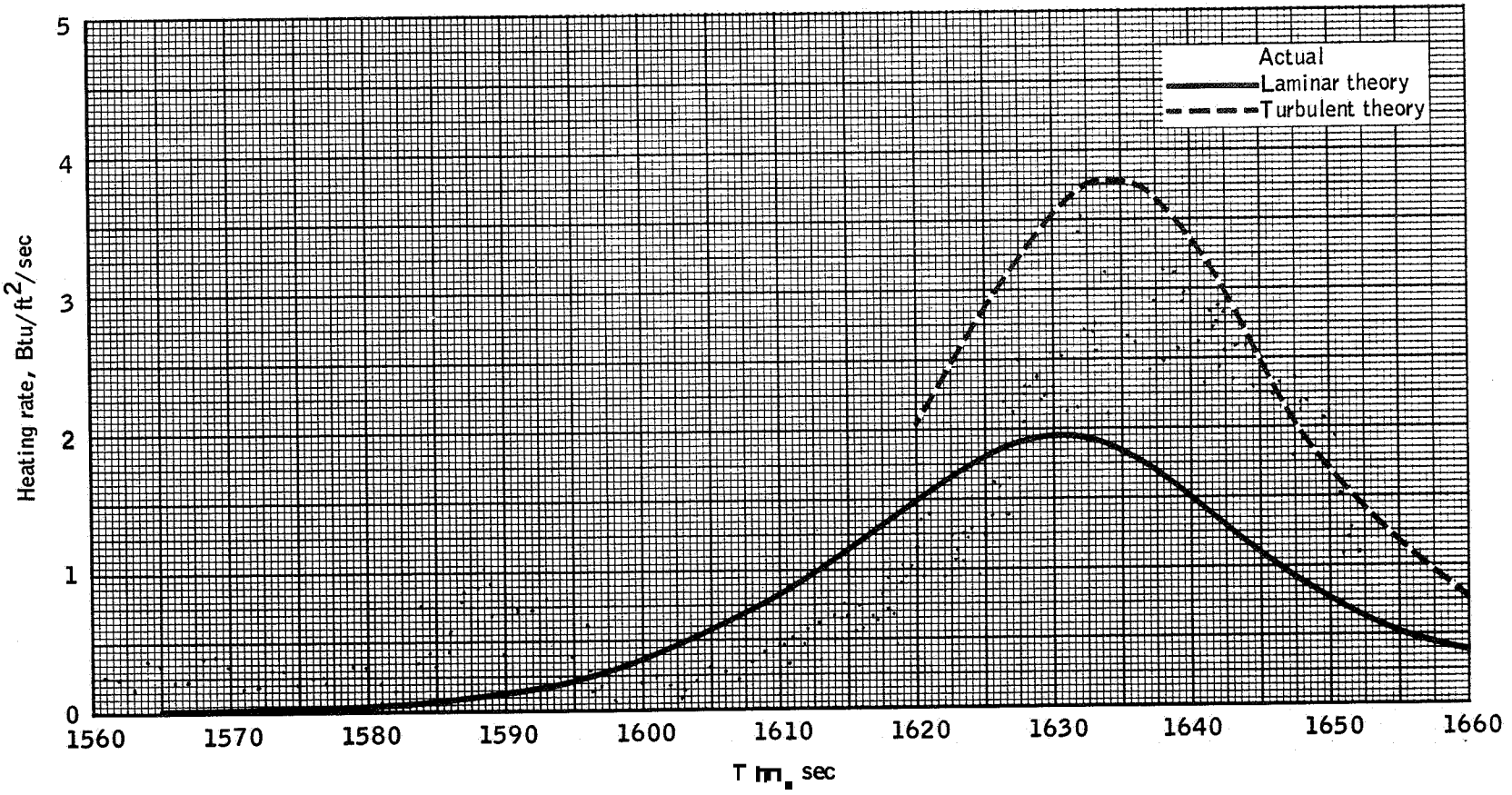
Figure 6.2-3.- Continued.

NASA-S-66-6200 MAY 6



(k) ∞1286R, α_c40, Z14°, S/R 1.36.

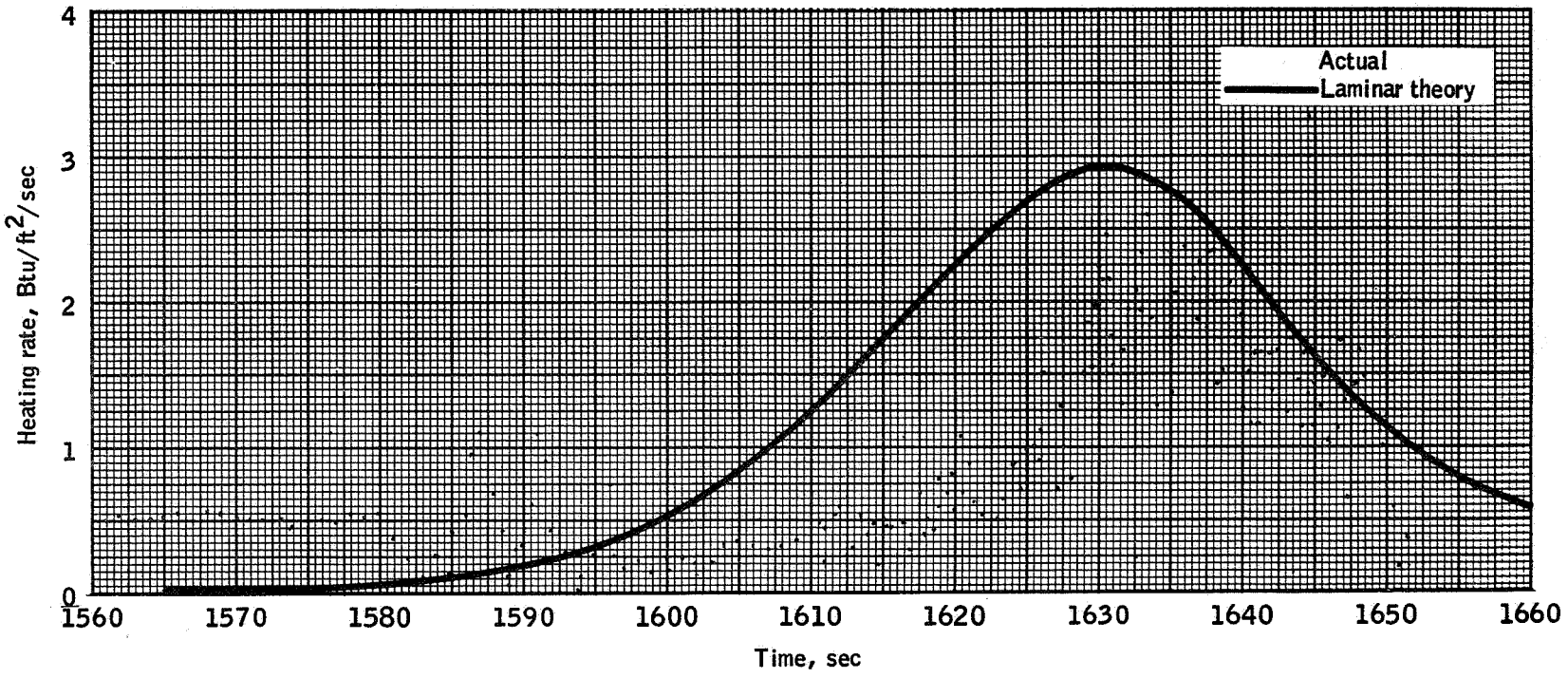
Figure 6.2ω.- Continued.



(l) CA1298R, X_C50, 228°, S/R 1.51.

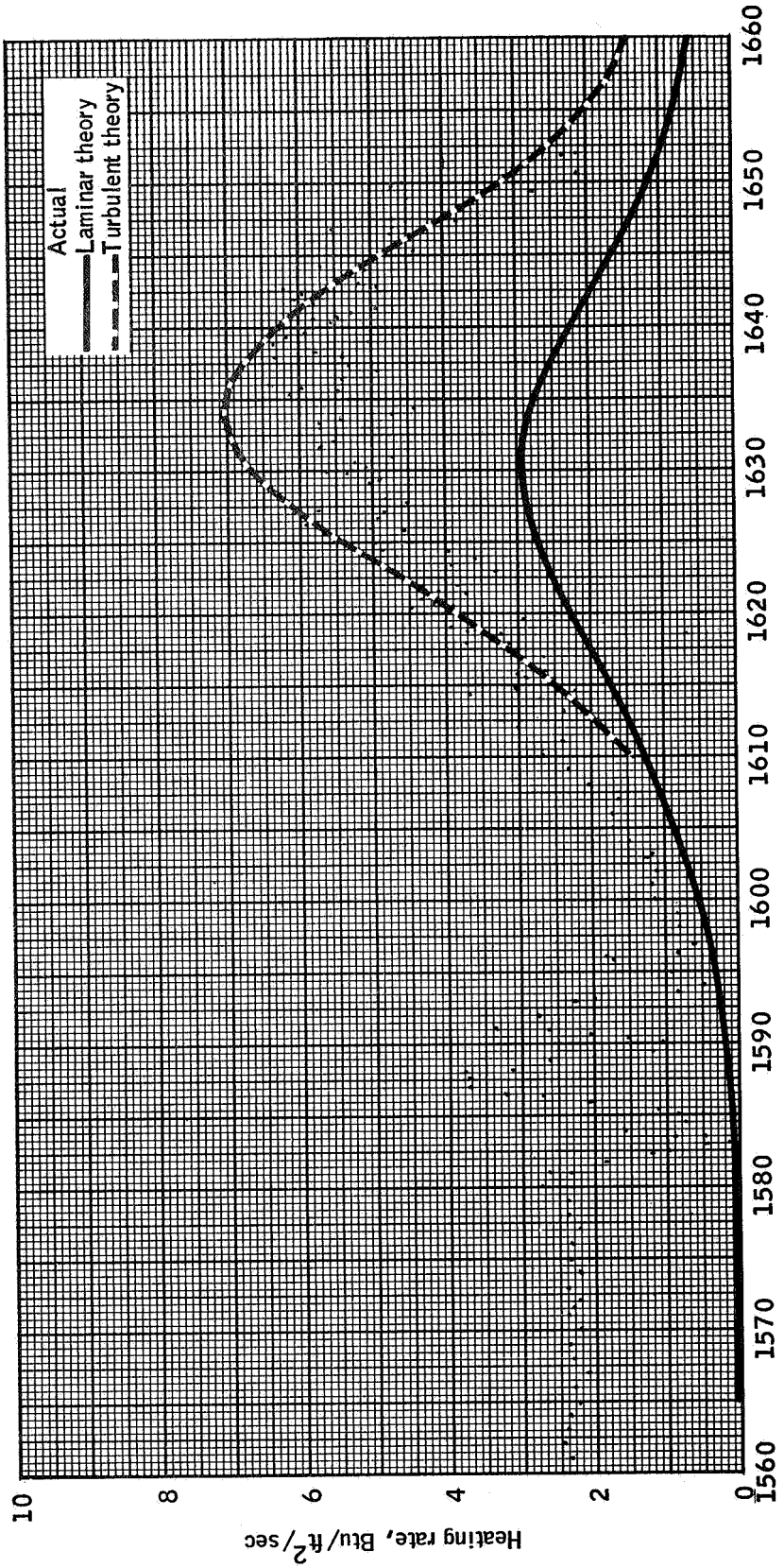
Figure 6.2-3.- Continued.

NASA-S-66-6202 MAY 6



(m) CA1332R, X_C67, 270°, S/R 1.77.

Figure 6.2-3.- Continued.

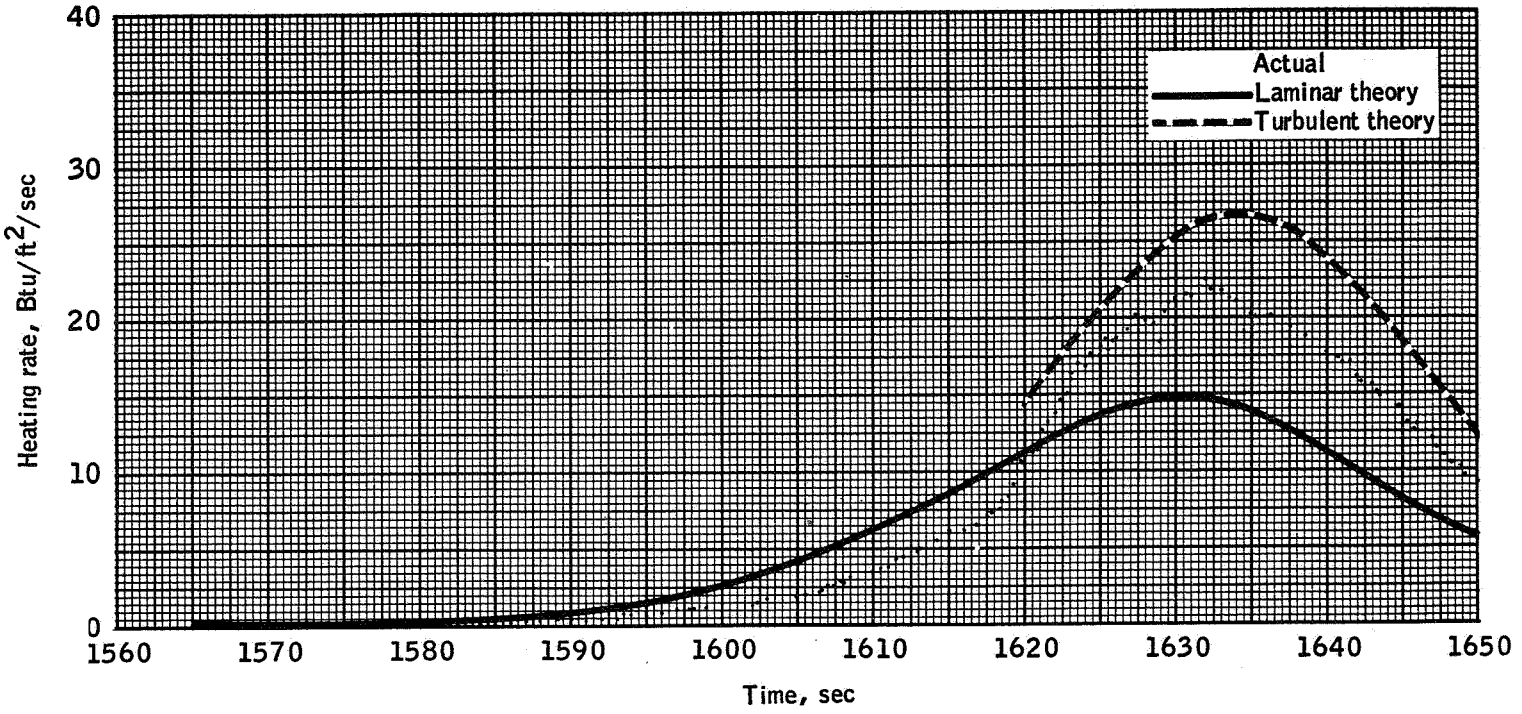


(n) CA1295R, X_C112.25, 270°, S/R Z.47.

Figure 6.2-3.- Continued.

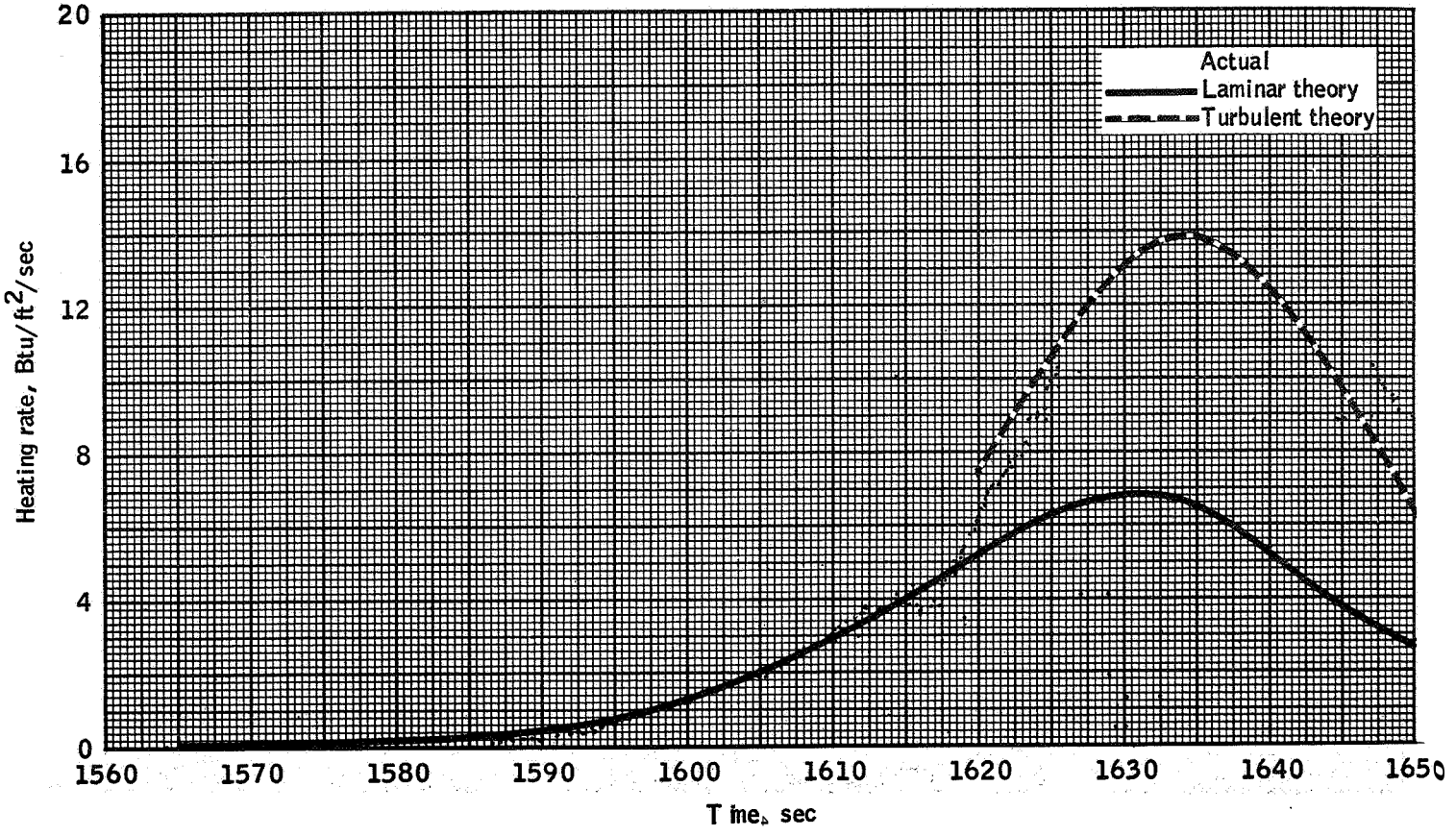
NASA-S-66-0203 ■AY 6

NASA-S-66-6204 MAY 6



(o) CA1277R, X_C 23.2, 180°, S/R 1.1.

Figure 6.2-3.- Continued.



(p) CA1283R, X_C21.5, 270°, S/π 1

Figure 6.2ω.- Concluded.

NASA-S-66-6206 MAY 6

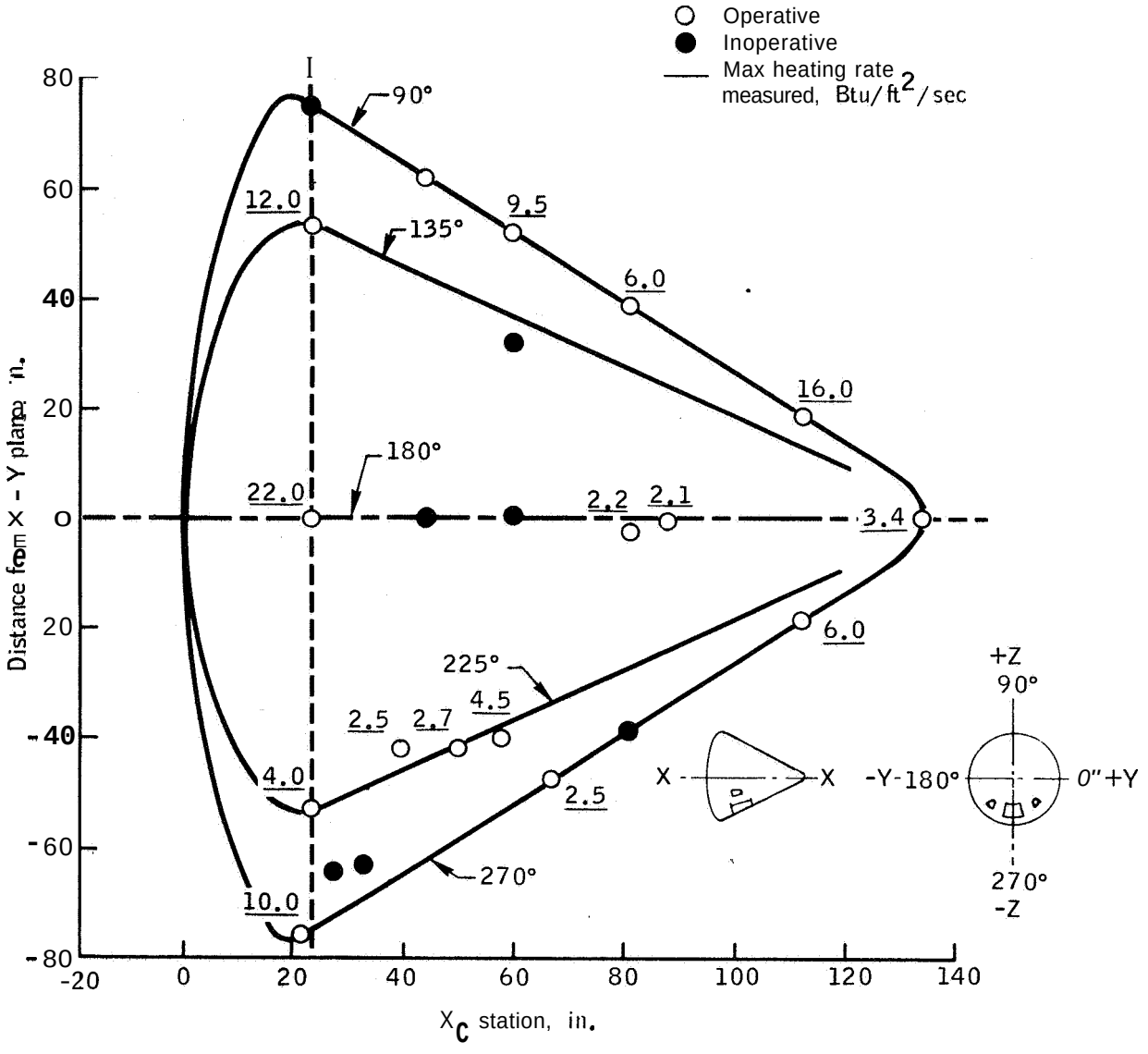
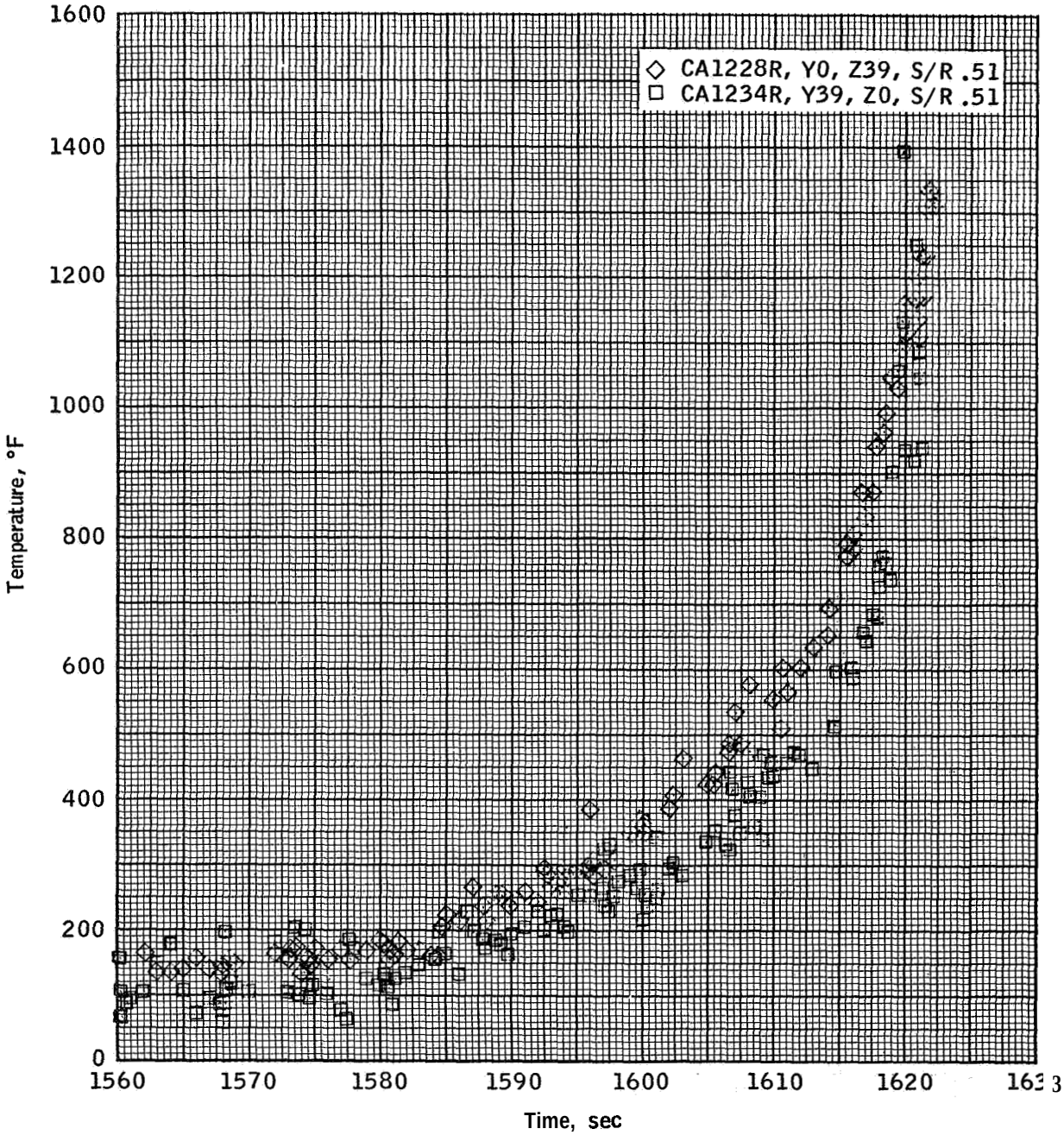


Figure 6.2-4.- Instrumentation locations on the conical surface of the CM, showing actual maximum heating rates, Mission AS-201.

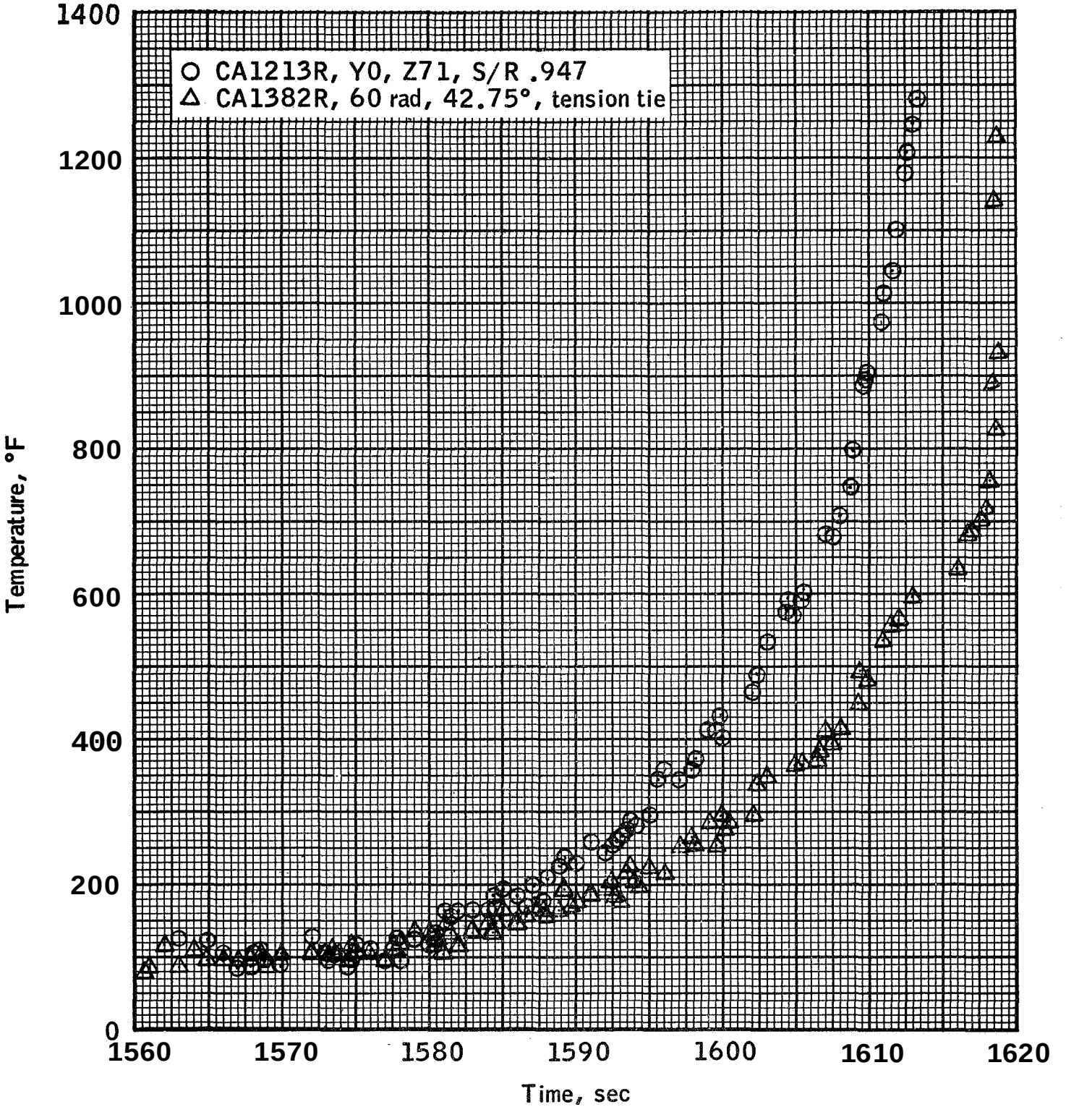
NASA-S-66-6207 MAY 6



(a) CA1228R and CA1234R.

Figure 6.2-5.- Time histories of high range calorimeter temperatures, Mission AS-201.

NASA-S-66-6208 MAY 6



(b) CA1213R and CA1382R.

Figure 6.2-5.- Concluded.

7.0 SPACECRAFT SUBSYSTEMS

7.1 structural Loads

Mission AS-201 was the first flight test of the Apollo Block I spacecraft structure under the Saturn IB launch environment, service propulsion subsystem operation, and reentry loading conditions. Critical loading conditions for the mission are summarized in table 7.1-I and were checked by two methods. Body loads at the command and service module (CSM) interface were determined and compared with design allowable loads (ref. 11). Internal loads in the command module (CM), service module (SM), and spacecraft - LEM adapter (SLA) structure were determined from strain gage readings, and compared with the allowable structural loads.

Description.- The spacecraft 009 structure included Block I type launch-escape subsystem (LES), CM, SM, and SLA.

Launch-escape subsystem: The Block I type LES tower used on Mission AS-201 was a titanium (alloy 6AL-4V) tubular truss structure, covered with Buna-N rubber for thermal protection. The tower was bolted to a structural skirt at the aft end of the launch-escape motor and to the CM by four single-mode explosive bolts. The Block I type launch-escape subsystem had been previously flown on Missions A-002, A-003, PA-2, and A-004 (refs. 6 to 9).

Command module: The Block I type CM structure was similar to that of spacecraft 002 (ref. 9) but included the complete ablator for the launch and reentry heating conditions planned for this mission. The ablator thickness varied along the three-piece heat shield (forward, crew, and aft compartment heat shield) according to the heat load expected from a lunar return trajectory. (See figs. 7.1-1 and 7.4-3.)

Boost protective cover: The Block I type boost protective cover, which was jettisoned with the LES, was in two portions. (See fig. 7.1-2.) Above $X_C 81$, the cover ("hard cover") consisted of fiberglass honeycomb sandwich material covered with cork ablator, and below $X_C 81$ the cover ("soft cover") consisted of teflon-impregnated glass cloth covered with cork ablator. The soft cover was constructed in eight gores which were attached to each other and to the hard cover by mechanical fasteners.

Service module: The Block I type SM structure was similar to that of spacecraft 002 (ref. 9), but included the installation of the service propulsion subsystem (SPS) and the service module reaction control subsystem (SM RCS) (fig. 7.1-3). The four main service propulsion subsystem propellant tanks were mounted on the aft bulkhead and supported against

lateral movement by the forward bulkhead. Blankets of insulation were installed between the CM and SM to maintain the temperature of the RCS propellants within operating limits. A heat shield was installed below the aft bulkhead to protect the SM interior from heat generated by the SPS engine. Nonfunctional radiator panels for the electrical puwer subsystem and environmental control subsystem were included in the service module outer shell structure.

The CM was attached to the SM by three tension ties and rested on three compression and three shear – compression pads. Each of the six SM bearing pads was mounted on the forward end of a SM radial beam truss. Each tension tie was bolted to a truss and extended through the CM aft heat shield to the inner structure of the CM (fig. 7.4-2). A fairing 26 inches in length enclosed the CM/SM interface.

Spacecraft – LEM adapter: The Block I type SLA structure was a truncated cone of monocoque construction (fig. 7.1-4). It was fabricated from aluminum honeyconib sandwich material 1.7 inches thick, with the face sheet thickness varying along the length of the adapter in proportion to the expected load variations. The forward portion of the adapter was composed of four panels with interfacing splice plates. At the time for SM/SLA separation, the panels and the splice plates were separated by pyrotechnics, and the four panels, each of which was strap-hinged at the aft end, were forced open by gas generator thrusters. The aft portion of the SLA structure remained in one piece, attached to the S-IVB instrument unit. Since no IEM was included in Mission AS-201, a stiffening member was installed in the SLA at the point for normal IEM attachment.

Body loads.- Loads were derived at the CM/SM structural interface for several critical loading conditions. These conditions were: lift-off, mid-boost, S-IB end boost (maximum axial acceleration), S-IB/S-IVB separation, and S-IVB end boost. Applied loads derived from flight data were compared to Saturn IB design loads for each critical condition. By making these comparisons, an evaluation of the design adequacy as well as increased confidence in the ability to predict loads is accomplished.

Lift-off: The spacecraft and launch vehicle were exposed to ground winds, defined in figure 7.1-5, prior to S-IB engine ignition. Very low values of vehicle response and loads were recorded during this time. Maximum lateral accelerations measured by the tuwer accelerometers before engine ignition were 0.13g peak-to-peak, well below the design level. No spacecraft loads of any significance were expected fromthe winds experienced (12.7 knots, maximum) since allowable ground winds for a free-standing Block I spacecraft, on the Saturn IB are 99.9 percent of those winds occurring in the worst ground wind month, which is 32.9 knots at the 60-foot level.

To find the worst loads condition at lift-off, loads were examined fromthe time of engine ignition until all significant structural response had decayed after the lift-off. Prior to lift-off large lateral accelerations were caused by the S-IB ignition sequence (see sections 7.2 and 7.20). These accelerations are larger than anticipated and were not included in the Saturn IB launch release design loads. (See fig. 7.1-6.)

Immediately after lift-off, the lateral elastic response of a flexible vehicle results from a transfer of elastic strain energy into kinetic energy. The strain energy is a result of the ground winds, unsymmetric thrust buildup, and thrust misalignments, and is transferred into kinetic energy as the hold-down arms are released. As seen in figure 7.1-6 spacecraft lateral transient accelerations were lower than those measured before lift-off and were damped out approximately 4 seconds after lift-off. A comparison of the maxim applied loads and accelerations with design values is shown in table 7.1-I(b) for this condition. The maximum loads could not be accurately measured because strain-gage readings at the CSM interface were commutated at 0.1-second intervals and the structural response was at approximately 10 cps. As a result, there is an apparent poor correlation shown in table 7.1-I(b) for this condition.

Saturn IB first-stage boost: To evaluate the spacecraft loads during the maximum dynamic pressure region of flight, body loads at the CM/SM interface were derived by the following three methods: (1) prelaunch flight simulation using T-0 winds which were measured by tracking an aluminized spherical balloon (jimsphere) with the FPS-16 radar (fig. 7.1-7), (2) MSC elastic body loads program using measured angles of attack and gimbal angles, and (3) reduction of measured strain readings. Values obtained by each of the three methods are compared with the design loads in table 7.1-I(c) to evaluate the design condition, the severity of the actual launch environment, and the loads prediction capability. The loads show good agreement, although the times of maximum load vary because of slight differences in the trajectories used in the calculations. The measured angle of attack at max q was 3.54° which is less than half the Block I design value of 8° for a Saturn IB trajectory*

S-IB/S-IVB staging: The loading conditions considered in this section are S-E3 end of boost; S-IB engine thrust decay, and S-IB/S-IVB separation.

Maximum axial accelerations and maximum compressive loads are experienced by the spacecraft structure near the end of S-IB boost. Shawn in table 7.1-I(d) is a comparison of predicted, measured, and design loads at the CSM interface for this condition. The predicted and measured values are lower than the design values. The lateral loads at this time were very low.

The X-axis acceleration shown in figure 7.1-8 very clearly indicates the inboard and outboard cutoff and thrust decay of the S-IB engines. No significant spacecraft vibrations or loads occurred during the time of S-IB thrust decay or S-IB/S-IVB separation.

A comparison of design and measured CM/SM interface loads during the time between OECO (T+146.9 sec) and S-IVB ignition (T+149.3 sec) is shown in table 7.1-I(e). The magnitude of the loads during this portion of the launch are not significant when compared with the maximum critical design loads.

S-IVB operation: The initial acceleration buildup during S-NB operation is shown in figure 7.1-8(b). The buildup from essentially 0g at T+151 seconds to 0.65g at TI-133.5 seconds is shown. From TI-153 seconds to TI-602.9 seconds, a slow buildup of axial acceleration was observed. The peak acceleration of 2.71g and the S-IVB thrust decay are shown in figure 7.1-9.

Table 7.1-I(f) shows a comparison of design and measured loads for the S-NB operation phase. The accelerations were as expected and show no significant load conditions for S-IVB operation when compared with the maximum critical design loads.

SPS burn and reentry: Command module accelerometer data recorded from S-IVB engine cutoff to touchdown were affected by a spacecraft puwer malfunction which lasted from TI-164.9 seconds to T+2121 seconds. The data recorded after the malfunction occurred were not considered reliable.

An evaluation of loads data between the S-IVB cutoff and the power malfunction indicated very low loading conditions which was as expected and no detailed structural analysis was made.

Internal loads.- Internal loads were determined from strain-gage instrumentation mounted on various structural components within the CM, SM, and SLA. See reference 1 for actual strain-gage locations and ranges.

Command module internal loads: Two strain gages on the aft heat shield were inoperative prior to the mission, and all of the gages on the forward longeron inner surfaces were either inoperative or produced invalid data during the mission, A voltage drop in the instrumentation system during the reentry blackout period resulted in invalid data from the remaining gages during the continued descent phase of the mission. Table 7.1-II shows the calculated stresses from the usable strain-gage measurements on the forward longerons and aft heat shield for the boost phase of the mission. These stresses indicate that during the boost the command module structure was lightly loaded, as expected.

Service module internal loads: Since all of the radial beam truss strain gages were reset to zero readings before lift-off according to the checkout procedures, the maximum loading these members carried during the mission was determined by making an analysis of the structure assuming that it was subjected to a 1g load prior to lift-off. Adjusting the flight-data strain values with those calculated prior to lift-off resulted in the actual structural loading during the mission. Comparison of these adjusted loads and those calculated by other means at the CM/SM interface resulted in a fair correlation which indicated that the assumptions made were very nearly correct.

The adjusted strain values for each radial beam truss member were converted to axial stresses and are shown in table 7.1-III. Also the calculated stresses for each member subjected to the 1g loading assumption are shown for comparison, as well as the maximum stresses experienced during the mission and the times at which they occur.

The axial strain on the radial beam caps and tension tie loads were also converted to axial stresses and are shown in table 7.1-IV along with maximum stresses experienced by these members during the mission. The times at which they occurred are shown for comparison.

In both tables, the maximum stresses were found to be less than the member design stress.

Spacecraft - LEM adapter internal loads: All SLA strain gages were balanced to zero before stacking the various spacecraft components with the exception of those on the stabilizing cable load-links. These cables were pretensioned after the stacking operation.

Table 7.1-V shows the stresses from the strain-gage measurements on the SLA shell skins and stabilizing structure. It should be noted that the maximum stresses do not necessarily occur during one of the significant phases shown in the table. Table 7.1-VI shows the loads measured on the SLA/LEM stabilizing cable load links, including the measured values of pretension in the cables just prior to the S-IB ignition, the maximum measured loads in the cables during the mission, and the times at which they occurred,

In both tables, the maximum stresses and loads were found to be less than those for the component design, indicating that the structure was lightly loaded during the mission. This was expected for this mission because of the off-loading of consumables and omission of some of the equipment normally included in the Block I configuration,

Table 7.1-VII shows the structural load comparison (maximum measured load versus the structural allowable load) for the various structural components listed in tables 7.1-II to 7.1-VI. It may be noted

from this table that the largest load in any member was only 43.2 percent of its allowable load, indicating that the structure was lightly loaded.

Conclusions.- Since the spacecraft; structural design criteria for lift-off did not include loads due to unsymmetric thrust buildup, the ground winds go-no-go procedure must be revised to include these effects. The present go-no-go procedure includes conservative estimates of vortex shedding and cantilevered vehicle dynamic loads.

The procedure is presently being revised in an effort to determine the actual on-pad loads due to winds. The modified procedure is expected to increase launch capability enough to offset a reduction due to unsymmetric thrust buildup. The new procedure is planned to be implemented on Mission AS-202 and subsequent missions. Unsymmetric thrust buildup will also be considered in all future spacecraft design load calculations.

Other than at lift-off, Mission AS-201 was nominal from the structural loads viewpoint. The body loads and internal loads were as predicted in all of the critical loading cases and were well within the structural capability of the vehicle. Postflight inspections have revealed no inflight structural damage to the command module,

TABLE 7.1-I.- EVENTS AND CONDITIONS SIGNIFICANT TO SIRUCTURAL ANALYSIS

a. Event Times	
Condition	Elapsed time, sec
Saturn IB engine ignition	-2.45
Lift-off	- 0.37
Mach 1	65.7
Maximum dynamic pressure region (qa)	77.7
Maximum axial acceleration	141.5
S-IB/S-IVB separation	147.7
S-IVB ignition	149.3
S-IVB end boost	602.9

b. hunch Release Maximum Bending Moment Conditions			
Condition	Predicted	Measured	Design (a)
Bending moment at CM/SM interface, in-lb	-13 000	-43 000	-13 000
Axial force at CM/SM interface at time of maximum bending moment, lb	-1.415×10^6	-0.416×10^6	-2.4×10^6
CM lateral acceleration at time of maximum bending moment, g	-0.876	-0.71	-1.48

[a] From reference SID 63-701, Feb. 1965.

TABLE 7.1-I.- EVENTS AND CONDITIONS SIGNIFICANT TO STRUCTURAL ANALYSIS - Continued

c. CSM Interface Conditions During Maximum $q\alpha$

Condition	Maximum values			
	Predicted (a)	Calculated (b)	Measured	Design
Time, sec	84.8	81.9	77.7	69.7
Dynamic pressure, lb/sq ft	584	617	605	653
Axial acceleration, g	2.14	[a]2.07	1.97	1.84
Bending moment at X_A1010, in-lb	0.66×10^6	0.657×10^6	0.616×10^6	1.97×10^6
Axial force at X_A1010, lb	-61 500	-59 400	-64 900	-80 800
Angle of attack, deg	2.0	2.84	3.54	8
Mach number	1.8	[a]1.6	1.42	1.25
Gimbal angle, deg	.85	2.04	-	-

[a]Based on measured launch wind conditions.
[b]Based on measured flight trajectory.

d. CSM Interface Conditions During S-IB End of Boost

Condition	Predicted	Measured	Design (a)
CM X-axis acceleration, g	4.04	4.1	4.4
Bending moment at X_A1010, in-lb		242 000	286 500
Axial force at X_A1010, lb	-80 000	-79 280	-84 500

[a]Based on measured launch wind conditions.

TABLE 7.1-I.- EVENTS AND CONDITIONS SIGNIFICANT TO STRUCTURAL ANALYSIS - Concluded

Condition	Design	Measured
Bending moment at X_A1010, in-lb	526 000	237 500
Axial force at X_A1010, lb	-26 800	-33 600

f. Conditions During S-IVB Operation		
Condition	Design	Measured
Longitudinal acceleration, g	3.35	2.71
Lateral acceleration, g	.39	-
Bending moment, in-lb	188 000	217 000
Axial force, lb	-38 000	-29 800

TABLE 7.1-II.- CM FORWARD LONGERON AND AFT HEAT SHIELD STRESSES FOR MISSION AS-201

Gage location	Lift-off (T=0.37 sec) stress, psi	Max. qα (T=77.7 sec) stress, psi	S-IB end boost (T=141.5 sec) stress, psi	S-IVB ignition (T=149.3 sec) stress, psi	Max. measured stress, psi	Time max. stress occurred, sec
Forward longeron 4, outer X_C77, 43°	2 660	-294	-602	1 323	2 660	0.37
Forward longeron 8, outer X_C77, 223°	3 260	2 540	805	2 320	3 260	.37
Forward longeron 4, outer X_C50.1, 43°	3 950	4 440	3 760	4 220	4 440	77.7
Forward longeron 8, outer X_C50.1, 223°	-262	2 020	1 323	1 410	2 020	77.7
Aft heat shield, outer Z-Z axis, center	5 390	9 050	8 250	8 080	9 050	77.7
Aft heat shield, inner Z-Z axis, center	4 250	5 180	6 420	5 490	6 420	141.5
Aft heat shield, outer Y-Y axis, center	3 720	6 840	9 600	8 000	9 600	141.5
Aft heat shield, inner Y-Y axis, center	1 930	5 070	4 070	2 560	5 070	77.7
Aft heat shield, outer tangential rad 46, 90°	1 140	4 740	3 620	2 800	4 740	77.7
Aft heat shield, inner tangential rad 46, 90°	21 100	20 400	23 100	23 400	23 400	149.3
Aft heat shield, outer tangential rad 47, 90°	19 450	17 100	11 800	13 320	19 450	.37
Aft heat shield, inner tangential, rad 47, 90°	23 100	18 450	18 650	20 100	23 100	.37
Aft heat shield, inner rad 46, 0°	14 600	12 480	7 640	10 850	14 600	.37
Aft heat shield, outer tangential rad 47, 0°	8 660	9 110	6 600	7 050	9 110	77.7

TABLE 7.1-II.- CM FORWARD LONGERON AND AFT HEAT SHIELD STRESSES FOR MISSION AS-201 - Concluded

Gage location	Lift-off (T=0.37 sec) stress, psi	Max. $q\alpha$ (T=77.7 sec) stress, psi	S-IB end boost (T=141.5 sec) stress, psi	S-IVB ignition (T=149.3 sec) stress, psi	Max. measured stress, psi	Time max. stress occurred, sec
Aft heat shield, inner tangential rad 47, 0°	9 560	15 280	11 100	9 280	15 280	77.7
Aft heat shield, inner tangential rad 46, 180°	-8 900	-17 650	-13 900	-9 700	-17 650	77.7
Aft heat shield, outer tangential rad 47, 180°	7 280	16 820	9 340	8 440	16 820	77.7
Aft heat shield, inner tangential rad 47, 180°	-17 450	-22 900	-22 600	-16 740	-22 900	77.7

TABLE 7.1-III.- SM RADIAL BEAM TRUSS STRESSES FOR MISSION AS-201[a]

Gage location	Calculated stresses before lift-off, psi	Lift-off (T=0.37 sec) stress, psi	Max. qα (T=77.7 sec) stress, psi	S-IB end boost (T=141.5 sec) stress, psi	S-IVB end boost (T=602.9 sec) stress, psi	Max. stress, psi	Time max. stress occurred, sec
Compression pad, inboard, beam 1	-6 020	-5 480	-7 750	-9 060	-7 900	-9 060	141.5
Compression pad, outboard, beam 1	-6 850	-6 820	-13 700	-13 900	-8 860	-13 900	141.5
Compression pad, inboard, beam 2	-5 880	-5 520	-8 850	-9 450	-6 880	-9 450	141.5
Compression pad, outboard, beam 2	-5 270	-6 690	-9 570	-10 990	-8 060	-10 990	141.5
Compression pad, inboard, beam 3	-6 020	-8 060	-9 890	-10 070	-8 330	-10 070	141.5
Compression pad, outboard, beam 3	-6 310	-7 760	-10 080	-11 750	-8 920	-11 750	141.5
Compression pad, inboard, beam 4	-5 880	-7 300	-11 400	-9 930	-6 980	-11 400	77.7
Compression pad, outboard, beam 4	-5 290	-5 980	-7 750	-8 930	-6 300	-8 930	141.5
Compression pad, inboard, beam 5	-6 020	-6 700	-8 690	-9 120	-7 960	-9 120	141.5
Compression pad, outboard beam 5	-6 780	-6 190	-9 660	-11 290	-7 460	-11 290	141.5
Compression pad, inboard, beam 6	-5 880	-5 940	-7 720	-8 660	-6 670	-8 660	141.5
Compression pad, outboard, beam 6	-5 290	-4 970	-9 140	-11 490	-10 200	-11 490	141.5

[a]All stress values are calculated from adjusted strain-gage data.

TABLE 7.1-IV.- SM RADIAL BEAM CAP AND CM/SM TENSION-TIE STRESSES FOR MISSION AS-201

Gage location	Lift-off (T=0.37 sec) stress, psi	Max. qα (T=77.7 sec) stress, psi	S-IB end boost (T=141.5 sec) stress, psi	S-IVB end boost (T=602.9 sec) stress, psi	Max. measured stress, psi	Time max. stress occurred, sec
Beam 1 outer cap, X_A983	-6 360	-7 350	-8 880	-6 850	-8 880	141.5
Beam 1 outer cap, X_A973	126	-1 512	-1 670	-336	-1 960	77.3
Beam 1 outer cap, X_A858	2 890	-1 050	-3 310	2 540	5 540	172.3
Beam 1 outer cap, X_A848	-630	-2 415	508	-1 312	-3 480	81.9
Beam 4 outer cap, X_A983	1 523	-1 890	-2 730	2 150	5 950	147.8
Beam 4 outer cap, X_A973	1 995	-894	-1 135	1 470	4 700	153.3
Beam 4 outer cap, X_A858	2 260	2 960	2 720	1 912	4 520	151.3
Beam 4 outer cap, X_A848	442	-525	1 323	105	3 470	156.3
Tension tie beam 2	26 800	12 480	7 540	22 000	37 500	151.3
Tension tie beam 4	25 200	14 750	12 950	25 000	37 600	150.5
Tension tie beam 6	31 600	17 480	13 560	24 100	35 000	150.0

TABLE 7.1-V.- SLA SKIN AND STABILIZING MEMBER STRESSES FOR MISSION AS-201

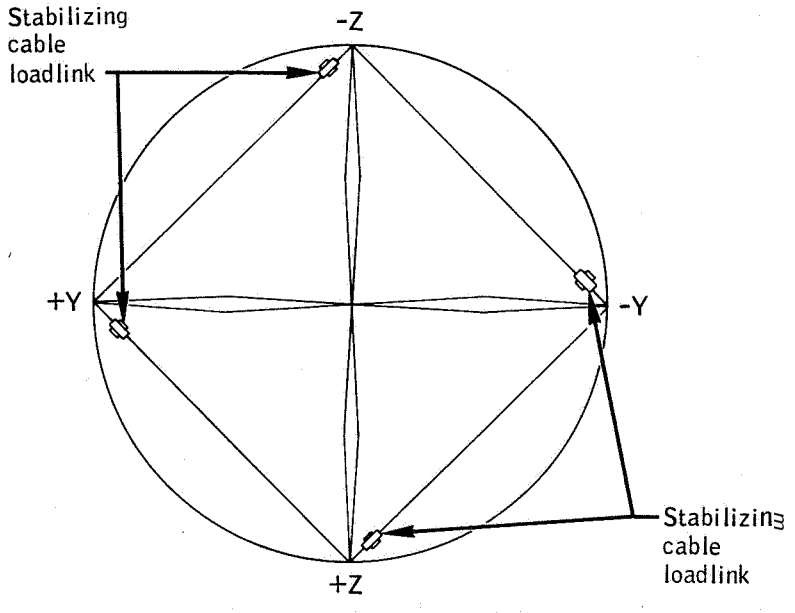
Gage location	Lift-off (T=0.37 sec) stress, psi	Max. qα (T=77.7 sec) stress, psi	S-IB end boost (T=141.4 sec) stress, psi	S-IVB end boost (T=602.9 sec) stress, psi	Max. calculated stress, psi	Time max. stress occurred, sec
Outer skin, longitudinal, X_A775, 34°	-3 520	-5 900	13 500	6 150	-13 500	141.5
Outer skin, circumferential, X_A775, 34°	-466	2 000	827	-2 180	-6 780	494.1
Inner skin, longitudinal, X_A775, 34°	-7 200	-11 600	4 850	10 520	-16 550	458.2
Inner skin, circumferential, X_A775, 34°	3 540	3 950	1 080	1 970	17 050	145.1
Outer skin, longitudinal, X_A775, 124°	-3 800	-5 250	-1 100	-7 550	-14 800	458.2
Outer skin, circumferential, X_A775, 124°	-5 750	-6 750	5 480	-7 290	-14 250	458.2
Inner skin, longitudinal, X_A775, 124°	-12 100	-15 650	-9 990	-16 980	-25 000	458.2
Inner skin, circumferential, X_A775, 124°	-5 990	-8 980	350	-9 010	-16 250	458.2
Outer skin, longitudinal, X_A775, 214°	-4 560	-4 070	600	-7 240	-12 100	460.5
Outer skin, circumferential, X_A775, 214°	4 240	5 150	4 470	2 890	8 190	120.9
Inner skin, longitudinal, X_A775, 214°	-4 100	-4 300	-2 310	-5 050	-6 440	86.3
Outer skin, longitudinal, X_A775, 304°	-2 760	-4 150	-8 560	5 140	-10 600	137.3
Outer skin, circumferential, X_A775, 304°	-5 480	-2 030	-3 500	4 650	-11 500	433.7

TABLE 7.1-V.- SLA SKIN AND STABILIZING MEMBER STRESSES FOR MISSION AS-201 - Concluded

Gage location	Lift-off (T=0.37 sec) stress, psi	Max. qα (T=77.7 sec) stress, psi	S-IB end boost (T=141.5 sec) stress, psi	S-IVB end boost (T=602.9 sec) stress, psi	Max. calculated stress, psi	Time max. stress occurred, sec
Inner skin, longitudinal, X_A775, 304°	-7 350	-13 300	-5 500	-11 940	-17 750	487.7
Inner skin, circumferential, X_A775, 304°	-722	-3 570	7 120	-5 400	-13 100	487.9
Stabilizing stiffener X_A584, Y_A0, Z_A-97	-1 260	-315	231	-2 310	-5 570	345.8
Stabilizing stiffener X_A584, Y_A97, Z_A0	210	105	420	-966	-4 460	574.4
Stabilizing stiffener X_A584, Y_A97, Z_A0	515	578	1 155	0	-5 280	483.5
Stabilizing stiffener X_A584, Y_A0, Z_A-97	-420	1 575	2 260	-399	2 260	141.5

TABLE 7.1-VI.- SLA STABILIZING CABLE LOADS FOR MISSION AS-201

Gage location	Pretension load prior to S-IB ignition, lb	Lift-off (T=0.37 sec) load, lb	Max. qα (T=77.7 sec) load, lb	S-IB end boost (T=141.5 sec) load, lb	S-IVB end boost (T=602.9 sec) load, lb	Max. measured load, lb	Time max. load occurred, sec
Stabilizing cable loadlink, +Z axis	36	240	195	320	260	582	501.6
Stabilizing cable loadlink, +Y axis	525	460	420	798	900	1 575	499.6
Stabilizing cable loadlink, -Z axis	416	340	530	563	340	1 104	575.0
Stabilizing cable loadlink, -Y axis	590	585	730	1 255	1 260	1 949	506.1



Looking aft from station $X_A = 584.7$

TABLE 7.1-VII.- STRUCTURAL LOAD COMPARISON FOR MISSION AS-201

Structural component	Percent maximum of allowable load	Allowable load bas on —	Allowab load
CM forward longerons	7.1	Material tensile yield, psi	62 000
CM aft heat shield	(a)	(a)	
SM inboard radial beam truss member	24.4	Critical buckling stress, psi	46 720
SM outboard radial beam truss member	19.6	Material compressive yield, psi	71 000
SM radial beam caps	13.05	Material compressive yield, psi	68 000
CM/SM tension ties	40.4	Material tensile limit stress, psi	93 400
SLA conical section skins	43.2	Material compressive yield, psi	58 000
SLA conical section skins	27.5	Material tensile ultimate, psi	62 000
SLA stabilizing structure chord member	17.1	Critical buckling stress, psi	32 500
SLA stabilizing structure chord member	4.92	Material tensile yield, psi	46 000
SLA stabilizing structure assembly[b]	12.8	Critical buckling load, lb	16 650
SLA stabilizing cable fittings	12.2	Ultimate tensile load, lb	16 000

[a]Stress in aft heat shield was considered insignificant for the brazed stainless steel honeycomb structure, i.e., less than 30 000 psi.

[b]The maximum compressive load experienced by the SLA stabilizing assembly as a whole was 2 124 lb and occurred at T+483.5 seconds. The percent of the allowable is based on the critical buckling load of the build-up column.

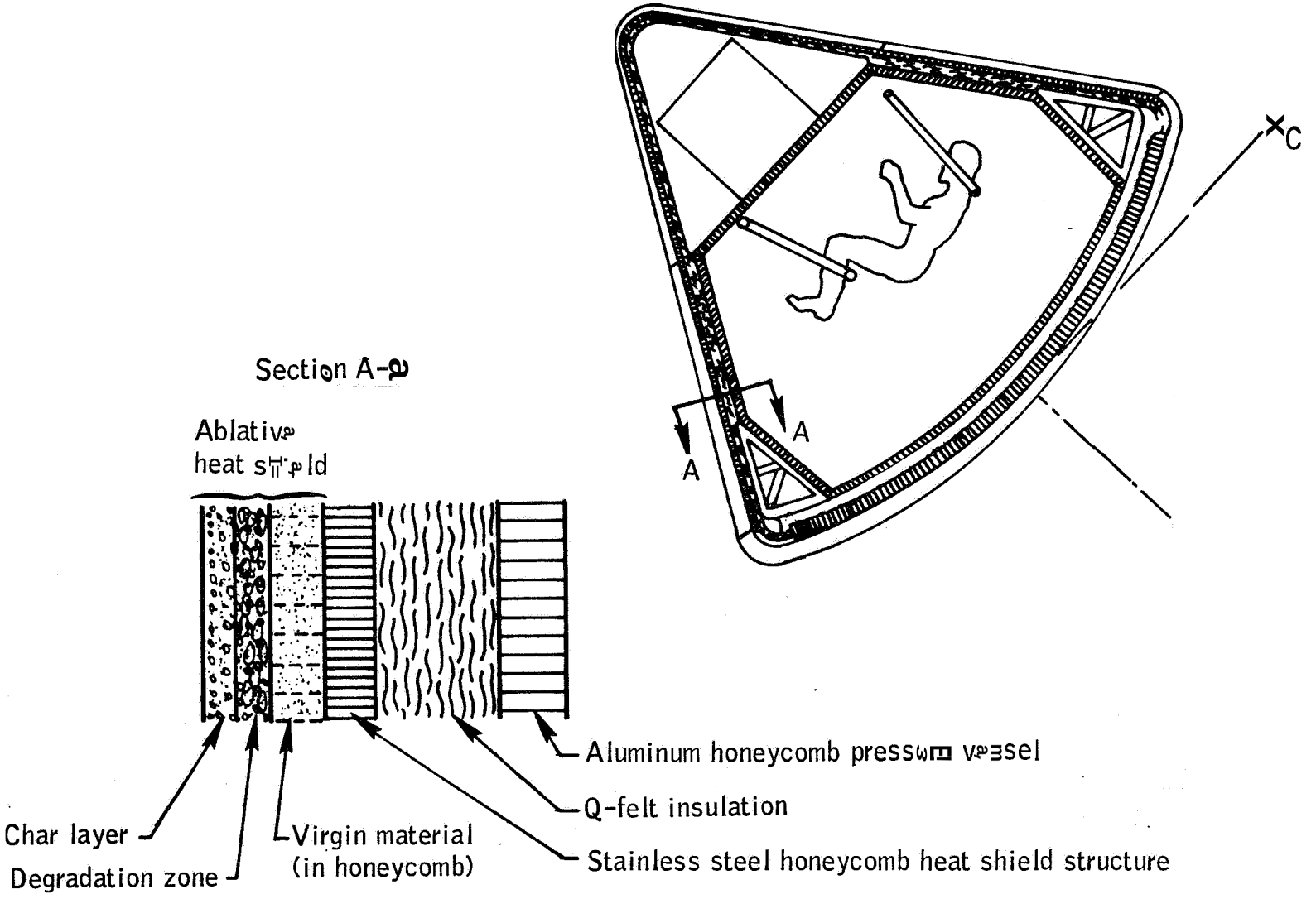


Figure 7.1-1.- CM heat shield, Mission AS-201.

NASA-S-66-6373 MAY 6

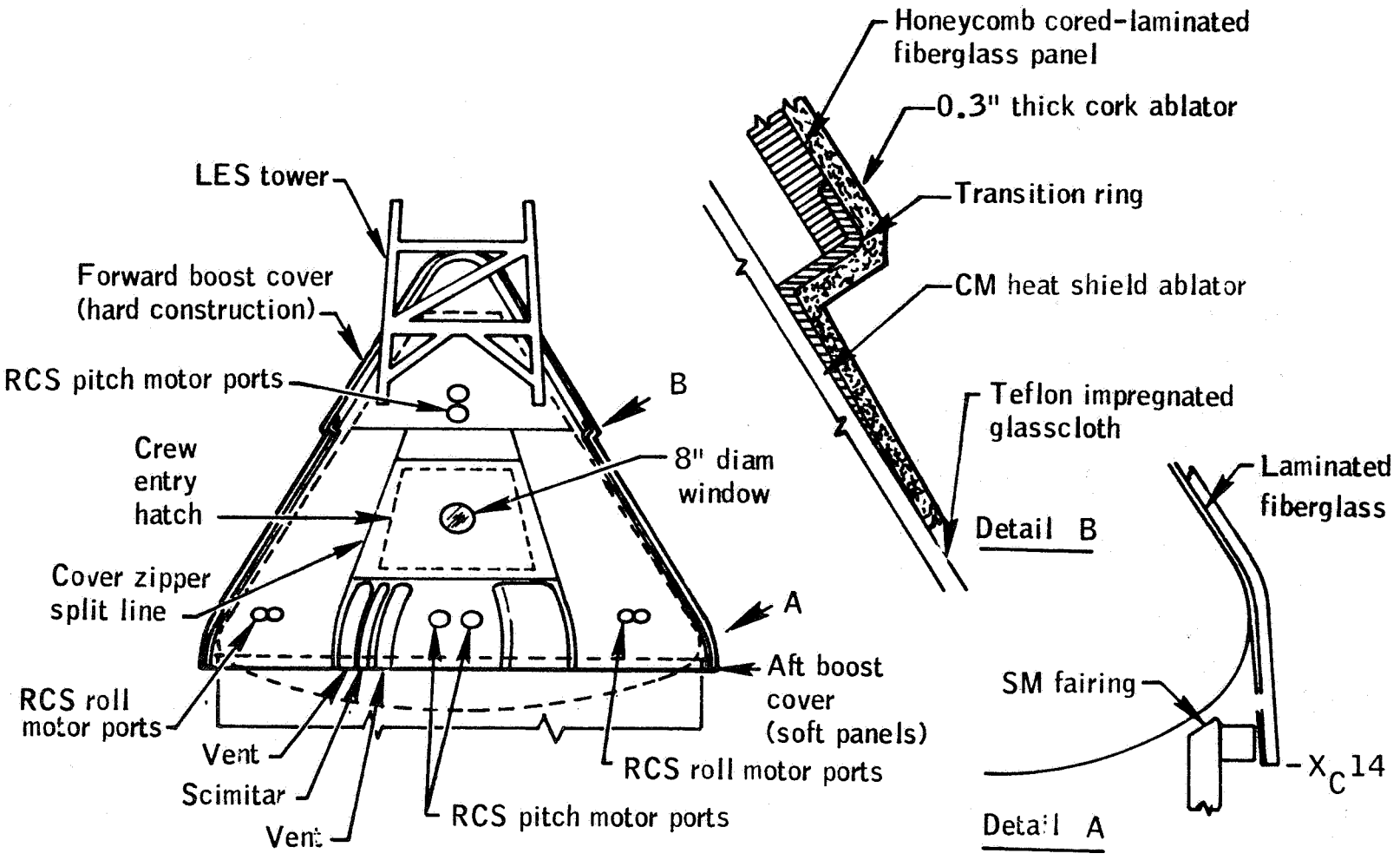
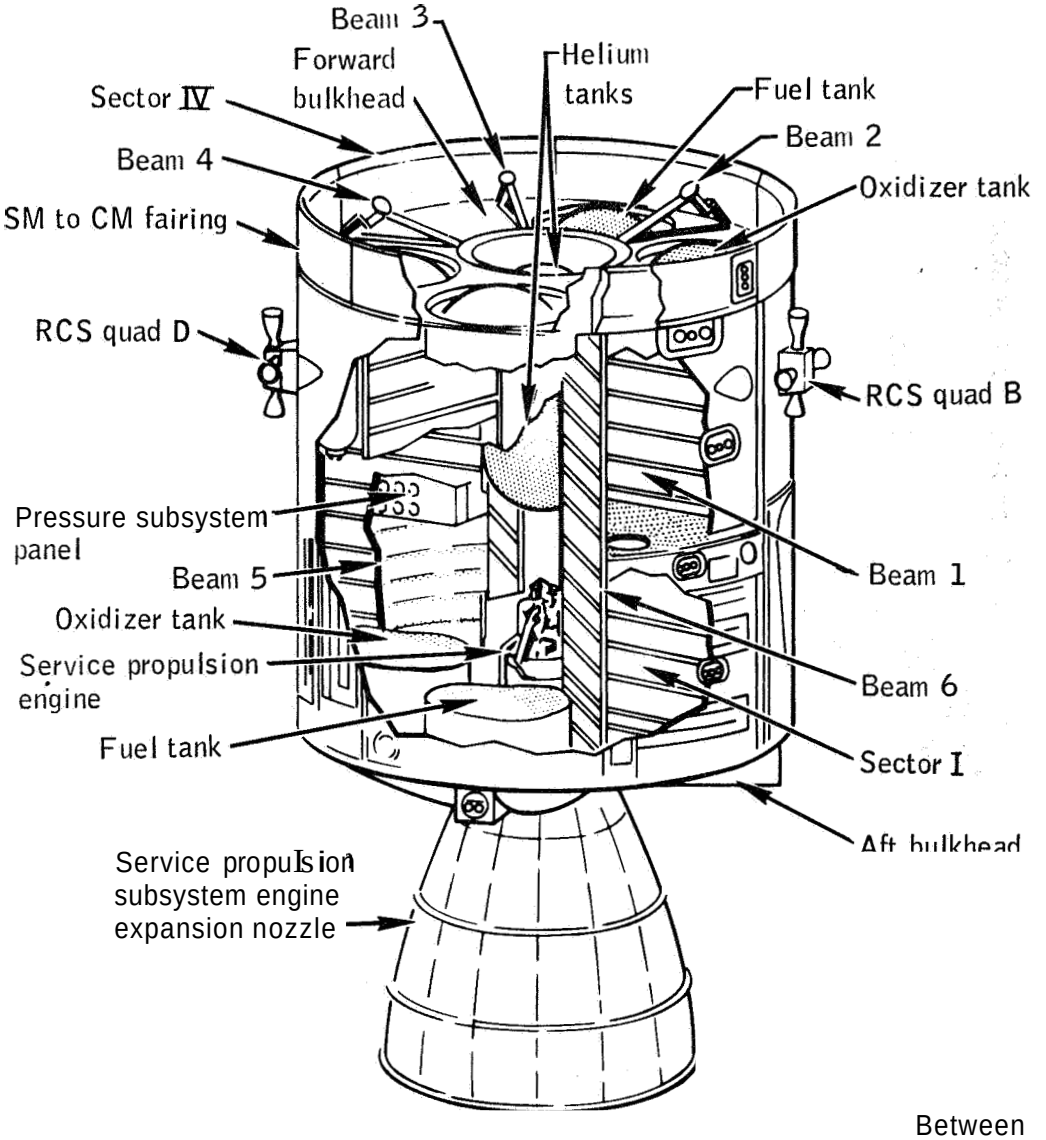
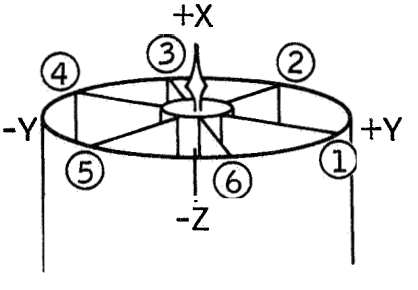


Figure 7.1-2.- Boost protective cover, Mission AS-201.

NASA-S-66-6374 MAY 6





Sector	Between beams	
I	⑥ - ①	(50°)
II	① - ②	(70°)
III	② - ③	(60°)
IV	③ - ④	(50°)
V	④ - ⑤	(70°)
VI	⑤ - ⑥	(60°)

Figure 7.1-3.- Service module structure, Mission **AS-201.**

NASA-S-66-6375 MAY 6

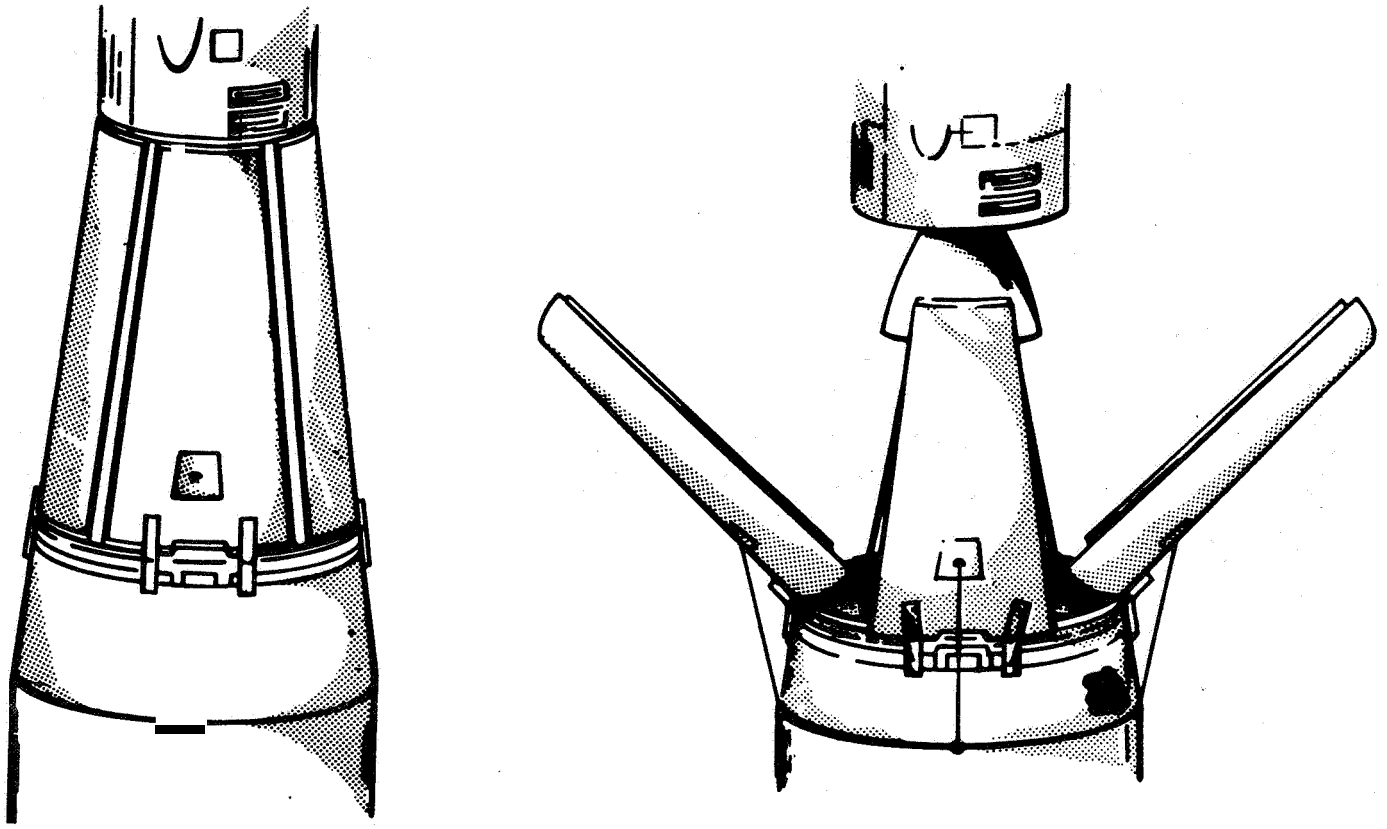


Figure 7.1-4.- Spacecraft – EM adapter, Mission AS-201.

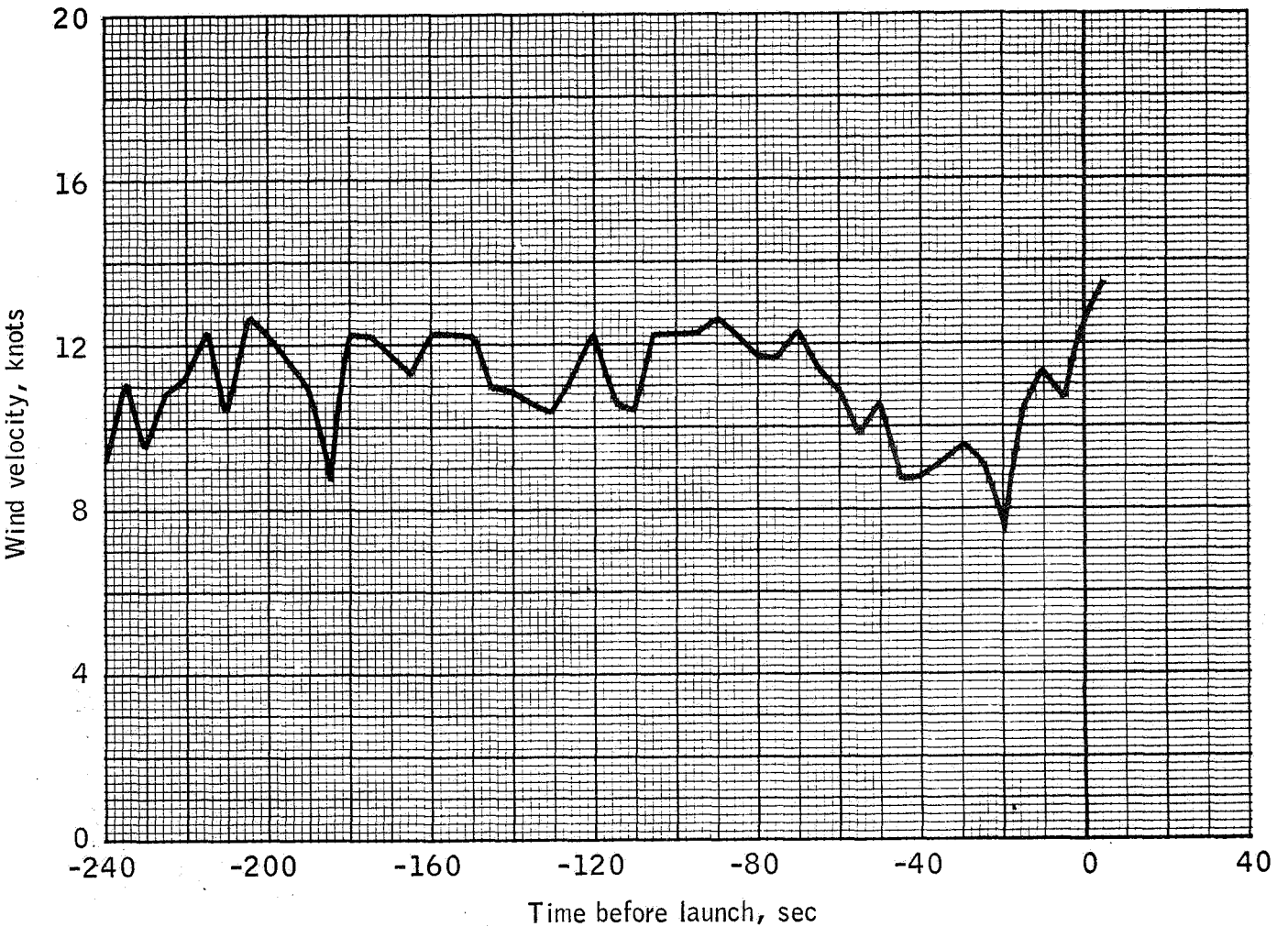


Figure 7.1-5.- Wind velocity obtained at 60 ft ≤v≤l dωring launch of Mission AS-201 at Complex 34.

NASA-S-66-6377 MAY 6

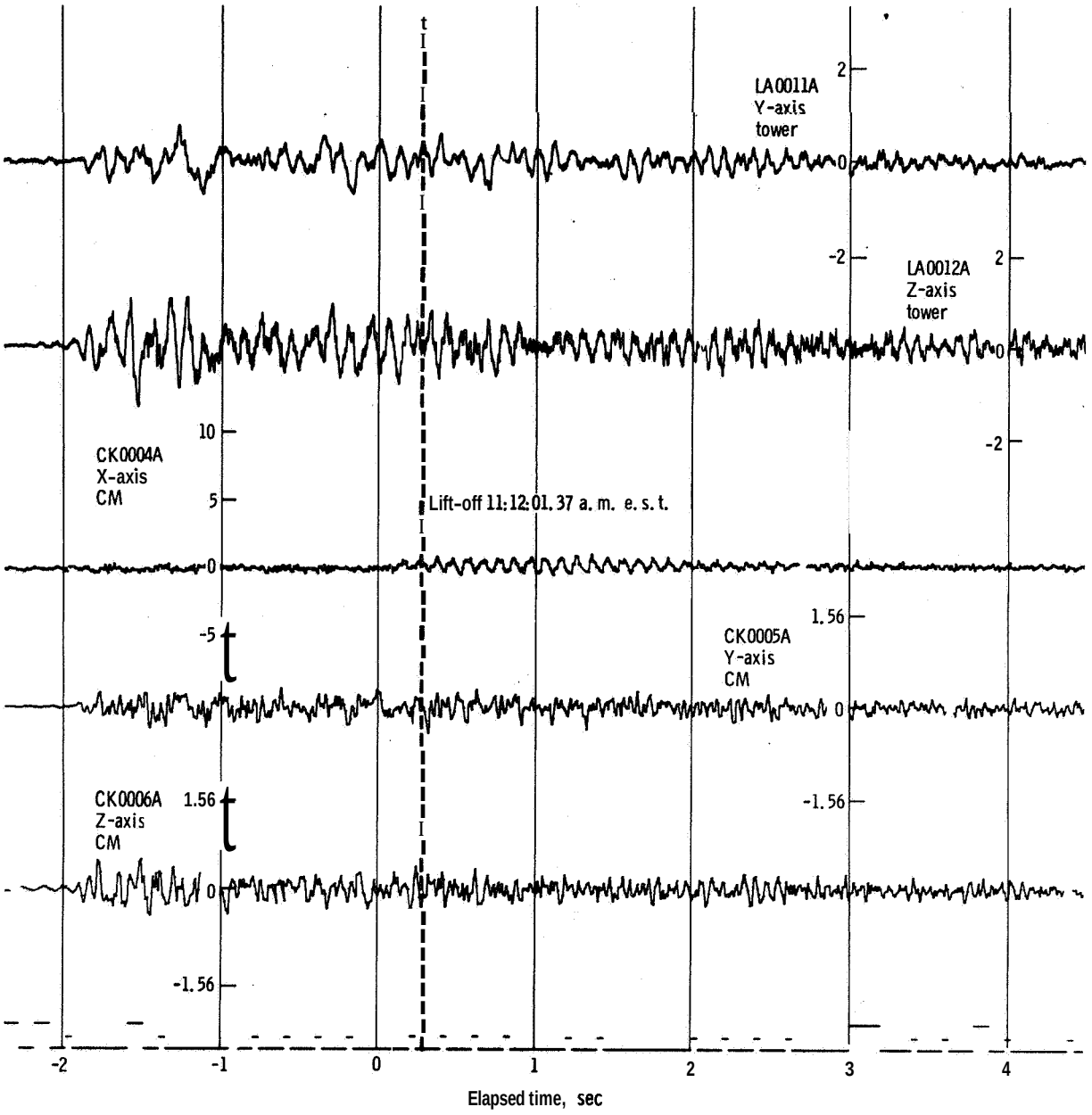
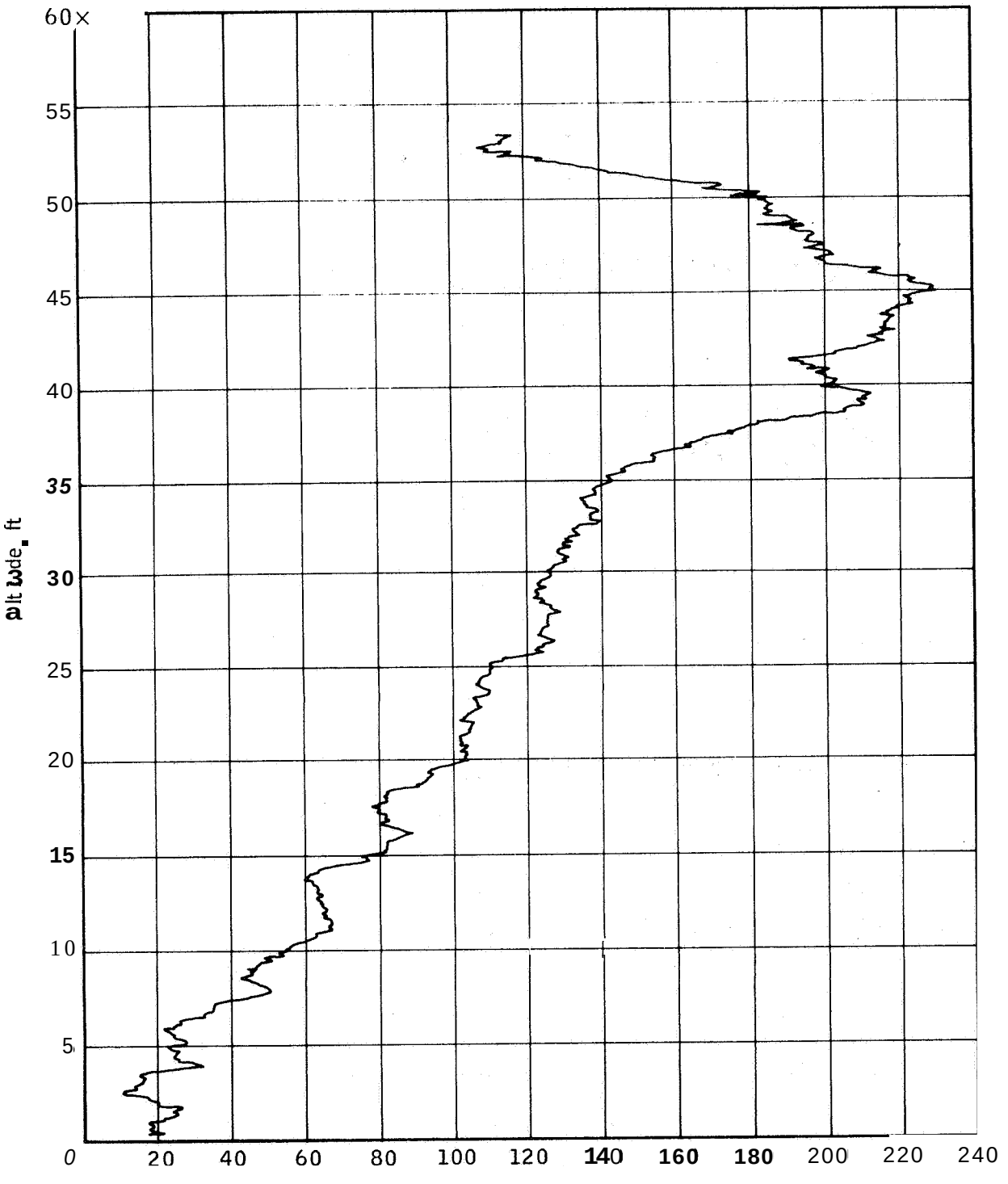


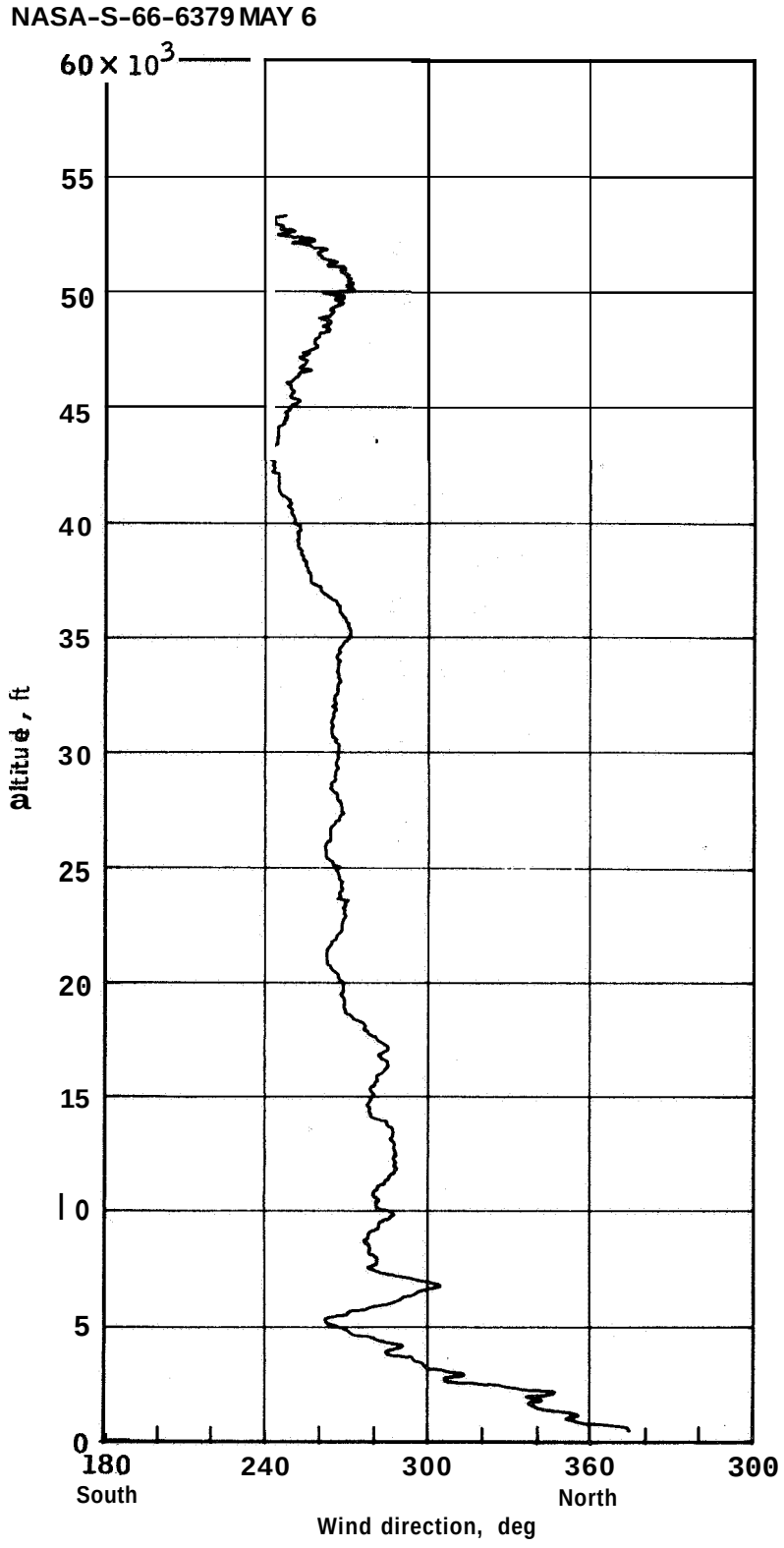
Figure 7.1-6. - Tower and CM lift-off accelerations, Mission AS-201.

NASA-S-66-6378 MAY 6



(a) Launch wind magnitude.

Figure **7.1-7.-** Launch winds, Mission **AS-201.**



(b) Launch wind direction.

Figure 7.1-7.- Concluded.

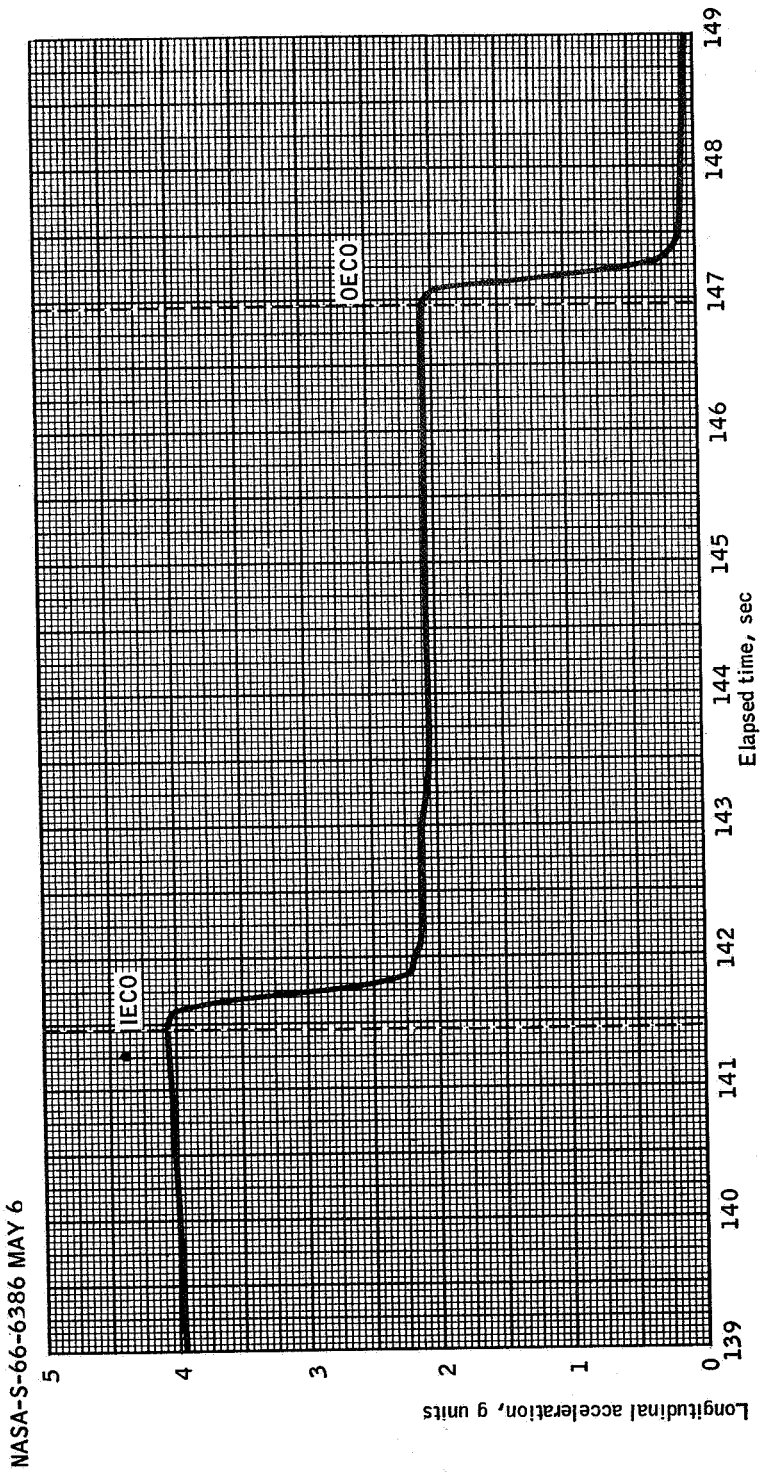


Figure 7.1-8.- Longitudinal acceleration time history, Mission AS-201.

NASA-S-66-6387 MAY 6

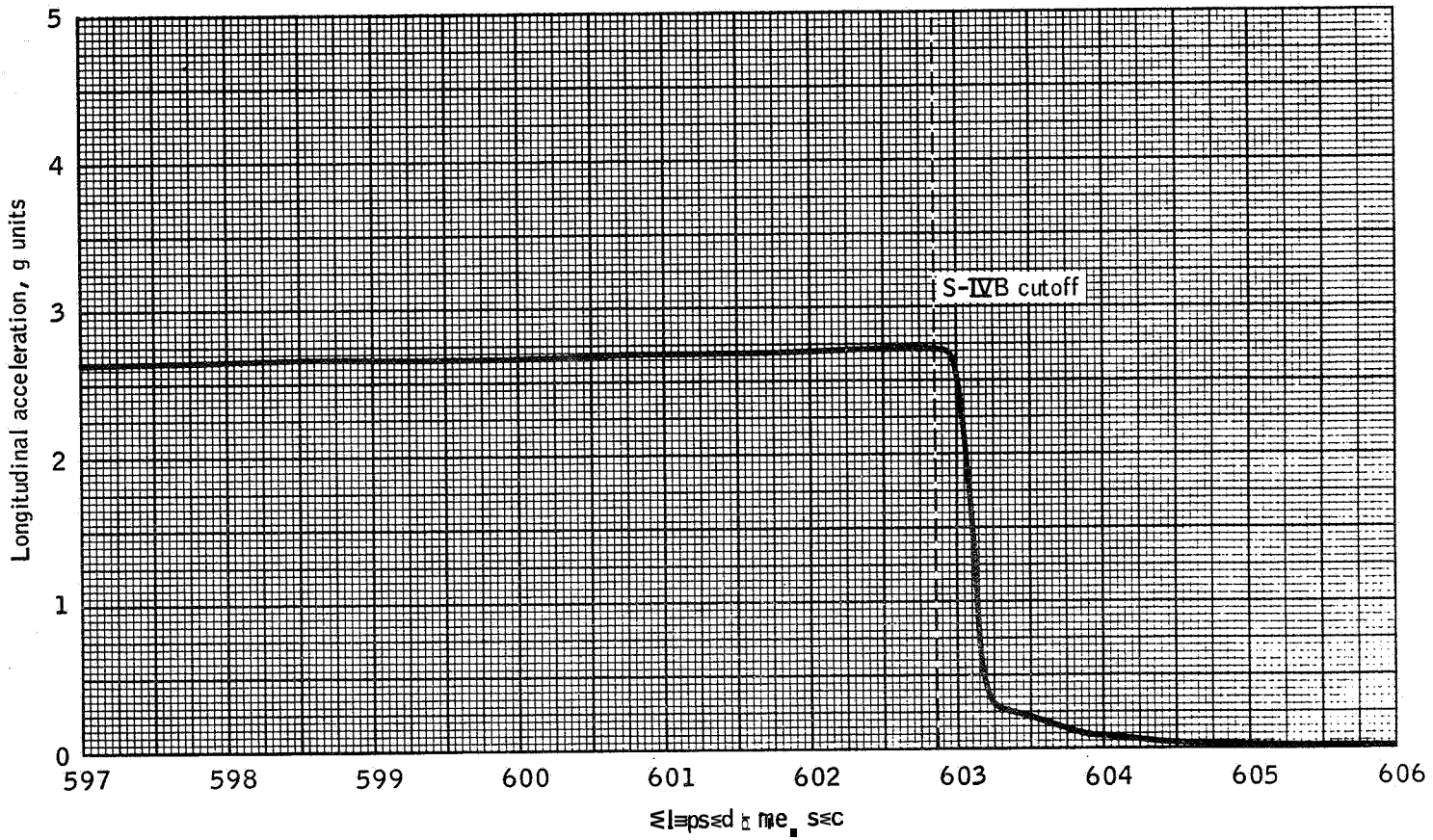


Figure 7.1-9.- Longitudinal acceleration time history, S-IVB engine cutoff, Mission AS-201

7.2 Structural Dynamics

Summary.- The spacecraft vibration data indicate that the spacecraft structure performed as required in the launch environment.

During lift-off, the command module (CM) longitudinal vibration reached a maximum of 1.1g peak-to-peak, The predominant frequency of oscillation was 10 cps. This oscillation damped out within 2 seconds and is considered to be of no consequence structurally. (See section 7.20.)

During S-IB ignition and lift-off, the tower lateral vibration reached a maximum of 2.5g peak-to-peak at a frequency of 10 cps. These oscillations were caused by the unsymmetric S-IB engine thrust buildup characteristics. This frequency is well above the natural frequencies of the four lowest cantilever and free-free lateral modes of the vehicle. During this period, the CM lateral vibration in the Y-Z plane reached a maximum of 1.4g peak-to-peak which, when coupled with the axial response, is within the design limits for lift-off.

Maximum vibration of the CM inner structure occurred between T+88 seconds and T+96 seconds. Vibration levels were lower than the established Apollo vibration criteria.

During the launch and service propulsion subsystem (SPS) burn periods, the service module (SM) interior structure vibration data showed very small response. The SPS engine dome vibration was between 6g and 8g (rms) during steady-state SPS burn, which is considered normal.

During lift-off, the spacecraft - LEM adapter (SLA) skin panel vibration levels exceeded the expected levels (vibration criteria, level A), but were more than adequately represented by the level B vibration criteria. During supersonic flight, the maximum vibration levels were as expected.

Low-frequency accelerations.-

X-axis accelerations: The CM was instrumented with accelerometer CK0004A to measure low-frequency accelerations in the X axis of the vehicle. This measurement was ranged from -2g to +10g with the data recorded at a rate of 100 samples per second.

Measurement CK0004A showed maximum oscillatory accelerations occurring at lift-off, with a maximum peak-to-peak amplitude of 1.1g. The predominant frequency of vibration was approximately 10 cps, which corresponds closely to the experimentally determined test vehicle first longitudinal frequency of 9.7 cps. This oscillation is believed to have been excited by the S-IB engine thrust buildup characteristics.

The oscillation damped out completely within 2 seconds and is considered to be of no consequence structurally. An oscillograph record of this acceleration during the lift-off period is shown in figure 7.1-6. (Also see section 7.20.)

Y-axis and Z-axis accelerations: Spacecraft 009 was instrumented with four accelerometers which measured low-frequency accelerations in the Y axis and Z axis of the vehicle. Two measurements, LA0011A and LA0012A, were provided in the forward extremity of the launch escape subsystem (LES), and two measurements, CK0005A and CK0006A, were in the CM. The tower accelerometers were ranged ±2g with a frequency response of 30 cps, while the CM accelerometers were ranged ±1.56g. Data from the CM accelerometers were recorded at a rate of 100 samples per second. This sampling rate was adequate to define the low frequency body bending moment up to 15 cps.

The Z-axis tower accelerometer showed maximum low-frequency accelerations occurring from T-2 seconds to T+3 seconds, with a maximum peak-to-peak amplitude of 2.33g at T-1.6 seconds. The acceleration had a predominant frequency of approximately 10 cps, as shown by the acceleration spectral distribution of figure 7.2-1. The Y-axis tower accelerometer exhibited maximum acceleration during the same time period and at approximately the same frequency. The maximum peak-to-peak Y-axis acceleration was 1.56g at T-1.3 seconds. Vector summation of the Y-axis and Z-axis vibrations indicates that a maximum acceleration of 2.5g peak-to-peak was incurred by the tower during the lift-off period. The 10-cps oscillation was excited by the S-IB engine unsymmetric thrust buildup characteristics (fig. 7.2-2). The mode of vibration associated with the 10-cps oscillation is unknown; however, this frequency is well above the natural frequencies of both the four lowest cantilever and the free-free lateral modes of the test vehicle. The CM Y-axis and Z-axis accelerometers measured maximum accelerations during the lift-off period of 0.80g and 1.2g peak-to-peak, respectively, as illustrated in figure 7.1-6. The magnitude of the CM acceleration, when coupled with the axial response, is within the design limit for the lift-off period, as specified in reference 15.

Response at the experimentally determined test vehicle second free-free bending frequency (2.9 cps) was noted from T+83 seconds through T+106 seconds. Response at the calculated second free-free bending frequency (7.8 cps) of the S-IVB/Apollo vehicle was noticed from T+149 seconds to T+172 seconds. These vibrations were of insignificant magnitudes.

Command module vibrations.- The CM was instrumented with four accelerometers, as shown in figure 7.2-3, to measure vibrations of the inner structure. Accelerometers CK0040D, CK0041D, CK0042D, and CK0043D measured vibrations of the forward bulkhead in the X direction, the inner aft sidewall in the Z direction, the aft bulkhead in the X

direction, and a cable tray, mounted on secondary structures within the lower equipment bay aft section, in the Z direction, respectively. Each measurement was ranged ±75g with a frequency response of 0 to 2500 cps.

Acceleration time histories in figure 7.2-4 show that maximum vibrations occurred between *Ti-88* seconds and T+96 seconds. This time period corresponds to a Mach number range of 1.9 to 2.4. Maximum response of the four measurements was indicated by the aft sidewall accelerometer and was shown to be 33g peak-to-peak at T+90 seconds.

Spectral distributions of vibratory energy during the period of maximum response are given in figures 7.2-5 to 7.2-8. Figure 7.2-9 gives the acceleration spectral distribution for the inner aft sidewall, measurement CK0041D, during the transonic flight regime. Comparison of figures 7.2-6 and 7.2-9 shows that the increase in inner aft sidewall vibration between Ti-60 seconds and T+90 seconds is primarily a result of the large increase in energy in the frequency range of 1000 cps to 1500 cps.

Acceleration spectral densities for the forward bulkhead, aft sidewall, and aft bulkhead during the period of maximum vibration (M = 2.1) are compared in figure 7.2-10 with the vibration criteria for atmospheric flight. In this figure the spacecraft 009 data have been scaled to the dynamic pressure of the vibration criteria (790 lb/sq ft), thereby enabling a direct comparison. These criteria are representative of average vibration levels developed during the spacecraft 007 CM acoustic tests. As shown in figure 7.2-10, the spacecraft 009 vibration levels lie within the criteria for these structural zones, with the exception of the aft sidewall vibration, which exceeds the criteria in the frequency range from 1000 cps to 2000 cps. This single high frequency spike would not be detrimental to the structure.

Service module vibration.- The SM was instrumented with nine accelerometers to measure vibrations of the aft helium tank mount in the X and radial directions, the aft bulkhead at the base of Sector II oxidizer tank in the X, Y, and Z directions, the helium pressurization panel in the radial and tangential directions, and the SM engine dome in the longitudinal and radial directions. Accelerometer locations are shown in figure 7.2-11 and details of instrument location, range, and frequency response are given in table 7.2-I.

Data from five of the nine measurements were not usable. Measurements SK0240D, SK0241D, SK0242A, SK0243A, and SK0244A recorded such small response during the launch phase that data were within 6 dB (a factor of 2) of the telemetry channel noise, causing a degradation of the data. The low frequency response of the telemetry channels (table 7.2-1) was a major cause of the small response measured, since the majority of vibratory energy was expected to occur at frequencies much higher than the available channel cutoff frequency.

The two most active vibration measurements in the SM were SK0245D and SK0246D, located on the SM helium pressurization panel in the radial and tangential directions, respectively. These measurements indicated maximum response during the transonic period from T+59 seconds to T+64 seconds. The acceleration spectral distribution of figure 7.2-12 indicates that the majority of vibratory energy in the radial direction was in the frequency range of 600 cps to 800 cps. Figure 7.2-13 indicates that the tangential vibration occurs at a predominant frequency of approximately 30 cps. The vibration levels for the transonic and supersonic maximum response periods fall considerably below the vibration criteria established during spacecraft 007 acoustic tests; however, this was to be expected since the spacecraft 007 measurement was mounted in the center of the panel, a region more susceptible to vibration than that of the spacecraft 009 measurement, which was mounted adjacent to a stiffener of radial beam 4.

The SPS engine dome was instrumented with two accelerometers, SK0020D and SP1023D, to monitor the rough combustion of the SPS engine. These data are used herein to evaluate the vibration induced into the SM and CM structure during SPS ignition and burn.

Measurements SK0020D and SP1023D, which measured vibration in the longitudinal and radial directions on the SPS engine dome, indicated maximum levels between T+90 seconds and T+92 seconds during atmospheric flight. Oscillograph records indicate peak-to-peak accelerations of 37.5g and 25g at this time period, respectively. These magnitudes were also indicated during stable burn of the SPS engine. During transient SPS burn conditions, ignition acceleration values were 144g and 200g peak-to-peak for the longitudinal and radial directions, respectively, with engine shutdown acceleration values of 50g and 62.5g peak-to-peak. The vibration levels on the SPS engine are approximately the same as those experienced during ground tests and are considered normal. Analysis of the vibration data for the CM and SM during the SPS burn period showed no significant acceleration. Figure 7.2-14 presents the acceleration density of SP1023D for a maximum response during S-IB boost. These data indicate the vibration energy to be within a frequency band of 175 cps to 275 cps, peaking at a frequency of approximately 225 cps. In the time period from T+1323 seconds to T+1325 seconds, during SPS burn, the vibration energy shifted to a higher frequency band of 750 cps to 2500 cps (fig. 7.2-15). Figures 7.2-14 and 7.2-15 show that the boost period radial rms acceleration on the SPS engine was 1.66 times that encountered during a stable burn of the SPS engine. Figure 7.2-16 illustrates the acceleration spectral density of SPS engine dome maximum longitudinal vibration during supersonic flight. These data indicate the vibratory energy in a frequency band of 150 cps to 350 cps, having an rms value of 4.6g. This value is approximately 1.6 times that of the radial vibration during this period.

In general, the magnitude of all vibration data in the SM is low during the transonic, supersonic, and SPS burn periods. No structural problems are anticipated from these low levels.

SLA vibrations.- Three accelerometers were located on the SLA to measure radial vibration of the skin panels. Measurement locations are shown in figure 7.2-17. These accelerometers, AK0250D, AK0251D, and AK0252D, were ranged ±100g with frequency responses of 160 cps, 220 cps, and 330 cps, respectively.

Time histories (rms) of shell panel accelerations are given in reference 1. These plots show vibration trends similar to those of the SM shell panels of earlier flights. Maximum vibration levels occurred during the lift-off, transonic, and supersonic periods of the launch phase.

Acceleration spectral densities for the SLA shell panel vibrations are compared with panel vibration criteria in figures 7.2-18(a) to 7.2-18(c) for periods of lift-off, transonic, and supersonic flight, respectively. The SLA shell panel vibration criteria were based on results from the spacecraft 007 SM acoustic tests a d are representative of average vibration levels expected on the SLA. The peak spectral density levels at lift-off exceeded the expected level A criteria by a factor of 4.0. However, comparison of the lift-off levels with the level B criteria of figure 7.2-18(b) shows that the level B criteria, although developed for the transonic condition, adequately encompasses the short duration lift-off levels. For the transonic period, the spacecraft 009 vibration levels were considerably lower than the level B criteria and, in fact, could be better represented by the level A criteria with the exception of the frequency range below 70 cps. For the supersonic period, the flight data were scaled to a dynamic pressure of 790 lb/sq ft to enable a direct comparison with the criteria. Figure 7.2-18(c) shows spacecraft 009 peak spectral density levels of 2 to 2.5 times the level A criteria; however, agreement between the measured levels and the level A criteria is considered to be reasonably good, since (1) a very narrow filter band width was used in the spacecraft 009 supersonic data reduction (a larger band width lowers the peak values considerably), and (2) spacecraft 009 supersonic rms accelerations were 50 to 60 percent of the criteria rms values over the frequency range of the spacecraft 009 data.

Based on spacecraft 009 data, updated environmental vibration criteria have been developed for the SLA shell panels.

TABLE 7.2-I.- STRUCTURAL DYNAMIC MEASUREMENTS, MISSION AS-201

Measurement number	Measurement description	Range	Response	Location			Channel or track
Low frequency accelerations							
LA0011A	Y-axis tower accelerometer	±2g	59 cps	X_L380	Y0	Z6	SEP 9
LA0012A	Z-axis tower accelerometer	±2g	81 cps	X_L380	Y6	Z0	SEP 10
CK0004A	X-axis CM accelerometer	-2g to 10g	100 s/s	X_C78	Y0	Z21	PCM
CK0005A	Y-axis CM accelerometer	±1.56g	100 s/s	X_C78	Y0	Z21	PCM
CK0006A	Z-axis CM accelerometer	±1.56g	100 s/s	X_C78	Y0	Z21	PCM
Command module vibrations							
CK0040D	Forward bulkhead, X-axis	±75g	2500 cps	X_C80.75	Y0	Z22	FQTR 5
CK0041D	Inner aft sidewall, Z-axis	±75g	2500 cps	X_C30.83	Y1.25	Z58.2	FQTR 13
CK0042D	Aft bulkhead, X-axis	±75g	2500 cps	X_C12.07	Y-1	Z47.7	FQTR 9
CK0043D	Lower equipment bay, Z-axis	±75g	2500 cps	X_C30.83	Y0.5	Z39.5	FQTR 11

TAB-< 7.2-I.- STRUCTURAL DYNAMIC MEASUREMENTS, MISSION AS-201 - Concluded

Measurement number	Measurement description	Range	Response	Location	Channel or track
	Service module vibrations				
SK0020D	SPS engine dome, longitudinal vibration	±250g	5 kc	SPS engine dome	
SP1023D	SPS engine dome, radial vibration	±250g	5 kc	SPS engine dome	
SK0240D	Aft He tank mount, X-axis vibration	±20g	110 cps	X_S286.5 145°	
SK0241D	Aft He tank mount, radial vibration	±20g	81 cps	X_S286.5 146°	
SK0242A	Aft bulkhead tank base, X-axis accelerometer	±20g	59 cps	X_S203 Y24	
SK0243A	Aft bulkhead tank base, Y-axis accelerometer	±10g	45 cps	X_S203 Y24	
SK0244A	Aft bulkhead tank base, Z-axis accelerometer	±10g	35 cps	X_S203 Y24	
SK0245D	He pressurization panel, radial vibration	±50g	600 cps	X_S259 152°	
SK0246D	He pressurization panel, tangential vibration	±50g	450 cps	X_S259 152°	
	Spacecraft – LEM adapter vibrations				
AK0250D	Skin panel, radial vibration	±100g	160 cps	X_A543.25 304°	SMMK 12
SK0251D	Skin panel, radial vibration	±100g	220 cps	X_A657.5 236°	SMMK 13
SK0252D	Skin panel, radial vibration	±100g	330 cps	X_A780 304°	SMMK 14

NASA-S-66-6209 MAY 6

SENSOR	LA0012A
TIME SLICE	.550 TO 3.010 SEC.
LOW-PASS FILTER	81. CPS
FILTER BW	2.5000 CPS
$LICE RMS VALUE	.230

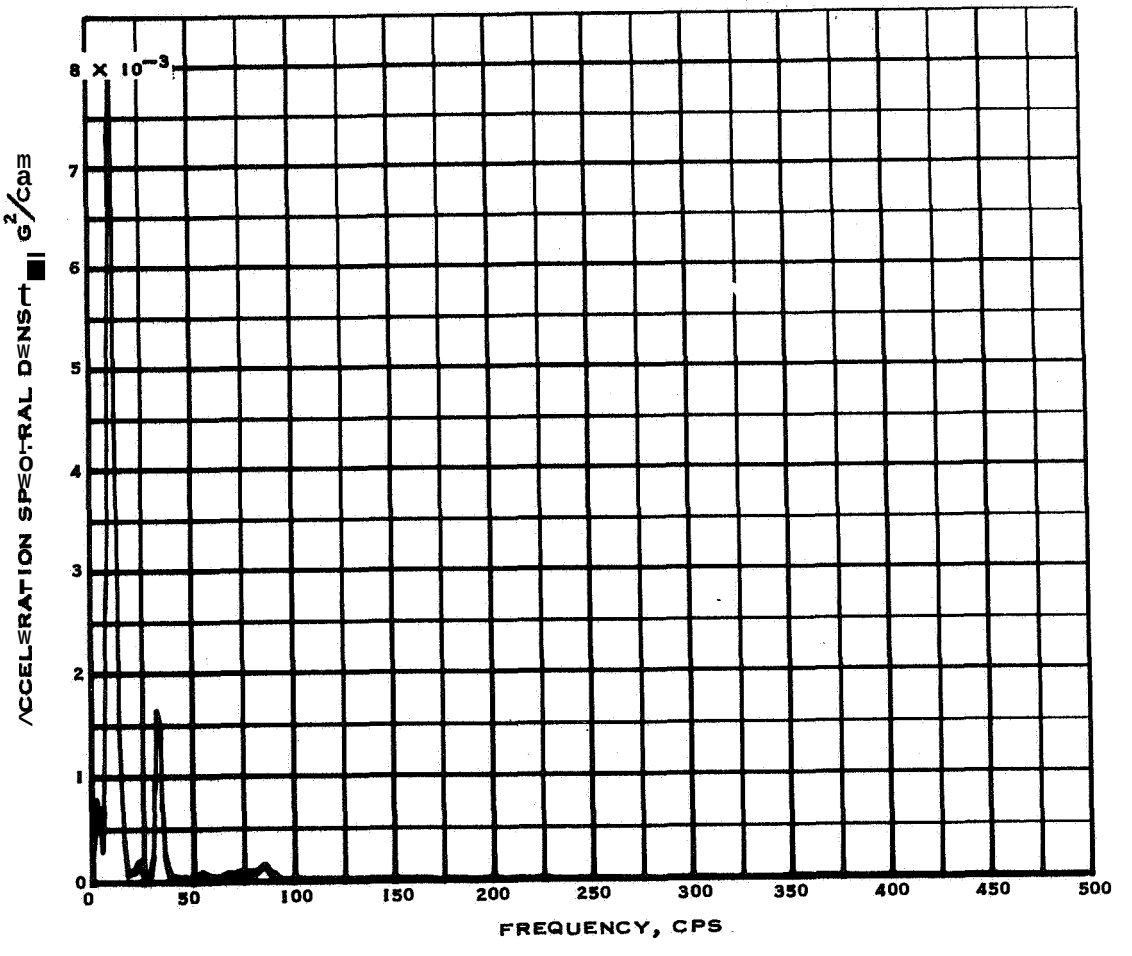
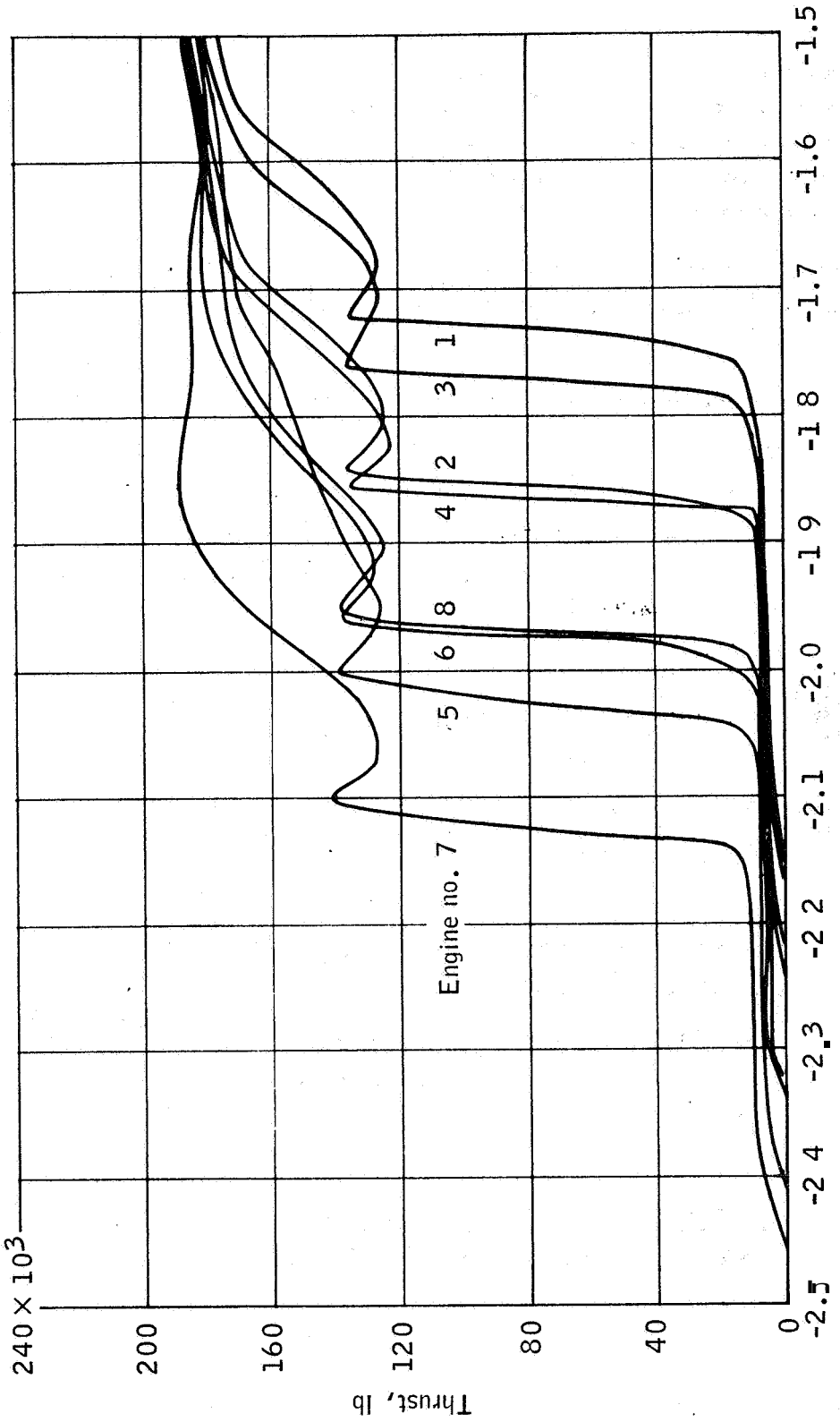


Figure 7.2-1.- Acceleration spectral density of Z-axis tower acceleration at lift-off, Mission AS-201.



NASA-S-66-6210 MAY 6

Figure 7.2-2.- S-IB engine thrust buildup, Mission AS-201.

NASA-S-66-6211 MAY 6

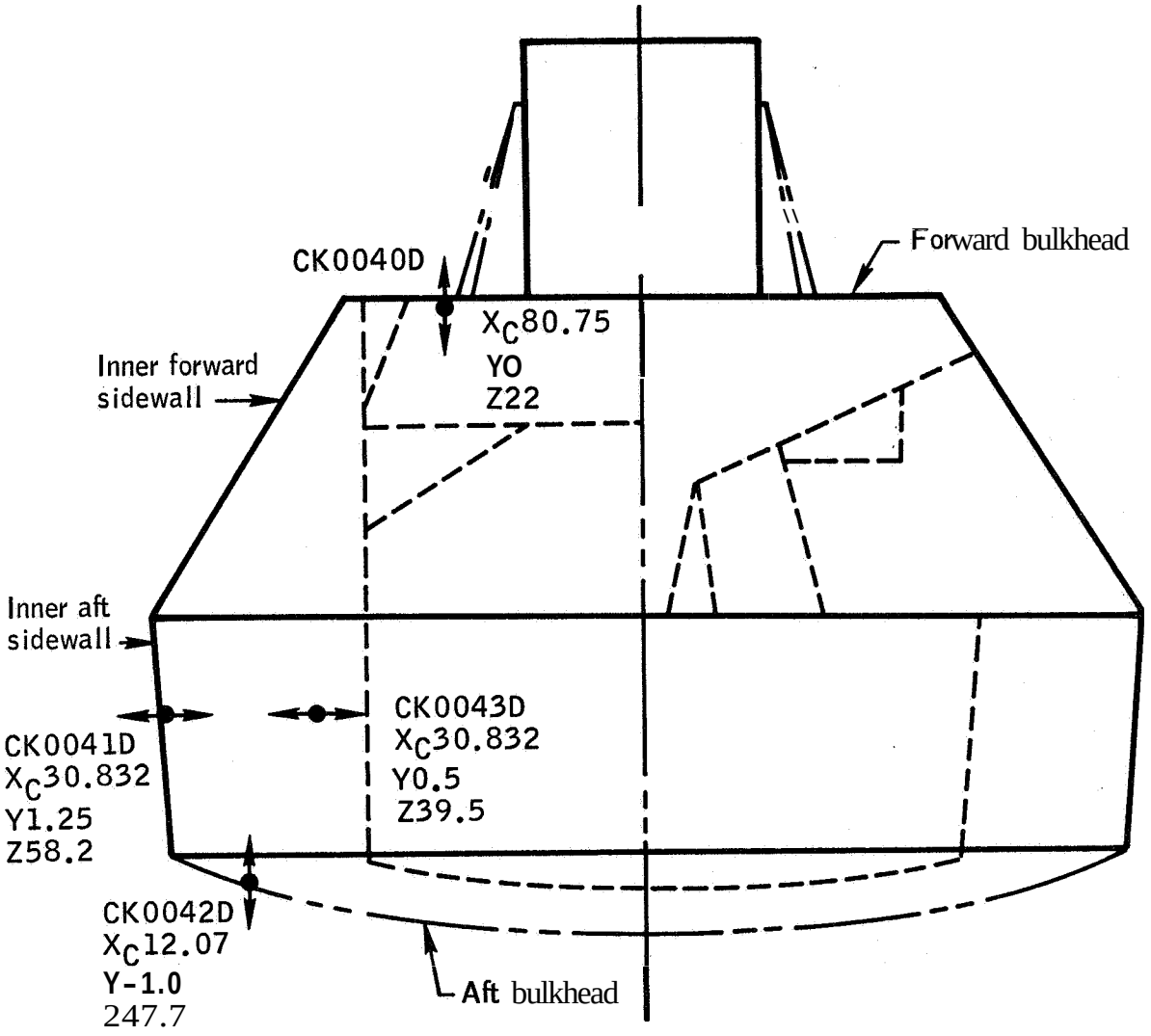
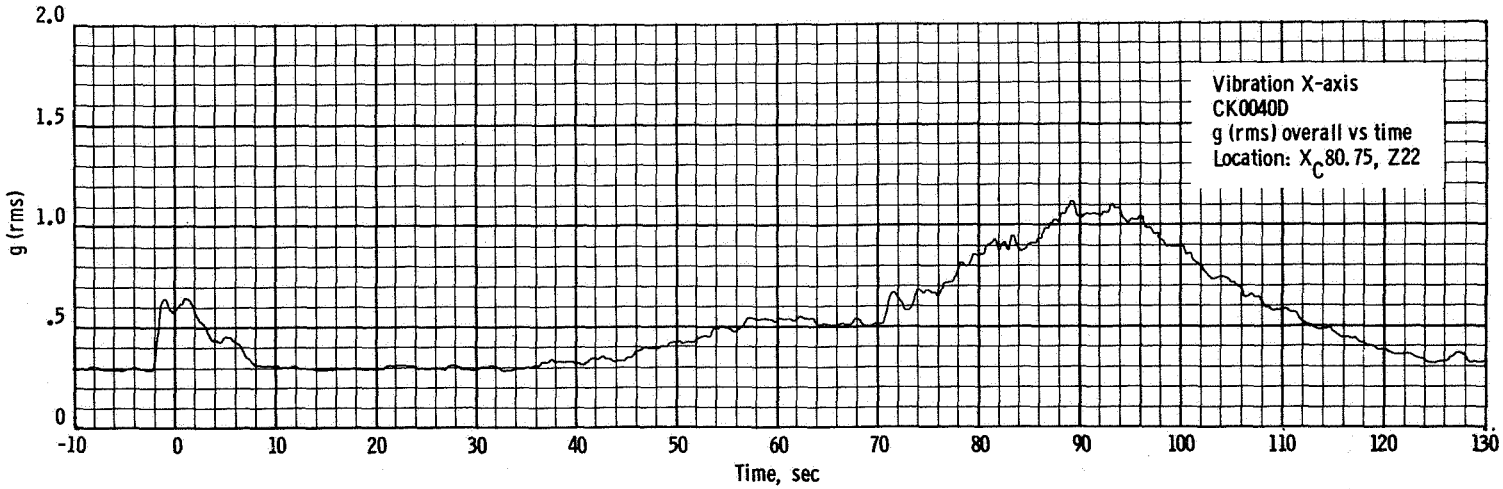
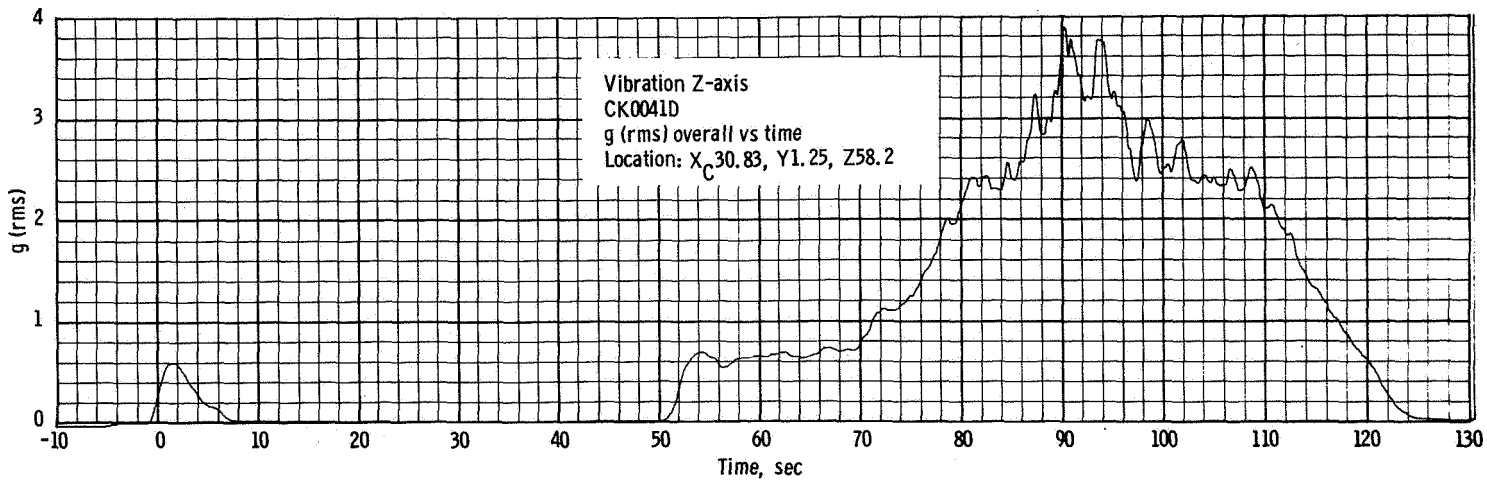


Figure 7.2-3.- Command module inner structure accelerometer locations, Mission AS-201.



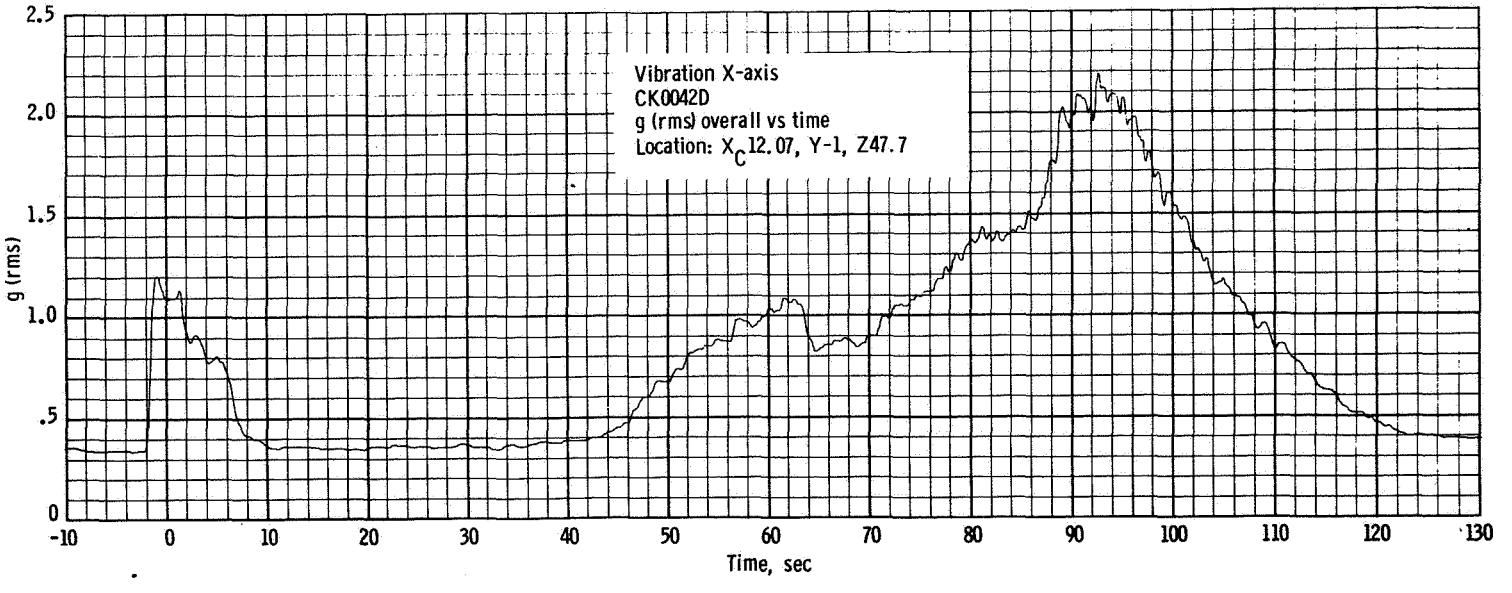
(a) Inner structure forward bulkhead X-axis acceleration.



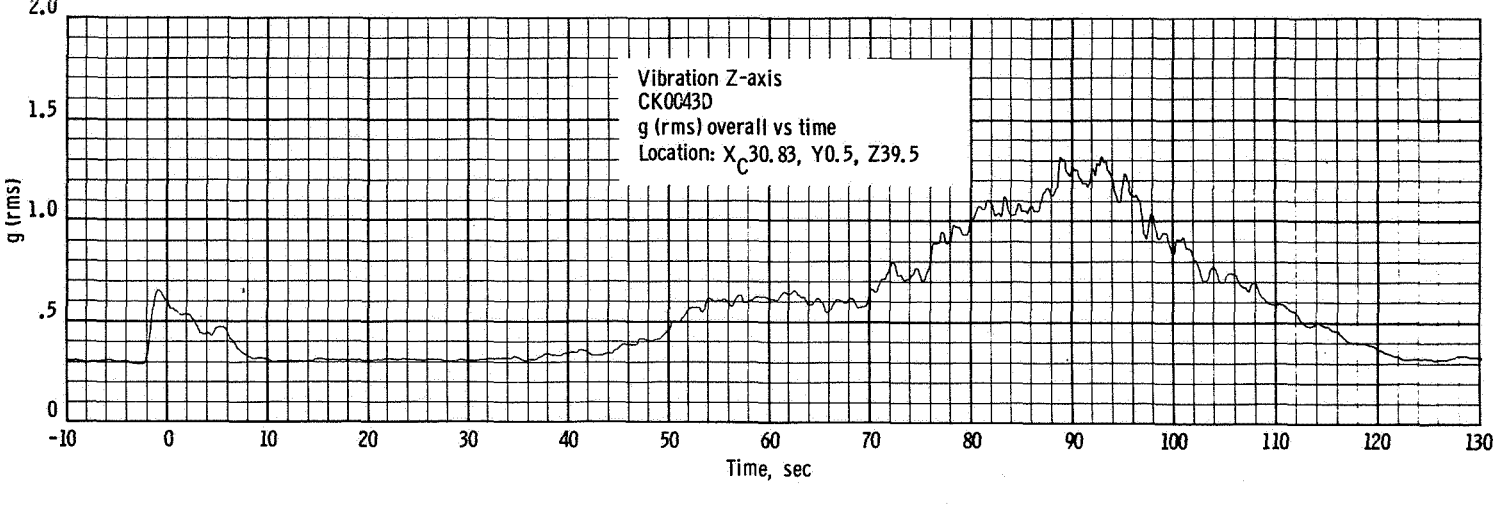
(b) Inner structure aft sidewall radial acceleration.

Figure 7.2-4.- Acceleration rms time history, Mission AS-201.

NASA-S-66-6213 MAY 6



(c) Inner structure aft bulkhead X-axis acceleration.



(d) Lower equipment bay cable tray Z-axis acceleration.

Figure 7.2-4. - Concluded.

NASA-S-66-6214 MAY 6

SENSOR	CK0040D
TIME SLICE	90.500 TO 92.500 SEC
LOW—PASS FILTER	2100. CPS
FILTER BW	5.0000 CPS
SLICE RMS VALUE	.957

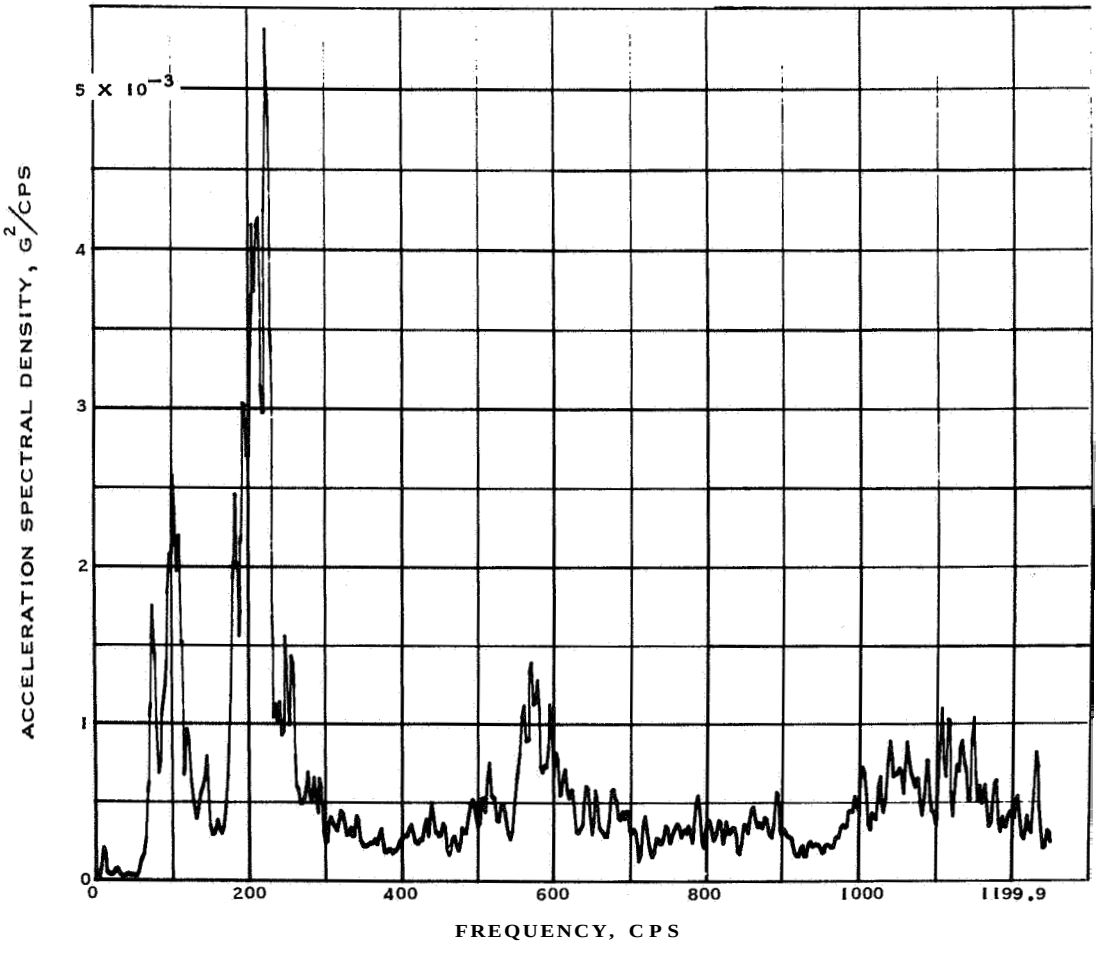


Figure 7.2-5.- Acceleration spectral density of CM inner structure forward maximum vibration, Mission AS-201.

NASA-S-66-6215 MAY 6

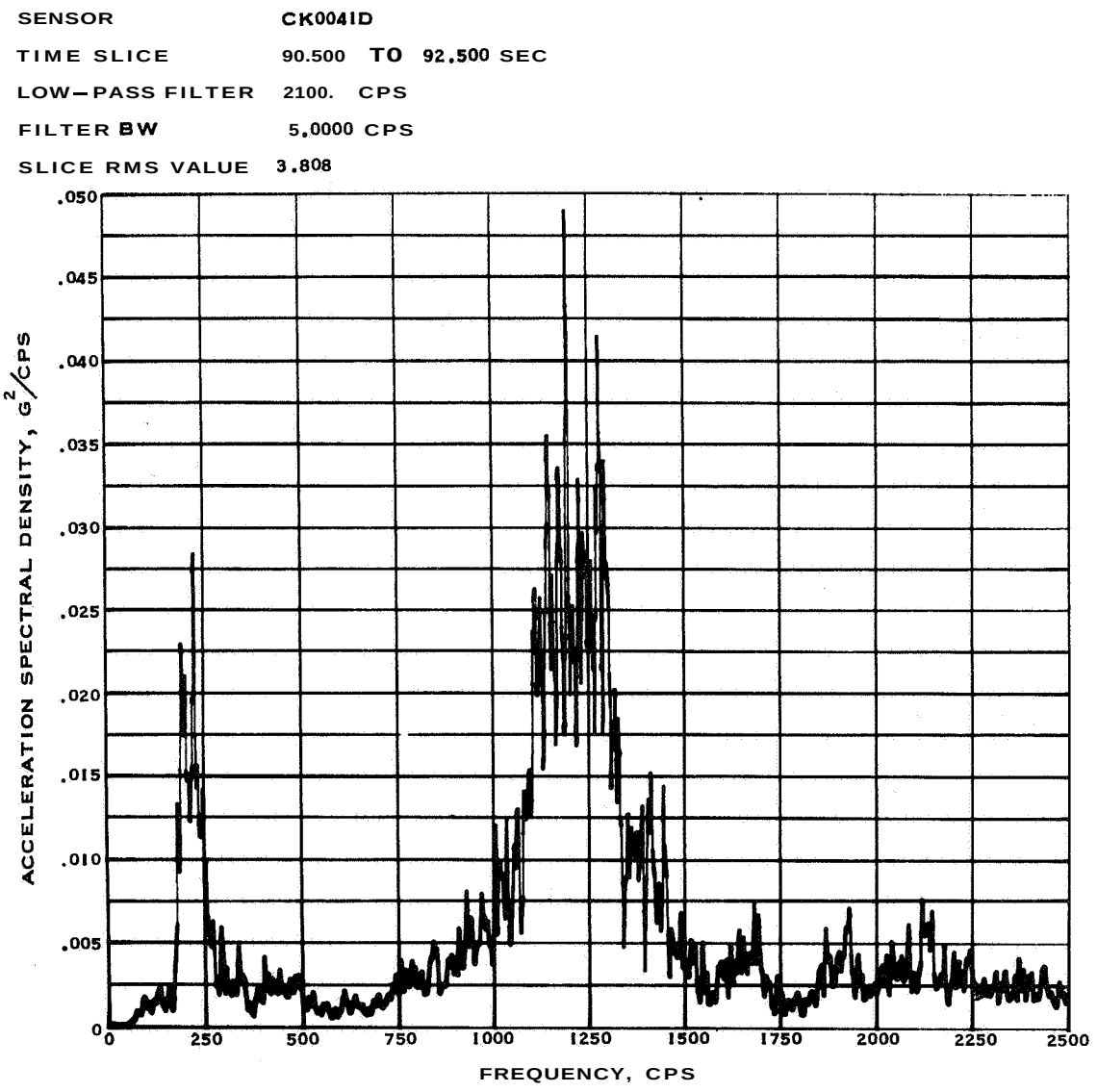


Figure 7.2-6.- Acceleration spectral density of CM inner structure of sidewall maximum vibration, Mission AS-201.

NASA-S-66-6216 MAY 6

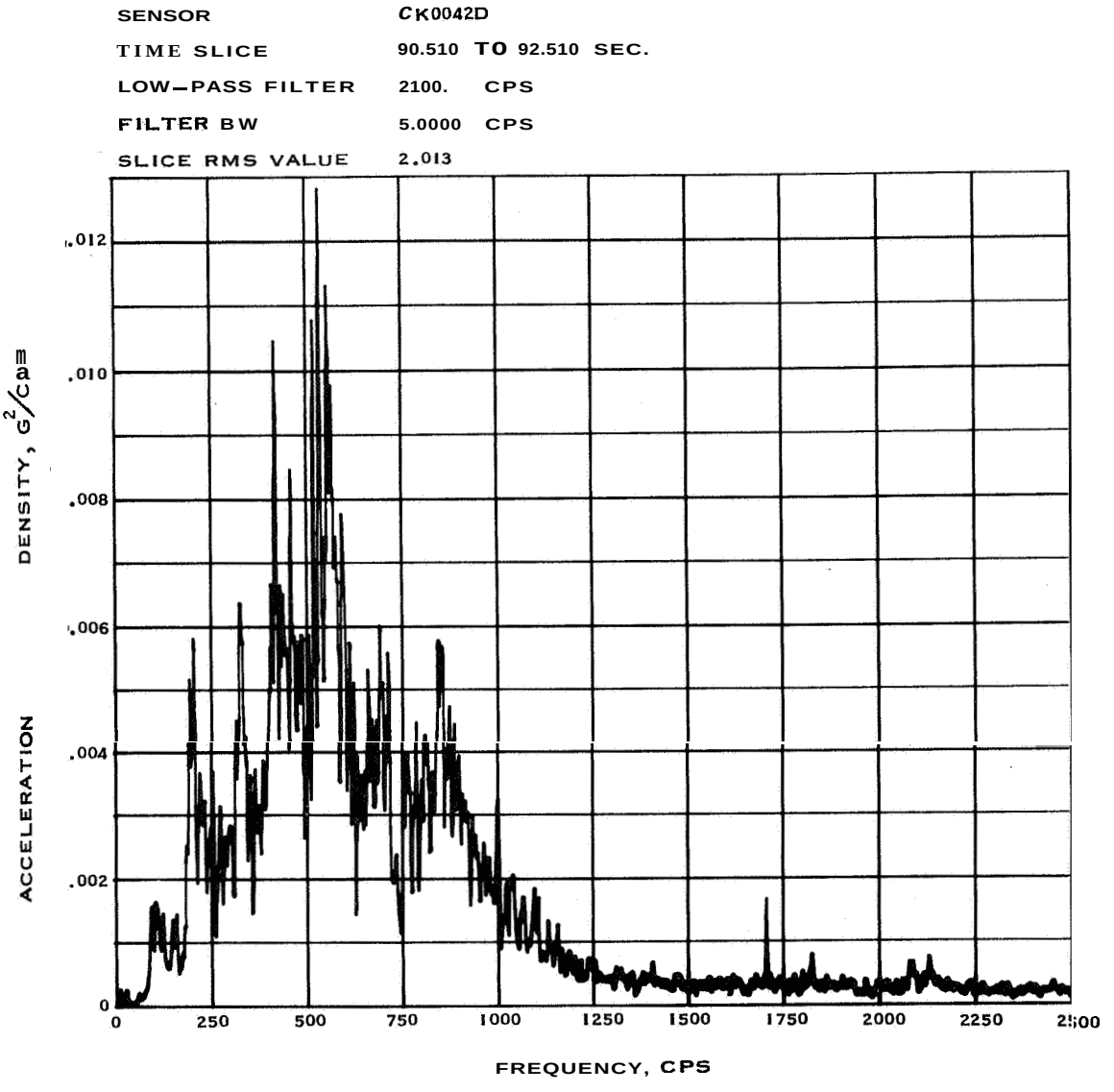


Figure 7.2-7.- Acceleration spectral density of CM inner structure aft bulkhead maximum vibration, Mission AS-201.

NASA-S-66-6217 MAY 6

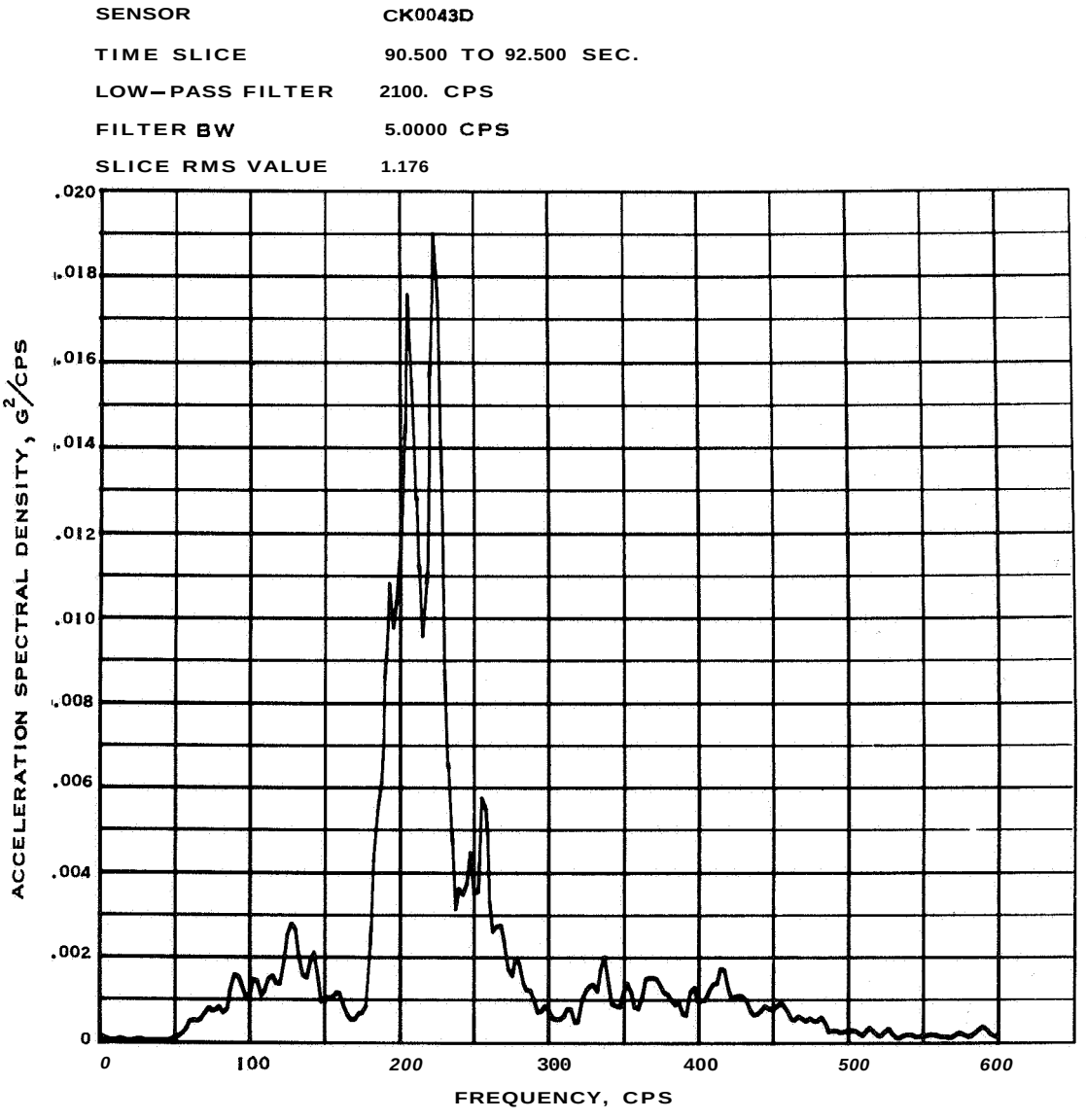


Figure 7.2-8.- Acceleration spectral density of lower equipment bay cable tray maximum vibration, Mission AS-201.

NASA-S-66-6218 MAY 6

SENSOR	CK0041D
TIME SLICE	60.010 TO 62.010 SEC
LOW-PASS FILTER	2100. CPS
FILTER BW	5.0000 CPS
SLICE RMS VALUE	.956

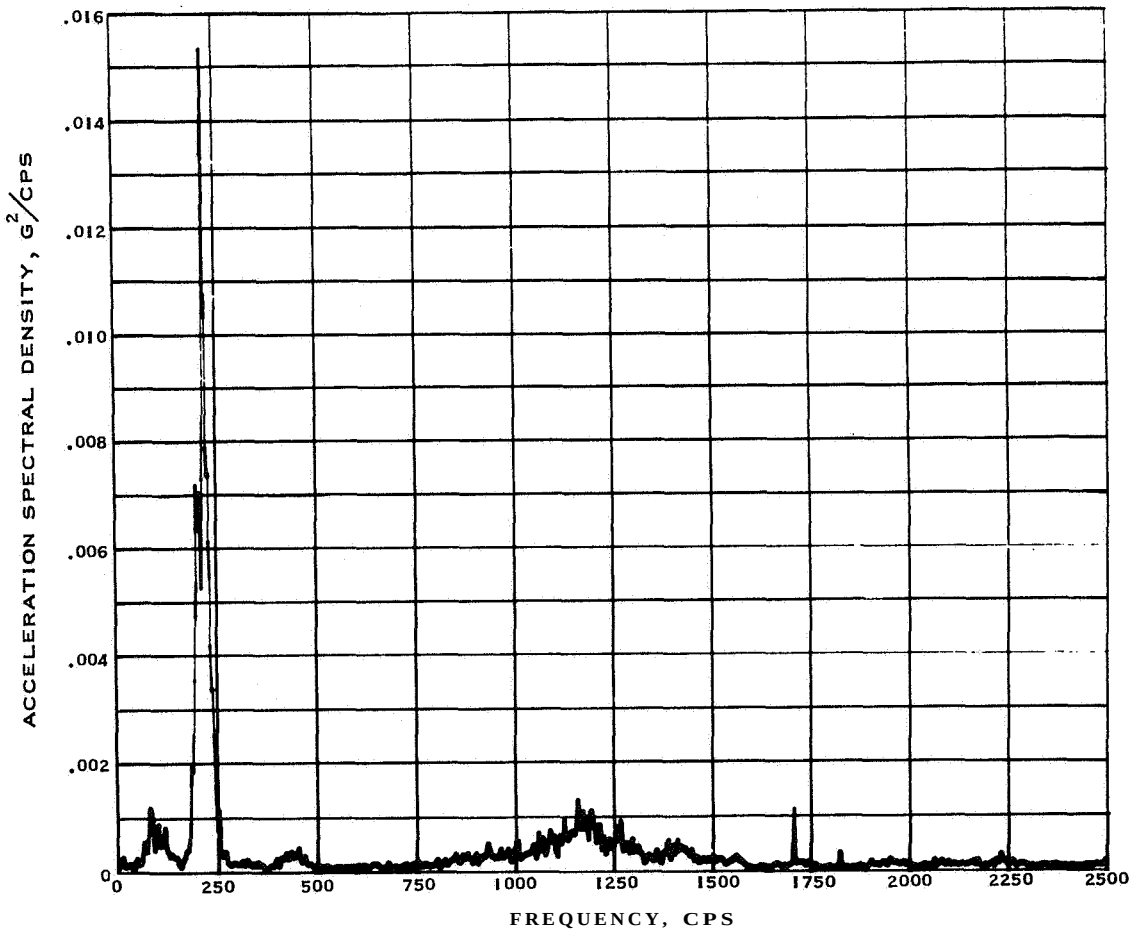


Figure 7.2-9.- Acceleration spectral density of CM inner structure aft sidewall vibration during transonic flight, Mission AS-201.

NASA-S-66-6219 MAY 6

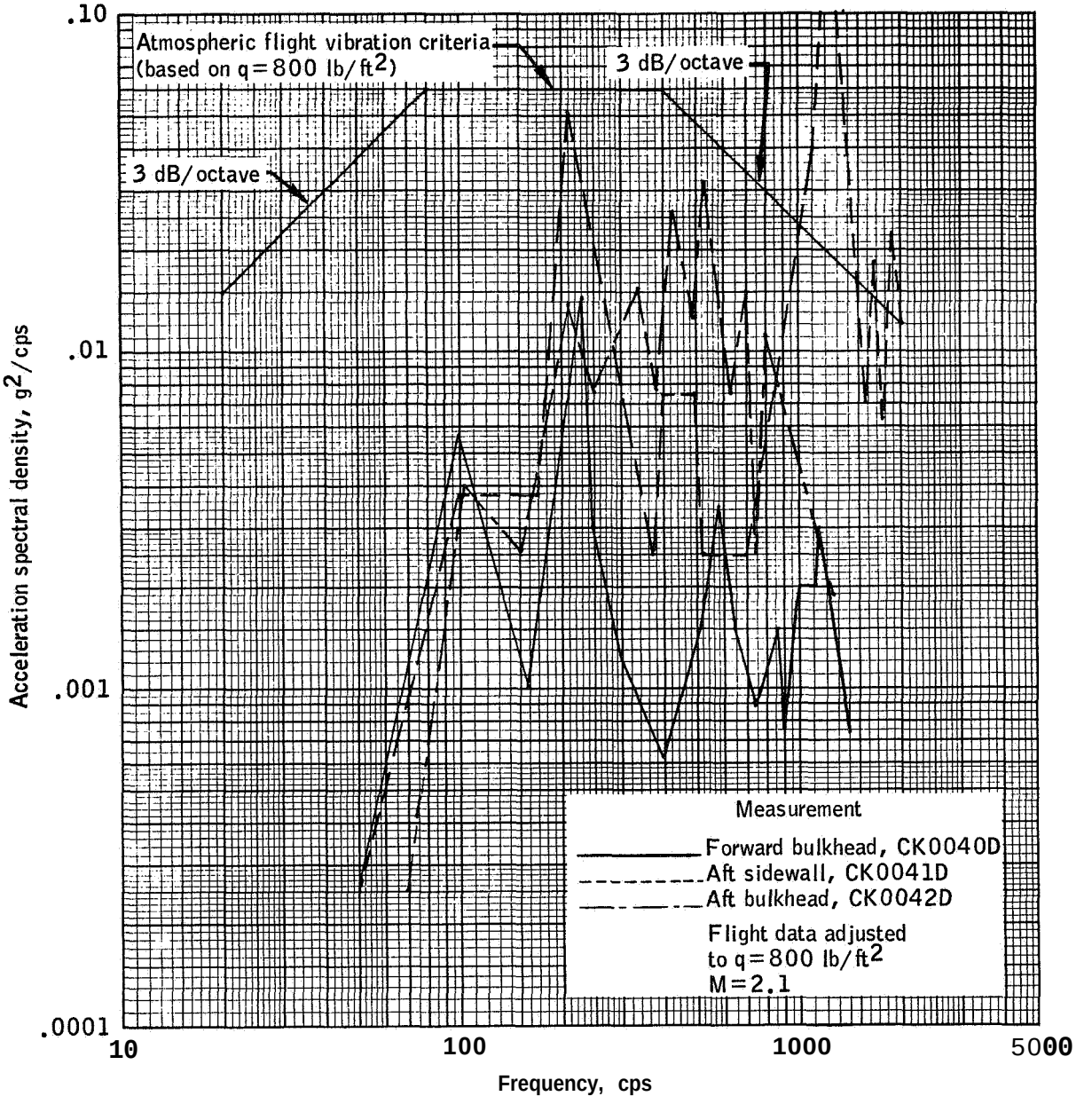


Figure 7.2-10.- Comparison of CM inner structure maximum vibration with criteria, Mission AS-201.

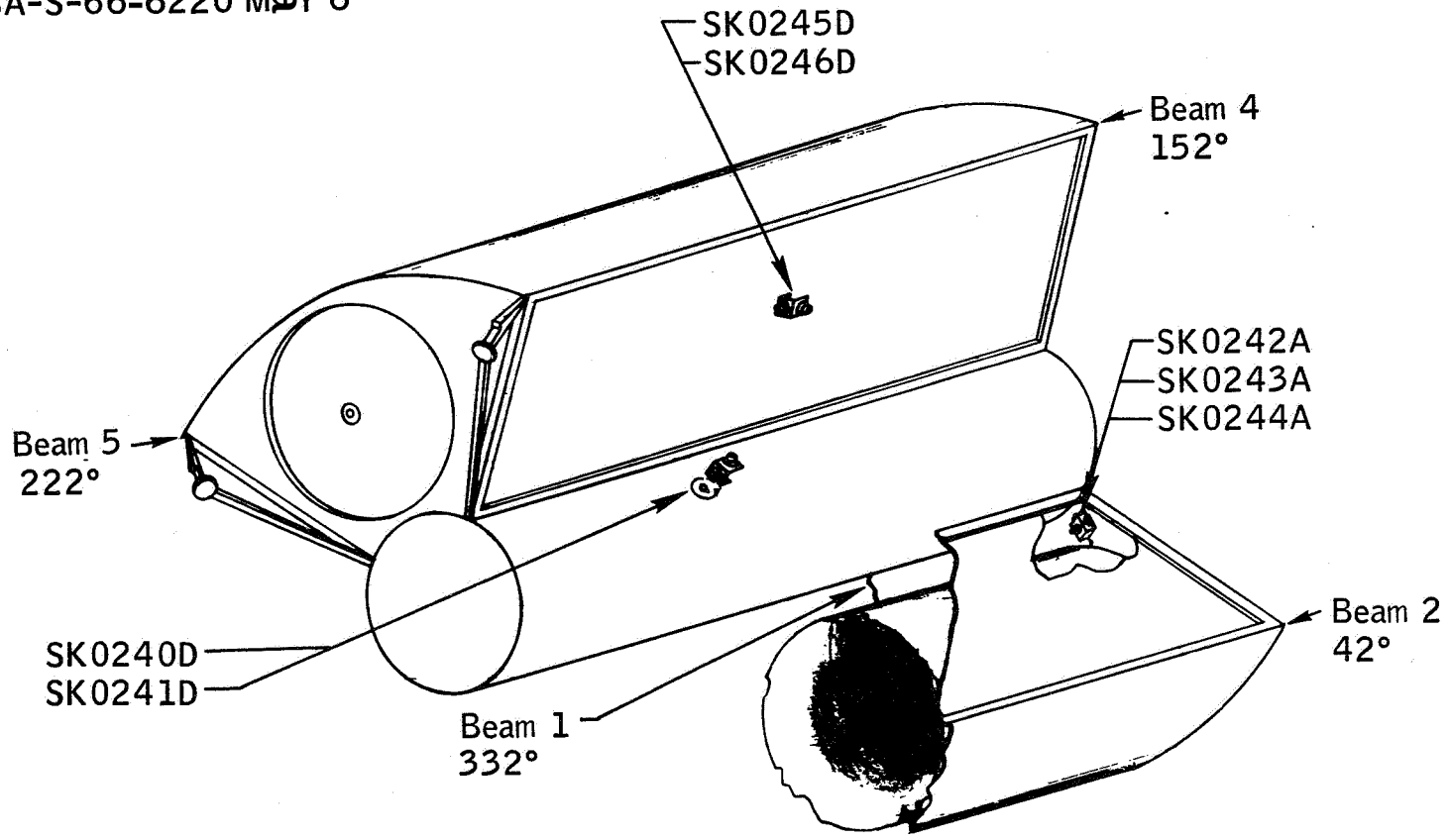


Figure 7.2-11.- SM accelerometer locations, Mission AS-201.
(SPS engine dome location not shown.)

NASA-S-66-6221 MAY 6

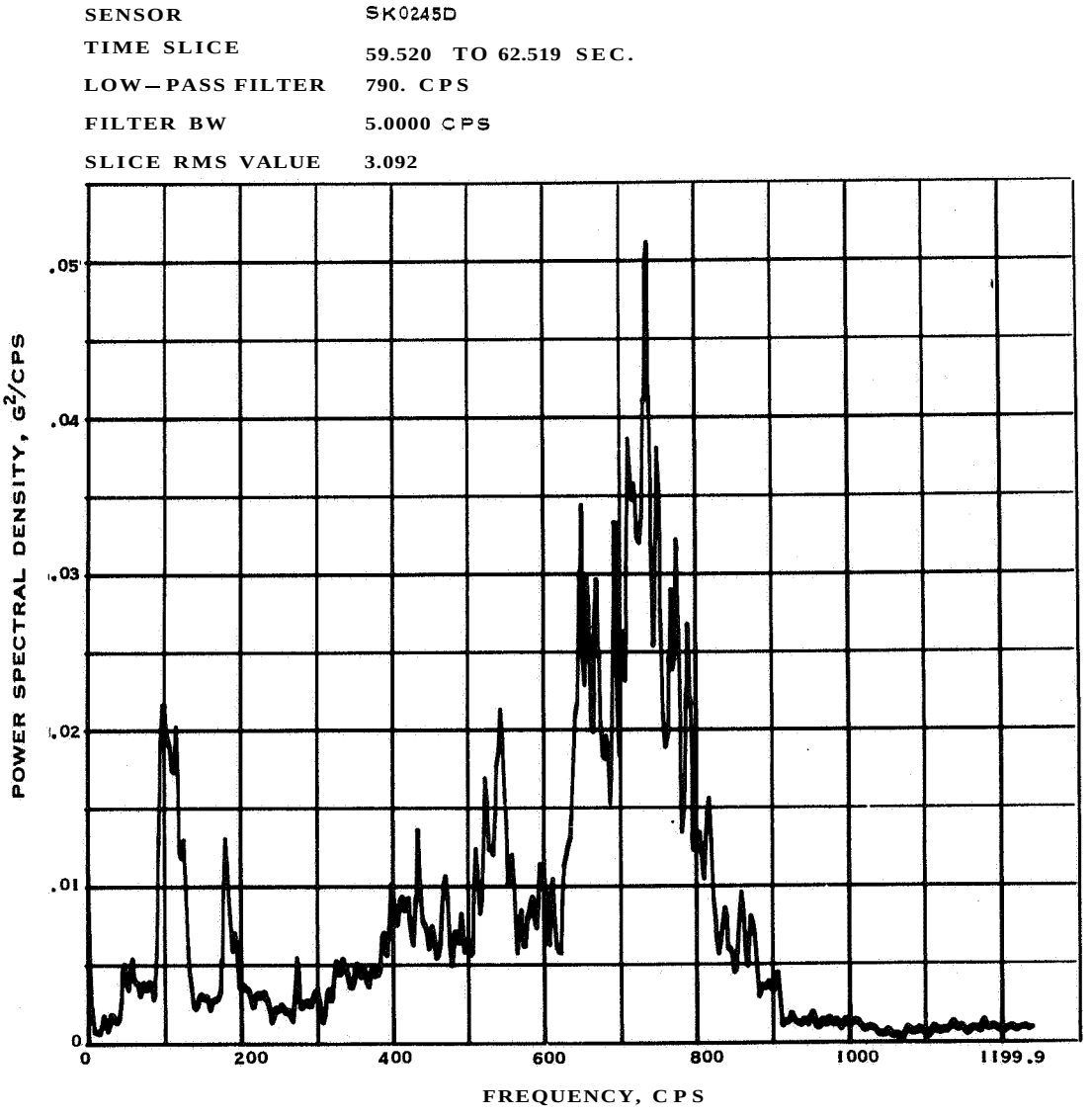


Figure 7.2-12.- Acceleration spectral density of SM helium pressurization panel radial vibration during transonic flight, Mission AS-201.

NASA-S-66-6222 MAY 6

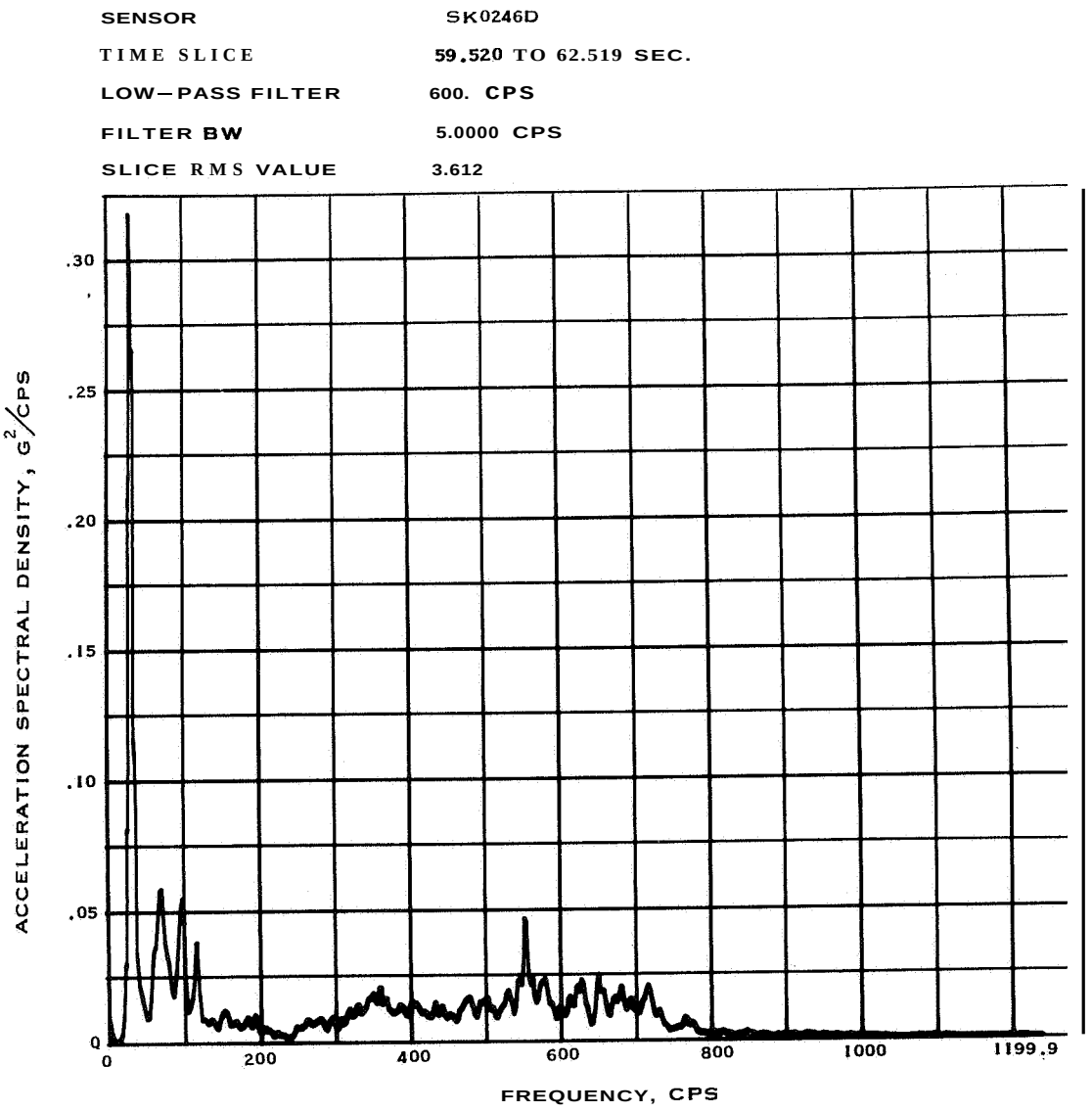


Figure 7.2-13.- Acceleration spectral density of SM helium pressurization panel tangential vibration during transonic flight, Mission AS-201.

NASA-S-46-4223 MAY 6

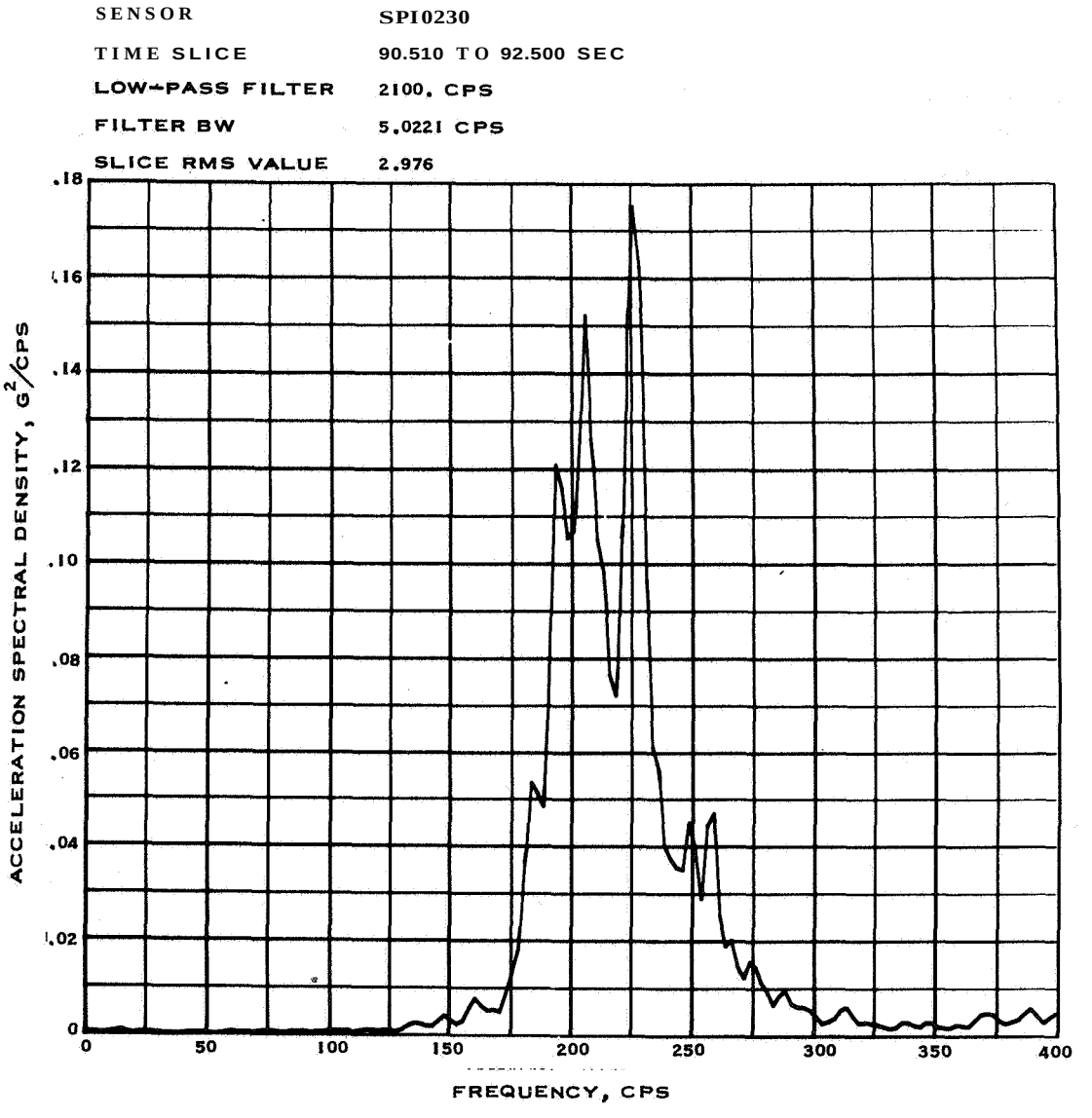


Figure 7.2-14.- Acceleration spectral density of maximum SPS engine dome, radial vibration, during supersonic flight, Mission AS-201.

NASA-S-66-6224MAY 6

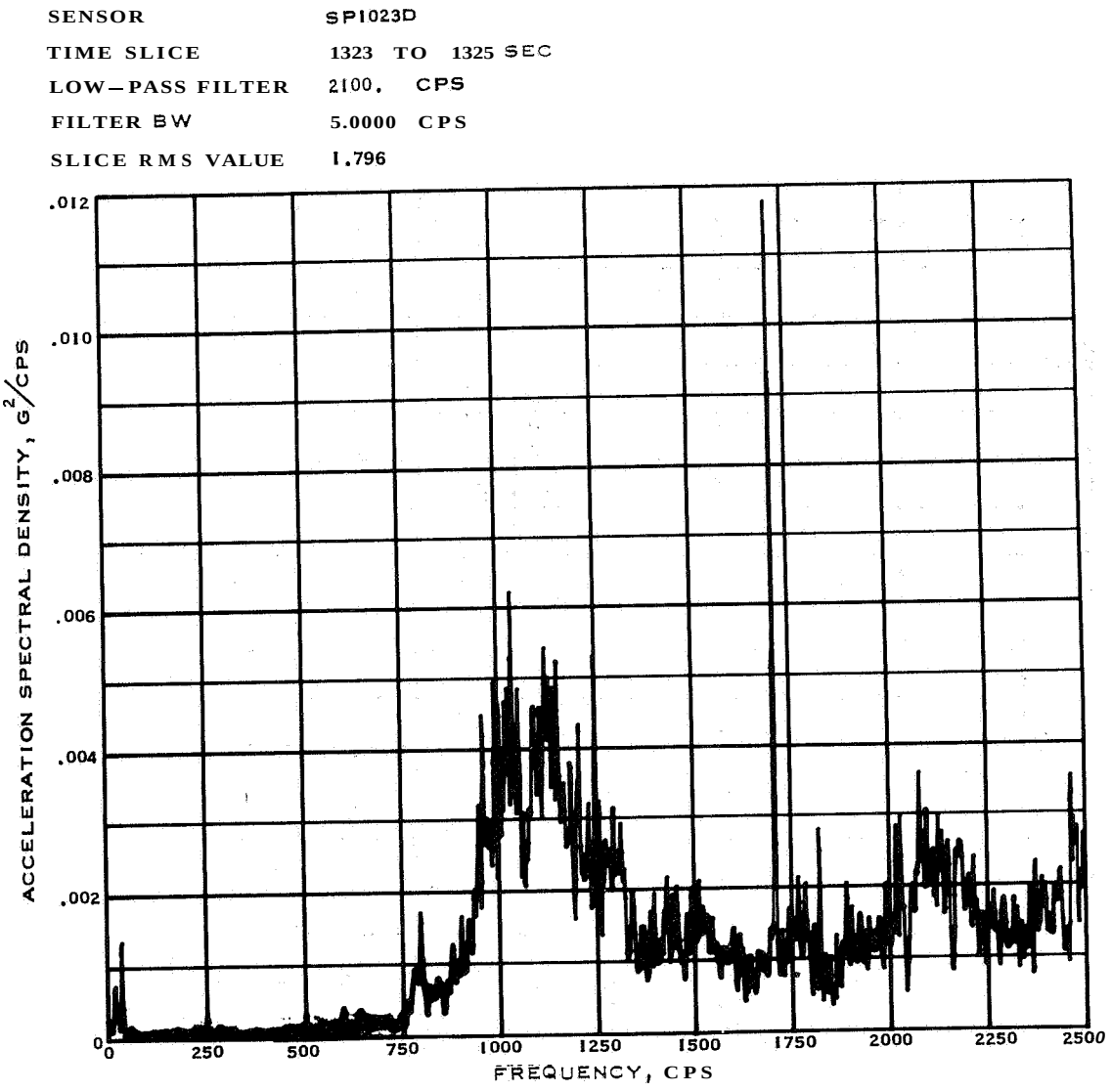


Figure 7.2-15.- Acceleration spectral density of SPS engine dome radial vibration during SPS burn, Mission AS-201.

NASA-S-66-6225 MAY 6

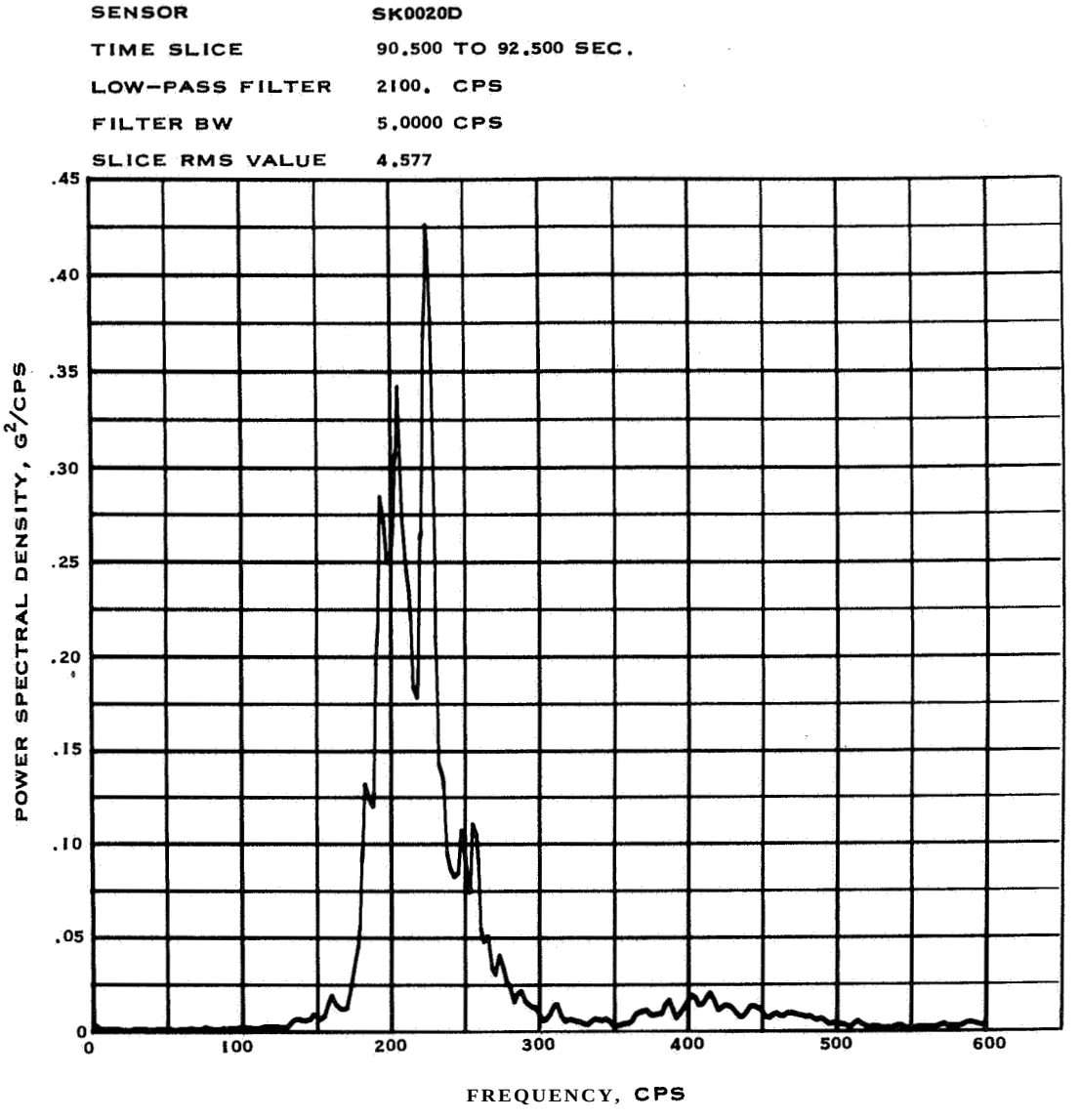


Figure 7.2-16.- Acceleration spectral density of maximum SPS engine dome longitudinal vibration during supersonic flight, Mission AS-201.

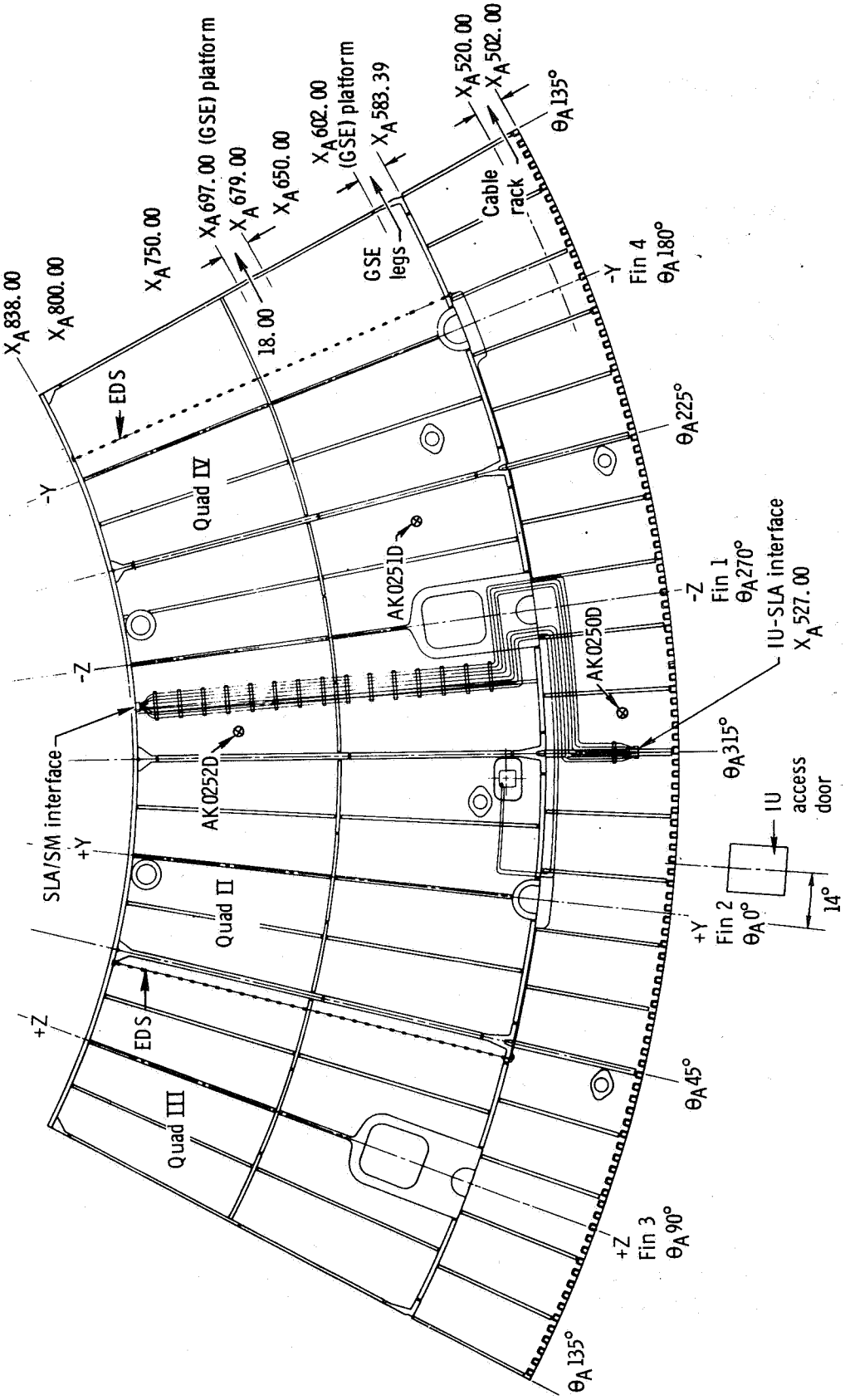
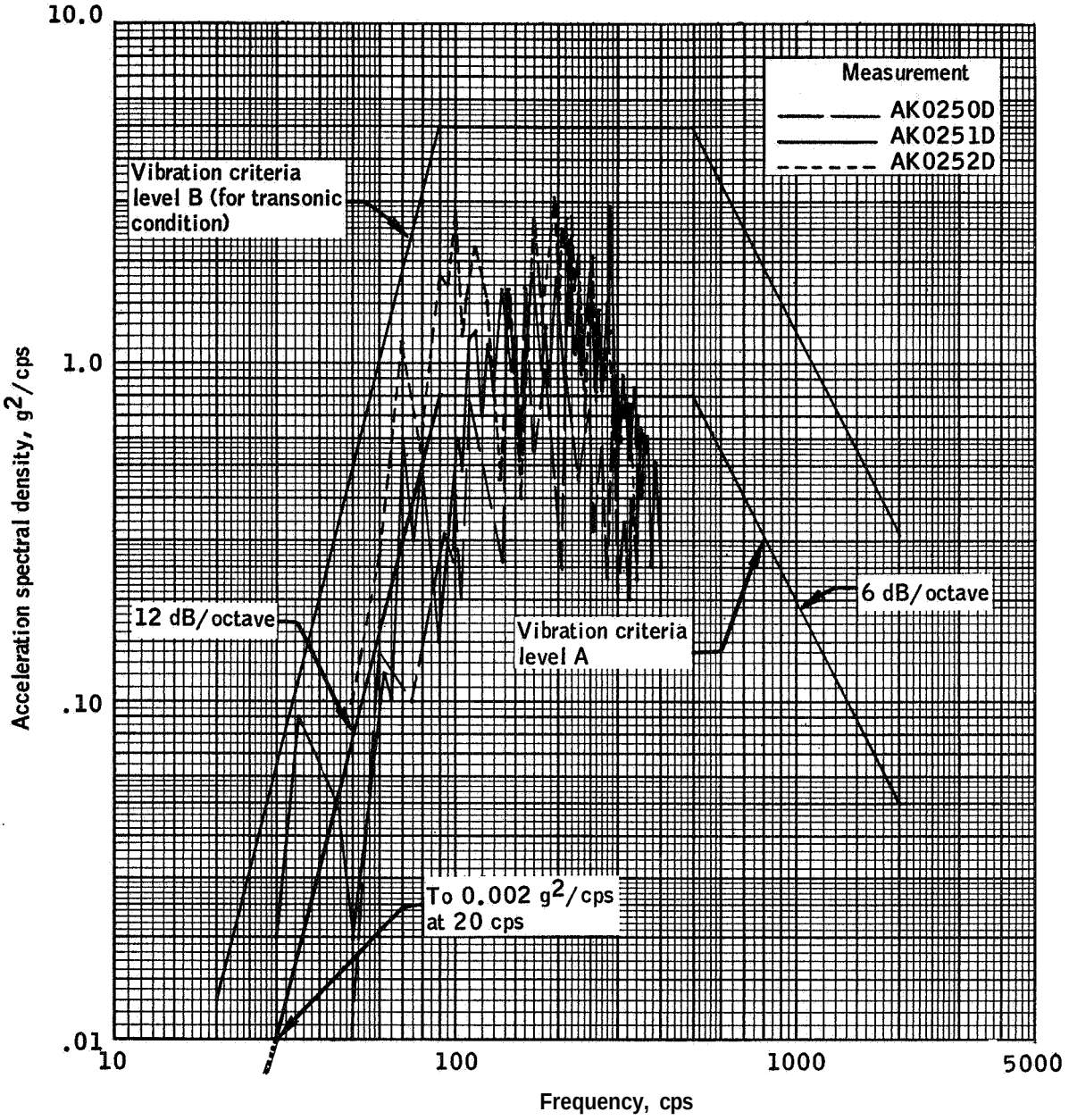


Figure 7.2-17.- Skin panel accelerometer locations, Station 2101.

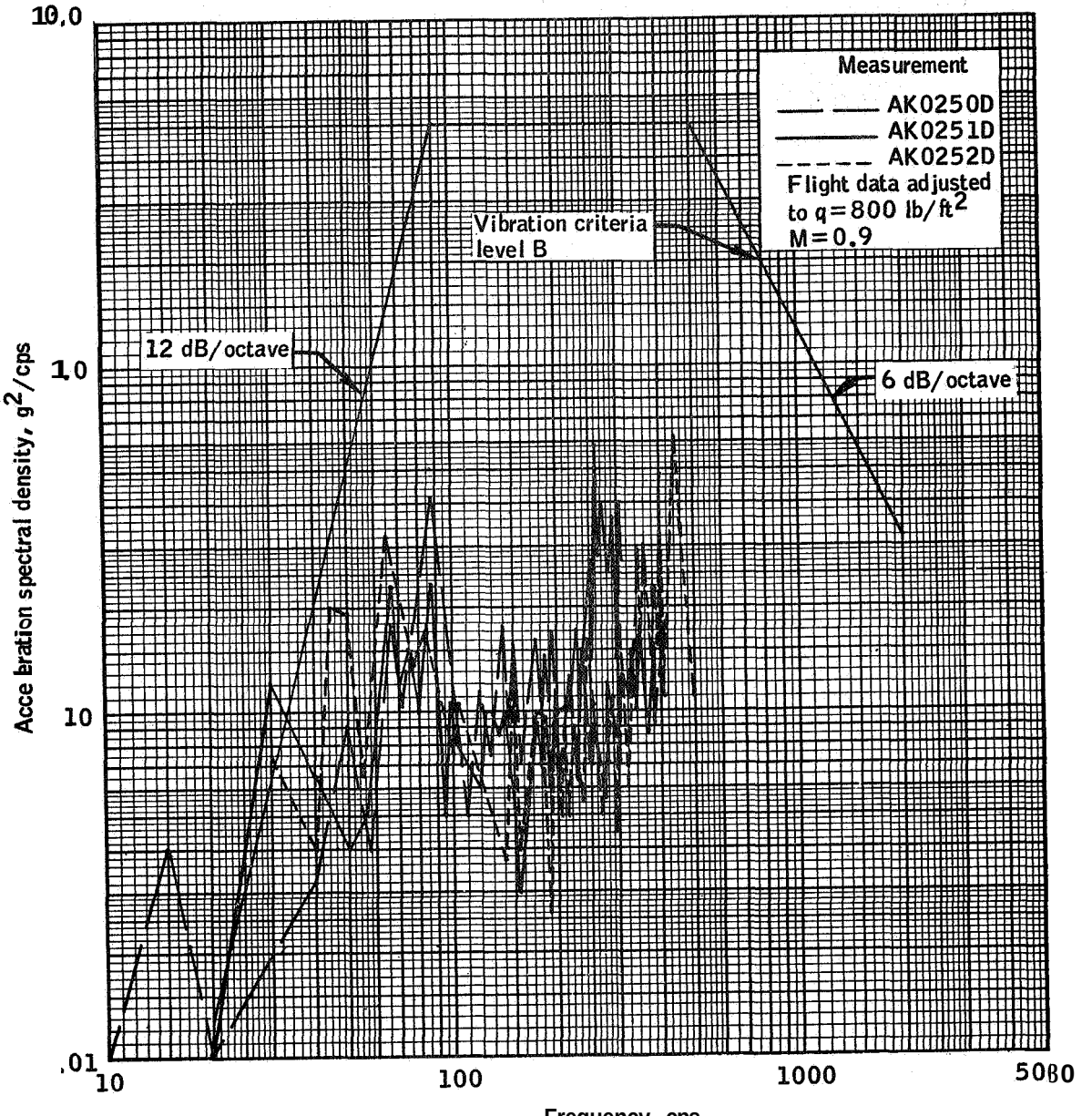
NASA-S-66-6227 MAY 6



(a) Lift-off.

Figure 7.2-18.- Comparison of SLA shell panel vibration with criteria, Mission AS-201.

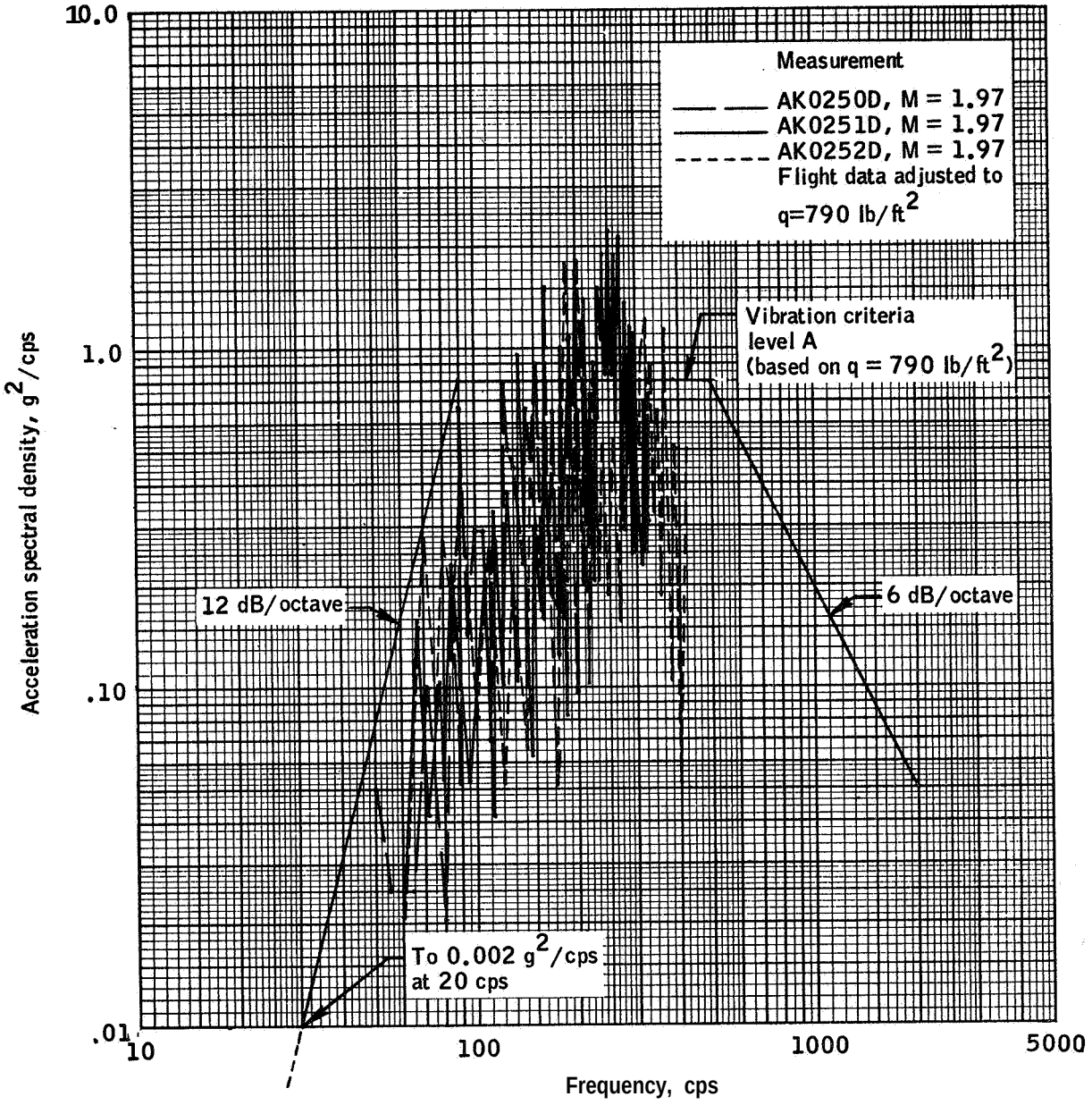
NASA-S-66-6228 MAY 6



(b) Transonic flight.

Figure 7.2-18.- Continued.

NASA-S-66-6229 MAY 6



(c) Supersonic flight.

Figure 7.2-18.- Concluded.

7.3 Heat Transfer

The thermal environment of the Mission AS-201 launch trajectory has been evaluated as pertains to the service module (SM) and the spacecraft – LEM adapter (SLA). The heating parameters were close to those predicted for the nominal mission trajectory.

The thermal environment was measured by temperature sensors located on the SM and SLA in areas which would best show longitudinal and circumferential temperature variations. This instrumentation measured both the inner and outer skin temperatures, and internal temperatures from lift-off through S-IVB/CSM separation at T+844.9 seconds, and to CM/SM separation at T+1455 seconds. In the following evaluation of temperatures, the discussion is limited to a representative number of significant temperature locations through the launch phase to about T+300 seconds, which is the only phase significant for launch heating. However, data beyond the launch phase are currently being evaluated.

Service module temperatures. - Figure 7.3-1 shows the distribution of peak temperatures measured on the SM outer skin during launch. Thermocouple locations were chosen to present a circumferential temperature distribution and a longitudinal temperature distribution as indicated.

The maximum launch temperature of 200° F was measured at Longitudinal station X_S350 at 253° from the +X axis at T+130 seconds. This high temperature is believed to be the result of shock impingement from flow past the nearby reaction control subsystem (RCS) quad A.

The low temperatures of 100° to 110° F measured for sensors SA7904T, SA7906T, SA7907T, SA7917T, and SA7918T located close to RCS quad A were the result of the protection afforded by the cork insulation on the SM surface around the quad and also due to the fact that the quad A engines did not function on this flight. (See section 7.9.) The cork protection covered the SM surface around each RCS quad for protection against plume impingement during RCS engine firing. Since quad A did not fire during the mission, there are no thermocouple data to indicate the effectiveness of the cork insulation.

Figure 7.3-2 shows peak launch temperatures measured on the SM as a function of longitudinal distance along the SM surface in two relatively smooth surface areas. The data indicate little longitudinal temperature variation in either area, although the peak temperatures for the area between -Y and -Z appear to be generally higher than the peak temperatures between -Z and +Y.

Figure 7.3-3 shaws peak launch temperatures measured on the SM as a function of circumferential location. Because of the programed pitch

of the launch vehicle, the area of highest boost heating (assuming a smooth body) was expected dong the -Z axis. The data in figure 7.3-3 indicate little circumferential variation, with somewhat higher temperatures near the -Y axis.

As predicted, the internal temperatures in the SM aft bulkhead, SA7931T and SA7914T, did not exceed 80° F. Sensors SA7910T and SA7912T on the inner surface of the SM skin did not exceed 150° F, as shown in figure 7.3-4.

Preflight temperature predictions for sensors SA7911T and SA7912T (X_S230 and 236°), outer and inner, respectively, were performed based on the maximum aerodynamic heating launch trajectory and were found to be slightly higher than the measured flight data. Postflight temperature predictions for sensors SA7911T and SA7912T, based on the actual launch trajectory and launch pressures which were obtained from wind-tunnel tests, are shown in figure 7.3-4 as the solid symbols and are compared to the measured values. The sensors, since they were in smooth areas away from major protuberances, were believed to be typical of the average SM outer skin temperature (160° F). As can be seen, good agreement exists between the measured and predicted values.

Spacecraft - LEM adapter temperatures.- Figure 7.3-5 shows the distribution of peak temperatures measured on the SLA outer skin during launch. The maximum temperature of 280° F was measured by sensor AA7937T (X_A775 and 304°) at T+150 seconds. Outer skin temperatures were as low as 80° F for sensor AA7934T located at X_A597.2 and 5°. All outer skin measurements aft of X_A610 show maximum temperatures below 110° F. These lower temperatures were the result of the protection afforded by the cork insulation on the surface of the SLA in this area and which covered these temperature sensors. The lower peak temperatures measured at X_A820 were possibly the result of the sensors being located in the potting compound on the pyrotechnic mild detonating fuse.

Temperatures on the inner surface of the SLA skin, sensors AA7932T, AA7936T, and AA7938T, did not exceed 130° F.

Figure 7.3-6 shows measured time histories for typical SLA sensors AA7931T and AA7932T. Temperature predictions were prepared, utilizing the actual spacecraft 009 launch trajectory and pressures obtained from wind-tunnel data. These predictions are shown as the solid symbols of figure 7.3-6 for outer skin temperature AA7931T and inner skin temperature AA7932T. As can be seen, good agreement exists between the predictions and actual for about the first 150 seconds from lift-off, but not during the cool-down portion of the curve which assumes radiation

to space. It has been determined that as the spacecraft pitched over to a flight-path angle of 24.52° at S-IB cutoff, and later to a flight-path angle of 4.13° at CSM/S-IVB separation, the SM +Z axis (90°) was pointed up. At launch time, about 11:12 a.m. e.s.t., the sun was almost overhead and was radiating to the +Z axis. Since sensor AA7931T was located at 124°, further analysis of the cool-down portion of the analytical investigation will now include the effects of solar heating based on the programed launch azimuth, flight-path angle, and longitude of the spacecraft.

Prediction of inner skin temperature was correct to within 20° F and conservative. The conservatism in the predicted inner skin temperature is believed to be largely due to the omission of consideration of heat exchange with the interior environment.

The SM and SLA temperatures measured on spacecraft 009 were well within their design values and thermally qualify these structures for future Saturn IB missions.

NASA-S-66-6230 Mod B

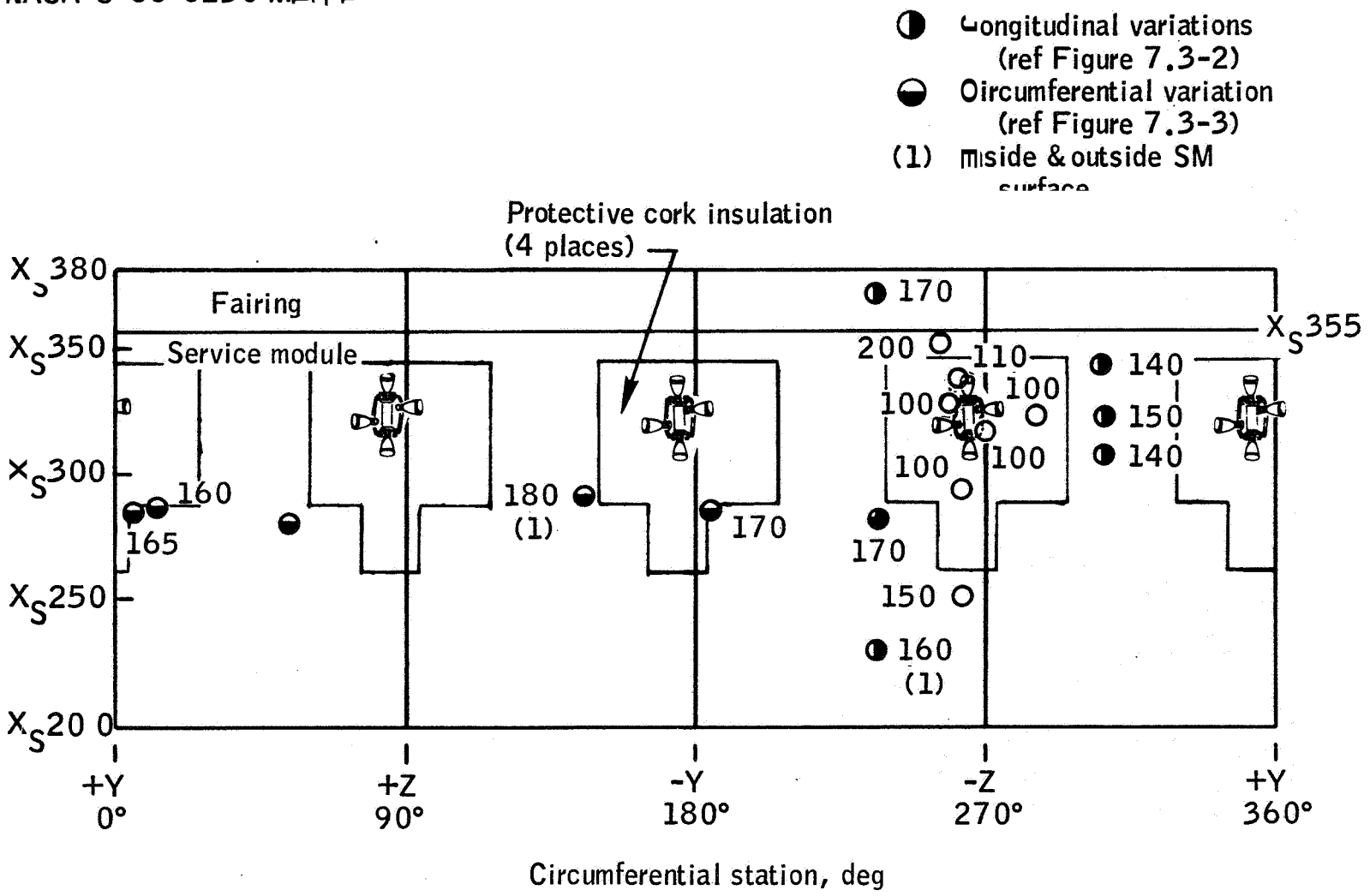


Figure 7.3-1.- Peak temperatures measured on service module outer surface during launch on Mission AS-201. (Sensors in cork insulated area are under the cork.)

NASA-S-66-6231 MAY 6

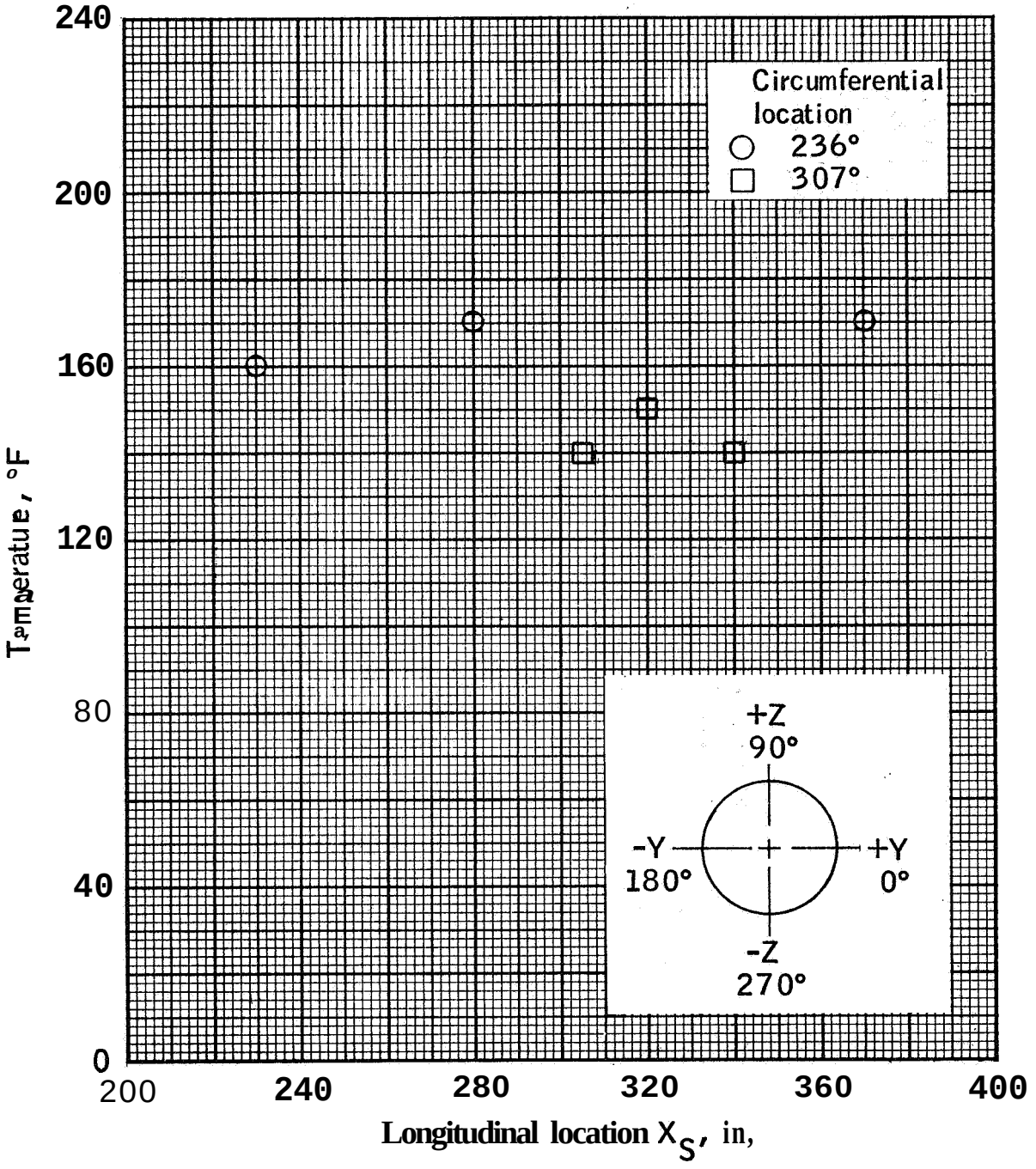


Figure 7.3-2.- Longitudinal variation of peak temperatures measured on the service module surface during launch on Mission AS-201.

NASA-S-66-6232 MAY 6

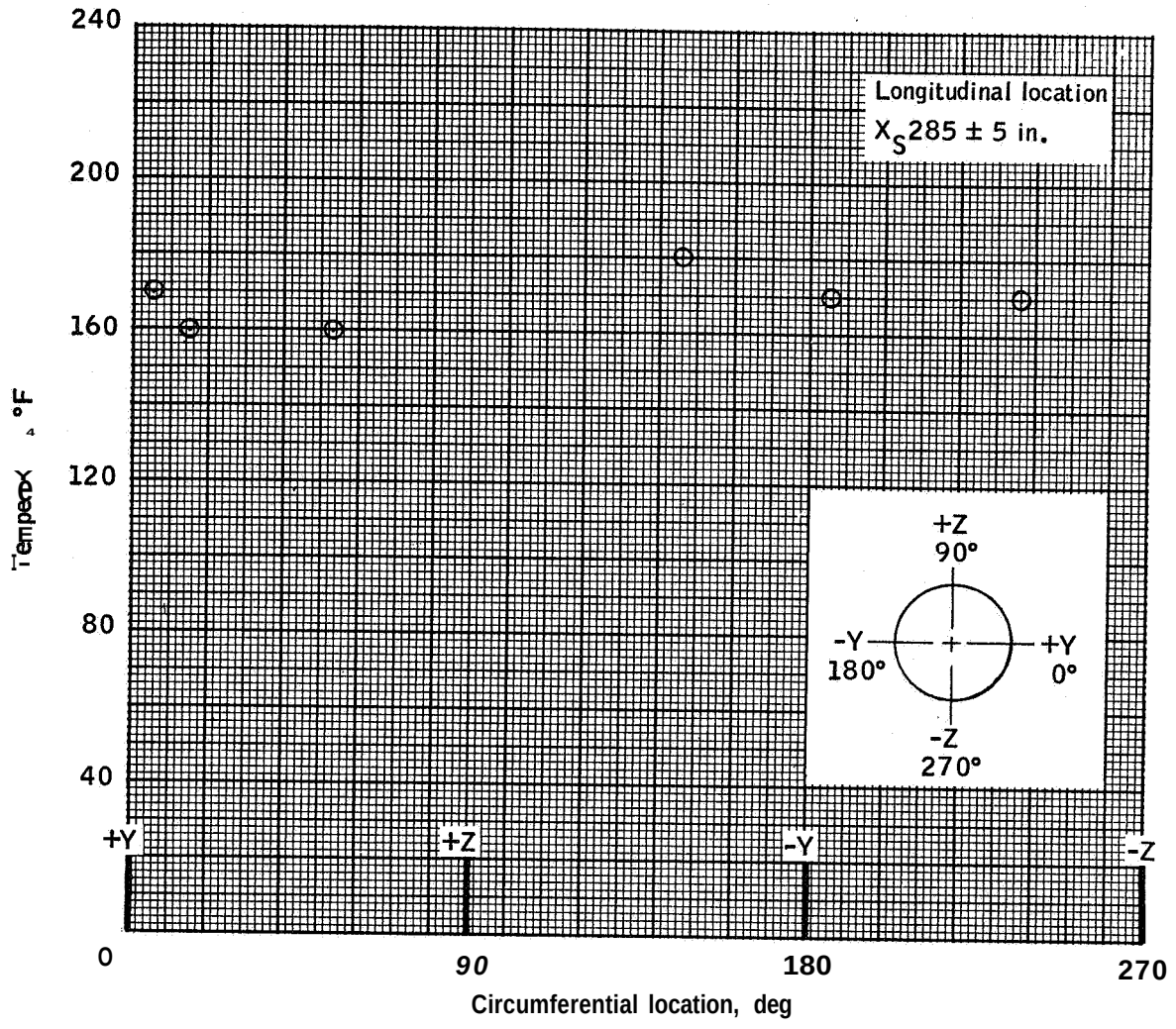


Figure 7.3-3.- Circumferential variation of peak temperatures measured on service module surface during launch on Mission AS-201.

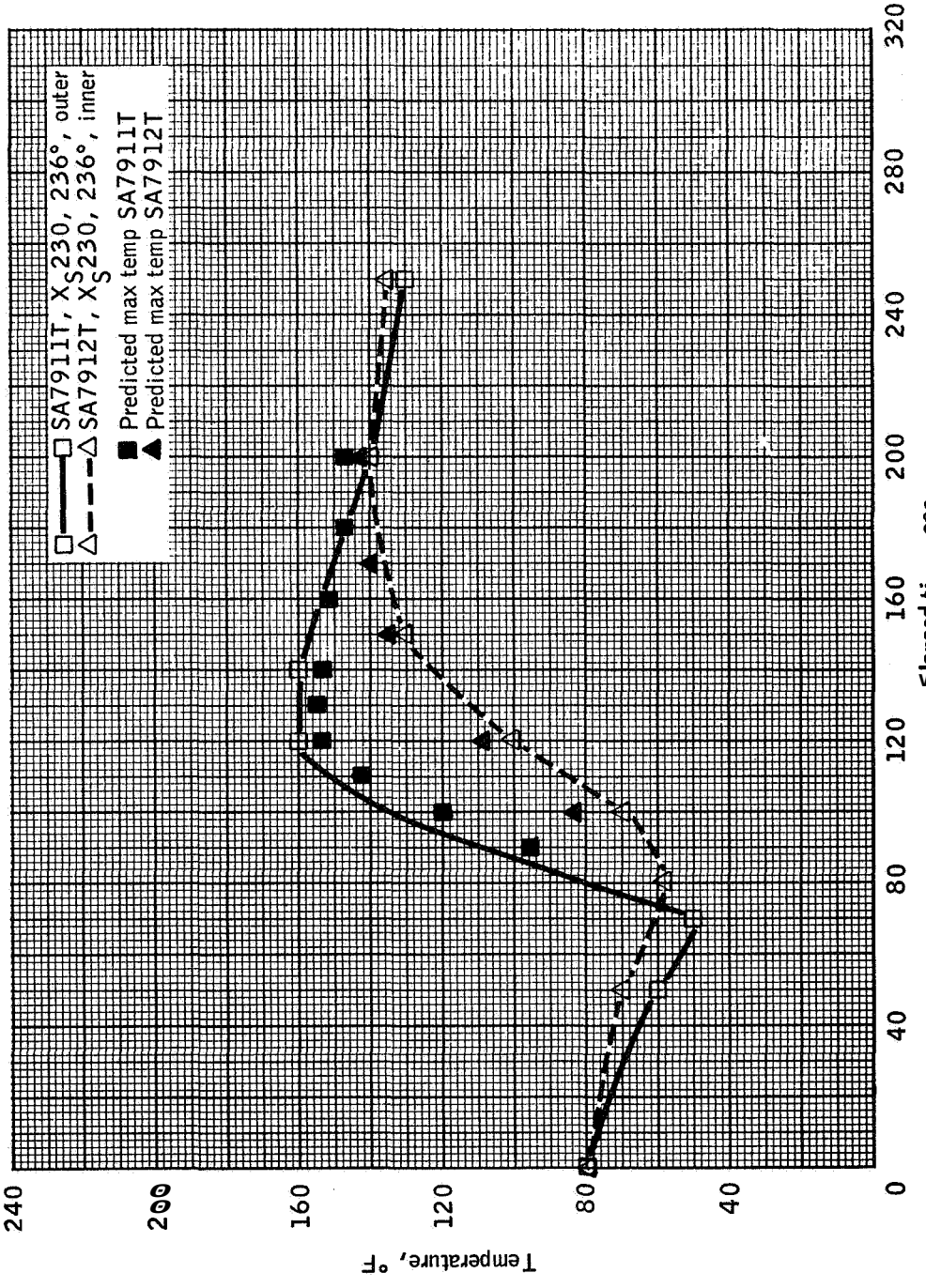


Figure 7.3-4.- Temperature time histories for service module sensors SA7911T and SA7912T, Mission AS-201.

NASA-S-66-6234 עמוד 6

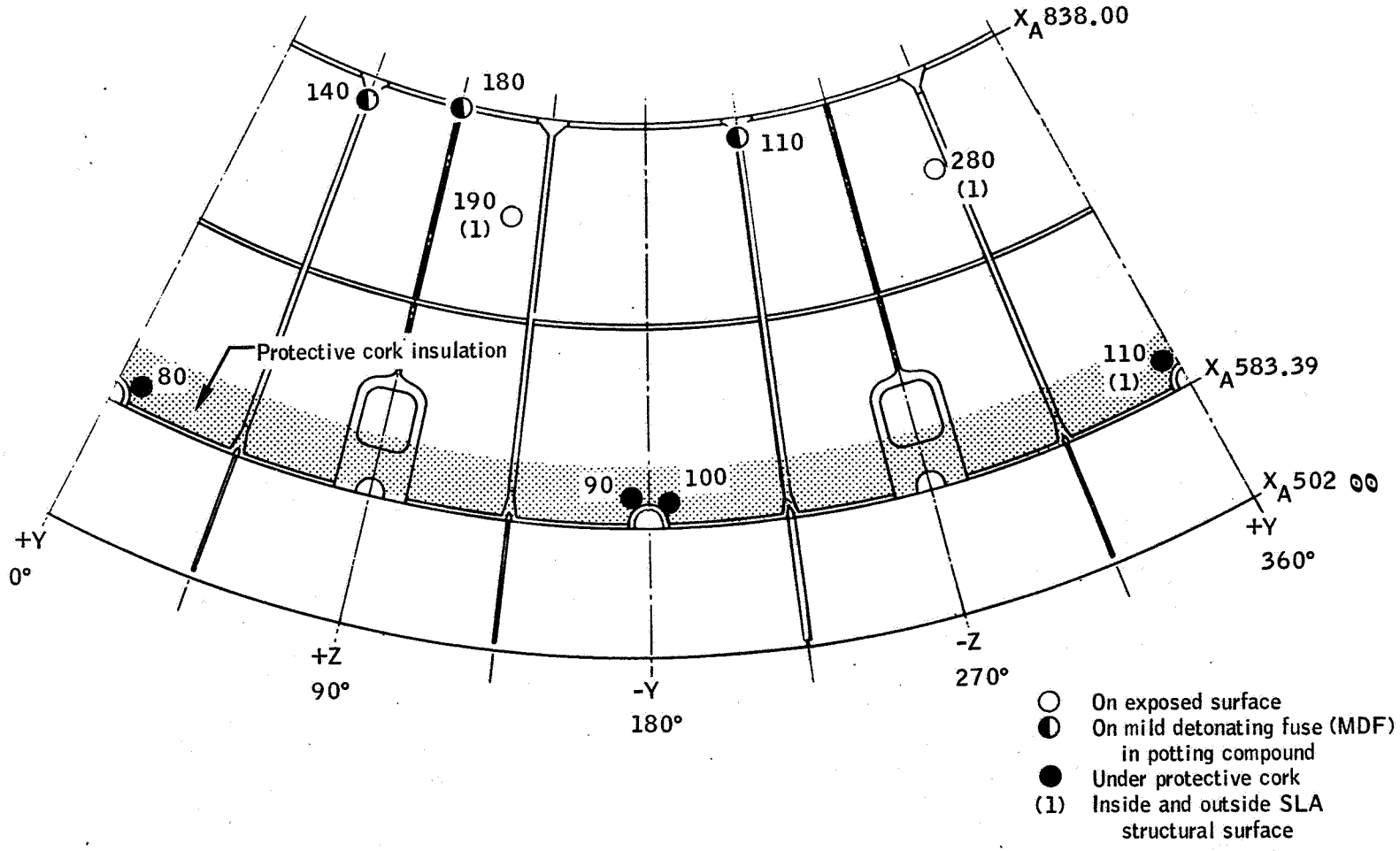


Figure 7.3-5.- Peak temperatures measured on spacecraft – LEM adapter outer surface during launch on spacecraft 009, Mission AS-201.

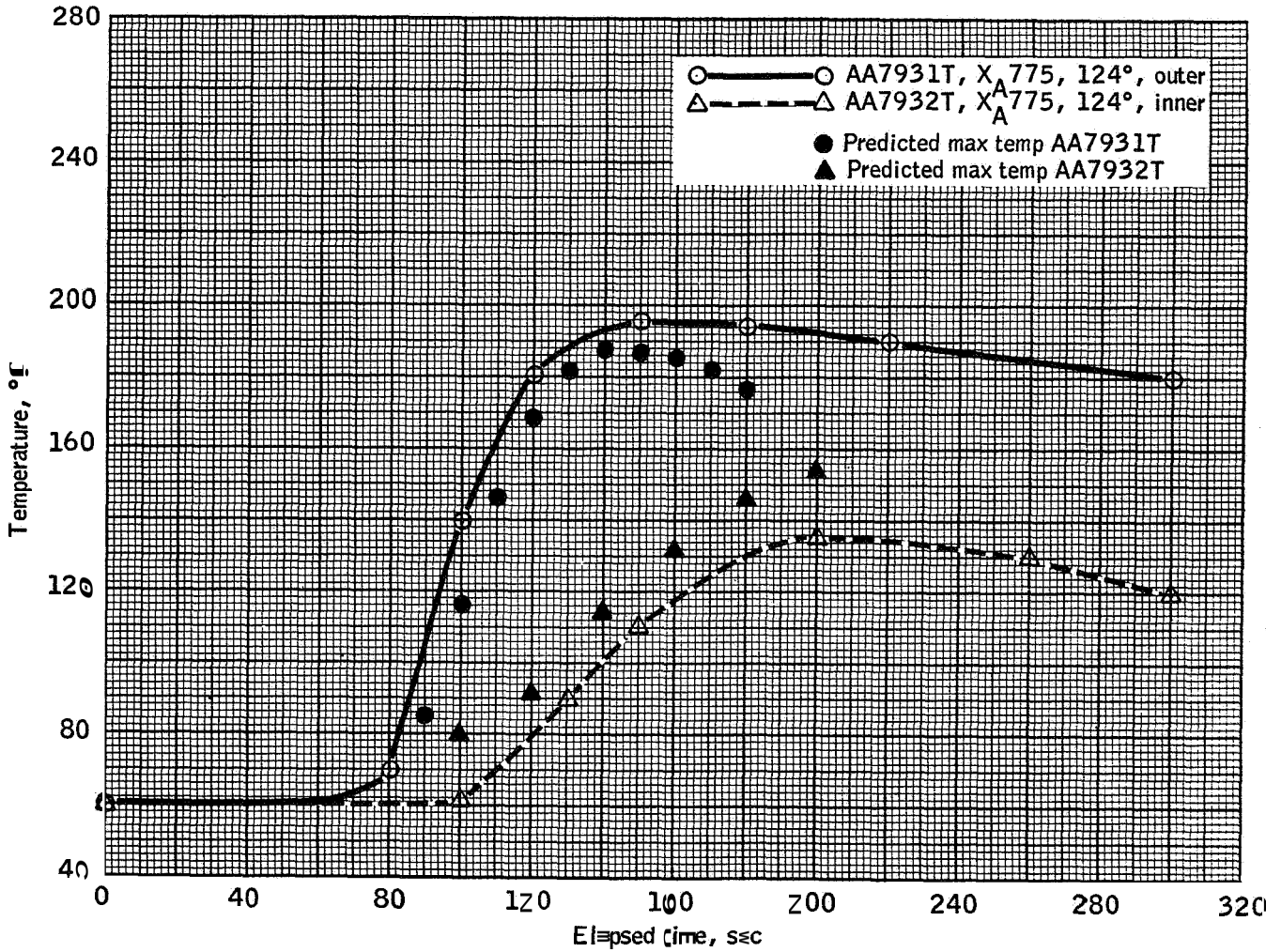


Figure 7.3-6.- Temperature time histories for SLA sensors AA7931T and AA7932T, Mission AS-201.

7.4 Heat Protection

Description.- The thermal protection subsystem protects the command module (CM) inner structure from the heat associated with reentry into the earth's atmosphere. This protection is accomplished by a planned degradation of the ablative heat shield in addition to insulation between the inner and outer structure. On spacecraft 009 the ablative heat shield consisted of epoxy novalac, phenolic microballoons, glass fiber, and hardeners mixed into a mastic and injected into a 3/8-inch phenolic honeycomb which was bonded to a brazed stainless steel honeycomb substructure. The conical section of the CM heat shield was attached to the inner structure by a floating stringer mechanism which allowed the outer structure to expand and contract with temperature changes, independent of inner structure expansion. Insulation type Q-felt was used between the inner and outer structure under the crew compartment heat shield on spacecraft 009 in place of the TG15000 insulation which will be used on subsequent spacecraft. Figure 7.4-1 shows the configuration of the CM, including a typical section of the thermal protection system in the crew compartment heat shield area. A typical section of the thermal protection system in the aft heat shield area is indicated in figure 7.4-2. Except for the windows and vents, the CM outer structure was completely covered with ablative material. The ablator varied in thickness over the CM to satisfy design heating distribution. A typical ablator thickness distribution is shown in figure 7.4-3.

The spacecraft 009 heat shield was originally designed for the lunar return using design trajectories HSE-3 and HSE-6 and the capsule oriented at an angle of attack of 33°. Because of the changes in the design angle of attack, the thicknesses for the operational Block I heat shield ablator had to be increased in several areas. The updated heat shield configuration will be flown on spacecraft 011, spacecraft 012, and spacecraft 014. Changes from the spacecraft 009 configuration to the updated heat shield configuration will include the following:

(a) Increased ablator thicknesses on the leeward side of the crew compartment

(b) Increased ablator thicknesses around the aft heat shield shear - compression and compression pads

(c) Increased ablator thicknesses on the aft heat shield, upstream of the umbilical.

Performance.- A first-order objective of the spacecraft 009 mission was to evaluate the performance of the heat shield ablator during a high heating rate atmospheric reentry. The mission was to serve a double purpose:

(a) To evaluate and verify the heat shield design methods, which in connection with future heat shield evaluation flights (SC-011, SC-017, SC-020) will be used to qualify the Block II heat shield for manned lunar return flights.

(b) To quality the Block 1 thermal protection subsystem for high heating rate type manned earth orbital reentries.

The evaluation of the heat shield performance is defined as the determination of the response of the ablator and its components to the reentry environment. It requires the definition of both the actual reentry environment and the ablator performance as a function of reentry time, and comparison of the test results with predictions for the actual reentry trajectory. It will allow verification of the design methods or may require their modification. Based on the calculated reentry trajectory conditions (see sections 5 and 6) the actual maximum heating rate was approximately 164 $Btu/ft^2/sec$ as compared with the minimum requirement of 160 $Btu/ft^2/sec$ (188 $Btu/ft^2/sec$, nominal).

Complete evaluation of the heat shield was not possible since temperatures and heating data were lost during the time of predicted peak heating and before the ablator could show a significant response to the heating environment. Detailed evaluation of the heat protection subsystem was therefore confined to the short; time period at the start of reentry and the last 100 seconds before landing. However, a measure of the overall performance of the heat shield has been obtained by using theoretical heating rates for the calculated reentry trajectory, and comparing the char penetration predicted to that measured from core samples taken from the heat shield. Figures 7.4-4 and 7.4-5 indicate the location of temperature measurements, and table 7.4-I shows the location of the aft heat shield cores measured.

Aft compartment heat shield: The aft heat shield ablator was charred all over, as predicted (fig. 7.4-6). Around the umbilical, the compression pads, the shear – compression pads, and the 59 plugs on the bolt circle, there was little evidence of erosion although protuberance heating patterns around the umbilical, shear – compression, and compression pads were clearly visible.

The three tension tie rods were melted flush with the pad surface, and, in the area where the three tie rods penetrated the aft heat shield, scorching or burning appeared to extend through to the substructure. Postflight examination of the rod area and heat shield installation procedures indicated that the room temperature vulcanizing sealant (RTV) between the marinite insulation sleeves and the heat shield had been omitted, presenting channels open to the flaw of hot gases (fig. 7.4-2).

A comparison of predicted ablator temperature response in in-depth ablator temperatures is shown in figure 7.4-7. All recorded temperature data are presented. As can be seen from the figure, the ablator temperature response during reentry was recorded in some cases for times less than 60 seconds and in no case for longer than 82 seconds.

A comparison of predicted and measured char depth and discoloration depth (600° F isotherm) at selected locations is shown in table 7.4-I. (Also see fig. 7.4-8.) A reasonable correlation is shown for the char and discoloration depth predictions. In general, the final position of the isotherms which correspond to char and discoloration have been predicted with a slight degree of conservatism; it is therefore considered that no gross deficiency exists in the overall ability to assess the adequacy of the thermal protection system for a given entry. A comparison of predicted and measured surface recession is also given in table 7.4-1. The surface recession measurements which were made on the core samples should be considered accurate only to +0.15 inches and -0.05 in inches because the original thickness was applied to an accuracy of +0.1 inch and -0.0 inch, and the postflight measurements were made to an accuracy of ±0.05 inch. Measured and predicted data for the cores are shown in figure 7.4-9, as a correlation with total heat at each location.

At Z71, the measured temperatures (during initial heat up), measured char depths, and discoloration depths all exceed predicted values. This could indicate that this location (near the stagnation heating area) received more heat than predicted based on wind-tunnel heating rate distributions. Other locations at Z71, Y39, and Y71 indicate a uniform conservatism in prediction for temperature, char depth, and discoloration depth.

The remaining high temperature thermocouples at other locations on the aft heat shield (see ref. 1) did not respond for the following reasons:

(a) The high range (2000' F to 5000° F) thermocouples did not respond because of losing emf bias.

(b) The high range (-100' F to 3000° F) thermocouples lost their insulative qualities to the high temperature and were inaccurate after reaching 1400° F because of oxidation.

The remainder of the thermocouples experienced no temperature rise prior to losing the emf bias.

Crew compartment heat shield: As a result of having to burn off the propellants for both the A and B systems of the CM reaction control subsystem (RCS) through the A system engines for the propellant depletion burn, the crew compartment heat-shield ablator adjacent to the A system roll engines experienced greater than normal charring and erosion. This effect is attributable to the plume impingement of the roll engines and the accompanying turbulence, along with the extended burn time. The maximum char depth occurred in the ablator material immediately below the intersection of the A system roll engine extensions. The maximum depth measured was 0.75 inch, which exposed the stainless steel honeycomb substructure of the crew compartment heat shield, This stainless steel structure was discolored but there was no evidence of subsequent degradation of either the cabin aluminum honeycomb structure or of the heat shield stainless steel honeycomb structure (see fig. 7.4-10).

Figure 7.4-11 shows surface char on the windward side, and only scorched paint around the conical section protuberances on the leeward side. The umbilical wires that extended approximately 1 inch in front of the umbilical after being severed were melted flush with the face, Thermocouples located in depth in the crew compartment heat shield had not responded at the time of loss of recorded data.

Results of the evaluation of the limited amount of ablator performance data indicated that fair to good agreement was obtained. The heat shield performed well during the mission and, since the reentry heating rates exceeded those predicted for manned earth orbital reentries, the Block I heat shield is now qualified for high heating rate (non-decay) type reentries from low earth orbits.

TABLE 7.4-I.- COMPARISON OF MEASURED AND PREDICTED HEAT SHIELD PERFORMANCE DATA

Location		Discoloration depth, in. (600° F Isotherm)		Char depth, in. (1000° F Isotherm)		Surface recession, in.	
Z	Y	Measured	Predicted	Measured	Predicted	Measured	Predicted
71	0	0.47	0.39	0.32	0.25	0.06	0.08
0	0	.35	.42	.21	.29	.02	.11
-71	0	.35	.38	.21	.26	.19	.08
0	39	.37	.45	.22	.32	.02	.13
0	71	.38	.45	.25	.32	.04	.13

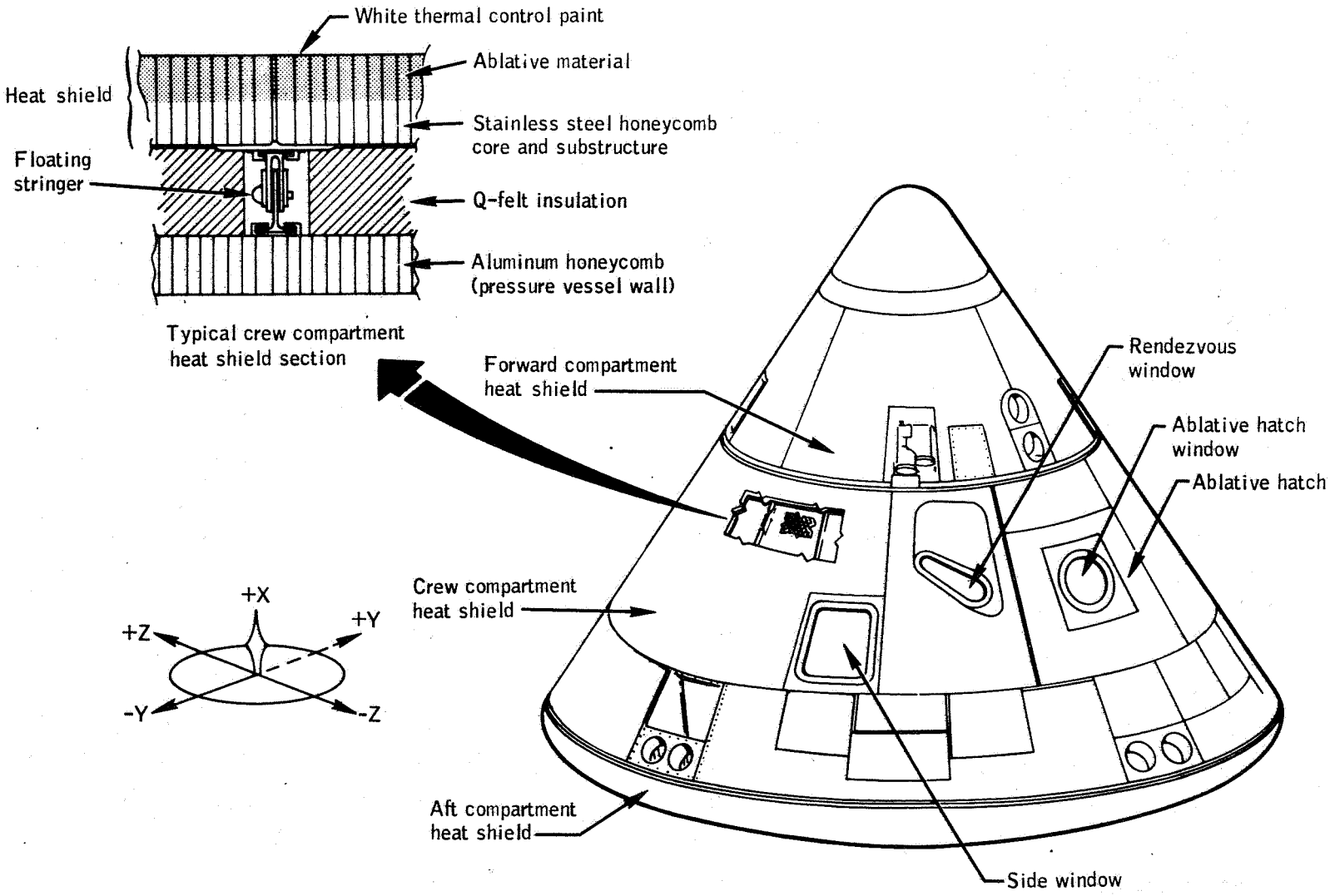


Figure 7.4-1.- Command module three-part heat shield, Mission AS-201.

NASA-S-66-6237 MAY 6

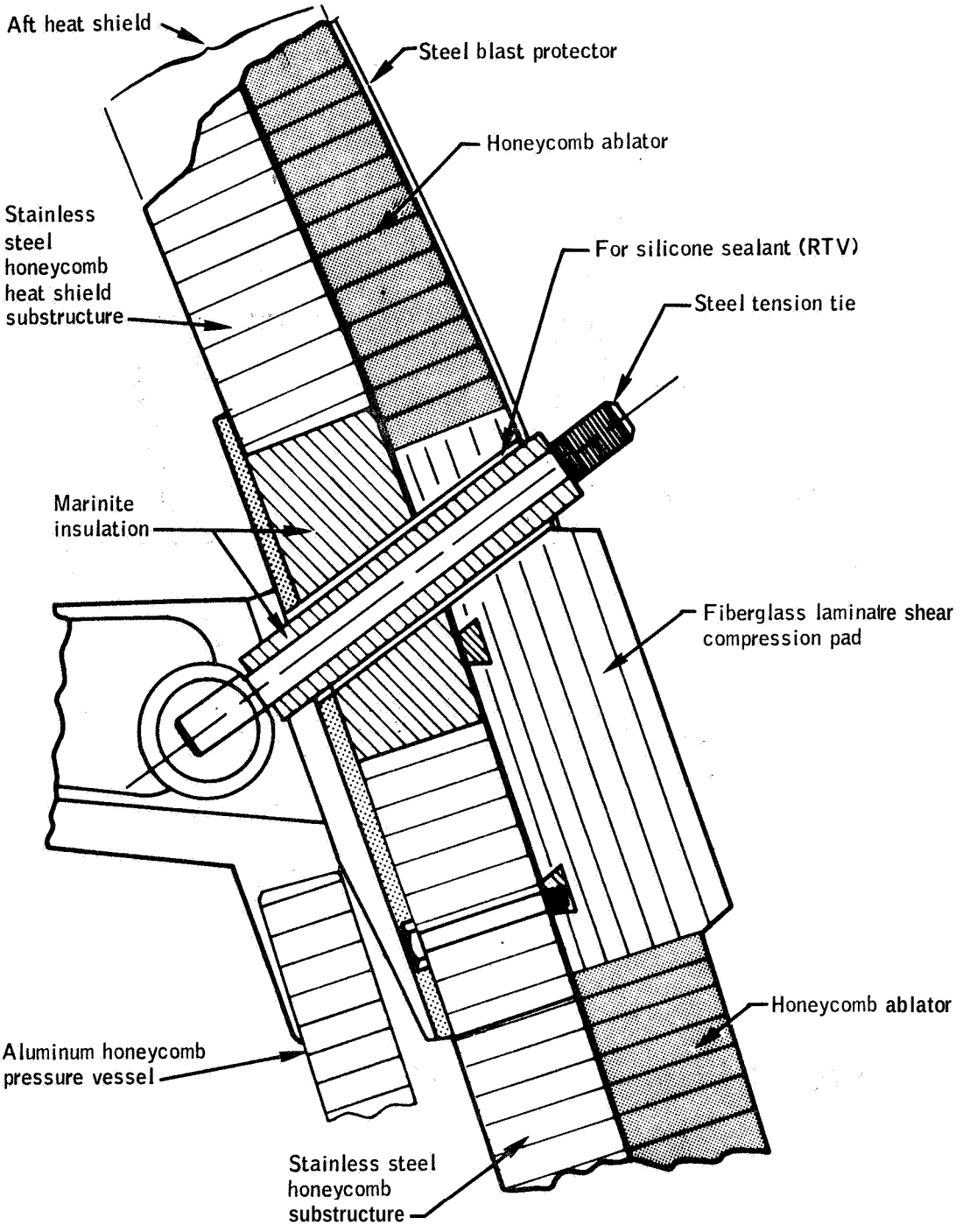
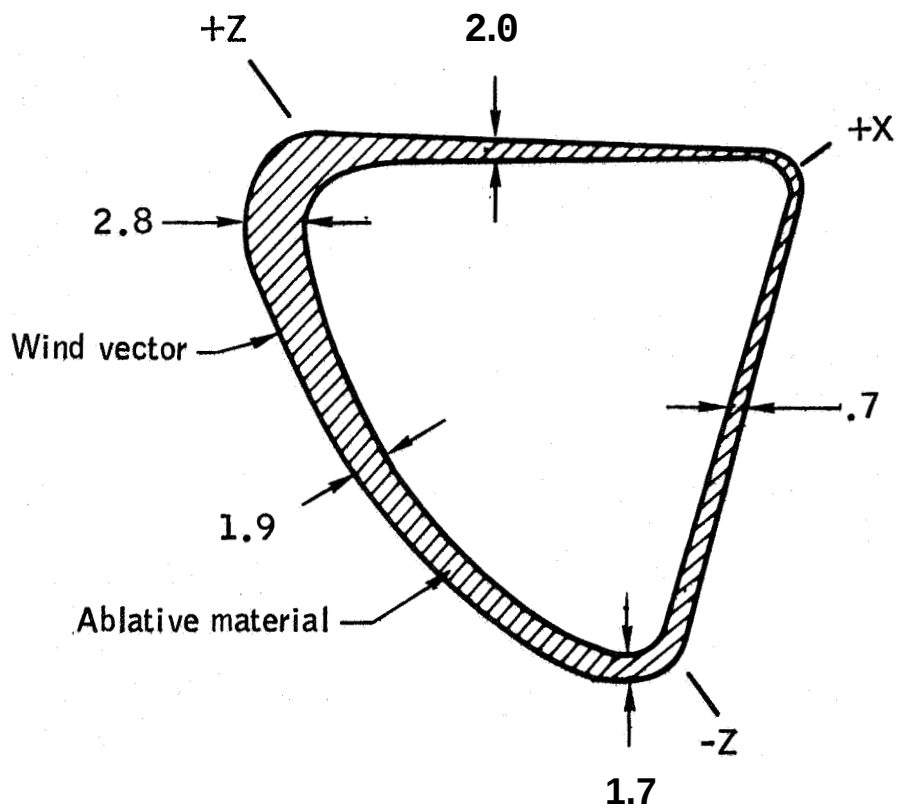


Figure 7.4-2.- CM/SM shear compression pad and tension tie - Block I type, Mission AS-201.

NASA-S-66-6238 MAY 6



Note: All dimensions are in inches

Figure 7.4-3.- CM ablator thickness distribution, Mission AS-201.

NASA-S-66-6239 MAY 6

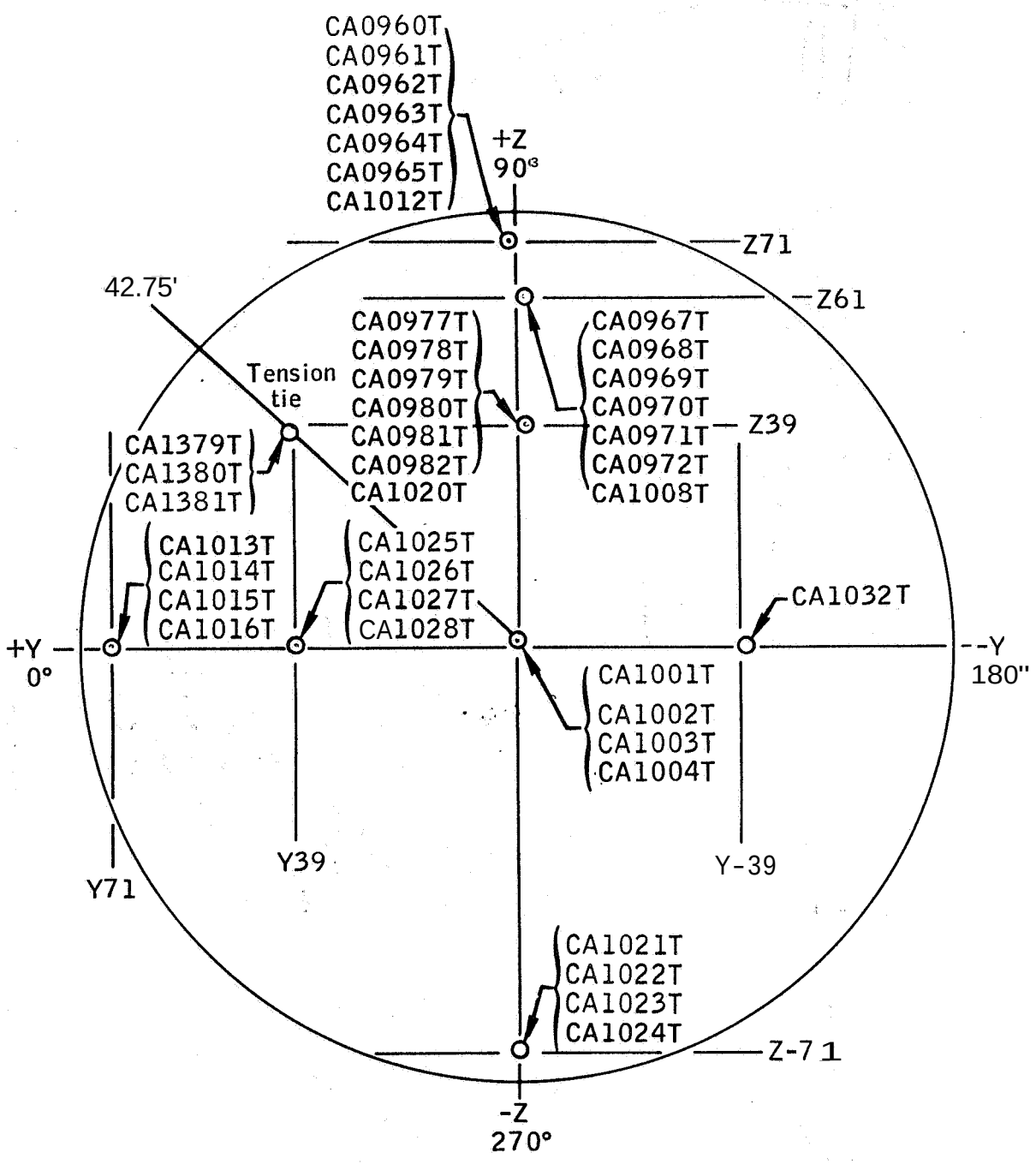


Figure 7.4-4.- Aft heat shield ablator measurement locations, Mission AS-201.

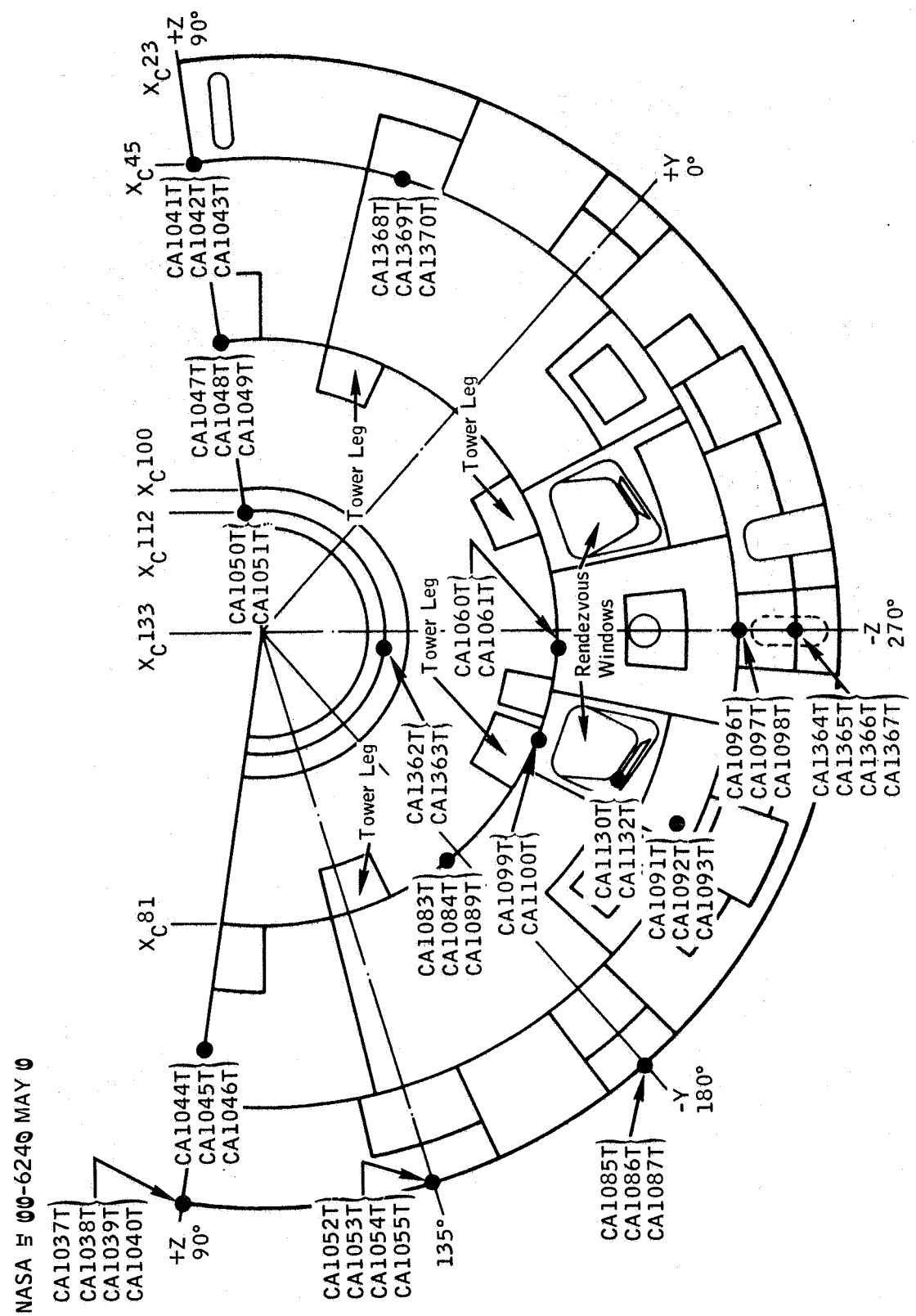
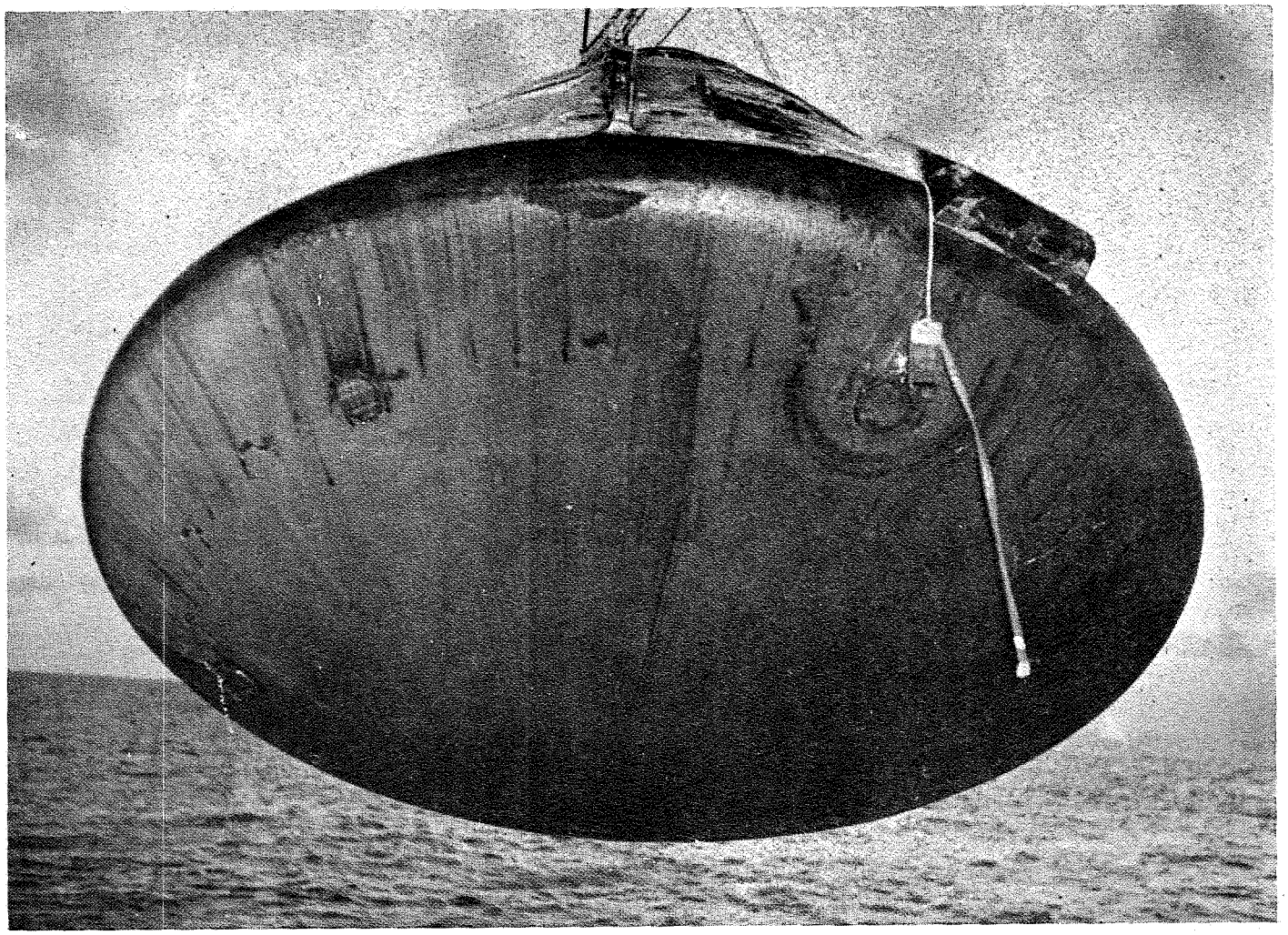


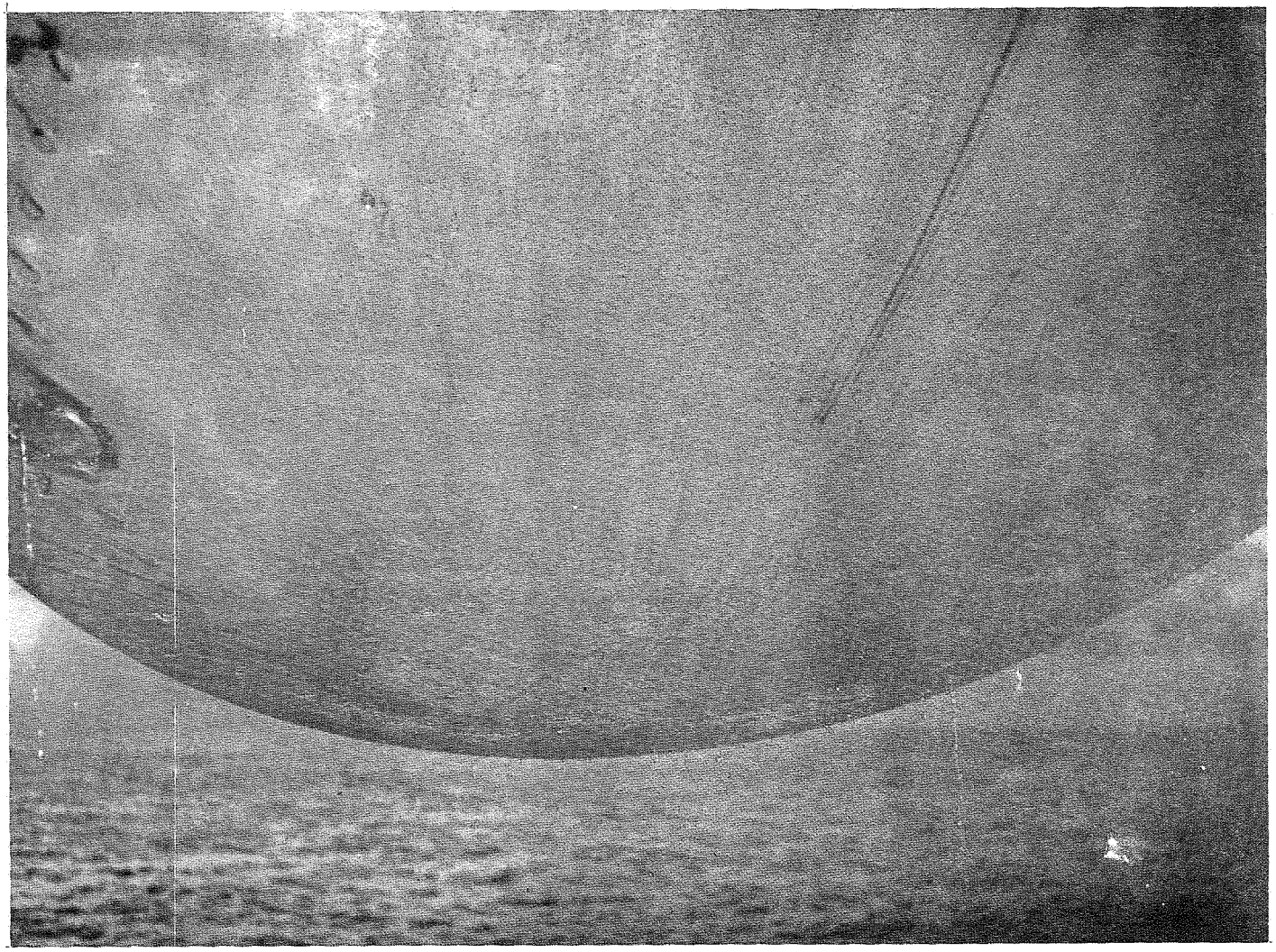
Figure 7.4-5.- Temperature measurement locations on CM forward and crew compartment, Mission AS-201

NASA-S-66-6241 MAY 6



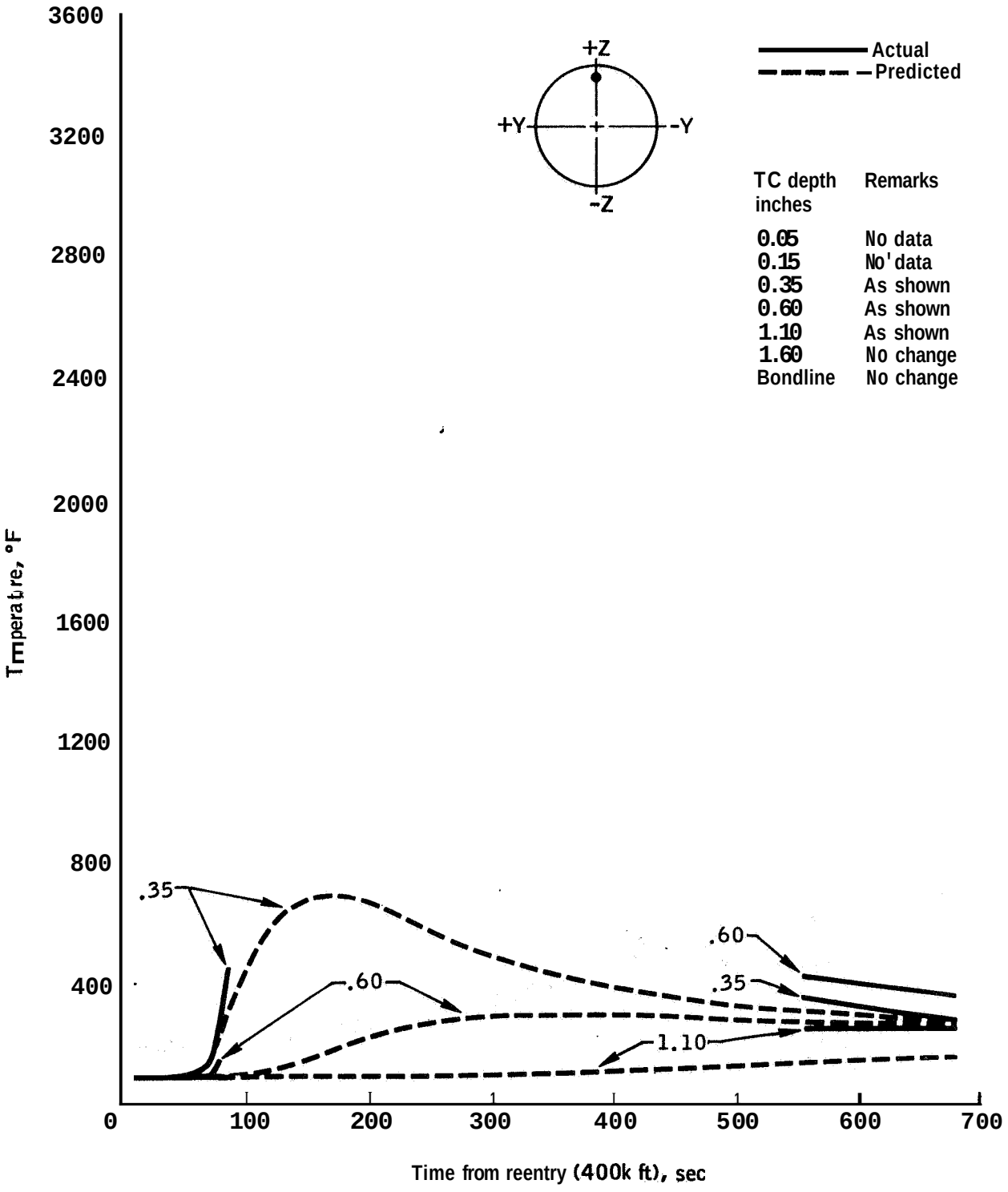
(a) General view from -Z-axis to -Y-axis.

Figure 7.4-6.- Char condition of aft heat shield, Mission AS-201.



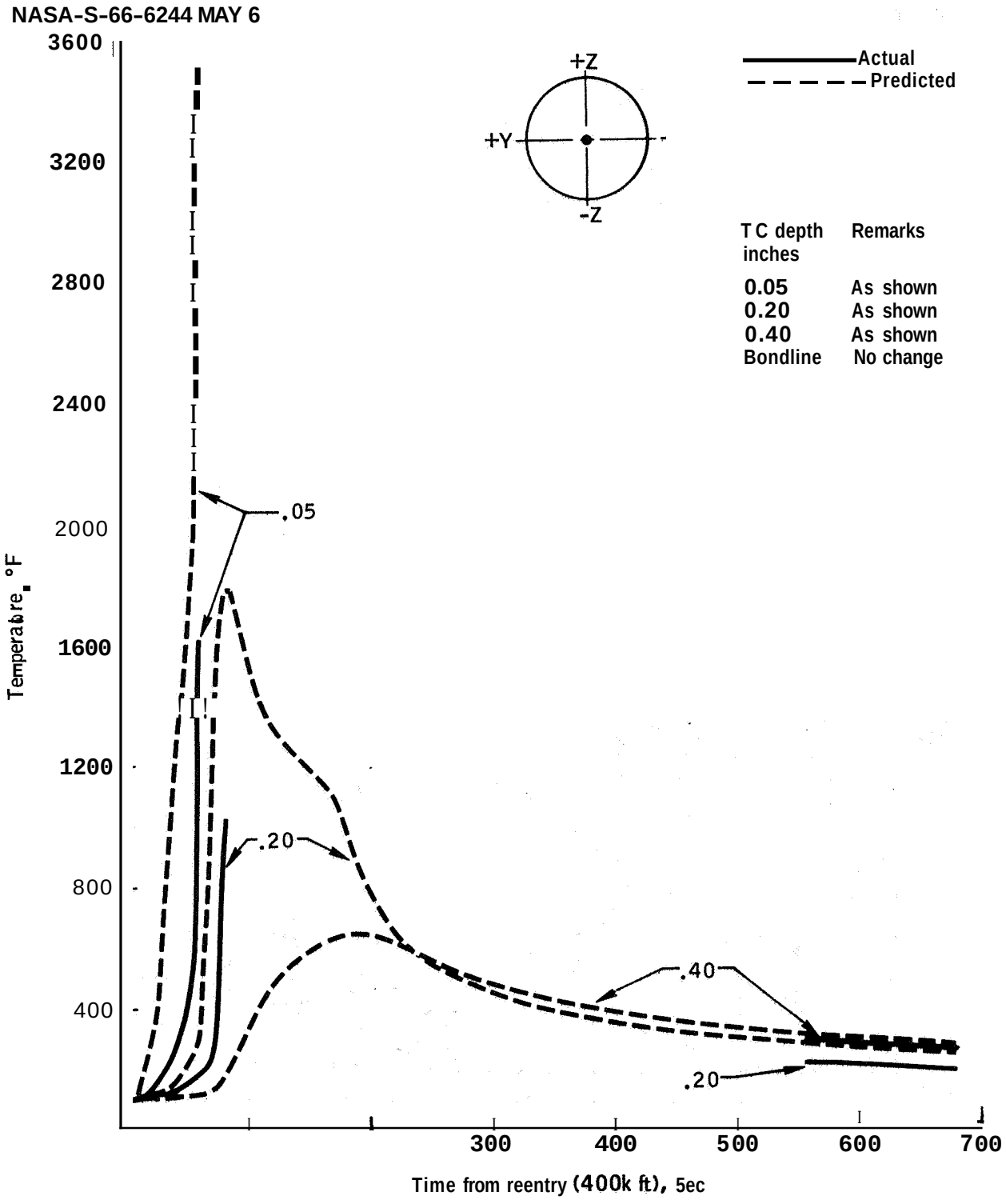
(b) View from center toward -Z axis

Figure 7.4-6.- Concluded



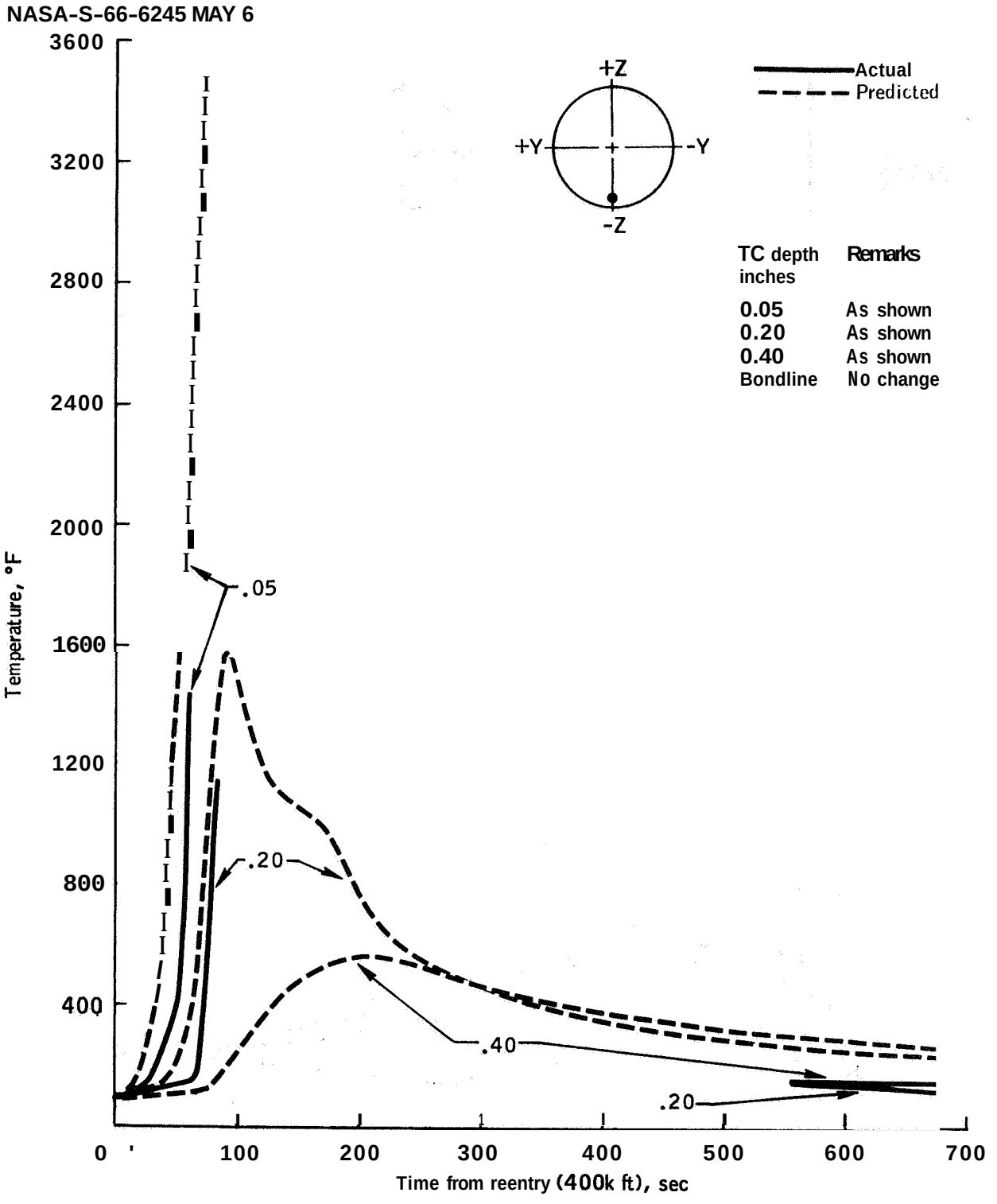
(a) Station 271, YO,

Figure 7.4-7.- Aft heat shield measurements, Mission AS-201.



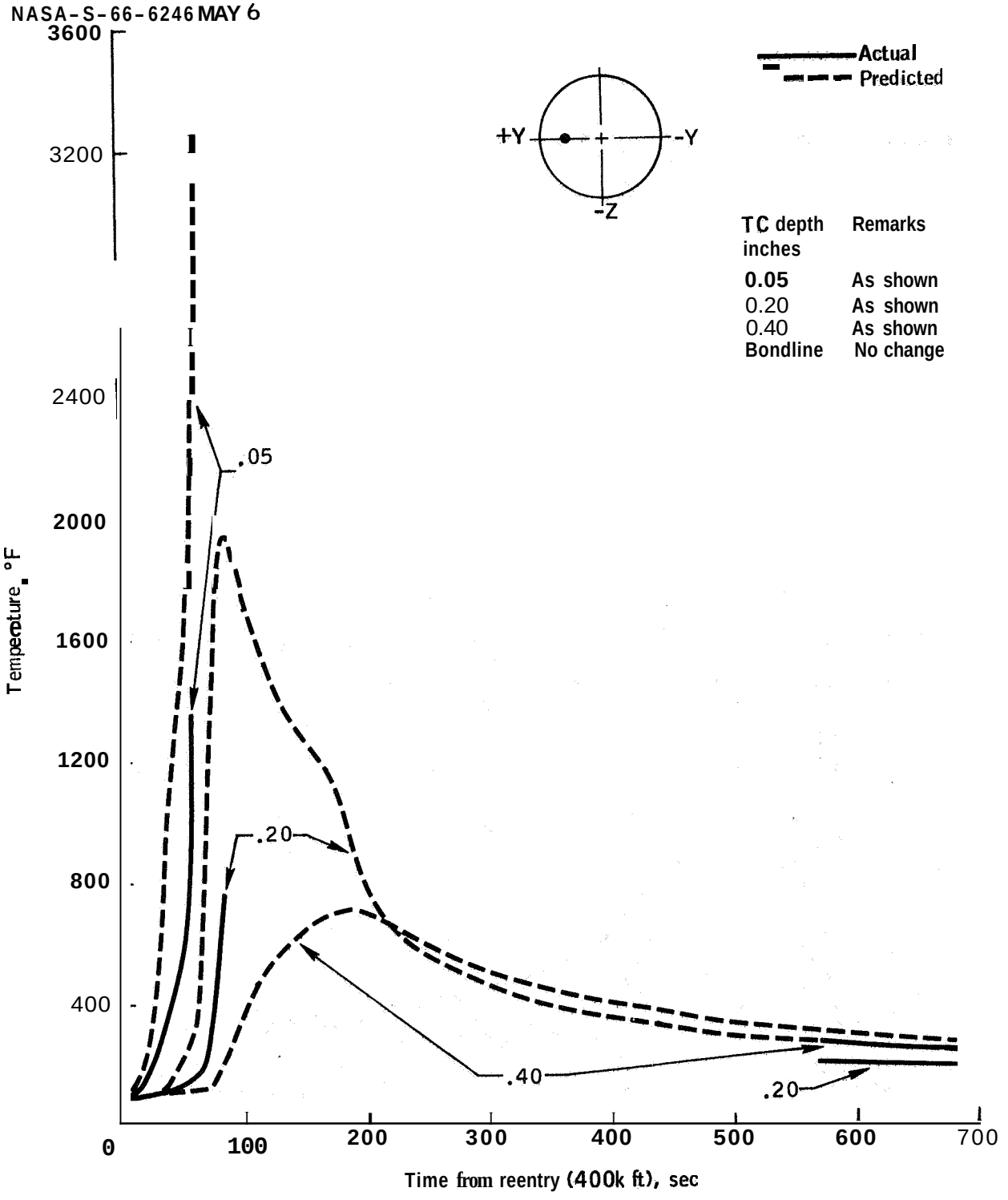
(b) Station ZO, YO,

Figure 7.4-7.- Continued.



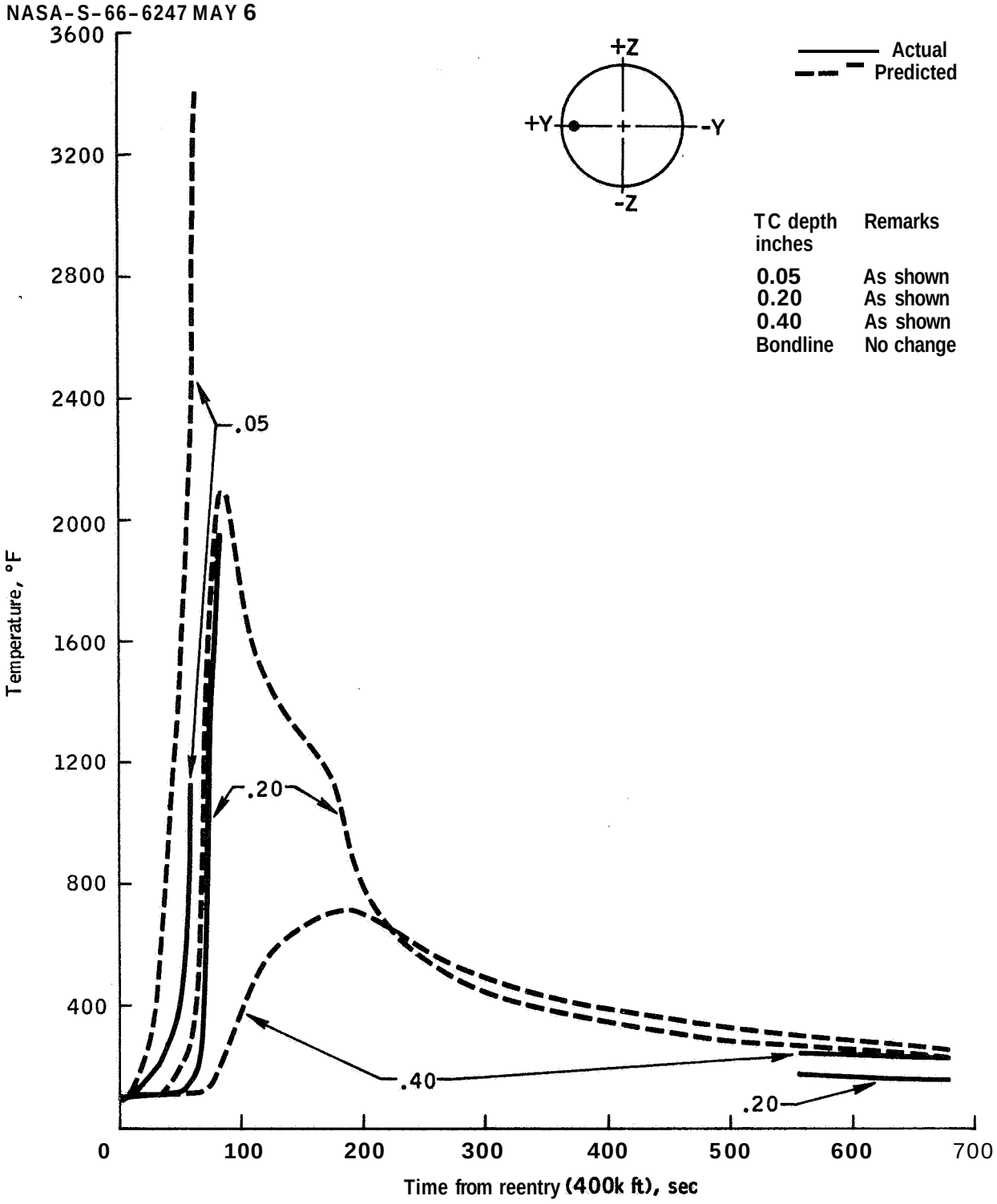
(c) Station 2-71, YO.

Figure 7.4-7.- Continued.



(d) Station Z0, Y39.

Figure 7.4-7.- Continued.



(e) Station ZO, Y71.

Figure 7.4-7.- Concluded.

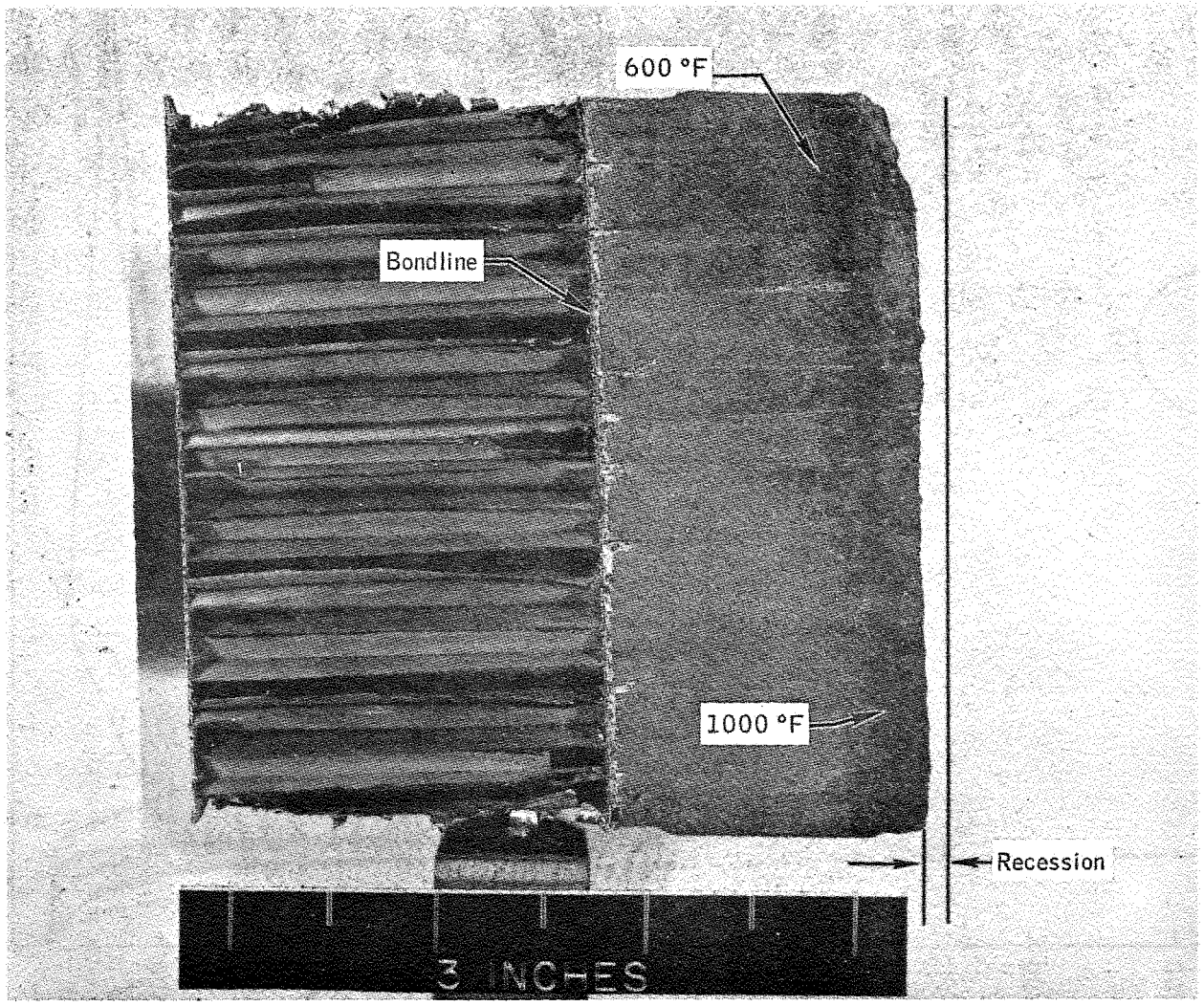


Figure 7.4-8.- Typical aft heat shield core (Z-71), Mission AS 201

NASA-S-66-6249 MAY 6

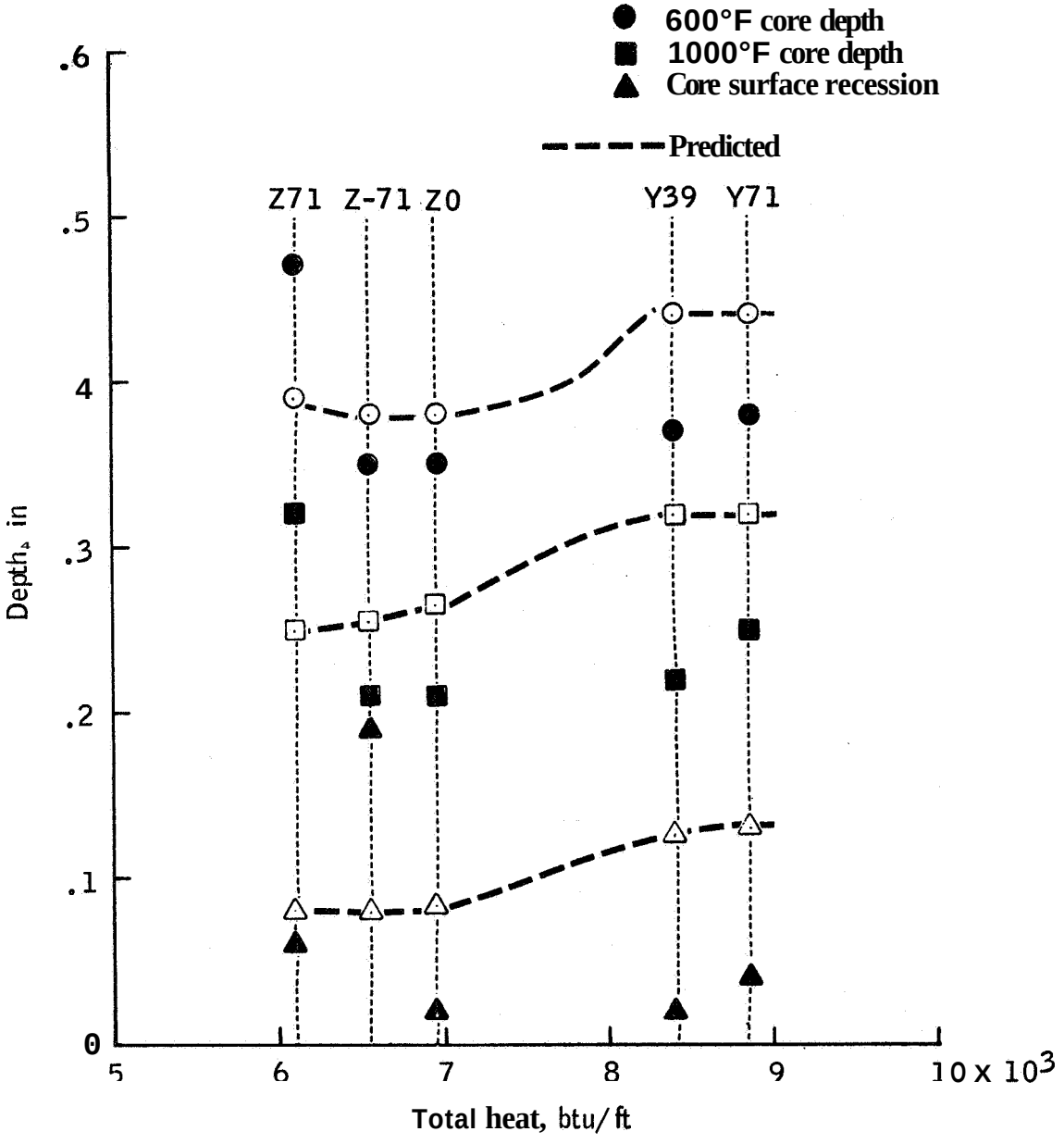


Figure 7.4-9.- Aft heat shield core measurements, Mission AS-201.

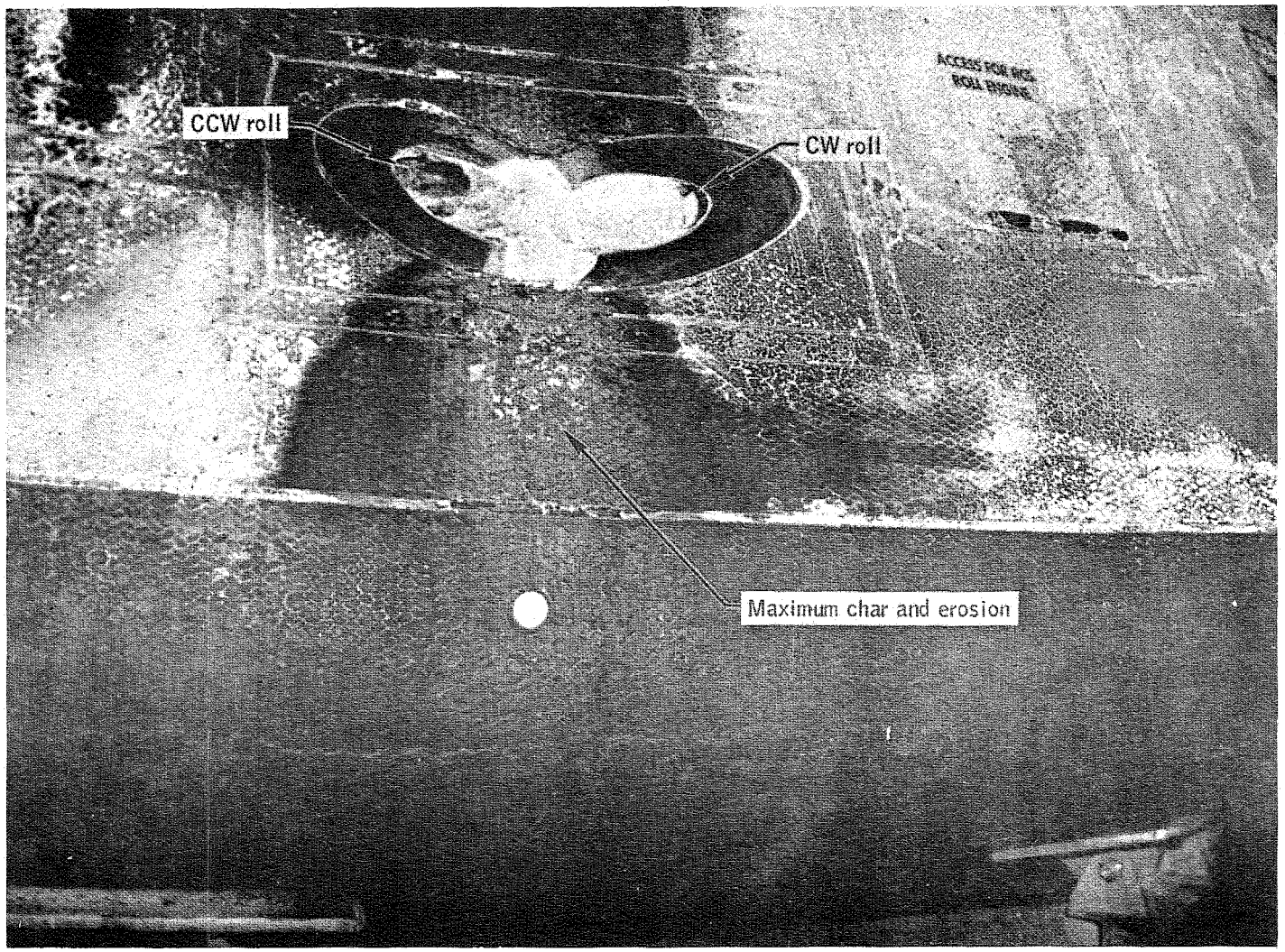
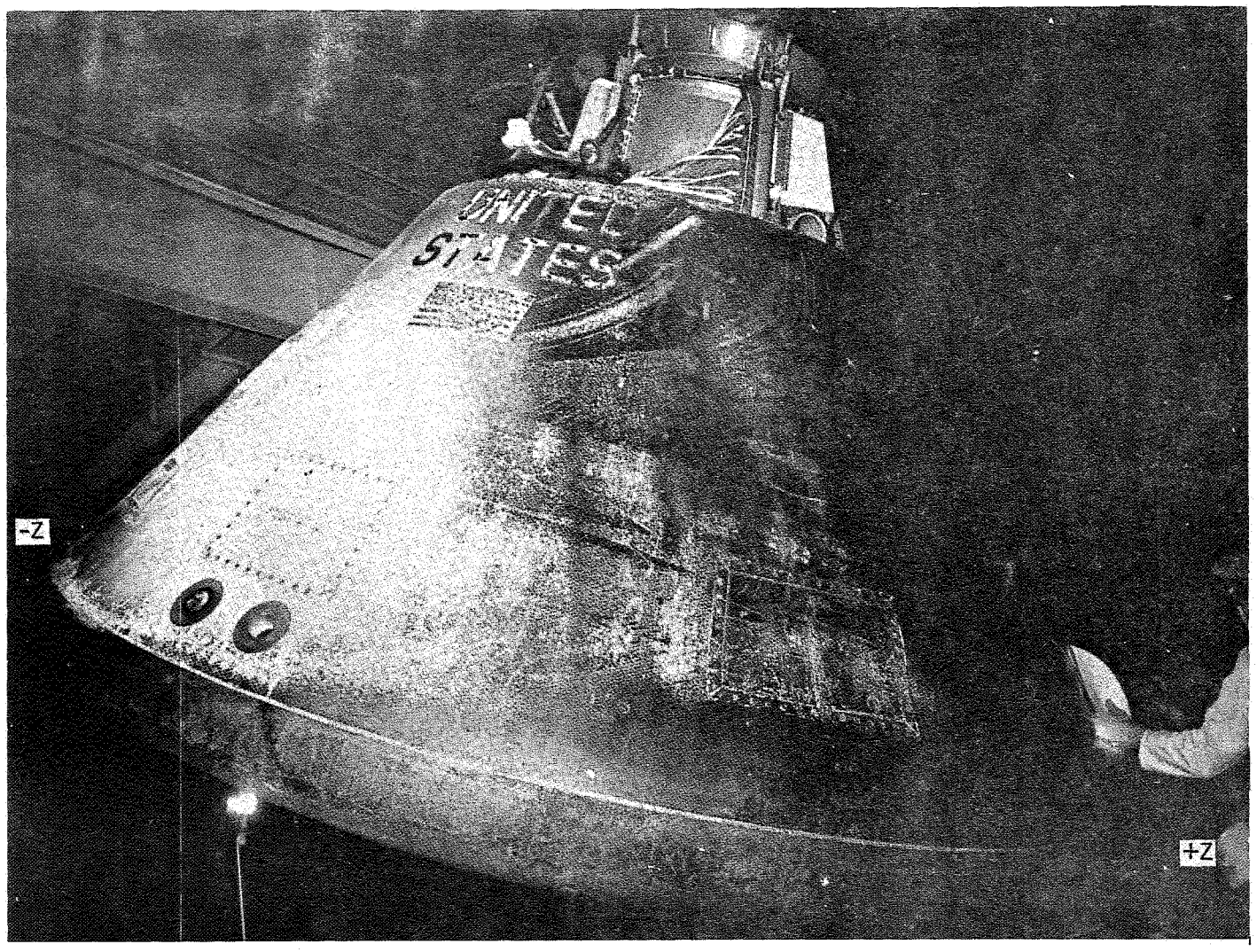


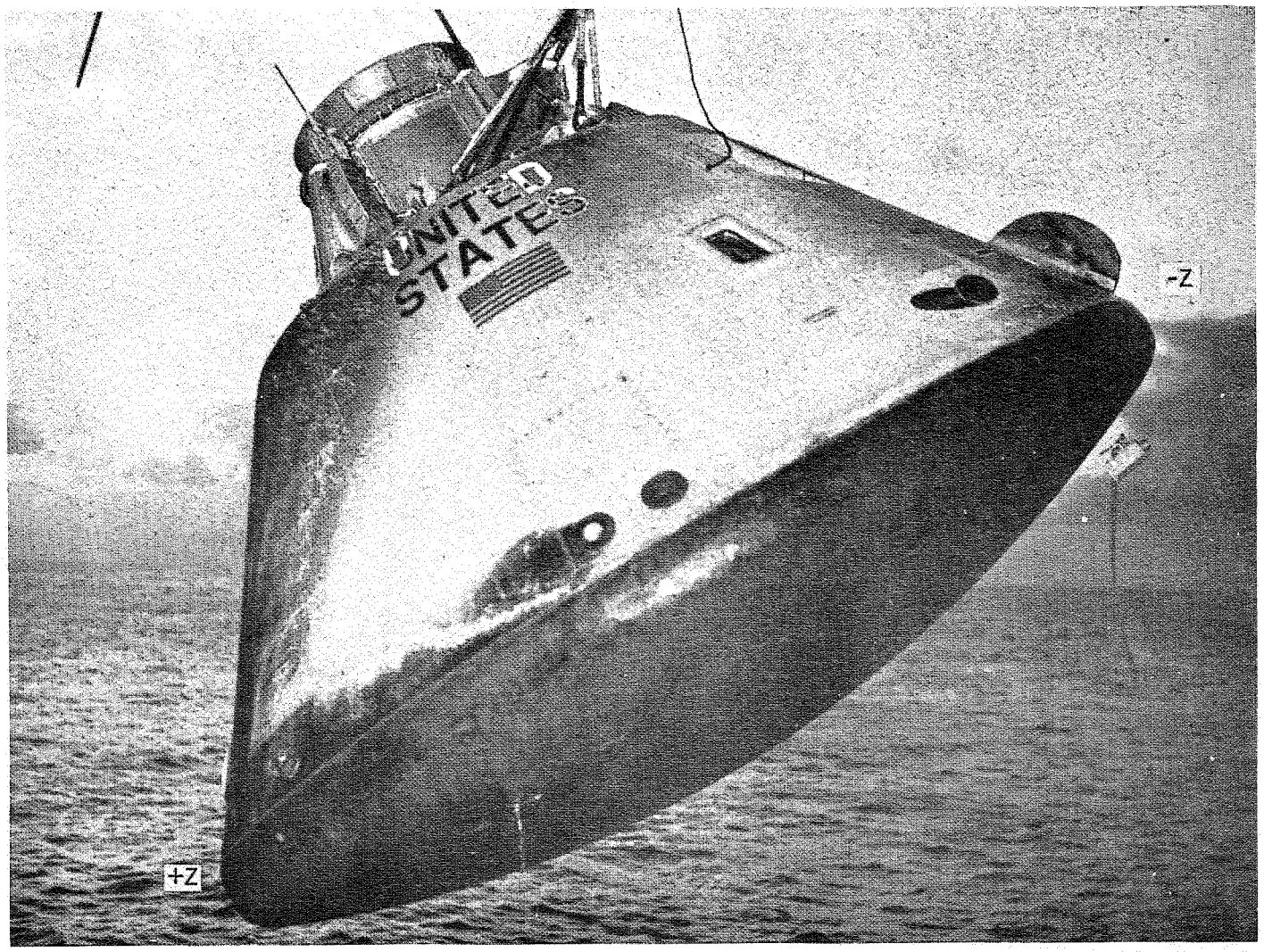
Figure 7.4-10.- Char and erosion around CM RCS system A roll engines after propellant depletion burn, Mission AS-201.

NASA-S-66-6251 MAY 6



(a) General view, +Z axis.

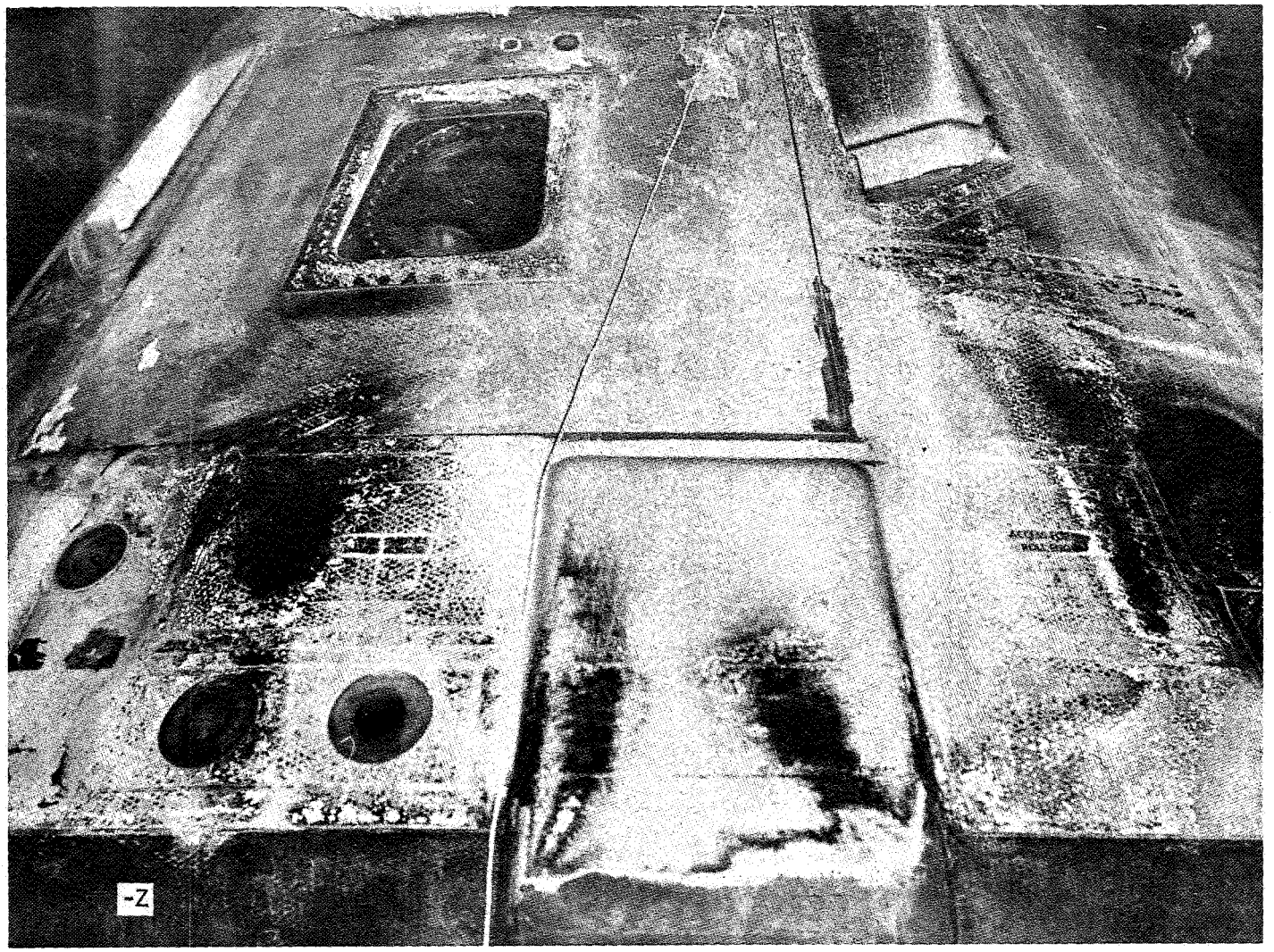
Figure 7.4-11.- Char condition of conical section, Mission AS-201



(b) General view, -Y axis

Figure 7 4-11 - Continued

NASA-S-66-6253 MAY 6



(c) General view, -Z axis.

Figure 7.4-11.- Concluded.

7.5 Mechanical Subsystems

Summary.- Components of the mechanical subsystems flown on Mission AS-201 included the canard subsystem, the uprighting subsystem, the deployment mechanisms for the recovery aids, the latching mechanisms for the side ablative, side pressure, and forward pressure 'hatches, a modified latching mechanism for the astro-sextant door, and an interim design latching mechanism for the boost protective cover (BPC) hatch. All components performed satisfactorily. The following paragraphs describe each component and its performance.

Subsystems description and performance.-

Canard subsystem: Mission AS-201 was the fifth mission to use the canard subsystem. This subsystem consisted of two deployable aerodynamic surfaces located between the forward end of the tower-jettison motor and the Q-ball assembly. A detailed description of the system is presented in references 6 and 7.

Since the launch-escape subsystem was not utilized in an abort mode during this mission, the canard subsystem was not required to function.

Uprighting subsystem: Mission AS-201 was the first mission to have an uprighting subsystem. The subsystem insures a proper flotation attitude of the command module (CM) after landing. An Apollo spacecraft is subject to floating in either of two trim attitudes: apex up (stable I) or apex down (stable 11) as shown in figure 7.5-1(a). The stable II attitude is unsatisfactory from the standpoint of recovery-aids performance, sea pickup; and for manned missions, crew safety, crew tasks, and postlanding ventilation. The uprighting subsystem is required to upright the command module to the stable I attitude if the command module should overturn because of impact dynamics or sea dynamics. The subsystem is not activated for spacecraft 009 unless the stable II position is sensed by an attitude switch in the postlanding sequence controller (PLSC).

The uprighting subsystem consists of three inflatable air bags stowed in two rigid metal canisters on the upper deck of the command module (figs. 7.5-1(b), 7.5-2, and 7.5-3). The design criterion requires that any two of the three bags when inflated must upright the command module. The bags are inflated by a motor-driven compressor located between the inner and outer structure in the aft compartment. Spacecraft 009 had only one compressor (near the +Y axis) as shown in figure 7.5-4. All subsequent spacecraft will have a second compressor also located in the aft compartment near the -Y axis. Also, the compressor case on spacecraft 009 was water-sealed externally with RTV; subsequent compressors will. have internal seals.

On Mission AS-201, the command module maintained the stable 1 attitude after Landing, and therefore the uprighting subsystem was not activated. Postflight inspection revealed no damage from contact with the earth landing subsystem (ELS) during parachute deployment. Also, the canisters remained latched and intact during flight and at landing.

Recovery aids deployment mechanisms: The deployment mechanisms for the postlanding recovery aids consisted of those used to deploy the VHF and HF antennas, the flashing light, and the sea dye marker/swimmer umbilical. All the mechanisms operated properly.

The deployment mechanisms for the antennas and flashing light were identical. Each was activated by a pyrotechnic cutter (section 7.10) actuated by means of a lanyard attached to the parachute riser. When the main parachutes were deployed, the lanyard pull caused the activation of the 8-second time-delay cutter device, which released the spring-operated deployment mechanisms. The deployment springs used on Mission AS-201 were of current Block I configuration which are stronger than the interim springs used on Mission A-004. The antennas and flashing light were located in the forward compartment as indicated in figure 7.5-2.

Postflight inspection of the antennas and flashing light confirmed that all had erected as planned, and examination of the mechanisms revealed no indication of damage during the flight or at landing. Signals were received from both VHF antennas after deployment on spacecraft 009. The flashing light as observed by the recovery forces was operating satisfactorily. Analysis of photographic coverage during recovery operations revealed that the light had a gross average flash rate of 12 flashes per minute, 2 to 3 hours after lauding.

The sea dye marker/swimmer umbilical deployment mechanism consisted of a rectangular canister which was spring loaded on a deployment platform located in the -Z bay of the CM upper deck (fig. 7.5-5). The sea-dye cake, contained in the canister, was not the present Block I cake. The Block I cake is required to last 12 hours after deployment, whereas the interim design cake used on spacecraft 009 would have lasted approximately 7 hours. The interim cake consisted of fluorescein dye with binder which was molded within a nylon mesh and then wrapped with water-soluble polyvinyl alcohol. In order to obtain a 7-hour life for the cake on spacecraft 009, many of the water-exposure holes in the canister were blocked by a shroud.

The deployment mechanism latch was triggered by a lanyard that was pulled when the HF antenna was erected after landing. The canister was deployed overboard by redundant springs but remained attached to the CM by a cable which included the swimmer telephone umbilical. Photographs taken from aircraft during recovery indicated that the size and color of

the slick formed by the sea dye marker were as planned. The lifetime of the dye marker was not determined.

Side ablative hatch-latching mechanism: The side ablative hatch is located on the -Z side of the outer structure of the CM conical surface. The hatch latches must retain the hatch in place to maintain the integrity of the structure and heat shield ablator. A detailed description is presented in section 5.5 of reference 9. The hardware was of a Block I design and was similar to that used on Mission A-004.

The side ablative hatch-latching mechanism performed satisfactorily on this flight in that the mechanism retained the hatch in place during flight and was operable after landing. Preflight torque required to latch the mechanism was not recorded, but difficulty was encountered during installation. The hatch edges had to be physically pushed in as the mechanism was latched. Postlanding torque required to unlatch the mechanism was 400 in-lb. The maximum operating torque should be 260 in-lb to either latch or unlatch the mechanism.

Side pressure hatch-latching mechanism: The side pressure hatch is located on the -Z side of the CM and relies on the inside cabin pressure for the "hard" seal against the CM inner structure. The hatch is held in place by machined edge members on three sides and a latch/release mechanism on the remaining side. A detailed description is presented in section 5.5 of reference 9. The hardware was a Block I design and was similar to that used on Mission A-004 except for the pinion gear as discussed in the following paragraphs. The side pressure hatch-latching mechanism performed satisfactorily for this mission in that the hatch remained latched during flight and released satisfactorily using the ground handling unit.

Before flight, lead tape had been applied to all the hatch edges to eliminate gaps between the hatch-seal surface and frame-seal surface so that an acceptable leak rate could be maintained around the hatch.

Several of the pinion gear teeth on the hatch-latching mechanism initially installed on the hatch were broken off during preflight ground handling (fig. 7.5-6). Because analysis indicated that a replacement pinion of the same material could present a similar problem during the final hatch installation of the launch countdown, the drive unit/pinion gear was replaced with the more ruggedly designed ground-handling drive unit. A new design will be incorporated on spacecraft 011 and subsequent spacecraft.

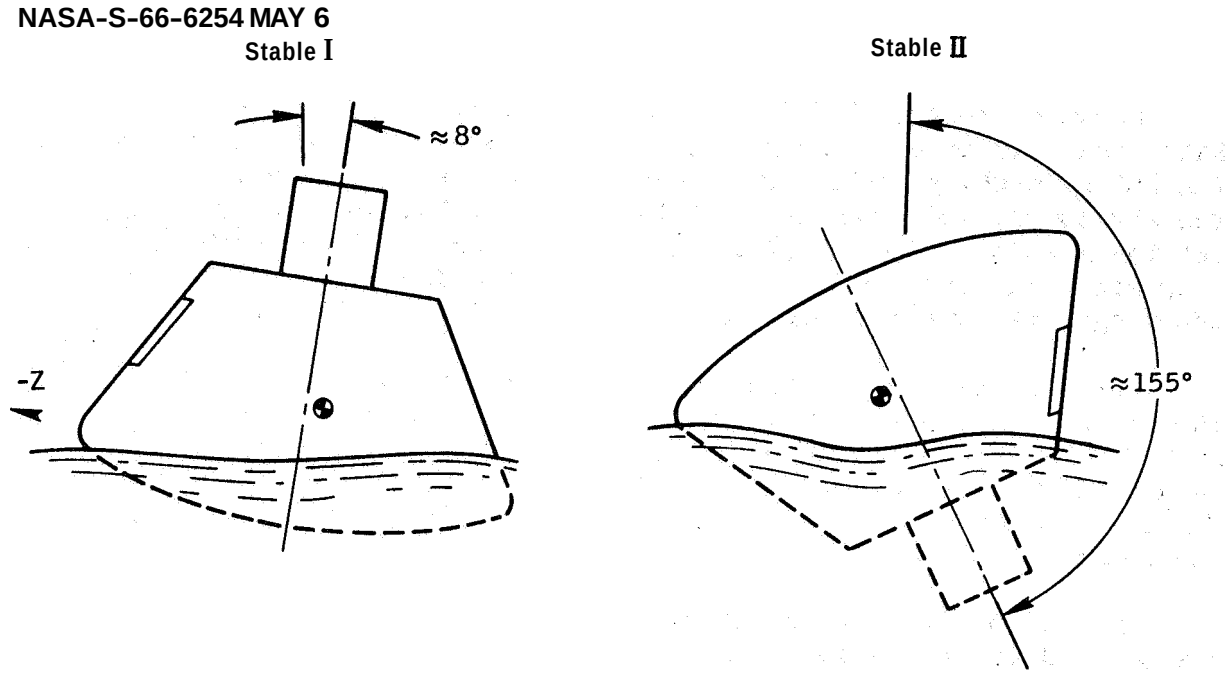
Preflight torque required to latch the mechanism was not recorded; but the mechanism required a torque greater than 600 in-lb to unlatch at recovery. The exact torque limit of the mechanism with the ground-handling unit was not known, but was considered to be greater than

1000 in-lb. The hatch was reinstalled and then removed a second time; both operations required 300 in-lb of torque.

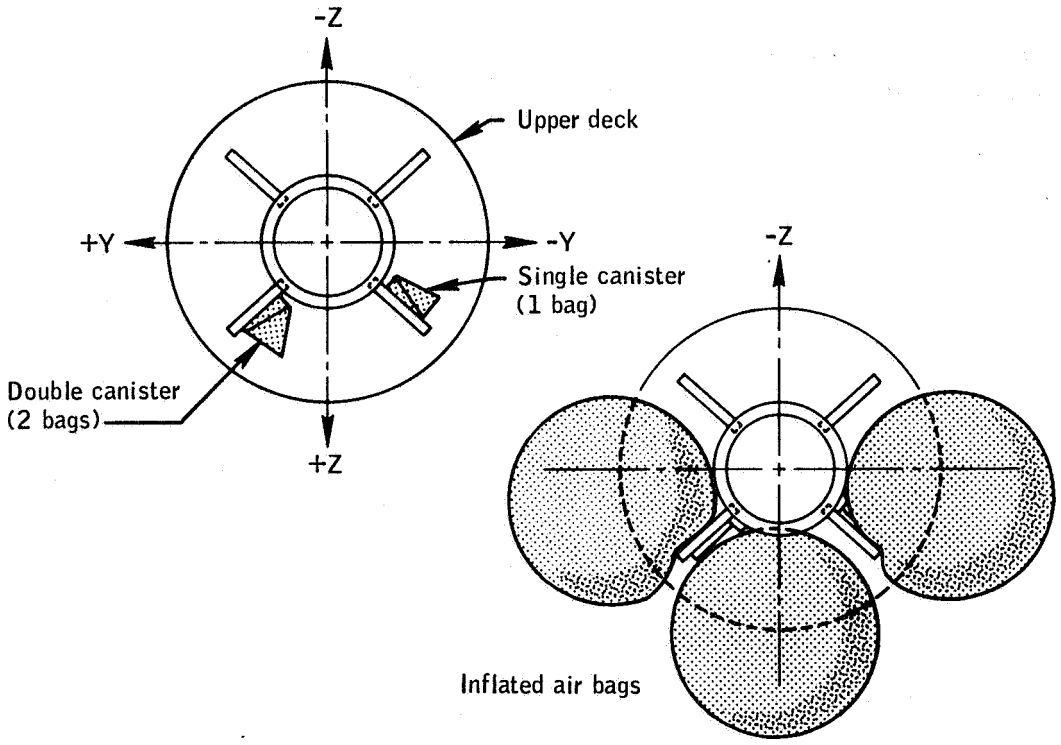
Forward pressure hatch-latching mechanism: The forward pressure hatch was located at the top of the tunnel on the upper deck of the CM. The hatch-latching mechanism locked the hatch in position to maintain the structural and pressure-seal integrity of the pressure vessel throughout the mission. The hatch provided a pressure seal seated by means of a breech lock configuration. A bolt-type looking mechanism retained the hatch against rotation and disengagement during the flight.

Astro-sextant door mechanism: The astro-sextant door mechanism of the command module was designed to latch and deploy the doors during manned missions. However, for Mission AS-201, only the latches were used, and these were not required to be operable at any time during the flight. The two latches satisfactorily held the doors in place during the flight.

BPC hatch-latching mechanism: The BPC hatch-latching mechanism hardware flown on Mission AS-201 was an interim design not intended for use on future spacecraft. No apparent problems occurred during flight with this configuration although during the preflight installation of the hatch, two of the multiple fasteners (of a quarter-turn, quick operating design) at the batch top broke loose and caused a small (1/8 inch) protrusion of the upper hatch edge for a length of approximately 6 inches. For flight, this protrusion was covered with three strips of tape.



(a) CM stable flotation attitudes.



(b) Location of air bags, stowed and deployed.

Figure 7.5-1.- CM uprighting subsystem, Block I, Mission AS-201.

NASA-S-66-6255 MAY 6

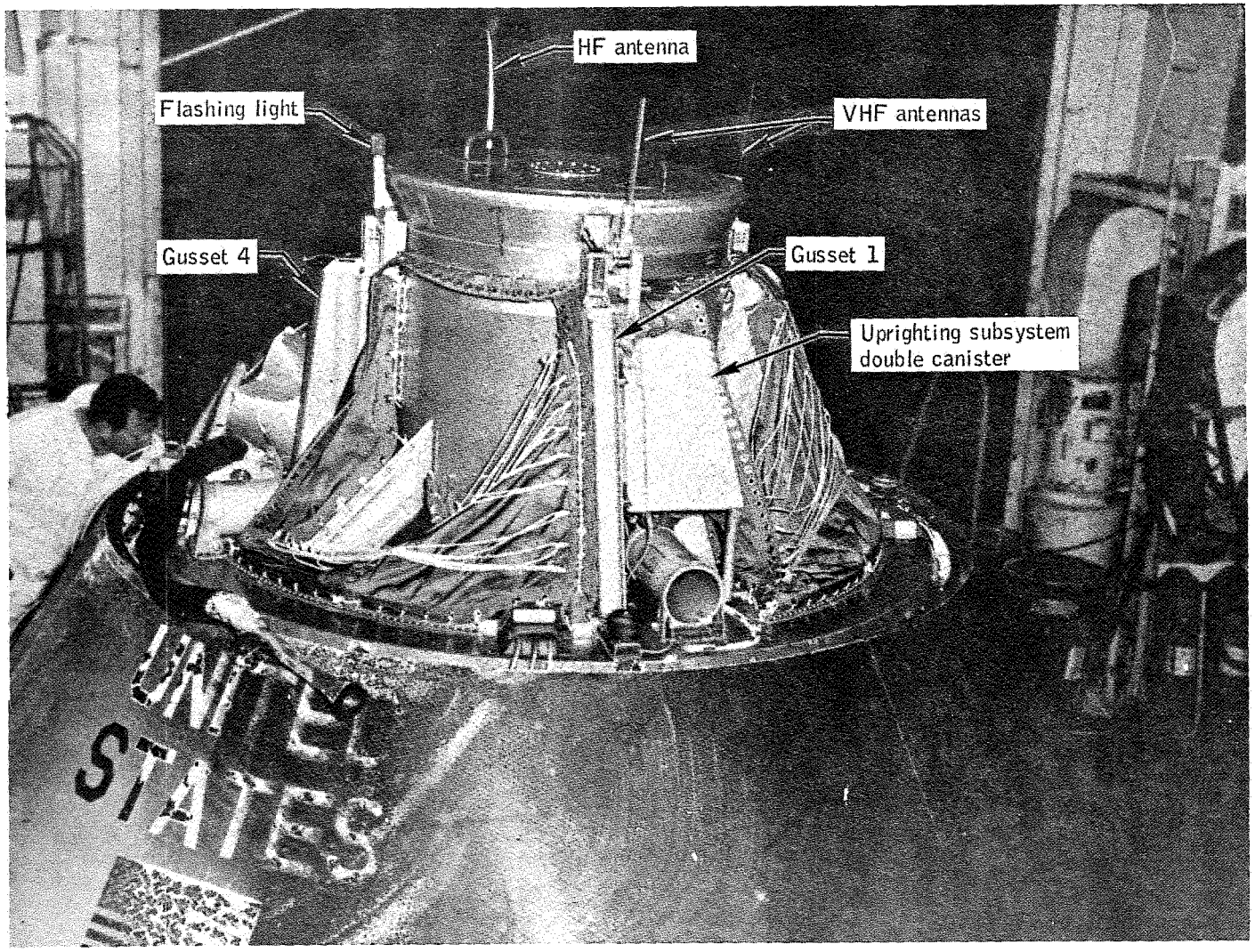


Figure 7.5-2.- Uprighting subsystem and recovery ≡Π components, Mission AS-201.

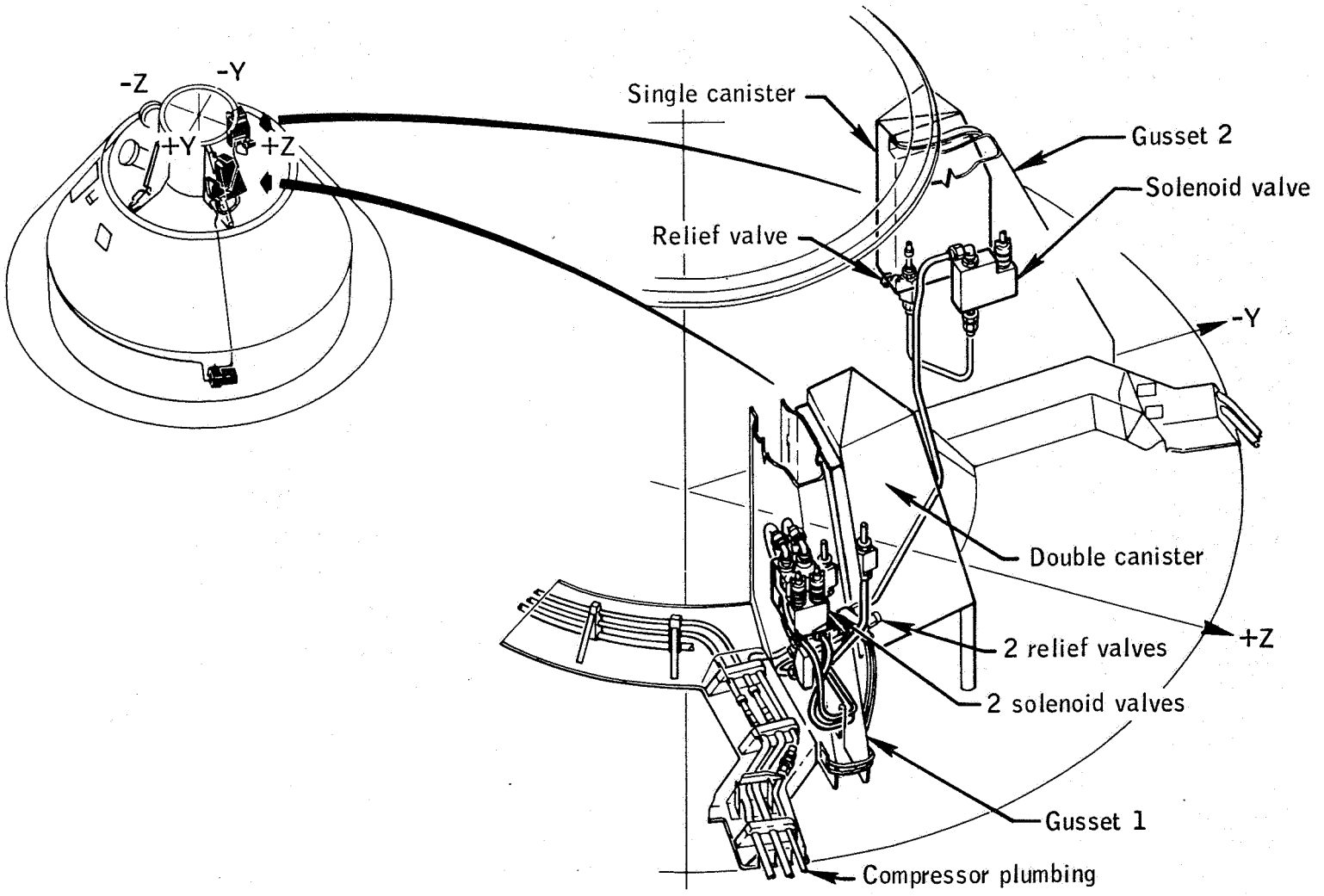


Figure 7.5-3.- Uprighting subsystem canister and valve location, Mission AS-201.

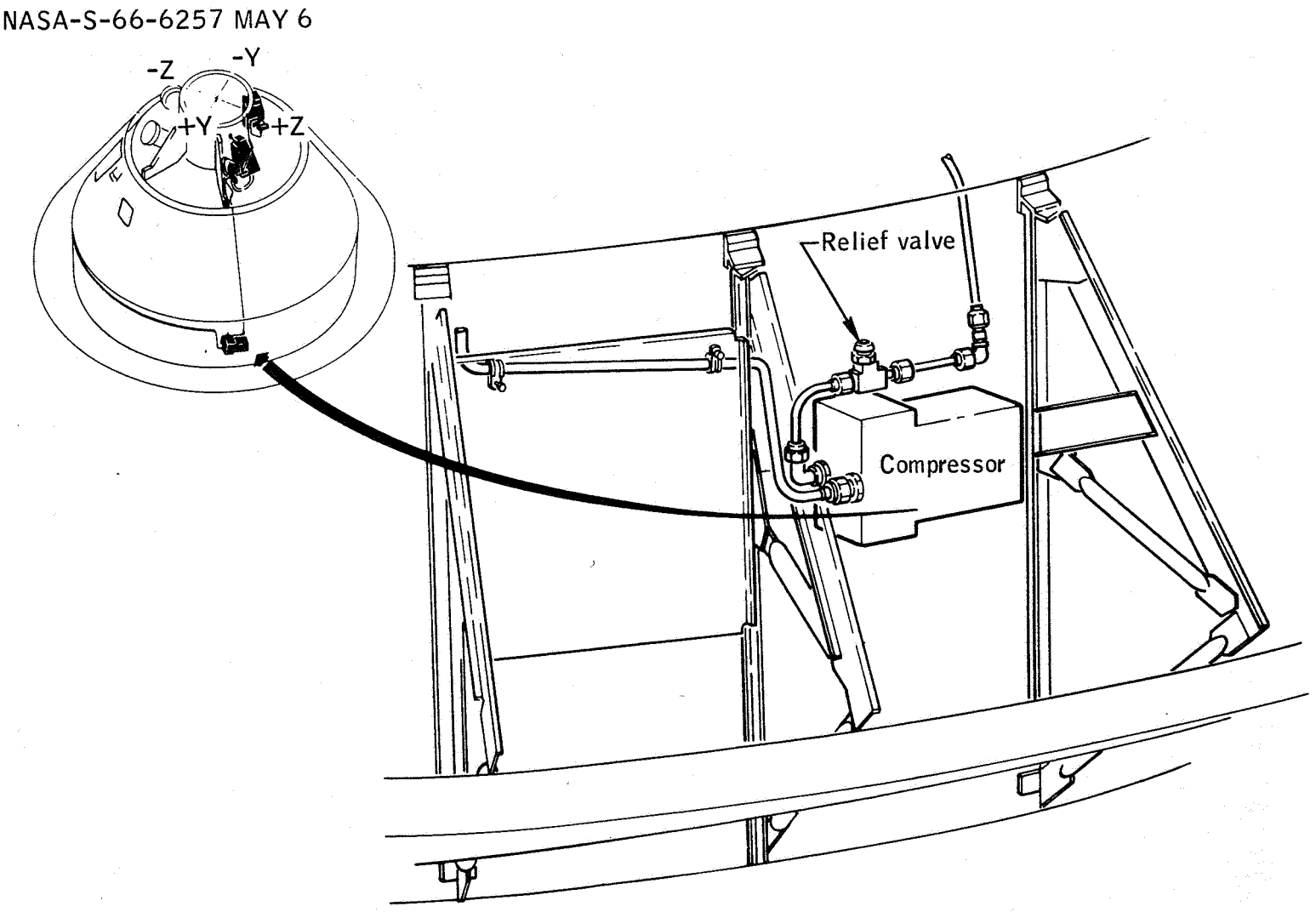


Figure 7 5-4 - Uprighting subsystem compressor location, Mission AS-201.

NASA-S-66-6258 MAY 6

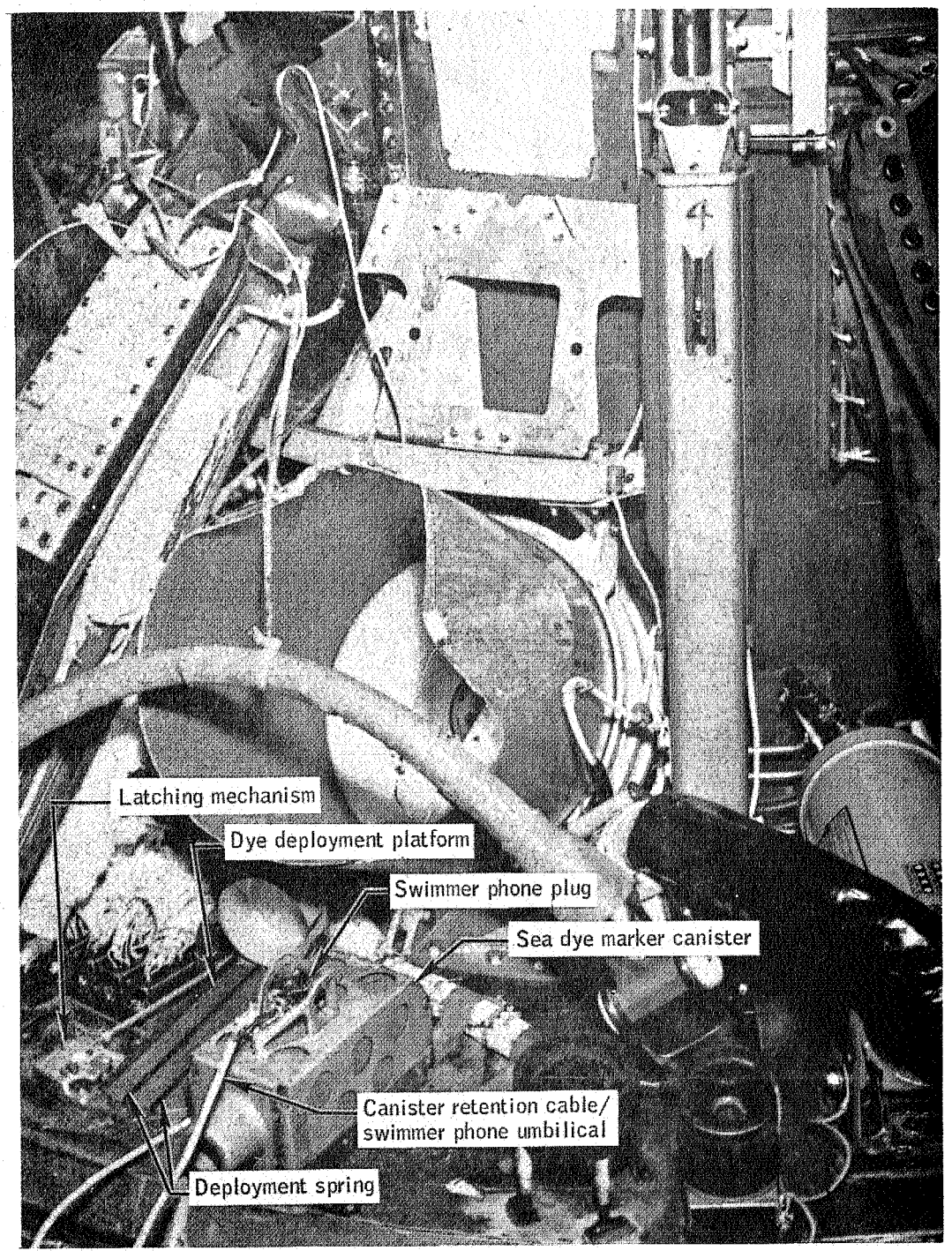


Figure **7.5-5.-** Sea dye marker canister and mechanism, Mission **AS-201.**

NASA-S-66-6259 MAY 6

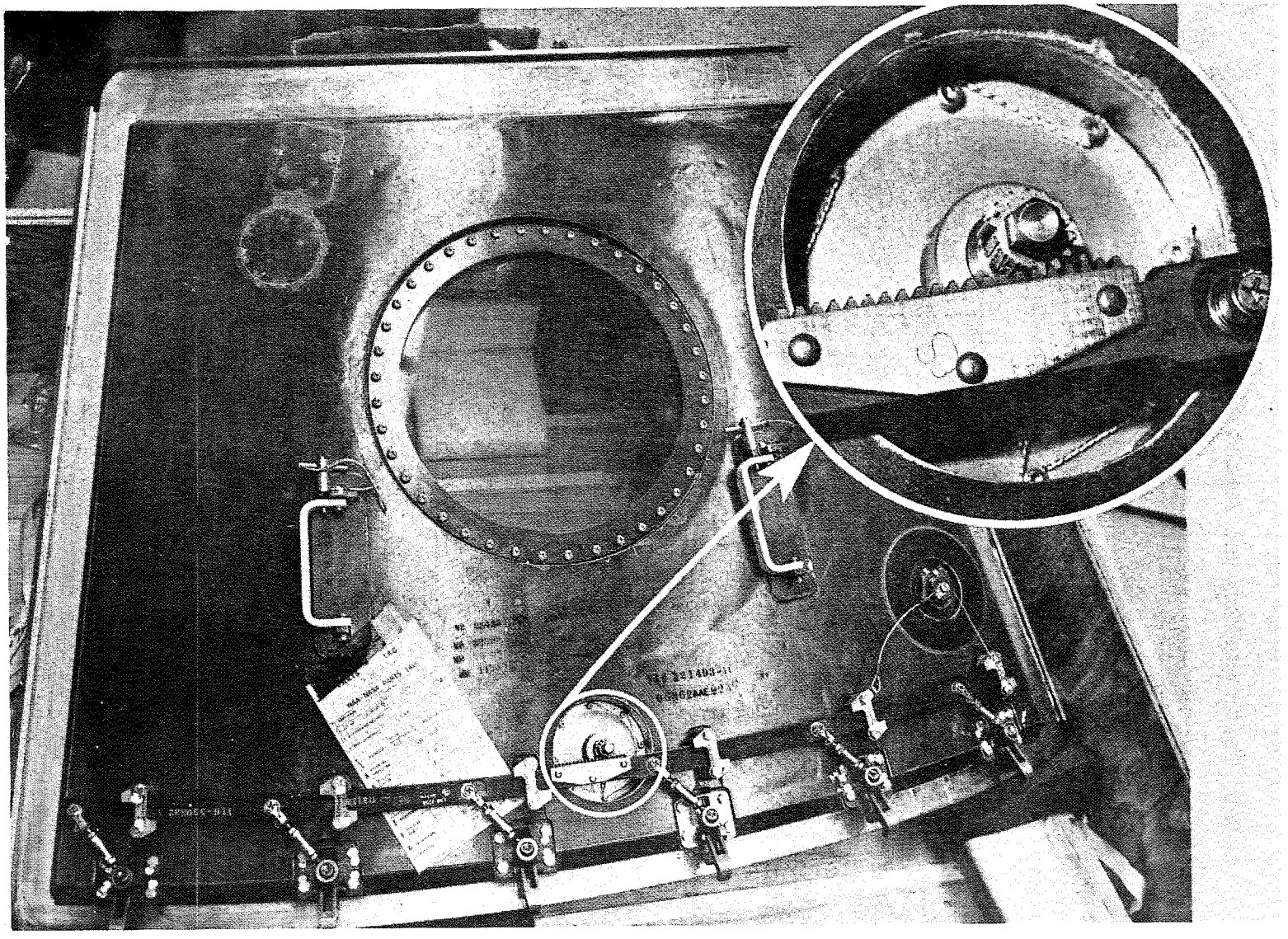


Figure 7.5-6.- Original pressure hatch pinion gear which was replaced with ground-handling unit for Mission AS-201.

7.6 Earth Landing and Impact Attenuation Subsystems

7.6.1 Earth landing subsystem.-

Description: The earth landing subsystem (ELS) used on this mission was of the same configuration as that flown on Mission A-004 and is described in the Mission A-004 Postlaunch Report (ref. 9). The exceptions to a Block I configuration are tabulated below:

Item	Mission AS-201	Block I
Drogue reefing line cutter lanyard knot	Two half-hitches	Chinese finger
Pilot parachute mortar lid	Retained	Expended
Pilot parachute deployment bag	Nylon	Dacron felt sleeve over nylon bag
Main parachute riser loop end boot	None	Dacron felt boot
Main parachute retention flaps	Nylon	High temperature nylon (Nomex) flaps with dacron felt liner

Operation of the ELS for Mission AS-201 was based on earth landing sequence controller (ELSC) baroswitch and logic functions. ELS functions are sequenced through two redundant ELSC's with crossover provided for all events except main parachute harness disconnect.

Performance: As planned for Mission AS-201 normal reentry recovery mode, closure of the high altitude baroswitches initiated logic power to the mission sequencer for initiation of forward-heat-shield jettison, and to the ELSC system A, starting the ELSC 2-second time-delay relay. Forward-heat-shield jettison occurred at Ti-1853.63 seconds, and drogue mortar fire was initiated after the ELSC 2-second time delay at T+1855.4 seconds. Drogue disconnect and pilot mortar fire were simultaneously initiated by closure of the low-altitude baroswitches at T+1908.4 seconds. Landing occurred at T+2239.7 seconds.

Main parachute harness leg no. 1 disconnect was initiated at touchdown by the ELS impact inertia switch through ELSC system A. Harness

leg no. 2 was not disconnected because no logic power had been received by ELSC system B (see section 7.12). Crossover circuitry for main parachute harness disconnect is not provided in order to preclude inadvertent disconnect of both harness legs prior to landing.

ELS event times were obtained from bilevel event data. No visual, optical, or radar reference data were available to evaluate ELS performance prior to landing.

A qualitative judgment was made of the spacecraft ELS dynamic performance by analyzing the amount of contact between components of the ELS and the spacecraft upper deck structure. Absence of marks from drogue cable risers on the tunnel lip indicated that the spacecraft was in the favorable attitude of aft heat-shield-forward at the time of drogue parachute deployment. Minimal contact of the main parachute harness legs with the drogue mortar cans and absence of evidence of undue abrasion on the main parachute deployment bags, uprighting system canisters, longerons, or tunnel also indicated a favorable attitude of aft heat-shield-forward at the time of main parachute deployment.

All ELS components appear to have functioned properly and the ELS successfully landed the spacecraft. The drogue and main parachutes were not recovered (see section 9.3).

6.2 Impact attenuation subsystem. -

Description: The Block 1 type impact attenuation subsystem used in Mission AS-201 was of the same configuration as reported in reference 9 for Mission A-004 except for the deletion of the lockout devices on the four X-X struts.

Lockout devices are provided on manned flights to prevent strut stroking under inflight loads and vibrations and to allow stroking to occur at lower accelerations on landing. Lockout devices were used on the unmanned abort Mission A-004 because the high pallet weight, when combined with expected high tumbling and landing accelerations, could result in loads that would stroke the unmanned strut. For Mission AS-201, spacecraft 009 had a pallet weighing 540 pounds and was qualified for a 20g reentry and landing load.

The strut stroking load for the unmanned X-X and Z-Z struts on spacecraft 009 was developed through the crushing of aluminum honeycomb and a friction device as illustrated in figure 7.6-1 and could operate in either tension or compression. The Y-Y strut load on spacecraft 009 was developed by the crushing of aluminum honeycomb alone, and operated only in compression.

The operation and attenuation capacity of the struts is indicated by the load stroke curves (fig. 7.6-2) as follows: The initial stroking load, for either the X-X or Z-Z struts, is developed by core crushing and friction. As long as a sufficient load is present the stroking in the applicable direction continues. If the vehicle were overturned, putting the load. on the struts in the opposite direction, the return load would be provided only by the friction device until honeycomb was encountered at the initial position of the strut piston. If the vehicle were to overturn again so that the load would be in the original direction, the friction device would again supply the load until the remaining core material was encountered, at which time the load would return to the initial stroking load. This cycle can continue until all core is crushed.

It is planned that the unmanned struts are to be used in spacecraft 011 (same as for spacecraft 009), and manned struts, with lockouts, are to be used on all manned flights, including spacecraft 012. The basic components are identical in the manned and unmanned struts with only the addition of lockout devices and a slightly lower stroking load being used in the manned struts.

Acceleration data at the time of landing for Mission AS-201 were lost. However, as no stroking of the struts occurred during the mission, landing accelerations must have been below 20g in the X axis, 14g in the Z axis, and 4g in the Y axis.

NASA-S-66-3260 MAY 6

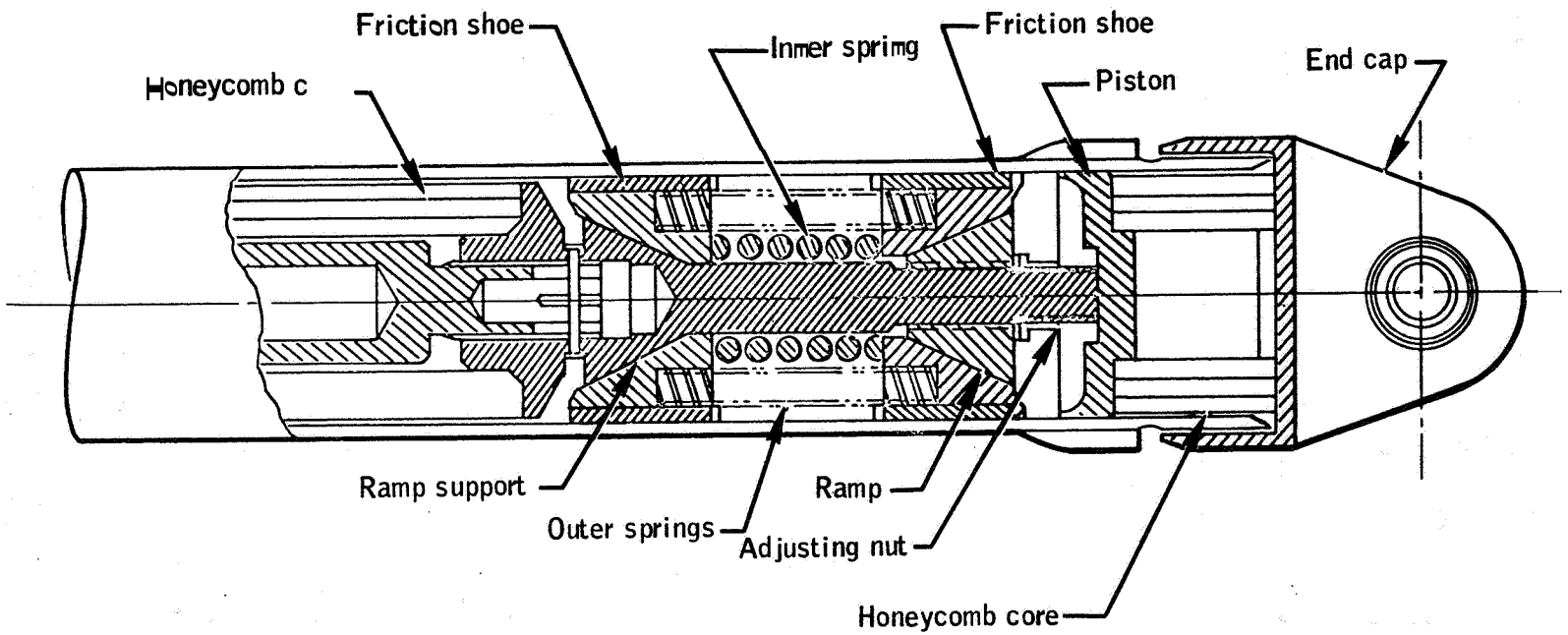


Figure 7.6-1.- Strut impact load mechanism, Mission AS-201.

NASA-S-66-6261MAY 6

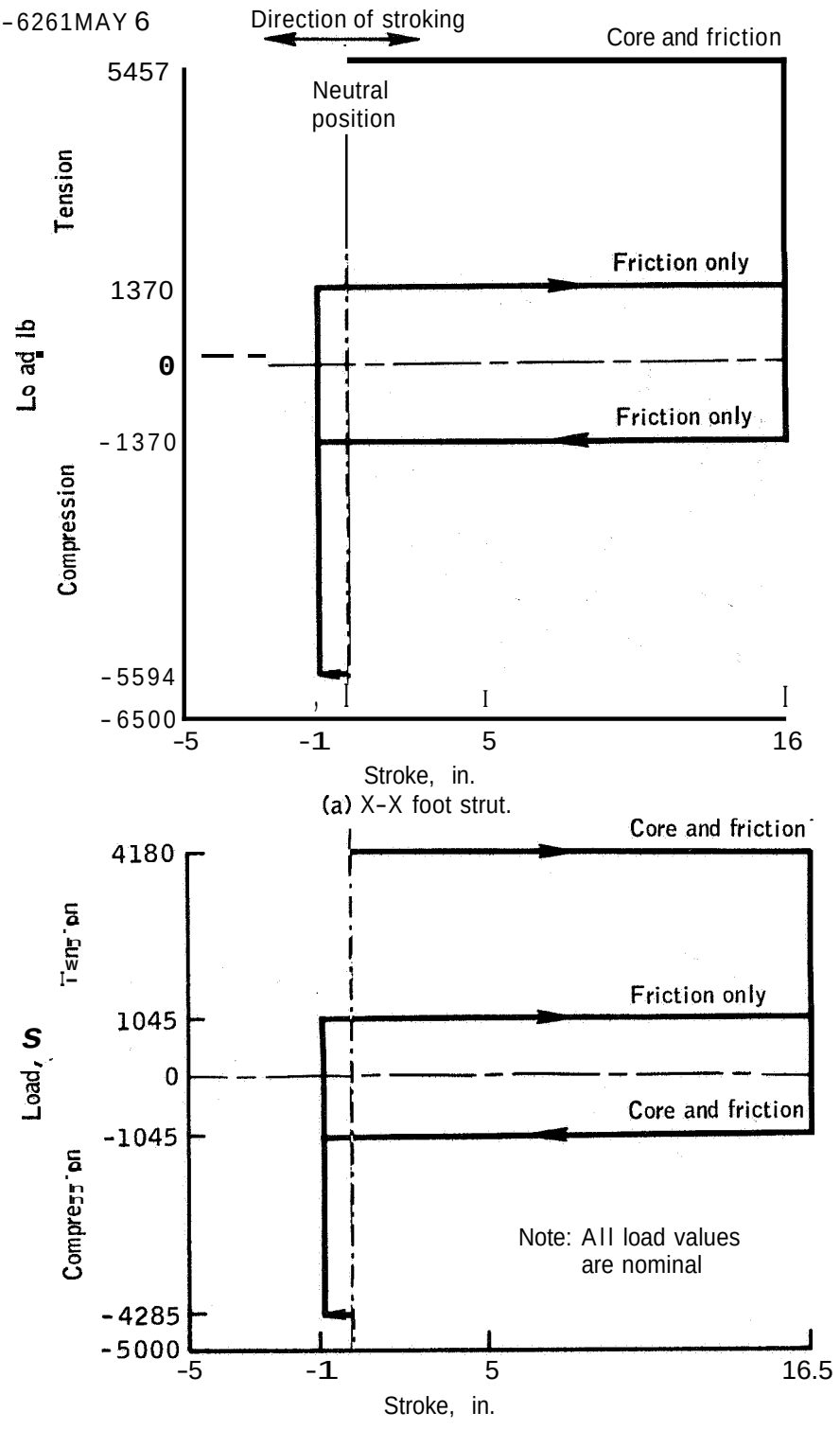
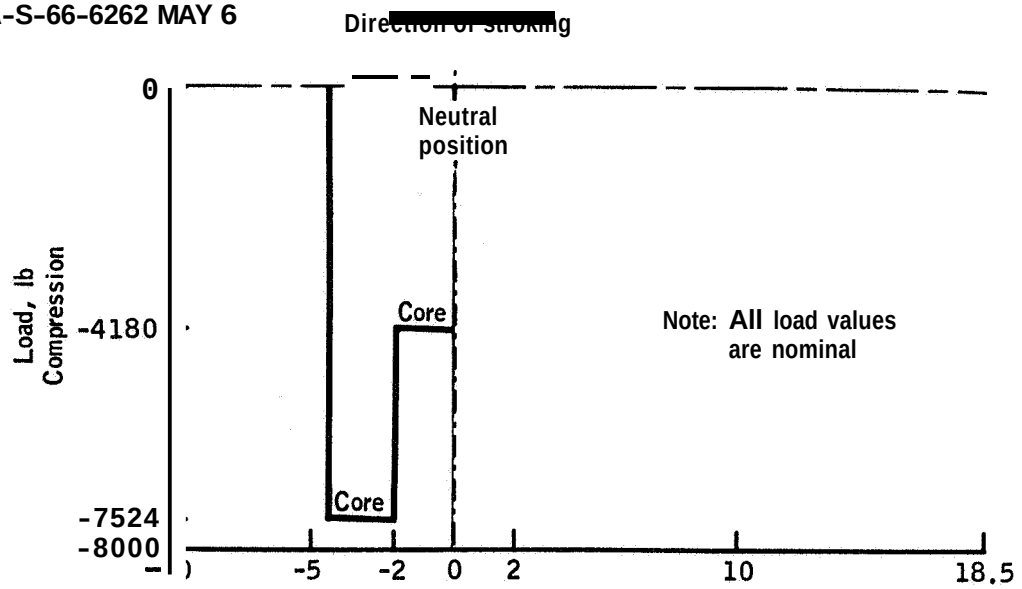
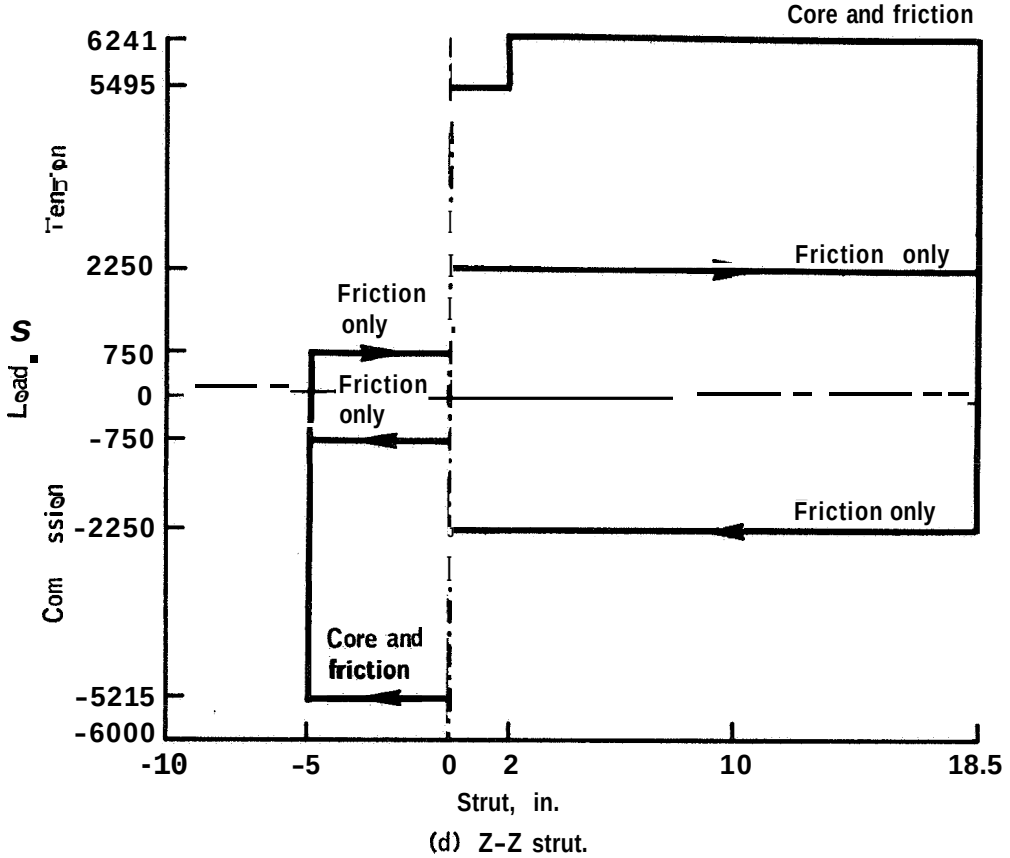


Figure 7.6-2.- Impact attenuation strut design load - stroke curves for unmanned mission, Mission AS-201.

NASA-S-66-6262 MAY 6



(c) Y-Y strut.



(d) Z-Z strut.

Figure 7.6-2.- Concluded.

7.7 Service Propulsion Subsystem

Summary.- Mission AS-201 was the first flight test of the service propulsion subsystem (SPS): One of the primary objectives of the mission was to verify SPS operation for a minimum of 20 seconds after at least 2 minutes in a space environment and verify restart capability.

The first burn of the SPS was initiated at T+1211.2 seconds. Although +X ullage translations by the service module reaction control subsystem (SM RCS) produced 25 to 45 percent of the ullage thrust expected (section 7.9.1), first burn ignition transients and performance of the SPS for the first 80 seconds of the burn were nearly nominal (fig. 7.7-1). The chamber pressure and oxidizer interface pressures were 2 psia and 3 psia below the minimum specification limits, respectively, after the transition from ignition transient to steady-state operation. The duration of the first burn was approximtely 184 seconds. However, SPS chaniber pressure had decayed (from nominal at 80 seconds) to approximately 70 percent of nominal at the time of engine shutdown. Engine shutdown was initiated by the control programer timed backup command rather than by the normal AV counter because the desired AV had not been achieved within the allotted time (table 7.7-I and section 7.11).

An erratic restart and second SPS burn of approximately 10 seconds in duration followed (fig. 7.7-2). The first 5 seconds showed chamber pressure oscillations to a low of 12 psia (102 psia nominal). The engine showed tendencies to recover for about 4 seconds, but then chamber pressure again decayed to about 70 percent of nominal at the time of engine shutdown.

The abnormal performance was primarily due to helium ingestion into the engine oxidizer feed line. The helium ingestion was made possible by the existence of a leak in the standpipe to the zero g propellant retention reservoir from which the engine oxidizer feed line was supplied. The leak had been observed previously in preflight tests.

Preflight test procedures and action guidelines are being studied for revision to insure the preflight integrity of the system for future missions.

An oxidizer storage tank pressure drop after each SPS firing termination was shown by the flight measurements, and no oxidizer crossover from storage to sump tank was evidenced during the first firing. These two observations indicated that a storage to sump tank pressure drop mechanismwas present. The cause of this pressure drop is hypothesized to be two-phase, two-component fluw between the storage and sump tanks.

Other than the abnormal conditions indicated, performance of the SPS was nominal. No rough combustion was recorded by the engine vibration monitors.

Description.- The Apollo spacecraft service propulsion subsystem (SPS) provides the thrust required for large changes in spacecraft velocity after spacecraft separation from the Saturn S-IVB.

The SPS for Mission AS-201 included the engine and nozzle assembly, propellant storage and transfer components, and the pressurization equipment (fig. 7.7-3). The propellant gaging equipment and propellant utilization control valves were omitted for this mission.

The SPS engine was a non-throttleable, restartable, liquid bipropellant, pressure-fed rocket engine designed to produce 21 500 pounds of thrust in a vacuum. The engine and nozzle assembly included an ablative combustion chamber, a radiation-cooled expansion nozzle, an aluminum injector, a thrust and gimbal mount, gimbal actuators, fuel and oxidizer propellant feedlines and pneumatic-operated valves.

The hypergolic propellants for the SPS were a 50:50 blend of UDMH and hydrazine for fuel, and nitrogen tetroxide (N_2O_4) for the oxidizer. Two oxidizer and two fuel tanks (upstream tanks being storage tanks, the downstream being sump tanks) are utilized for propellant storage. For Mission AS-201, the propellant load, being only 28 percent of capacity, was loaded in the sump tanks.

The high pressure helium supply required to pressurize the propellant tanks was contained in two spherical pressure vessels, each with a volume of 19.4 cubic feet. Each vessel was filled to a pressure of 4000 psia ± 50 psi, and both vessels were connected to a common helium distribution line. Two solenoid-operated valves, installed in parallel downstream of the helium storage vessels, isolated the helium supply when the propulsion system was inoperative. Helium pressure was regulated by parallel pressure regulator assemblies, which reduced the helium pressure to 185 psia ± 4 psi. Downstream of the helium pressure regulators, parallel check-valve assemblies were installed to prevent the backflow of propellants or vapors into the pressurization lines.

Gaseous nitrogen (GN_2) for the engine pneumatically operated valves was contained in two spherical storage tanks, one for the primary valves and one for the secondary valves. Tank pressure for the GN_2 was 800 ± 25 psia.

All SPS components were certified for the short duration mission. Critical problems encountered during the buildup, static firing, and subsystem checkouts at Kennedy Space Center (KSC) are shown in table 7.7-II.

Propellant and gas servicing, accomplished from T-10 days to T-4 days, is indicated in table 7.7-III, and the results of the analyses of the materials loaded are presented in table 7.7-IV.

During the preparation for flight readiness firing on T-99 days, it was discovered that oxidizer from the loaded sump tank had leaked into the storage tank by way of the helium standpipe and crossover line. Oxidizer interface pressure indicated that a fluid crossover occurred during the flight readiness test. (See table 7.7-V.) All other measurements of the subsystem showed normal conditions, including pneumatic and solenoid valve positions.

The expanded life status of time/cycle sensitive components at the time of launch is shown in table 7.7-VI.

Performance.- Figures 7.7-4(a), (b), and (c) show the behavior characteristics of the SPS critical measurements through the S-IB and S-IVB boost phases.

Figure 7.7-4(c) shows the effects upon the propellant pressures by the various g fields experienced through the S-IB and S-IVB phases. Comparison of the oxidizer interface pressure and the oxidizer tank pressure, under the several g fields with those same parameters for the fuel side, indicates the movement of oxidizer into the storage tank from the sump tank during boost. Figure 7.7-5 shows the arrangement of the oxidizer retention reservoir. (Also see fig. 7.7-3.)

At each of the zero g conditions a certain amount of the storage tank propellant was transferred back to the sump tank by way of the crossover line and standpipe (data quality prevents exact calculations). However, a positive amount of oxidizer was indicated as being transferred and retained in the storage tank after the boost phase.

Between S-IVB separation and SPS ignition, no unexpected changes in any of the SPS measurements occurred. Table 7.7-VII lists the SPS temperature and pressure measurements at approximately 11 seconds before the first burn.

Steady-state first SPS operation: The first SPS burn can be broken into two distinct periods. From ignition at T+1211.2 seconds to approximately T+1291 seconds, the performance was about as expected with indicated chamber pressure and oxidizer tank and inlet pressure slightly low. The 20-psi pressure drop between oxidizer storage tank and oxidizer inlet pressure was similar to the normal pressure drop in the flight support firing tests at the White Sands Test Facility with spacecraft 001. These values are summarized in table 7.7-VIII.

During the remainder of the burn a definite degradation of oxidizer and fuel inlet pressures, chamber pressure, and oxidizer feed line temperature (see fig. 7.7-6) occurred together with a marked increase in pressure oscillations.

The faired plot of the chamber pressure during the first burn, indicated slightly low values (98 psia compared to expected 102 ± 2 psia) during the first 80 seconds (fig. 7.7-1). At T+1290 seconds, the chamber pressure began to drop rapidly, reaching 84 psia at T+1294 seconds, gradually climbed to 88 psia at T+1318 seconds, then began a downward trend to an indicated 69 psia for the last 15 seconds prior to shutdown. Increasing chamber pressure oscillations were experienced from T+1318 seconds to shutdown. The maximum oscillation reached just prior to shutdown was approximately ±9 psia. Oxidizer tank pressure, oxidizer interface pressure, fuel tank pressure, and fuel interface pressure during the first bum are presented in figure 7.7-7.

Helium tank pressure, divided by absolute helium tank temperature (fig. 7.7-8) maintained a steady decline until approximately T+1291 seconds (the time of chamber pressure drop), when the decrease deviated from the normal straight line function and became increasingly steeper, indicating increased helium consumption.

An accelerometer mounted on the injector indicated a vibration of ±10g to ±15g throughout the first burn except for two spikes (possibly pops) of ±40g at T+1385.3 seconds and T+1385.8 seconds. Ignition vibration levels were ±65g maximum, which was within the ±90g specification value, and in agreement with results of spacecraft 001 firings at White Sands Test Facility.

Two modes of shutdown were provided in spacecraft 009: AV cutoff when the desired 4570 ft/sec velocity change had been obtained, and a backup command shutdown based on total burn time. Because of the abnormal performance of the SPS the desired velocity was not achieved and engine shutdown was initiated by the control programer backup command (see section 7.11) with a AV of approximately 863 ft/sec yet to be gained.

When the helium isolation valve was closed at engine shutdown, the oxidizer tank pressure measurement, located just downstream of the helium check valve, showed an immediate drop from 174 psia (during helium flow) to 158 psia, representing the oxidizer ullage pressure. A very small drop was expected. However, a drop of this magnitude under the existing conditions would be the result of helium loss from the oxidizer tanks during the burn. In addition, there were small Y-axis and Z-axis accelerations which could result in sloshing or vortexing of the propellants. There was no indication that a clean crossover ever occurred during the burn. This was probably due to sloshing or vortexing such that a small

intermittent inflow of oxidizer from the storage tank into the crossover line existed during both firings. This could cause a two-phase, two-component flow pressure drop (ref. 16). At engine shutdown at zero g conditions, the tank presaures would equalize when fluid flow stopped; however, the tank pressure drop occurred when the helium isolation valves were closed rather than at 300 msec later, as would be expected, when the propellant valves closed.

Coast period: During the coast conditions between first and second SPS burns (T+1395.2 sec to T+1410.7 sec), all parameters were about as predicted except for the oxidizer tank and the oxidizer interface pressures (table 7.7-IX) mentioned previously.

Second SPS steady-state operation: The second SPS burn was very erratic. Chamber pressure (fig. 7.7-2) oscillated radically during the second burn, reaching a low of 12 psia, then recovered slowly to about 95 psia, only to fall again to 73 psia by the time shutdown was initiated.

Oxidizer interface pressure fluctuated between approximately 148 psia and 103 psia for 2 seconds after ignition (fig. 7.7-9); recovered to 145 psia for approximately 3 seconds then began decaying erratically, reaching a minimum of 106 psia at T+1416 seconds (5 sec into the second burn). Then the interface pressure started to recover and reached a maximum of 148 psia at about T+1420 seconds. After shutdown, the interface pressure stabilized at 156 psia.

At ignition, the oxidizer tank pressure increased approximately 8 psi from 158 psia, then climbed erratically to 175 psia (fig. 7.7-7). At the second SPS shutdown, the pressure again dropped, this time to approximtely 157 psia. The helium regulator performed normally under the existing flight conditions.

Fuel tank pressure decreased from 172 psia to 168 psia during the first 5 seconds of operation, rising again to 173 psia after about 6 seconds from ignition (fig. 7.7-10).

Fuel interface pressure reacted in a manner similar to oxidizer interface pressure, although at much less amplitude (fig. 7.7-10). A low of 137 psia was measured at T+1415 seconds (4 sec into the second burn). At T+1418 seconds, it had recovered to 150 psia and held steady for 2 seconds before starting to decay prior to shutdown.

The changes, or fluctuations, in fuel tank and fuel interface pressures resulted from the chamber pressure fluctuations. The fuel flow increased with the decreased chamber pressure and the fuel interface pressure reacted inversely to the fuel flow rate.

Temperature measurements were taken in both the oxidizer and fuel feed lines. Fuel temperature remained constant throughout both SPS operations. The oxidizer experienced an unanticipated drop in temperature during the first burn (fig. 7.7-6) and rapid fluctuations in temperature throughout the second burn. During the second burn, two temperature cycles occurred with maximum and minimum readings of 64" F and 55" F for one cycle, and 65° F and 59° F for the other. The dip to 55° F occurred slightly before the low points on both chamber pressure and oxidizer interface pressure. It is thought that the dips in oxidizer temperature measurements occurred because helium bubbles, which were 10° F to 20" F cooler than the oxidizer, were present in the oxidizer feed line.

During the second burn, the accelerometer mounted on the injector recorded nominal vibration levels during ignition, a ±65g peak, damping to ±10g through the first 5 seconds. At 5.2 seconds after ignition, a ±20g peak occurred which damped to ±10g and remained there until shutdown.

Ignition and shutdown transients: Figures 7.7-11 and 7.7-12 show chamber pressure start transients for the first and second SPS firings in Mission AS-201.

The first firing exhibited excellent start transients for all affected parameters. All transient characteristics were typical and normal with the exception of slightly low chamber and oxidizer interface pressures. Analysis of flight data has indicated low effective longitudinal thrust (25 to 45 percent) by the SM RCS during the propellant settling (ullage) maneuver prior to SPS ignition. The nominal SPS first ignition transients indicated a satisfactory demonstration of the functioning of the propellant retention reservoir (zero g can) under these conditions. The first ignition impulse resolved into a starting impulse of 235 lb-sec, a value well within the specification tolerances.

The second engine ignition was erratic and stabilized burning was not reached. No valid starting impulse value could be determined. Figure 7.7-12 shows an initial chamber pressure drop almost immediately after the pressure rise had started.

The erratic second ignition was not due to poor propellant valve timing. Figures 7.7-13(a) and (b) show that the propellant valves opened normally except for valve 4, which opened in approximately 450 msec. Since the minimum feed line opening time is 250 msec, this fast value was not a problem.

Figures 7.7-14 and 7.7-15 show the chamber pressure shutdown transients for both SPS firings. Both shutdowns were determined to be good considering that both were initiated from an oscillating engine chamber

pressure condition and were initiated from a low level of chamber pressure. The pneumatically operating propellant valves shutdown sequence operated within specifications (figs. 7.7-16(a) and (b)).

No shutdown impulses were calculated since the shutdown initiation conditions were so far off nominal as to make comparison of flight to static test shutdown impulses meaningless.

Thrust characteristics: An empirical best estimate of propulsion parameters analysis was conducted with the SPS data to determine the actual flight thrust and specific impulse values (ref. 17). This approach used the vehicle thrust-acceleration as the controlling parameter to determine propulsion performance.

The ΔV remaining to be gained (CH3184) was the only parameter available to determine the thrust acceleration of the spacecraft. This particular measurement had a resolution of 55 ft/sec, and exhibited considerable scatter when differentiated to arrive at acceleration. The SPS thrust determined by this analysis was 21 668 pounds thrust at a 2.02 oxidizer to fuel mixture ratio during the first 80 seconds of burn. This was within specification limits (21 500 lb ± 400 lb).

The resolution of specific impulse (I_{sp}) from the data was ±10.3 seconds, which is greater than the specification tolerance. The analytical engine model used in the analysis was invalid for times after the first 80 seconds of burn, because after this time chamber pressure was governed by factors other than the normal mechanisms of tank pressures, inlet pressures, and line resistances (fig. 7.7-17). As a result, accurate values for SPS thrust, I_{sp}, mixture ratio, and flow rate are not available beyond the first 80 seconds of operation.

Malfunction analysis: Twenty-eight probable malfunction modes were investigated. Initial analyses determined that the probable malfunction modes would be confined to the oxidizer feed side of the system, since the fuel engine interface pressure was governed by the chamber pressure while the oxidizer interface pressure was not (ref. 17), and that fuel tank pressures were nominal throughout the mission. The malfunction mode was required to fit within the following boundary conditions:

(a) The engine fuel interface pressures, measured in flight, were the result of the reduced chamber pressure.

(b) Fuel flow was in an "all liquid" state.

(c) Oxidizer engine interface pressure was at a lower value than would be caused by low chamber pressure.

(d) No engine damage or excessive throat erosion occurred since the engine performance recovered to near nominal values during the last few seconds of the last firing.

(e) A large pressure loss in the oxidizer storage and sump tanks occurred during firing as shown by the flight measurements of oxidizer tank and interface pressures after each engine shutdown.

(f) Helium consumption increased when the engine performance began to decay during firing.

(g) No oxidizer crossover was sham by the flight measurements.

Failure modes that could not satisfy the foregoing features and those that could not withstand quantitative and logical investigations were eliminated. Table 7.7-X contains brief remarks on the more probable SPS malfunction modes that were evaluated.

Of the malfunctions considered, the mechanism which explains the burn characteristics observed during flight was primarily helium ingestion together with some possible effect of two-phase fluw between the storage tank and the sump tank.

Equations were derived which would determine the approximate location of the helium leak point. When flight values were inserted into the equations, the results indicated the leak point to be located someplace along the standpipe length within the zero g propellant retention reservoir (fig. 7.7-5). Suspect locations along the pipe within the reservoir included each weld location.

Testing with a 1/5-scale model of the SPS oxidizer tankage and reservoir at the Manned Spacecraft Center Thermochemical Test Area demonstrated that a helium leak would. occur with the propellant level above the reservoir, and that gas flow would increase 'considerably, even through a very small hole, as propellant outflow occurred. The leak hole positions and sizes were investigated during testing by replacing the portion of standpipe within the reservoir with similar lengths having either a 0.055-inch or 0.013-inch diameter hole drilled at one of three positions: at the center, approximtely 0.5 inch from the top, and the bottom of the reservoir.

Analysis of the results of these tests is not yet complete. Mitional tests of a similar nature were conducted by the contractor at Dmey, and ground test firings with spacecraft 001 configured with a leak condition are being scheduled for the White Sands Test Facility.

TABLE 7.7-I.- SPS PERFORMANCE FOR MISSION AS-201

Event	Elapsed time, sec		Space-fixed velocity, ft/sec	
	Planned	Actual	Planned	Actual
Beginning +X translation	1 170.7	1 181.2	21 853.19	21 850.77
First SPS thrust on	1 200.7	a 211.2	21 864.59	21 855.55
End of 80 seconds of burn	1 280.7	1 291.2	23 889.59	23 896.75
ΔV ending shutdown	1 380.4	NA	26 423.19	NA
Timed engine shutdown	1384.7	1395.2	NA	25 557.77

TABLE 7.7-II.- CRITICAL SPS PROBLEMS DURING KSC CHECKOUT OF SPACECRAFT 009

Problem	When and where discovered	Possible effect upon SPS performance	Disposition
Primary helium check valve, on oxidizer side leaking. Leak rate measured at 132 cc/hr. (Specification allowable: 9 cc/hr.)	During performance of OCP-K-4074 at KSC, Nov. 2 to Nov. 9, 1965, before static firing at pad 16.	Concentrated N_2O_4 vapors could affect helium ullage regulator operation.	Waived. Rationalized as being satisfactory for flight because the secondary check valve was in series with the leaking primary check valve. Test subsequent to the pad 16 static firing showed a leakage rate of 7.22 cc/hr. A subsequent leak check at Manned Spacecraft Operations Building (MSOB), KSC, using GN_2, showed a leakage rate of 4.25 cc/hr.
The oxidizer sump tank standpipe leaked oxidizer into the transfer line and the storage tanks.	During OCP-K-4077 at pad 16; static firing test on Nov. 19, 1965.	Inadvertent pressure unbalance in storage and sump tank ullages could cause a greater than anticipated shift of oxidizer into the storage tank, thus affecting c.g. location and possibly allowing engine oxidizer starvation.	Waived. The engine had operated satisfactorily with this condition and had been concluded to be no constraint to flight. Leakage rate on the standpipe was measured to be 3 and 2/3 lb/min. The contractor recommended loading at 25 ± 5 psia and pressurization to 175 psia prior to flight. This procedure would allow a maximum of 231 lb of oxidizer to be transferred to the storage tank. This shift of propellants would not disturb the c.g. travel nor the propellant requirements for SC-009. It was recommended that since X-raying the propellant tank might not yield sufficient detail to locate the above leak point, X-ray would not be required.
Ball valve opening time checks before and after pad 16 static firing showed actuator 3 to be faster opening than specification allowance. Opening travel time was 225 msec. (Minimum specification value was 250 msec.) Closing travel time was 345 msec and specification value was 430 msec.	Post-static firing functional tests at KSC per OCP-K-4074 and OCP-K-4623 between Nov. 19 and Nov. 23, 1965.	Incorrect valve timings could cause rough ignitions and long tailoff shutdowns.	Waived. Rationalized as having no effect upon engine ignition because actuator 4, being slower and within specifications would be the propellant flow governing actuator. The out-of-specification condition was accepted for spacecraft 009 by changing requirements per ED 434322.
Propellant contamination – During preparation for tanking the spacecraft, the oxidizer GSE transfer and conditioning unit filters exhibited excessive ΔP (pegged 25 psid gages). Filter units were replaced and oxidizer was circulated and sampled again. Samples contained black rubber type contaminate which was found to be O-ring seals from GSE. Several GSE O-ring seals were replaced in the sample valve and in the valve boxes. Freon MF (oxidizer system) and methyl alcohol (fuel system) were used to flush and purge. Approximately 12 hr elapsed between freon tanking and detanking.	During OCP-K-4075 preparations at pad 16, KSC, dated Nov. 13 to Nov. 19, 1965.	Contamination of the engine interface propellant screens could restrict propellant flow to the engine.	Obtain propellant samples during loading to determine cleanliness.

TABLE 7.7-II.- CRITICAL SPS PROBLEMS DURING KSC CHECKOUT OF SPACECRAFT 009 - Concluded

Problem	When and where discovered	Possible effect upon SPS performance	Disposition
A dent in the bellows of the SPS oxidizer inlet line measuring 0.013 in. deep by 1/8 in. long by 1/32 in. wide. (Station 200, section 5 of SM.)	(Reference: DR SC-009-SC-0134, paragrapn 14350.)	Gimbaling actuation and engine vibrations through boost and SPS burn could flex the bellows such that an oxidizer leak could develop.	Zyglo tests indicated no removal of metal or cracks in metal. Aerojet-General specification ETD 5.1-2.5 stated a depth of 0.020 in. was acceptable for such a dent. This dent with depth of 0.013 in. and no evidence of cracks or metal removal was acceptable as is for flight. In addition, the bellows attachment welds were X-rayed and subjected to dye-penetrant tests. No cracks were indicated.
Pressure measurement SP0003P oxidizer tank pressure, and SP0009P, oxidizer engine interface valve inlet pressure, read low and did not calibrate consistently.	During OCP-K-4074, OCP-K-4623, and OCP-K-4077 at KSC, repeated errors in these two measurements were evidenced at various times between Oct. 31 and Nov. 19, 1965.	Data obtained from these measurements would not allow sufficient accuracy to determine oxidizer storage and transfer analysis to level required. An additional malfunction in the oxidizer storage and transfer system during flight could not be properly analyzed by direct data methods if only invalid data were available from these two measurements.	Requested change of transducers. Transducers were not changed and only subsequent calibration was single-point reading after flight servicing.

TABLE 7.7-III.- PROPELLANT AND PRESSURANT SERVICING OF SPS FOR MISSION AS-201

Propellant and pressurant	Value	Start	Complete
Oxidizer load, lb	10 476	Feb. 16, 1966, 9:15 a.m. e.s.t.	
Fuel load (second service), lb	4 737	Feb. 18, 1966, 10:00 a.m. e.s.t.	
Oxidizer/fuel service			Feb. 18, 1966, 9:00 a.m. e.s.t.
Measurement (during loading)	Reading, psia		
SP0003P Oxidizer tank pressure	51		
SP0009P Oxidizer engine interface pressure	50		
SP0006P Fuel tank pressure	48		
SP0010P Fuel engine interface pressure	51		
Helium load		Feb. 22, 1966, 8:47 a.m. e.s.t.	Feb. 22, 1966, 9:43 a.m.
Propellant and pressurant service			Feb. 22, 1966, 10:00 a.m.
Measurement (lockup)	Reading		
SP0001P Helium tank pressure	4 050 psia		
SP0002P Helium tank temperature	60° F		
SP0003P Oxidizer tank pressure	182 psia		
SP0009P Oxidizer engine interface pressure	178 psia		
SP0006P Fuel tank pressure	182 psia		
SP0010P Fuel engine interface pressure	184 psia		
SP0600P Primary GN_2 pressure	800 psia		
SP0601P Secondary GN_2 pressure	820 psia		

TABLE 7.7-IV.- RESULTS OF CLEANLINESS ANALYSES OF PROPELLANTS AND PRESSURANT FOR MISSION AS-201

	Constituents											
	N_2O_4, percent	N_2H_4, percent	UDMH percent	He percent	H_2O, percent	Chlorides, percent	NO, percent	H_2, ppm	N_2, ppm	O_2/ Ar ppm	H_2O, ppm	Hydro-carbon, ppm
Oxidizer (N_2O_4)												
Purge loop (Pad 34)	98.8				0.07	0.01	0.75					
Spacecraft bleed unit	99.1				.09	.01	.74					
Fuel												
Purge loop (Pad 34)		50.7	47.7		1.6							
Spacecraft bleed unit		51.5	47.2		1.3							
Helium												
(SPS-FDS: 2-1-66)				99.99≡				1.3	31.0	5.4	8.0	1.0

	Particle count (500 ml. sample from purge loop, Pad 34)						
	25 to 50μ	50 to 100μ	100 to 175μ	175 to 350μ	over 350μ	100 to 180μ	over 180μ
Oxidizer (N_2O_4)	44	9	5	0	[a]1		
Fuel	0	0				0	1

[a]A metallic flake 600μ long by 25μ wide.

TABLE 7.7-V.- ON-PAD MONITORING OF SPS SERVICE SUBSYSTEMS FOR MISSION AS-201

Measurement	Time, e.s.t. (a)	T-4 days 9:00 p.m.	T-3 days 7:00 a.m.	T-3 days 5:00 p.m.	T-2 days 3:00 a.m.	T-2 days 1:00 p.m.	T-2 days 11:00 p.m.	T-1 day 9:00 a.m.	T-1 day 7:00 p.m.	T-0 day T-8 min
SP0006P	Fuel tank pressure, psia	181	181	181	181	181	181	181	181	181
SP0010P	[illegible]-engine interface pressure, [illegible]ia	185	184	184	185	185	185	184	184	185
SP0003P	Oxidizer tank pressure, psia	182	182	182	182	182	182	182	182	182
SP0009P	Oxidizer-engine interface pressure, psia	178	178	178	178	178	178	178	178	178
SP0001P	Helium tank pressure, psia	4010	4010	4010	4010	4010	4010	4010	4010	4010
SP0002T	Helium tank temperature, °F	72	72	72	72	72	72	72	72	72
SP0600P	Nitrogen pressure, primary, psia	800	800	800	800	800	800	800	800	800
SP0601P	Nitrogen pressure, secondary, psia	820	820	820	820	820	820	820	820	820

[a]Measurements presented at 10-hour intervals.

TABLE 7.7-VI.- CRITICAL LIFE COMPONENTS, MISSION AS-20)

Part number	Serial number	Nomenclature	Allowable operation (lifetime)	Expended time
ME901-0484-003	001890000026	Engine, SPS, lifetime, sec	450	63.6
AGC118931		Ball valve, propellant, cycles		
		Wet	250	26
		Dry	50	
		Ball valve, oxidizer, cycles		
		Wet	250	26
		Dry	50	
AGC712952		Pilot valve, oxidizer, cycles	960	33
AGC712953		Pilot valve, fuel, cycles	960	33
ME901-0615-0005	001390000009	Gimbal actuator motor, pitch, hr		
		P_1	5	4 hr 17 min 56 sec
		P_2	5	4 hr 18 min 49 sec
ME901-0615-0006	001390000009	Gimbal actuator assembly, yaw, hr		
		Y_1	5	3 hr 38 min 46 sec
		Y_2	5	3 hr 51 min 37 sec

TABLE 7.7-VII.- PRE-IGNITION SPS MEASUREMENTS, MISSION AS-201

[At T+1200 seconds]

Measurement no.	Measurement	Value
SP0001P	He tank pressure, psia	3 978
SP0002T	He tank temperatwe, °F	67
SP0003P	Oxidizer tank pressure, psia	174
SP0005T	Oxidizer line temperature, °F	66
SP0006P	Fuel tank pressure, psia	179
SP0008T	Fuel line temperature, °F	65
SP0009P	Oxidizer interface pressure, psia	175
SP0010P	Fuel interface pressure, psia	181
SP0020T	Thrust chamber outer skin temperature, °F	60
SP0040T	Fuel at interface temperature, °F	67
SP0041T	Oxidizer at interface temperature, °F	65
SP0050T	Nozzle outer skin temperature	lost
SP0060T	Injector manifold temperature, °F	64
SP0060P	GN_2 tank (primary) pressure, psia	813
SP0601P	GN_2 tank (secondary) pressure, psia	lost
SP0661P	Thrust chamber pressure, psia	0

NOTE: All propellant valves were closed.

TABLE 7.7-VIII.- FIRST SPS BURN, MISSION AS-201

a. Steady state (first 80 seconds)

Measurement	Parameter	Indicated value	Expected value
SP0003	Oxidizer tank pressure, psia	172	175
SP0005	Oxidizer temperature in feed line, °F	67	67
SP0006	Fuel tank pressure, psia	175	175
SP0008	Fuel temperature in feed line, °F	65	67
SP0009	Oxidizer inlet pressure, psia	152	156
SP0010	Fuel inlet pressure, psia	156	159
SP0661	Chamber pressure, psia	98	102

b. Comparison: First 80 seconds with next 100 seconds

Parameter	Oscillations, psia	
	First 80 seconds	Next 100 seconds
Oxidizer inlet pressure	±0.8	±4
Fuel inlet pressure	±1.0	±2
Chamber pressure	±2.0	±9

TABLE 7.7-IX.- COAST CONDITIONS (T+1395.2 to T+1310.7 SECONDS),

MISSION AS-201

Measurement no.	Identification	Indicated value, psia
SP0001P	He tank pressure	2 650
SP0003P	Oxidizer tank pressure	158
SP0006P	Fuel tank pressure	172
SP0009P	Oxidizer inlet pressure	158
SP0010P	Fuel inlet pressure	174
SP0661P	Chamber pressure	0

TABLE 7.7-X.- MALFUNCTION MODE EVALUATION MATRIX, MISSION AS-201

Malfunction \ Observed SPS instrumentation data	Chamber pressure (First burn)	Oxidizer tank pressure	Oxidizer interface pressure	Chamber pressure (Second burn)	Helium storage tank pressure	Oxidizer tank pressure decay at cutoff	Oxidizer engine feed line temperature (First burn)	Oxidizer engine feed line temperature (Second burn)	Remarks
Helium ingestion from leak near	X	X	X	X	X		X	X	Probable failure mode. (See discussion of malfunction modes in text.)
Helium ingestion through faulty seal in oxidizer standpipe	X	X	X	X	X		X	X	Possible failure mode. (See discussion of malfunction modes in text.)
Oxidizer storage tank not depleting completely during crossover; rather, having a continuous two-phase (liquid and gas) generated pressure drop between the two tanks	X	X	X	X		X			Probable failure mode. (See p-[illegible] on of malfunction modes in text.
Partial constriction in helium supply line downstream of pressure transducer		X	X			X			Improbable failure mode. Chamber pressure was not driven by oxidizer interface pressure. Does not explain engine chamber pressure data.
Complete constriction in helium supply line downstream of tank pressure transducer		X							Improbable failure mode. Oxidizer pressures did not respond as expected for a blowdown mode on that side; therefore, the oxidizer tanks were receiving helium.
Partial constriction in transfer line between oxidizer storage and sump tanks		X	X			X			Improbable failure mode. Chamber pressure was not driven by oxidizer inlet pressure. Does not explain oxidizer feedline temperature drop during SPS operation.
Complete constriction in transfer line between oxidizer storage and sump tanks		X							Improbable failure mode. Chamber pressure was not driven by oxidizer inlet pressure. Does not explain oxidizer feedline temperature drop during SPS operation.
Clogging or restriction of oxidizer feed line at interface filter		X	X	X					
Clogging or restriction of oxidizer feed line at bellows upstream of interface flange		X	X	X					[illegible] oxidizer inlet pressure.
Oxidizer leak upstream of propellant shutoff valves	X	X	X		X				
Oxidizer leak downstream of propellant shutoff valves	X	X	X		X				

TABLE 7.7-X.- MALFUNCTION MODE EVALUATION MATRIX, MISSION AS-201 - Concluded

Observed SPS instrumentation data / Malfunction	Chamber pressure (First burn)	Oxidizer tank pressure	Oxidizer interface pressure	Chamber pressure (Second burn)	Helium storage tank pressure	Oxidizer tank pressure decay at cutoff	Oxidizer engine feed line temperature (First burn)	Oxidizer engine feed line temperature (Second burn)	
Thrust chamber throat erosion	X	X	X		X				Impossible failure mode. Does not explain any of observed data during second burn. Analysis of ablative chamber material rules out possibility of required 68 percent increase in throat area to duplicate first 185 seconds of burn.
Engine injector failure	X	X	X		X				Impossible failure mode. Chamber pressure could not have recovered to near nominal performance during second burn if the injector had failed, and fuel engine interface pressure would have been more erratic than the oxidizer side.
Oxidizer freezing in the helium line in the heat exchanger area		X	X			X			Impossible failure mode. Helium Btu transport capability too low. Does not explain excessive helium consumption.

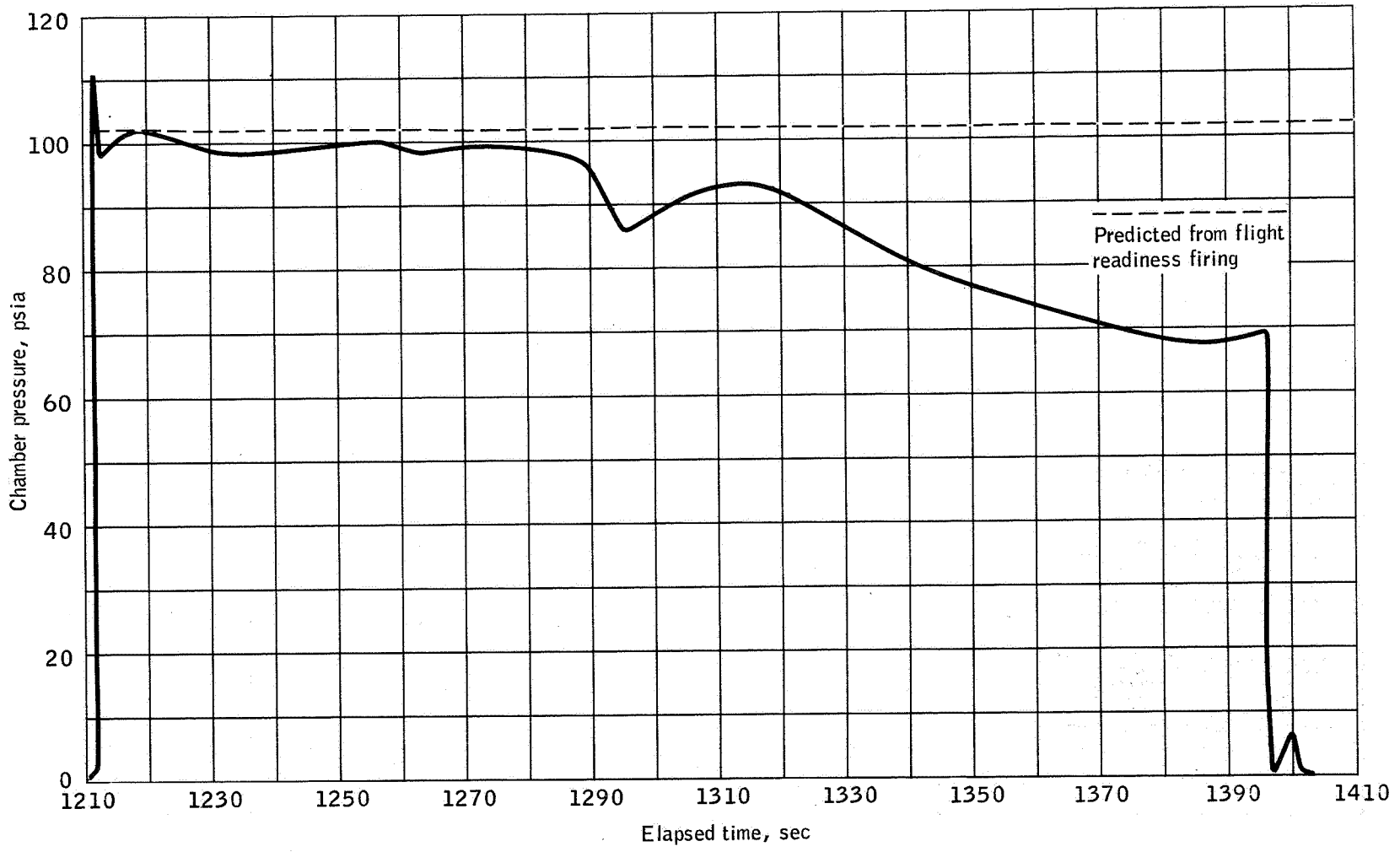


Figure 7.7-1.- Chamber pressure during first burn, Apollo Mission AS-201.

NASA-S-66-6264 **MAY 6**

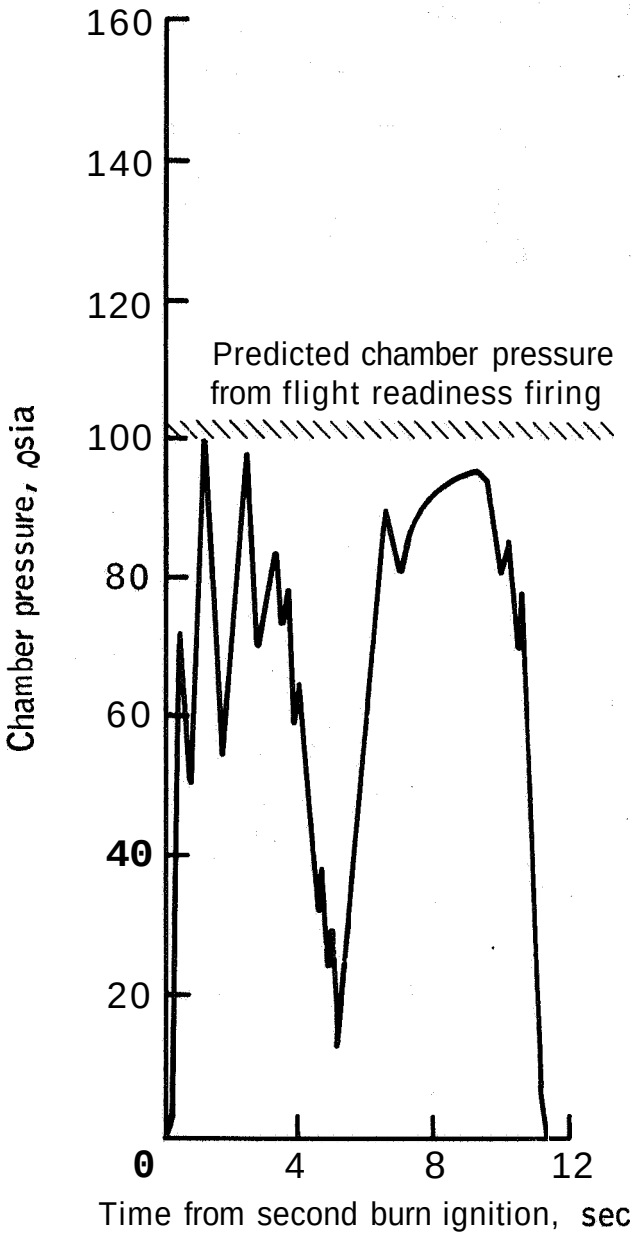


Figure 7.7-2.- Second **SPS** burn, Mission AS-201.

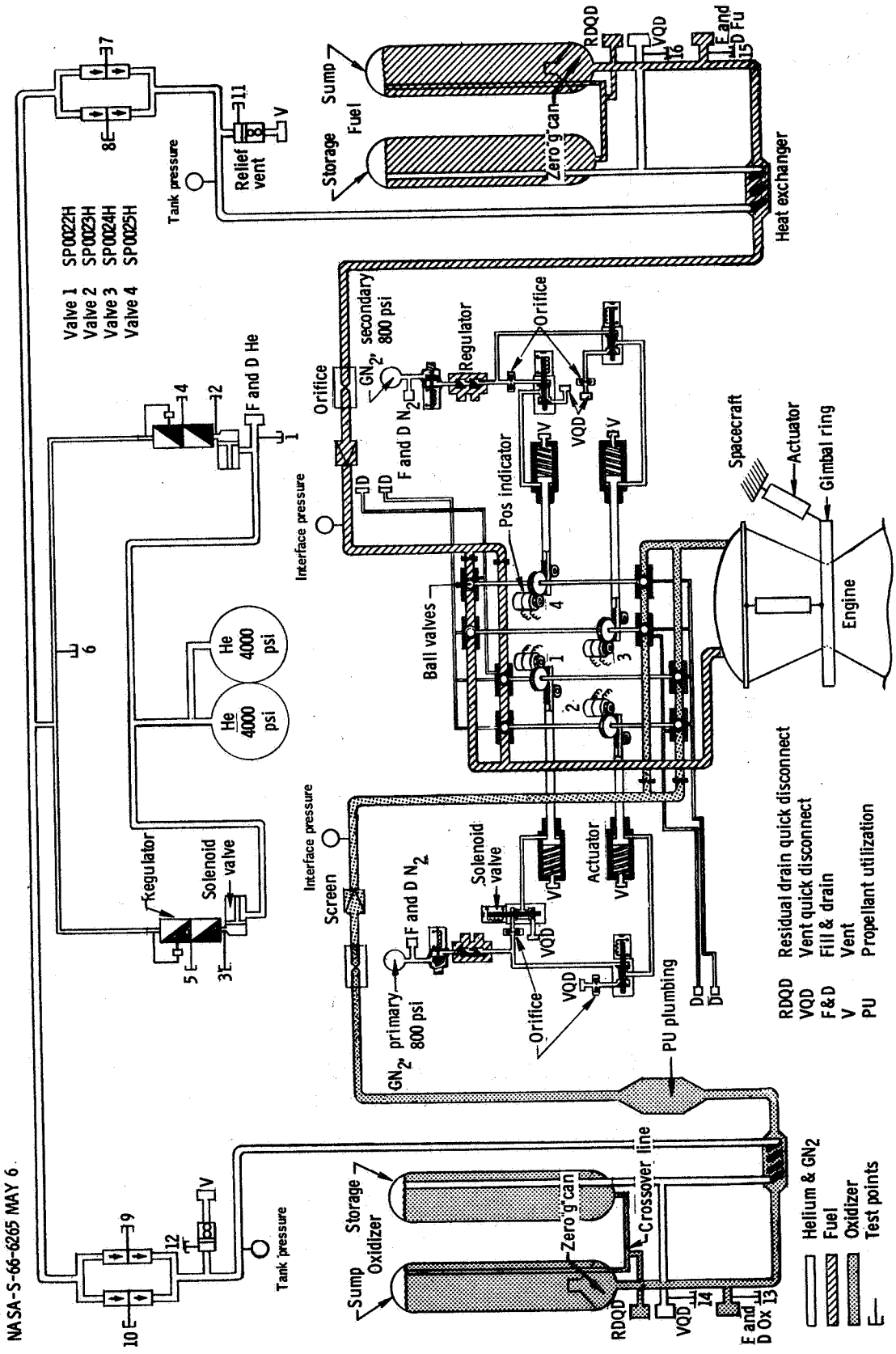
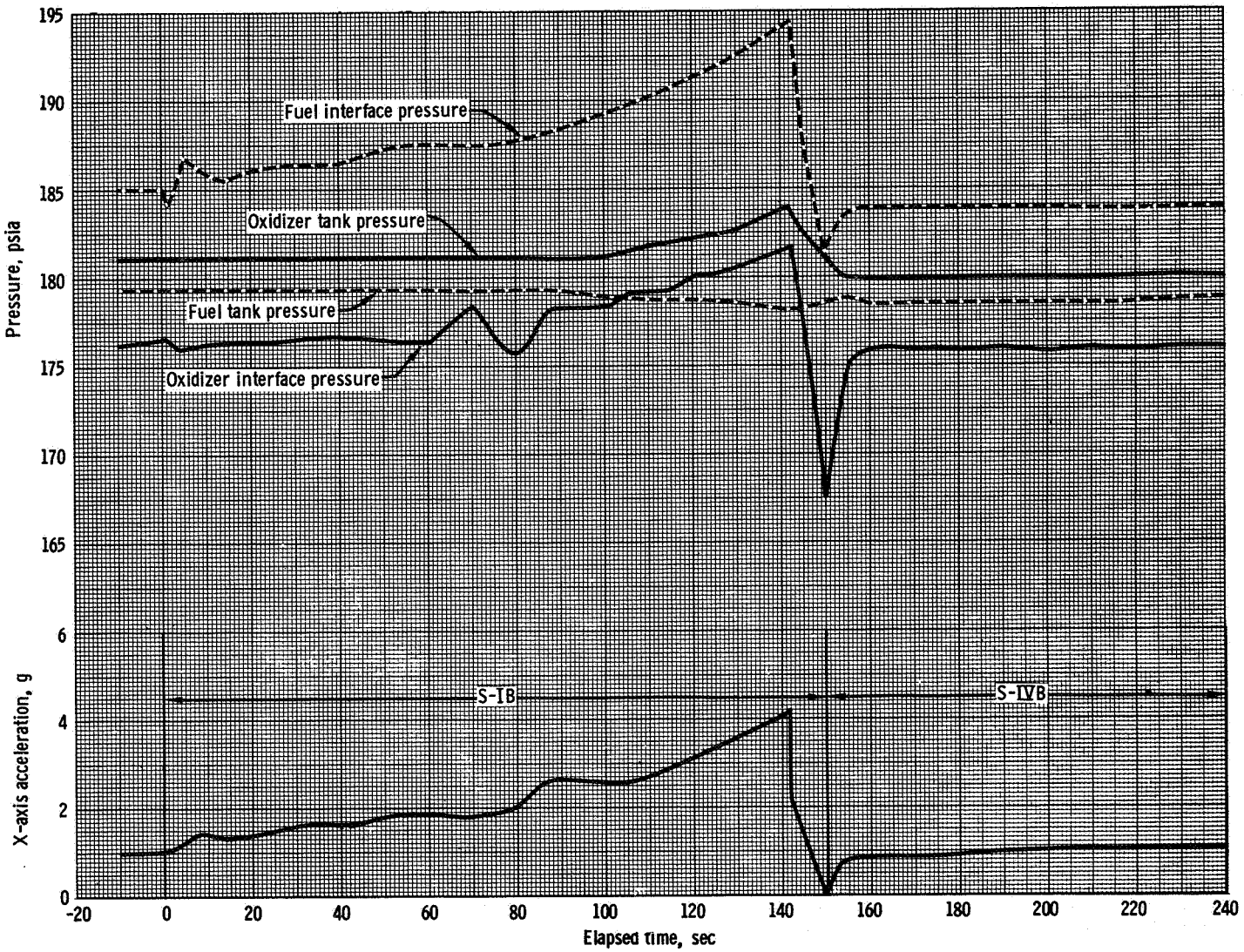


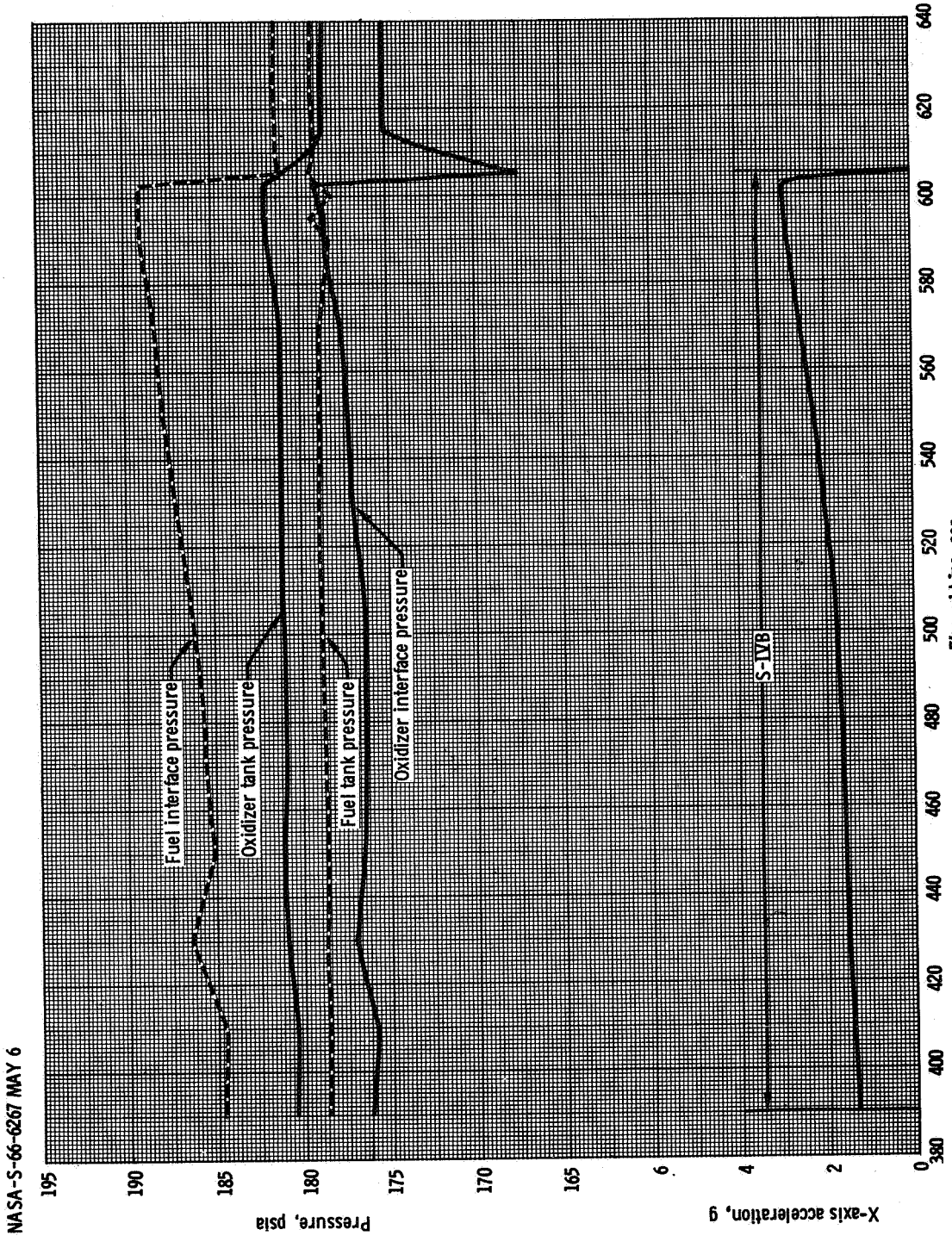
Figure 7.7-3.- Service propulsion subsystem, Mission AS-201.

NASA-S-66-6266 MAY 6



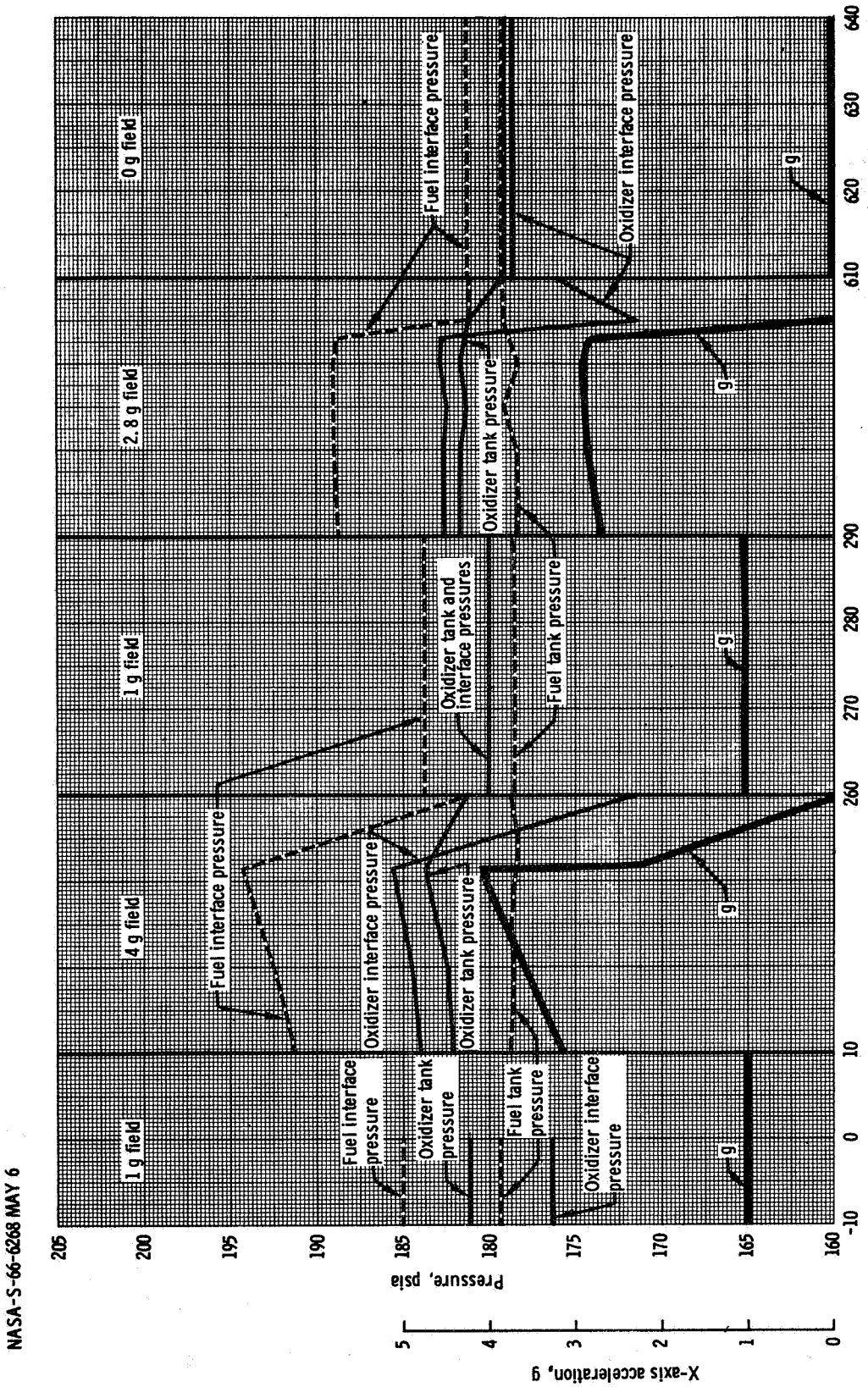
(a) S-IB booster effects.

Figure 7.7-4.- SPS critical measurements during launch and exit, Mission AS-201.



(b) S-IVB booster effects.

Figure 7.7-4. - Continued.



(c) Various g effects.

Figure 7.7-4.- Concluded.

NASA-S-66-6269 MAY 6

All dimensions are in inches

A = 2.87 I.D.
B = 6.94 I.D.
C = 5.24 O.D.
D = 3.00 O.D.
E = 2.93 I.D.
F = 14.78 O.D.

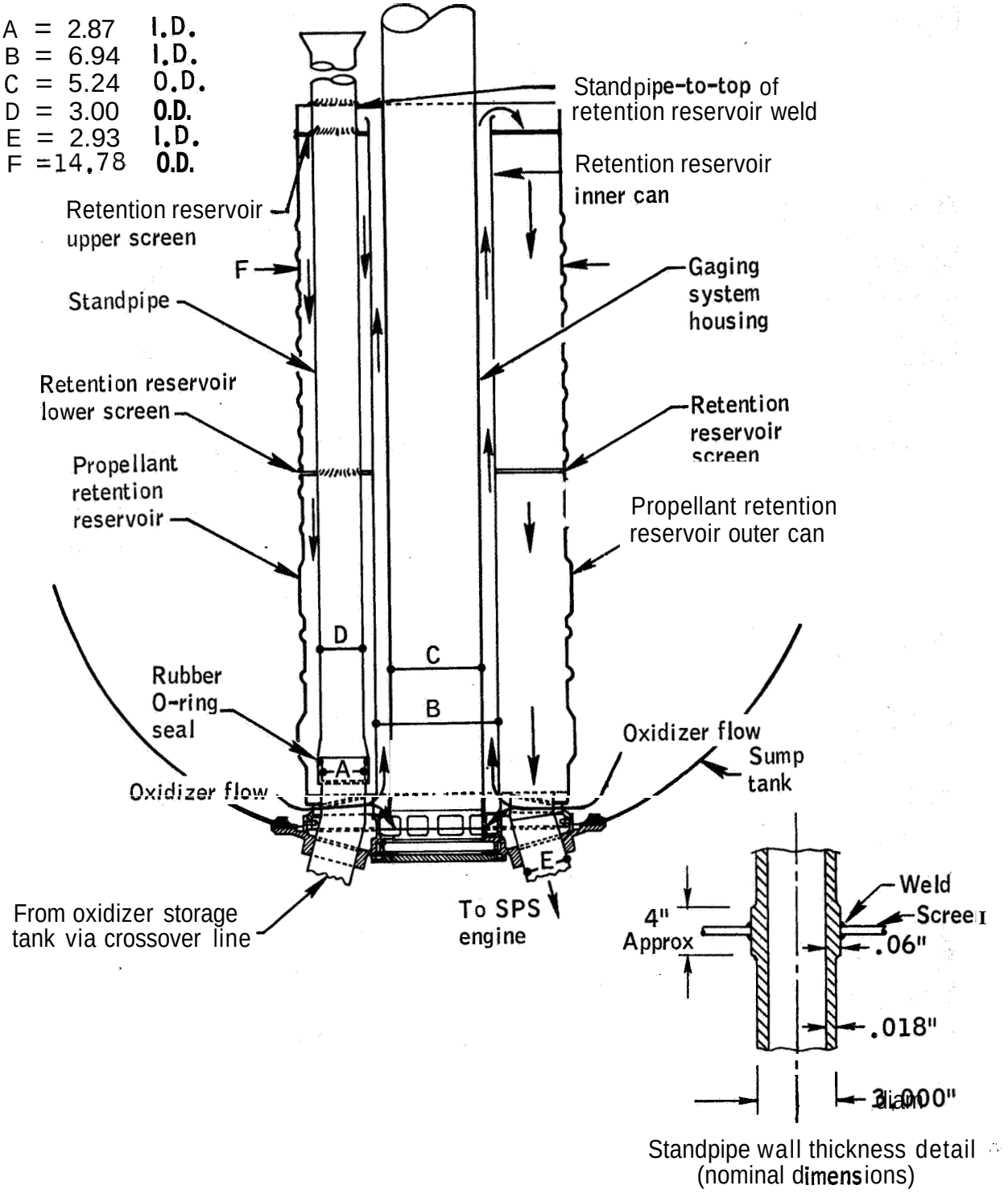
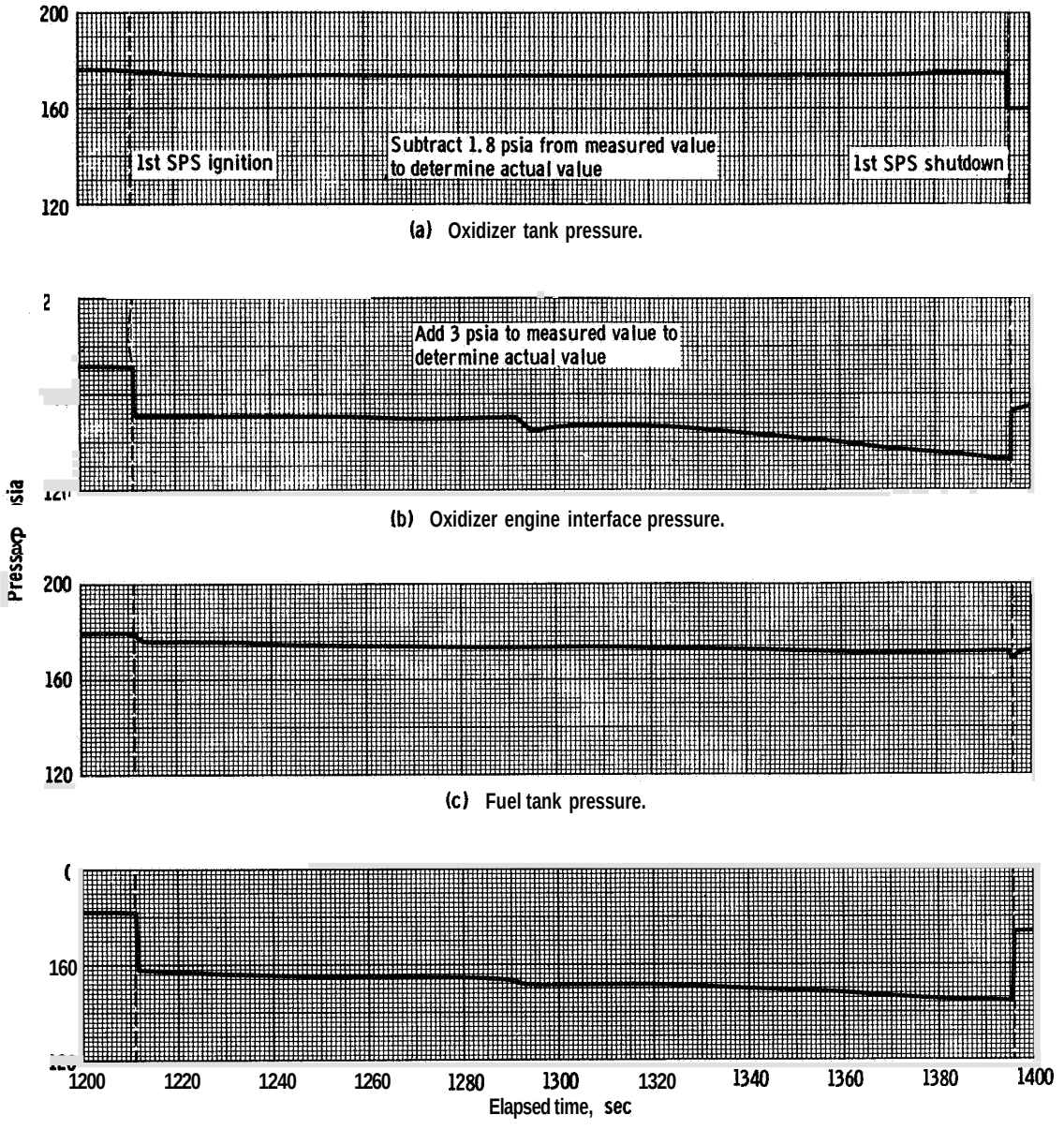


Figure 7.7-5.- Oxidizer retention reservoir (zero g can), Mission AS-201.

NASA-S-66-6270MAY 6



(a) Oxidizer tank pressure.

(b) Oxidizer engine interface pressure.

(c) Fuel tank pressure.

(d) Fuel engine interface pressure.

Figure 7.7-6. - Propellant tank and interface pressures during first burn, Mission AS-201.

NASA-S-66-6271MAY 6

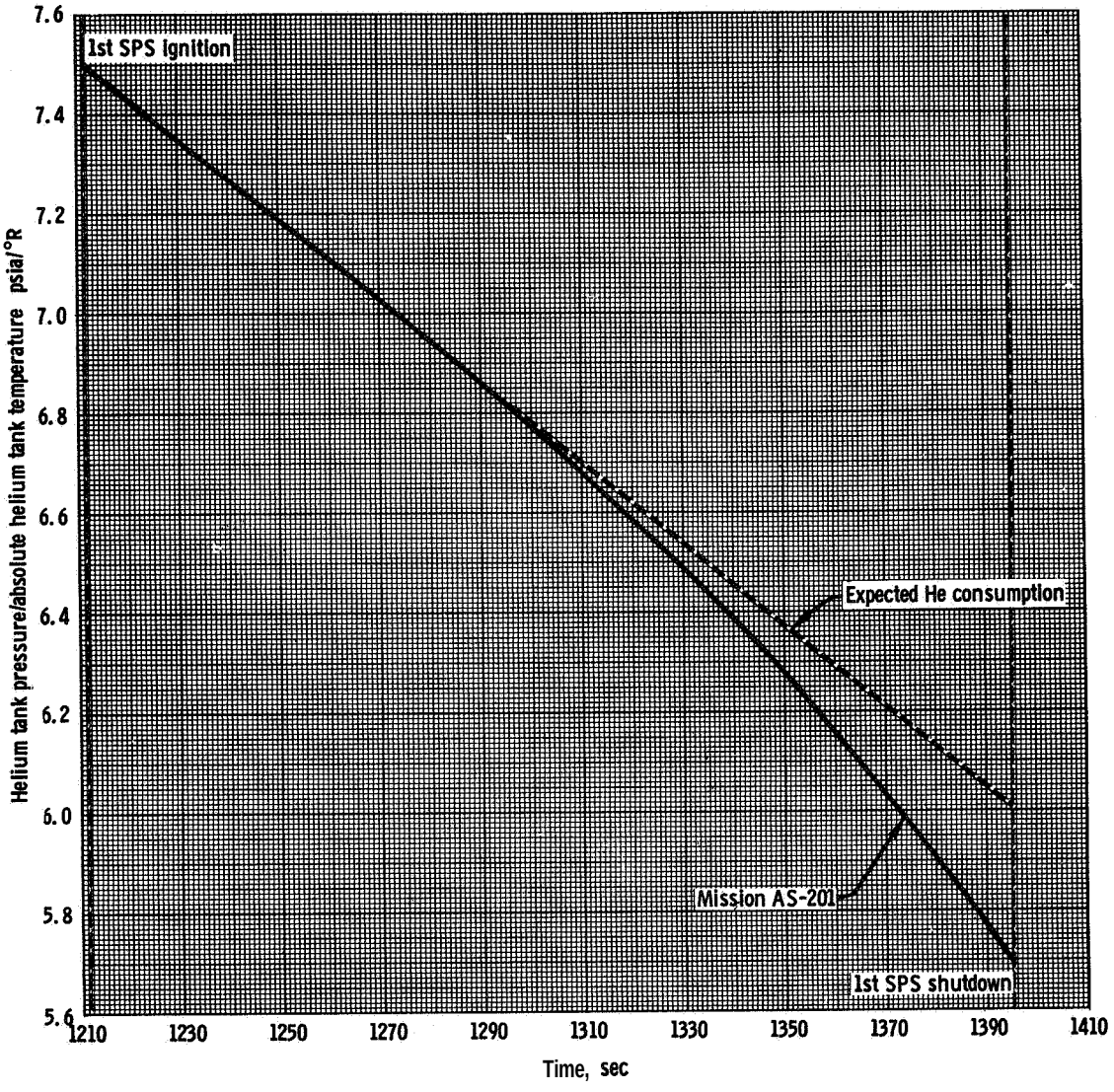


Figure 7.7-7. - SPS helium consumption during first burn, Mission AS-201.

NASA-S-66-6272 MAY 6

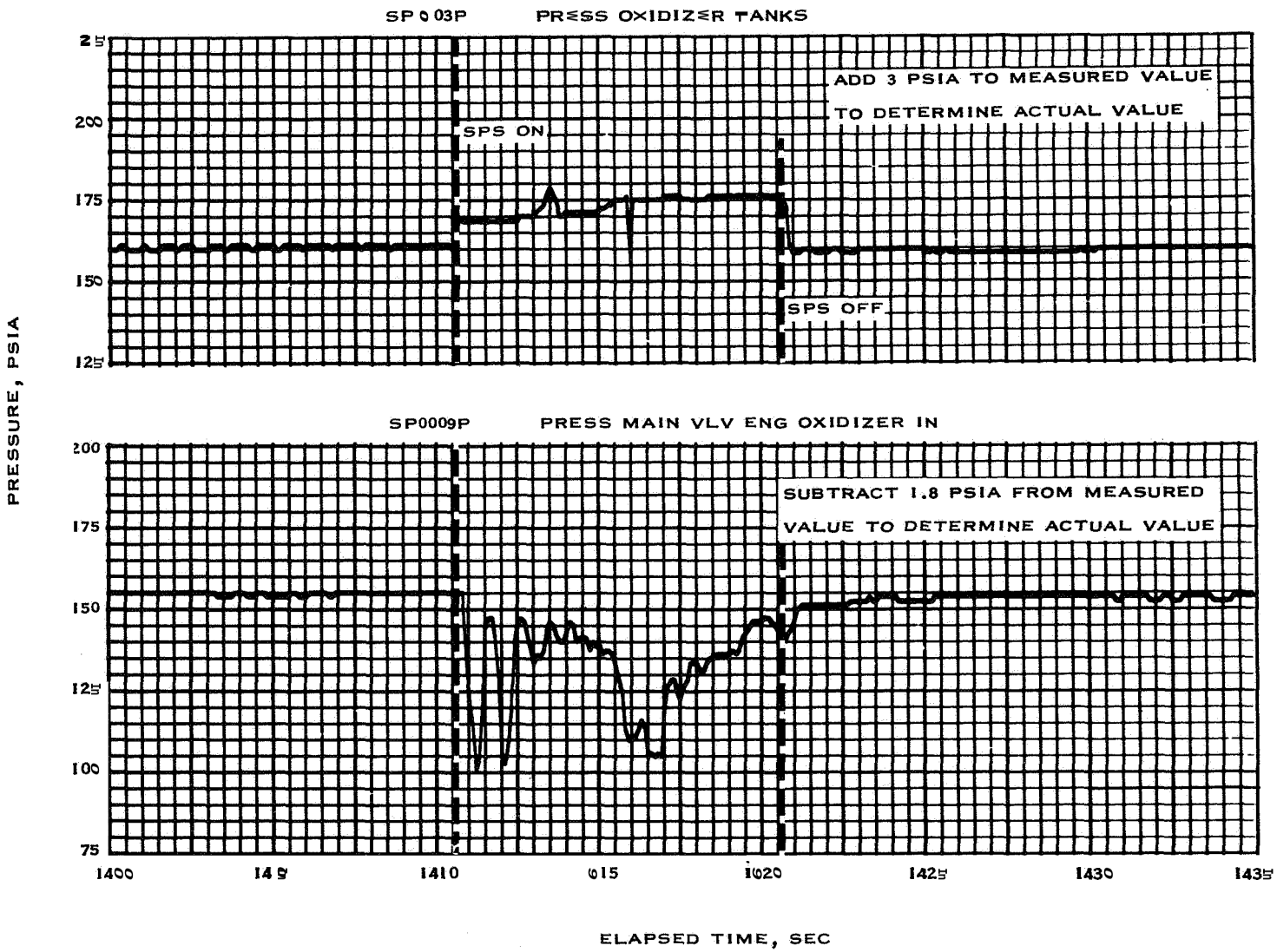


Figure 7.7-8.- Oxidizer tank and interface pressure plotted against time, second SPS burn. Mission AS-201.

NASA-S-66-6273 MAY 6

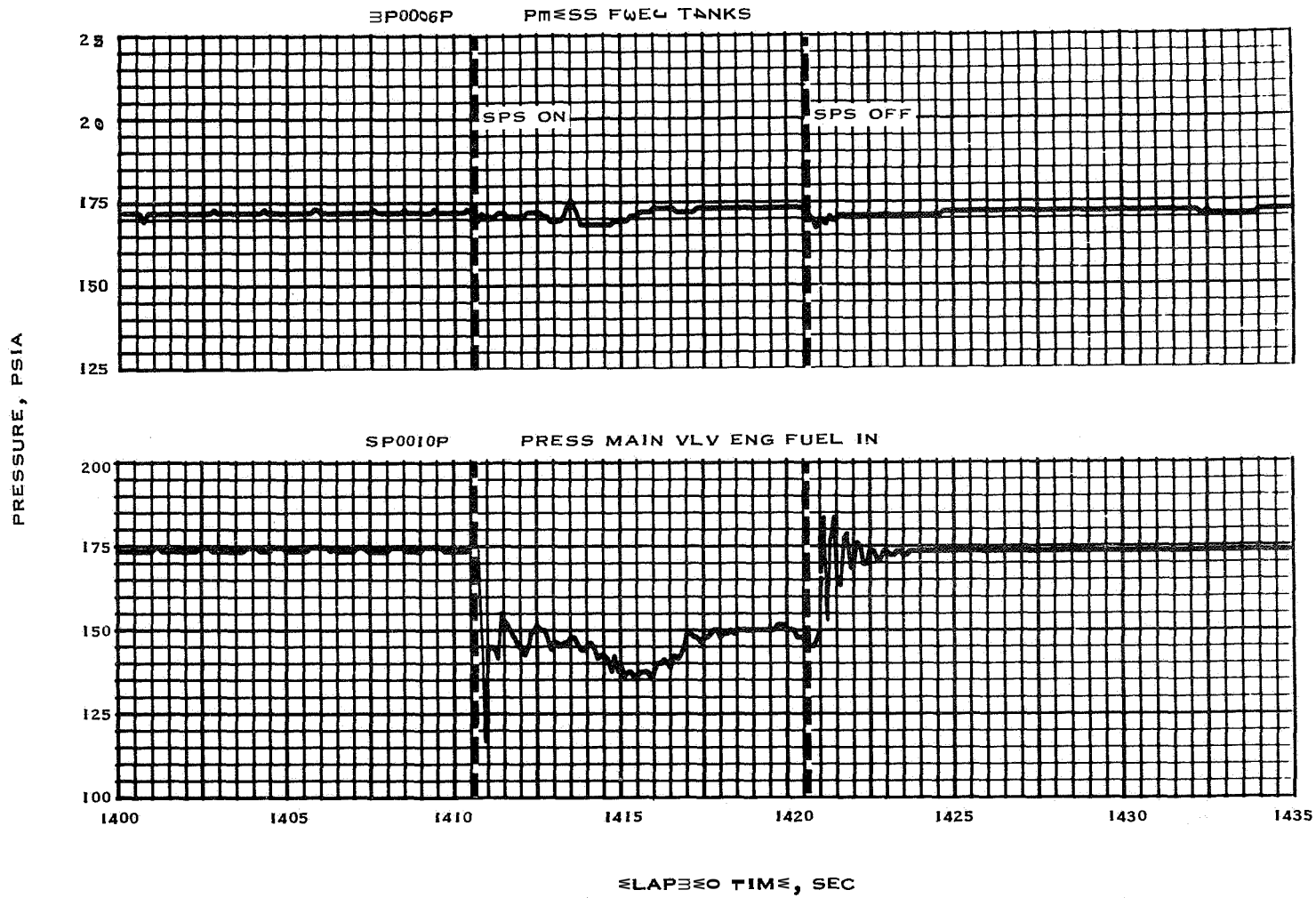


Figure 7.7-9.- Fuel tank and interface pressures plotted against time, (second SPS burn), Mission AS-201.

NASA-S-66-6274 MAY 6

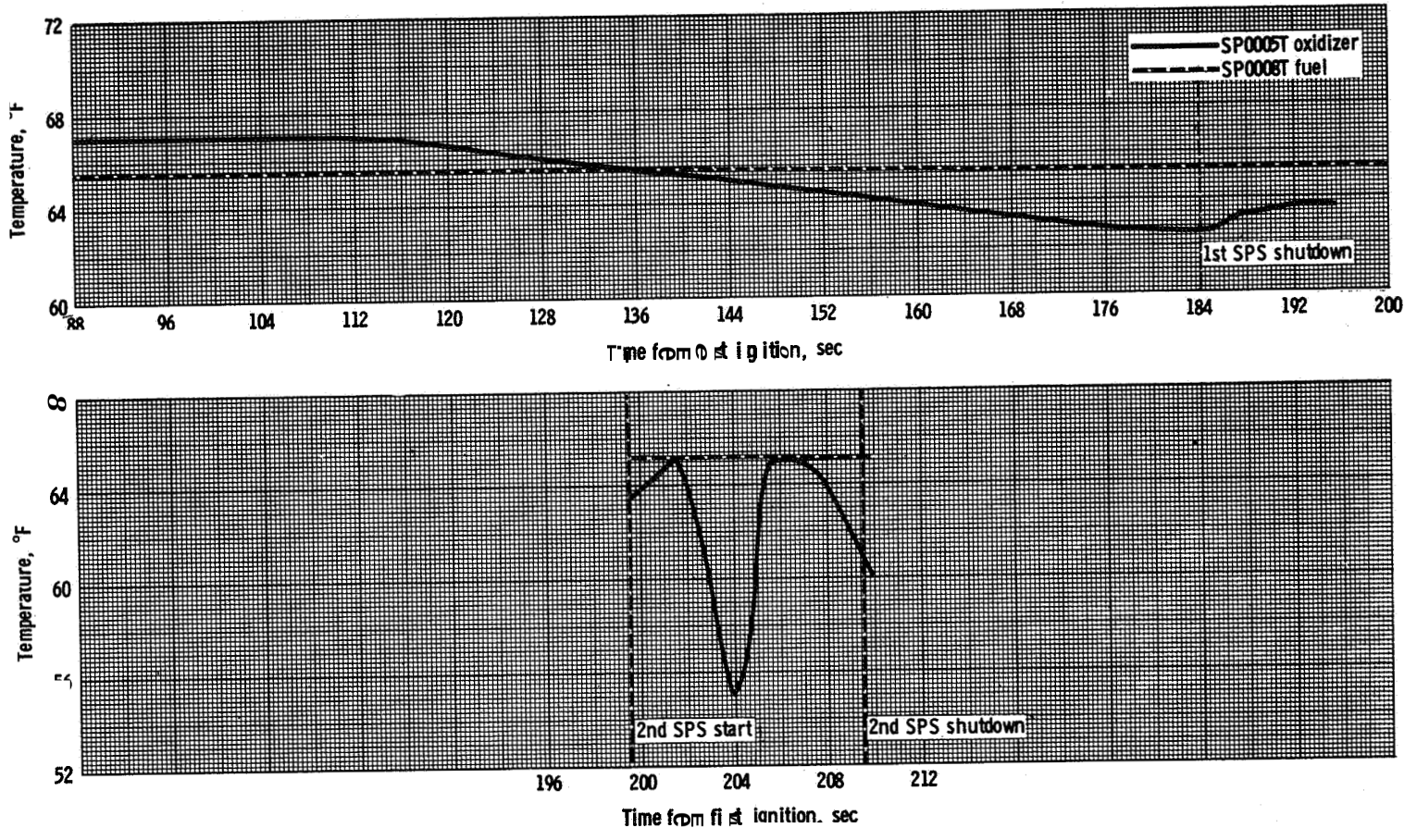


Figure 10.- Engine feed line temperatures (SP0005T and SP0008T) plotted against time, Mission AS-201.

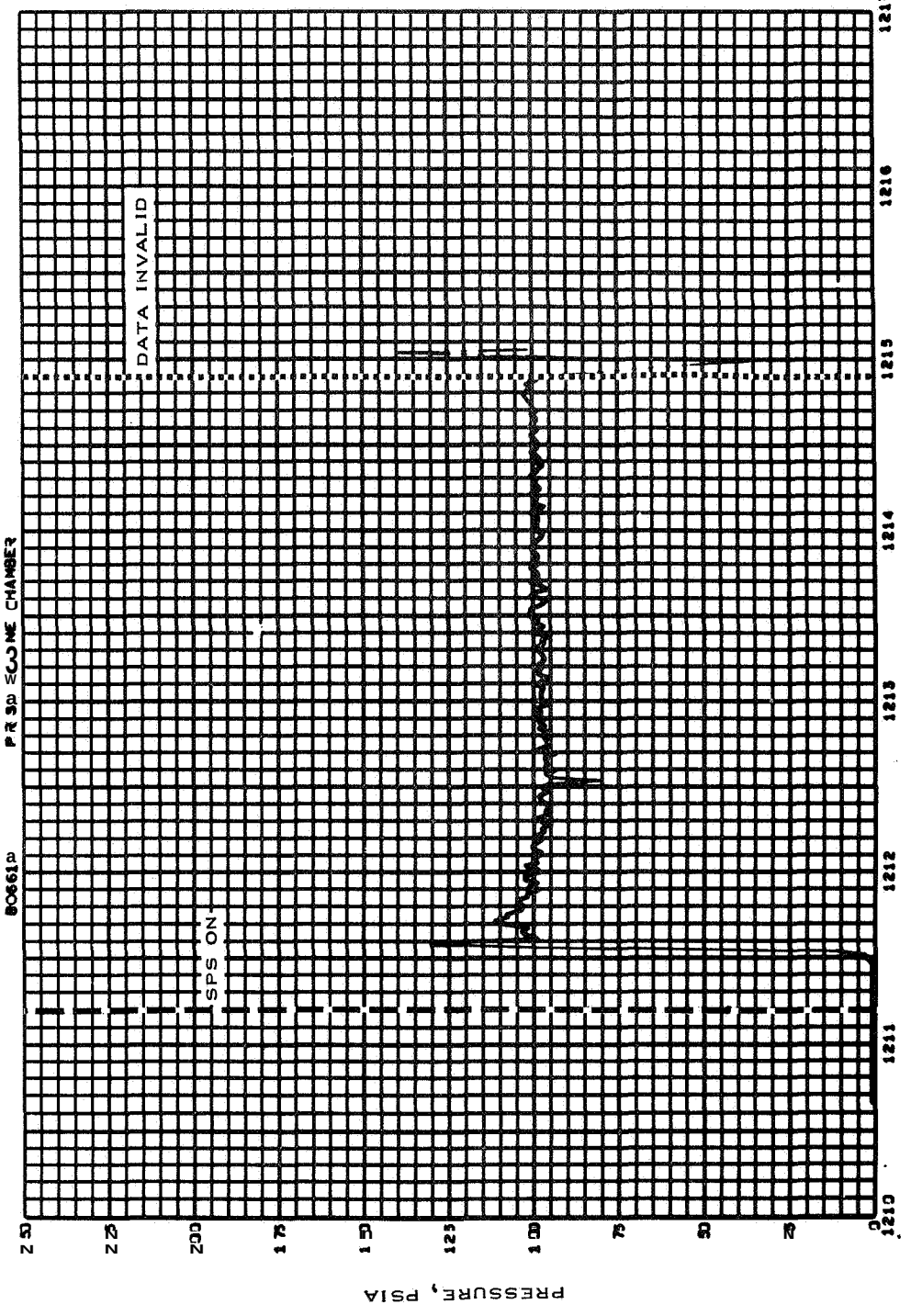


Figure 7.7-11.- First SPS ignition chamber pressure transient (SPS on at 1211.2 sec), Mission AS-201.

NASA-S-66-6276 MAY 6

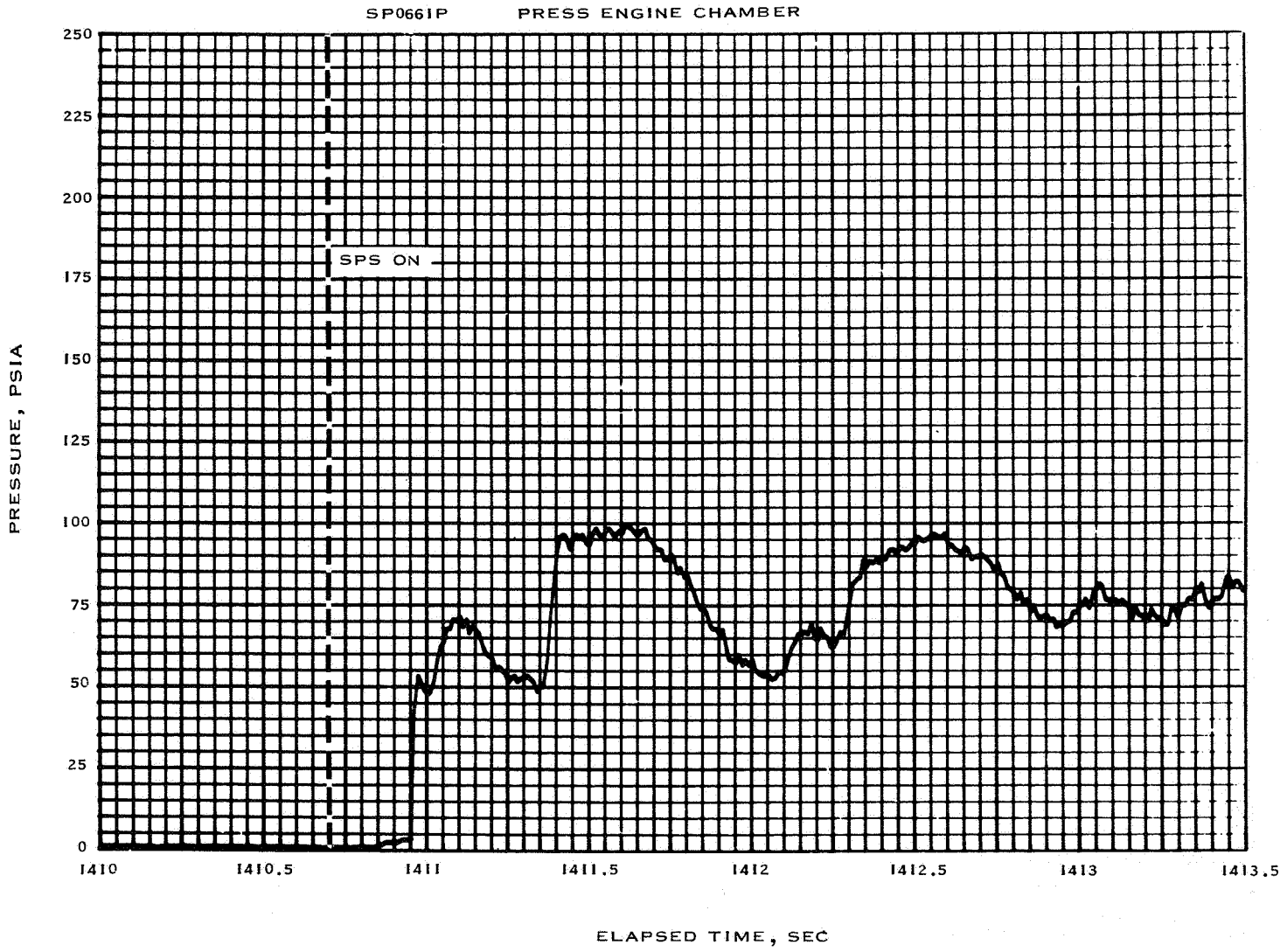
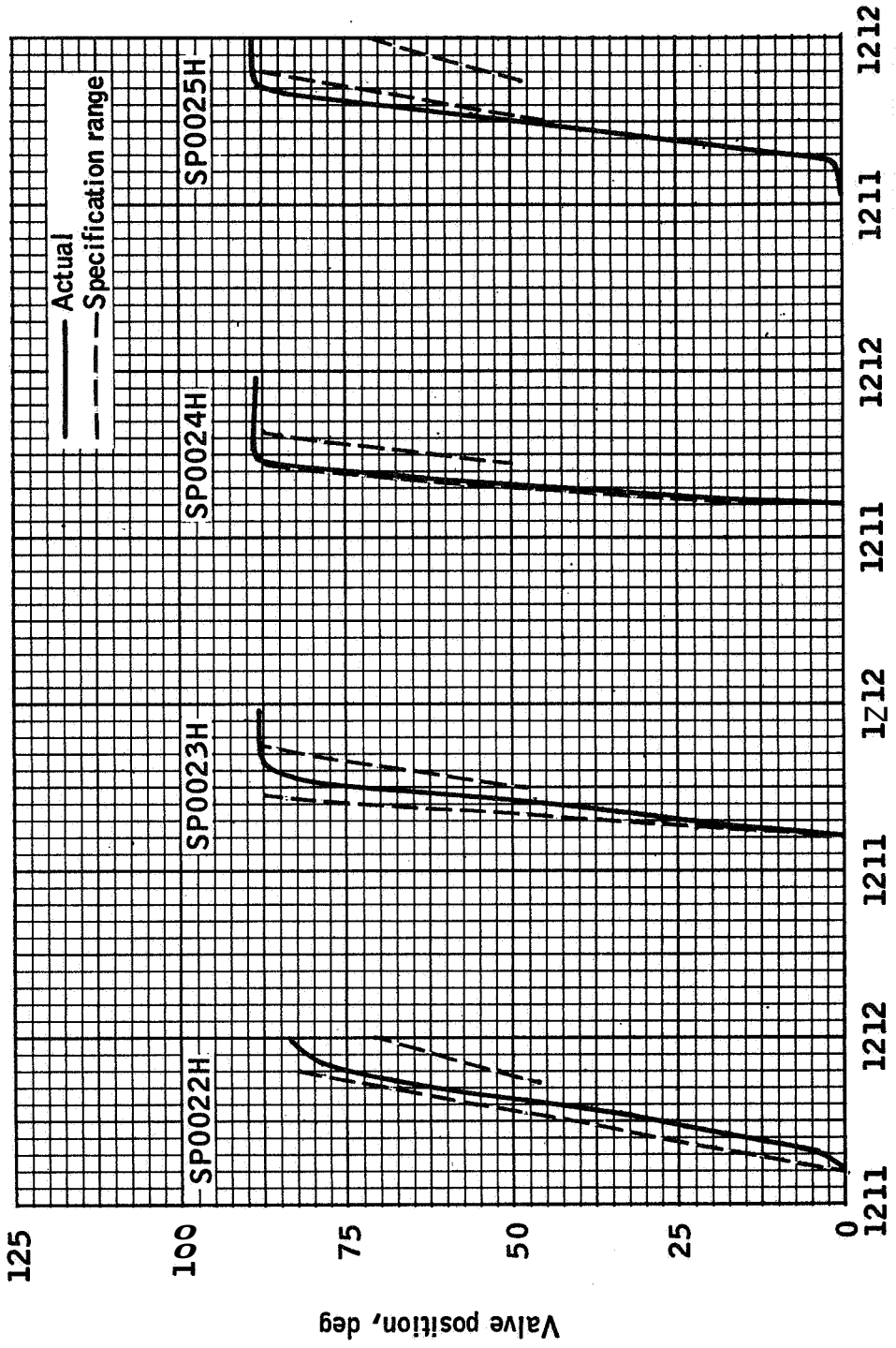


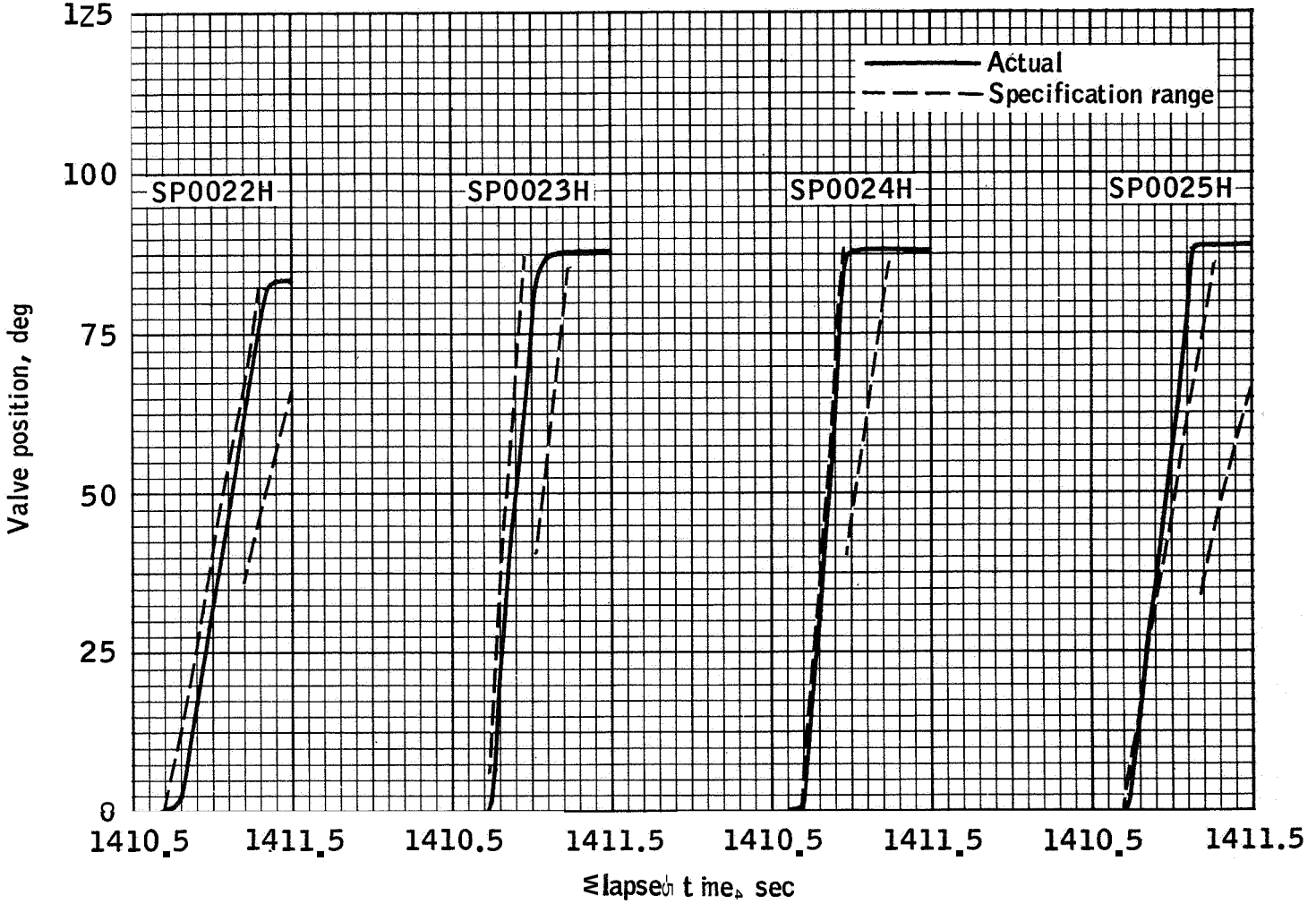
Figure 7.7-12.- Second SPS ignition chamber pressure transient, Mission AS-201.



(a) First SPS ignition.

Figure 7.7-13.- Propellant valve opening times, Mission AS-201.

NASA-S-66-6278 M Y 0



(b) Second SPS ignition.

Figure 7.7-13.- Concluded.

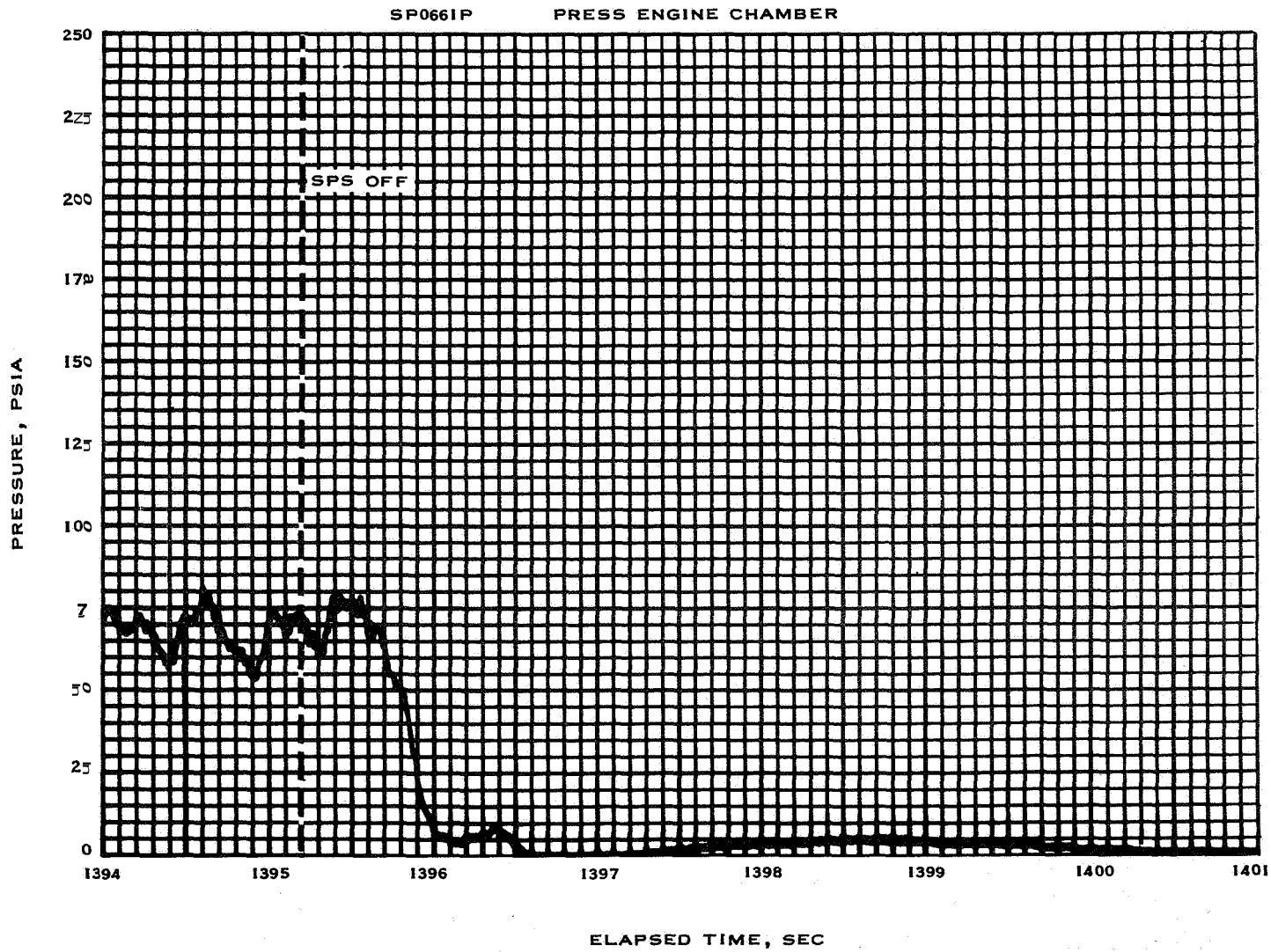


Figure 7.7-14.- First SPS shutdown chamber pressure transient, Mission AS-201.

NASA-S-66-6280 MAY 6

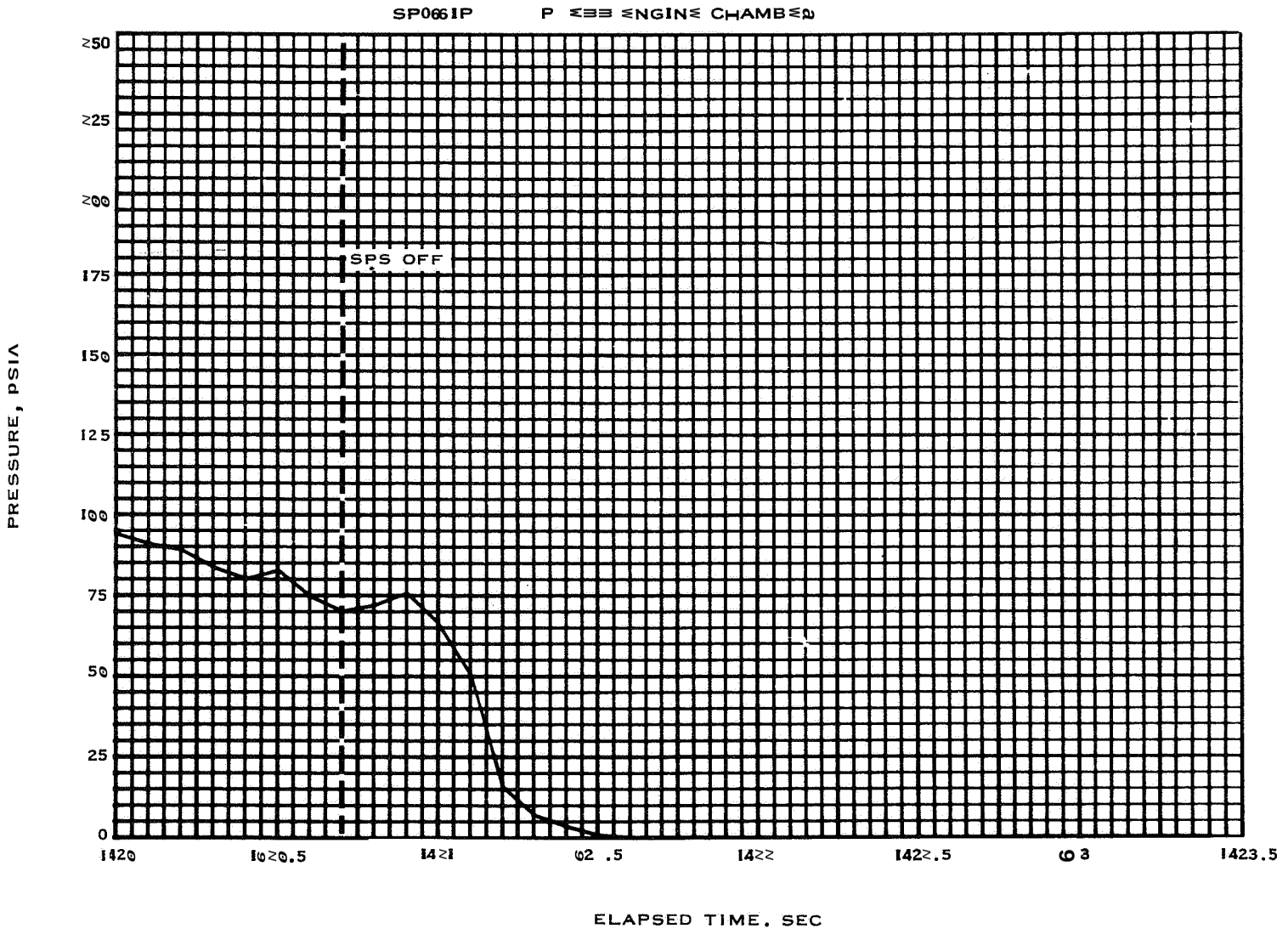
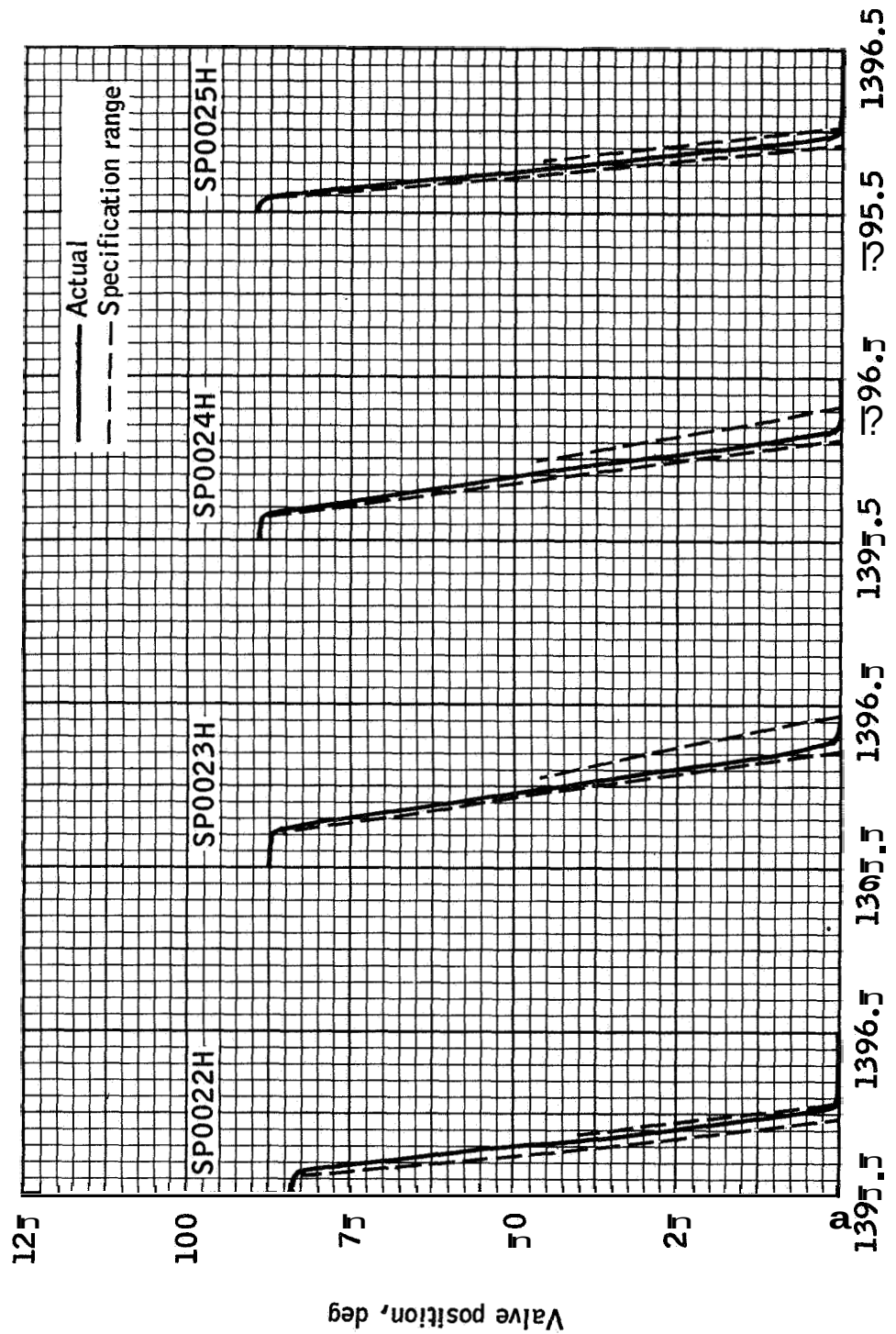


Figure 7.7-15.- Second SPS shutdown chamber pressure transient, Mission AS-201.

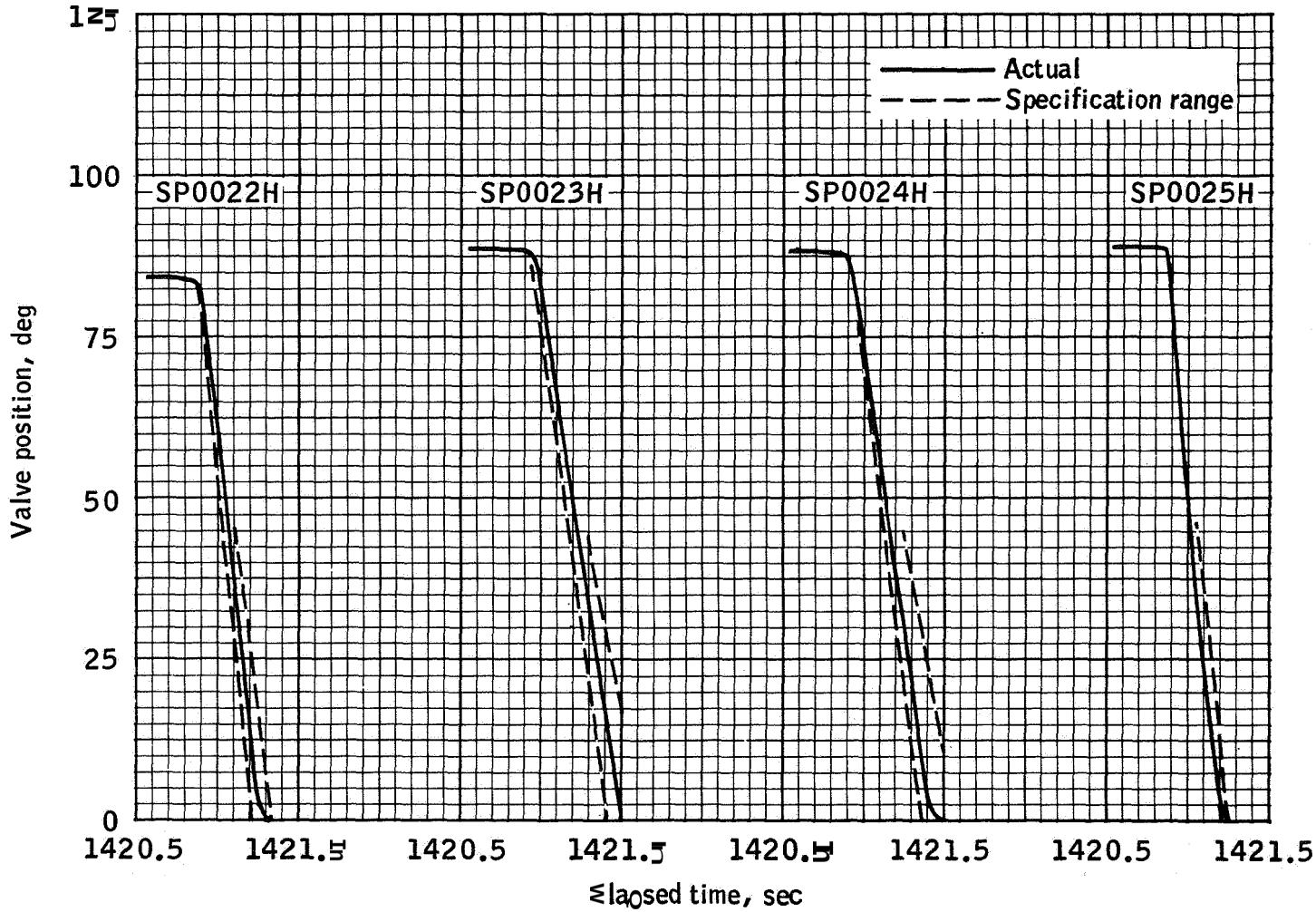


(a) First SPS shutdown.

Figure 7.7-16.- Propellant valve closing times, Mission AS-201.

NASA-S-66-6281 MAY 6

NASA-S-60-6282 MAY 0



(b) Second SPS shutdown.

Figure 7.7-16.- Concluded.

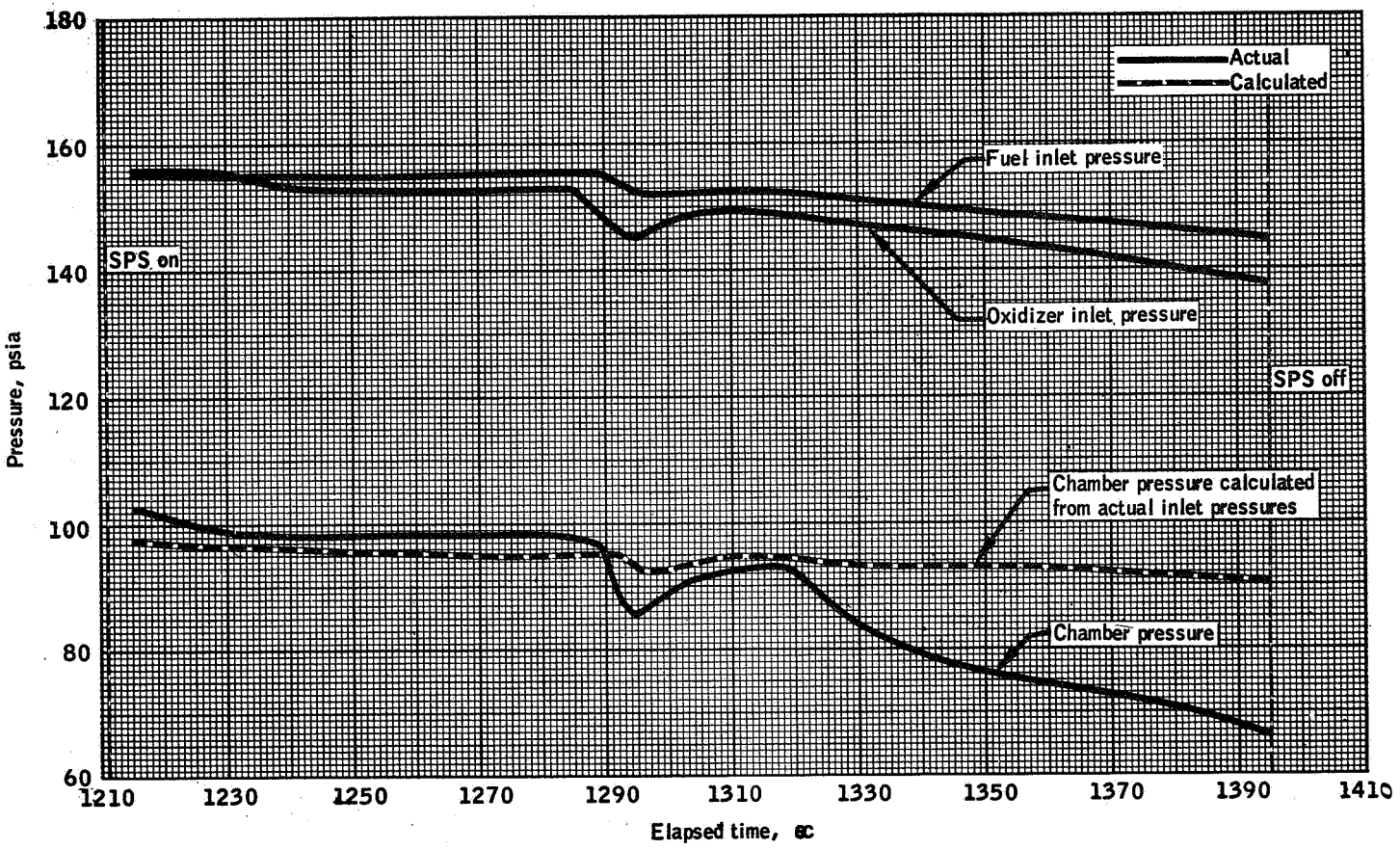


Figure 7.7-17.- Comparison of calculated chamber pressure and observed chamber pressure during first SPS burn, Mission AS-201.

7.8 hunch-Escape Subsystem

Description.- The launch-escape subsystem (US) for Mission AS-201 was a Block I type configuration; however, provisions for abort initiation by ground radio command and initiation of tower jettison by a launch vehicle instrument unit signal or a ground radio command were added for this unmanned mission. The Block I type U S has been flight tested successfully on previous Apollo missions. The LES consisted of a nose cone with Q-ball, canard assembly, ballast enclosure, pitch-control motor, tower-jettison motor, hunch-escape motor, and the launch-escape-tower structure. (See fig. 7.8-1.) The boost protective cover was attached to the U S tower legs.

Performance.- Analysis of tracking camera film indicated that performance m s satisfactory and that the tower-jettison motor fired as programmed (20 seconds after S-IVB ignition), removing the LES and boost protective cover from the command module as planned.

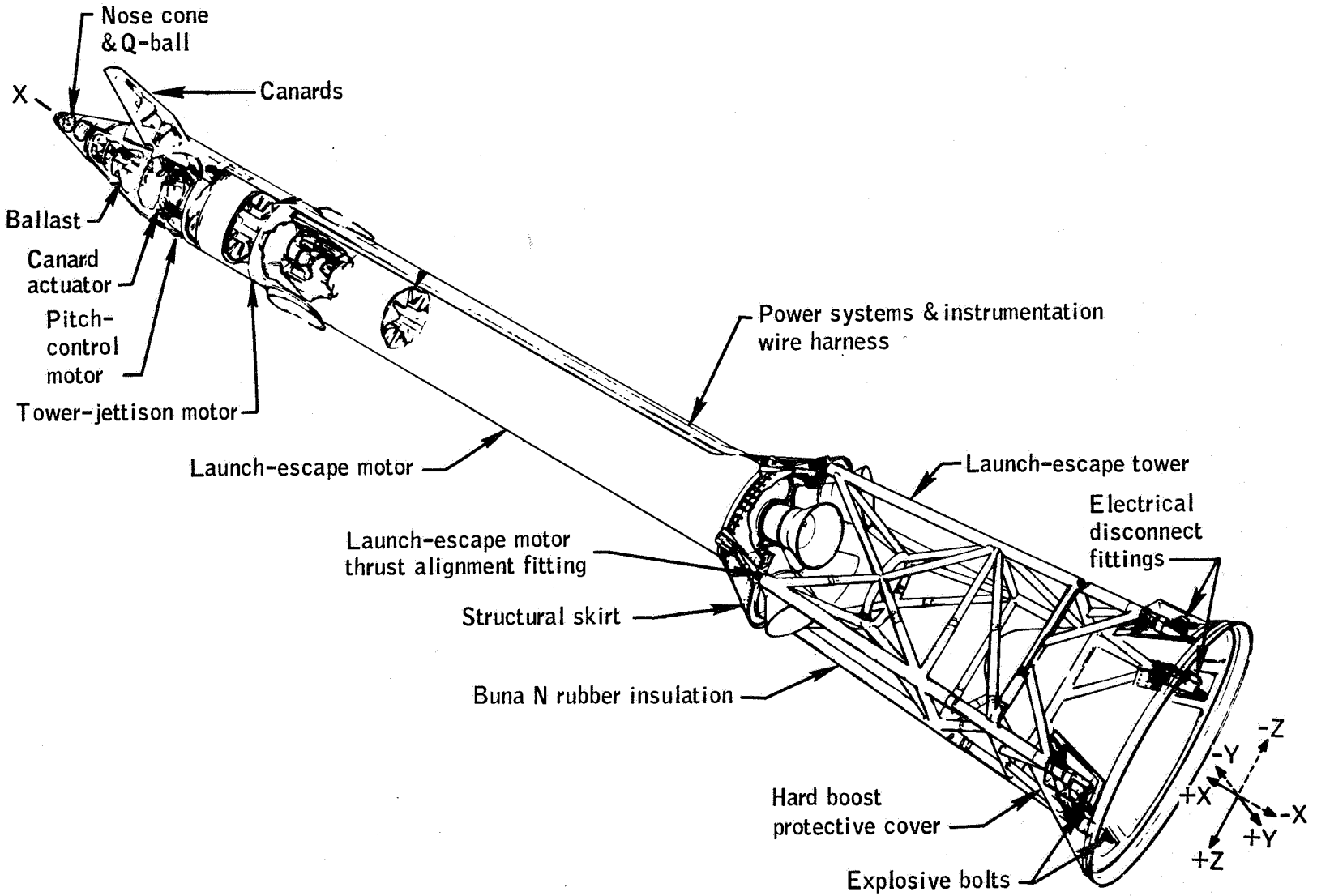


Figure 7: 8-1.- Launch escape subsystem, Block I configuration, mission AS-201.

7.9 Reaction Control Subsystems

Summary. - The service module reaction control subsystem (SM RCS) successfully performed the pitch maneuver required before SM/CM separation and maintained proper attitude control even though quad A was completely inoperative and one of the negative yaw (-Y) engines was either inoperative or producing only partial thrust. However, as a result of the quad A and -Y engine problems, the +X translation maneuvers produced somewhat less than nominal velocity change when spacecraft attitudes and rates were maintained. Performance compared favorably with that predicted (considering the effects of the disabled engines), indicating that nominal engine thrusts were produced by the operating engines.

The command module reaction control subsystem (CM RCS) successfully performed all required maneuvers and maintained proper spacecraft control until electrical problems disabled the B system at T+1641 seconds and the A system at T+1649 seconds, maintaining CM control through the max. q region. Both CM RCS systems performed nominally up to the time of the electrical failure.

Failures incurred during the mission were: (1) failure of the SM quad A to operate because of a malfunction in the oxidizer supply system, (2) partial, or possibly complete, loss of thrust from one of the -Y engines when the automatic coils were used (the engine involved and the cause of this failure could not be definitely determined from the available data, (3) loss of both CM RCS systems after blackout because of the transfer of the RCS control motor switches from the CM to the SM position, (4) loss of the use of CM RCS system B for the propellant depletion burn as a result of the B system logic power failure, (5) loss of the use of the A and B system helium interconnect valves, and the A system fuel tank and the B system oxidizer tank helium bypass pyrotechnic valves as a result of the B system logic power failure, and (6) failure of the CM RCS oxidizer isolation valves to close during the postflight deactivation due to incompatibility between the valves and the oxidizer. The sequence of RCS events is given in table 7.9-I.

7.9.1 Service module reaction control subsystem. -

Description: The Block I type SM RCS on spacecraft 009 consisted of four identical RCS quads equally spaced at 90° intervals around the service module. (See fig. 7.9-1.) Each of the four RCS quads was mounted on a hinged panel of the SM. Each quad included four 95-pound thrust radiative-cooled rocket engines, an oxidizer tank, a fuel tank, a helium tank, and associated components such as valves and regulators. (See fig. 7.9-2.)

High pressure helium, used to pressurize the propellants, was routed from a storage tank through parallel isolation (shutoff) valves, parallel

regulators, and check valves into the propellant tanks. The check valves were used to prevent contamination of the helium by propellant vapors.

The hypergolic propellants, nitrogen tetroxide (oxidizer) and a 50:50 mixture of N_2H_4 and UDMH (fuel), were stored in positive expulsion teflon bladders mounted inside the propellant tanks. The propellants were forced from the bladders through isolation valves to the SM RCS engines. Each engine included electrically operated fuel and oxidizer valves with an automatic coil operated by signals from the stabilization and control subsystem (SCS) and a direct coil operated by signals from automatic sequencers.

All SM RCS components on spacecraft 009 were certified for the short. duration mission. No components were known to be malfunctioning or failed on the SM RCS prior to lift-off except the propellant-quantity-*gaging* system, which was deleted because of problems encountered during checkout, and some primary-stage helium check valves. All secondary-stage check valves were functioning normally.

The SMRCS propellant servicing was accomplished on T-11 to T-9 days. (See table 7.9-II,) The results of the chemical analysis performed on the propellants prior to servicing are shown in table 7.9-III. The SM RCS helium servicing was accomplished on T-4 days. (See table 7.9-IV.)

Performance: Analysis of data showed that no thrust was obtained fromthe engines on quad A and that one -Y engine was inoperative. This caused the quad C positive and negative pitch (+P and -P) engines to alternately fire and the quad D positive and negative yaw (+Y and -Y) engines to alternately fire to maintain proper attitudes and rates. As a result of this duty cycle, the net +X ΔV produced during the ullage maneuvers was 25 to 45 percent of that expected. (See section 7.11 and figs. 7.11-4 and 7.11-5.) With the pitch engines on quad A disabled, control authority for the CSM pitch-dawn maneuver was reduced; however, the maneuver was satisfactorily completed.

The first evidence of a failure in the SM quad A was noted when the SM RCS was initially operated at T+843.7 seconds for a 3-second, direct coil, +X translation maneuver that provided thrust for the CSM/S-IVB physical separation. A pitch-up disturbance torque was generated during the maneuver (see section 7.11 and fig. 7.U-2) which required a pitch-down correction. This pitch-dawn correction overshot and required a pitch-up correction to return the spacecraft to the desired attitude, Analysis of the spacecraft data revealed that, during the initial maneuver, quads B, C, and D fired normally using the direct coils, but no thrust was generated by the +X/-P engine on quad A, resulting in the pitch-up error. The pitch-down correction rate and the pitch-up

correction rate for the overshoot were one-half that anticipated indicating that the positive and negative pitch engines on quad A were both inoperative (see section 7.11).

The second maneuver programmed was an 18-second +X translation with SCS automatic attitude and rate control. Data showed that the -P and +P engines on quad C were alternately firing during this maneuver with a duty cycle of approximately 50 percent on and 50 percent off, again indicating that no thrust was being produced by the +X translation engine on quad A (see section 7.11 and fig. 7.11-2).

The third and fourth maneuvers were automatic coil +X translation maneuvers used to settle the SPS propellant prior to SPS firing. The third maneuver was initiated from nominal spacecraft attitudes. Data again showed alternate firing of opposing quad C pitch engines. (See fig. 7.11-4.) The fourth maneuver was started with substantial pitch and yaw attitude errors introduced by the SPS during tailoff. (See fig. 7.11-5.) Pitch corrections were made at half rate and the same alternate firing of opposing engines was experienced, verifying the earlier indication that quad A was inoperative.

The last maneuver performed by the SM RCS was the 90° pitch-down pre-entry attitude change. The pitch-rate data again indicated the quad A failure. (See section 7.11 and fig. 7.11-7.)

The quad A failure was further evidenced by decreases in temperatures where temperature should have increased if the quad was firing. Temperature decreases were noted on the quad A package, the quad A minus pitch engine injector head, the quad A CCW roll engine injector head, the quad A minus pitch engine fuel solenoid valve, and the quad A CCW roll engine fuel solenoid valve (see figs. 7.9-3 and 7.9-4). These temperature drops indicated that one propellant was flowing and providing evaporative cooling, but no engine was firing. The -P and CCW roll fuel solenoid temperatures decreased to the same temperature as the fuel supply and stabilized there, indicating that fuel, rather than oxidizer, was flowing. In addition, indications are that the quad A helium supply tank pressure drop corresponded to a calculated "fuel flow only" value (based on flow into a vacuum without combustion chamber back pressure) which was approximately 62 percent of a normal firing pressure drop.

The only logical way to stop oxidizer flow to all four engines simultaneously is to close the oxidizer propellant isolation valve. During postflight decontamination of the CM RCS, it was determined that the oxidizer isolation valves had seized in the open position after 11 days exposure to nitrogen tetroxide (N_2O_4). These CM valves are identical to valves used on the SM. As presented in the servicing section, the SM RCS propellant isolation valves were exposed to propellants on the launch pad for 10 days prior to being opened. This evidence indicates

that the quad A oxidizer isolation valve seized in the closed position prior to launch, disabling the system. This compatibility problem of the valve with oxidizer has been recognized for some time and previously experienced in tests. Consequently, a completely new valve has been designed, qualified, and is being used on spacecraft 011 and all subsequent spacecraft.

The first evidence of a failure of an SM yaw engine was noted during the first automatic mode +X translation by an alternate firing duty cycle of the quad D engines. This duty cycle ranged from approximately 50 percent on, 50 percent off to 90 percent on, 10 percent off, indicating a control problem in the yaw engines (see section 7.11).

A similar duty cycle was noted during the third and fourth +X translations. During the fourth +X translation (ullage maneuver prior to second SPS firing) the SPS tailoff from the previous SPS firing introduced a +Y rate error requiring -Y engines of the RCS to fire for correction. This correction rate was one-half that anticipated. A similar yaw rate disturbance was introduced at the completion of the second SPS burn with similar RCS correction rates (see section 7.11 and fig. 7.11-5), indicating that one yaw engine was inoperative. Data again showed the same alternate firing of opposing engines as in the two preceding +X translation maneuvers. Analysis of the yaw rate data and realized duty cycles showed that these conditions could have been produced by malfunctions in either or both -Y engines. Even though these conditions could possibly have been produced by partial thrust degradation in both -Y engines, the more probable failure mode would be failure of only one engine. Analyses showed that, assuming nominal performance of the -Y/-X quad D engine, the -Y quad B engine would have had to perform at approximately 70 percent thrust early in the mission and constantly degrade to approximately 20 percent thrust at the end of the mission. Conversely, assuming nominal performance of the -Y/+X quad B engine, the -Y quad D engine would have had to produce essentially no thrust to produce the realized conditions. The most probable of these assumptions is the complete failure of the quad D engine. Also, yaw engine duty cycles produced during the +X translation burns indicated that the torque required to displace the spacecraft through the rate deadband zone to the positive limit was an order of magnitude of that produced by the center-of-gravity offset in the Y axis with +X engines of both quads B and D firing. Similarly, the torque required to displace the spacecraft from the +Y limit to the -Y limit, when holding the ±0.2 deg/sec limit cycle, was an order of magnitude of the torque produced by only one -Y engine firing. These considerations again indicate that the -Y/+X quad D engine was inoperative. The conclusion is further substantiated by analysis of the quad engine package temperature (see fig. 7.9-3). From CSM/S-IVB separation to CM/SM separation, quad D shawed a temperature increase that was 20° F less than that in quad B and 70° F less than that in quad C. In light of the duty cycles, this again indicates that the -Y quad D engine was not firing when commanded.

In conclusion, the analysis of available data indicates that the -Y/-X quad D engine was inoperative or malfunctioning, but the failure mode could not be determined due to lack of information. It can be deduced, however, that since bilevel indications of firing were recorded, electrical continuity existed in at least one of the automatic coils in the engine that was malfunctioning. Also, if both propellants would have been flowing but not producing thrust, as in the case of a combustion chamber failure, the overall quad pressure drop would have been approximately twice that of the normal pressure drop of the other quads, which was not the case. Since no other data were available for further analysis, it can only be concluded that for some unknown reason, when the SCS signaled the -Y engines to fire using the automatic coils, either the fuel or oxidizer valve of one of the -Y engines, most probably the -Y/-X quad D engine, failed to respond, thus disabling the engine. Postflight analysis of the data has led to no remedial action.

Attitude control was satisfactorily maintained during the mission, and attitude hold limit cycle control was nominal. (See section 7.11 and fig. 7.11-3.) Attitude corrections resulting from major attitude disturbances were accomplished with somewhat reduced authority (section 7.11 and fig. 7.11-5); however, all corrections were satisfactorily accomplished.

The SM RCS pressurization subsystem, including all valves and regulators, was activated on the ground prior to launch. Data shown in table 7.9-V indicate that regulated pressures at initiation of the first SM RCS burn were initially 15 psi above operating values of 181 ± 4 psia because activation reference pressure was sea level rather than space. During the burn, pressures dropped to normal and, after the burn, returned to regulator lockup values, which were approximately 3 to 4 psi above the regulated pressures. The pressures were considered nominal throughout the mission.

All helium source pressures dropped at first SM firing. However, for quad A, the drop corresponded to that expected for fuel flow only. The source pressures measured during the ullage maneuvers and the CSM pitch-down maneuver support the first burn data. (See fig. 7.9-5.)

With the exception of quad A where indications are that the oxidizer isolation valve seized in the closed position, all propellant supply systems functioned normally.

The SM RCS quad temperature rise due to boost heating was near the predicted values (see fig. 7.9-3) and verified those established on Mission A-102 (ref. 5). Quad temperatures due to soakback after engine firings were also near anticipated values. Temperature profiles of valves and injectors on both the roll and pitch engines on quad A all showed definite cooling effects after the first burn at CSM/S-IVB

separation in contrast to the expected temperature rises due to soakback as experienced in the other quads. (See fig. 7.9-4.) Propellant tank temperatures and propellant manifold temperatures were nearly invariant at 70° + 5° F throughout the mission, as was expected. Quad B valve and injector head temperatures measured were nominal for the realized duty cycles. Boost heating, as expected, was most pronounced in the forward-firing engines, reaching a maximum of 200° F on the injector head. (See fig. 7.9-6.)

7.9.2 Command module reaction control subsystem.-

Description: The Block I type CM RCS consisted of two identical redundant systems, A and B, which operated simultaneously. Each system of the CM RCS consisted of six 93-pound thrust ablative-cooled rocket engines, an oxidizer tank, a fuel tank, a helium tank, and associated components such as filters, valves, and regulators. (See figs. 7.9-7 to 7.9-9.) The propellants used were nitrogen tetroxide (oxidizer) and monomethylhydrazine (fuel). The only purpose of the CM RCS was to control CM attitude after CM/SM separation.

The CM RCS components and operating principles were similar to those in the SM RCS except for the engines. The CM RCS engines were ablatively cooled, whereas the SM RCS engines were radiatively cooled, The CM RCS engines included both automatic and direct coils in the electrically operated propellant valves. The automatic coils were operated by signals from the SCS and the direct coils were operated by signals from the propellant dump sequencer installed in spacecraft 009 to control the disposal (dump) of propellants before the CM landed; on manned missions the crew will perform this function.

All CM RCS components were certified for the short duration mission. The only CM component known to be failed prior to lift-off was the CM B system relief valve burst diaphragm on the fuel side. This was found to be ruptured during checkout testing and was not replaced for the mission. (The burst diaphragm provides redundant sealing not required for this short duration mission.) As in the SM, some primary helium check valves were again leaking out of tolerance, but were not replaced since the secondary valves were functioning normally.

The CM RCS propellant servicing was accomplished on T-11 day to T-9 day; however, the system B helium relief valve vent port on the fuel side was not sealing properly and the system required pressurizing to approximately 107 psia to effect proper sealing. (See table 7.9-VI.)

On T-4 day the CM RCS helium servicing was accomplished, and at T+1454.75 seconds the CM RCS system was activated. (See table 7.9-VI.)

Performance: Control by the CM RCS was initiated following SM/CM separation at T+1455 seconds, and operation was nominal until T+1649 seconds and T+1641 seconds when electrical malfunctions disabled automatic operation of systems A and B, respectively.

Failure of the B system logic power caused the B system engine direct coils to be inoperative at the time of propellant depletion burn (T+1915 to T+2050 seconds). Therefore, both A and B system propellants were burned off through the A system engines (with the exception of the +P engine which is normally disabled) resulting in greater than nominal charring of the A system engines, particularly the roll engines. Satisfactory propellant jettison was accomplished, however, with nominal propellant residuals.

During the purge operation, data indicated that the A system fuel and B system oxidizer tank pressures did not decay. (See fig. 7.9-10.) Postflight inspection of the A and B system helium interconnect squibs, the A system fuel tank helium bypass squib, and the B system oxidizer tank helium bypass squib, showed that these squibs had not fired, thus preventing depressurization. These valves were also disabled by the B system logic power anomaly. (See section 7.12.)

All component temperature measurements, including the propellant tank, the helium tanks, engine valves, and the engine outer wall, remained constant at launch temperatures of 600 to 65° F, as expected, from launch to system activation. Helium and propellant tank pressures remained constant, within telemetry accuracies, at loaded conditions from launch to system activation with no indication of helium leakage. (See table 7.9-VI.)

Decay in helium source pressures due to system activation was nominal, agreeing with theoretically calculated values. (See table 7.9-VI.) Following system activation, small propellant usage resulted in no noticeable change in source pressure prior to the depletion burn at T+1915 seconds. Pressure decay due to the depletion burn is shown in figure 7.9-11.

Within expected instrumentation accuracies, propellant tank pressures reached nominal values of 294 ± 5 psia following system activation. These pressures remained stable during all CM RCS activity, indicating nominal system operation through the propellant depletion burn.

Eased on measured propellant residuals and nominal propellant flow rates during burnoff, propellant usage was estimated to be nominal (approximately 12 to 15 pounds). The following amounts of propellants were removed during deactivation: 5 pounds of fuel were removed fromthe helium side and purge lines of the CM systems A and B; 2 pounds of fuel were removed fromthe propellant side of both systems; 1 pound of oxidizer

was removed from the helium side and purge lines of both systems; and $1\frac{1}{4}$ pounds of oxidizer were removed from the propellast side of both systems. The propellants removed from the helium side of the systems were not unexpected since the B system fuel and A system oxidizer tank bypass lines were opened during purging.

All measured temperatures showed nominal and, in some cases, less than expected effects of reentry heating and depletion burn on the CM RCS components. The propellant tank temperatures remained nearly constant at about 60° to 65° F.

The data are questionable from T+1649 seconds until T+2125 seconds because of the low voltage on the spacecraft main buses. The dashed lines on figures 7.9-10 and 7.9-11 represent estimated nominal traces at correct spacecraft bus voltage.

During recovery of the spacecraft after landing, no problems were reported with the CM RCS or with propellants or propellast fumes. During deactivation, which began 5 days later at Norfolk, Virginia, the B system +Y oxidizer valve failed to open when the direct coil was commanded. A short to ground was found on both sides of the coil. During decontamination operations, the electrical leads to the coil were inadvertently reversed on the spacecraft side of a terminal strip such that both sides of the coil were connected to ground. The automatic coil was found to be in proper working order.

When the A and B system oxidizer isolation valves were cycled to the closed position during the deactivation procedures, the valve indicators showed the valves to be closed but a gas flow through the valves did not decrease, indicating that both valves were seized in the open position. Since they were normally open during the flight and had no inflight function, this failure had no effect on the flight. Similar problems during development and qualification of this valve indicated incompatibility between the oxidizer and the valve. This valve has been replaced on spacecraft 011 and all subsequent spacecraft. There was no problem with the fuel isolation valves.

Postflight inspection also revealed that the fuel bypass valves on both the A and B systems were incorrectly wired in that the system A valve was wired to the B pyro battery instead of the A battery, and the system B valve was wired to the A pyro battery instead of the B battery. As a result of this condition the helium pressure in both A and B systems was able to bleed down during purging. In the normal configuration the high pressure helium would have been trapped in the B system.

Requested postflight testing of the CMRCS consisted of propellant bladder leak checks, electrical integrity checks of the CM B system +Y

engine direct oxidizer coil., oxidizer isolation valve failure analysis, functional checks of the engine valves, char analysis of the A system CCW and -Y engines, and relief valve leakage tests.

The *only* tests completed to date were those concerning the direct coil short. These tests revealed that the electrical leads to the coil were incorrectly wired to the spacecraft, side of *a* terminal strip such that both sides of the coil. were connected to ground. When the wiring was corrected, the coil performed normally.

Results of all other postflight tests were not available for this report but will be documented in a supplemental report.

TABU 7.9-I.- RCS EVENT TIMELINE, MISSION AS-201

Event	Time, sec	
	On	off
1. SM 3-second direct coil +X translation	843.7	846.7
2. SM 18-second automatic coil +X translation with attitude control	846.7	864.6
3. SM attitude control only as required	864.6	1181.2
4. SM 30-second automatic coil +X translation with attitude control (SPS ullage no. 1)	1181.2	1212.2
5. SM roll control only during SPS burn	1212.2	1395.2
6. SM attitude control only as required	1395.2	1395.7
7. SM 15-second automatic coil +X translation with attitude control (SPS ullage no. 2)	1395.7	1411.7
8. SM roll control only during SPS burn	1411.7	1420.7
9. SM attitude control only as required	1420.7	1424.2
10. SM preentry 90° pitch maneuver with roll and yaw attitude control	1424.2	1442.1
11. SM attitude control only as required	1442.1	1454.7
12. CM-SM separation (SM control transferred to SM jettison controller) and CM activation	1454.7	NA
13. CM attitude control as required	1456.0	1462.6
14. CM pitch maneuver with roll and yaw attitude control as required	1462.6	1479.1
15. CM attitude control as required	1479.1	1479.2
16. CM roll maneuver with pitch and yaw attitude control as required	1479.2	1515.1
17. CM attitude control as required	1515.1	1580.7

TABLE 7.9-I.- RCS **EVENT TIMELINE, MISSION** AS-201 - Concluded

Event	Time sec	
	On	Off
18. CM **roll.** attitude control and pitch and yaw rate damping	1580.7	1649.
19. Loss of effective CM RCS control[a]	1649	NA
20. CM RCS pyro interconnect valve firing[b]	1915	NA
21. CM RCS propellant depletion burn[c]	1915	2050
22. CM RCS pyro bypass valve firing[b]	2175	NA
23. CM RCS helium purge[d]	2175	2250

[a] RCS control motor switches switched from CM to SM position disabling the CM RCS.

[b] All pyrotechnic valves operated from the A pyro bus were fired including the fuel and oxidizer interconnect valves and the B system fuel and A system oxidizer tank bypass valves. All pyro valves operated from the B pyro bus were disabled by the B system logic power anomaly.

[c] The propellant depletion burn was completed using only the CM RCS A system engines. The B system engine direct coils were disabled by the B system logic power anomaly.

[d] The helium purge was completed using the B system fuel and A system oxidizer tank bypass lines.

TABLE 7.9-II.- SM RCS PROPELLANT SERVICING, MISSION AS-201

System	Oxidizer loading date, 1966	Oxidizer, lb (a)	Tank pressure, psia	Fuel loading date, 1966	Fuel, lb (a)	Tank pressure, psia
A	Feb. 15 to 16	137.4	29	Feb. 16 to 17	69.1	40
B	Feb. 15 to 16	136.1	30	Feb. 16 to 17	68.6	37
C	Feb. 15 to 16	136.4	30	Feb. 16 to 17	67.2	37
D	Feb. 15 to 16	134.6	30	Feb. 16 to 17	68.0	36
Calculated nominal parameters		137.4			69.3	

[a]Fuel and oxidizer quantities were verified by pressure-volume calculation to an estimated accuracy of ±2 percent.

TABLE 7.9-III.- RCS PROPELLANT ANALYSIS, MISSION AS-201

Propellant	Specification requirement		Service	
	SM	CM	SM	CM
Fuel	N_2H_4 - UDMH	MMH	N_2H_4 50.6 percent UDMH 47.6 percent	MMH
Purity, percent	98 min.	98 min.	98.2	98.7
H_2O equivalent, percent	2 max.	2 max.	1.8	1.3
Density, gm/ml	-	0.872±0.002 max.	-	0.8707
Transmittanoy, percent	-	90 min.	-	92
Filterable solids, mg/liter	1.0 max.	1.0 max.	0	0.5
sample extract date	-	-	Feb. 16, 1966	Feb. 16, 1966
Sample analysis date		-	Feb. 16, 1966	Feb. 16, 1966
Oxidizer	N_2O_4	N_2O_4	N_2O_4	N_2O_4
Purity, percent	99.5 min.	99.5 min.	99.2	99.8
H_2O equivalent, percent	0.1 max.	0.1 max.	0.1	0.1
Chloride, as nitrosylchloride, percent	0.08 max.	0.08 max.	0.05	0.04
Filterable solids, mg/liter	1.0 max.	1.0 max.	0	.5
Nitrogen oxide, percent	0.85 max.	0.85 max.	0.8	.8
Sample extract date	-	-	Feb. 15, 1966	Feb. 14, 1966
Sample analysis date	-	-	Feb. 15, 1966	Feb. 14, 1966

TABLE 7.9-IV.- SM RCS HELIUM SERVICING, MISSION AS-201

System	Loading date, 1966	Pressure, psia	Temperature, °F	Helium manifold, psia	Preflight date, 1966	Pressure, psia	Temperature, °F	Helium manifold, psia
A	Feb. 22	4190	73	167	Feb. 26	4090	73	200
B	Feb. 22	4170	69	184	Feb 26	4020	67	212[a]
C	Feb. 22	4190	73	168	Feb 26	4080	72	197
D	Feb. 22	4140	76	191	Feb 26	4060	74	211[a]
Nominal parameters		4150±50	70±5			4150±50	70±5	

[a]Preflight pressure transducer calibration check at KSC showed these parameters were indicating 8 psi higher than actual.

TABLE 7.9-V.- SM RCS INITIAL OPERATION PARAMETERS, MISSION AS-201

System	Initial operation time, actual, sec	Helium source pressure at -		Helium manifold pressure at -	
		Preactivation (845.7 sec)[a]	Postactivation (847.7 sec)[a]	Preactivation (845.7 sec)[a]	Postactivation (847.7 sec)[a]
A	846.7	4062	4041	198	187
B	846.7	4008	3987	208[b]	191[b]
C	846.7	4072	4051	197	178
D	846.7	4061	4018	209[b]	193[b]

[a]One second before actual, initial operation time.

[b]Preflight pressure transducer calibration check at KSC showed these parameters were indicating 8 psi higher than actual.

TABLE 7.9-VI.- CM RCS PREPARATION, MISSION AS-201

a. CM RCS Propellant Servicing

	Oxidizer loading date, 1966	Oxidizer, lb (a)	Tank pressure, psia	Fuel loading date, 1966	Fuel, lb (a)	Tank pressure, psia
System A	Feb. 15	88.3	59	Feb. 16 to 17	44.5	65
System B	Feb. 15	88.4	50	Feb. 16 to 17	44.5	107
Calculated nominal parameters		88.7			44.9	

[a]Fuel and oxidizer quantities were loaded by weight with an accuracy of ±1 percent.

b. CM RCS Helium Servicing

	Loading date, 1966	Pressure, psia	Temperature, °F	Helium manifold, psia	Preflight date, 1966	Pressure, psia	Temperature, °F	Helium manifold, psia
System A	Feb. 22	4160	74	25	Feb. 26	4140	71	25
System B	Feb. 22	4210	67	15	Feb. 26	4170	64	15
Nominal parameters		4150±50	70±5			4150±50	70±5	

c. CM RCS Activation

	Activation time, actual, sec	Helium source				Fuel tank				Oxidizer tank			
		Pressure, psia		Temperature, °F		Pressure, psia		Temperature, °F		Pressure, psia		Temperature, °F	
		Pre-activation	Post-activation	Pre-activation	Post-activation	Pre-activation	Post-activation	Pre-activation	Post-activation	Pre-activation	Post-activation	Pre-activation	Post-activation
System A	1454.7	4104	3500	69	69	66	290	63	65	61	286	-	-
System B	1454.7	4131	3478	62	60	105	285	-	-	50	285	63	65

NASA-S-66-6285 MAY 6

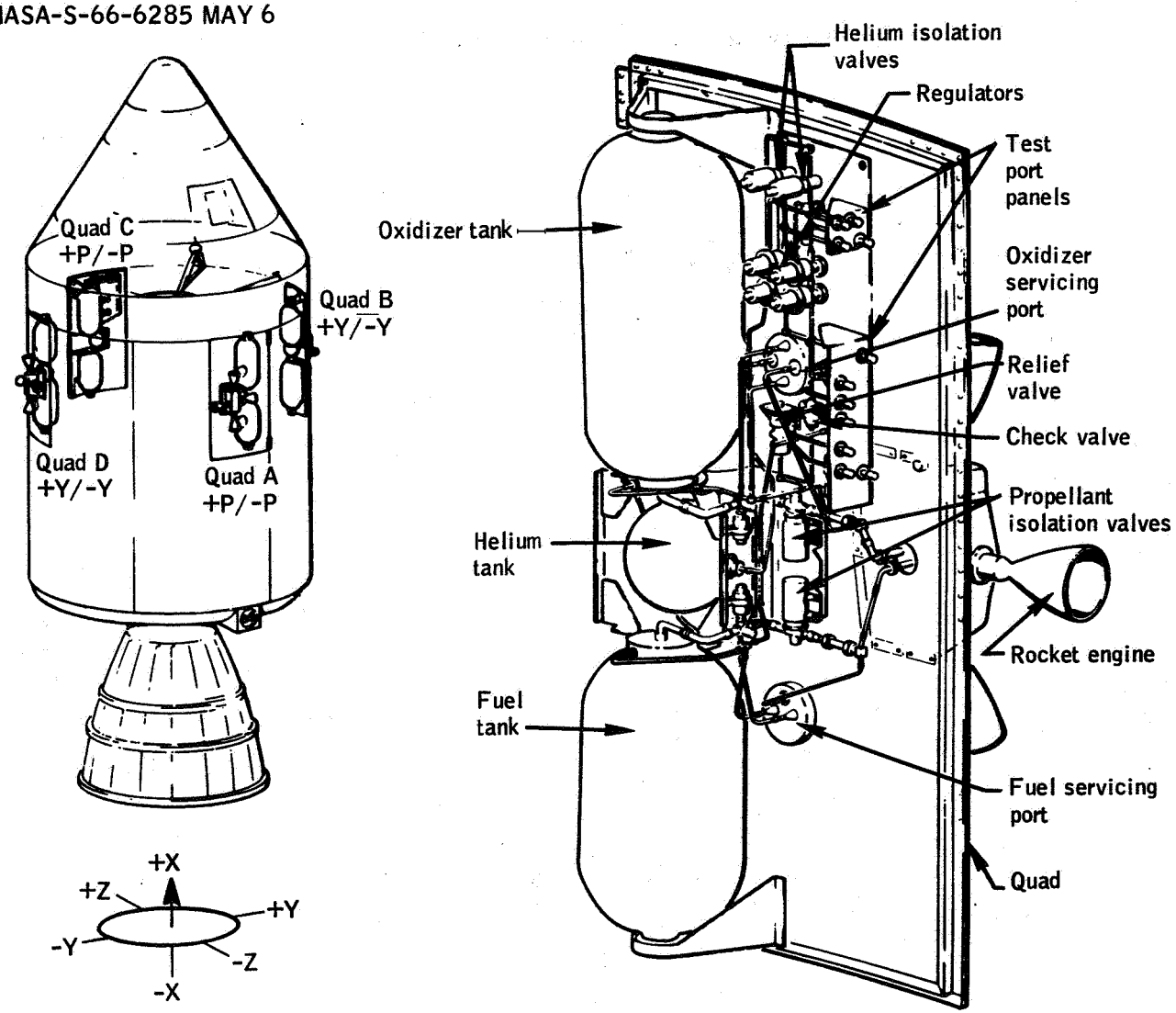


Figure Service module reaction control subsystem, Mission AS-201.

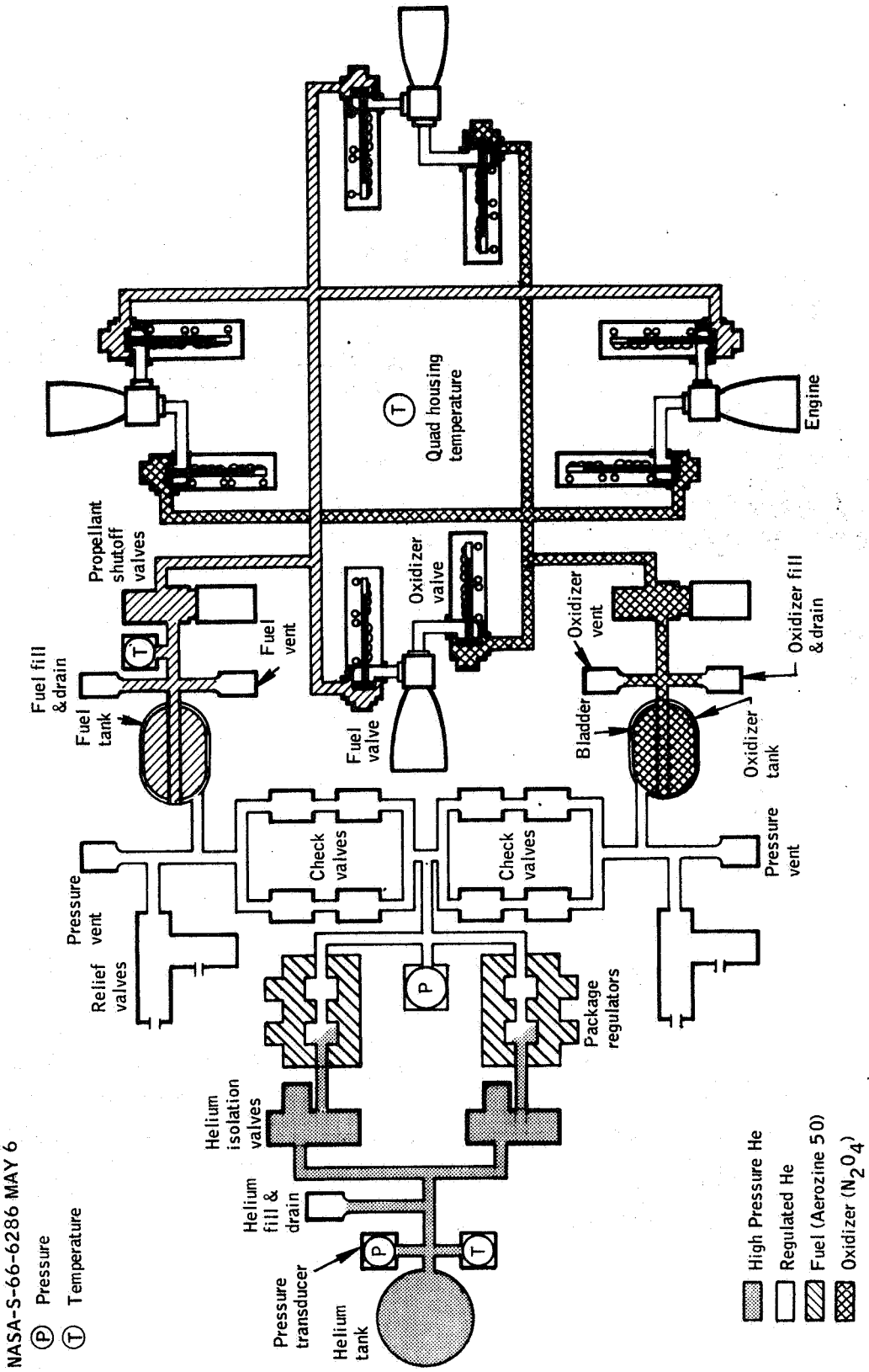
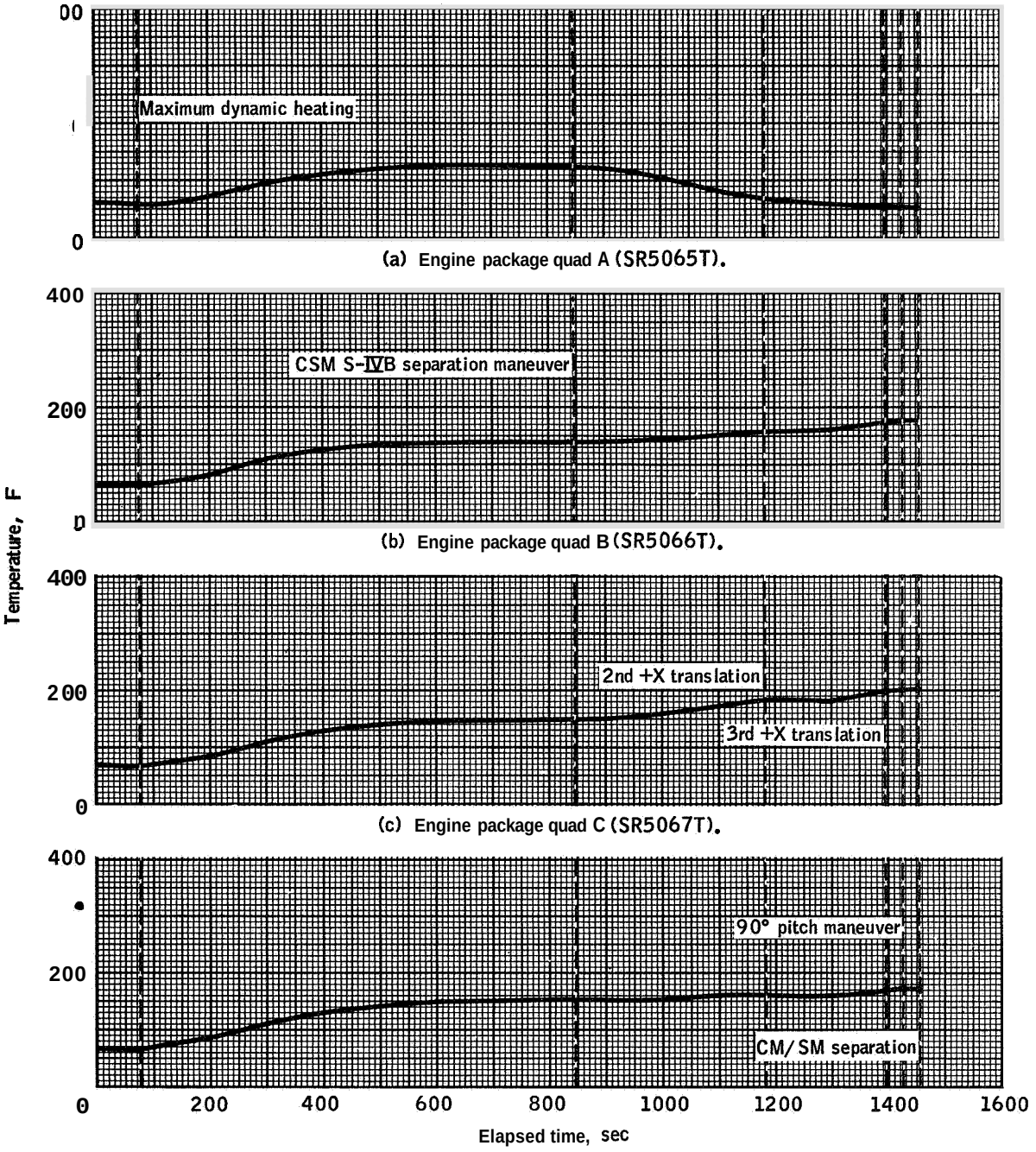


Figure 7.9-2.- Schematic of typical SM RCS quad, Mission AS-201.

NASA-S-66-6287 MAY 6



(a) Engine package quad A (SR5065T).

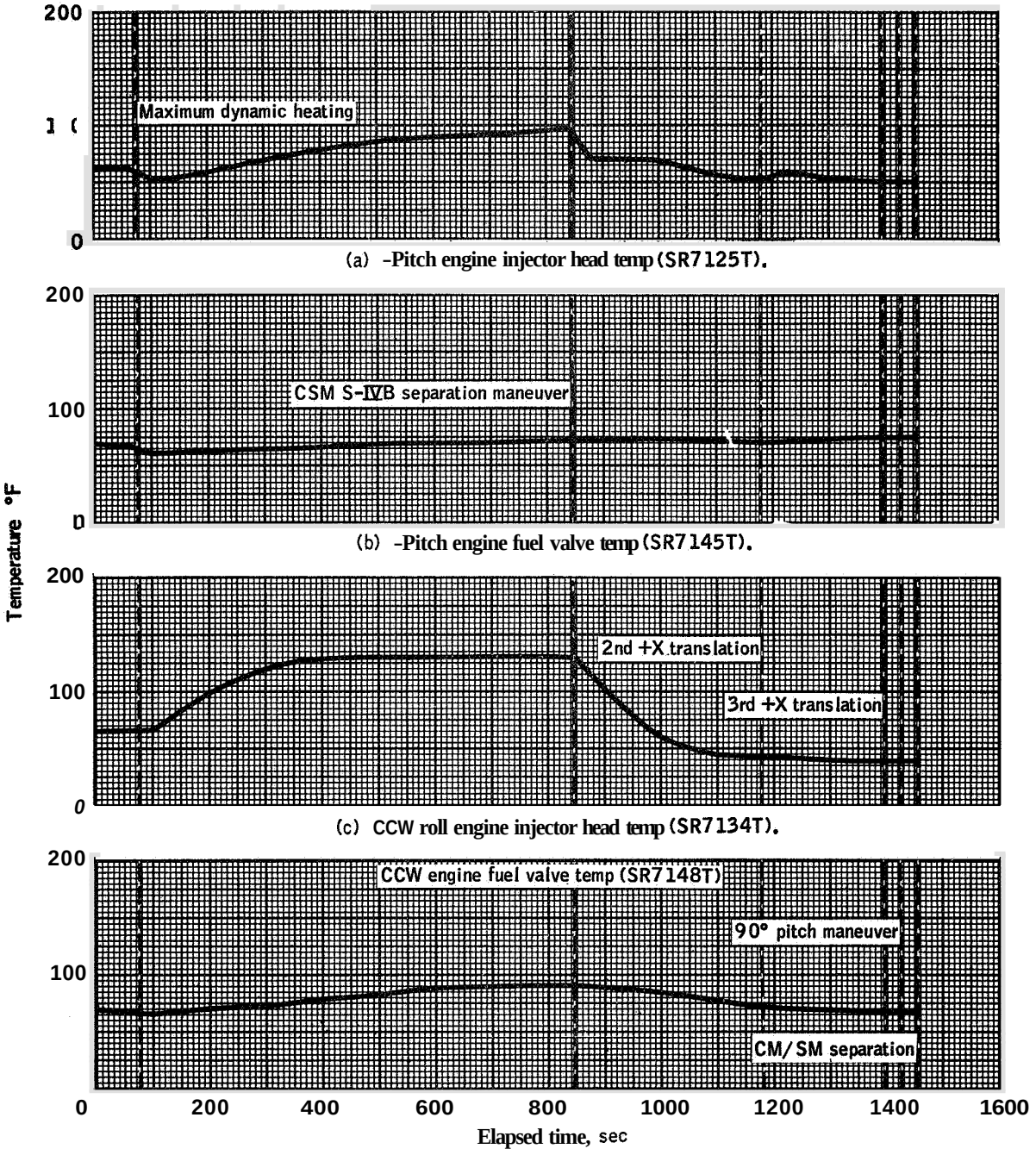
(b) Engine package quad B (SR5066T).

(c) Engine package quad C (SR5067T).

(d) Engine package quad D (SR5068T).

Figure 7.9-3.- SM RCS quad engine package temperatures, Mission AS-201.

NASA-S-66-6288 MAY 6



(a) -Pitch engine injector head temp (SR7125T).

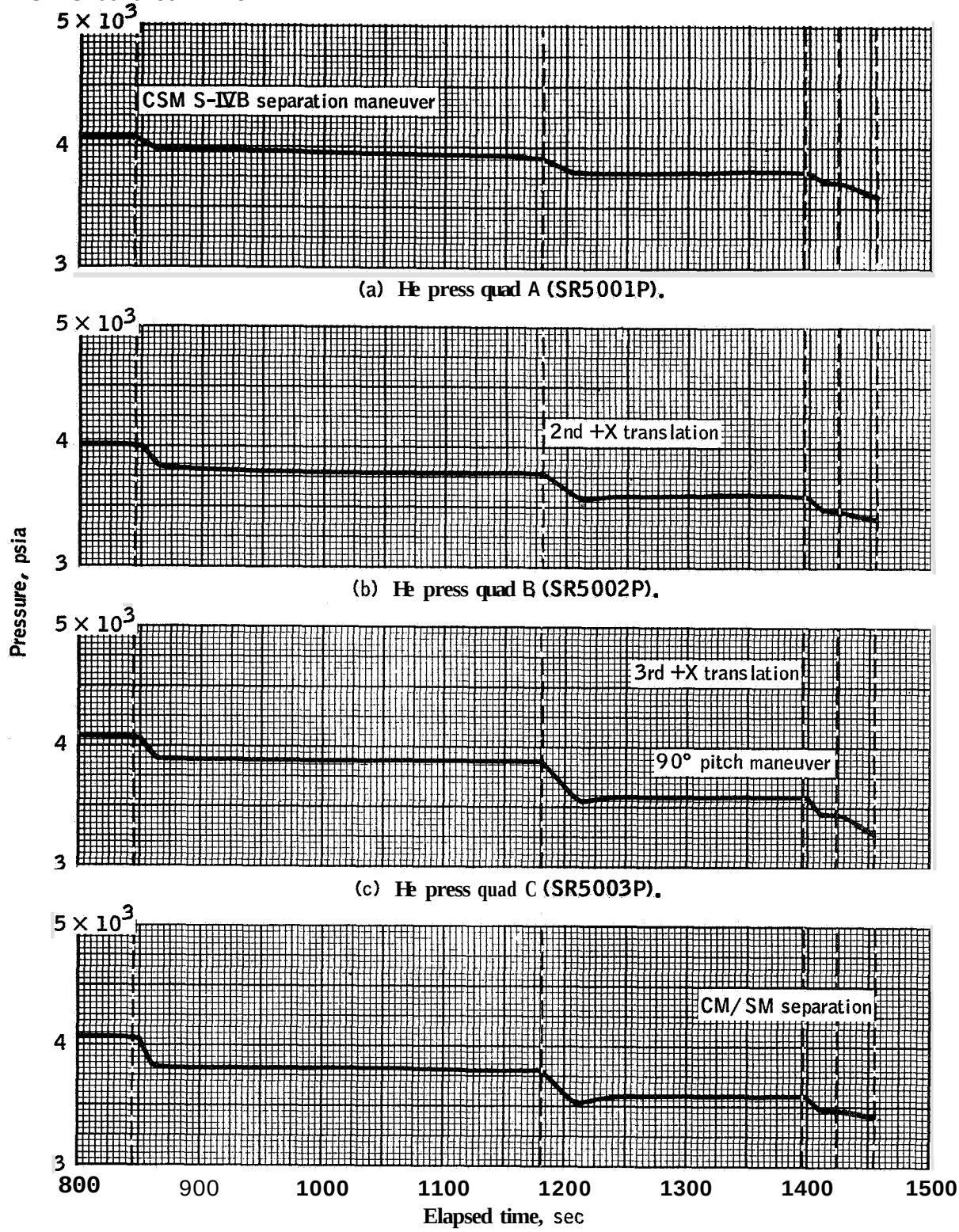
(b) -Pitch engine fuel valve temp (SR7145T).

(c) CCW roll engine injector head temp (SR7134T).

(d) CCW roll engine fuel valve temp (SR7148T).

Figure 7.9-4.- SM RCS quad A fuel valve and injector head temperatures, Mission AS-201.

NASA-S-66-6289 MAY 6



(a) He press quad A (SR5001P).

(b) He press quad B (SR5002P).

(c) He press quad C (SR5003P).

(d) He press quad D (SR5004P).

Figure 7.9-5.- SM RCS helium source pressures, Mission AS-201.

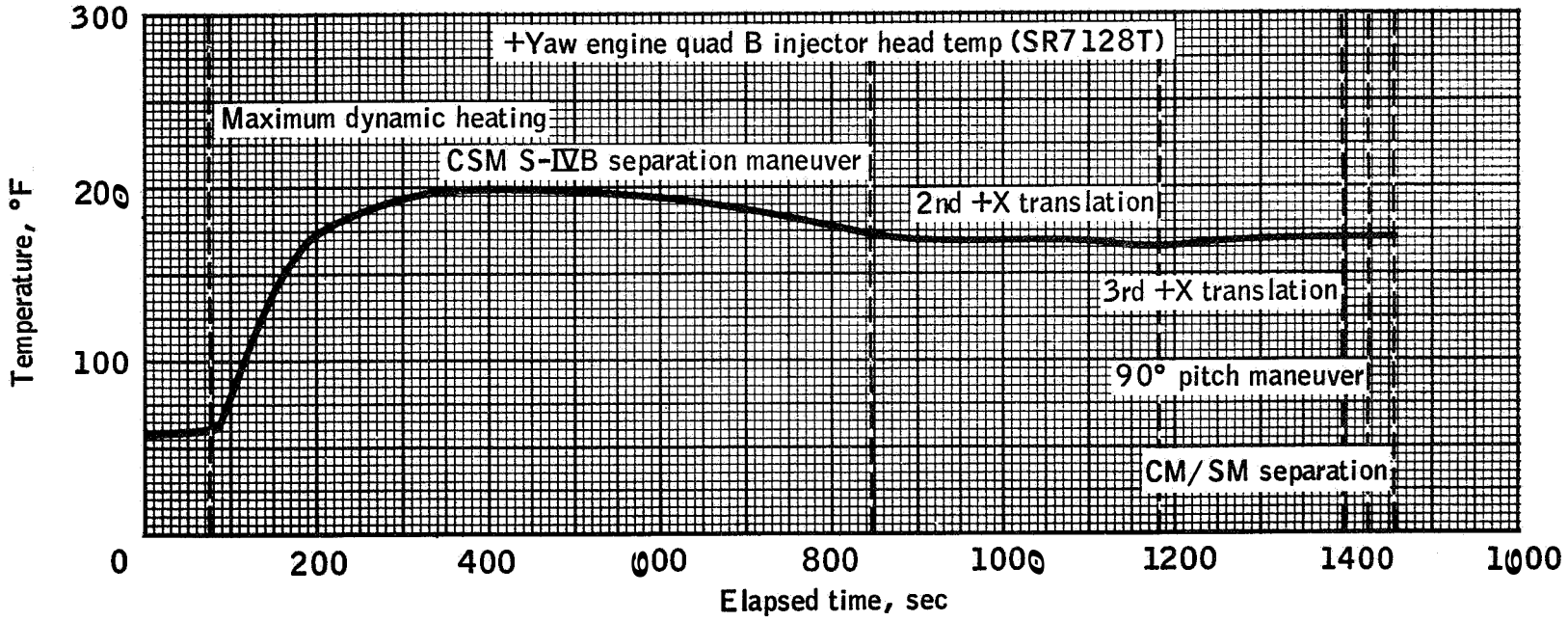


Figure 7.9-6.- SM RCS quad B forward firing engine injector head temperature, Mission AS-201.

NASA-S-66-6291 MAY 6

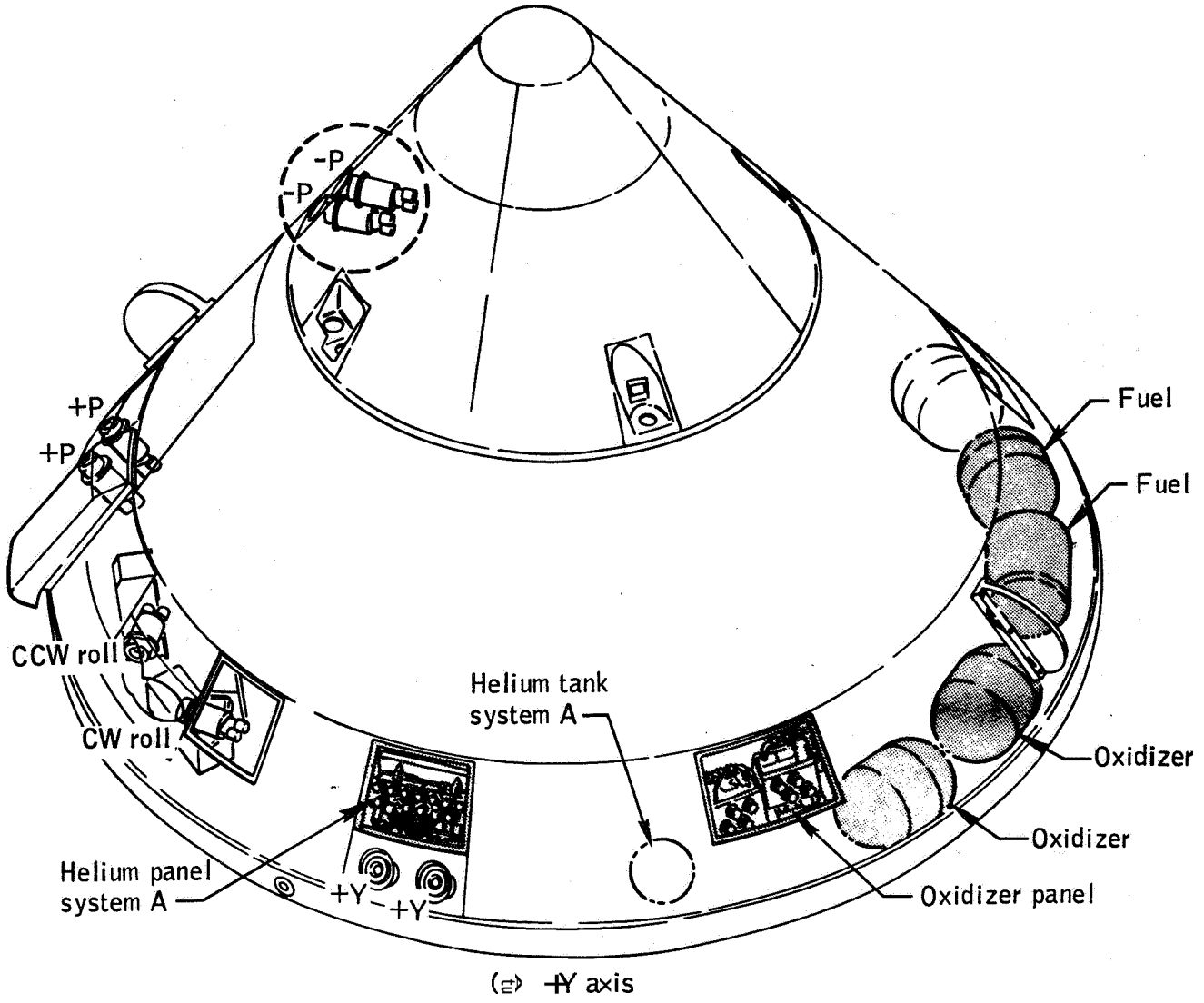
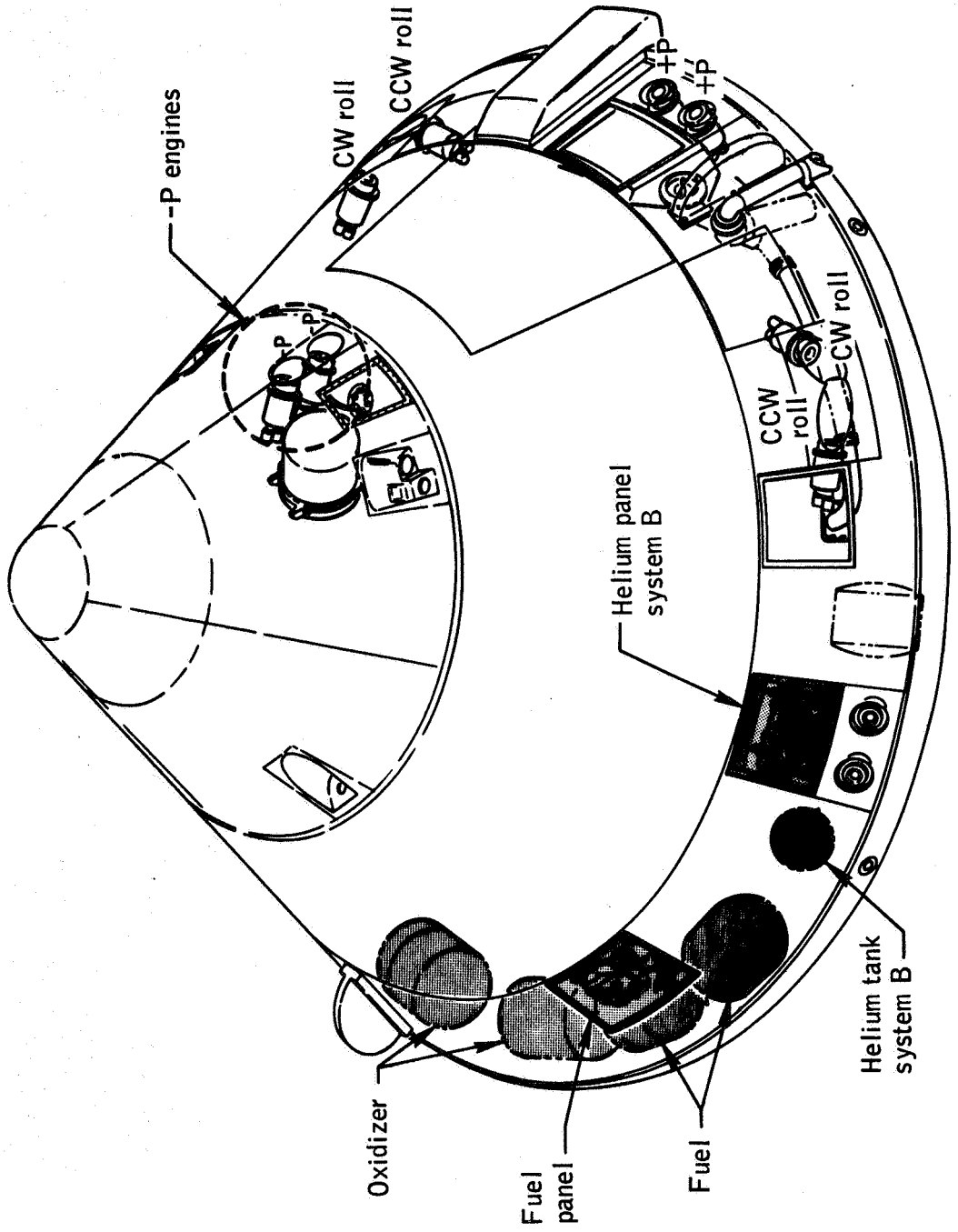


Figure 7.9-7.- CM RCS component location, Mission AS-201.



(b) -Y axis.

Figure 7.9-7.- Concluded.

NASA-S-66-6292 MAY 6

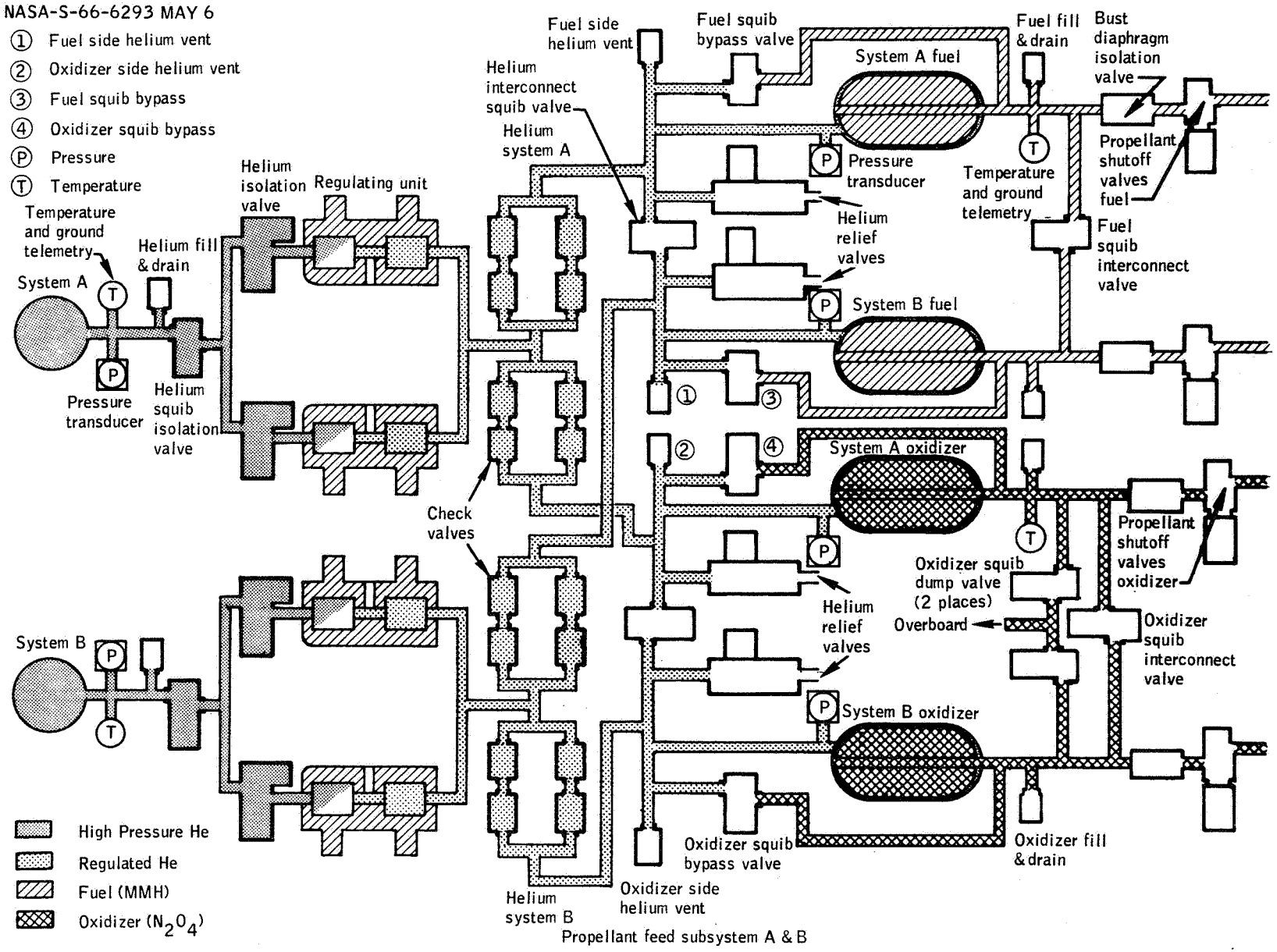


Figure 7.9-8.- Schematic of CM RCS propellant distribution, Mission AS-201.

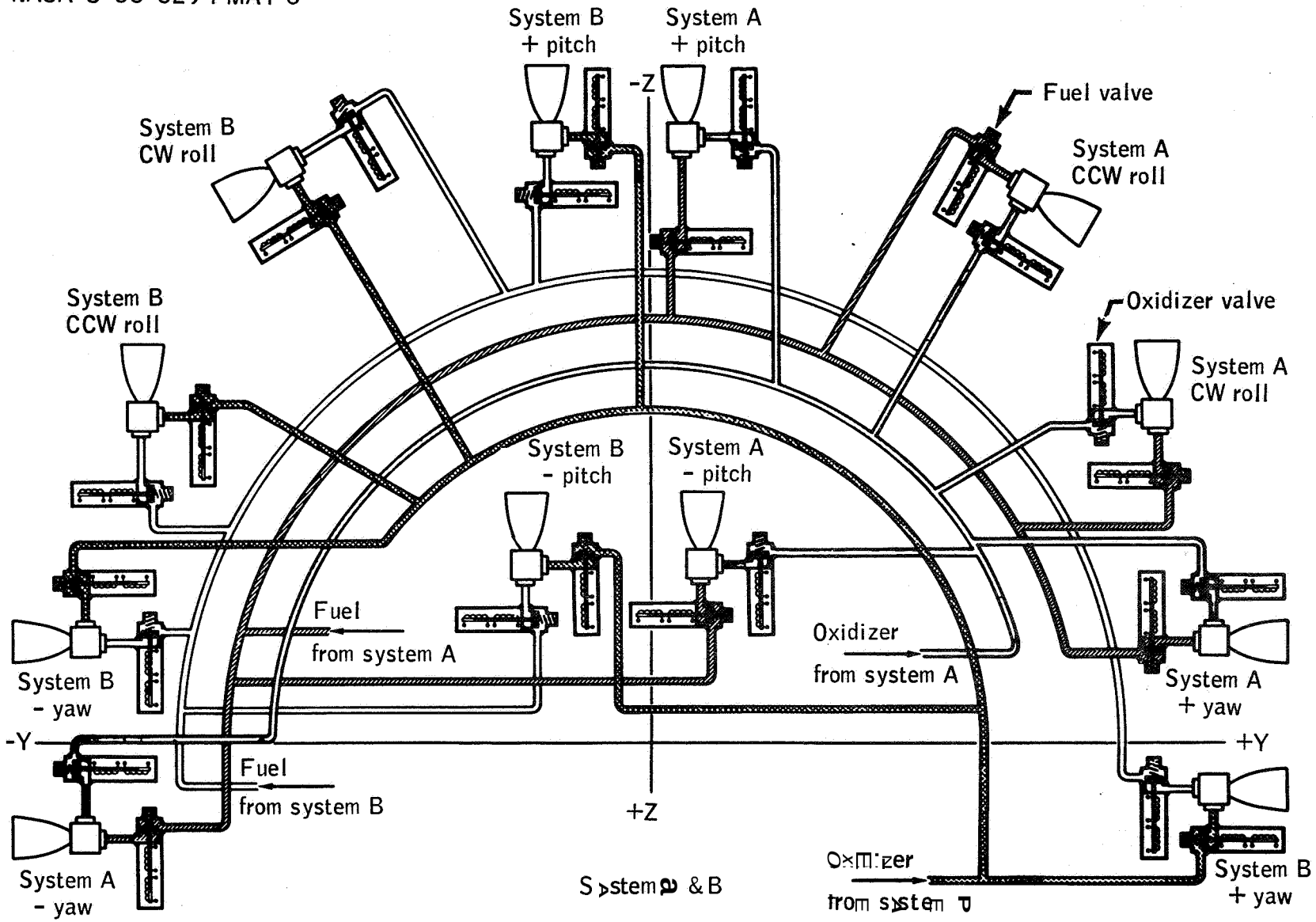


Figure 7.9-9.- Schematic of CM RCS engines, Mission AS-201.

NASA-S-66-6295 MAY 6

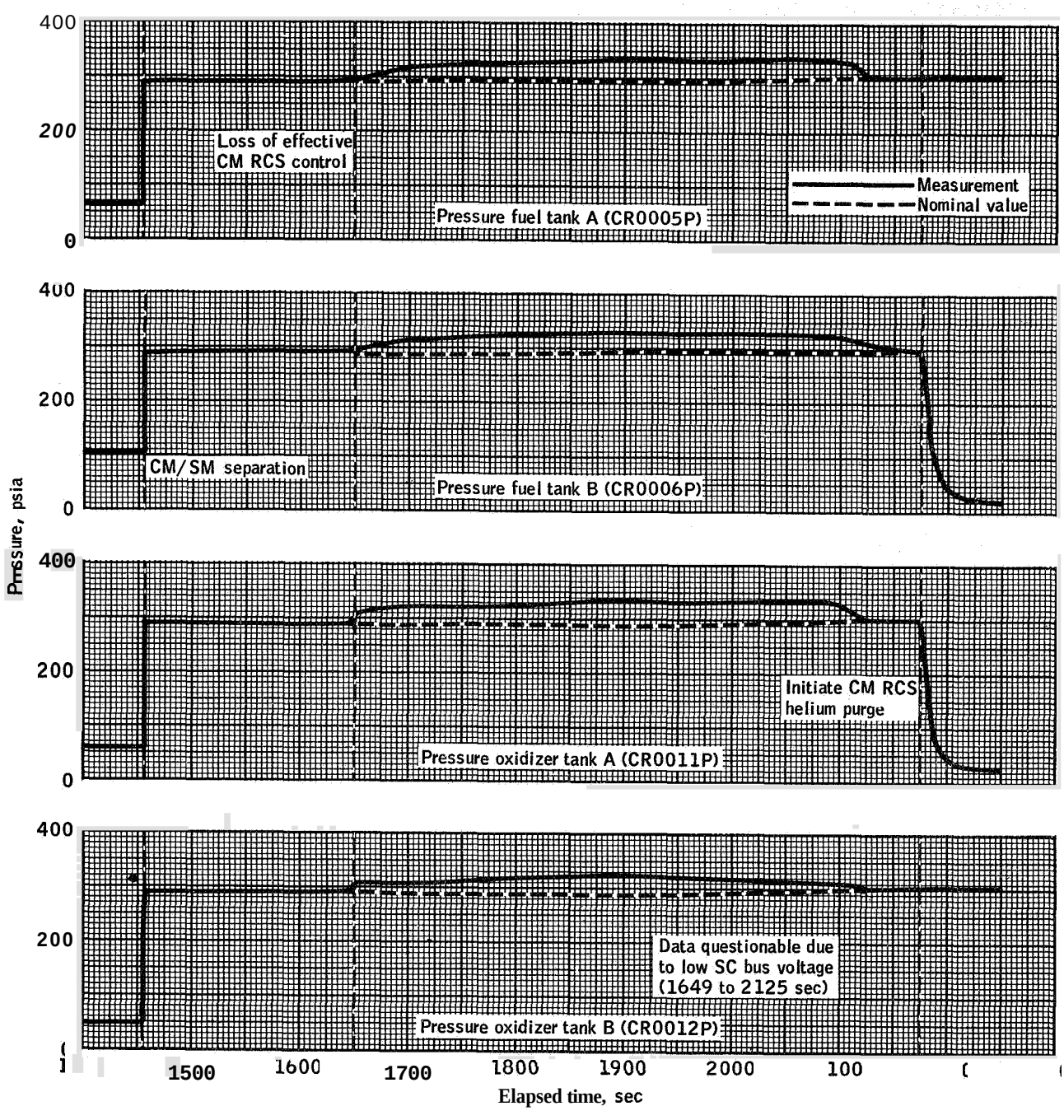


Figure 7.9-10.- CM RCS propellant tank pressures, Mission AS-201.

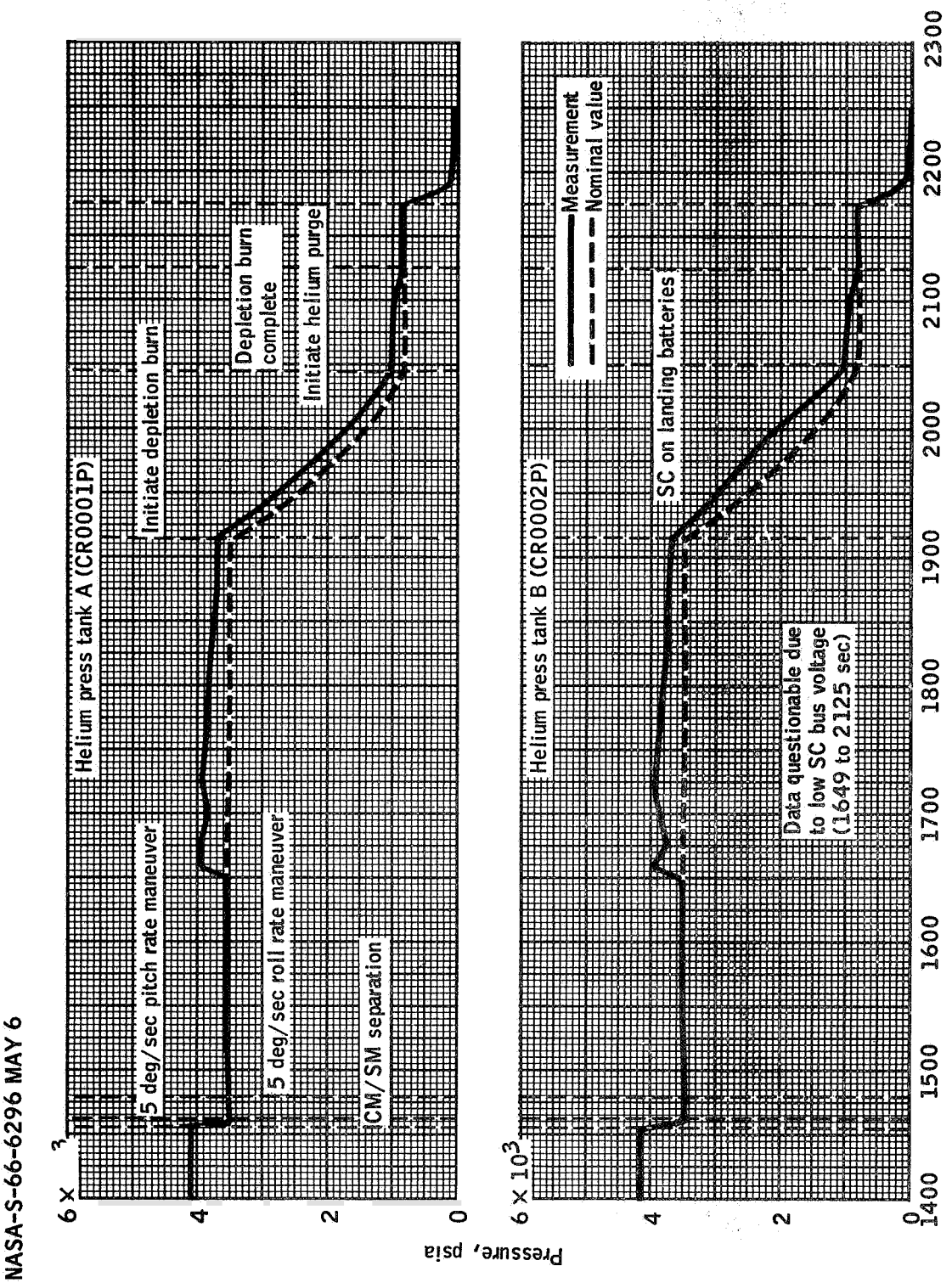


Figure 7.9-11.- CM RCS helium source tank pressures, Mission AS-201.

7.10 Pyrotechnic Devices

Description.- The pyrotechnic devices used on Mission AS-201 were of the same type as those used on Mission A-004 (ref. 9), but also included the addition of the spacecraft - LEM adapter (SLA) separation subsystem, the type 100 pressure cartridges for the 1/4-inch reaction control subsystem (RCS) valves, the type IV pressure cartridges for the 5/8-inch RCS valves, swimmer umbilical and die marker deployment, and HF antenna deployment release.

The function of the SLA separation subsystem was to sever the four SLA panels from each other and from the service module (SM) simultaneously, to initiate the SM/SLA umbilical disconnect, and to initiate the panel thruster pressure cartridge upon separation command. (See figs. 7.10-1 and 7.10-2.) As the panels are thrust outward, they are protected from possible rebound by a spring reel assembly. After 38° deployment, panel attenuators begin to slow dam. panel movement (fig. 7.10-3).

The SLA separation system included the Apollo standard initiators to initiate the explosive components upon receipt of signal, the explosive train to sever the structural interface splice plates, the charge holders to hold the strands of mild detonating fuse (MDF), the MDF of lead sheathed RDX class G, the cross-over boosters for detonation across joints (fig. 7.10-4), the confined detonating cord (CDC) for SM/SLA umbilical disconnect (fig. 7.10-5), the SM/SLA umbilical disconnect (fig. 7.10-6), splice plate severance debris catchers, panel thrusters, panel attenuation and retention devices, and pressure cartridges (fig. 7.10-7).

Two other items which were flight tested for the first time on Mission AS-201 were the RCS valve cartridges, type 100 and type IV. The type 100 pressure cartridge, used in the 1/4-inch RCS valves, generates a pressure of 9000 ± 1650 psi within 5 milliseconds when fired into a 0.05-cc volume. The type IV pressure cartridge, used in the 5/8-inch RCS valves, generates a pressure of 2260 ± 478 psi within 8 milliseconds when fired into an 8.8-cc volume.

Performance.- Pyrotechnic devices functioned satisfactorily on Mission AS-201 for the proper operation of the appropriate subsystems. Six pressure cartridges, which are normally "fired" during a mission, were rendered inoperative during Mission AS-201 following a malfunction in the electrical parer subsystem. This malfunction, which caused the pyro bus B to be de-armed, is discussed in detail in sections 7.12 and 7.13. Postflight tests of these devices indicated that all bridgewire resistances were within tolerance and that they would have functioned properly if they had received the proper electrical signal. The six pressure cartridges consisted of one type VI ME453-0005-0056 in the apex cover jettison system, one type 200 ME453-0005-0232 in the main

parachute disconnect assembly, one type 100 ME453-0005-0111 in the command module (CM) RCS fuel bypass valve, one type 100 ME453-0005-0111 in the CM RCS Oxidizer bypass valve, and two type-100 ME453-0005-0112 in the CM RCS helium interconnect valves.

Postflight tests of the two CM RCS oxidizer dump valve cartridges (type IV, ME453-0005-0024), which were intended to be activated *only* in the event of a low altitude abort, confirmed these conclusions.

NASA-S-66-6297 MAY 6

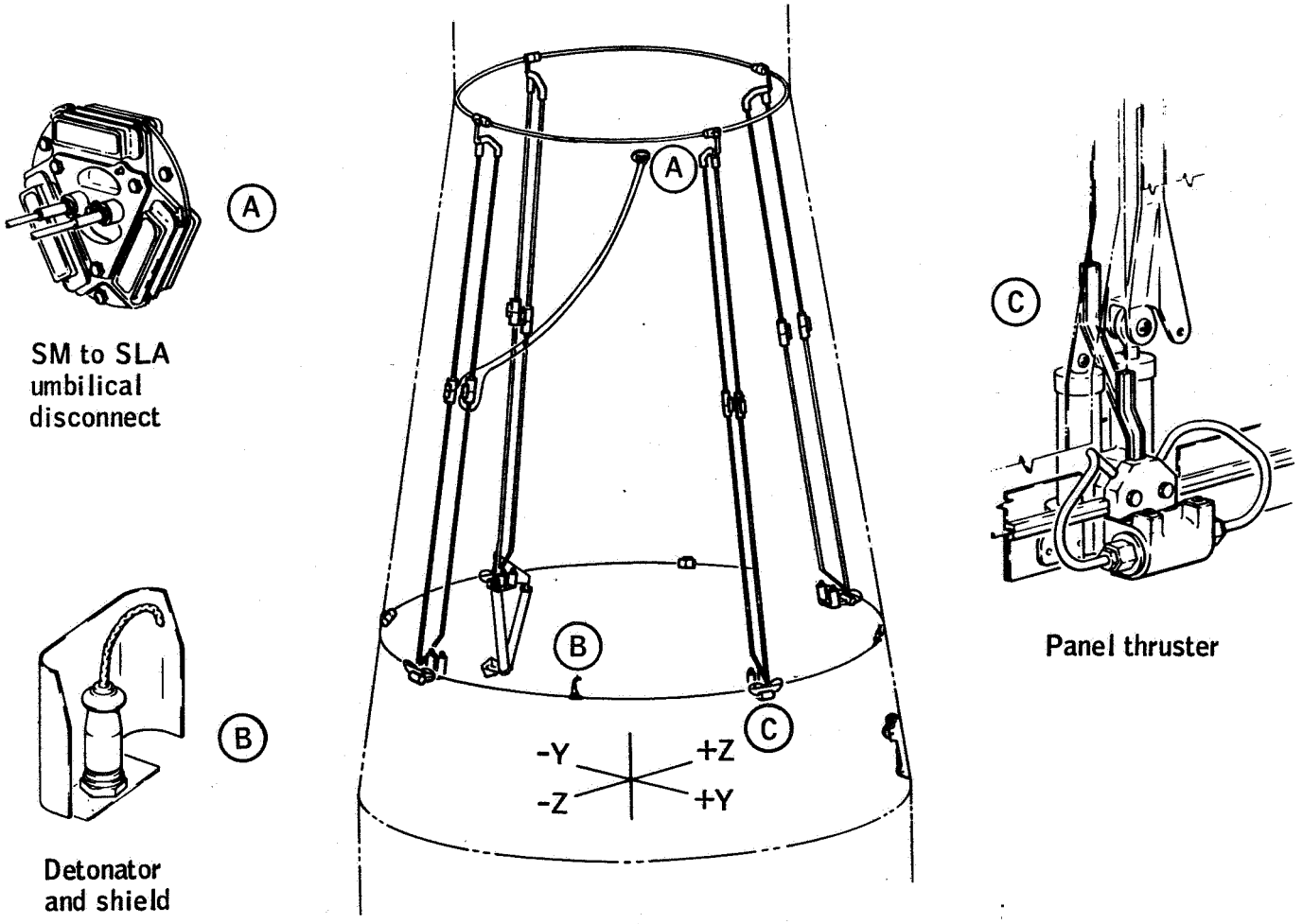


Figure 7.10-1.- Spacecraft – LEM adapter separation system Mission AS-201.

NASA-S-66-6298MAY 6

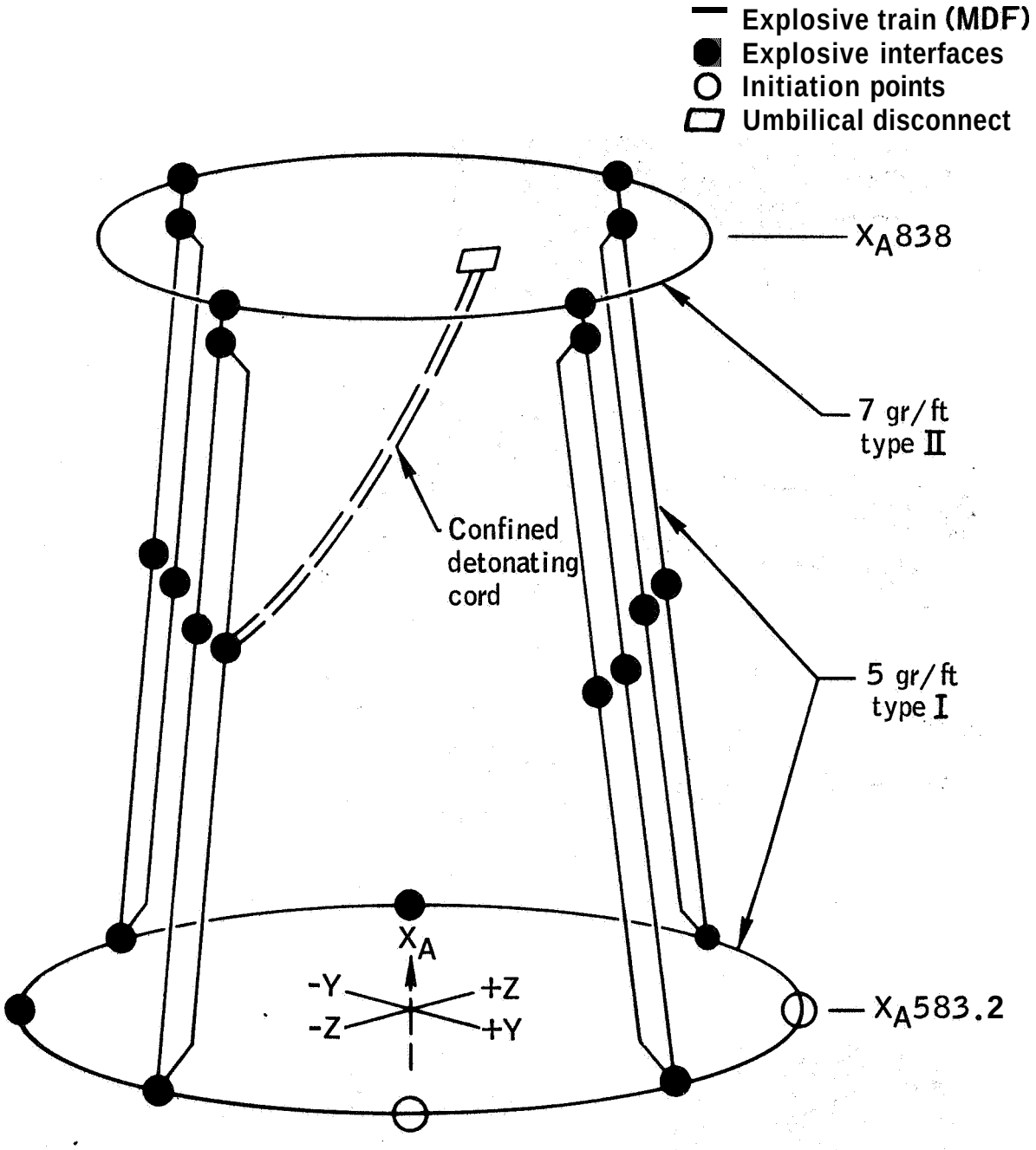


Figure 7.10-2.- .Spacecraft – LEM adapter separation system, explosive train schematic, Mission AS-201.

NASA-S-66-6299 MAY 6

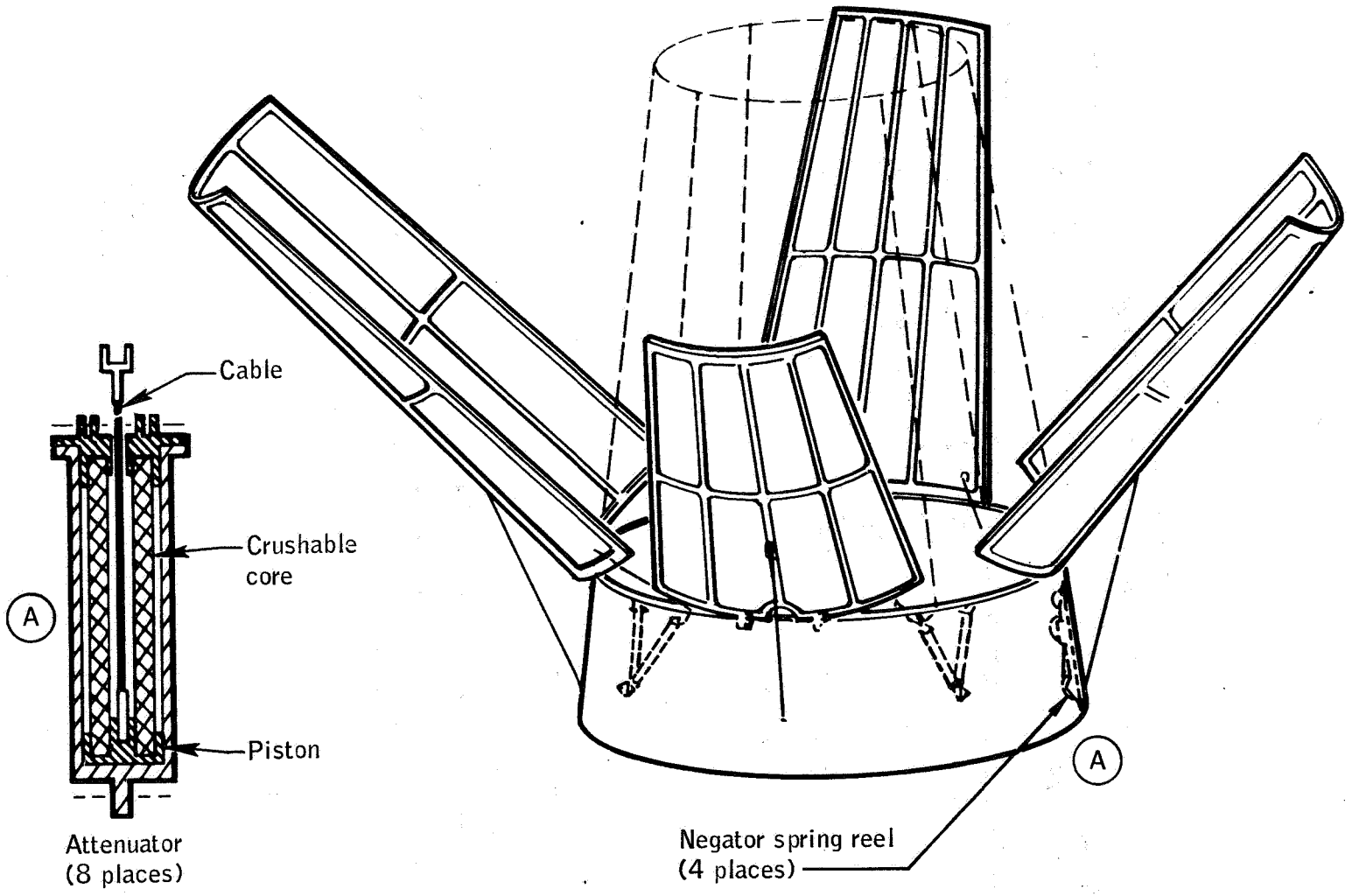
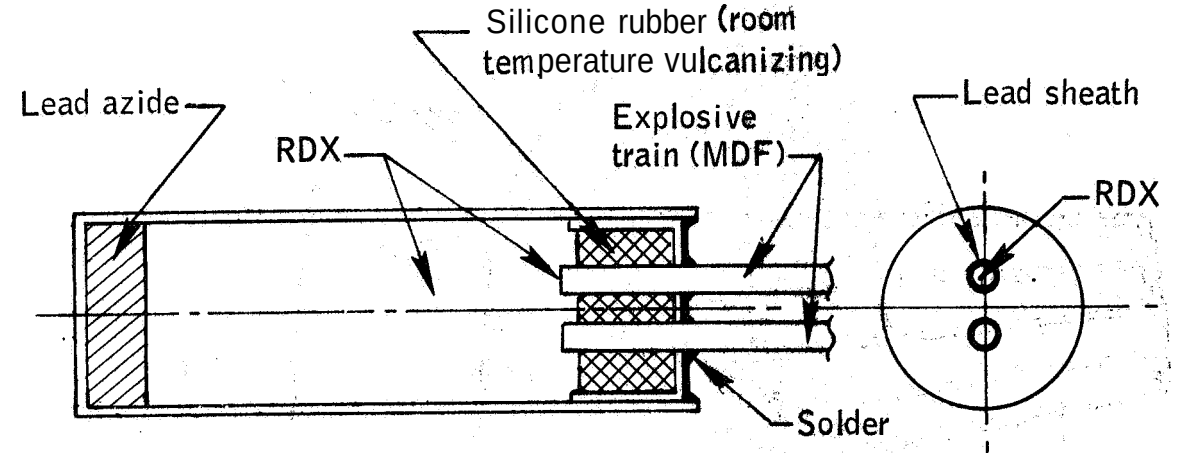
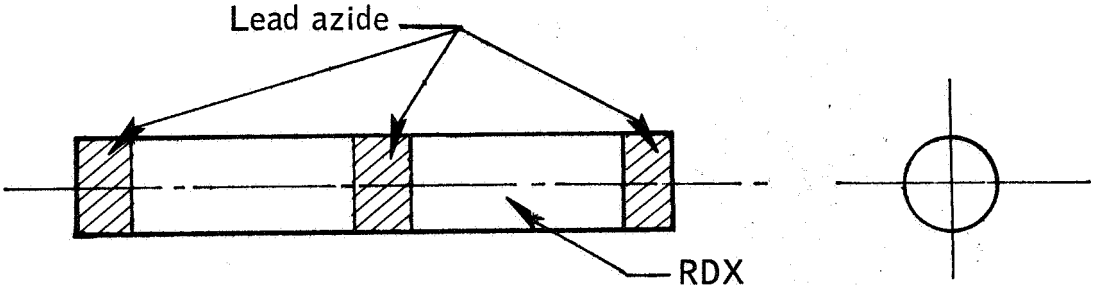


Figure 7.10-3 - Spacecraft – LEM adapter panel attenuation and retention, Mission AS-201

NASA-S-66-6300 MAY 6



Booster



Crossover booster

Figure 7.10-4.- Charge, explosive train, Mission **AS-201.**

NASA-S-66-6301 MAY 6

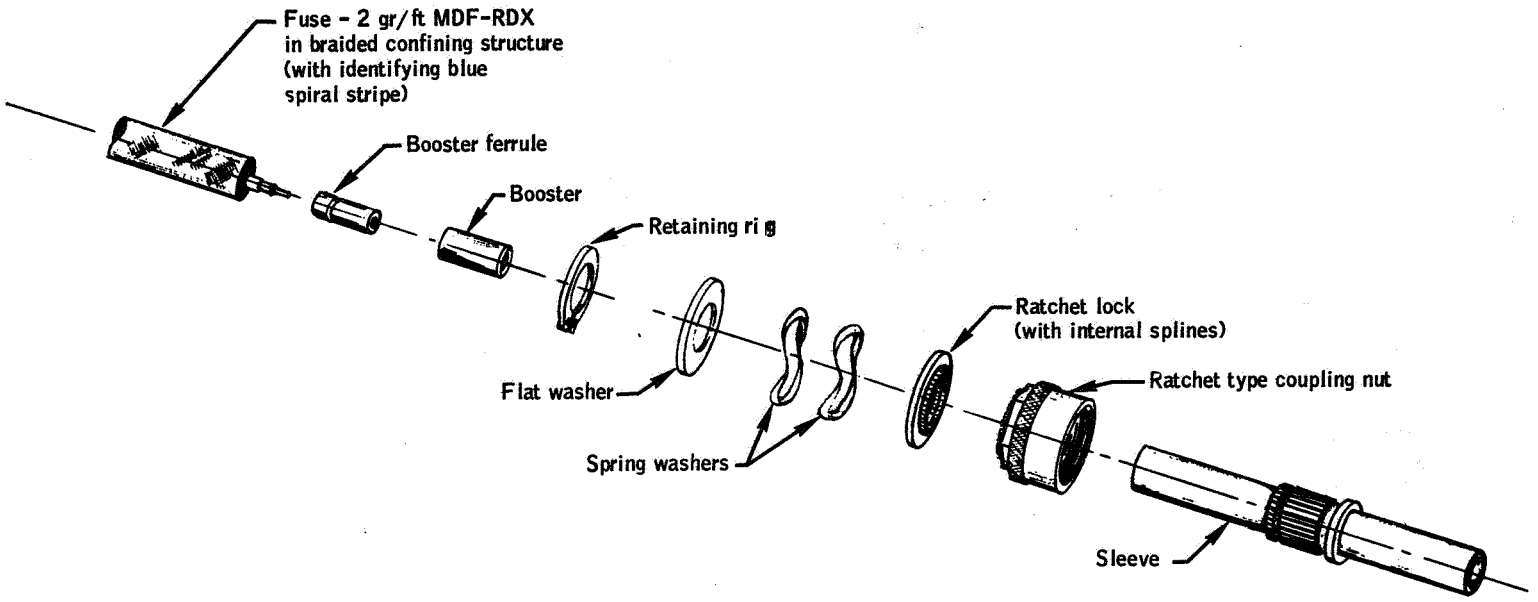


Figure 7.10-5.- Confined detonating cord assembly, Mission AS-201.

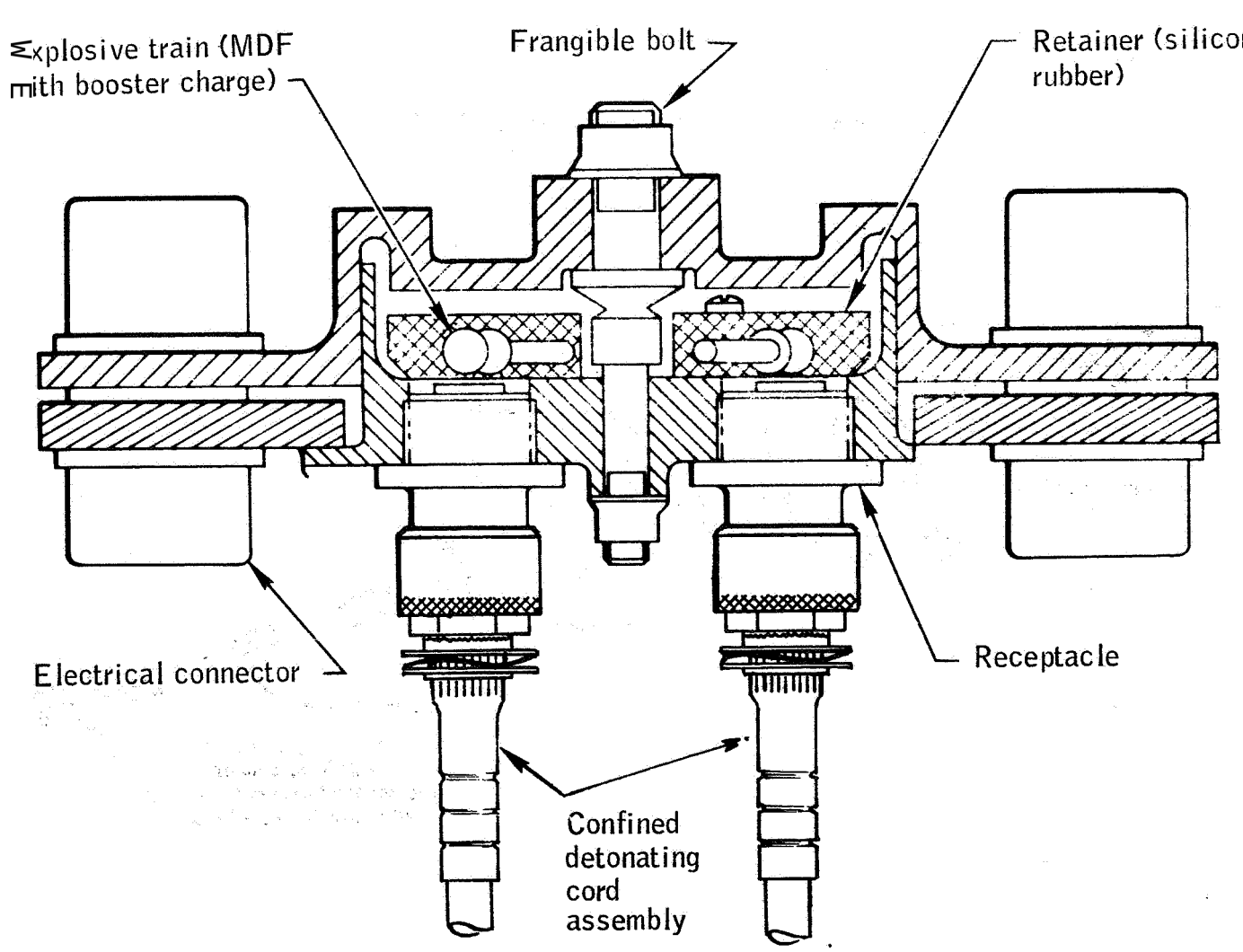


Figure 7.10-6.- Umbilical disconnect, service module to SLA, Mission AS-201.

NASA-S-66-6303 MAY 6

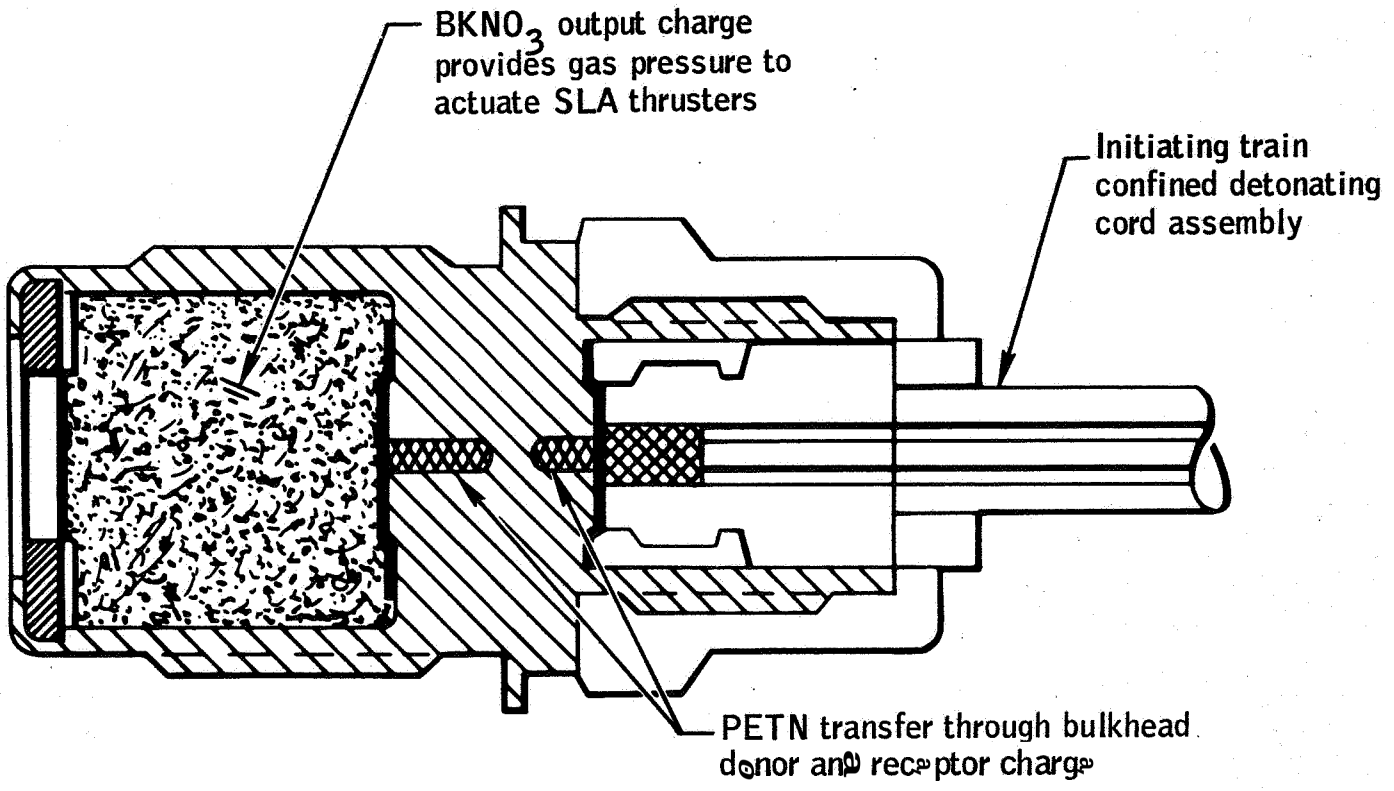


Figure 7.10-7.- Pressure cartridge, explosive transfer initiation, mission AS-201.

7.11 Stabilization and Control Subsystem and Control Programmer

Summary.- The stabilization and control subsystem (SCS) demonstrated the capability for performance of all mission objectives. Attitude control was maintained adequately from CSM/S-IVB separation until the electrical power subsystem (EPS) failure occurred at T+1649 seconds. The SCS performed adequately during both the CSM/S-IVB and CM/SM separations. Three precise attitude maneuvers were performed: one maneuver utilized the service module reaction control subsystem (SM RCS), and two maneuvers utilized the command module reaction control subsystem (CM RCS). Two service propulsion subsystem (SPS) firings were properly controlled despite abnormal engine performance. Reentry control was exercised through the peak g region and well into blackout (until approximately T+1649 sec), at which time the RCS control motor switches were transferred from the CM to the SM position as a result of EPS problems.

The control programmer (CP) performed properly throughout the mission although all events were delayed approximately 10 seconds from the nominal timeline because of a late initiation signal from the launch vehicle. The attitude reference subsystem (ARS) performed as expected with relatively high gyro drifts appearing under g loads.

Description.- The stabilization and control subsystem on spacecraft 009 was a Block I type configuration, modified to allow commands normally provided by the guidance and navigation system or the pilot to be initiated by the control programmer and master events sequence controller (fig. 7.11-1). Mission AS-201 was the first flight test of the Block I hardware.

The spacecraft 009 SCS included:

(a) A rate gyro package, which contained three miniature rate *gyros* mounted orthogonally to sense angular rates about the three spacecraft body axes.

(b) An attitude gyro and accelerometer package, which consisted of three body-mounted *gyros* mounted orthogonally to sense angular displacements about the three spacecraft body axes, and a hinged pendulum accelerometer mounted to sense acceleration along the spacecraft X axis.

(c) Electronic control assemblies which contained the circuit elements required for resolving, summing, shaping, and switching the signals necessary to control the reaction control thrusters and the propulsion engine thrust vector subsystem.

(d) A velocity change indicator which provided the capability for manually inserting the desired velocity change required for SPS thrusting.

(e) An attitude set/gimbal position indicator which provides a means of selecting the desired position of the SPS engine gimbals for the first SPS AV maneuver.

The automated control subsystem on spacecraft 009 included the CP, the radio command control (RCC) unit, the ARS, and the backup reentry sensor.

The CP included a normal and abort timer and the logic networks necessary to provide, in the proper sequence, commands to the spacecraft subsystem. Backup ground control of selected spacecraft events was provided through the up-data link and the RCC unit.

The ARS provided, by way of telemetry link, spacecraft pitch, roll, and yaw attitudes for backup information for ground control activities and for postflight evaluation. The backup reentry sensor provided backup for the 0.05g switch which commanded the SCS to the reentry configuration.

Stabilization and control subsystem performance evaluation.

Ascent, S IVB, Minimum orbit phase. At S-IB ignition (approximately T+ 5 sec) the spacecraft rate gyros indicated oscillations (oscillation) in all axes. These oscillations continued for approximately 5 seconds, then returned to a negligible value on all axes for the remainder of the flight. The roll rate telemetry signal nulled at a constant 0.12 deg/sec. This value in instrumentation bias noted during flight tests and throughout the mission, did not affect SCS performance.

The body-mounted integrating gyros were uncaged simultaneously with the S-IVB separation command (T+843.2 sec) to establish a spacecraft attitude reference. The separation sequence, starting at this time, is shown in figure 7.11-2. Physical separation was effected by a direct ullage command which applied power to the +X RCS direct coils. At physical separation (T+844.9 sec), a positive pitch (+P) disturbance was observed. When attitude control was enabled (0.8 sec later), the appropriate negative pitch (-P) thruster counteracted the disturbance and stabilized the rate at 0.8 deg/sec. Direct ullage was replaced by +X translation at T+846.7 seconds. *During* +X translation, attitude control took priority, and the rate decreased with an acceleration typical of single thruster performance. (See section 7.9.1.) The +P/+X and -P/-X thrusters fired alternately throughout the +X translation to correct for the inoperative thruster.

Yaw-axis transients were negligible during direct ullage, indicating proper operation of the +Y/+X and -Y/+X thrusters. During +X translation, however, the positive yaw (+Y) and negative yaw (-Y) thrusters fired

alternately to counteract inoperative or degraded yaw thrusters. (See section 7.9.1.) The inoperative thrusters had no adverse effect on attitude control of the CSM; however, the capability for the +X translation maneuvers (ullage) was degraded.

Command and service module coast phases: Attitude hold control was excellent throughout the coasting periods. Both body attitudes and rates were controlled within specified limits (±2° and ±2 deg/sec), and thruster activity was minimal with short duration firings in all cases. Representative limit cycles during attitude control are shown in figure 7.11-3. Pitch-axis cycles were both asymmetrical and variable in period (12 to 57 sec). Amplitudes were approximately 0.4° peak-to-peak. Yaw-axis periods were also variable (13 to 88 sec) with peak-to-peak amplitudes of approximately 0.35°. The asymmetry and varying periods in these axes are normal reactions to variations in thrust levels, center-of-gravity locations, and initial conditions. In the roll axis, the cycles were relatively symmetrical and stable with an amplitude and period of approximately 0.3° peak-to-peak and 2.5 seconds, respectively.

Service propulsion subsystem translations: Spacecraft response during +X translations preceding each SPS ΔV maneuver was similar to that observed at S-IVB/CSM separation. (See figs. 7.11-4 and 7.11-5.) The RCS thrusters identified in section 7.9.1 remained inoperative and ullage capability was degraded.

Transients were negligible at ignition for the first SPS translation, indicating proper SCS performance and accurate center-of-gravity location estimates (fig. 7.U-6). All SPS control axes were stable during the maneuver. The low-frequency transient response which developed was normal. The trim follower loop performance demonstrated the ability to adjust spacecraft attitude automatically as required by spacecraft center-of-gravity shifts. After engine ignition, the roll thruster duty cycle increased significantly, although the duration of thruster impulses remained at the minimum level.

The SPS thrust level decreased approximately 80 seconds after ignition (see section 7.7). No effect was noted in control system operation; however, the low acceleration resulted in a timed backup CP thrust-off command rather than a thrust-off command from the normal ΔV counter.

The ΔV counter performed as expected, based on actual SPS thrust profiles. The initial preflight ΔV setting was 4570 ft/sec. At SPS thrust termination, commanded by the CP, the remaining ΔV was 863 ft/sec. A zero reading is necessary for a normal automatic SPS thrust-off.

The +X translation and gimbal position set preceding the second SPS translation were commanded simultaneously with first burn cutoff and were performed during the thrust tail-off period. Because RCS attitude

control was inhibited at this time, pitch and yaw transients occurred. The disturbances caused by the thruster outages noted previously remained in effect.

The thrust profile during the second SPS translation was erratic (see section 7.7). The commanded gimbal trim settings were based on preflight estimate of center-of-gravity location assuming a nominal first SPS translation, and, therefore, were not correct for the actual location. Because of the improper trim setting, an approximately 3° initial thrust misalignment occurred in the yaw axis and a significant transient developed. Despite these conditions, adequate control was maintained throughout.

An analog computer simulation of the second burn with all system parameters nominal was performed and the time histories of pertinent parameters obtained from the simulation were compared with data obtained fromthe flight. The low-frequency response of spacecraft rates, attitude errors, and gimbal positions agreed, indicating that no significant degradation in the performance of the gimbal actuators occurred during the first burn. The rather erratic high-frequency (1 to 2 cycles/sec), small-amplitude oscillations noted in the data (particularly in the gimbal position feedback signals) during the first 6 seconds of the burn were not reproduced in the nominal simulation. These oscillations were most probably a result of the fluctuations in SPS thrust, particularly in the variation of thrust-vector orientation relative to the engine centerline resulting from unsymmetrical propellant flow in the SPS nozzle. Such a variation would produce an oscillatory torque on the SPS engine which, in turn, would produce a direct force on the gimbal actuator clutches (as opposed to torques on the spacecraft which affect the actuators only through the feedback loops). This effect was demonstrated in the analog simulation by applying a sinusoidal force of 200 pounds peak at a frequency near that observed in the data. Two hundred pounds is estimated to be a "worst case" force which would be expected. from thrust-vector displacement from the engine centerline. This forcing function resulted in oscillations of the gimbals about the trim point comparable in magnitude to those shown by the data (±0.2° to ±0.4°).

Other attempts were made in the simulation to reproduce the high-frequency oscillations by varying different system parameters such as clutch force gains, and rate and attitude feedback gains; however, these variations in system parameters, in general, caused the low-frequency response to differ significantly from the flight data. This further substantiates the conclusion that the system performed normally, and that the high-frequency oscillations were forced, apparently by the fluctuating thrust-vector orientation relative to the engine centerline, as opposed to inherent oscillations in an underdamped system. As in the first SPS burn, a small oscillation was noted, particularly in the yaw gimbal position feedback, at approximately slosh frequency during the last 4 seconds of the second burn.

CSM separation orientation: After the second SPS thrust termination, a 90° pitch maneuver was accomplished by utilizing the SM RCS to achieve proper CM/SM separation attitude. Figure 7.11-7 contains a time history of spacecraft pitch rates, attitude errors, and thruster firing commands during this period. Roll and yaw disturbances were negligible and are not shown. The maneuver commands were initiated by the CP, and the RCS responded with positive and negative angular accelerations slightly less than half the predicted value for dual thruster operation, indicating that the pitch thrusters in quad A remained inoperative. In addition, the rate response (fig. 7.11-7) matched that obtained from a preflight simulation with this quad inoperative. The total angular change achieved was 91.4°, when calculated by integrating the rate curve, and 90.7°, as measured by the ARS (fig. 7.11-8). The maneuver was precisely performed although CM/SM separation was initiated before the spacecraft stabilized within the rate and attitude deadbands.

CM/SM separation: At CM/SM separation, a pitch rate transient of -3.5 deg/sec was imparted to the CM; roll and yaw rate transients were negligible. The pitch disturbance was controlled, as indicated in figure 7.11-9. The performance of the SCS at CM RCS activation was nominal and pitch accelerations indicated normal dual system performance.

CM reentry orientation: After CM/SM separation, an 82.5° pitch maneuver was accomplished utilizing the CM RCS to achieve proper pitch orientation. Figure 7.11-10 contains a time history of spacecraft pitch rates, attitude errors, and firing commands during this period. Roll and yaw disturbances were again negligible and are not shown. A comparison of spacecraft response with the predicted angular accelerations and with preflight simulations indicates dual system performance. The total angular change achieved was 86° when calculated by integrating the rate curve, and 80° as measured by the ARS (fig. 7.11-8).

After completion of the pitch orientation the CP initiated a nominal 180° roll maneuver. Figure 7.11-10 contains a time history of spacecraft roll rates, attitude errors, and firing commands during this period. Comparison of spacecraft response with the predicted angular accelerations and with preflight simulations again indicates dual system performance. The total angular change achieved, calculated by integrating the rate curve, was 190°. The discrepancy is due to the null bias in the rate data. The total maneuver measured by the ARS indicated 176.9° (see fig. 7.11-11).

CM coast phase: Representative pitch, yaw, and roll rate and attitude error time histories are presented in figure 7.11-12. The peak-to-peak amplitudes of the limit cycles were 1.9° in pitch, 1.65° in yaw, and 1.82° in roll. The periods were approximately 10 seconds in pitch, 22 seconds in yaw, and 21 seconds in roll.

The SCS performed satisfactorily during this phase.

CM reentry: Proper spacecraft control was maintained through peak g and well into blackout. All SCS 0.05g functions occurred as expected (T+1580.72 sec). Normal thruster firings during reentry indicated near-trim attitudes and rates which reflect proper SCS performance and negligible drift in the body-mounted integrating gyros. Transfer from the CM to the SM position of the RCS system B CSM transfer switch occurred at T+1641 seconds, and control of system B CM thrusters was lost (see section *7.12).* The CM system A thrusters properly controlled the spacecraft until T+1649 seconds when system A CSM transfer switch also transferred and all spacecraft control was lost. The only discrepancy noted in SCS environmental parameters during the mission occurred at this time when the combined temperature indication in the body-mounted integrating gyros decreased below limits. Aerodynamic loading caused the spacecraft to start rolling at T+1649 seconds (see fig. 7.11-13(a) to (d)). The roll rate increased to 26 deg/sec at T+1778 seconds at which time the rate signal output saturated and remained saturated until after drogue parachute deployment when all spacecraft rates were damped.

Control programmer performance.- The control programer performed nominally throughout the mission, providing a series of commands in the correct sequence and at the proper times within the limits of the timer. The planned and actual times of events commanded by the control programer are shown in table 7.11-I. An initial error in starting the timer, due to a delay in the S-IVB cutoff, caused an approximate 10-second difference between planned and actual times.

Attitude reference subsystem performance evaluation.- The attitude reference system provided a means of monitoring spacecraft attitude throughout the mission. The spacecraft pitch and roll maneuvers as measured by the ARS were:

	ARS measured rate, deg	Integrated rate, deg	Nominal rate, deg
First pitch	90.7	91.4	go. 0
Second pitch	80.0	86.0	82.5
Roll	176.9	179.0	180.0

Figures 7.11-8, 7.11-11, and 7.11-14 are time history plots of ARS gimbal angles, Saturn (ST-124) gimbal angles, and nominal preflight simulation. With the exception of a pitch transient prior to **S-IVB** shutdown, the **ST-124** data compare favorably with the preflight simulation.

At **S-IVB** shutdown, the pitch and yaw gyro indicated a relatively large error, -166 in pitch and +6° in yaw. These values remained constant throughout CSM coast, indicating large g-sensitive drift. Further drifts were noted during SPS translations. Fixed drift for this gyro was within specification tolerance throughout the flight, with errors at entry of 10° in **roll** and 5° in yaw, compared **with** the nominal trajectory.

TABLE 7.11-I.- CONTROL PROGRAMMER COMMANDS SEQUENCE

Number	Event	Time from range zero, sec	
		Planned	Actual
1	Start normal timer	652.7	663.1
2	Tape recorders off	654.7	665.2
3	S-IVB/SC separation signal on	832.7	(a)
	Uncage SCS gyros	832.7	843.2
4	S-IVB/SC separation signal off	836.2	(a)
	+X translation on	836.2	846.7
5	+X translation off	854.2	864.6
6	+X translation on	1170.7	1181.2
	First gimbal position set	1170.7	(a)
7	Primary SPS gimbal motors on	1185.7	1196.1
8	Secondary SPS gimbal motors on	1186.7	(a)
	Remove primary motors on command	1186.7	(a)
9	Remove secondary motors on command	1187.7	(a)
10	Arm SPS thrust solenoids	1200.7	1211.2
	SPS thrust on "On"	1200.7	1211.2
11	Tape recorders on	1311.2	1321.9
12	+X translation off	1384.7	1395.2
	SPS thrust on "Off"	1384.7	1395.2
13	SPS thrust off "On" (AV backup)	1385.0	1395.4
14	+X translation on	1385.2	1395.7
	SPS thrust off "Off"	1385.2	(b)
	Second gimbal position set	1385.2	1395.7
15	SPS thrust on "On"	1400.2	1410.7
16	SPS thrust on "Off"	1410.2	1420.7
	+X translation off	1410.2	1420.7
17	Pitch rate (-5 deg/sec) on	1413.7	1424.1
18	Pitch rate (-5 deg/sec) off	1431.7	1442.1

[a] No measurement available to determine time.

[b] Could not be determined from intermittent data.

TABLE 7.11-I.- CONTROL PROGRAMMER COMMANDS SEQUENCE - Concluded

Number	Event	Time from range zero, sec	
		Planned	Actual
19	CM/SM separation start	1443.7	(a)
	SCS entry mode on	1443.7	1454.2
20	Pitch rate (-5 deg/sec) on	1452.2	1462.6
21	Pitch rate (-5 deg/sec) off	1468.7	1479.1
	Roll rate (+5 deg/sec) on	1468.7	1479.2
22	Roll rate (+5 deg/sec) off	1504.7	1515.1
	Arm 0.05g backup	1504.7	(a)
	ELS activate	1504.7	(b)

[a]No measurement available to determine time.

[b]Could not be determined from intermittent data.

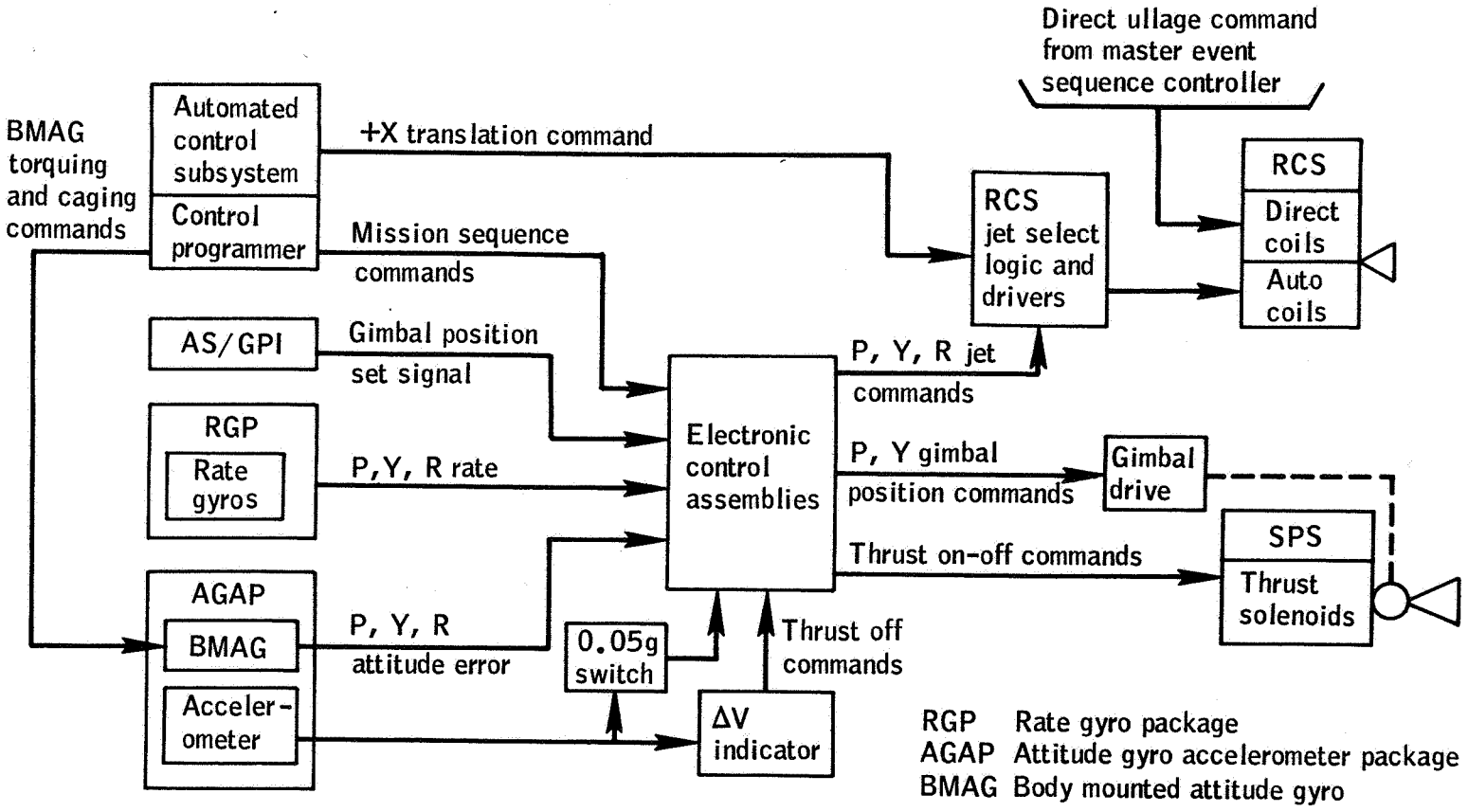


Figure 7.11-1.- Stabilization and control subsystem mission AS-201.

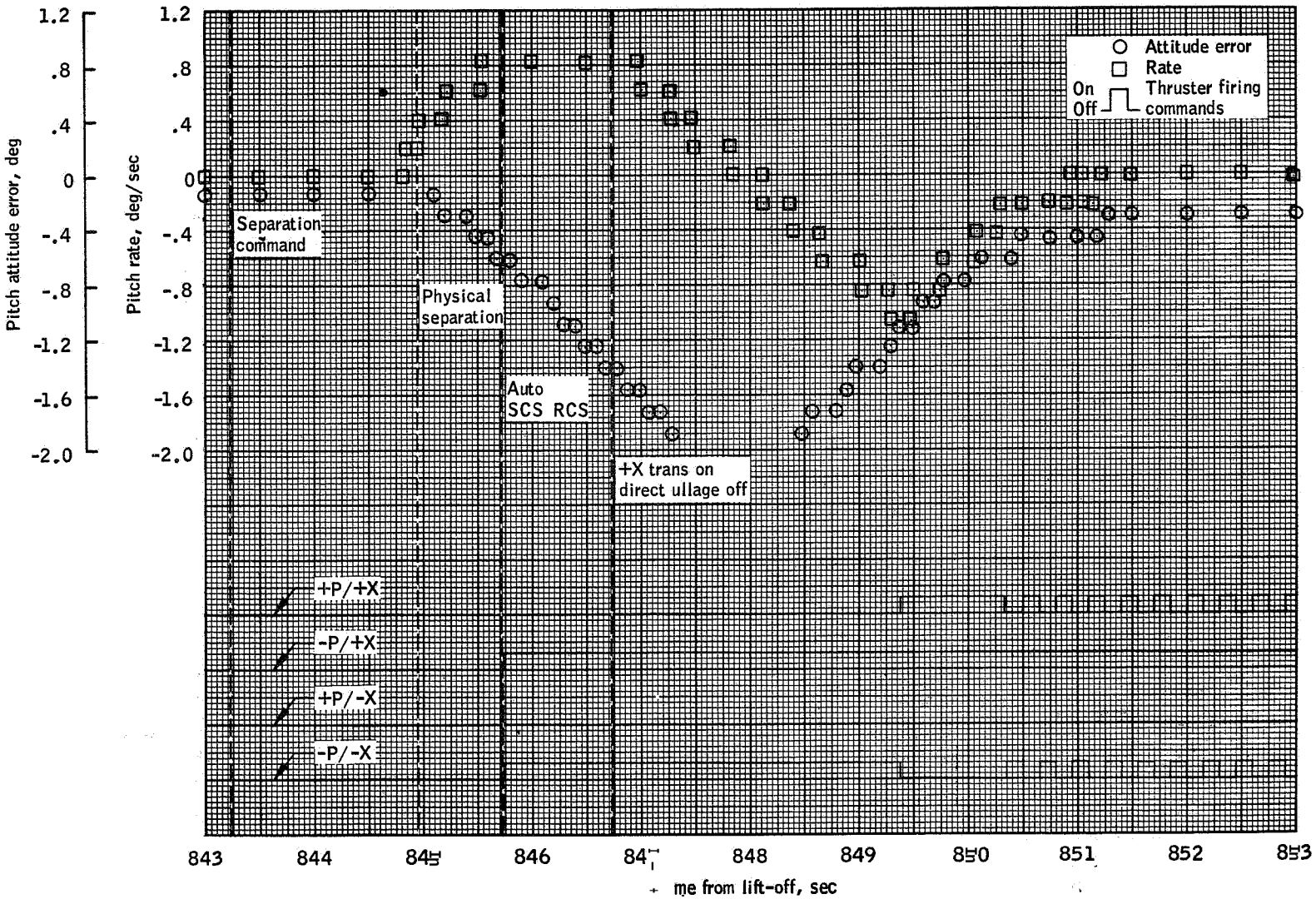


Figure 7.11-2.- Pitch rate and attitude transients during S-IVB/CSM separation Mission AS-201

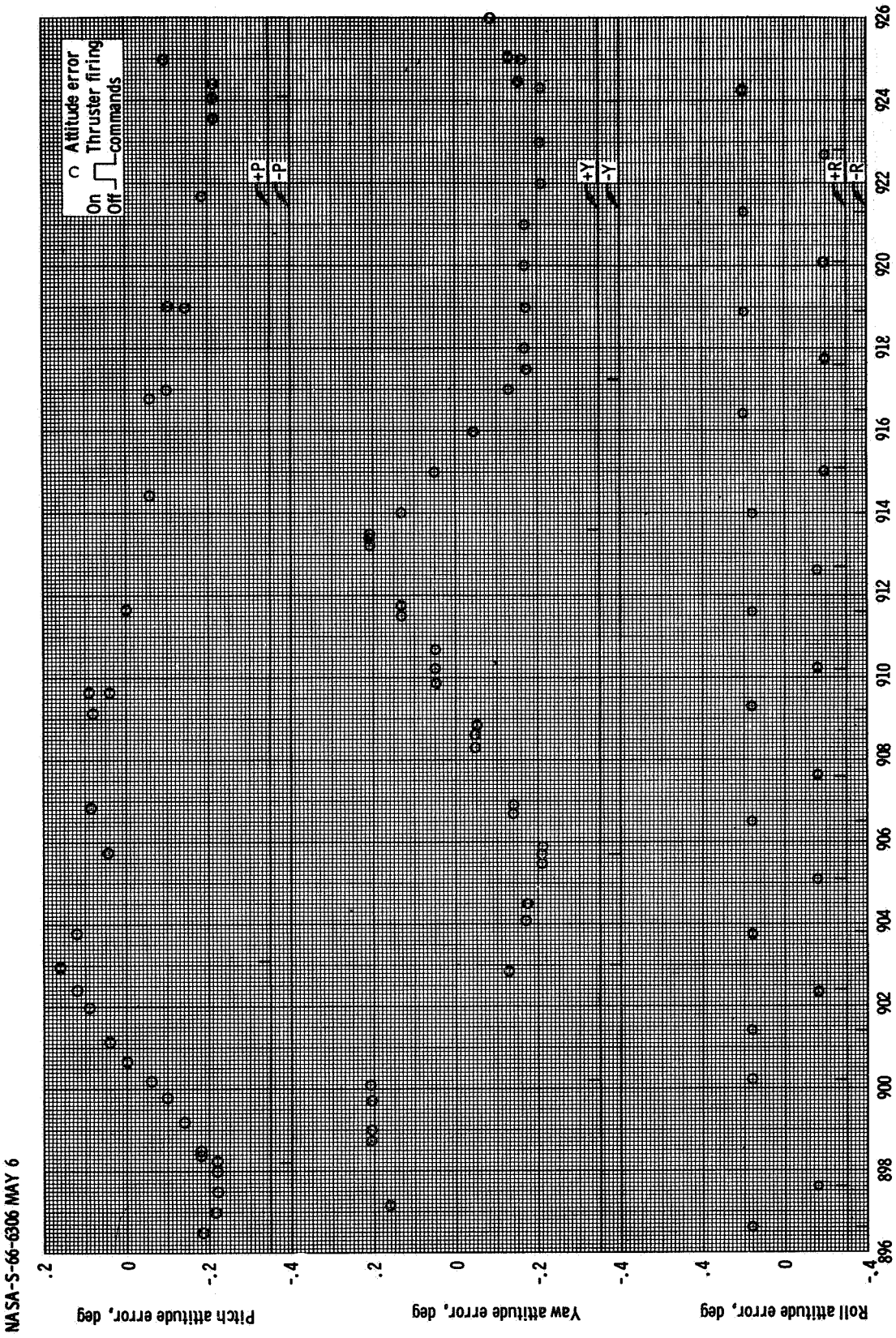


Figure 7.11-3. - CSM coast phase limit cycles. Mission AS-201.

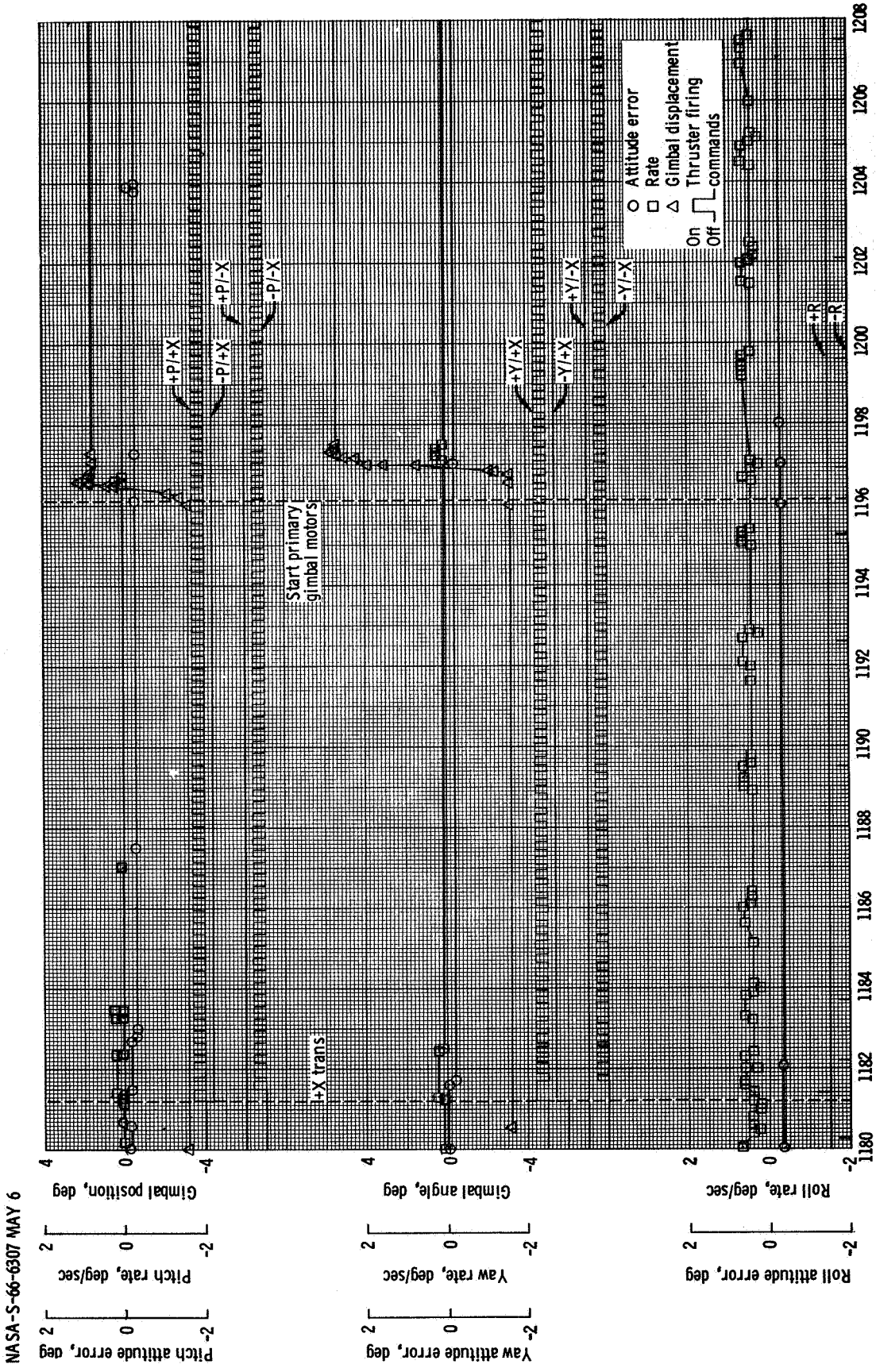


Figure 7.11-4.- Thrust vector control operation, second +X translation, 1st gimbal position set, Mission AS-201.

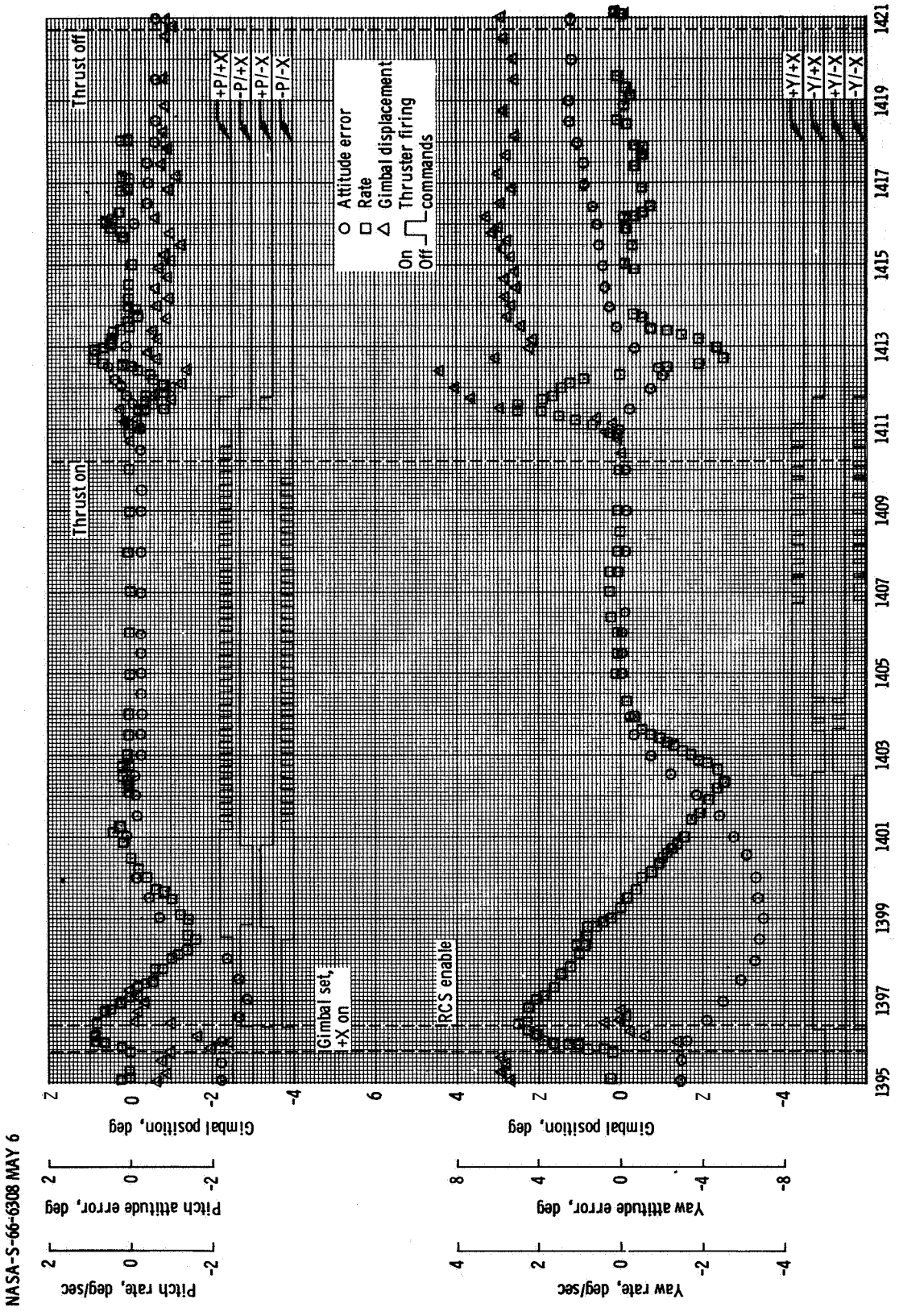


Figure 7.11-5.- Thrust vector control ...tion, +X translation 2nd gimbal positi... set, 2nd SPS ΔV ...neuv... Mission AS-201.

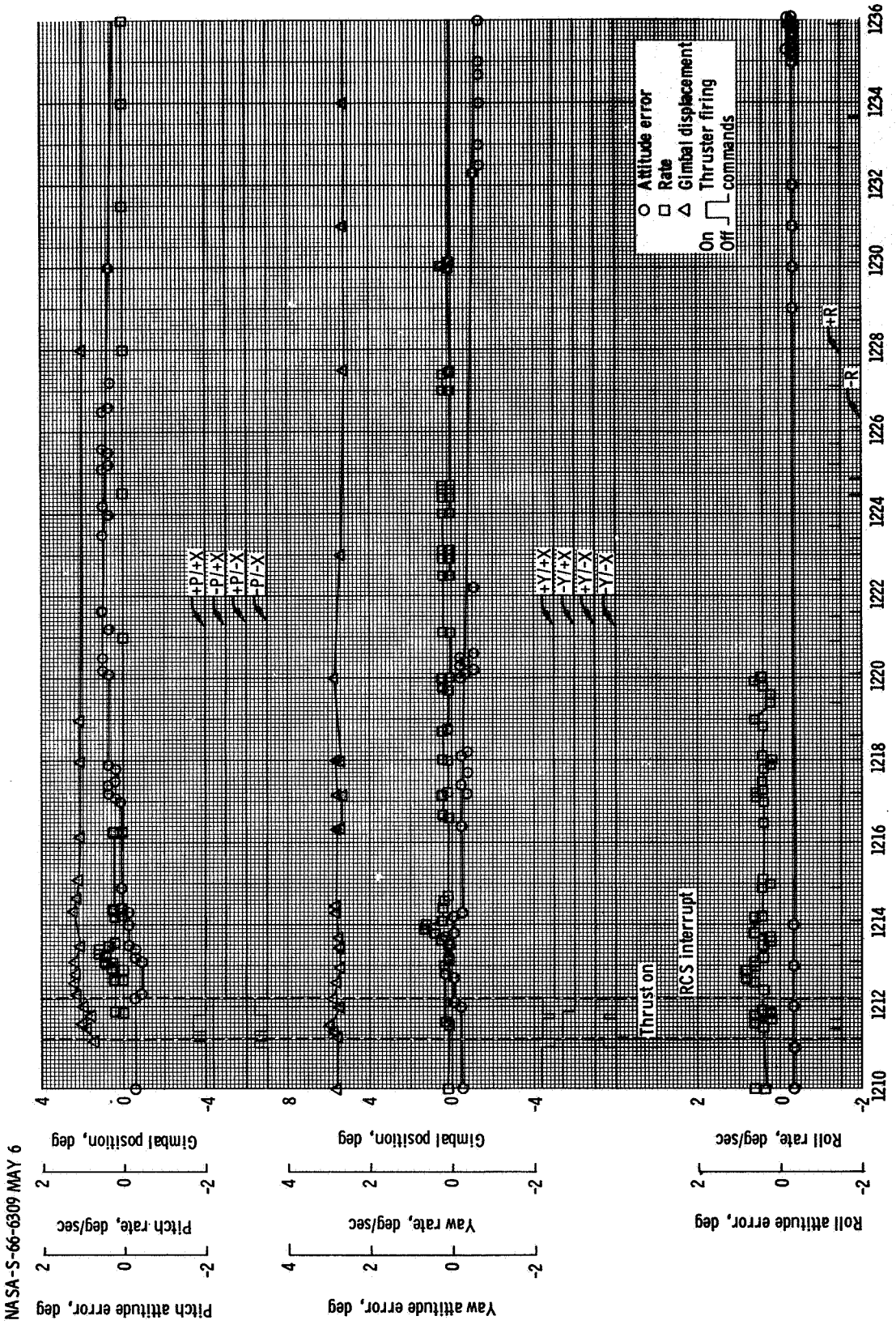


Figure 7.11-6.- Thrust vector control operation, 1st SPS ΔV maneuver, Mission AS-201.

NASA-S-66-6310 MAY 6

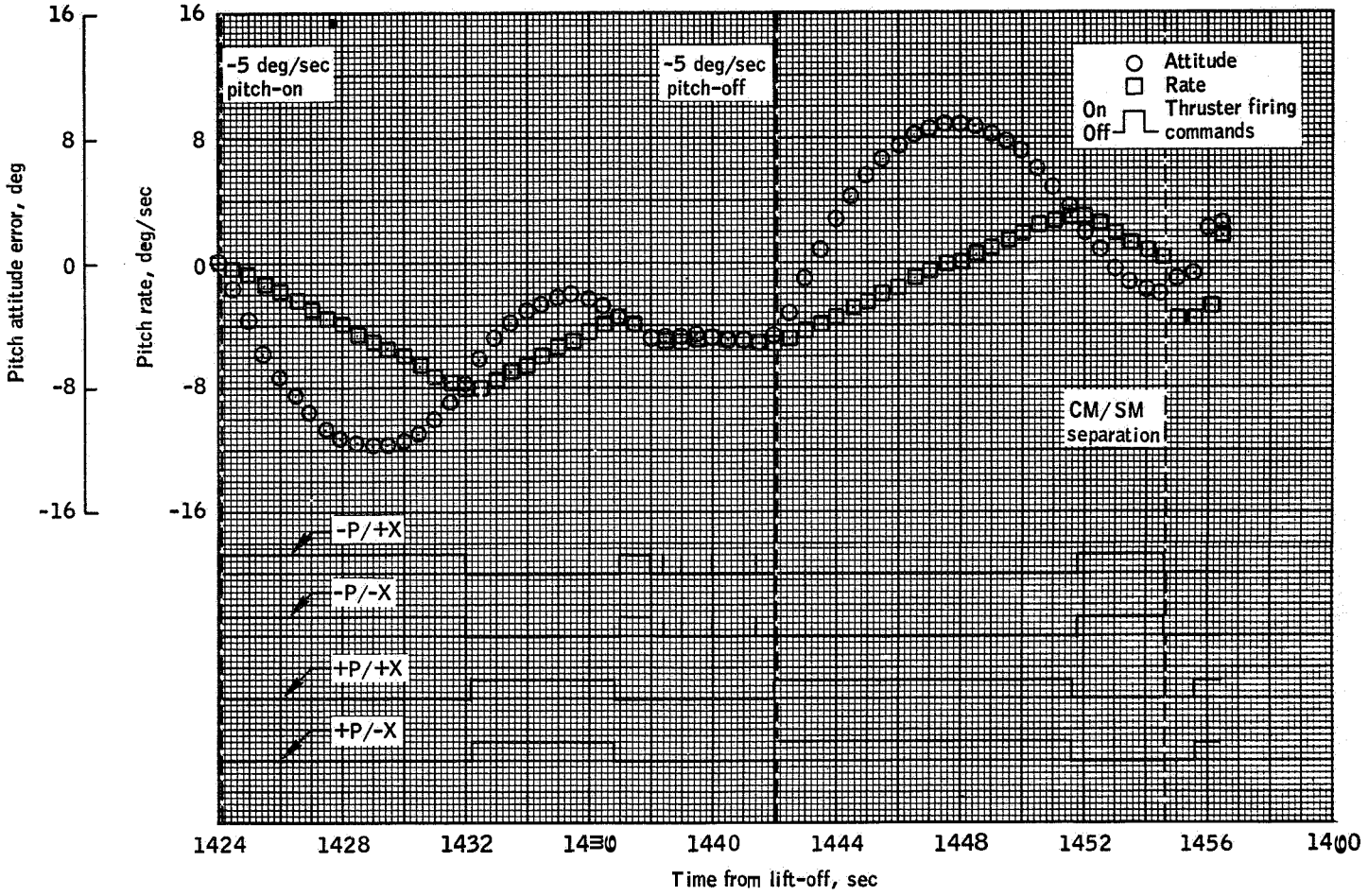


Figure Pre-separation pitch maneuver, SC rate and attitude errors, Mission AS-201.

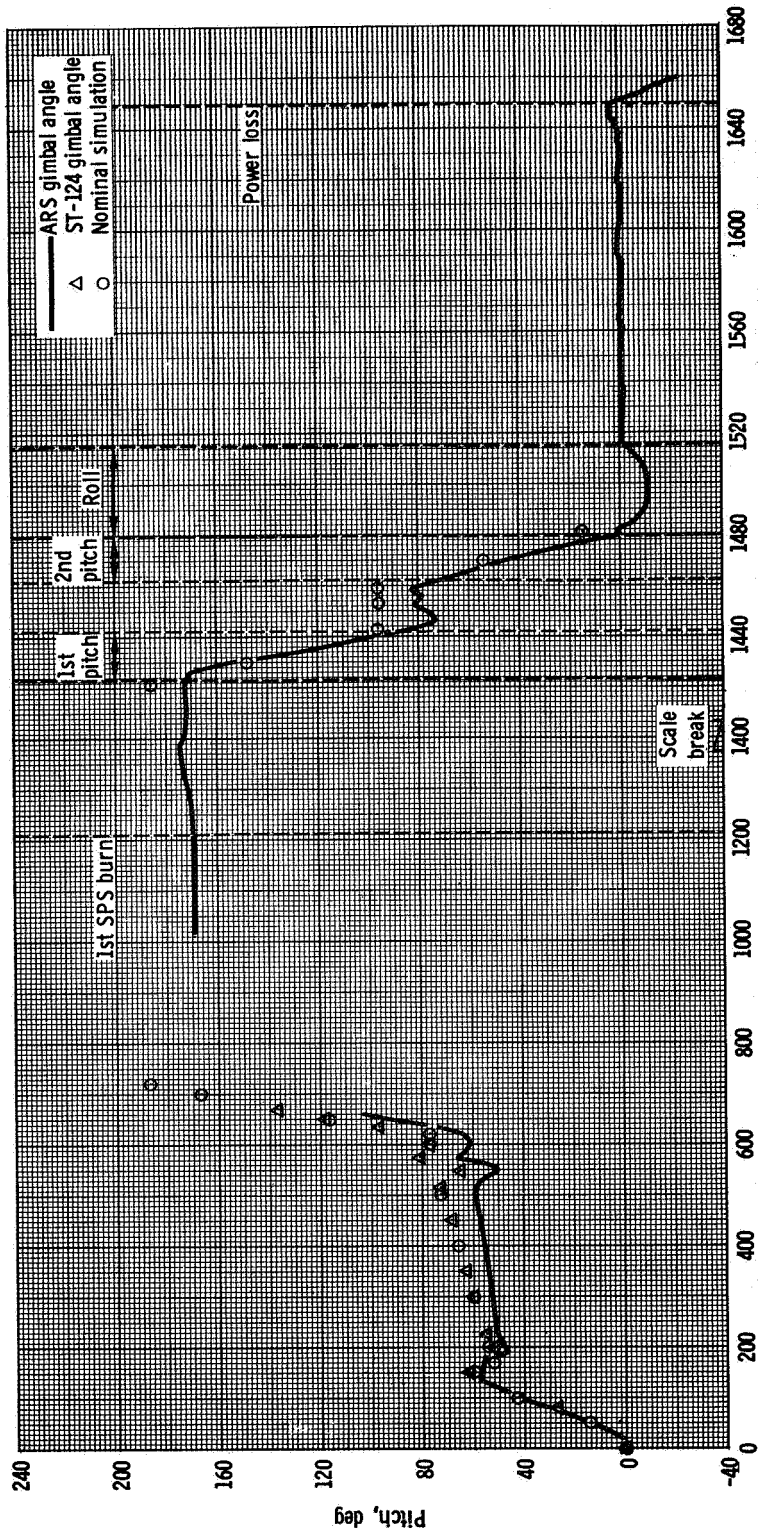


Figure 7.11-8. - Pitch ARS gimbal angle, Mission AS-201.

NASA-S-66-6311 MAY 6

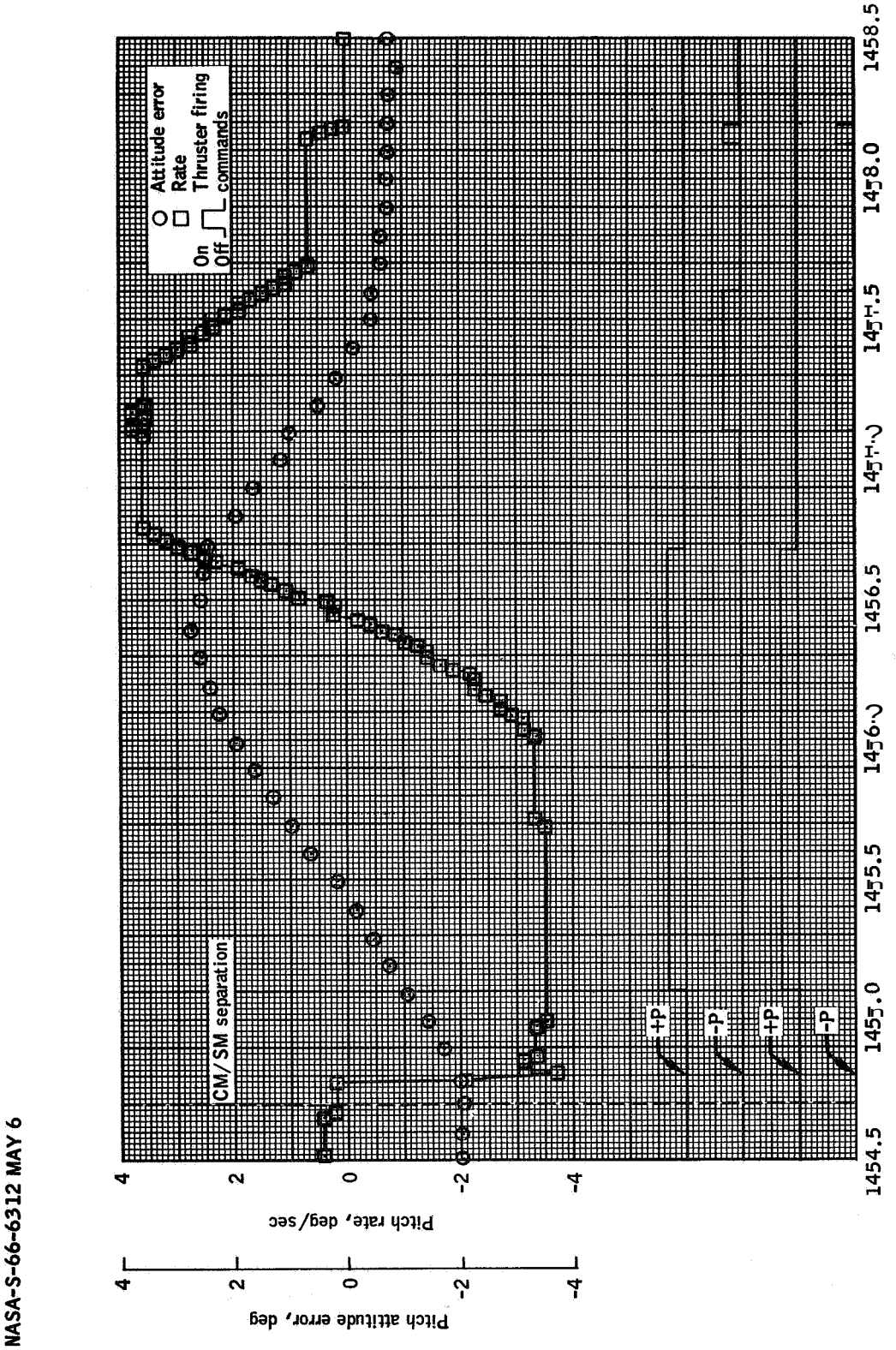


Figure 7 11-9.- Spacecraft rates and attitude errors at CM/SM separation, Mission AS-201.

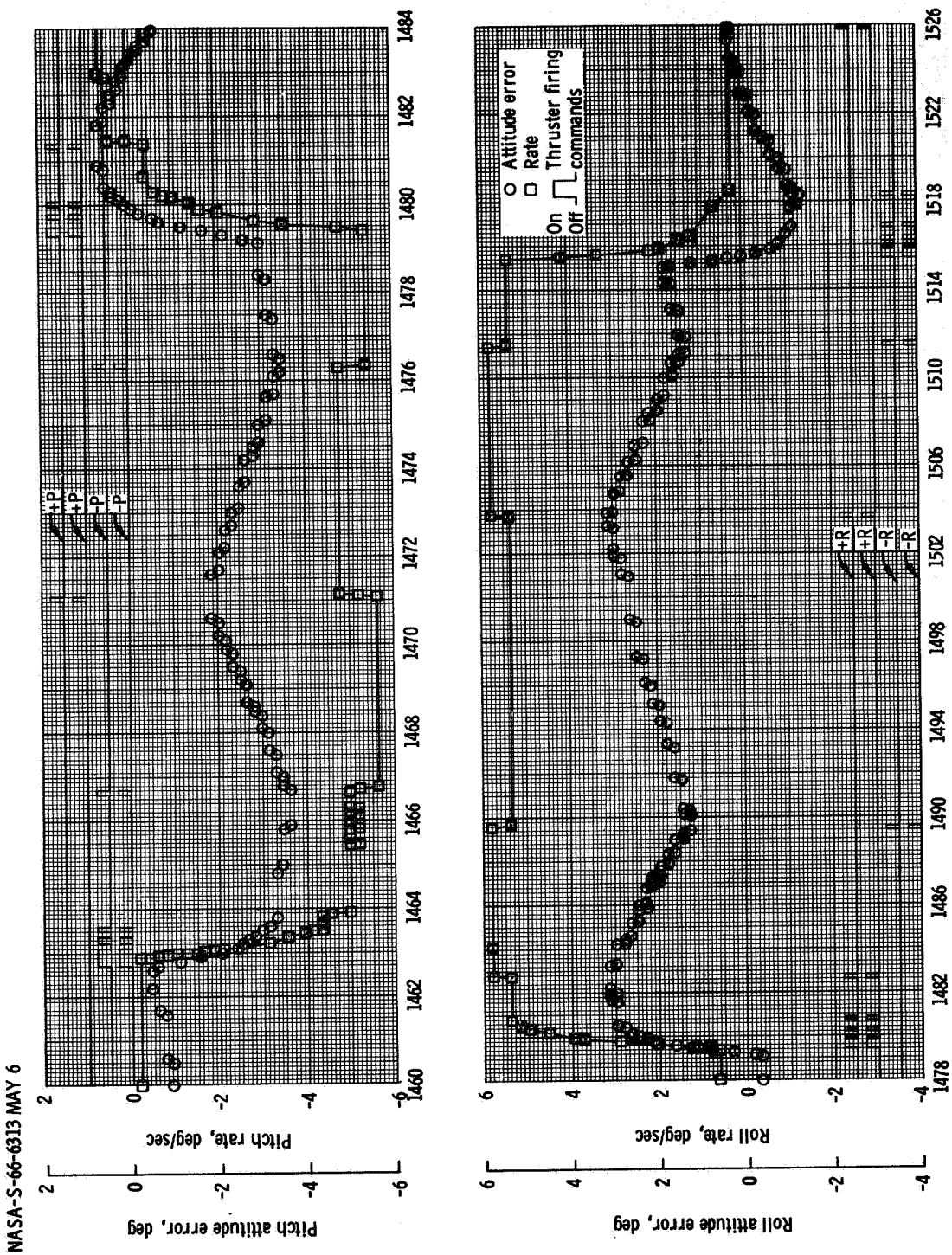
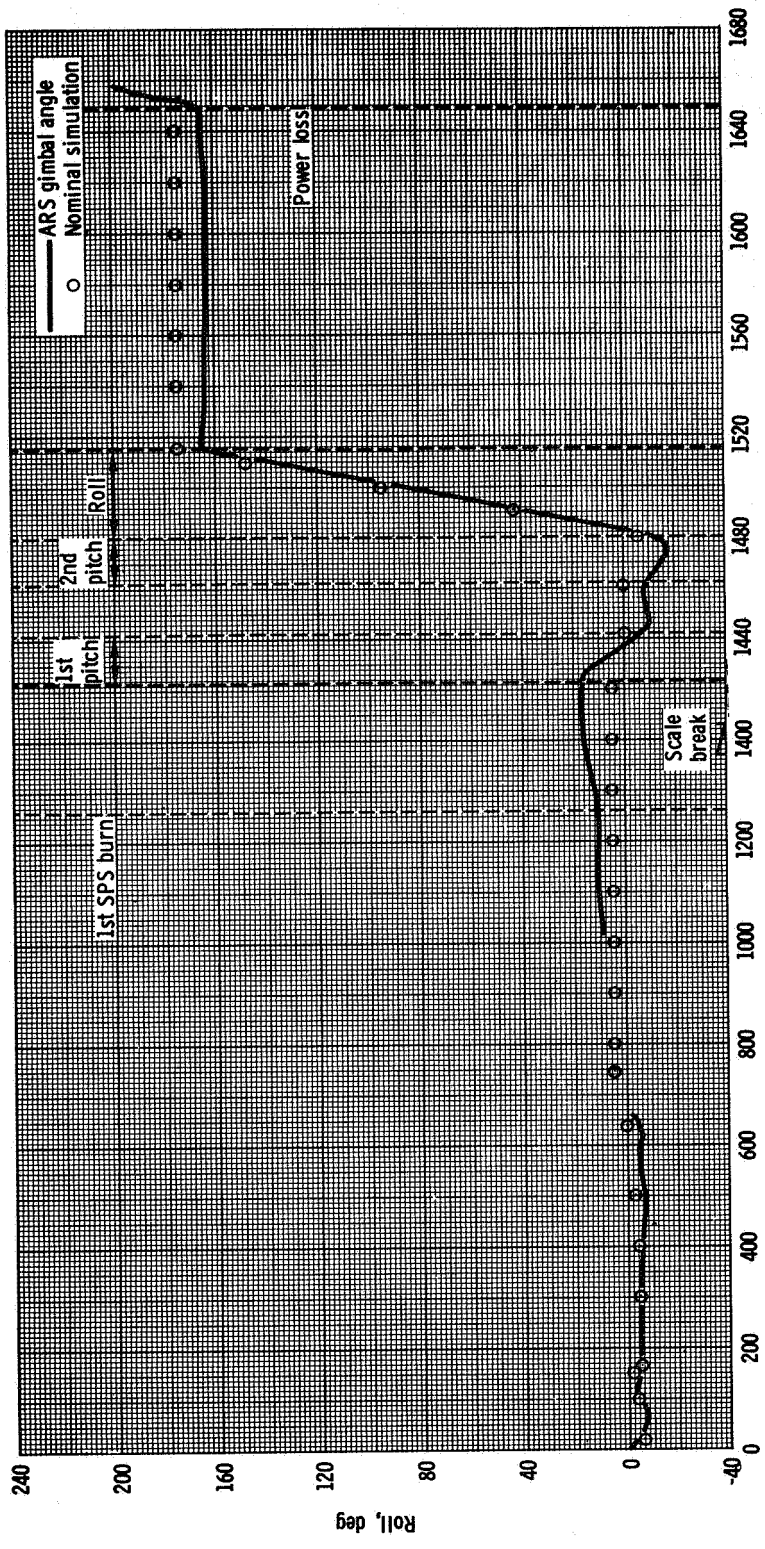


Figure 7.11-10. - GO pitch and roll man euvers, SC rates and attitude errors, Mission AS-201.



NASA-S-66-6314 MAY 6

Figure 7.11-11.- Roll ARS gimbal angle, Mission AS-201.

NASA-S-66-6315 MAY 6

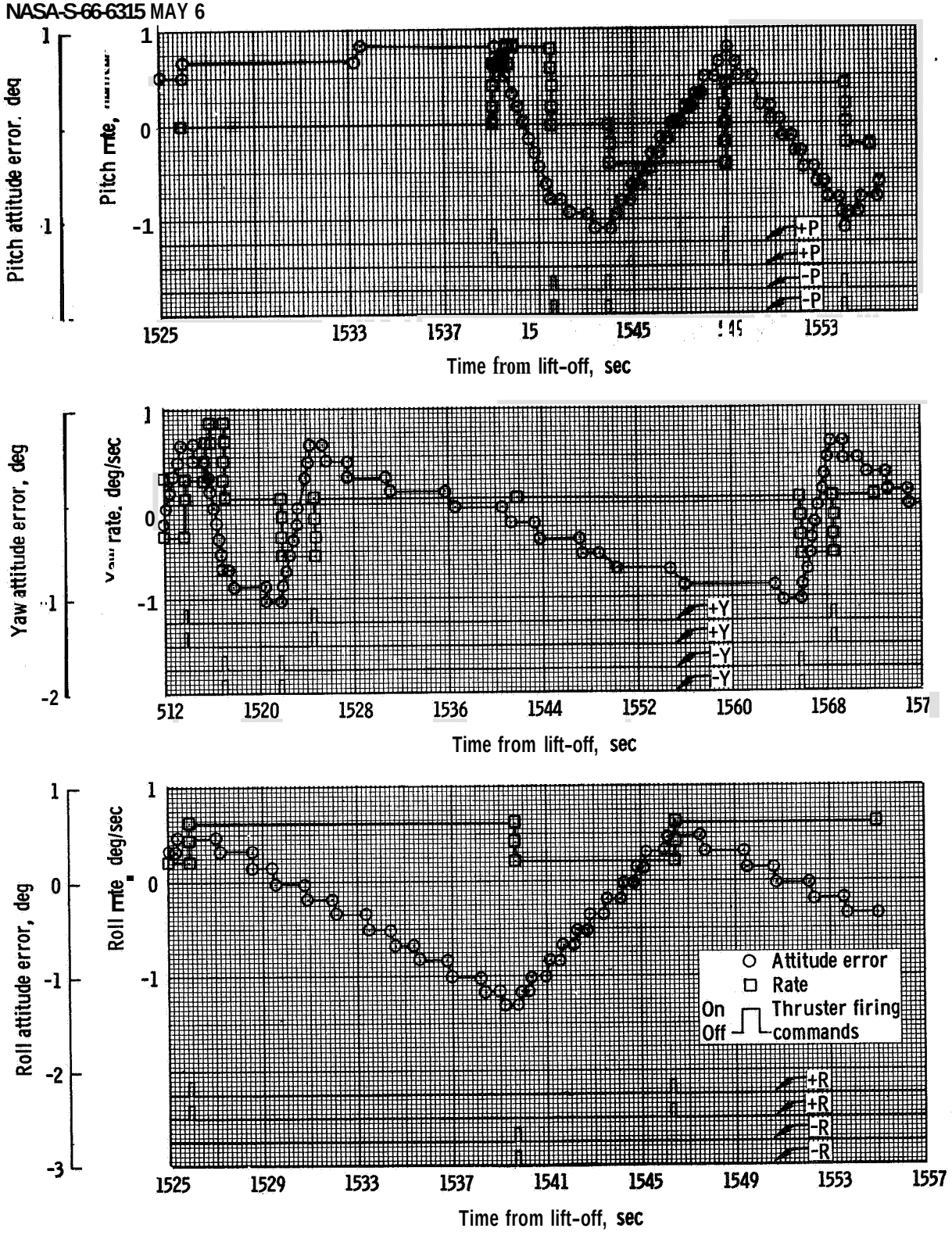
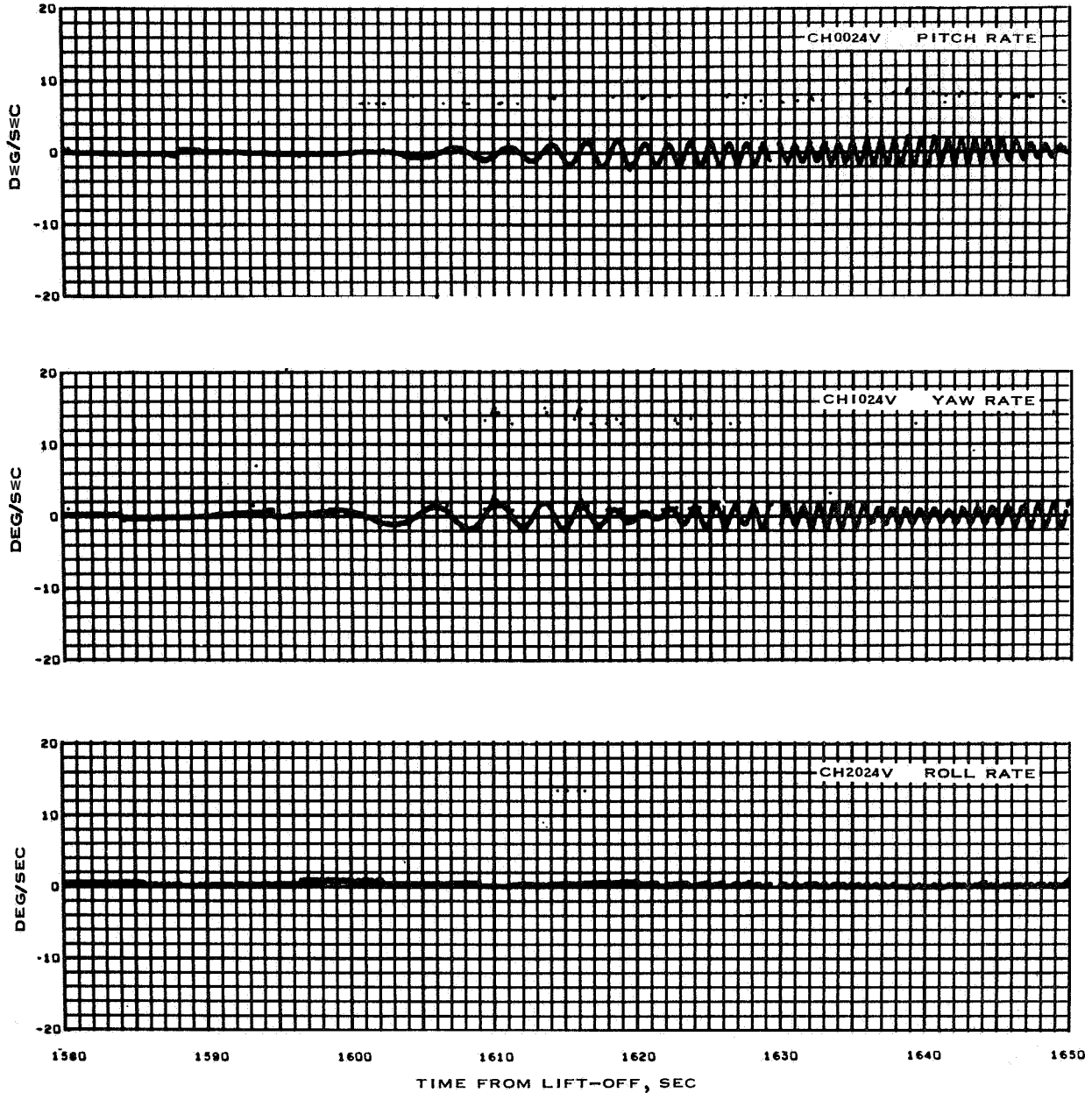


Figure 7.11-12 - CM coast phase limit cycles, Mission AS-201.

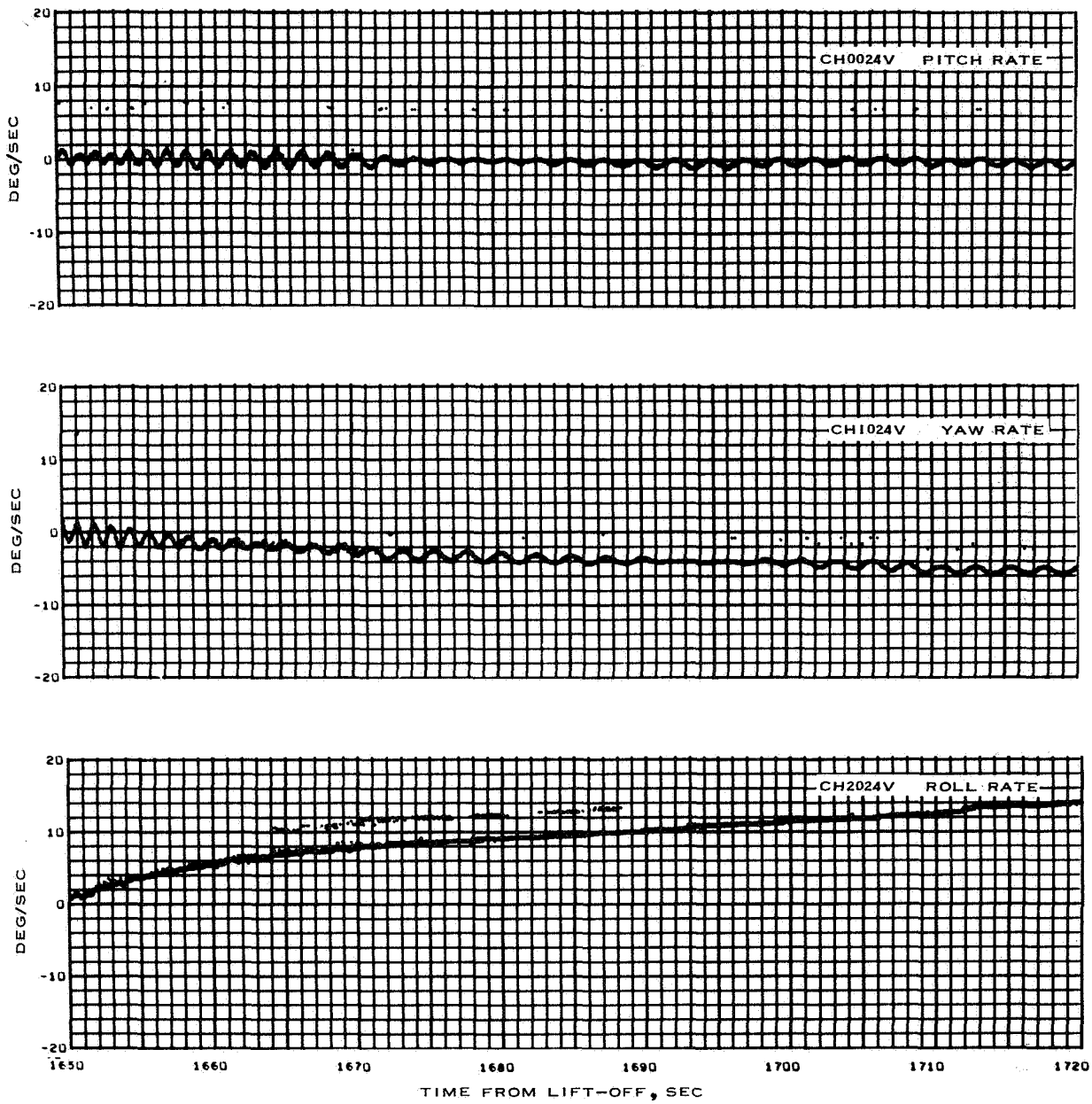
NASA-S-66-6316 MAY 6



(a) 1580 to 1650 seconds.

Figure 7.11-13.- CM reentry rate time histories, Mission AS-201.

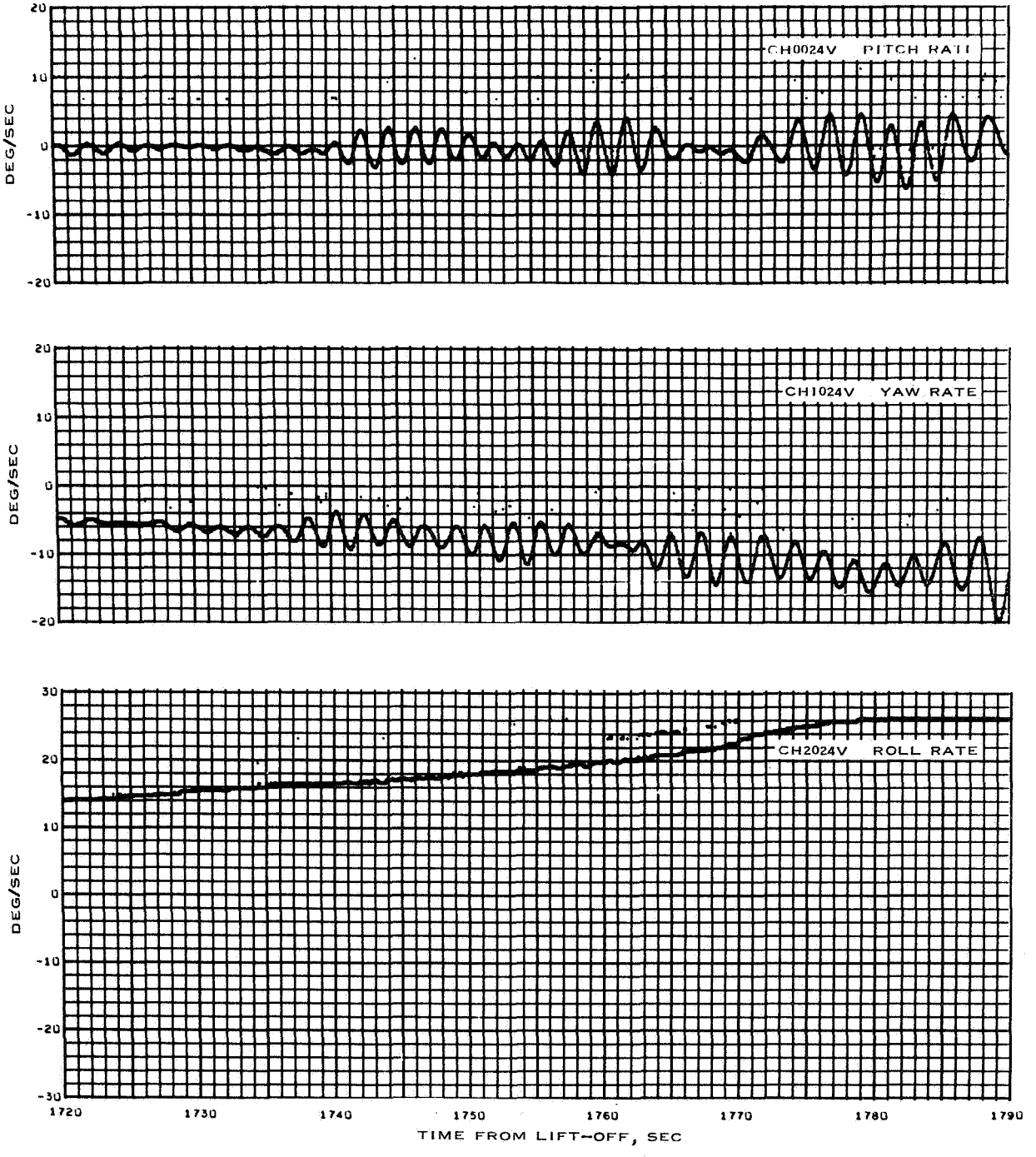
NASA-S-66-6317 MAY 6



(b) 1650 to 1720 seconds.

Figure 7.11-13.- Continued.

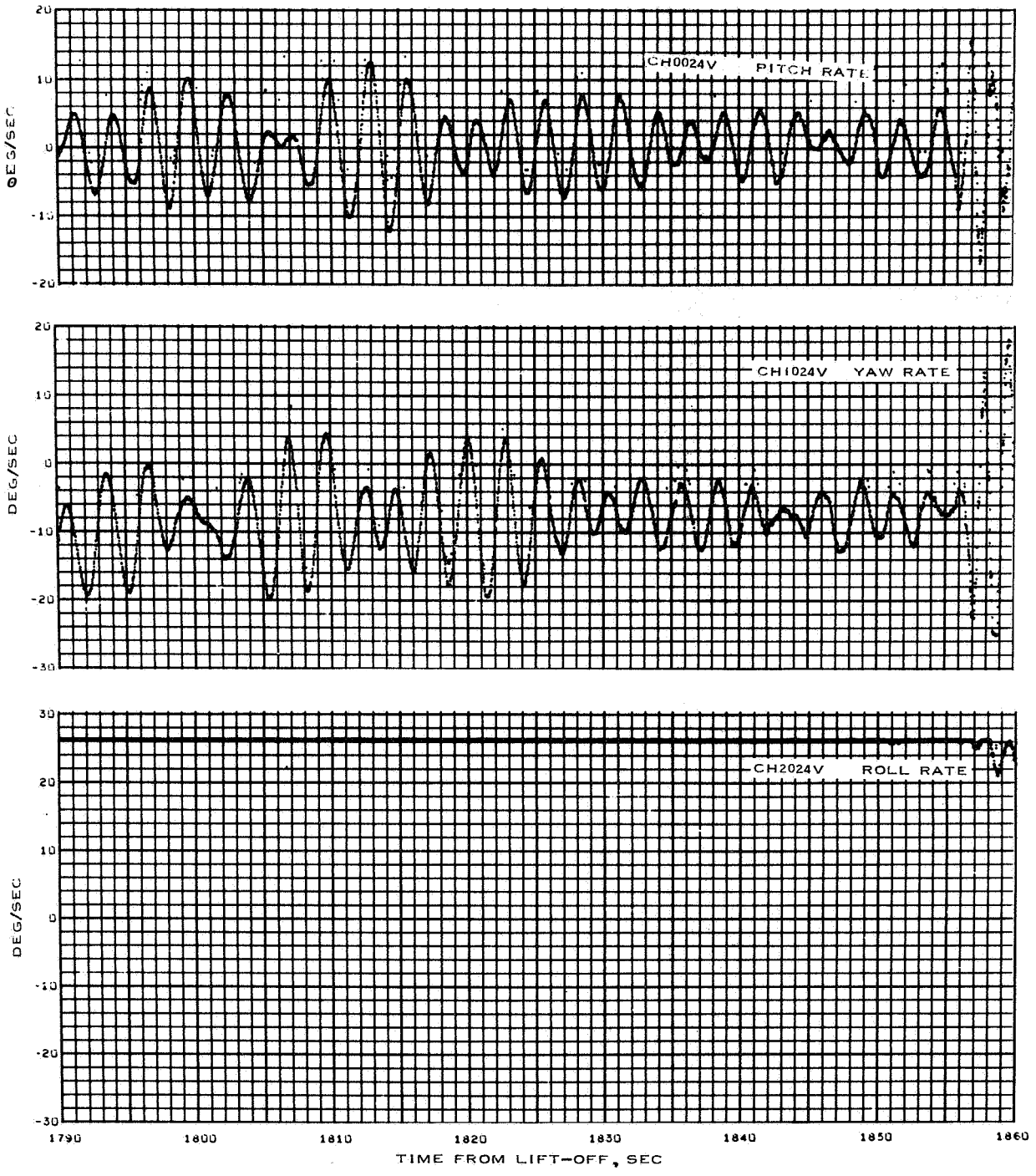
NASA-S-66-6318 MAY 6



(c) 1720 to 1790 seconds.

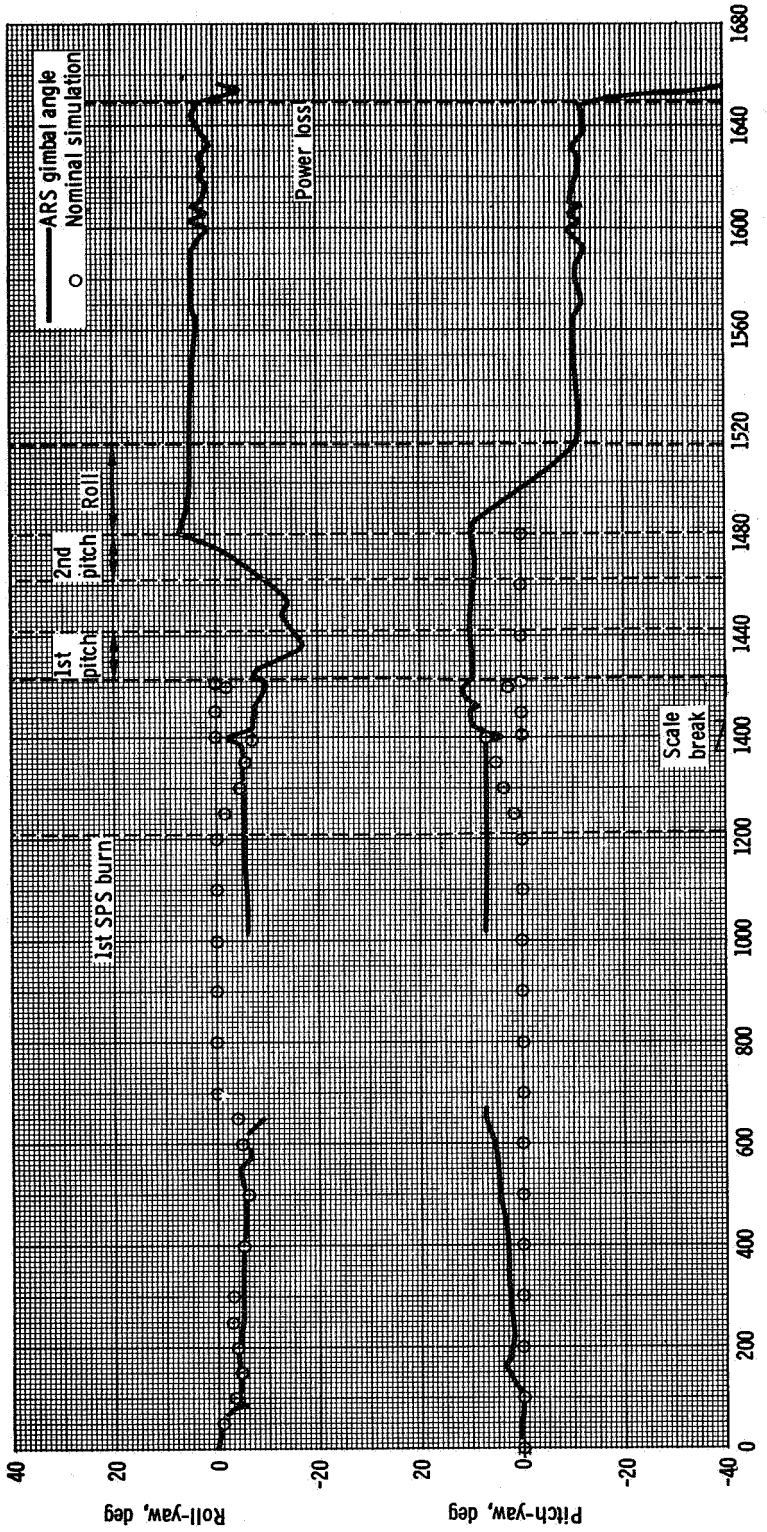
Figure 7.11-13.- Continued.

NASA-S-66-6319 MAY 6



(d) 1790 to 1860 seconds.

Figure 7.11-13.- Concluded.



NASA-S-66-6320 MAY 6

Figure 7.11-14.- Yaw ARS gimbal angle, Mission AS-201.

7.12 Electrical Power Subsystem

Description.- The electrical power subsystem (EPS) supplied, controlled, and distributed all electrical power in the spacecraft from lift-off through recovery. Three major differences existed between the EPS aboard spacecraft 009 and the Block I configuration: (1) batteries were included rather than fuel cells, (2) a power transfer control unit was included to perform part of the power switching that will be performed by the flight crew on manned missions, and (3) only two inverters were used. (See fig. 7.12-1.) In addition, the battery charger was not installed on spacecraft 009, and although the EPS radiators were installed, they were not utilized.

Main dc power was supplied by three batteries (ME461-0012-003) located in the service module and distributed through two redundant dc buses (A and B). Two 400-cycle inverters which received power from dc buses A and B were connected to the ac buses prior to flight; one inverter supplied power to ac bus 1 and the other supplied power to ac bus 2. The essential ac loads received power from ac bus 1. The power-transfer control unit automated the electrical power subsystem controls normally operated manually by the flight crew. If inverter 1 or ac bus 1 had failed during flight, the power transfer control unit would have disconnected the essential loads from ac bus 1 and reconnected them to ac bus 2.

Immediately prior to separation, command module (CM) batteries A, B, and C were connected to main dc buses A and B and the postlanding bus to supply power to CM loads after the service module (SM) was separated. Approximately 11 seconds after the CM landed, batteries A, B, and C were disconnected from main buses A and B to prevent unnecessary battery drain. Batteries A and B were also disconnected from battery buses A and B. All postlanding loads received power from the postlanding bus. Pyrotechnic devices were powered by two pyro batteries (ME461-007) in the CM, and two additional batteries (ME461-007) were installed in the SM to power the SM jettison controller after CM/SM separation.

Performance.- The electrical power subsystem operated normally until T+1454.7 seconds (CM/SM separation) at which time a short transient occurred on both main buses, A and B. Main bus A voltage dropped to 21.8 volts and main bus B dropped to 22.9 volts and total current rose to a maximum of 209.9 amperes compared with a nominal value of approximately 60 amperes. The total transient occurred in less than 0.5 second. Figure 7.12-2 shows this transient on battery bus A and main bus A.

Analysis indiceted that hot wires existed in the CM umbilical when it was guillotined. Postflight testing verified that SM RCS propellant isolation lines A and B and an obsolete line for SM RCS quad temperature control system were not deadfaced before going through the umbilical.

These lines were fed through circuit breakers CB15, CB16, and CB18 located on panels 25 and 22. The transient was too short to effect an opening of the circuit breakers and therefore the lines remained hot after CM/SM separation. This has been confirmed by postflight testing.

Data show the loss of pyro B and logic B bus voltages at T+1635 seconds (see fig. 7.12-3). Analysis indicated that CB18 on panel 22 had opened. Postflight inspection verified this. Data showed an overload on the system which was cleared when CB18 opened. Figures 7.12-4(a) to 7.12-4(c) show the three battery currents during the period of T+1631 seconds to T+1636 seconds. A composite of these shows an abnormal current beginning at T+1632.8 seconds ramping to a maximum of 27 amperes at approximately T+1633.3 seconds and abruptly decreasing at T+1635.1 seconds. The current distribution among the three batteries was what would be expected for the abnormal current through CB18. Further, the magnitude of abnormal current shown and the time that it lasted, compared with the circuit breaker characteristics, show that CB18 performed exactly to specifications. Figure 7.12-5 shows the effect of the circuit breaker opening.

From T+1635 seconds to T+1649 seconds, main buses A and B began to show transient excursions from nominal values. These transient excursions continued until approximately T+1650 seconds when a major short occurred which dropped the main bus A and main bus B voltages sharply, reaching a low of approximately 18 volts on each bus with a total current of approximately 266 amperes at T+1693 seconds. Figure 7.12-6 shows the sequence of events associated with this failure.

As individual circuit breakers opened, distinct voltage rises occurred at T+1693 seconds, T+1728 seconds, T+1770 seconds, T+2065 seconds, T+2103 seconds, T+2113 seconds, and T+2121 seconds. Each voltage rise was accompanied by a distinct decrease in total current. The last rise brought both buses back to nominal voltage and current levels. Figures 7.12-7 and 7.12-8 show this series of events on main buses A and B voltage and battery A and B current.

Postflight inspection revealed that the following circuit breakers which were closed prior to flight were open after flight:

Panel	Circuit breaker	Measurement
25	CB15	Propellant isolation main B
	CB16	Propellant isolation main A
	CB31	Yaw main B
	CB32	Yaw main A
	CB33	B and D roll main B
	CB34	B and D roll main A
	CB40	Pitch main B
	CB39	Pitch main A
22	CB18	Master event sequence controller arm B

The data analysis and postflight testing have led to the conclusion that the series of events was caused by the following:

As the spacecraft entered the high heat period of reentry the two propellant isolation lines, which were not run through any deadfacing facility, applied voltage through the GSE reset lines to the RCS transfer switches in the RCS controllers. This transferred the switches back to the SM position. The reset switches connected additional hot lines to the umbilical, which fused to the spacecraft ground, resulting in a heavy current drain. The total current flaring through the affected breakers averaged 204 amperes as opposed to the total breaker capacity of 205 amperes. The high current drain lasted for a significant time period (approximately 472 seconds) before the noted breakers opened and terminated the short. After the last of the listed circuit breakers opened, the electrical power subsystem operated normally with the exception of the permanent loss of pyro bus B and logic bus B when circuit breaker CB18 opened.

As a result of this analysis, the following changes have been made:

(a) Corrected wiring on subsequent spacecraft.

(b) Provided ground support equipment to verify umbilical deadfacing.

(c) Isolated A and B buses.

The following actions have been taken on spacecraft 011:

(a) A rearrangement of the SCS diode circuits was made in order to prevent a failure in one bus from overloading the other bus.

(b) In the SCS circuit utilization box C15A1, contacts for K3, 4, 5, 6, and 7 were jumpered. This bypasses the SCS channel disable relays to eliminate a possible single point failure.

(c) Two SM RCS positive yaw (+Y) jets were rewired such that S19A4 B1 is now transferred by the B RCS motor transfer switch and S19A2 B3 is now transferred by the A RCS motor transfer switch.

(d) The umbilical for spacecraft; 011 was reexamined and cleared of all unnecessary non-deadfaced wires that were identified as potential problem areas. Approximately 11 wires remain which are hot but these are current-limited annunciator wires.

(e) A physical examination of spacecraft wiring associated with CB18 and C23TB1 has revealed that these circuits are clean.

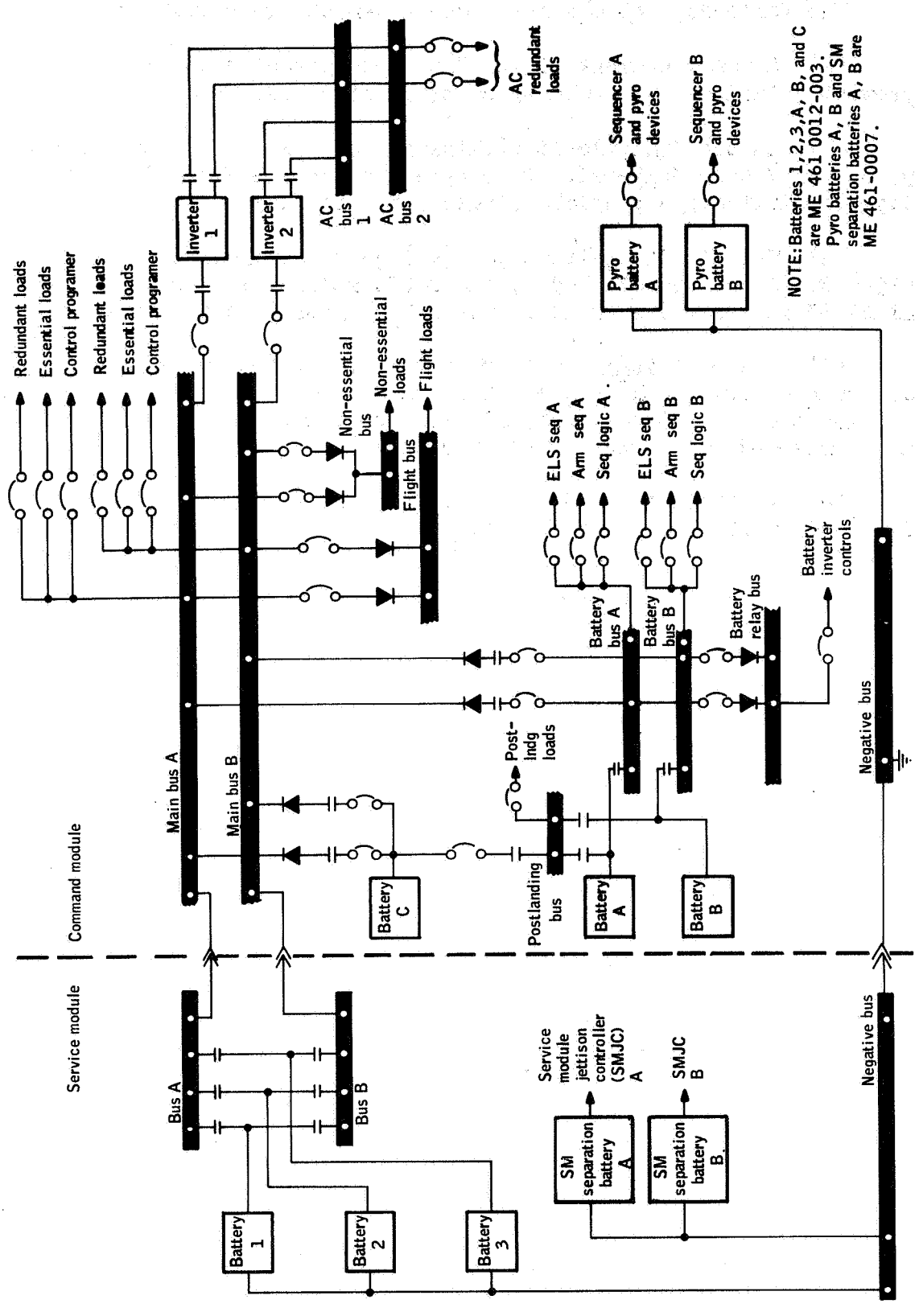


Figure 7.12-1.- Electrical power subsystem, Mission AS-201.

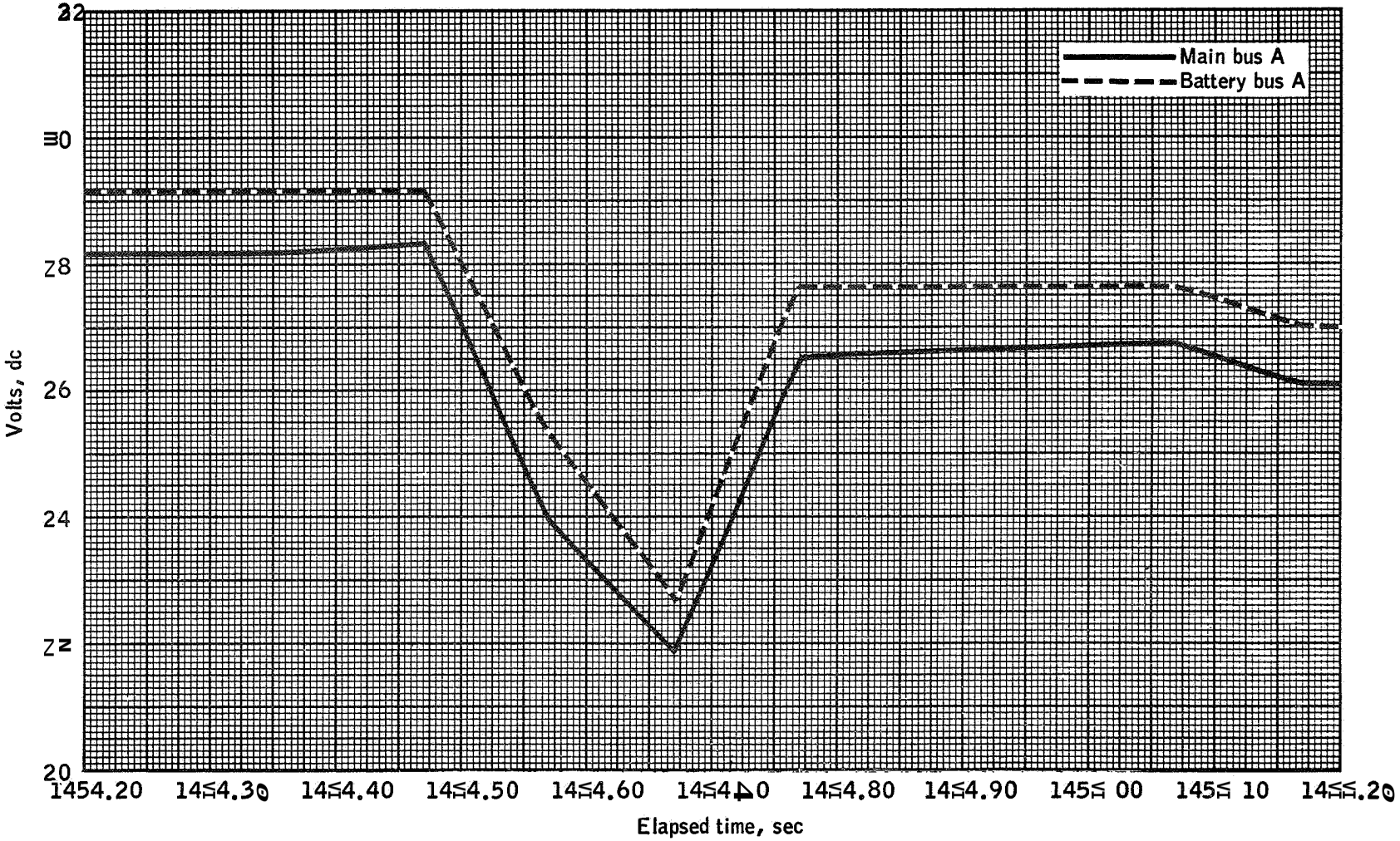


Figure 7.12-2.- Battery bus A and main bus A during CM/SM separation, Mission AS-201.

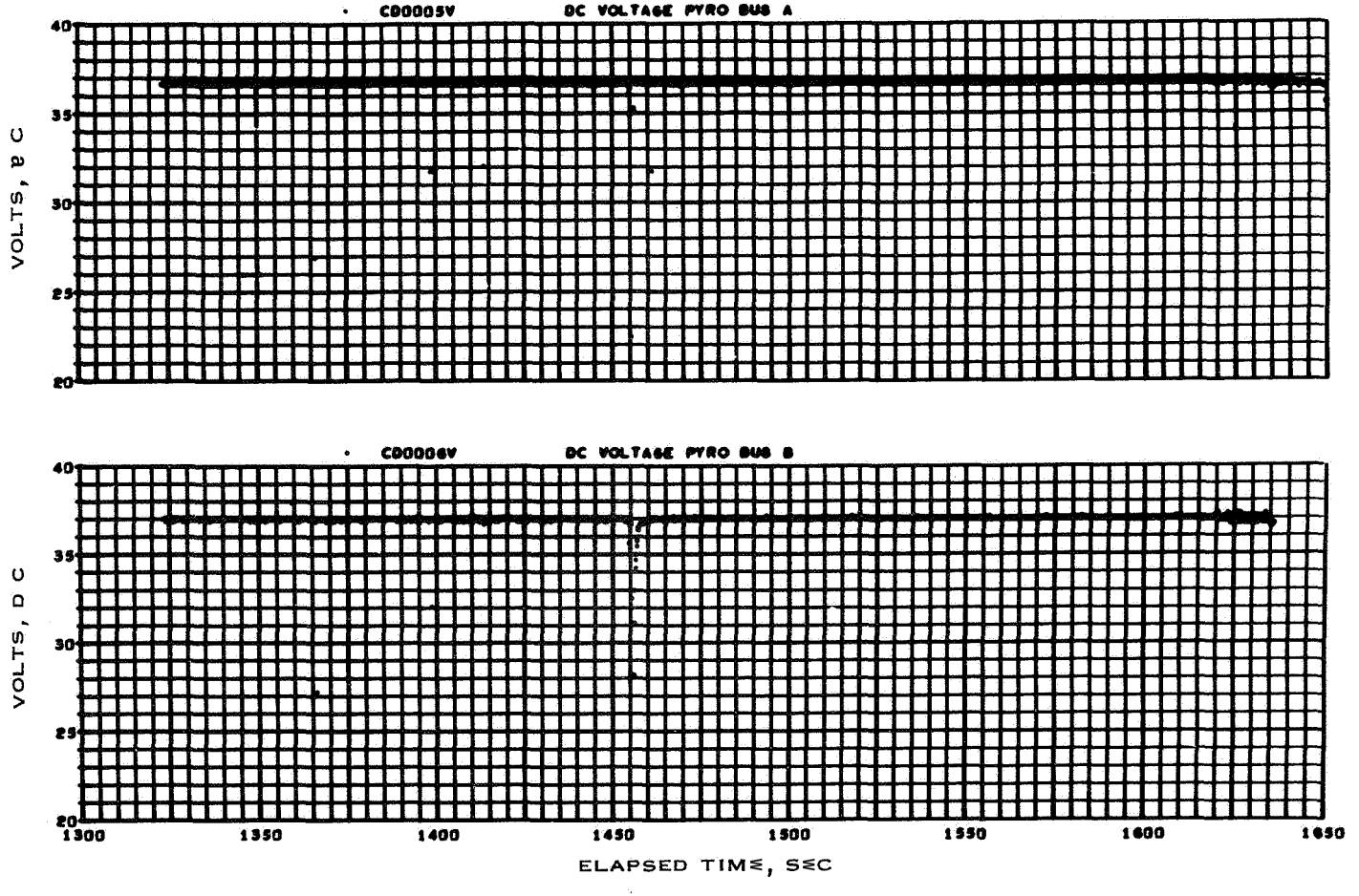
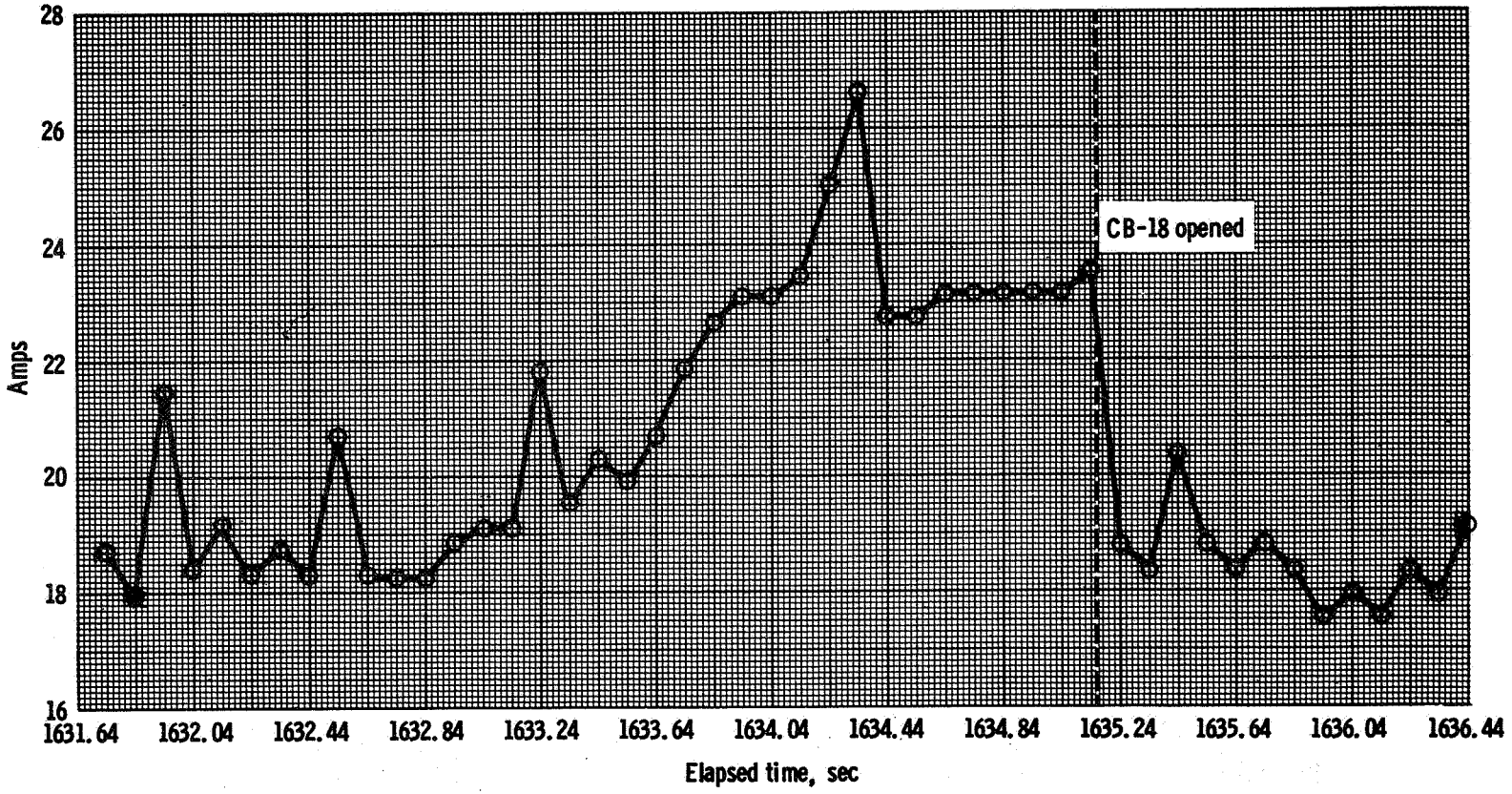


Figure 7.12-3.- Pyro bus B voltage from T-1300 to 1650 seconds, Mission AS-201.

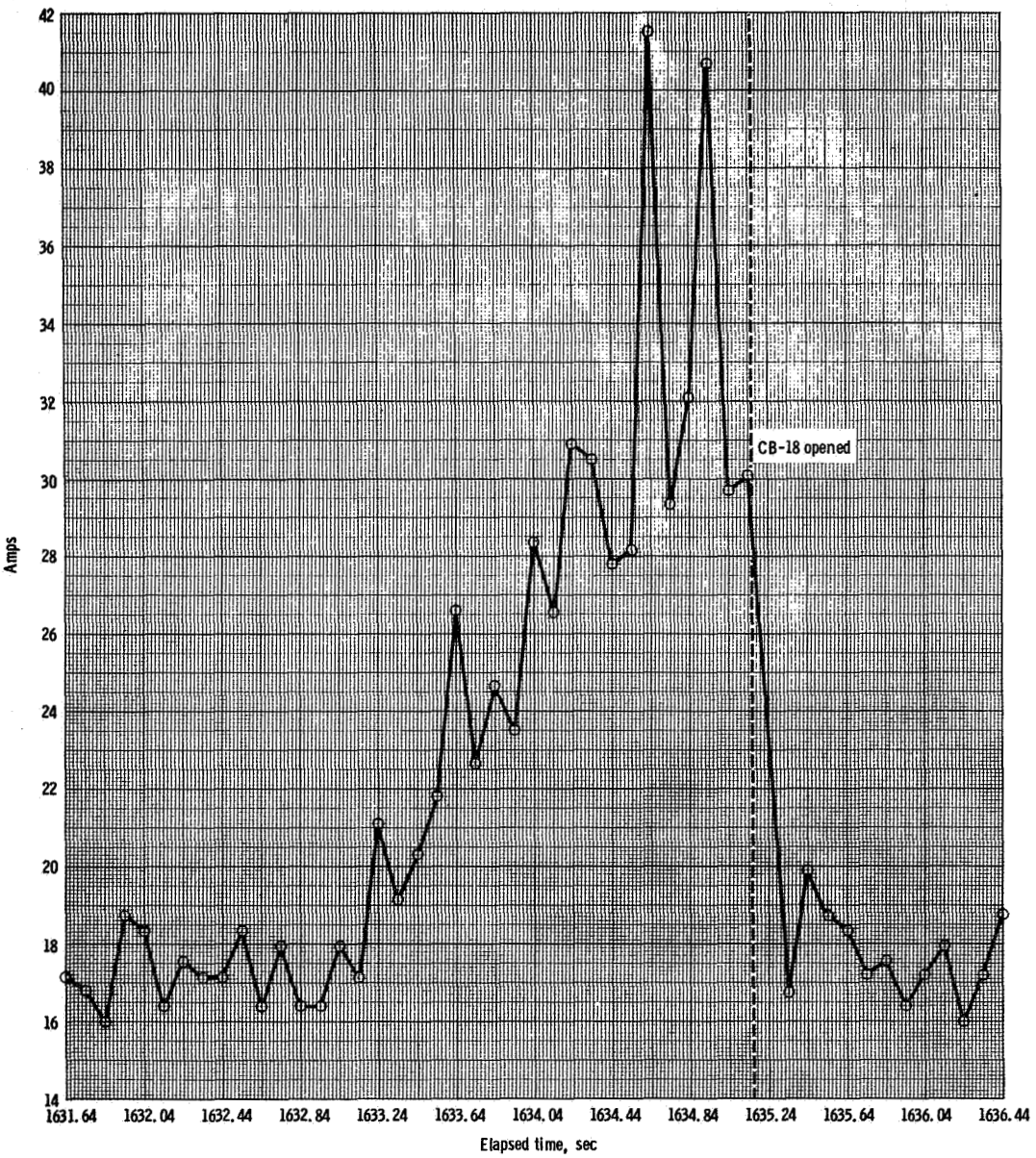
NASA-S-66-6324 MAY 6



(a) Current battery A.

Figure 7.12-4.- Three battery currents during the period from T+1631.64 to 1636.44 seconds, Mission AS-201.

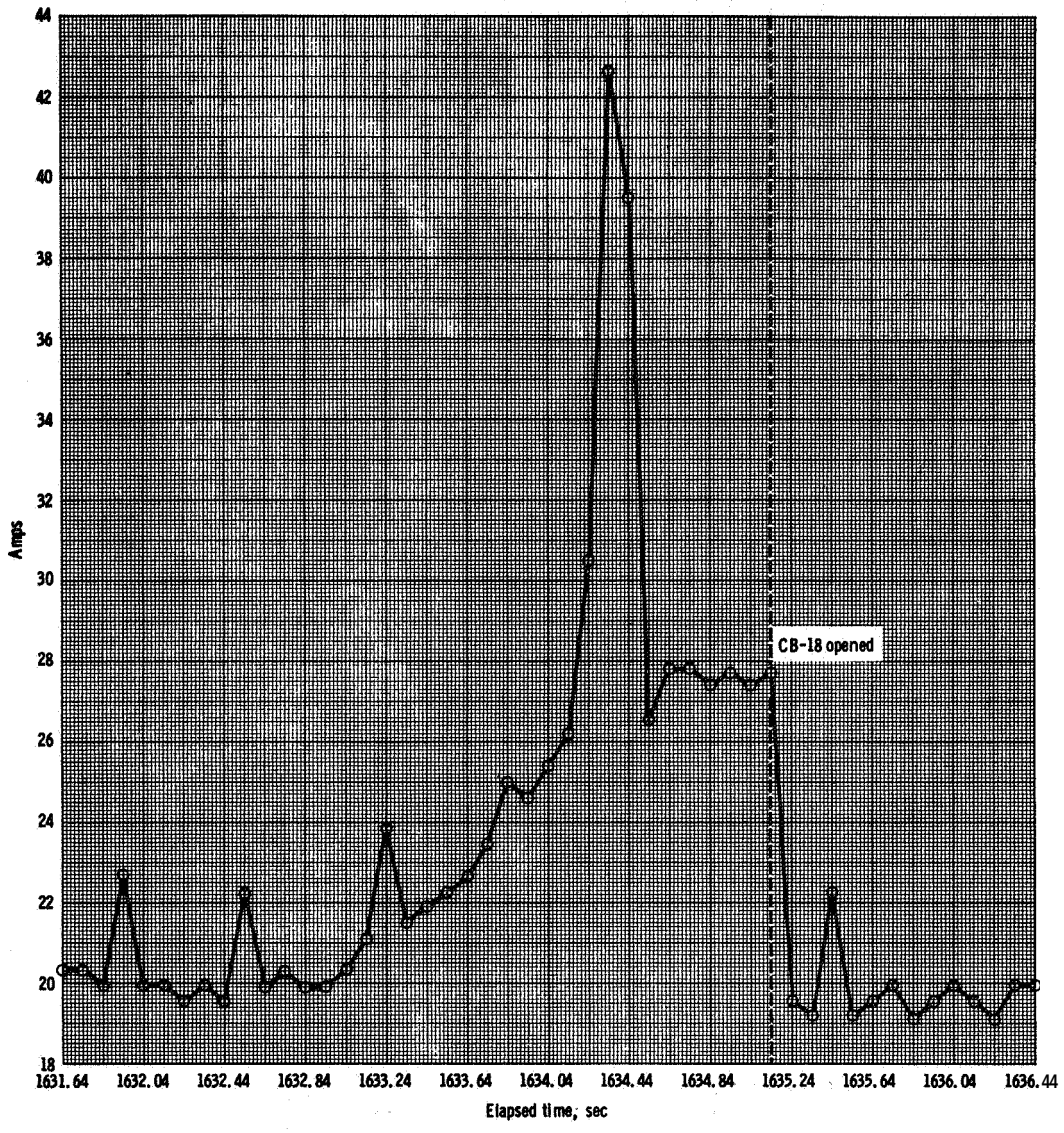
NASA-S-66-6325 MAY 6



(b) Current battery **B.**

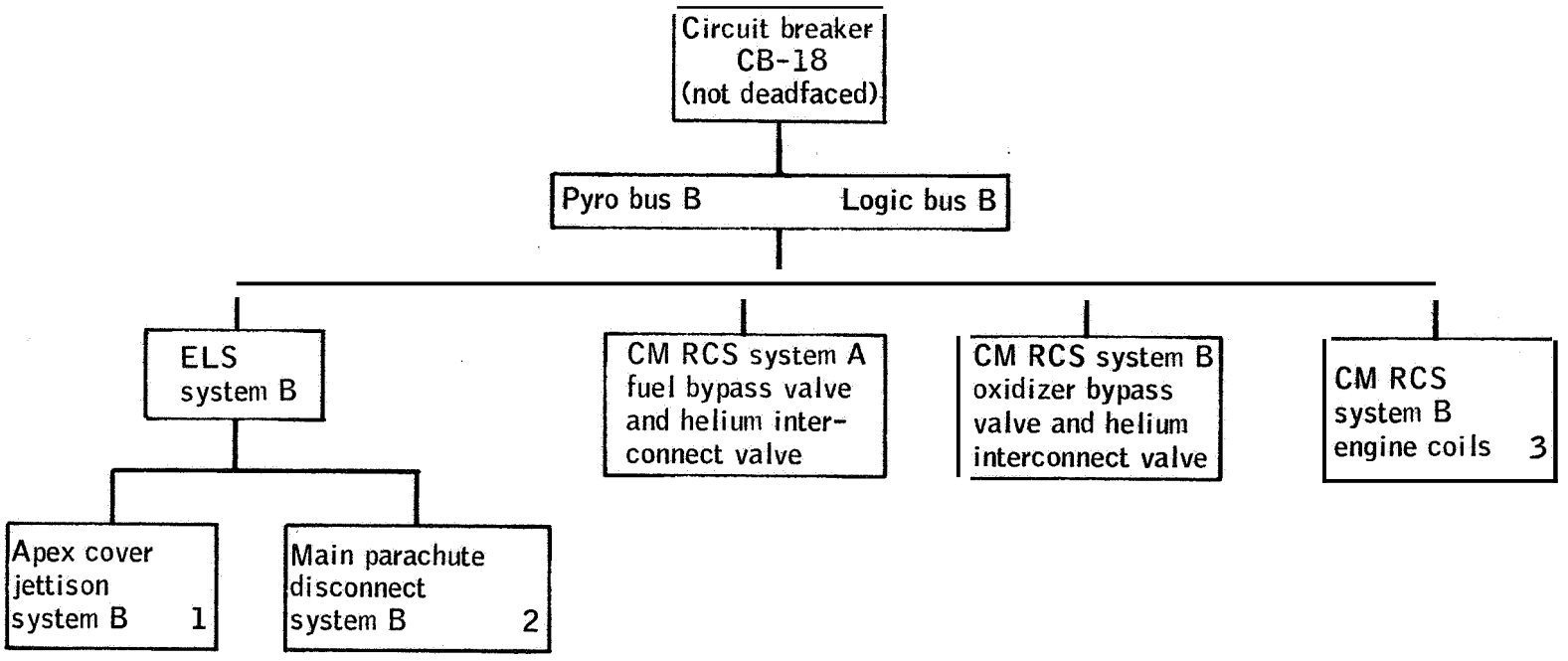
Figure 7.12-4.- Continued.

NASA-S-66-6326 MAY 6



(c) Current postlanding battery.

Figure 7.12-4.- Concluded.



Functions completed by redundant system

1. Apex cover jettisoned by system A
2. Depletion burn by system A

Function completed by semi-redundancy

3. One of two legs disconnected by system A

Figure 7.12-5.- Effects of circuit breaker 18 opening, Mission AS-201.

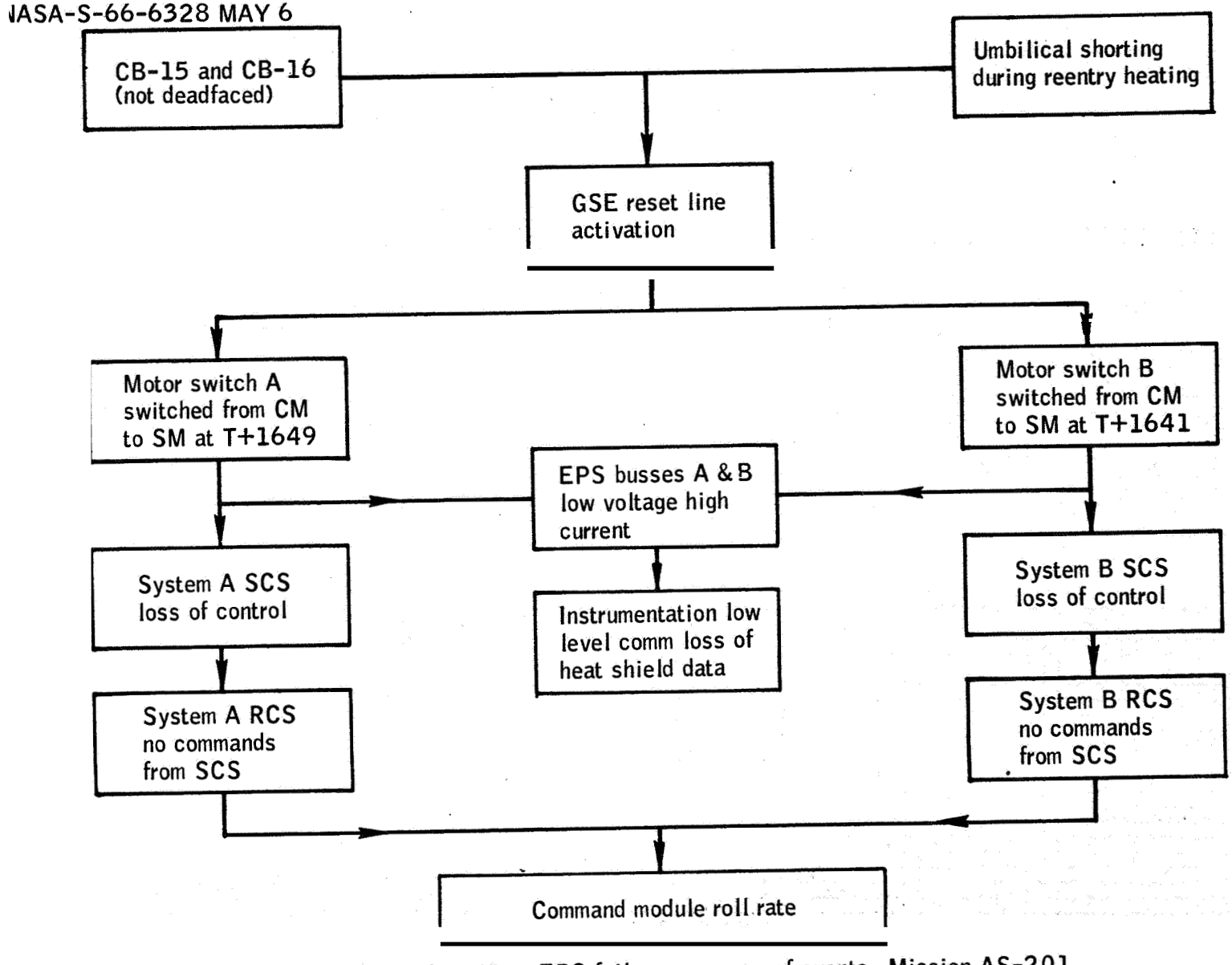
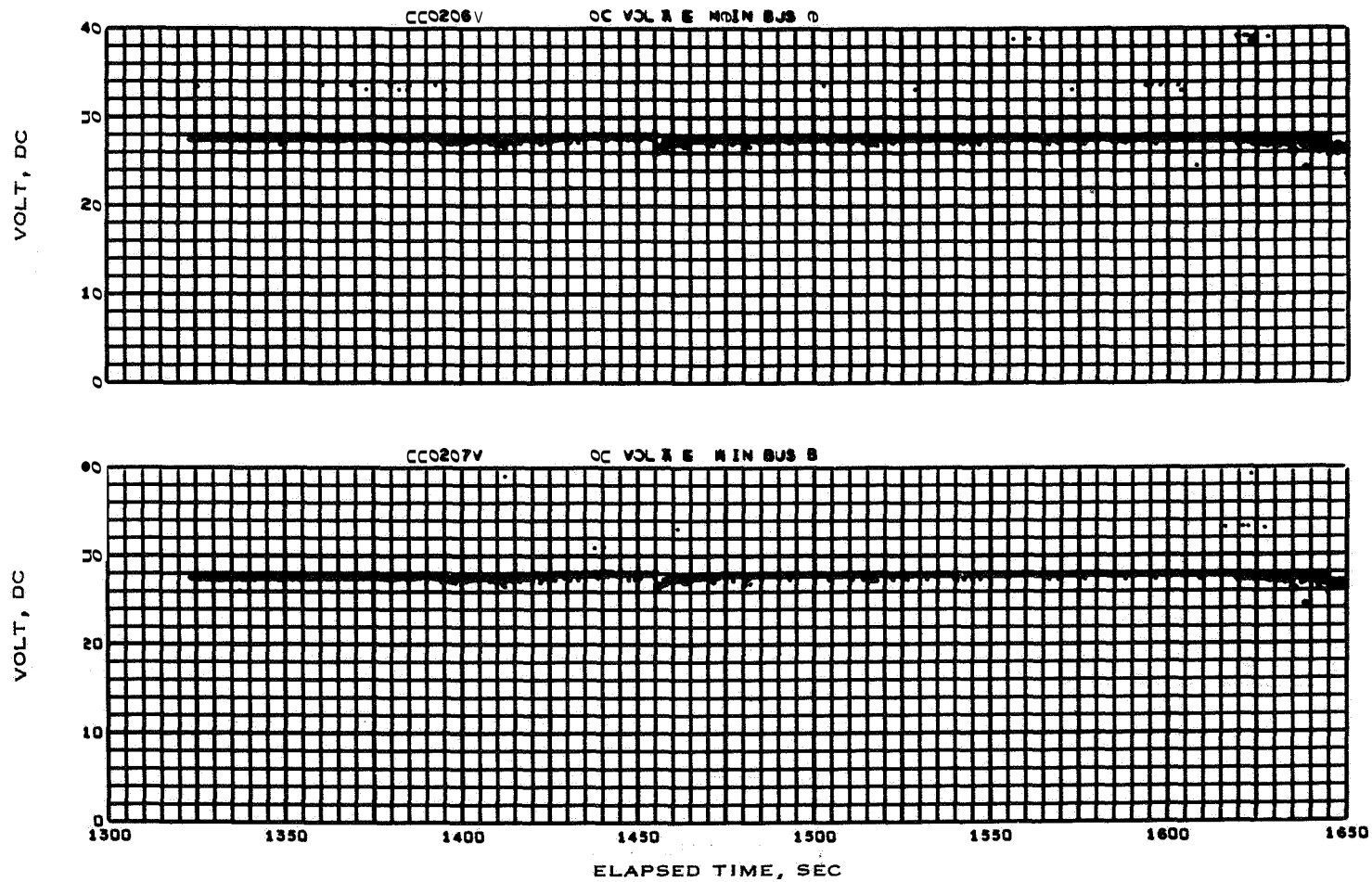
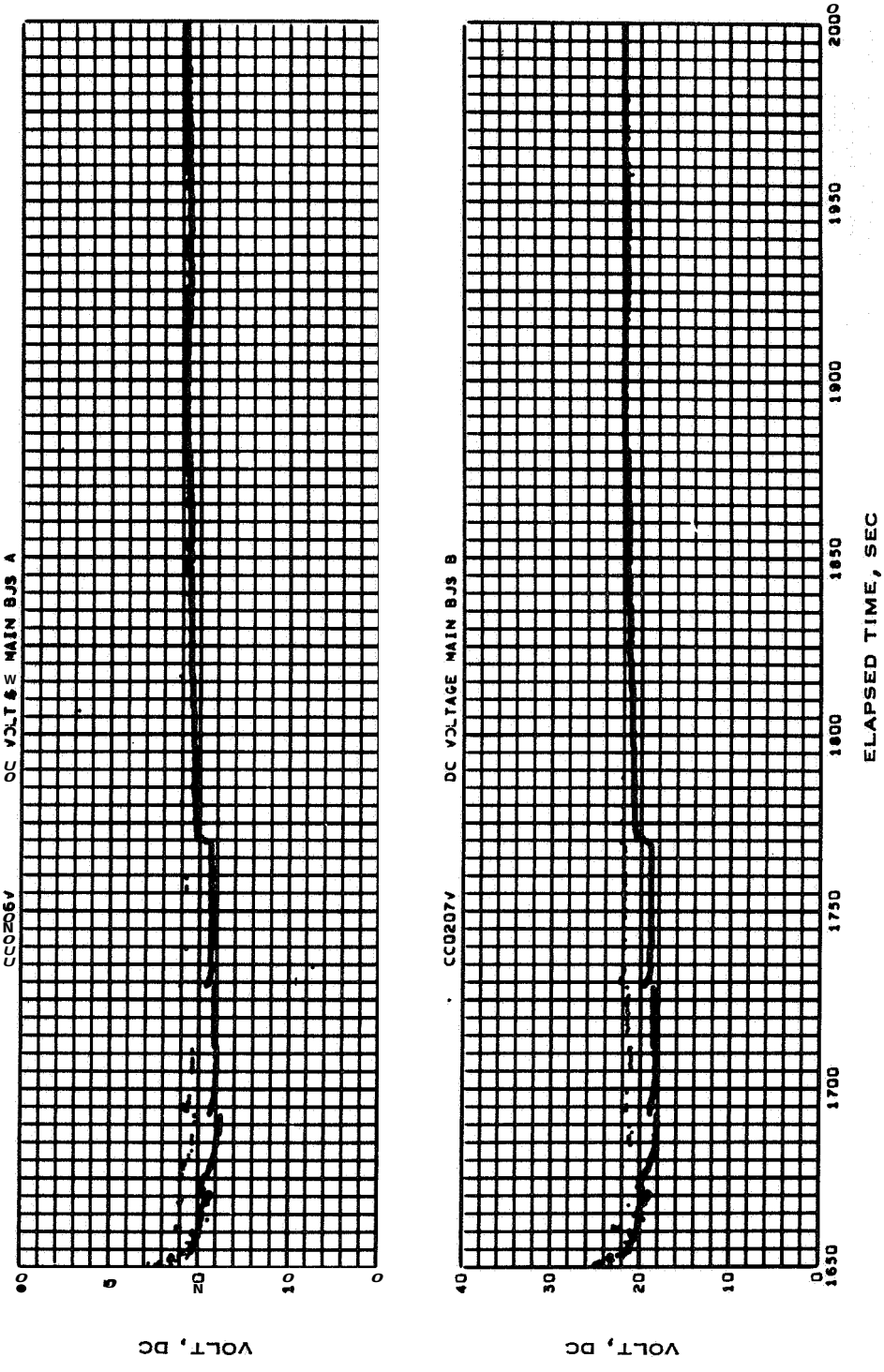


Figure 7.12-6.- Main EPS failure sequence of events, Mission AS-201.



(a) 1300 to 1650 seconds.

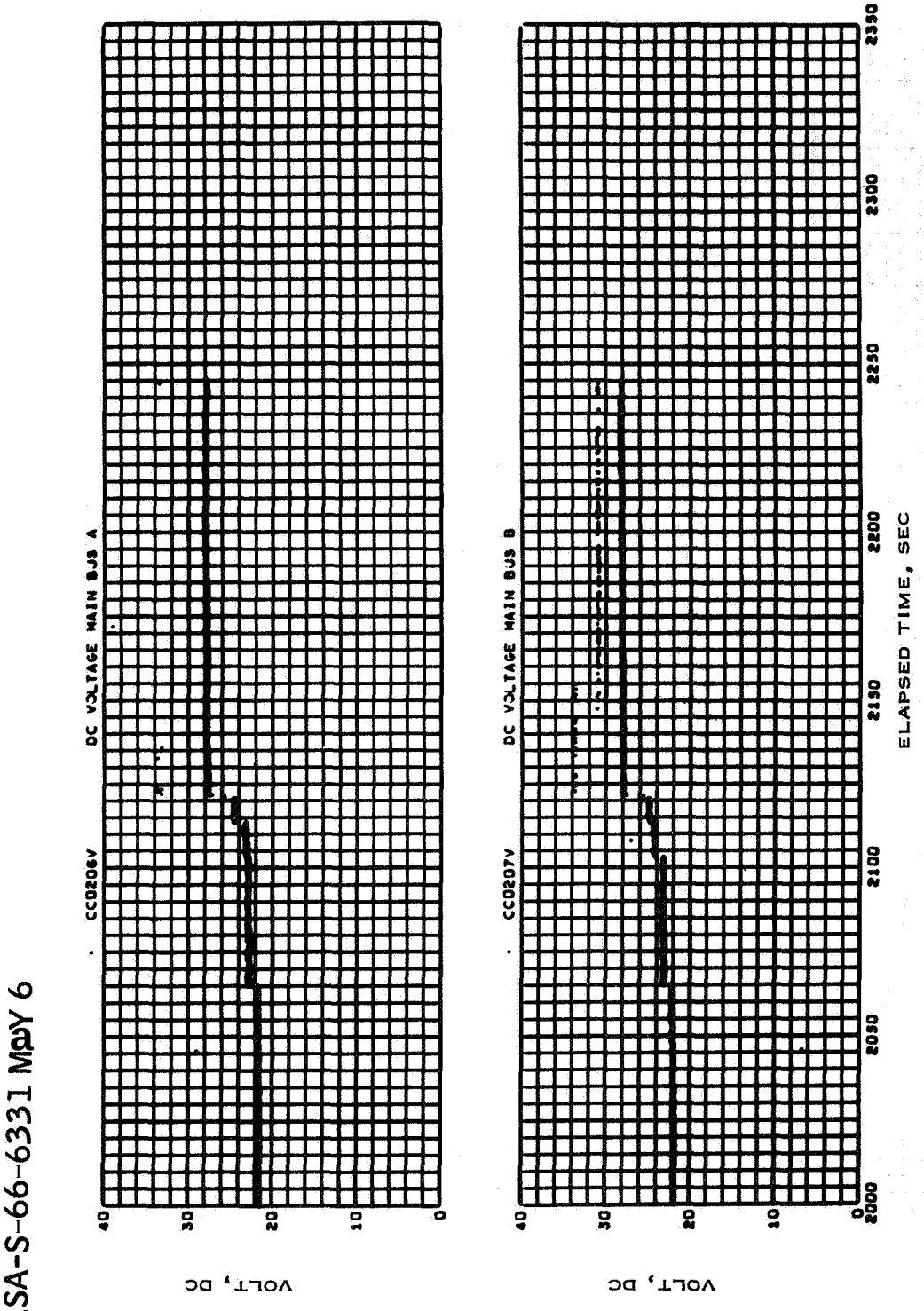
Figure 7.12-7.- Main bus A and main bus B voltage, Mission AS-201.



NASA-S-66-6330 MAY 6

(b) 1650 to 2000 seconds.

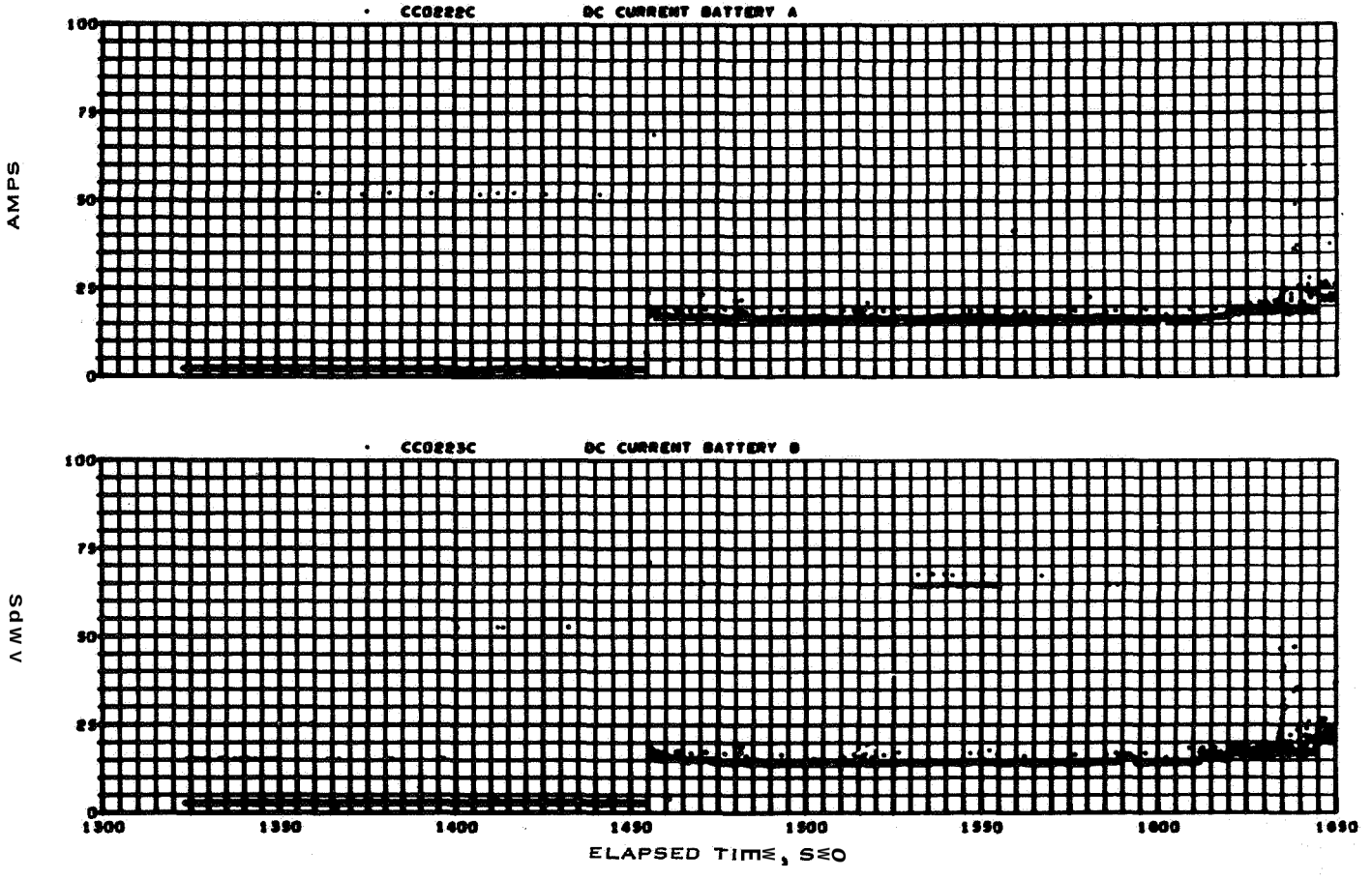
Figure 7.12-7.- Continued.



(c) 2000 to 2350 seconds.

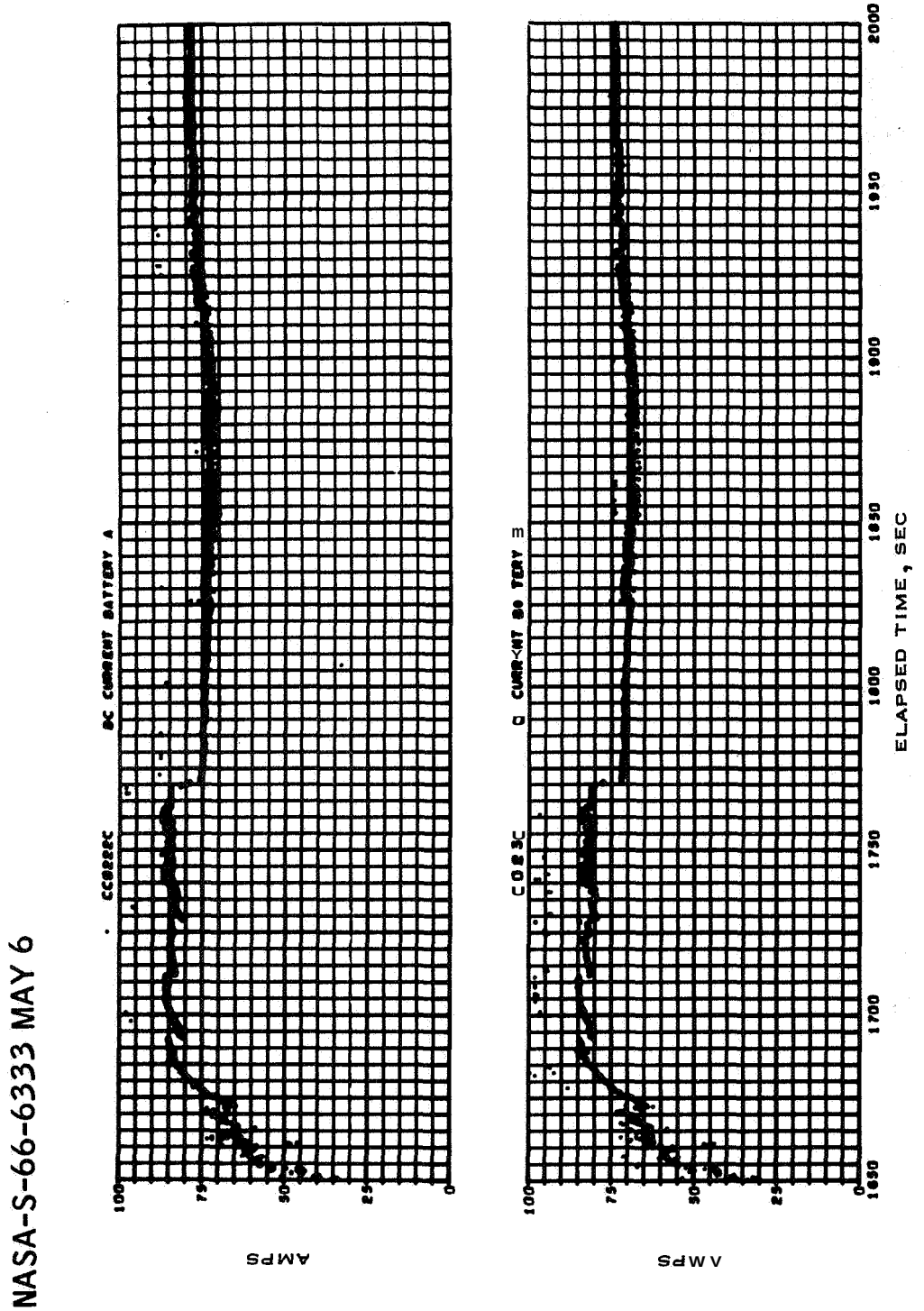
Figure 7.12-7.- Concluded.

NASA-S-66-6332 MAY 6



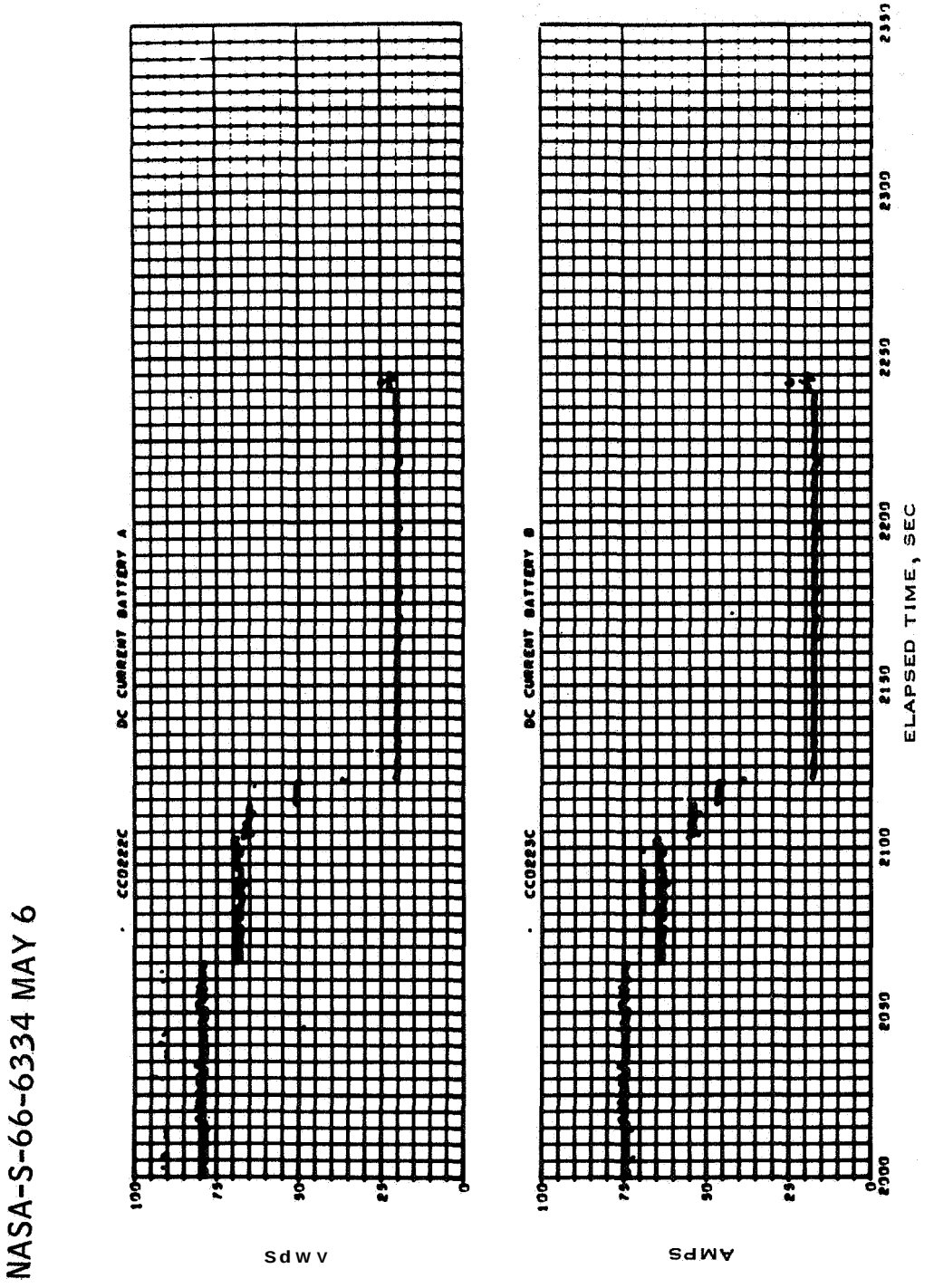
( ) 1300 to 1650 seconds.

Figure 7.12-8.- Batteries A and B dc currents from T-1300 seconds to impact, Mission AS-201.



(b) 1650 to 2000 seconds.

Figure 7.12-8.- Continued.



(c) 2000 to 2350 seconds.

Figure 7.12-8.- Concluded.

7.13 Sequential Subsystem

Description. - The sequential events control subsystem (SECS) aboard spacecraft 009 consisted of a master events sequence controller (MESC), service module jettison controller (SMJC), earth landing sequence controller (ELSC), reaction control subsystem controller (RCSC), postlanding sequence controller (PLSC), pyro continuity verification box (PCVB), impact switch, and fuel dump box. The PLSC, impact switch, and fuel dump box are not standard Block I equipment. These were added to spacecraft 009 to perform automatically the following functions which are normally controlled manually: main parachute disconnect, RCS fuel dumping and postlanding functions. The PCVB on spacecraft 009 differed from standard Block I in that it did not contain the relays to preclude premature operation of ELSC functions. Service module batteries powered the SMJC while all other controllers received power from batteries in the command module (CM). Only the ELSC and PCVB had been previously flight tested (ELSC and PCVB on SC-002 and ELSC on SC-002 and BP-22, refs. 6 and 7).

The MESC controlled the logic power, pyrotechnic power, and timing functions required to initiate and terminate events associated with ascent, abort, and separation. Control of CM RCS fuel and oxidizer dumping, purging, and transfer of the RCS electrical control from the SM to the CM during LES abort or normal CM/SM separation was provided by the RCSC and the fuel dump box. The SMJC programed the SM maneuvers required to minimize the probability of recontact of the two modules after separation. Events associated with drogue parachute deployment and release, and pilot parachute deployment were controlled by the ELSC; main parachute disconnect was initiated by the impact switch. The PLSC provided for automatic control of uprighting the spacecraft (if in an apex-down attitude in the water) and initiated deployment of the HF recovery antenna. Figure 7.13-1 shows the SECS together with major related spacecraft items.

Performance. - The sequential events control subsystem (SECS) functioned satisfactorily throughout the flight except for those functions disabled by the opening of CB18 on panel 22 at T+1635 seconds (see section 7.12). This removed power from the SECS system B and prevented the following events from occurring:

(a) CM RCS system B propellant depletion burn

(b) CM RCS fuel system A and B helium interconnect

(c) CM RCS oxidizer system A and B helium interconnect

(d) CM RCS system A fuel tank bypass

(e) CM RCS system B oxidizer tank bypass

(f) System B forward heat shield jettison thruster fire

(g) System B main parachute disconnect

For further discussion of these disabled circuits, see sections 7.9, 7.10, and 7.11.

A complete list of significant flight events with planned and actual times is given in table 2.0-I.

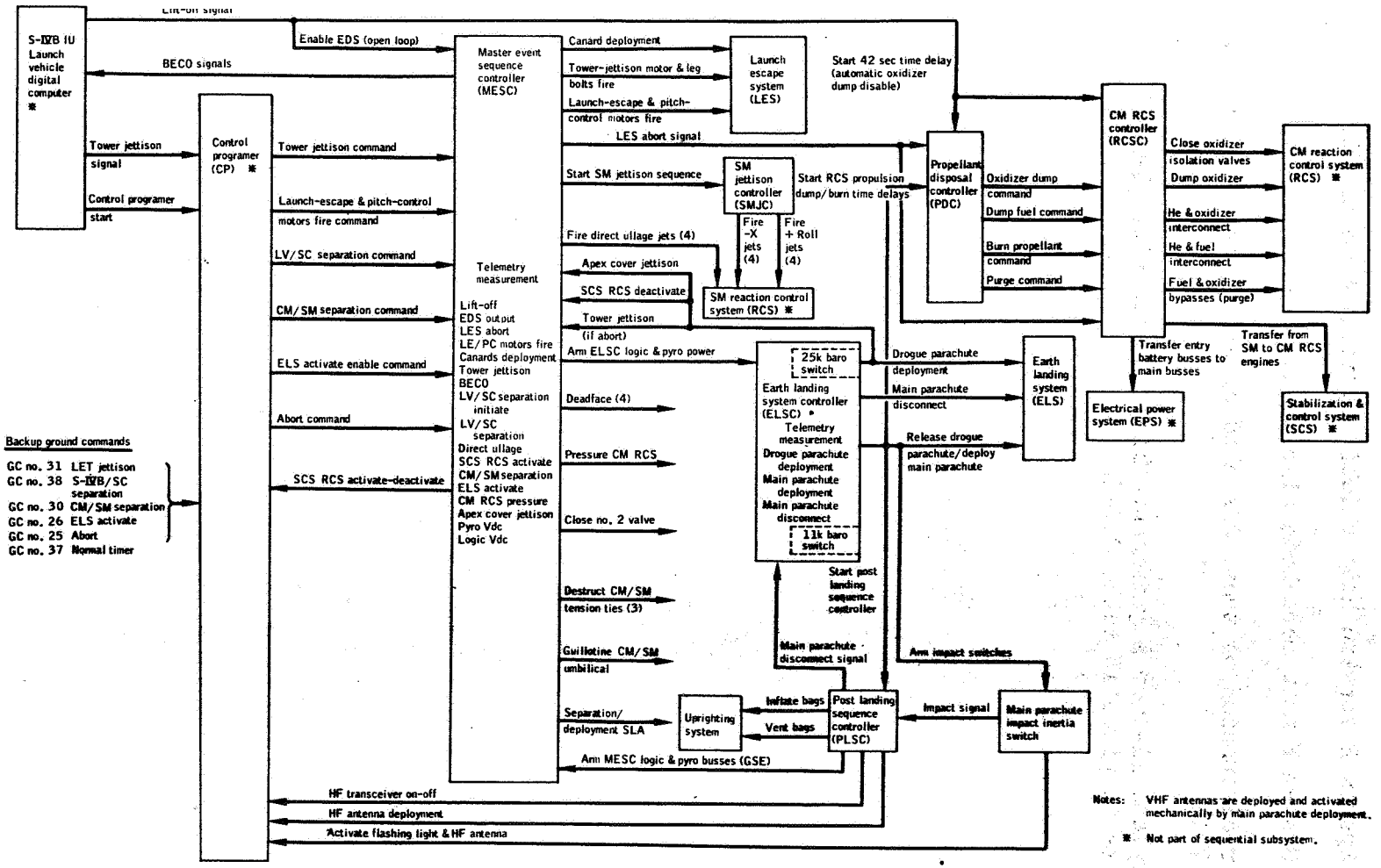


Figure 7.13-1.- Sequential events control system block diagram, Mission AS-202.

7.14 Emergency Detection Subsystem

Summary.- A primary objective of Mission AS-201 was to evaluate the performance of the emergency detection subsystem (EDS) in the open-loop configuration (automatic abort circuit not enabled in the spacecraft). The open-loop EDS performed nominally in all respects, with no abort signals generated by the subsystem.

Description.- The emergency detection subsystem in the spacecraft was designed to receive indications of emergency during the launch phase fromthe launch vehicle, from spacecraft systems, and from the Q-ball mounted at the apex of the launch-escape tower. The command module (CM) interfaces with the launch vehicle and the Q-ball are shown in figure 7.14-1.

Crew displays of EDS parameters were omitted in Mission AS-201, with system A bilevel display parameters telemetered for flight evaluation. Q-ball output of pitch and yaw angle of attack vector sum was also telemetered. The guidance and navigation subsystem and the flight director attitude indicator were omitted; therefore spacecraft angular rates and attitude errors were unavailable. Provisions for tower jettison and nonautomatic abort, which normally would be pilot functions, was included in the control programmer. Tower jettison was commanded to the control programmer by the launch vehicle sequencer with backup fromthe spacecraft tone command link. Abort could only be commanded to the control programmer by the spacecraft tone command link.

The automatic abort circuitry installed in spacecraft 009 was placed in the open-loop configuration by leaving the automatic abort mode switch in the OFF position (figs. 7.14-2 and 7.14-3). In the closed-loop configuration an automatic abort would have been commanded by the launch vehicle in the event of loss of thrust of two first-stage engines, excessive angular rate in *any* control plane, or by loss of at least two of the three hot-wire automatic abort interface signals between the CSM and the instrument unit (IU),

Performance.- No automatic abort or display signals were generated during the mission. The Q-ball output was smooth, continuous, and within expected limits throughout the period of interest, T+30 seconds through T+100 seconds, as shown in figure 7.14-4.

The mission demonstrated proper performance of the launch vehicle engine status circuits, the Q-ball, and launch vehicle lift-off signals to the spacecraft.

The excessive noise in the outputs of the rate gyros during the period of high dynamic pressure is discussed in section 8.

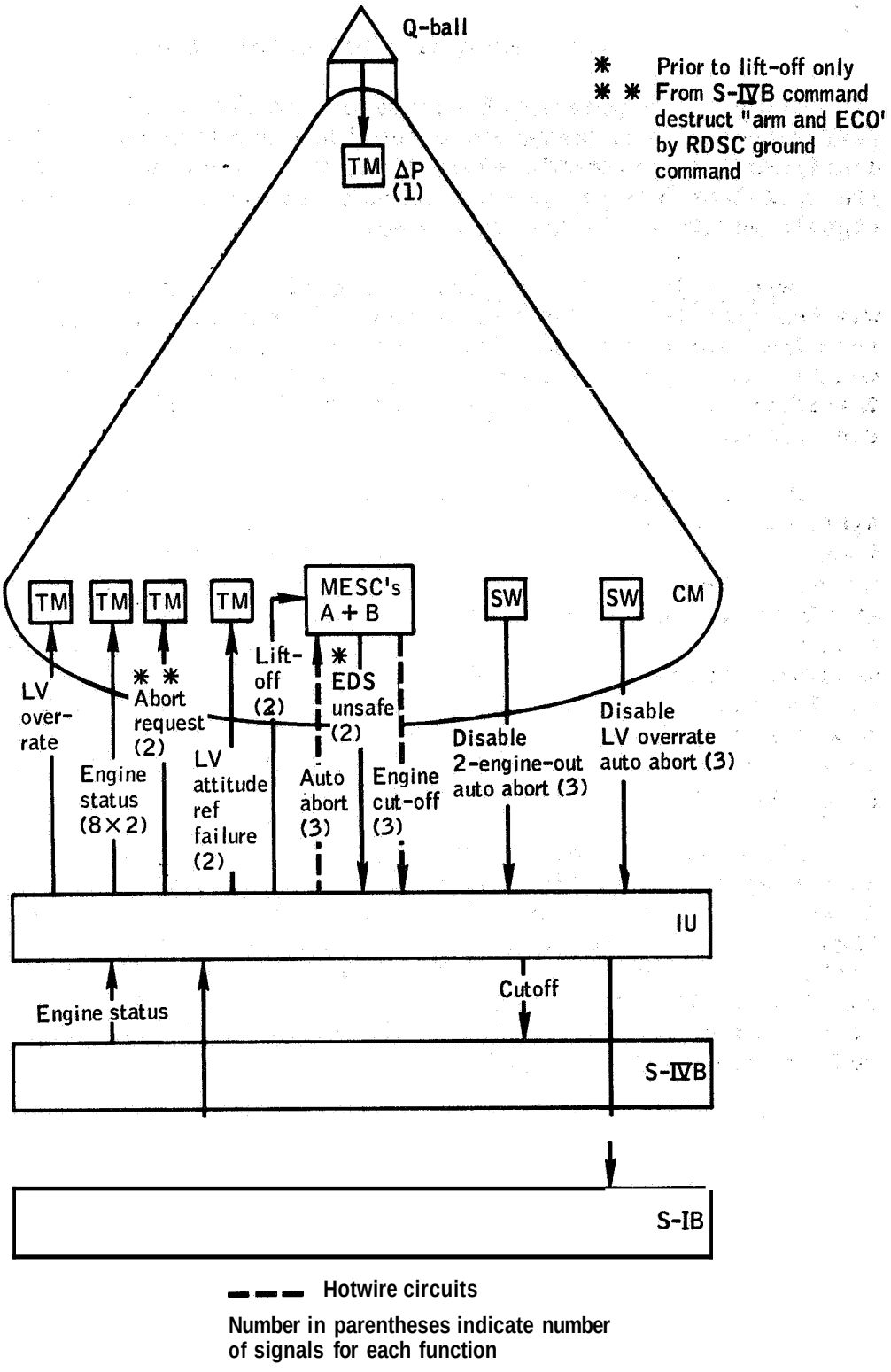


Figure 7.14-1.- EDS launch vehicle and Q-ball interface, Mission AS-201.

NASA-S-66-6337 MAY 6

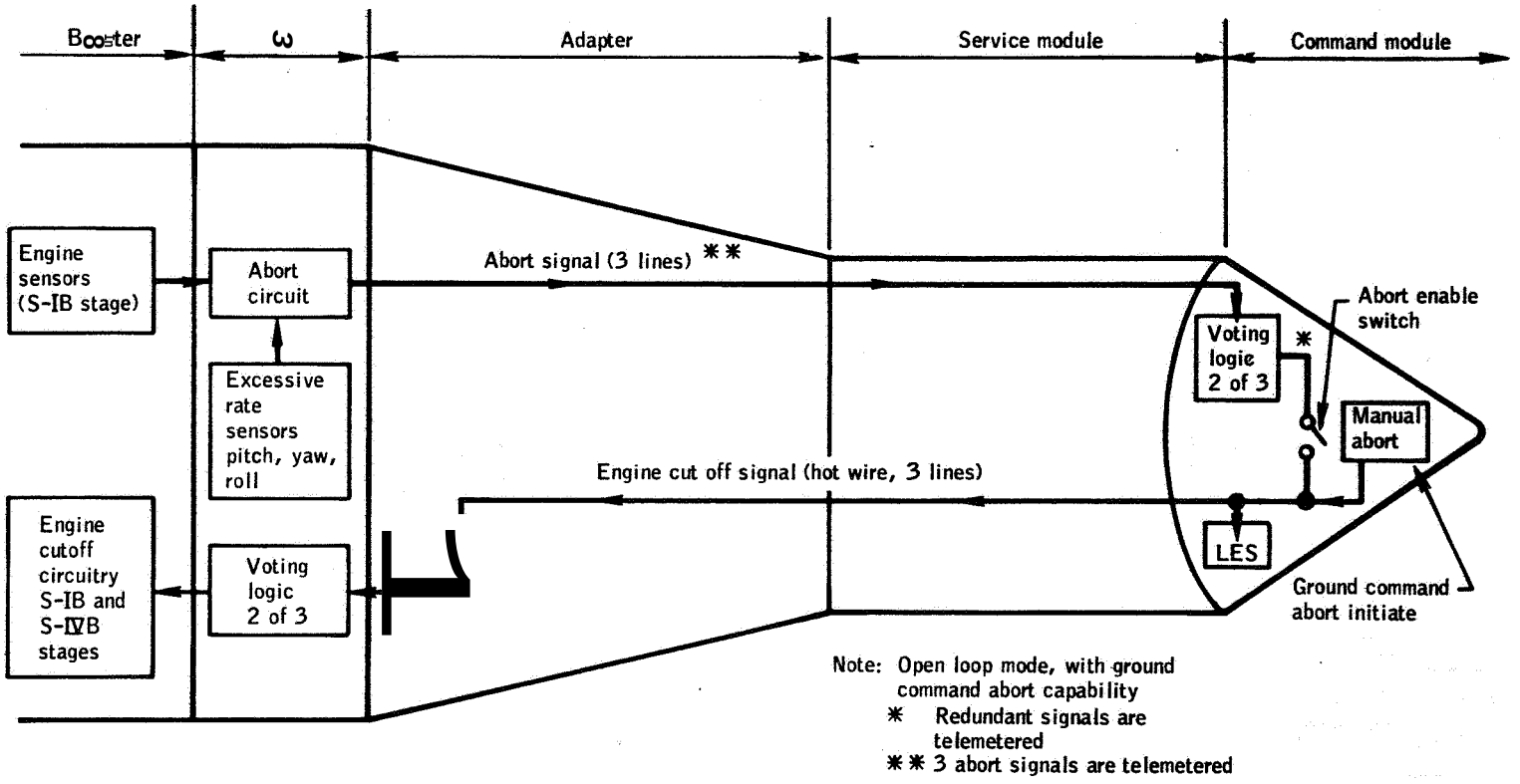


Figure 7.14-2.- Emergency detection subsystem automatic abort circuit, showing open-loop configuration, Mission AS-201.

NASA-S-66-6338 MAY 6

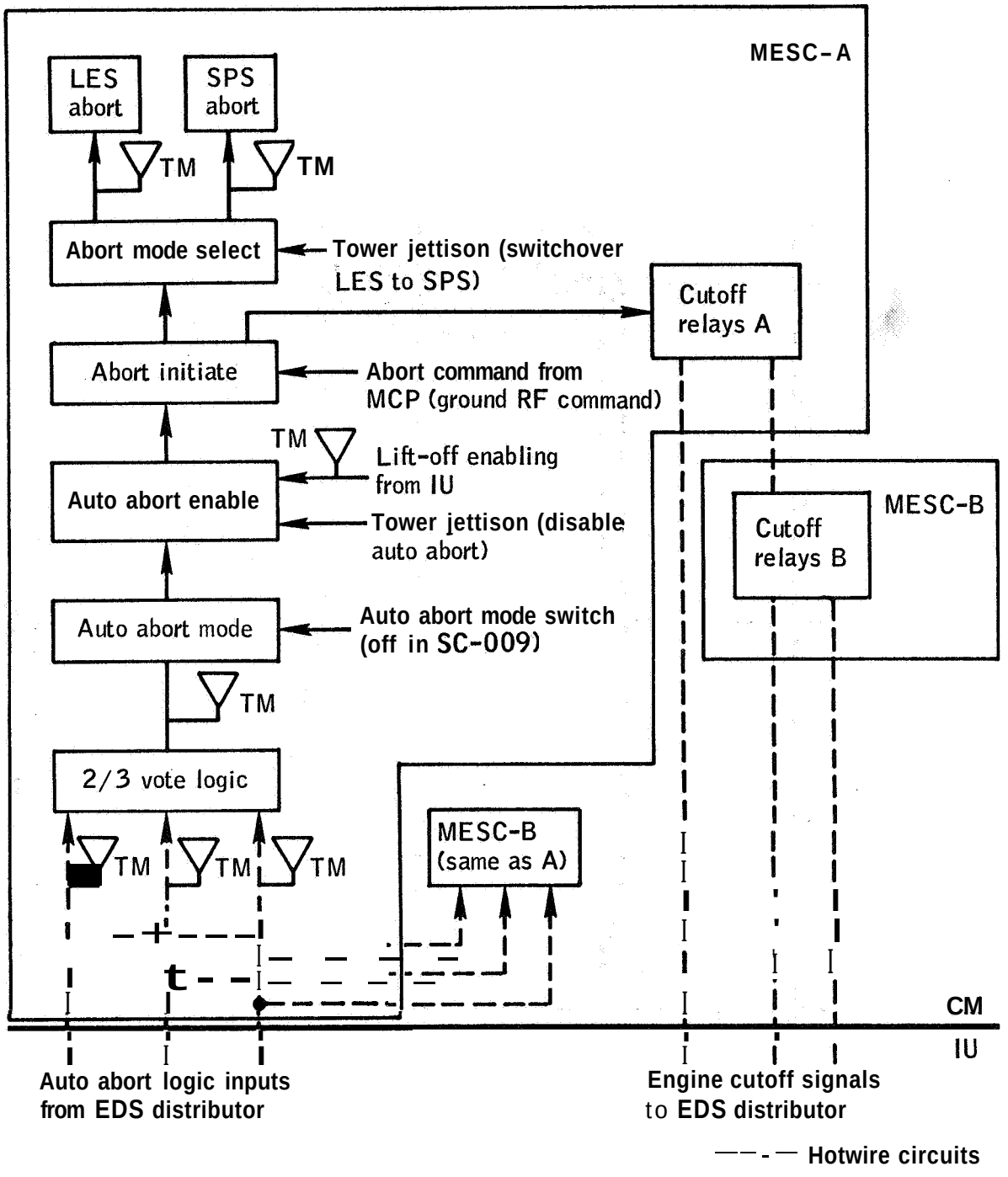


Figure 7.14-3.- Spacecraft automatic abort and LV engine cutoff, Mission AS-201.

NASA-S-66-6339 MAY 6

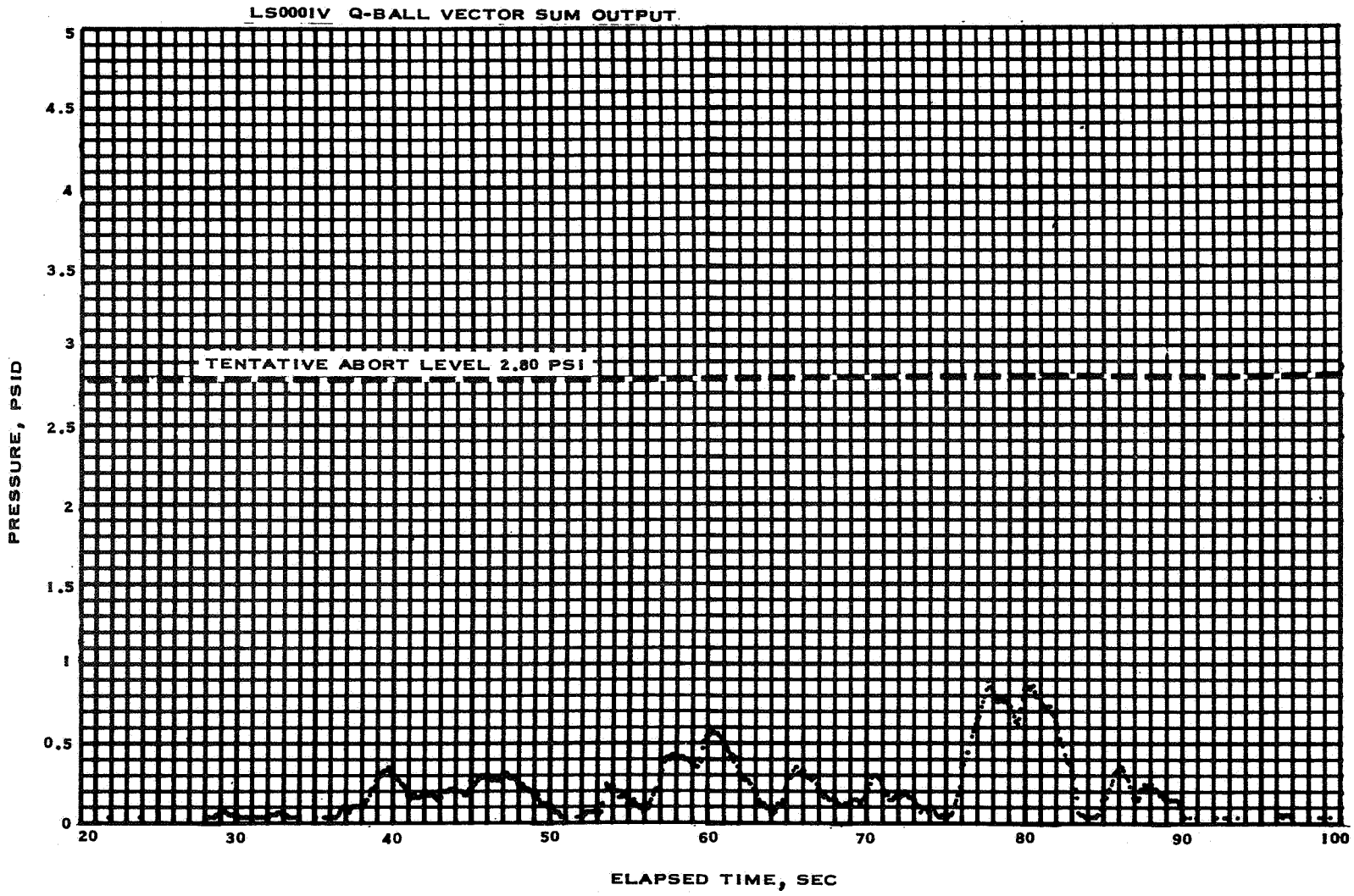


Figure 7.14-4.- Q-ball vector sum output, Mission AS-201.

7.15 Instrumentation

7.15.1 Operational and flight qualification instrumentation.- The instrumentation subsystem included four separate categories: the measuring systems, the timing equipment, the magnetic tape recorders, and the special telemetry equipment. The interfaces between the instrumentation and other spacecraft subsystems are shown in figures **7.15-1** and **7.15-2.** A measurement summary is presented in table **7.15-I.**

Operational instrumentation: The operational instrumentation consisted of transducers and matching components which were used to measure temperatures, pressures, currents, voltages, frequencies, quantities, flow rates, and events necessary to the management of spacecraft 009.

Some operational transducers are an integral part of hardware in other subsystems. The measurements described in the following paragraphs are a part of the spacecraft and therefore are in the instrumentation subsystem.

The temperature measurements system made use of solid-state sensing elements which changed resistivity with temperature. The sensing element was one leg of a bridge. The associated signal conditioner provided bridge power and amplified the signal.

The pressure measurements system was similar to the temperature system except that a solid-state stress sensitive element was mounted on a pressure-sensing diaphragm.

The CM/SM separation monitor, mounted on the CM, contained a roll of glass tape, one end of which was attached to the service module. The tape was coded for separation distances of 5, 10, and 15 feet with a conductive coating so that as the tape unrolled during separation, rate and distance data were generated.

night qualification instrumentation: The flight qualification instruments were used to measure the physical performance of the command module, service module, spacecraft – LEM adapter and included signal conditioners, power supplies, current limiters, power control modules, zone boxes, and a data distribution panel. The measurements were made and conditioned for telemetry and for recording on magnetic tape. Measurements were made of strain, vibration, acceleration, acoustics, char, ablation, pressure, heat flux, and temperature. The instruments are described briefly as follows:

Acceleration was measured by a system which employed a mass loaded, zero-length strain gage, power supply, and amplifier.

The acoustic levels were measured by a system which used a condenser microphone and a signal conditioner.

The strain measurements system was composed of a bridge and signal conditioner which supplied 5- or 10-volt puwer from a de-to-de converter.

Vibration was measured by a mass loaded piezo-electric sensor and a charge amplifier.

The ablation measurement system consisted of a Geiger counter mounted near the bondline, with radioactive pellets imbedded at seven depths in each of three plugs in the ablative heat shield. A signal conditioner was included to convert the Geiger counting rate to a dc voltage such that the voltage would drop approximately 0.7 V for each radioactive pellet lost to ablation.

The technique of char measurement was based on the high increase in conductivity of the ablator when it carbonizes or chars. The probe contained seven leads, each separated by 0.25-inch of ablator material from a common lead. As the char advanced to each lead, conductivity was sensed by a voltage increase across a resistor common to all seven stages.

Standard asymptotic calorimeters determined law-range heat flux by measuring the temperature difference between the center and periphery of a metal foil.. The high-range heat flux was measured by sensors which were composed of a stack of graphite slug type calorimeters. The temperature of each layer was measured by tungsten rhenium thermocouples. As the range of each calorimeter was exceeded, it was automatically switched out of the circuit, and the next one in the stack switched in so that the heat flux could be determined from the rate of temperature rise and radiation balance established. The calorimeters were stacked so as to be approximately flush with the ablator surface. Associated components included the zone boxes, the parer supplies, and the sequencer.

The ablation temperature measurement system was composed of sheathed thermocouples, zone boxes, power supply, amplifiers, and temperature gradient sensors. The temperature gradient sensor, used for the bondline temperature and the temperature gradient measurements in the heat shield, was a plug of ablator material with embedded hafniumoxide-coated thermocouples.

The data group equipment provided the interface between instrumentation and communication equipment and included data storage, spacecraft timing, and data signal conditioning functions.

Data generated on the spacecraft were either recorded on magnetic tape or transmitted to ground stations, or both. There were two onboard tape recorders: the data storage equipment (DSE) and the flight qualification recorder (FQR).

The data storage equipment, a hybrid recorder, carried 2250 feet of 1-inch tape to record digital and analog data on 14 channels at 15 in/sec for a total recording time of 30 minutes. The five digital tracks were used to record the PCM telemetry signal. Four of the nine analog tracks were used to record the output of four 90 x 10 commutators. Two tracks were used to record acoustic data. One track carried a composite timing signal which originated in the FQR and was a mixture of a 25-kc reference signal and mission elapsed time in the MSC decimal format. The remaining two tracks on the DSE were unused,

The flight qualification recorder carried 2325 feet of 1-inch tape to record 14 channels of analog data at 15 in/sec for a possible total of 31 minutes. Six tracks were used for vibration data and two for acceleration measurements. Two tracks were used to record the composite timing signal. This composite signal was a mixture of a 50-kc reference signal and the same time signal recorded on DSE. Three tracks were used to record three of the four commutator outputs recorded on DSE, and one track was unused.

Central timing equipment - The primary clock on future Apollo spacecraft will be within the guidance and navigation (G&N) equipment. On spacecraft 009 the primary time source was the central timing equipment (CTE) because the G&N equipment was omitted for this mission. The CTE supplied a 512-kc signal to the PCM telemetry package, 6.4 kc to the power inverters, 4 kc to the SCS AV control circuitry, and 1 pulse/sec to the controls and displays subsystem. The CTE consisted of a temperature compensated crystal oscillator of high frequency stability and a series of flip-flop dividers. It derived puwer fromthe 28 V dc buses which it converted and regulated for internal use. The CTE also provided a 32-bit digital word to PCM which measured mission elapsed time in binary coded decimal format.

Signal conditioning equipment - The signal conditioning equipment (SCE) consisted of a nmber of plug-in modules containing electronic circuitry which accepted signals from sensors and converted signals into a standardized 0 to 5 V dc signal suitable for telemetry or display. The modules included dc amplifiers, active attenuators, frequency to dc converters, phase sensitive demodulators, ac-to-dc converters, and a power supply.

The SCE derived power from the 400-cps inverters and, in addition to its own +20 V dc and -20 V dc requirements, supplied reference voltages of +5 V dc and +10 V dc to instrumentation in this and other subsystems.

Performance.- The performance of the majority of the operational and flight qualification instrumentation during the mission was satisfactory. One operational measurement was waived because the measuring

system was inoperative. Two were lost in flight. The remaining 240 operational measurements yielded high quality data. Fifteen flight qualification measurements were inoperative before launch and had been waived. An additional 13 did not operate during the mission. Four more thermocouples in the heat shield failed during reentry. Five measurements indicated errors but not failures. The remaining 258 flight qualification measurements operated properly.

The acoustic measurement systems recorded properly for a limited duration. There was evidence that the damage to the microphones could have occurred before or during the flight.

A large number of structure measurements were ranged so that the maximum excursions were below 10 percent of full scale throughout the mission. Failures occurred in the heat-shield instrumentation measuring system with thermocouples ranged from 4000° F and above failing at temperatures of 2700° F or below. The failures were caused by inadequate insulation which allowed shorting of the thermocouples in the charring ablator. The high range calorimeters failed because the sequencer was triggered by voltage fluctuations during the main bus anomaly.

The data group equipment functioned throughout the mission without exception.

Measurements CT0012X and CT0013X monitor tape motion of DSE and FQR, respectively. Examination of these events indicated that both units were running at T-9.606 seconds. As planned, the DSE stopped motion at T+665.4 seconds and FQR at T+665.2 seconds. Both recorders were turned on again at T+1321.9 seconds and operated until T+2251 seconds (after CM landing).

The data storage equipment (DSE) operated satisfactorily throughout the mission. Wow and flutter were between 2 and 3 percent as determined after recovery from the reference signal recorded on track 14. The data from the four commutators were recorded satisfactorily on tracks 6, 8, 10, and 12. However, data from the low-level commutators on tracks 6 and 8 were lost while main bus voltage was down to 18 volts. The recorder, which derived all but control power from the 400-cps lines, operated correctly through this period. The acoustic measurements on tracks 7 and 9 were recorded properlywithin the systems limitations. PCM data recorded on tracks 1 through 5 have been recovered and processed, No dropouts of *any* consequence were shown.

An examination of vibration, acceleration, and time measurements recorded on the flight qualification recorder (FQR) wide-band tracks indicated that the FQR operated normally throughout the mission. Several mission events including landing, LES jettison, and main parachute deployment were time verified by reference to the vibration and acceleration measurements.

The proper operation of PCM during the mission proved that the oscillator in the CTE operated properly. Accurate performance of the countdown circuitry was demonstrated by review of the 400-cps frequency measurements. It has been verified by study of a translated oscillograph record that the time accumulator of mission-elapsed-time was reset at launch and updated correctly thereafter.

No failures of the signal conditioning equipment (SCE) modules were indicated. The 1.20 V dc and -20 V dc levels were nominal throughout the flight, including the period of reduced voltage, since SCE derives power from the 400-cps lines. Also, the +10-volt and +5-volt reference levels were within 2.5 percent of nominal. The SCE package temperature was also nominal.

7.15.2 Government furnished instrumentation equipment. - Flight qualification instrumentation included three 90 × 10 commutators, a command module (CM) PAM/FM/FM telemetry package, a service module (SM) PAM/FM/FM telemetry package, a time code generator, and a five-point calibrator. All were of a type previously flight tested.

The CM PAM/FM/FM telemetry package interfaced with the communications subsystem (fig. 7.15-3) and processed 37 measurements from the structural subsystem, the communication and instrumentation subsystem, the service propulsion subsystem, and the reaction control subsystem. The package consisted of the following standard IRIG components: a 90 x 10 high-level commutator, a five-point calibrator, a nine-channel modulation package, and a 5-watt, 247.3-mc, FM transmitter. The components were mounted internal to a spacecraft electronic package (SEP) which was installed in the lower equipment bay of the CM. A redundant commutator differentiated pulse duration modulation (DPDM) output was also recorded on the data storage equipment (DSE).

The SM PAM/FM/FM telemetry package interfaced with the communications subsystem (7.15-4) and processed 93 measurements from the structural subsystem. The package consisted of the following standard IRIG components: a 90 x 10 law-level commutator, a five-point calibrator, a fifteen-channel modulation package, and a 5-watt, 257.3-mc, FM transmitter. The components were mounted on a plate attached to the bottom side of the shelf between beams 3 and 4 in the SM. This package was added to the original flight qualification subsystem as a modification kit for collecting SM and SLA structural integrity data.

The three CM 90 x 10 commutators, two low-level mechanical and one high-level electronic type, were utilized to process 191 heat-shield measurements from the structural subsystem. Each commutator data channel was sampled 10 times per second. The DPDM output of these commutators was recorded on both the data storage equipment (DSE) and flight qualification recorder (FQR). The commutators were mounted in the aft equipment bay.

The time code generator and five-point calibrator, installed internal to the FQR, were utilized to provide a timing reference on the FQR and DSE flight tapes and to provide preflight calibration to the FQR wideband FM record amplifier modules. The time code generator provided an output coded to one-tenth of a second and recycles each hour. (See ref. 18 for performance characteristics of both components.)

Performance.- All government furnished equipment (GFE) instrumentation components and packages performed satisfactorily except for the period of the electrical power subsystem (EPS) anomaly (see section 7.12 of this report).

The performance of the CM PAM/FM/FM telemetry package was nominal throughout the flight. Two continuous and 37 PAM commutated measurements were transmitted over the telemetry link. The two continuous channels monitored Y-axis tower acceleration, measurement LA0011A, and Z-axis tower acceleration, measurement LA0012A), from launch through launch escape subsystem (LES) tower jettison at 172.64 seconds. The PAM commutated data were telemetered, received, and decommutated satisfactorily. The DPDM output of this commutator was also recorded on the DSE, track 12. During the preflight calibration the telemetry package operated properly, and the package exhibited good characteristics with minimum crosstalk and intermodulation.

The reentry RF blackout period of T+1580 seconds to T+1695 seconds prevented reception of the CM PAM/FM/FM data, but since the commutator DPDM output from this package was redundantly recorded on the DSE, no data were lost.

The SM PAM/FM/FM telemetry package transmitted 10 continuous and 83 PAM commutated measurements. The SM telemetry package performed satisfactorily until transmission was terminated, at CM/SM separation (T+1455 seconds). The temperature of the SM telemetry package transmitter, measurement ST1490T, averaged 110° F from lift-off to CM/SM separation. The calibrator of the telemetry package operated properly to provide preflight calibration.

The performance of the three CM commutators processing heat-shield data were satisfactory. The low-level commutators were mechanical motor-driven switches and lost 10 revolutions per second motor speed regulation when input power dropped below 22 V dc. The drop in speed regulation resulted in a degraded DPDM output. The high-level commutators performed satisfactorily during the EPS anomaly period.

The time code generator and five-point calibrator in the FQR performed satisfactorily prior to and during the flight. The five-point calibrator provided preflight calibration of the FQR wideband subcarrier

oscillators. The time code generator read 36 minutes 11.2 seconds (± 0.05 sec) at lift-off. It was not planned for the time code generator to reset to zero time at lift-off. The FQR, due to internal packaging limitations, did not include a reset command capability.

TABLE 7.15-I.- FLIGHT MEASUREMENT SUMMARY

System	Operational measurements					Flight qualification measurements					PCM total	System total
	PCM			Display	Total flight measurements (a)	PCM		PAM	Tape recorder	Total		
	Analog	Event	Digital			Anloog	Even					
Structures	6	0	0	0	6	8	0	0	190	200	14	206
Electrical power	21	1	0	[b]21	35	3	5	0	0	9	31	44
Launch escape	7	32	0	0	39	0	0	0	0	0	39	39
Earth landing	1	8	0	0	9	0	0	0	0	0	9	9
Environmental	15	0	0	0	15	0	0	0	0	0	15	15
Guidance and navigation	0	0	0	0	0	0	0	0	0	0	0	0
Stabilization and control	23	26	0	5	54	19	5	0	0	25	74	79
Life	0	0	0	0	0	0	0	0	0	0	0	0
Flight technology	0	0	0	0	0	3	0	0	9	12	3	12
Propulsion	15	0	0	4	17	0	0	7	1	8	15	32
Reaction control	20	0	0	16	36	0	0	28	0	28	20	64
Crew safety	1	15	0	0	16	0	0	0	0	0	16	16
Communications and instrumentation	13	1	2	0	16	1	4	4	4	13	21	29
Total	122	83	2	56	243	21	25	41	204	295	257	545

[a]This total is the number of individual flight measurements.

[b]Includes nine flight qualification measurements. These measurements are to be taken on the backup batteries that replace fuel cells 1, 2, and 3.

NASA-S-66-6340 MAY 6

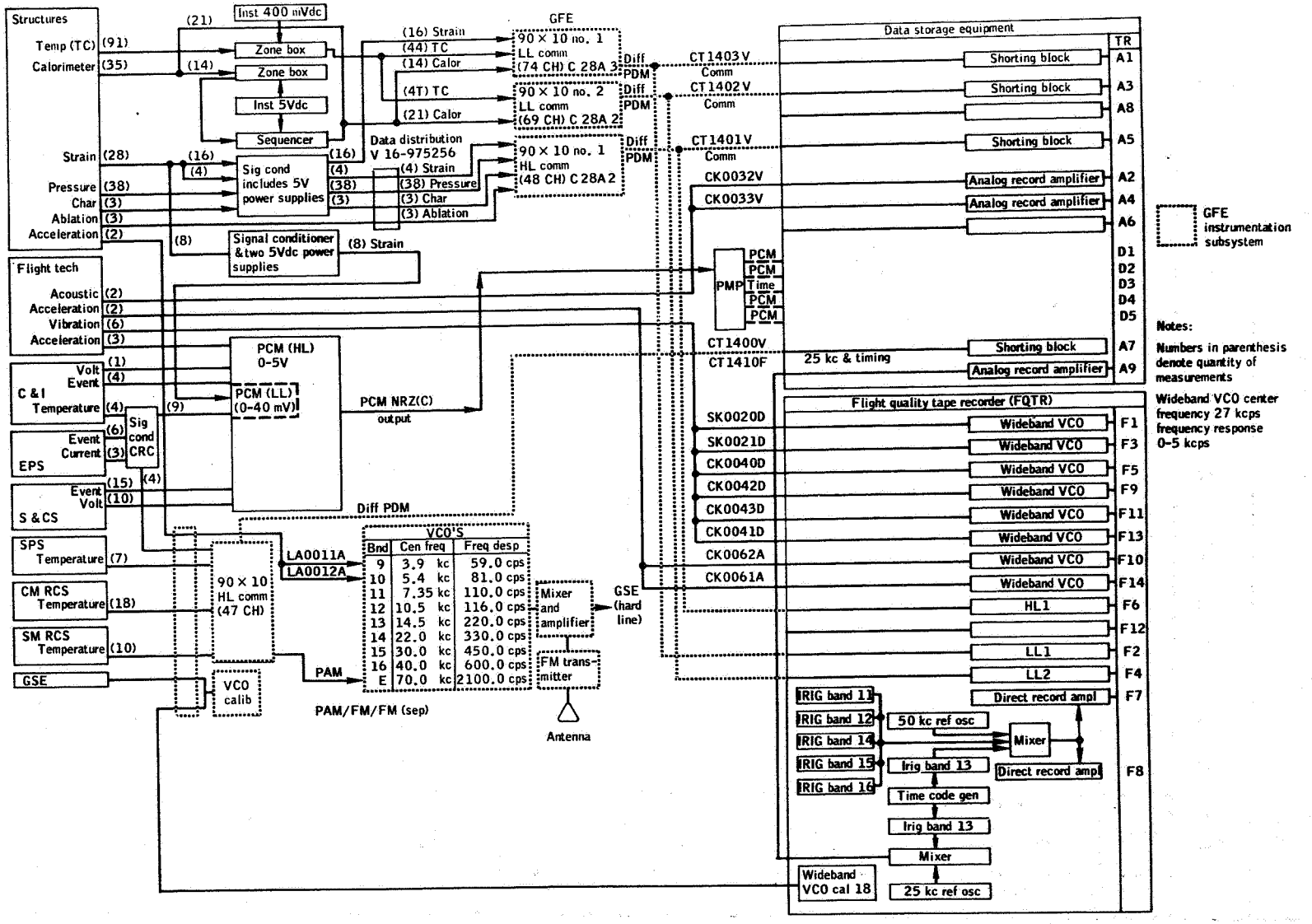


Figure 7.15-1.- R &D instrumentation subsystem for command module, Mission AS-201.

NASA-5-66-6341MAY 6

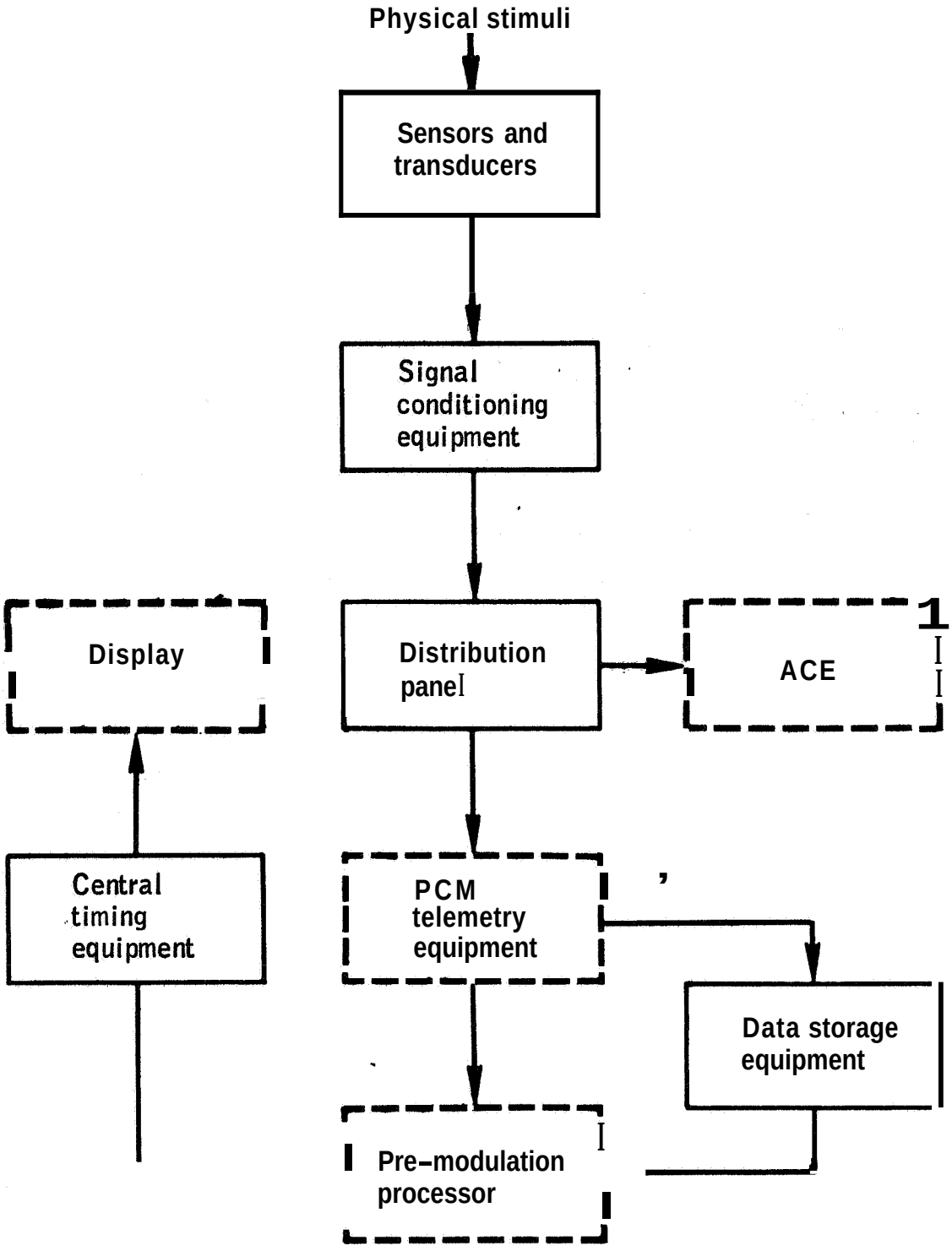


Figure 7.15-2.- Instrumentation system block diagram for Mission AS-201.

NASA-S-66-6342MAY 6

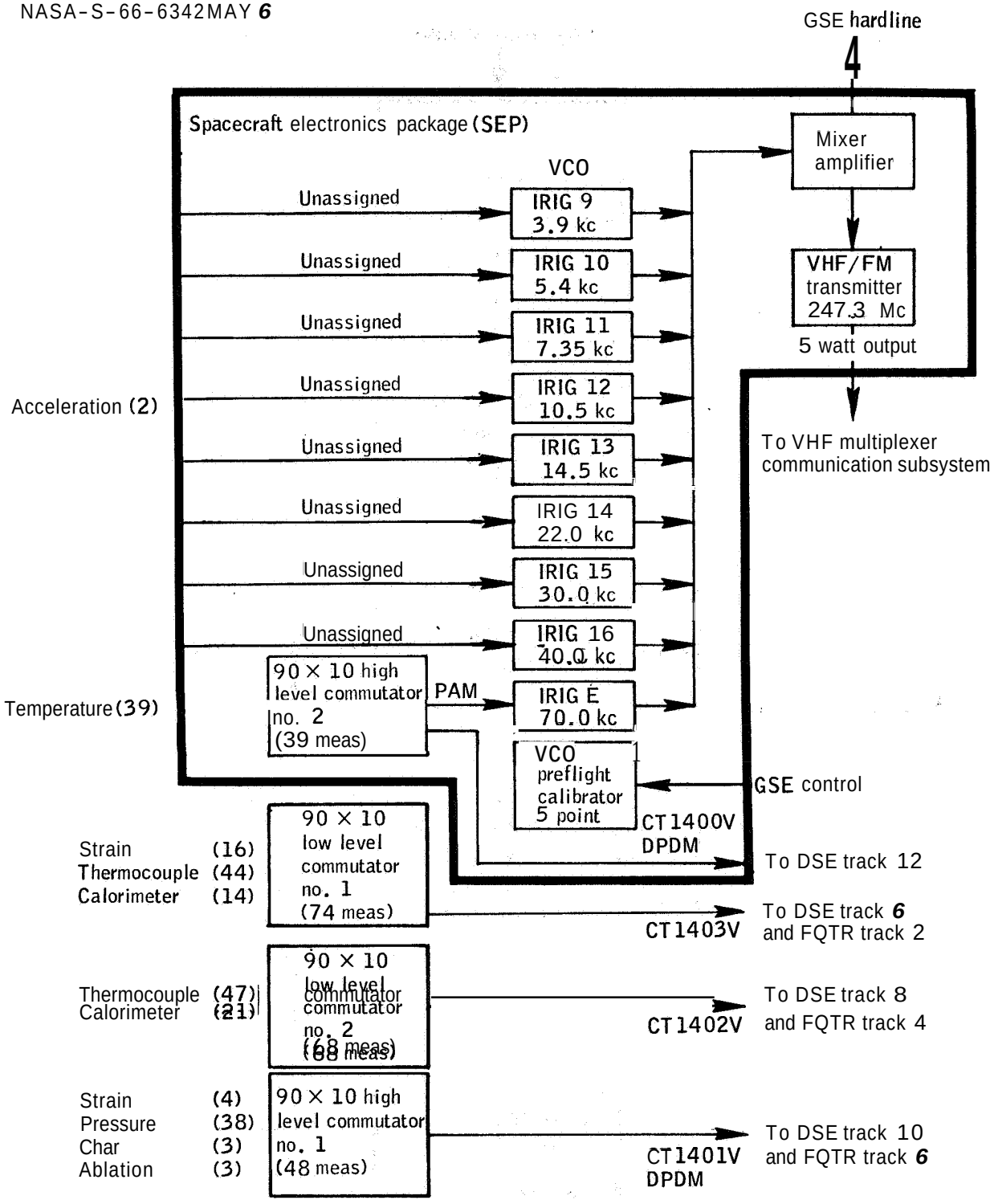


Figure 7.15-3.- GFE instrumentation CM PAM/FM/FM telemetry package and 90 x 10 commutators, Mission AS-201.

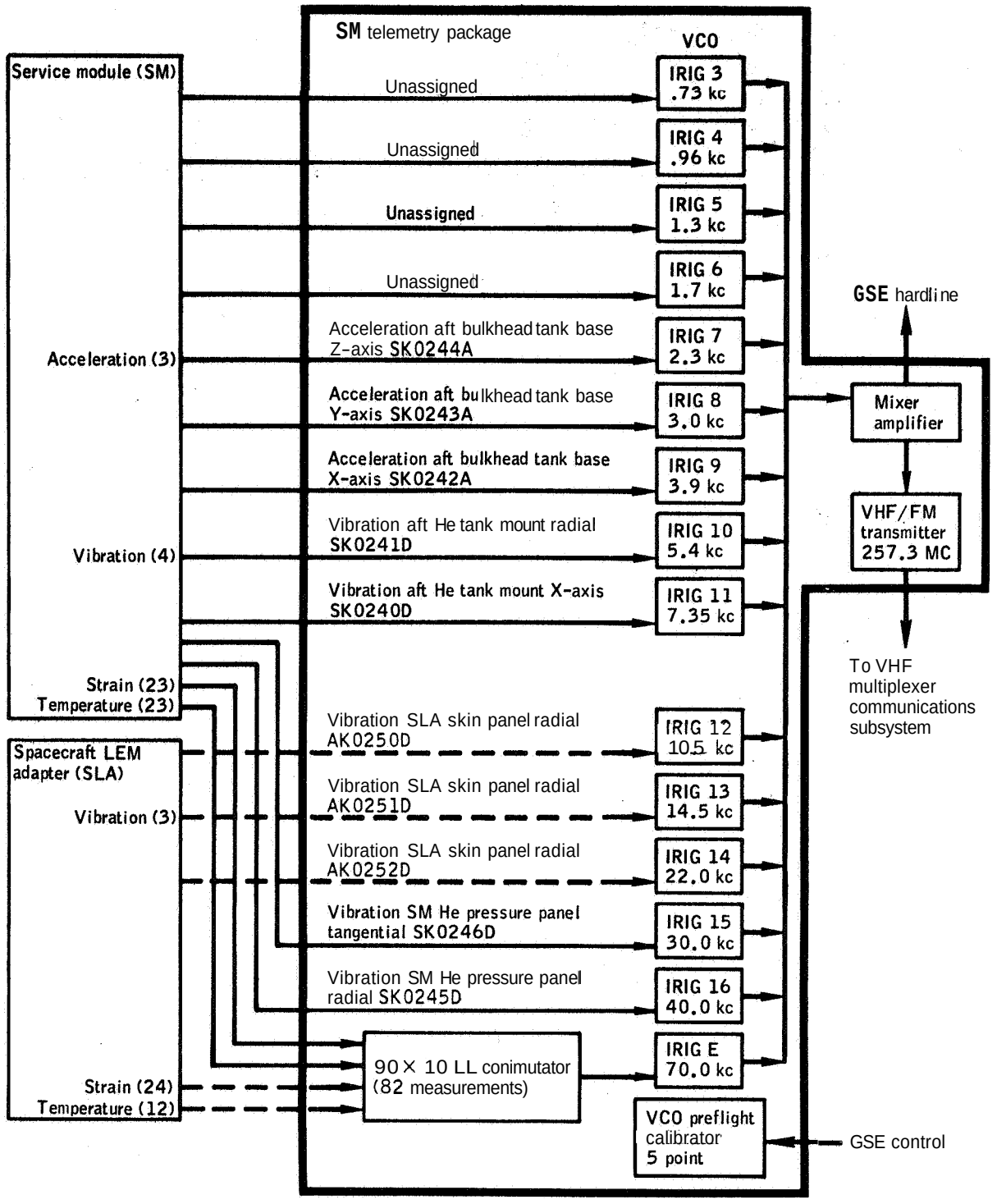


Figure 7.15-4.- GFE instrumentation SM PAM/FM/FM telemetry package, Mission AS-201.

7.16 Communications Subsystem

Summary.- The communications subsystem provided the operational communication links and the radio command equipment (RCE). The pulse code modulation (PCM) encoder and its VHF/FM transmitter encoded and transmitted spacecraft measurements throughout the mission. The VHF recovery and survival beacons provided the recovery aircraft with the initial contact with the spacecraft. The C-band transponder operated properly during the mission. The performance of the RCE was considered proper even though only one command was transmitted to the spacecraft,

The HF transceiver beacon mode signal was not received. The results of postflight tests indicated this could have been due to sea water causing a short circuit in the HF antenna. The reception of the VHF/AM transmitter-receiver signal was poor when compared to the reception of the VHF telemetry links.

The effect of the electrical power subsystem (EPS) anomaly was minor with the RF output levels of the VHF/FM transmitter and the VHF/AM transmitter being reduced only 7 watts and 2.4 watts, respectively.

Description.- The operational communications subsystem aboard spacecraft 009 was basically a Block I subsystem without the S-band equipment, television equipment, and up-data link equipment. The communications subsystem equipment (fig. 7.16-1) was installed on liquid-cooled coldplates in the lower equipment bay of the command module (CM), and antennas were installed on the external-surface of the CM.

C-band transponder: A C-band transponder was used in conjunction with ground radars to track the spacecraft. The transponder received double-pulse interrogations from the ground radar and responded with a single RF pulse. Pulses of proper spacing and width triggered the transponder, which received the interrogation code pulses on a frequency of 5690 ± 2.0 Mc and responded on a frequency of 5765 ± 4.0 Mc.

Telemetry: The PCM telemetry encoder converted spacecraft data into a serial, time division, non-return-to-zero change (NRZ-C) format for transmission to ground receiving stations. The PCM encoder was capable of generating two PCM digital-data rates, 51.2k bits/sec and 1.6k bits/sec. However, Mission AS-201 utilized only the 51.2k bits/sec rate. Four types of data inputs were multiplexed into the PCM wavetrain as follows:

a. Analog high level

[Data input range: 0 to 5 V full scale]	
No. of channels	samples/second
4	200
16	100
25	50
125	10
100	1

b. Analog Low level

[Data input range: 0 to 40 mV]	
No. of channels	samples/second
50	1

No. of channels	samples/second	bits/channel
1	200	[a]16
1	50	16
1	10	32
1	10	24
12	10	8
16	10	8

[a]Requires transfer pulses.

d. Serial digital

[Binary 0 : ± 0.5 V; binary 1 : 3.5 to 10.0 V]		
No. of channels	samples/second	bits/channel
1	50	[a]40

[a]Requires transfer pulses.

The PCM wavetrain was routed to the VHF/FM telemetry transmitter via the premodulation processor.

One PCM telemetry transmitter, which transmitted operational instrumentation subsystem data, was included in the communications subsystem. The VHF/FM transmitter sent PCM telemetry data through the active VHF antenna to ground receiving stations during all phases of the flight up to landing. Transmitter frequency was 237.8 Mc and power output was 10 watts.

The radio command equipment was included on spacecraft 009 to receive and decode ground command information on a frequency of 450 Mc and to send the discrete commands to the CM control programmer. It will be replaced by operational updata link equipment on manned flights.

Recovery beacons: Two VHF recovery beacons were included in spacecraft 009 to assist in locating the spacecraft during the postlanding phases of the mission. Operating on an output frequency of 243.0 Mc with a power output of 3 watts, the first beacon provided line-of-sight, direction-finding capability within a minimum range of 150 nautical miles. The transmitter operated through VHF recovery antenna 1. A redundant VHF survival beacon that operated through VHF recovery antenna 2 was also provided. Both VHF recovery antennas were located on the forward tunnel exterior and deployed by a pyrotechnic charge after main parachute deployment.

An HF transceiver was included on spacecraft 009 to provide direction-finding capability beyond line of sight during recovery operations. Operating on a frequency of 10.006 Mc with a power output of 5 watts, it was designed to transmit only an unmodulated carrier beacon signal during the postlanding phase of the mission through the HF recovery antenna. The antenna, an extendible monopole, was stowed on the parachute deck and released by a pyrotechnic charge after the CM landed.

Audio center: On spacecraft 009 the audio center was used for voice communications only during checkout; during the flight a 400-cps tone was applied to the audio center to modulate the VHF/AM transmitter.

VHF/AM transmitter-receiver: The VHF/AM transmitter-receiver operated during all phases of the flight up to landing. A 400-cps signal was transmitted for evaluation of signal characteristics. Output frequency was 296.8 Mc; power output was 5 watts.

VHF multiplexer: The VHF multiplexer allawed simultaneous transmission of the VHF/AM transmitter, VHF/FM transmitter, UHF radio command receiver, CM PAM/FM/FM flight qualification telemetry transmitter, and service module (SM) PAM/FM/FM flight qualification telemetry transmitter through the -Z axis VHF scimitar antenna.

Premodulation processor: In spacecraft 009 the only function of the premodulation processor was to provide a law-pass filter between the PCM telemetry set and the VHF/FM transmitter.

Scimitar antennas: Two scimitar-shaped antennas were located approximately 180° apart on the CM mold line approximately 3 feet from the base of the aft heat shield. The antenna near the -Z axis was complete Block I type configuration, including ablative covering for reentry heating, and was the only one which was electrically functional. Only the VHF/UHF portion of the -Z axis antenna was used on spacecraft 009. The scimitar antenna near the +Z axis was inoperative on spacecraft 009.

Performance.-

C-band transponder: During the launch phase five ground-based radars simultaneously interrogated the transponder from different locations. The transponder replied to each interrogation. Where a number of radar sites time-shared the transponder and there was the possibility of interference between interrogators, it was necessary to schedule the radar sites accordingly. In some cases interference did occur (see section 9.2). Later in flight, the interference was eliminated since few downrange radars are available to track the spacecraft.

The CM and instrument unit (IU) C-band transponders were scheduled to transmit at 5765 Mc so as to be interrogated simultaneously by ground radars. The CM transponder frequency was measured at 5763.6 Mc by the Eastern Test Range (ETR), and the Saturn IU transponder frequency at 5757 Mc by ETR. The frequency difference and the ground radar IF bandpass of 18 Mc prevented successful simultaneous interrogation.

Telemetry: The PCM encoder sampled and encoded a total of 257 operational and flight qualification measurements into the pulse code

format. The PCM output wavetrain was successfully transmitted to, and recorded at, each of the ETR telemetry receiving stations associated with the flight. The PCM encoder and the VHF/FM radio frequency link operated continuously throughout the flight, including the period of the EPS anomaly. In addition, the PCM output interfaced with the instrumentation subsystem and was recorded on the data storage equipment (DSE) as reported in section 7.15.1.

The RF output of the VHF/FM transmitter maintained a level of 10 watts from lift-off until the EPS anomaly at T+1650 seconds. At this time, the RF output dropped following the EPS voltage drop. The minimum RF output of 7 watts occurred between T+1710 seconds and T+1770 seconds, when the EPS voltage was at 18 V dc. Between T+1770 seconds and T+2121 seconds the RF output increased to 8 to 9 watts. At T+2121 seconds the RF output returned to the normal 10 watts output and maintained this level throughout the remainder of the flight.

The calibration references at 15 percent and 85 percent of full scale for each of the high-level, 0- to 5-volt channels and low-level, 0- to 40-millivolt channels provided excellent data on the performance of the PCM encoder.

The RF blackout period during reentry caused the loss of the PCM/FM data between T+1580 seconds and T+1692 seconds. At S-IB/S-IVB staging the signal strength dropped to 3 microvolts, but data reception was continuous through this period.

A data processing problem occurred with the PCM tape record from the DSE tape recorder. This was because the PCM data processing equipment required bit transitions to maintain the ground station bit-rate clock synchronization with the airborne PCM encoder bit rate. The major cause was the DSE wow and flutter in conjunction with the open computer word. On spacecraft 009, the 40-bit digital guidance computer word was not programmed since no guidance and navigation subsystem was flown on this mission. Therefore, the 40-bit computer word period contained all binary zeros, a case of no-bit transitions. This could occur on future missions when the Apollo guidance computer is in the standby condition or when the computer word is nearly all ones or zeros. Consideration is being given to methods of eliminating this data retrieval ground station problem on future missions.

Recovery beacons: The two VHF recovery antennas were extended at approximately T+1916 seconds and the two VHF recovery beacons were turned on at approximately T+1926 seconds. Recovery personnel reported that both VHF recovery beacons were operating after spacecraft landing. The initial contact with the spacecraft was made with the VHF beacon signals and the recovery aircraft were guided to the landing site using these signals. The initial VHF beacon acquisition was made at a

distance of 400 nautical miles from the spacecraf't. No permanent records were made of the beacon modulation.

No transmission was received by the recovery forces from the HF transceiver. Upon recovery, the HF antenna was found extended and apparently undamaged. During recovery operations, the HF antenna was bent as the spacecraft was being lifted from the water. Prelaunch checkout at KSC indicated proper beacon mode operation of the transceiver. Postlaunch testing at Dmey, California also indicated proper operation of the transceiver, including the power and control circuitry. The damaged portion of the HE' antenna was replaced with a spliced-in member to simulate the original flight configuration for transmission checks under salt water spray and salt water immersion conditions. Transmission was satisfactory when the unit was *dry,* both before and after the tests. On the other hand, the salt water spray and salt water immersion each resulted in severe RF losses and an antenna mismatch which reduced the output level from 5 watts down to 0.5 milliwatt. This was apparently the reason for the lack of reception of the HF transceiver beacon.

Design changes on the HF antenna, which are planned for spacecraft 011, include waterproofing the antenna and providing increased drainage area for the antenna base.

In addition to the waterproofing requirement two fundamental HF transceiver signal acquisition problems were:

(a) Possible difficulty in identifying the HF transceiver operating in the unmodulated beacon mode.

(b) Possible difficulty of broadband type receivers on recovery aircraft to discriminate adjacent radio frequency signals, such as WWV at 10 000 Mc and the HF transceiver at 10.006 Mc.

VHF/AM transmitter - receiver: The received signal level at each ground station was lower than the telemetry signal strength resulting in later signal acquisition, more frequent dropouts of the carrier, and earlier signal loss. This was attributed to the lack of high quality range-receiving equipment at this frequency, as compared to the telemetry equipment. The 400-cps modulation was recovered at each of the range stations. The 400-cps modulation overdrove the VHF/AM modulator, saturating the input by at least 10 dB. This caused severe clipping of the 400 cps, resulting in a 400-cps, square-wave modulation of transmitter. An extraneous 10-cps signal also modulated the recovered 400 cps to modulation depths of 100 percent. The source of the 10 cps is not known.

The RF output of the VHF/AM transmitter maintained a level of 10 watts from lift-off until the EPS anomaly at T+1650 seconds. Following the EPS voltage drop, the RF output dropped to a minimum RF output of 2.4 watts between T+1710 seconds and T+1770 seconds when the EPS main bus voltage was at 18 V dc. Between T+1770 seconds and T+2120 seconds the RF output increased to 4.5 watts. At T+2121 seconds the RF output returned to the normal 10-watts output and maintained this level throughout the remainder of the flight,

VHF multiplexer: All spacecraft VHF carriers were received at the ground receiving sites, indicating proper operation. The radio command equipment operation consisted of a single command from the Rose Knot Victor (RKV) as planned at T+1515.1 seconds to provide the only test of the 450-Mc reception.

Scimitar antennas: The -Z scimitar antenna was successfully utilized for the transmission of all the VHF/RF carriers and provided for the reception of the UHF radio command equipment ground commands. The -Z scimitar showed minimum damage to the ablator material in surviving the reentry conditions. Figure 7.4-9 indicates the condition of the scimitar antenna after landing.

NASA-S-66-6344 MAY 6

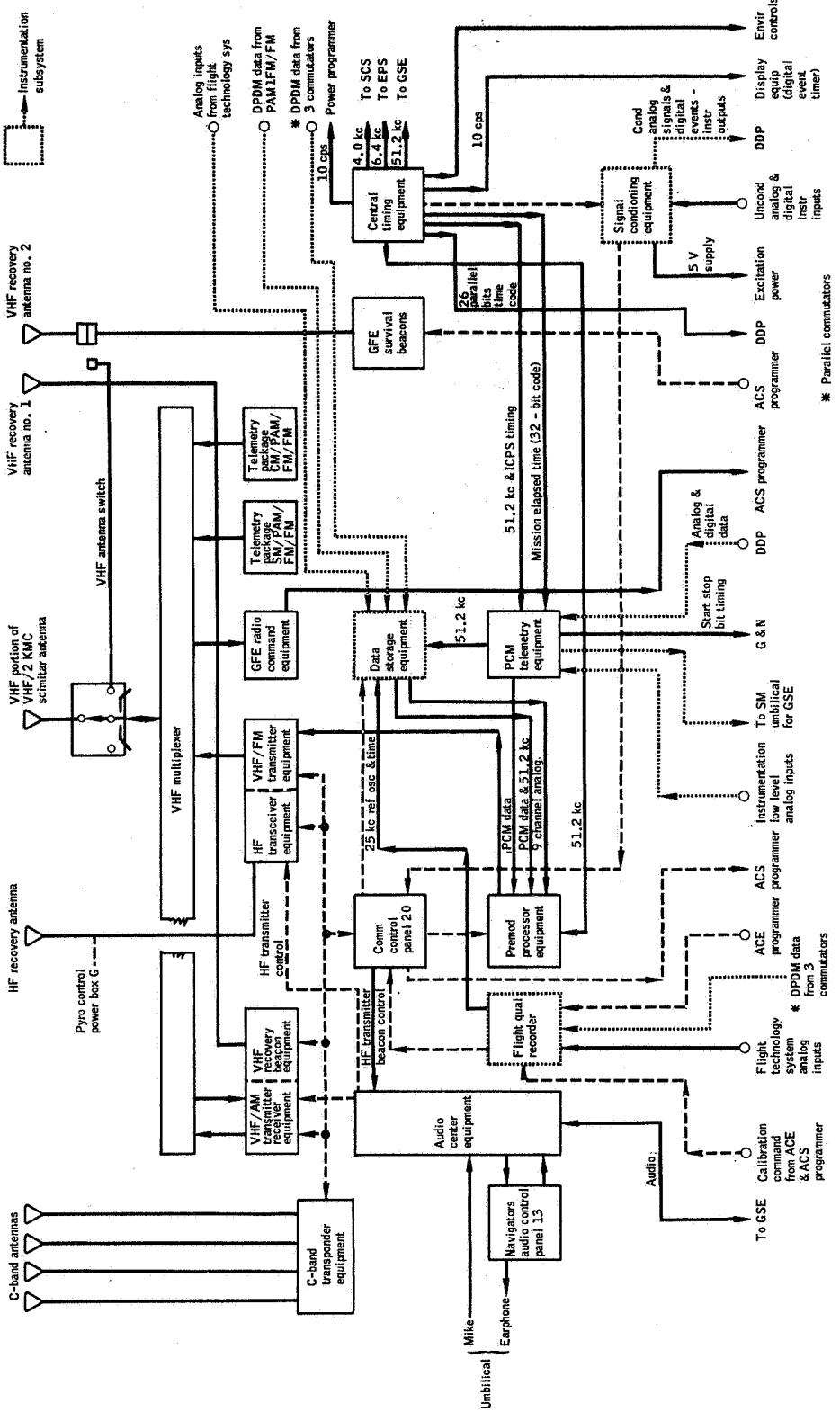


Figure 7.16-1.- Communication subsystem, Mission AS-201.

7.17 Environmental Control Subsystem

Description.- The components of the environmental control subsystem (ECS) installed in spacecraft 009 were a Block I type configuration. The waste management system (WMS), postlanding ventilation system, radiator valves and associated plumbing, and pressure suit circuit distribution ducting usually included in the complete ECS (ref. 12) were omitted for Mission AS-201. The ECS radiators were installed in spacecraft 009 but were inoperative because of the omission of the associated valves and plumbing. The suit circuit compressors were installed but not activated during the mission. The most significant difference between the components on spacecraft 009 and the comparable ones on spacecraft 012 was the coolant circuit evaporator and associated control system. Design changes to the evaporator and control system were implemented late in the program to correct attitude sensitivity problems discovered during development testing. These changes are incorporated in spacecraft 012 and subsequent systems.

The purpose of the ECS on Mission AS-201 was to provide cooling to the cabin and electronic equipment and to control the cabin pressure rather than flight qualify the complete Block I configuration.

The water-glycol (37.5 percent water, 62.5 percent ethylene glycol) circuit included the coolant circuit evaporator, suit circuit heat exchanger, cabin heat exchanger, glycol pump assembly, glycol reservoir, and the coldplate network (see fig. 7.17-1). The total heat load absorbed by the water-glycol coolant was rejected by water evaporation in the coolant circuit evaporator. Water was supplied to the coolant circuit evaporator from the waste water tank.

Cabin pressure was controlled by the cabin pressure relief valve (fig. 7.17-2) and cabin pressure regulator. The cabin pressure relief valve provided positive pressure relief during spacecraft ascent and negative pressure relief during spacecraft descent. The cabin pressure relief valve operates on a differential pressure principle, ceasing to relieve cabin pressure at a nominal value of 6.0 psid, which is equivalent to a cabin pressure of 6.0 psia when the ambient pressure is essentially zero. The cabin pressure regulator was required to maintain cabin pressure at 5.0 psia ± 0.2 psia after cabin pressure had decayed to a nominal value of 5.0 psia. In addition, the demand pressure regulator provided suit circuit pressure relief during spacecraft ascent and repressurization during spacecraft descent.

The oxygen surge tank supplied oxygen to the high pressure oxygen regulator assembly and hence to the cabin pressure regulator, demand pressure regulator, and to the positive expulsion bladders in the potable water tank, waste water tank, and glycol reservoir. The oxygen

surge tank served as the only source of ECS oxygen because the cryogenic oxygen storage system was not installed in spacecraft 009.

Performance.- The ECS performed the functions required for Mission AS-201 with the following deviations:

(a) The water-glycol temperature measured at the evaporator outlet dropped to a minimum of 26.4° F by T+580 seconds as compared to the 45" ± 3" F specification control range (fig. 7.17-3).

(b) Cabin pressure was regulated at approximately 5.65 psia as compared with the 5 psia ± 0.2 psia specification range (fig. 7.17-4).

Evaporator outlet temperature: The water-glycol evaporator outlet temperature, after a temporary rise from 52.5° F at lift-off to 57" F at T+105 seconds, decreased to a minimum of 26.4° F at T+580 seconds. At T+920 seconds the outlet temperature returned to 47.4° F at maximum excursion, which was within specification units, before starting to decrease again. This decline in temperature indicated that the temperature control circuit was operative. The temperature then dropped to 40" F and remained approximately at that temperature until reentry.

As programmed, the wetness control and the glycol inlet temperature control were not activated by the control programmer until T+172 seconds. During the prelaunch spacecraft closeout procedures, the manual override knob had been turned to the "full cool" position, as scheduled, and left in that position. As a result the back gressure control was enabled to open (or close) the back pressure control valve in response to signals from the pressure and temperature sensors (fig. 7.17-5).

Activation of the back-pressure control by the glycol temperature control valve was thus independent of mission control programmer operation. The back pressure of the steam in the coolant circuit evaporator was controlled to a pressure necessary to maintain the outlet water-glycol temperature at 45" ± 3" F, which is normally about 0.10 psia or less. With a pressure of 14.7 psia at the launch pad, and an evaporator outlet liquid temperature of 52.7° F at the time of lift-off, both the back-pressure and the glycol temperature sensors would have signalled the enabled back-pressure control to open the back-pressure control valves. Since the back-pressure control was fully enabled, the back-pressure control valve was open prior to lift-off as the back-pressure sensor, sensing 14.7 psia at sea level, signalled the back-pressure control to open the back-pressure control valve. In addition, the glycol temperature sensor sensed an evaporator outlet liquid temperature of 52.7" F at lift-off, which also signalled the back-pressure control to open the back-pressure control valve.

The evaporator was serviced with 0.8-pound water during the countdown, to allow evaporation to occur upon reaching the proper altitude. Water evaporation and the resulting temperature decrease in the coolant circuit evaporator outlet liquid began at approximately T+100 seconds. The minim outlet liquid temperature of 26.4° F, reached at T+580 seconds, indicated that some of the water in the coolant circuit evaporator metal wicks froze. This resulted in law coolant temperatures at the evaporator outlet. The law temperatures and freezing were the result of the back-pressure control valve being in the open position during the early minutes of the flight. The back-pressure control valve appears to have closed prior to the temperature increase in coolant circuit evaporator outlet liquid, thus allowing conditions to warm in the evaporator steam passages and metal. wicks. The decrease in the coolant temperature after it reached 47.4° F is attributed to reopening of the back-pressure control valve and additional water evaporation.

The inherent freezing in the coolant circuit evaporator and associated control system difficulties was well known prior to this mission, and the Block II type configuration was scheduled for use on Mission AS-204 (spacecraft 012).

Postflight test results indicated that the cabin pressure regulator responded at a pressure of 5.4 psia, which is slightly higher than the specification value of 5.0 psia ± 0.2 psia. Allowing for the accuracy of the telemetry and instrumentation, and assuming that the landing impact had no effect on the cabin pressure regulator, the higher regulator operating pressure of 5.4 psia could account for the higher cabin pressure of 5.65 psia attained during the mission after T+405 seconds.

Cabin pressure relief valve: At T+53 seconds, the cabin pressure relief valve relieved cabin pressure at a maximum differential pressure between the cabin and aft compartment of 6.13 psi (see fig. 7.17-4). (Specification requirements for positive pressure relief are 6.0 psid (+0.2 psi, -0.4 psi).) Cabin pressure relief continued through the cabin pressure relief valve until a pressure of 5.65 psia was reached at T+405 seconds. Cabin pressure was .controlledat 5.65 psia for the remainder of the flight.

During descent, the cabin pressure relief valve opened at a differential pressure of 0.39 psi between cabin and ambient, permitting repressurization of the cabin at T+1863 seconds. (Specification requirements for negative pressure relief are 0.36 to 0.90 psid.) The cabin pressure relief valve operated within the specification control range for both ascent and reentry.

Following touchdown, approximately 1 1/2 quarts of sea water leaked into the cabin via the steam duct outlet port and through the cabin pressure relief valve.

Cabin temperature: No attempt was made to control cabin temperature within the specification temperature range of 75° ± 5" F. Cabin temperature was 60° F at lift-off, decreased to 52° F during spacecraft ascent, and rose to 59.5" F at T+625 seconds (see fig. 7.17-4). Cabin temperature was maintained between 59.5° F and 60.1° F until reentry. The maximum cabin temperature of 67° F experienced during the mission occurred during cabin repressurization.

The temperatures on the inoperative ECS radiator during the launch phase were reviewed for possible indicating of degradation of the radiator thermal coating as a result of heating from the S-IB/S-IVB separation retrorockets. A temperature rise of approximately 10" F was noted, indicating service module heating from the retrorocket plume. The cooling trend following this heating was not markedly different from the cooling trend during the period just before S-IB retrofire. However, the data were insufficient to establish any indication of the status of the thermal coating.

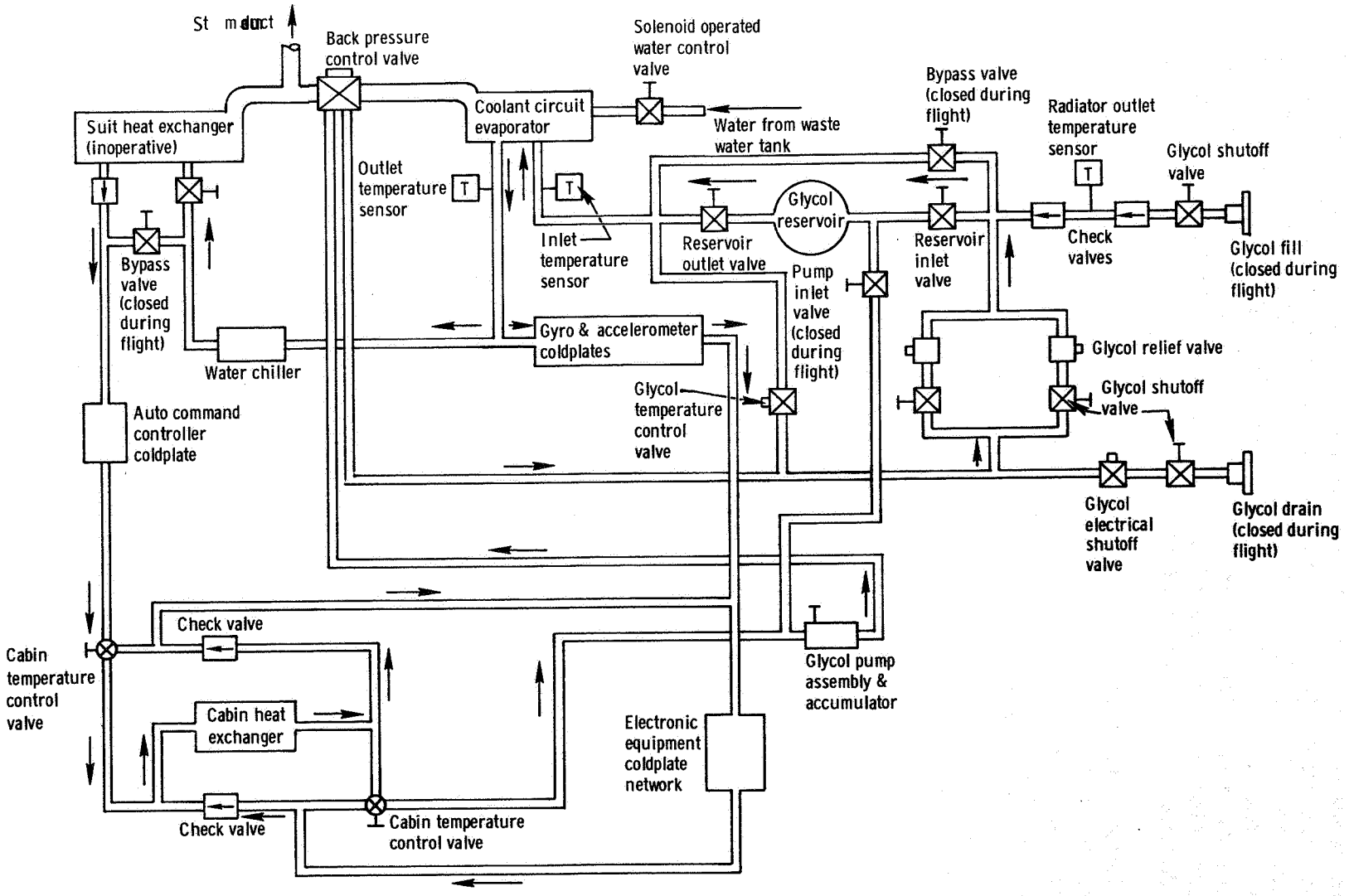


Figure 7.17-1. - Flow diagram of GOS water/glycol coolant circuit, Apollo AS-201.

NASA-S-66-6346 MAY 6

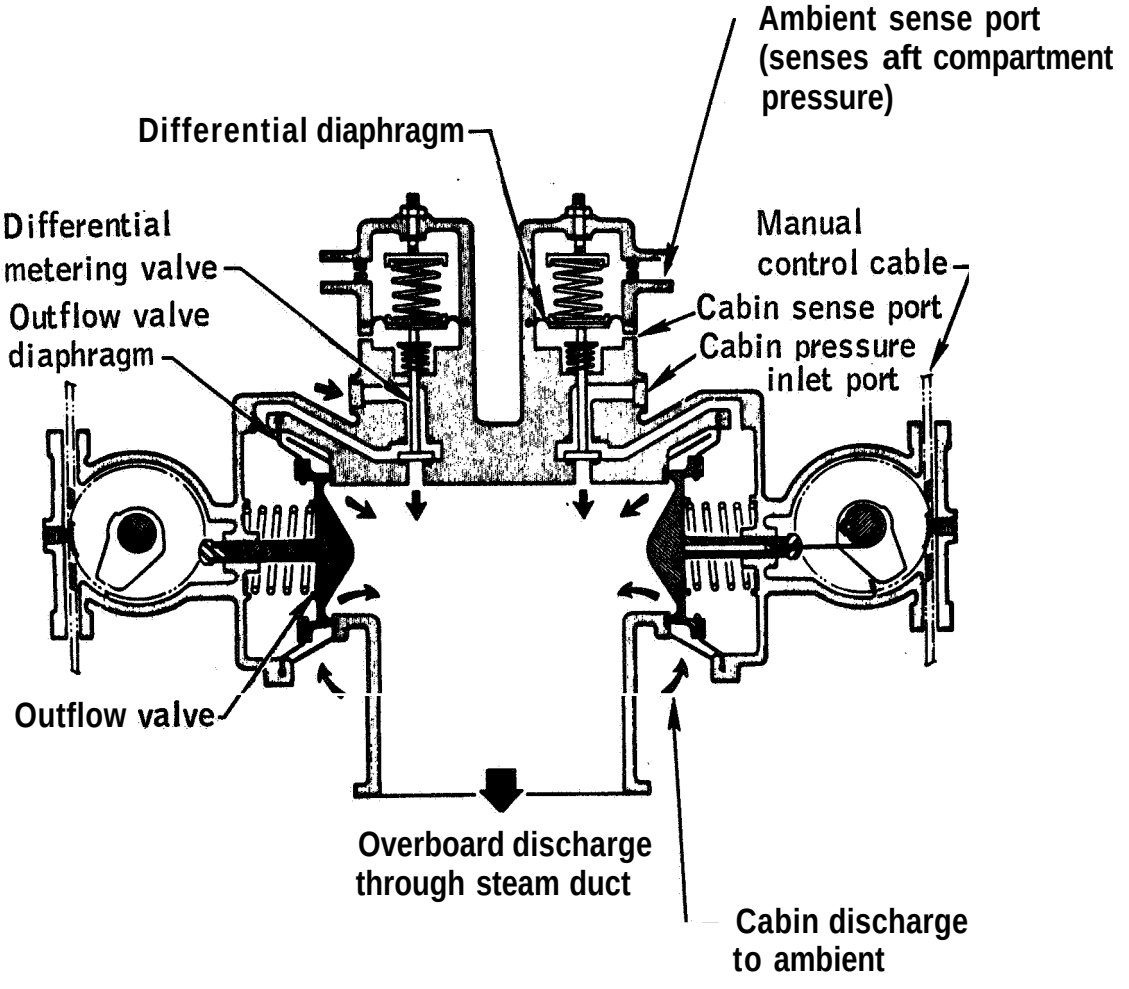
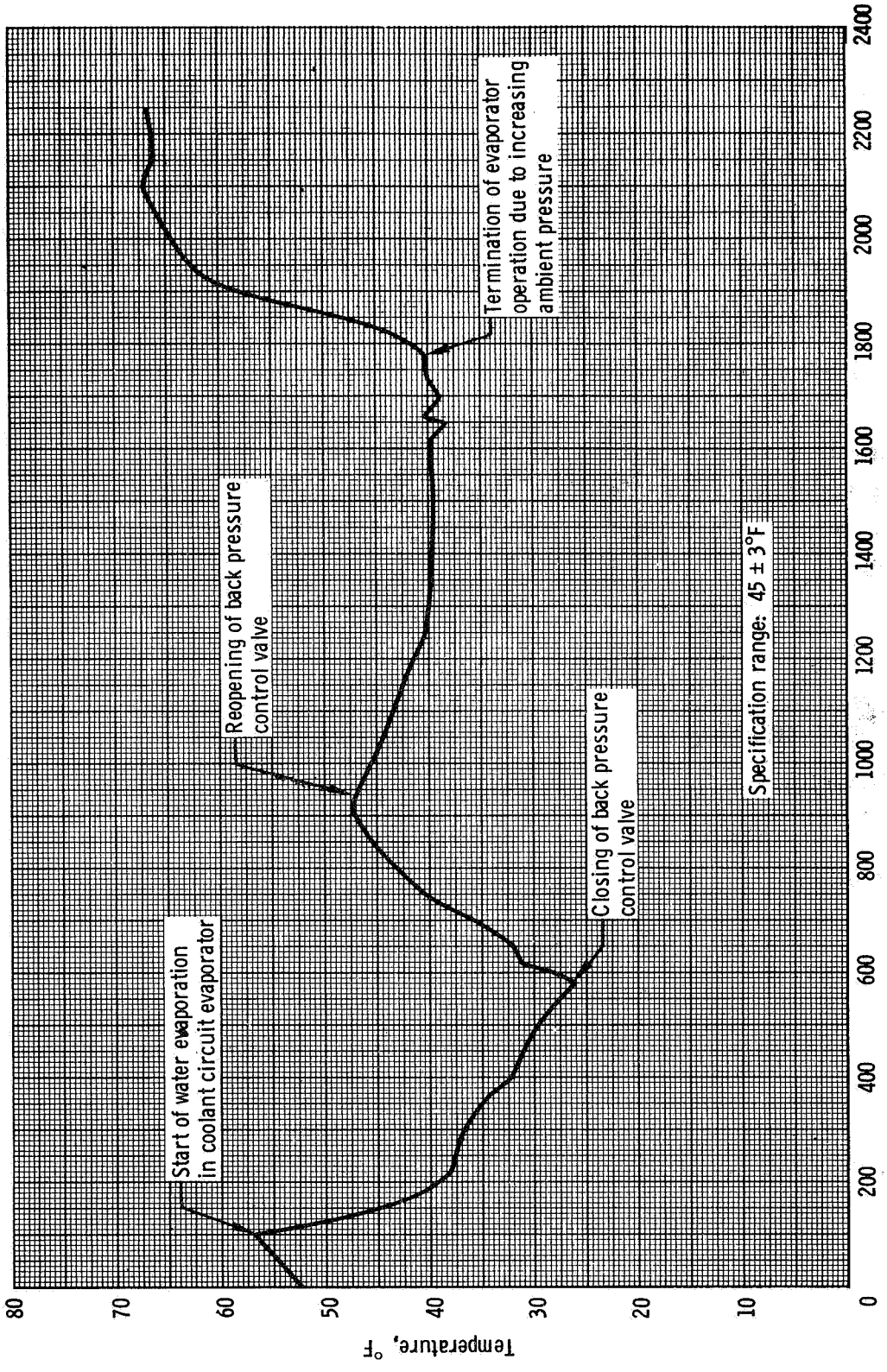
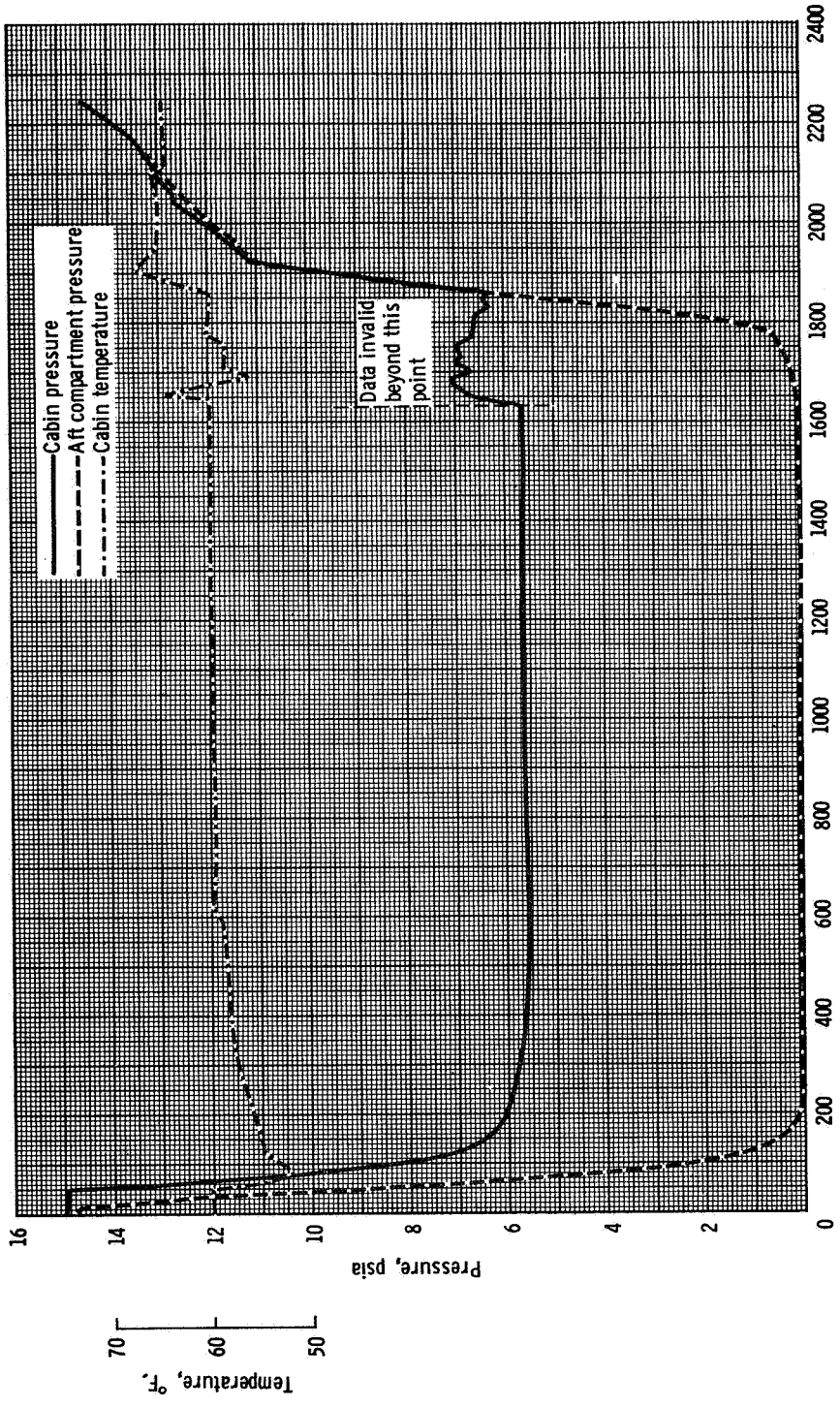


Figure 7.17-2.- ECS cabin pressure relief valve, Mission AS-201.



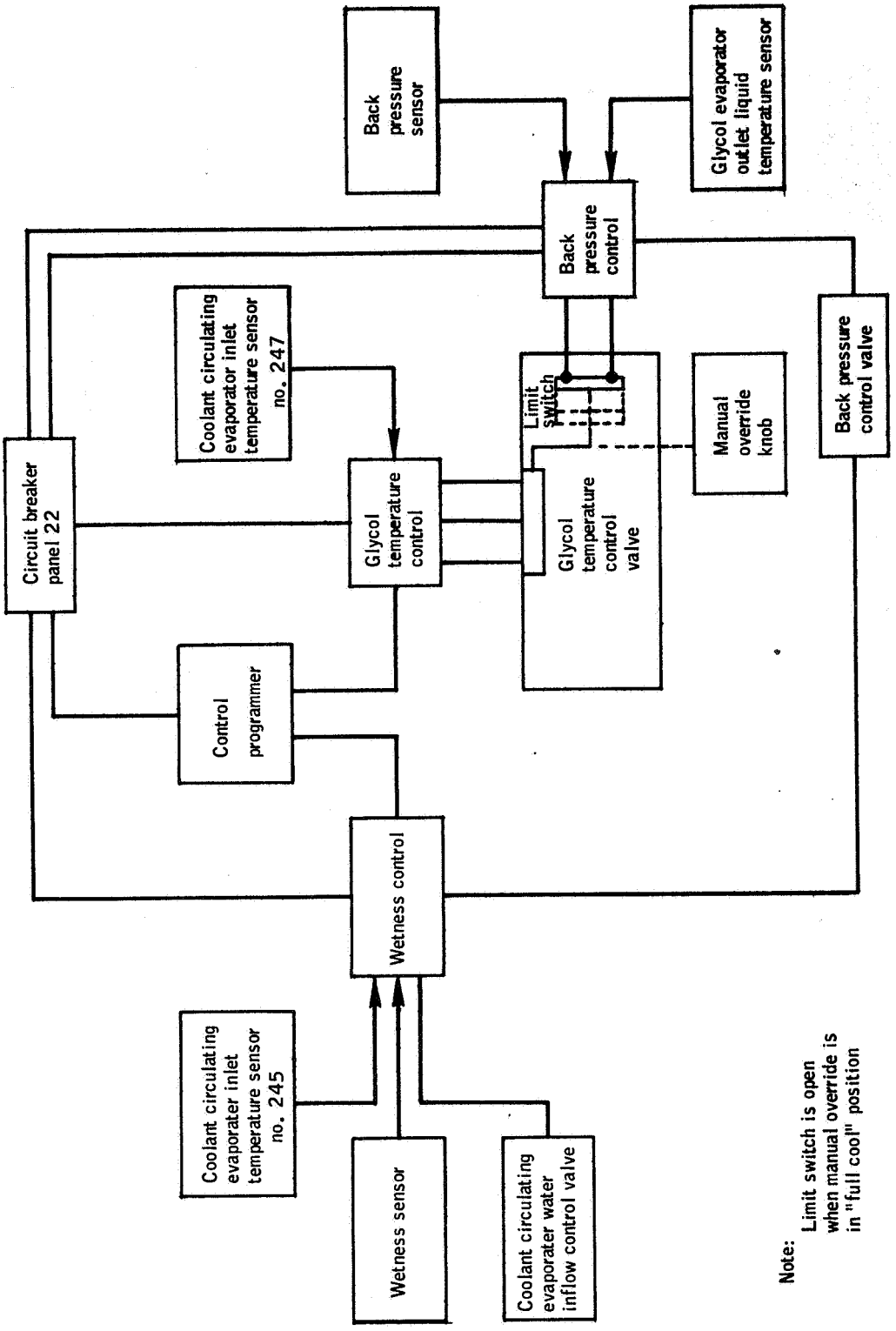
NASA-S-66-6347 MAY 6

Figure 7.17-3. - Coolant circuit evaporator outlet liquid temperature, Mission AS-201.



NASA-S-66-6348 MAY ≤

Figure 7.17-4.- Command module cabin environment, Mission AS-201.



NASA-S-66-6349 MAY 6

Figure 7.17-5.- Power and control diagram for ECS back pressure control, Mission AS-201.

7.18 Crew Station Acoustics

Description.- Two condenser microphones were mounted in spacecraft 009 to measure crew station acoustics. The environment of interest was the noise generated during the region of maximum dynamic pressure. From the available wind-tunnel data (ref. 19) for the Apollo spacecraft configuration, a maximum overall sound pressure level (SPL) of 168 decibels (dB, Re: 0.0002 dynes/cm^2) was predicted at the CM/SM exterior interface for a nominal Saturn IB trajectory. Sound pressure levels of 166 dB and 158 dB, respectively, were measured at the CM/SM exterior interface of the instrumented boilerplate spacecraft with the Saturn I launch vehicles during Apollo Missions A-101 and A-102 (refs. 4 and 5).

Instrumentation.- Microphone CK0033Y, located at X_C 50.0, Y -0.5, Z -18.0, and microphone CK0032Y, located at X_C 50.0, Y 0.5, Z -18.0, were mounted on the equipment platform in the crew compartment. Preflight calibrations showed that the microphones were linear with SPL and had a flat frequency response (±1dB) from 10 to 5k cps. Both measurements were recorded on the DSE recorder, which did not have a flat frequency response. As a result, a data correction, based on preflight testing, was required. In addition, the acoustic measuring system did not have end-to-end calibrations produced before flight, and so calibrations were added to the data processed at the MSC Computation and Analysis Division. The recorded data from both measurements were reduced in an analog format using an rms meter, octave band analyzer, and X-Y plotter. The reduced data consisted of overall SPL time histories, one-third octave band time histories, and power spectral density analysis.

Performance.- The usable data from the acoustic measurements are presented in figure 7.18-1. This figure presents the overall SPL's from T-10 to T+12.3 seconds (booster noise) and from T+45 to T+51 seconds (aerodynamic noise). Except for these flight periods, the noise levels were not accurately recorded because the noise was not within the instrument range of either measurement. In addition, measurement CK0033Y became erratic after T+51 seconds.

The total ranges of both acoustic measurements (70 to 110 dB for CK0032Y and 100 to 140 dB for CK0033Y) were not realized because the combination of ambient noise and electronic systems noise limited the ranges from 87 to 110 dB for CK0032Y and 115 to 140 dB for CK0033Y. Postflight tests conducted at the contractor's facility showed that the epoxy bond between the microphone diaphragm and the diaphragm mounting ring failed. From the character of the data, it would appear that this failure occurred after T+51 seconds. (See section 7.13.) A failure analysis could not be determined.

For the acoustics measured, the noise levels during the time where data were collected during Mission AS-201 will not be detrimental to the crew.

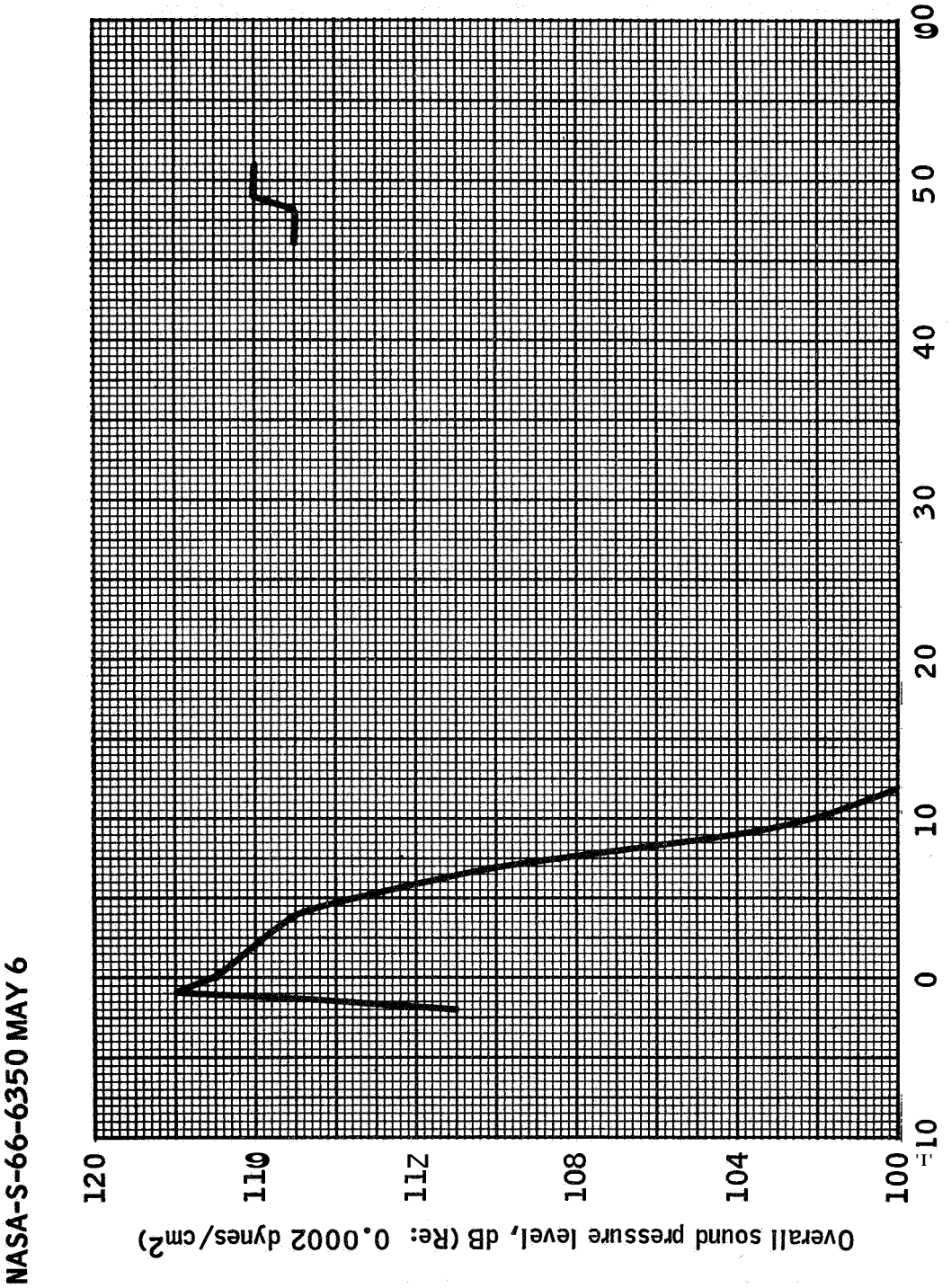


Figure 7.18-1.- Overall sound pressure level time histories of crew station acoustics, Mission AS-201.

7.19 Spacecraft Windows

Summary.- In general, all five of the command module windows on spacecraft 009 had the same postflight appearance. Each of them had a uniform light-gray film deposit. Visibility through the windows was much better than through the windows on spacecraft 002 after flight (ref. 9). Black soot smudges were not found on any of the windows. Without photographic data from an onboard camera looking through a window, it was not possible to determine at what time in flight the contamination occurred. The visual degradation was due to the combined effects of the thin contamination layer and crystallization of the minerals found in sea water after the spacecraft was recovered from the Atlantic Ocean.

Description.- The spacecraft 009 command module windows were of a Block I type configuration and included one hatch window, two side windows, and two rendezvous windows (see fig. 7.4-1). Each window consisted of three panels: two inner panels, each 0.20-inch thick with a 0.175-inch air space between them, installed in the pressure cabin structure; and one outer panel, 0.70-inch thick, installed in the CM outer (heat shield) structure, approximately 1 inch from the inner panels. The two inner panels were aluminum silicate (Corning code 1723) and were coated on both sides with a multilayer, antireflective coating. The outer panel was amorphous fused silica (Corning Code 7940, optical grade). The outer surface of this panel was coated with a magnesium fluoride antireflective coating, and the inner surface had a blue-red (W-IR) reflective coating. The left rendezvous window did not have the optical coatings that were used on the other windows.

Postflight inspection.- The outer heat-shield windows were removed for visual examination and spectrographic analyses. Visual examination revealed that all windows had a deposit of a light-gray material that varied in thickness from window to window. The typical black spots which were deposited on the windows during the previous boilerplate and the spacecraft 002 launch abort tests were not present on any of the windows. The right side window appeared to have been washed by wave action while the spacecraft was in the water, and the remaining residue on the window had a salt-like appearance. The left side window had a light film deposited uniformly over about 80 percent of the total area. The clear area appeared to have been manually wiped. The right rendezvous window was contaminated with a light-gray film. The majority of this film had been abraded away, as though the Window had been used as a step. The left rendezvous-window contaminate was similar to that found on the left side window. The hatch window had been scraped clean for the rubber suction cups used for removing the outer hatch.

Postflight analysis.- Spectral transmission, reflection, and light-scattering measurements were conducted on the left side and the left

rendezvous windows. Emission spectrographic analyses were conducted on contamination smears taken from all the windows except the right rendezvous window, Analyses were not conducted on the right rendezvous window because the contamination had been so badly abraded that the results would be arbitrary.

Figure 7.19-1 shows the five spacecraft windows and the location fromwhich each contamination sample was taken. Sample 9 was a small piece of the ablative material that was found on the left rendezvous window. sample 10 was rust.

Table 7.19-I presents the results of the emission spectrographic analyses studies for all window samples. Contamination samples included ocean water residue and products from the tower-jettison motor propellant burning.

Figure 7.19-2 shows the spectral transmission and the reflection (forward and aft) characteristics of the left crew window. The high reflection at 3500 to 3800 angstroms would be expected from the blue-red (W-IR) coating. This high reflection is in the near UV and blue end of the spectrum and the contamination had very little effect on the magnesium fluoride antireflective coating. Normal reflectivity of the coating is 4 percent from 3750 to 7000 angstroms. 'Figures7.19-3(a) and (b) represent the light-scattering and diffused light transmission characteristics of the left side and the left rendezvous windows. The direct-light transmission through the window and contaminate ranged from 5 percent at 3750 angstroms to 50 percent at 6500 angstroms through the left side window and 24 percent to 32 percent through the left rendezvous window.

The light-scattering characteristics of the windows indicate that approximately 35 percent of the impinging light on the left window and 40 percent on the left rendezvous window was scattered. .

Subjective analysis of the window transmission and light-scattering characteristics indicate that with the light source (sunlight) to the rear there would be small. degradation in visual acuity through the window; however, with the light source in front of the window visual acuity would be quite difficult.

An evaluation of the Gemini VIII and Gemini IX windows, which is being conducted at this time, is expected to result in a basic measure which can be used in the evaluation of all Apollo windows.

TABLE 7.19-I.- EMISSION SPECTROGRAPHIC ANALYSIS OF WINDOW CONTAMINATES FOR MISSIONS A-004, AS-201, AND AEDC ENGINE TESTS

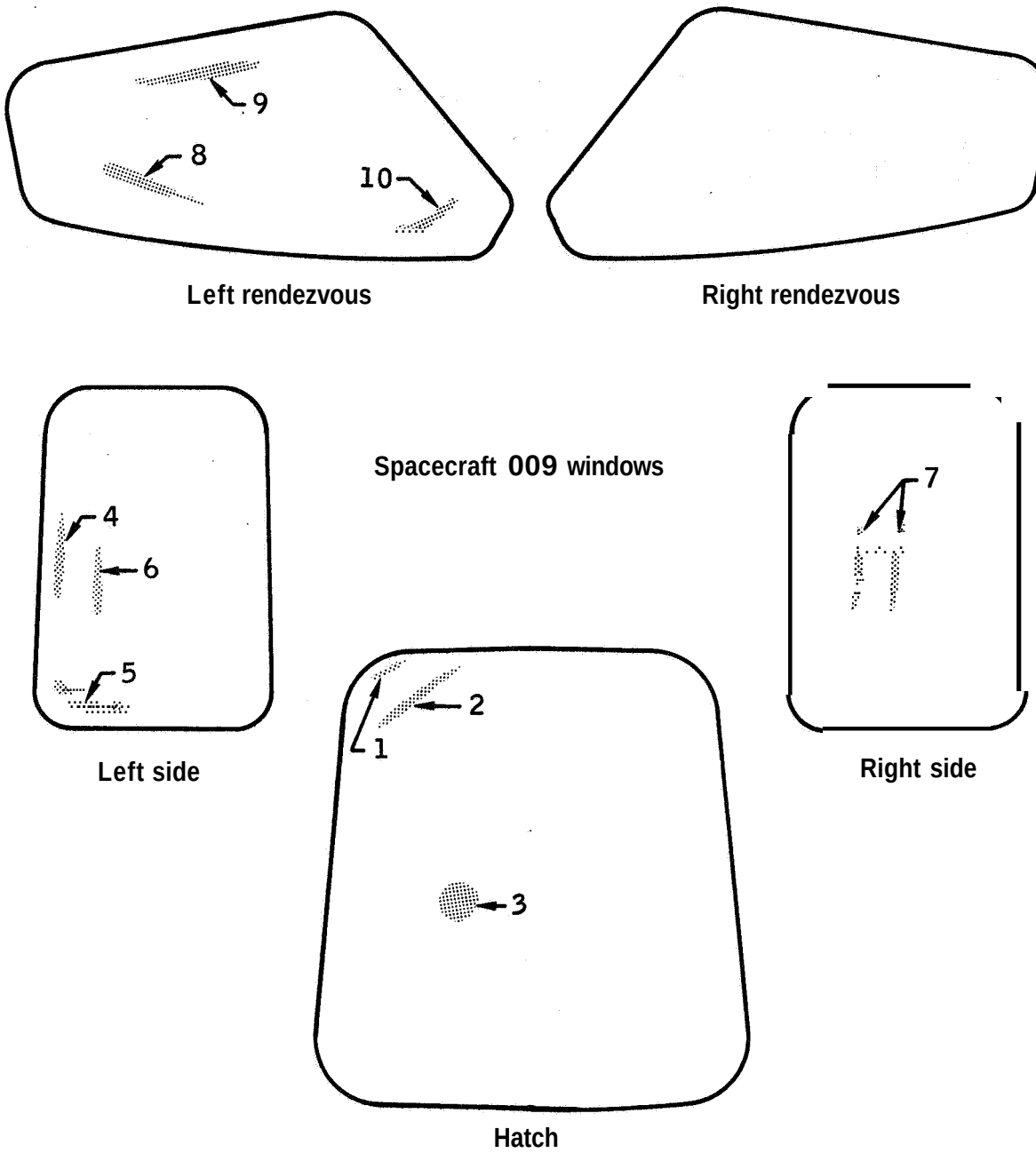
[Elements are listed in order of amounts found on the Spacecraft 009 windows]

Element	Spacecraft 009	Spacecraft 002	AEDC engine test	Possible source
Silicone	Heavy major	Minor	-	RTC
sodium	Heavy major	Major	None	Sea & binders
calcium	Heavy minor	Base	Trace	Sea
Lead	Heavy minor	Heavy major	Light major	LET leadliner
Magnesium	Heavy minor	Base	Base	LET & sea
Aluminum	Major	Light minor		LET
Iron	Major	Major	Light major	LET
Copper	Minor	Base	Light major	Wire
Titanium	Light major	Light major	None	Ablator
Zinc	Light major	Heavy major		Ablator
Chromium	Light major	Trace	Trace	Cork liner-binders
Boron	Light minor	Light minor	Light minor	Igniter (LET)
Cadmium	Base	None	Base	Bolts (LET)
Manganese	Base	Trace	Trace	SEA & LET
Tin	Base	Base	Base	Solder
Vanadium	Base	None	None	Steel structure
Antimony	Trace	None	None	Fire retardant
Barium	Trace	None	None	TJM
Molybdenum	Trace	None	None	RCS nozzle lining
Nickel	Trace	Trace	Trace	Structure
Silver	Trace	None	Trace	Solder
Zirconium	Trace	None	None	-
Bismuth	None	Trace	None	WSMR environment

Key to weighted code
(in descending order)

Heavy major
Heavy minor
Major
Minor
Light major
Light minor
Base
Trace

NASA-S-66-6351 MAY 6



Note: Numbers identify contaminate smears taken for emission spectographic analysis

Figure 7.19-1.- Window contaminate smear locations, Mission AS-201.

NASA-S-66-6352 MAY 6

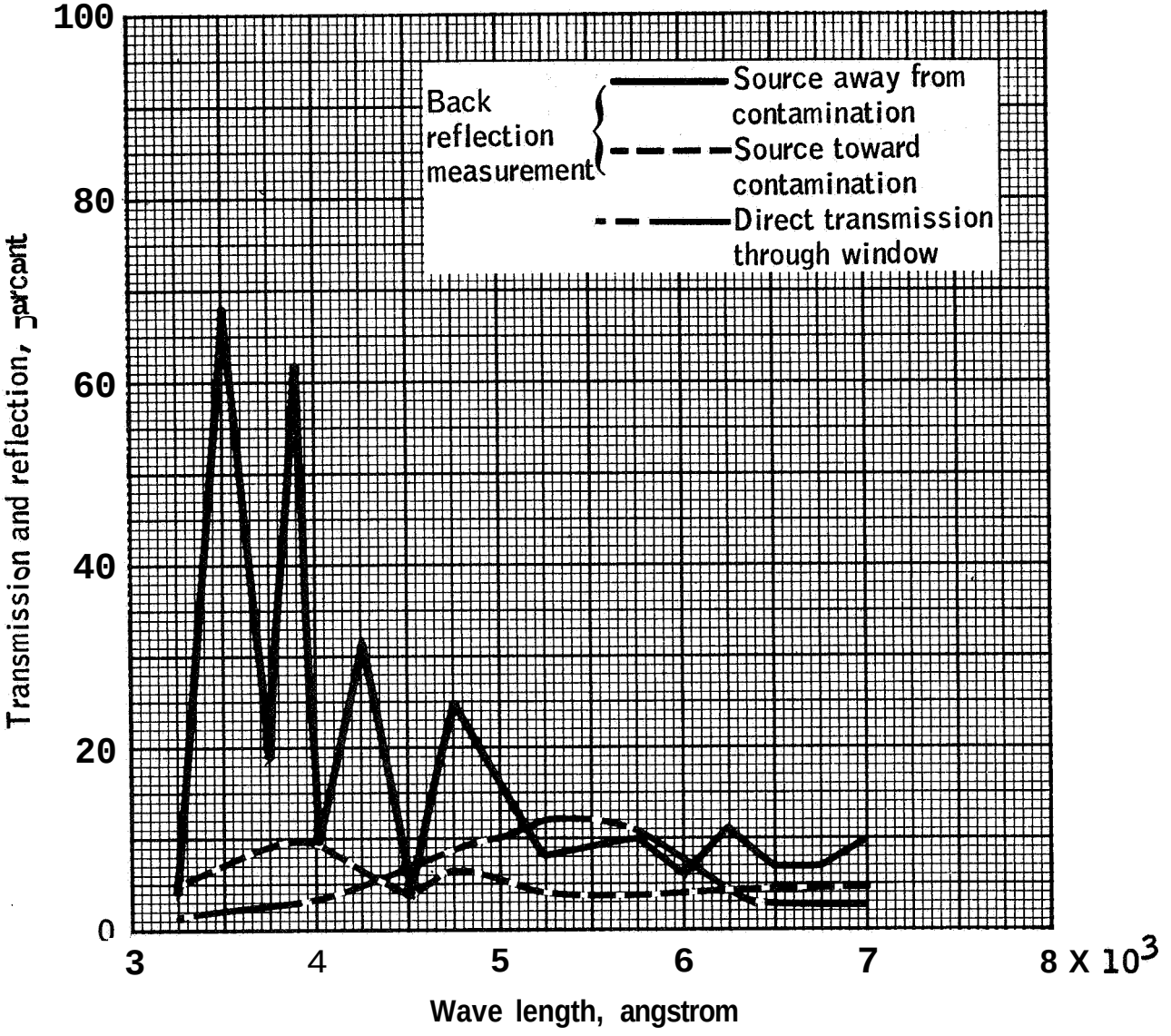
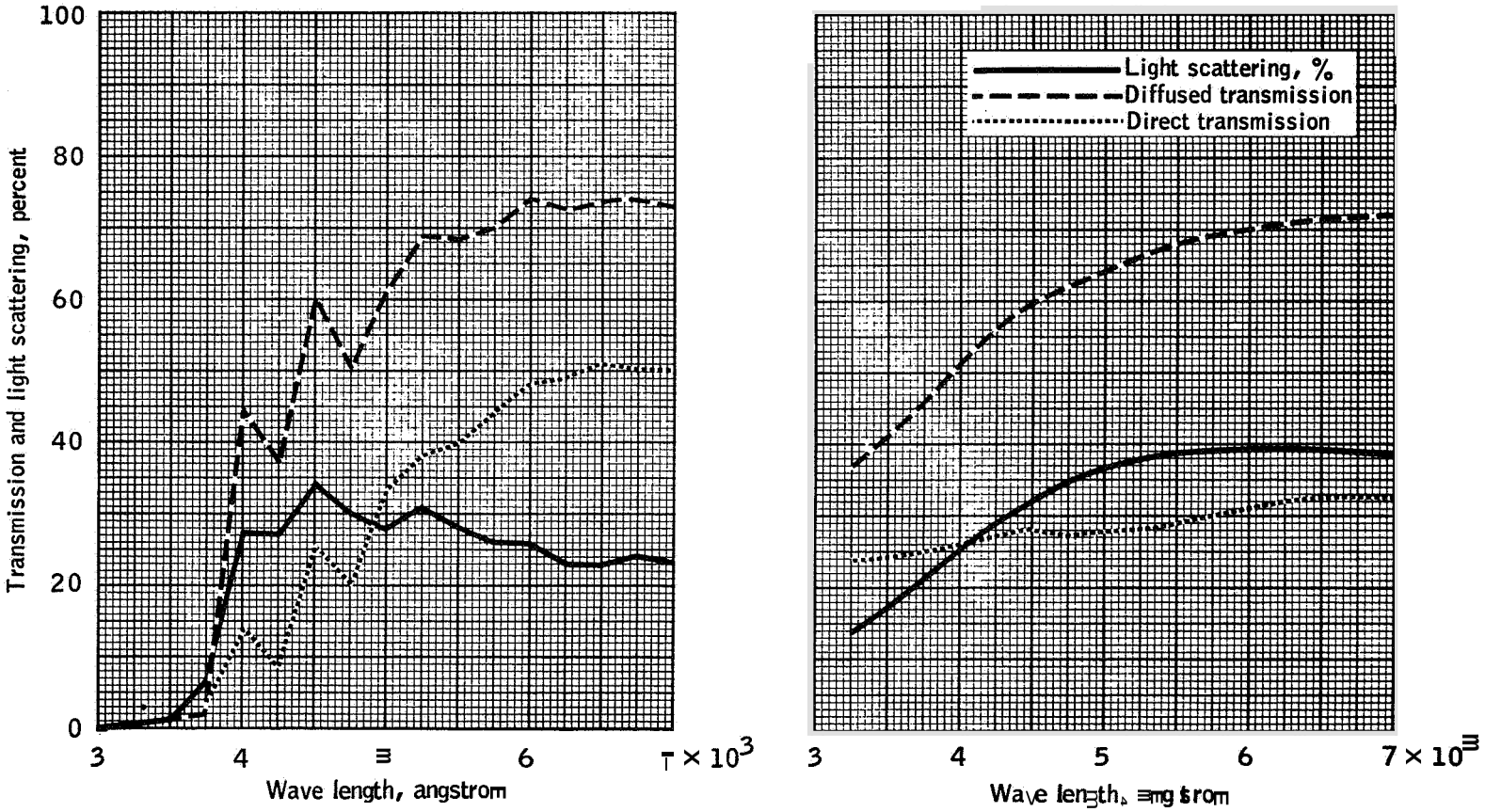


Figure 7.19-2.- Spectral transmission and reflection characteristics of left side window, Mission AS-201.



(a) Left side window.

(b) Left rendezvous window

Figure 7-190 - Integrity sphere spectral transmission and light scattering characteristics, Mission AS-201.

7.20 Crew Related Dynamics

Summary.- The vibration levels, which were measured on Mission AS-201 on the forward bulkhead of the crew compartment and which indicated a measure of cabin environment to which crew members could be exposed during a manned mission, exceeded the nominal Apollo limits for approximately 2 seconds at lift-off, and were higher than anticipated between T+76 seconds and T+96 seconds and at the time of S-IB engine cutoff.

During these periods, the physical well-being of the crew would not have been jeopardized. Crew members would have experienced a noticeable degradation in visual acuity in the monitoring of cabin display meters, dials, et cetera, to determine instantaneous status. Because instrument panel and crew vibration phase relationship is unknown, it must be assumed that the crew's visual acuity would not be improved.

Data.- Acceleration measurements CK0004A, CK0005A, and CK0006A (located on the forward bulkhead of the crew compartment) and their resultant were used to determine the Vibration environment. The resultant acceleration and the azimuth and elevation angles of the resultant were computed as shown in figure 7.20-1.

At lift-off, the resultant vibration reached a maximum of 1.1g peak-to-peak at T+1.4 seconds. The 10-cps, longitudinal vibration (fig. 7.20-2) was the major contributor. The amplitude of the resultant vibration had decreased to 0.5g peak-to-peak at T+2.8 seconds and was insignificant between T+3 seconds and T+53 seconds. Between T+53 seconds and T+76 seconds, the resultant vibration increased to an average level of 0.5g peak-to-peak with several bursts reaching 0.7g peak-to-peak. During this period the major component was lateral (Y axis) vibration.

From T+76 seconds to T+96 seconds the average peak-to-peak g level of the resultant was approximately 0.9g and reached, 1.4g to 1.6g peak-to-peak several times (See figs. 7.20-3 to 7.20-9.) & this period, the major components were longitudinal and lateral vibration. At T+96 seconds, the amplitude began to decrease and was insignificant until inboard engine cutoff (T+142 sec). Immediately following inboard engine cutoff, between T+142 seconds and T+143 seconds, a 0.75g peak-to-peak, 10-cps, primarily longitudinal, vibration developed. This vibration decreased to 0.25g peak-to-peak in 2 seconds. A similar vibration developed at the time of outboard engine cutoff (T+147 sec) reaching a maximum amplitude of 0.5g peak-to-peak.

Analysis of periods of significant vibration indicates that the 10-cps longitudinal Vibration noticed at lift-off continued to be a significant frequency through T+96 seconds. In addition, analysis of ten 3-second time slices between T+55 seconds and T+99 seconds shows

significant 23- to 26-cps lateral and longitudinal vibrations (table 7.20-1). The vibration immediately following inboard and outboard engine cutoff was predominantly longitudinal at 10 cps.

Effect on crew.- None of the vibrations observed were of sufficient magnitude and duration to cause pain or to jeopardize directly the physiological well-being of the crew. However, the vibrations would noticeably degrade the ability of the crew to perform the required visual monitoring of vehicle systems. Low-frequency vibration (5 to 35 cps) at levels well below pain threshold generally cause blurred vision. For example 11-cps longitudinal vibration at levels above 0.5g peak-to-peak (0.177g rms) has been reported to impair vision (ref. 20). Also, lateral vibration (Y axis) degrades visual ability more than longitudinal vibration (X axis) of the same level (ref. 21). Although the crewman's ability to read a given dial or meter may not be completely eliminated, he must concentrate on the reading for a longer period of time than normally required to interpret it. Having to concentrate on each meter for a longer period of time interrupts the established scan pattern and results in incomplete or late monitoring for the time normally allowed. During lift-off, max q, and staging, critical periods during which the crew may be required to make decisions quickly, the ability to obtain the required visual data on which to base these decisions would have been degraded.

If the vibration environment indicated at the forward bulkhead on this mission is representative of the condition at the crew position on manned flights, it will be necessary to adjust scan patterns to the expected degraded visual acuity.

The phase relationship between the vibration of the instrument panel and the crew is unpredictable. It must be assumed that this would not improve the crew's ability to read the instruments.

TABLE 7.20-I.- SUMMARY OF POWER SPECTRAL DENSITIES

Time slice, sec	X axis (CK0004A)			Y axis (CK0005A)			Z axis (CK0006A)		
	Major frequency, cps	Major frequency amplitude, cps	Time slice, rms value (a)	Major frequency cps	Major frequency amplitude, cps	Time slice, rms value (a)	Major frequency, cps	Major frequency amplitude, cps	Time slice, rms value (a)
0.029 to 3.01	10	0.212	0.243	8 24	0.053 .052	0.139	14	0.68	0.157
4.01 to 7.00	10	0.038	0.096			0.088			0.082
55.00 to 58.01	10 to 11 24 to 25	0.045 .053	0.134	25	0.076	0.160	25	0.068	0.118
60.51 to 63.52	10 to 11 24	0.04 .048	0.129	24 to 26	0.065 to .070	0.167			0.112
65.21 to 68.22	10 to 11 24	0.055 .048	0.129	24 to 25	0.076	0.160	26	0.058	0.121
70.01 to 73.00	10 to 11 16 23 28	0.056 .053 .050 .043	0.165	26	0.105	0.213	25	0.070	0.134
73.52 to 76.51	8 10 23 to 25	0.043 .044 .064	0.170	6 25	0.062 .12	0.231	25	0.063	0.144
78.01 to 81.00	11 23	0.062 .073	0.204	4 14 23	0.048 .053 .085	0.229	25	0.067	0.145
82.00 to 85.01	6 11 23	0.05 .075 .106	0.246	13 to 14 23 20 to 30 46 to 47	0.054 .104 .054 .053	0.242	23	0.052	0.125

[a]Frequency content of time slice, approximately 0 to 50 cps.

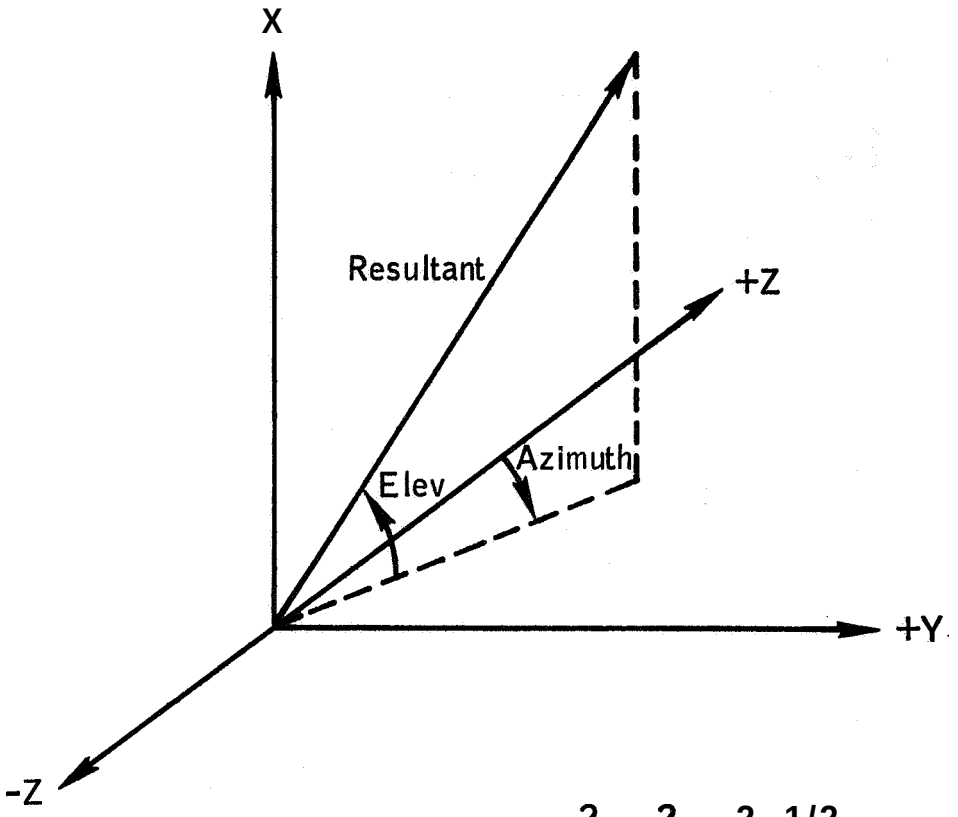
TABLE 7.20-I.- SUMMARY OF POWER SPECTRAL DENSITIES - Concluded

Time slice, sec	X axis (CK0004A)			Y axis (CK0005A)			Z axis (CK0006A)		
	Major frequency, cps	Major frequency amplitude, cps	Time slice, rms value (a)	Major frequency, cps	Major frequency amplitude, cps	Time slice, rms value (a)	Major frequency, cps	Major frequency amplitude, cps	Time slice, rms value (a)
86.01 to 89.01	0 to 32 21 to 22 28 31	[b]0.048 .072 .059 .068	0.248	9 to 11 16 to 18 23 27 33 38 to 42 0 to 42	0.048 .050 .076 .063 .050 .053 [b].044	0.244			0.121
90.52 to 93.52	10 16 to 19 22 28 41	0.054 .058 .072 .056 .066	0.250	0 to 35 23	[b]0.043 .065	0.255			0.114
95.51 to 98.52	2 21 28 42	0.062 .051 .052 .056	0.224	23	0.049	0.154			0.082

[a]Frequency content of time slice, approximately 0 to 50 cps

[b]Average amplitude over indicated frequency.

NASA-S-66-6354 MAY 6



$$\text{Resultant} = (X^2 + Y^2 + Z^2)^{1/2}$$

$$\text{Azimuth} = \tan^{-1}\frac{Y}{Z}$$

$$\text{Elevation} = \sin^{-1}\frac{X}{(X^2 + Y^2 + Z2)^{1/2}}$$

Figure 7.20-1.- Determination of accelerometer resultant for CM forward bulkhead conditions, Mission AS-201.

NASA-S-66-6355 MAY 6

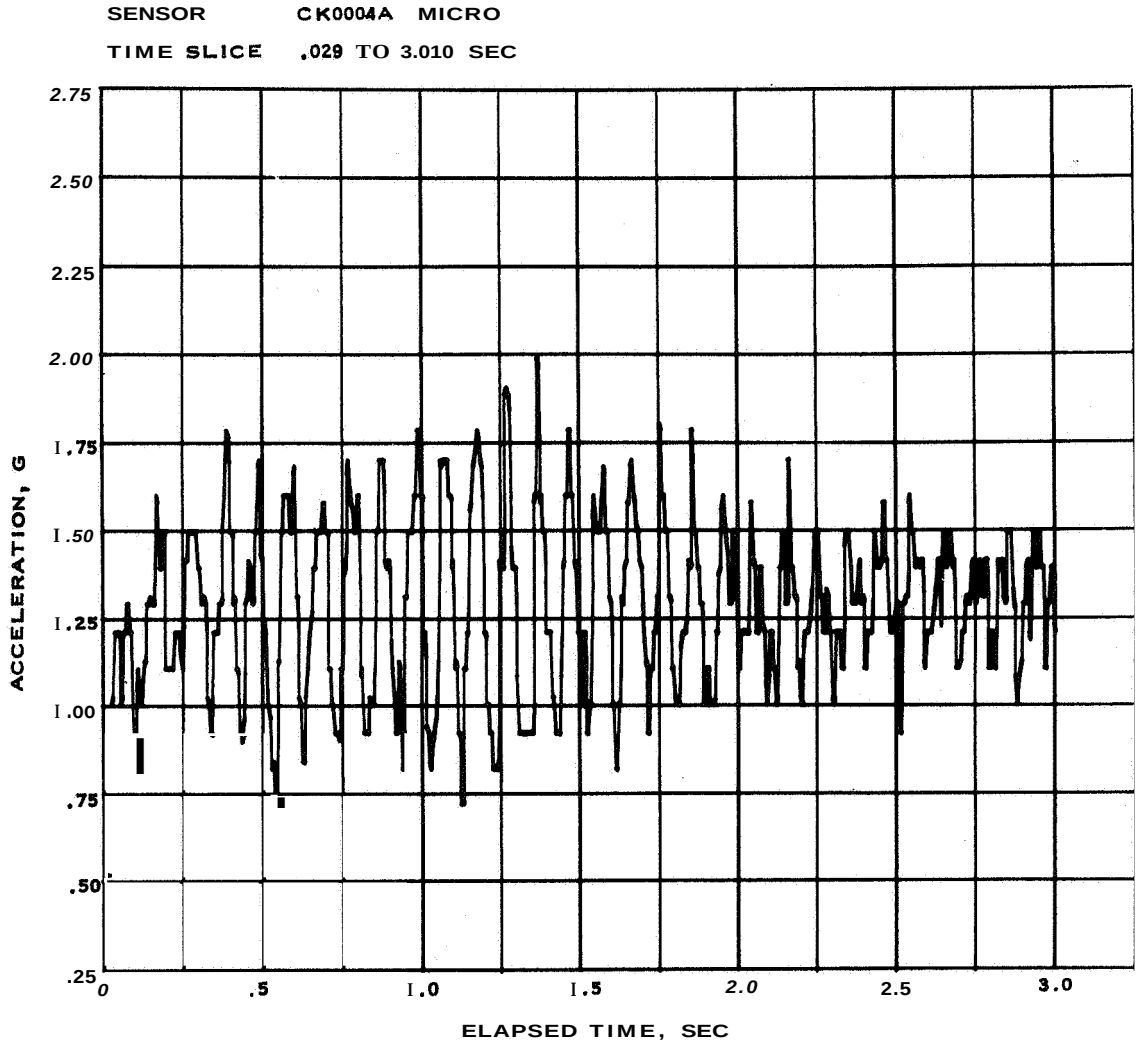


Figure 7.20-2.- Lift-off X-axis vibration, Mission AS-201.

NASA-S-66-6356 MAY 6

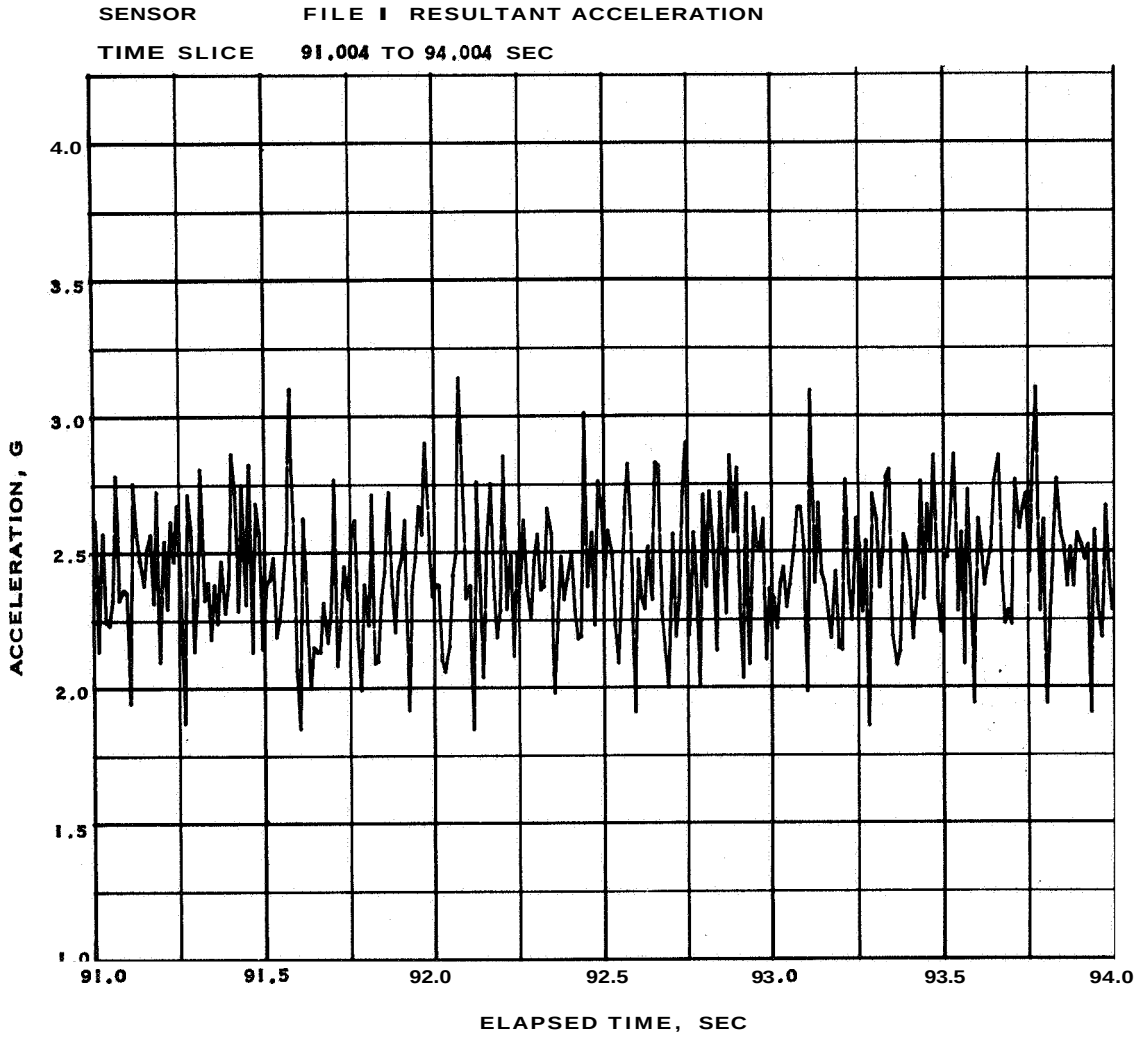
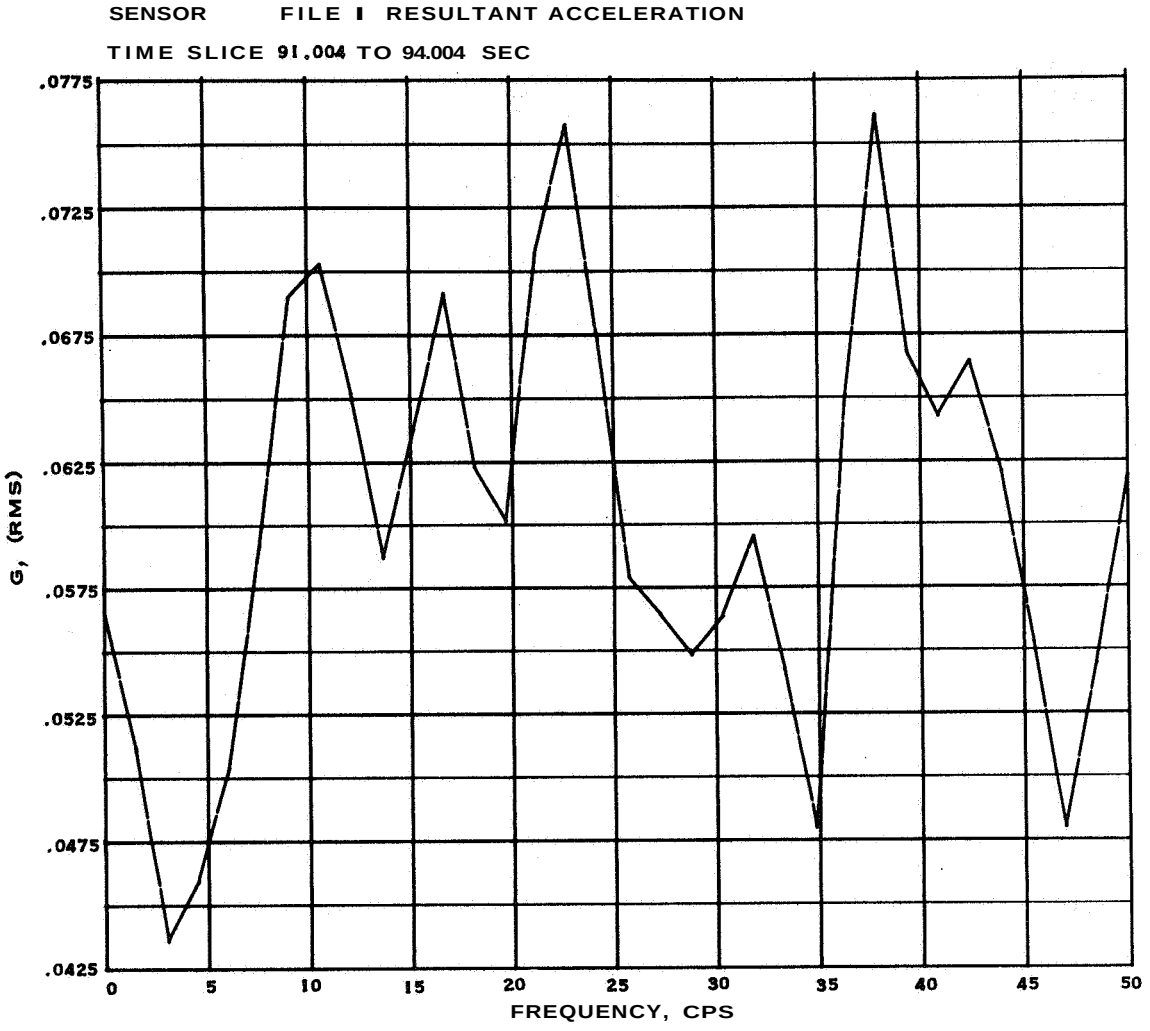


Figure 7.20-3.- Resultant acceleration (CK0004A, CK0005A, and CK0006A), Mission AS-201.

NASA-S-66-6357 MAY 6



E9

Figure 7.20-4.- Resultant acceleration amplitude spectral density, g (rms), Mission AS-201.

NASA-S-66-6358 MAY 6

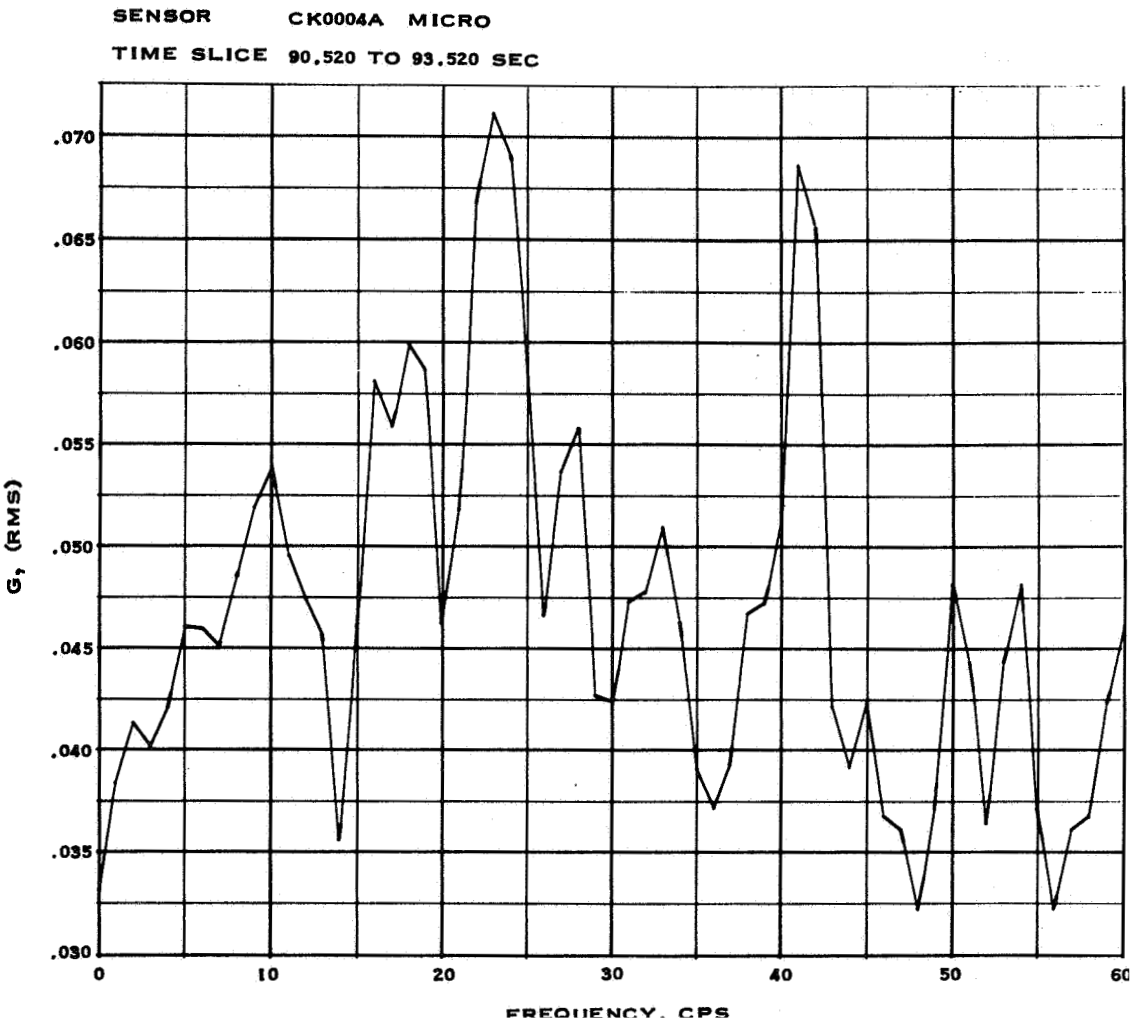


Figure 7.20-5 .- X-axis vibration amplitude spectral density, g (rms), Mission AS-201.

NASA-S-66-6359 MAY 6

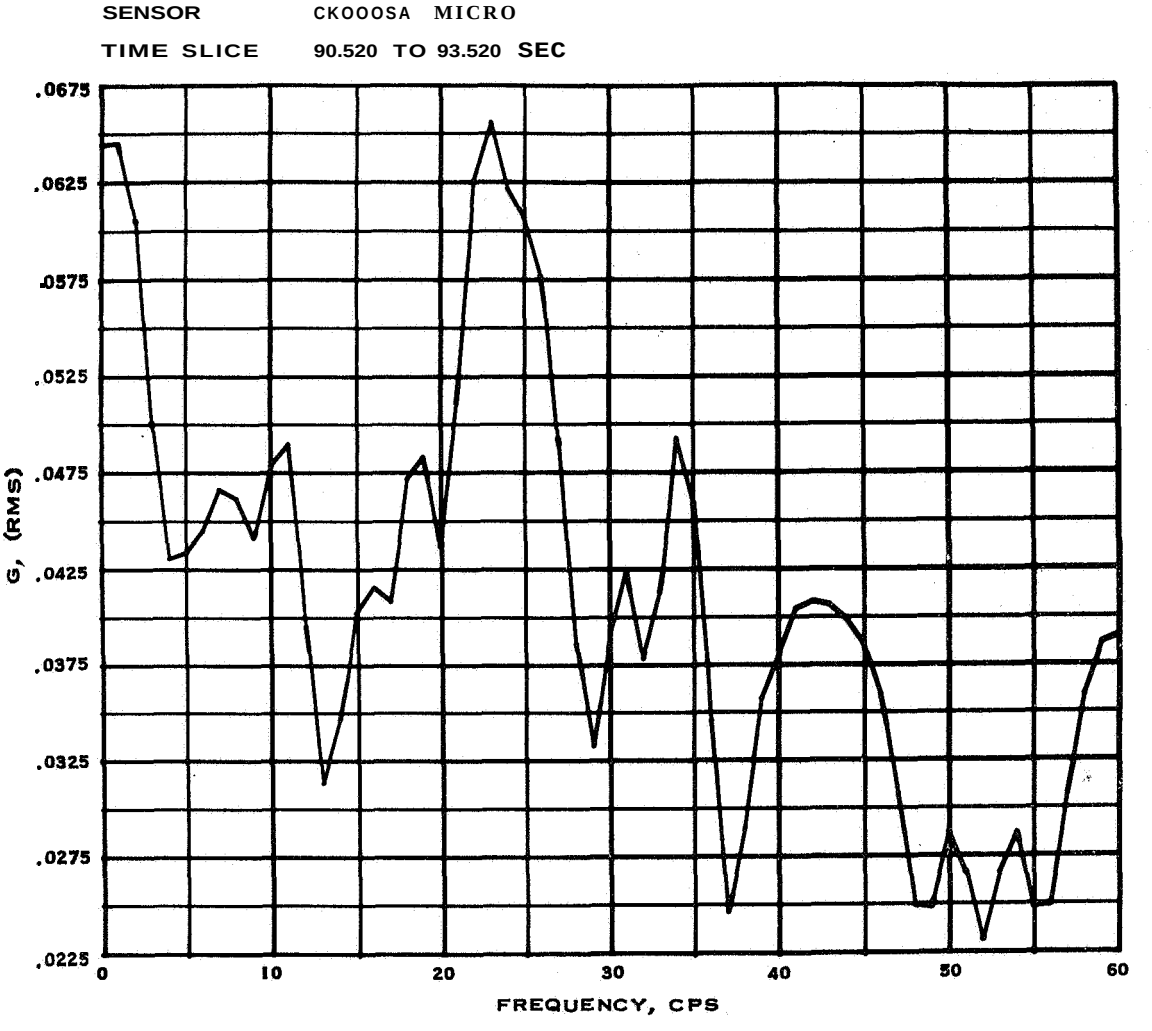


Figure 7.20-6.- Y-axis vibration amplitude spectral density, g (rms), Mission AS-201.

8.0 LAUNCH VEHICLE PERFORMANCE

After 11.2 seconds of vertical flight, the launch vehicle began to roll from the 100° east of north launch azimuth to the proper flight azimuth of 105° east of north and completed the maneuver at T+16.2 seconds. At T+11.2 seconds, the programed pitch attitude profile was initiated and continued until T+134.39 seconds, at which time an essentially constant pitch attitude was maintained until the initiation of active guidance. Active guidance was initiated successfully 28.4 seconds after separation of the S-IB/S-IVB stages. Shutdown of the S-IB stage occurred at T+146.9 seconds which was only 0.3 second later than nominal. At S-IB cutoff, the actual trajectory parameters as compared with nominal were 26.3 ft/sec high in space-fixed velocity, 0.40 nautical mile low in altitude, and 0.55 nautical mile greater in range.

Separation of the S-IB and S-IVB stages occurred at T+147.7 seconds, followed by ignition of the S-IVB stage 1.6 second later. All ullage rockets functioned as expected and were successfully jettisoned.

S-IVB stage cutoff occurred at T+602.9 seconds, 10.2 seconds later than predicted. The pitch-aver maneuver was initiated 11.1 seconds after S-IVB cutoff, which was 11 seconds later than predicted. The spacecraft separation sequence was started at T+663.1 seconds and was completed approximately 180 seconds later. Both events were about 10.2 seconds later than predicted.

At S-IVB stage cutoff, the actual trajectory parameters as compared with nominal were 1.6 ft/sec less in space-fixed velocity, 0.38 nautical mile high in altitude, and 16.1 nautical miles greater in range. At spacecraft separation space-fixed velocity was 1.6 ft/sec less, altitude was 1.3 nautical miles high, and range was 22.2 nautical miles greater.

The overall performance of the S-I3 propulsion system was satisfactory. Preliminary reconstruction data shuw the average thrust to be approximately 0.8 percent lower, fuel flow rate 0.5 percent higher, LOX flowrate 1.0 percent lower, and specific impulse 0.2 percent lower than predicted. All four retrorockets performed as expected. Outboard engine cutoff was initiated by a fuel depletion sensor. The GN_2 control pressure system functioned properly during flight, after having some difficulty during countdown.

The performance of the guidance system was adequate and the control system deviations were about as expected. During maximum dynamic pressure (max q) the attitude errors were 2.2° nose up in pitch, 2.5° nose right in yaw, and 0.8" counterclockwise from the rear in roll. Maximum angles of attack during max q were 1.6° nose up in pitch and 3.6° nose

left in yaw. Maximum actuator position movements were 1.15° in pitch and 2.1° in yaw.

Disturbances during S-IB/S-IVB separation were quite small. Maximum S-IVB attitude errors during separation were 0.8° in pitch and 0.7" in both yaw and roll. Maximum S-IVB actuator response was, 0.8" in pitch, occurring at the initiation of active guidance.

Beginning around 30 seconds after S-IB/S-IVB separation and lasting through S-IVB burn, there was a positive torque on the roll axis of about 15 to 20 ft-lb. The torque caused a 0 to 0.7° clockwise roll (viewing from the rear), which was well within the 1° deadband in the auxiliary propulsion system (APS). Only 20 percent of the total APS fuel was used up to spacecraft separation.

There were no structural. loads of sufficiently high magnitude to threaten the structural integrity of the launch vehicle. The maximum load was encountered at inboard engine cutoff in one of the S-IB radial beams located in the spider beam. Seventy-seven percent of the design limit stress was experienced. Overall vibration levels were slightly above expected while overall acoustic levels were slightly below expected.

Environmental heating rates and temperatures on the launch vehicle were somewhat cooler than expected, except *on* the fins, outboard engine aspirator, and S-IVB base. Fin heating rates on the trailing edge went slightly outside the Saturn I Block II band and fin side panel temperatures were higher than expected. Heating rates were somewhat high on outboard engine aspirator at outboard engine cutoff and on the S-IVB base due to retrorocket impingement.

A high differential pressure occurred on several fins during Mach 1 phase caused by a 3" yaw angle of attack. Common bulkhead pressure in S-IVB was nominal at 0.07 psi.

In the instrument unit (IU) a new system was used for cooling components. Equipment was mounted on cold plates with H_2O/methanol circulating through the plates. The heat was dissipated overboard through a sublimator. The instrument unit was cooler than expected during the early portion of flight. However, during subsequent portions of the flight, the temperature stabilized properly. This indicated proper operation of the cooling system and sublimator.

Temperature of the GN_2 supply system to the ST-124 platform air bearings was normal (15.6" C) up to T+70 seconds. At this time the temperature began to decay and was out of the 10" C telemetry range limit by T+110 seconds. No structural problems were indicated in the IU.

All electrical systems on the launch vehicle performed as expected and operated within appropriate limits, including the emergency detection subsystem (EDS). The launch vehicle portion of the EDS is deemed to have performed properly based only on telemetry data from the IU. The three EDS buses were energized properly, automatic abort enable and disable were commanded at the proper times, and the engine-aut measurements indicated ignition, the events of staging, and the cutoff of both stages, (Note: IU measurements only indicated when one or more S-IB engines were out; therefore, inboard cutoff only was indicated by these measurements.) The 40-second timer timed out properly, no angular overrates were sensed, and because no abort conditions were witnessed and the launch vehicle portion of the EDS performed properly, the automatic abort bus was not energized.

It should be noted that the angular rates sensedby the EDS sensors approached the EDS limit in the pitch plane. At approximately T+62 seconds an angular rate of approximately -5 deg/sec was experienced in the pitch plane. The nominal abort setting for Mission AS-201 was ±5.5 deg/sec. The inaccuracies of the instrument result in a deadband of 4.725 deg/sec to 6.275 deg/sec. The most predominant frequencies were about 19 cps.

A disturbance was witnessed also in the roll axis of about ±6 deg/sec. This is considerably below the roll abort threshold of 20 deg/sec. A small rate of such low magnitude as to be of no consequence was also witnessed in the yaw axis. All three sensors indicated essentially the same disturbance in each respective axis, and none of the nine (3 per axis) overrate switches closed during the boost phase. Marshall Space Flight Center (MSFC) plans to provide filters in the output circuits of the EDS rate gyros to suppress noise, modification to be effective in Saturn SA-203 and subsequent vehicles, Evaluation of this flight will support closed-loop EDS flight test in Mission AS-202.

Seven launch vehicle measurements were deleted during launch preparation. Of the 1220 active measurements at lift-off, 13 failed completely and 34 were partially successful. The remaining measurements were successful.

A detailed analysis of the Saturn mission is contained in reference 13.

9.0 FLIGHT OPERATIONS

The information in this section is based on real-time observations, and, as a result, may differ from some of the detailed evaluations in other sections of the report which are based on final reduced data. Mission AS-201 was the first Apollo mission in which the Mission Control Center (MCC-H) at the Manned Spacecraft Center, Houston, Texas, was used for mission support.

9.1 Flight Control

Flight-control operational procedures established during preflight simulations allowed smooth operation of the Mission Operations Control Room (MOCR) and System Support Room (SSR) activities during the mission. Launch pad support activities were monitored to acquaint personnel with the type of data available during the various launch pad tests. These tests provided the systems engineers with an opportunity to view systems verification of all systems and to exercise the command link.

During the countdown the MCC-H and its interfaces, which included the MCC/network flight-control operations, were exercised at the proper times. The overall AS-201 mission operation and support plan is presented in figure 9.1-1.

Launch phase.- Lift-off occurred at 11:12:01 a.m. e.s.t. No radar tracking plots were available at MCC-H as a result of a power failure at Kennedy Space Center (KSC) at lift-off which caused both of the range safety impact predictor computers to fail. However, the Saturn instrument unit (IU) inertial data were used for driving the trajectory displays and plotboards for flight control. Power was restored to the range safety computers, and tracking data were available to the MCC-H 5 minutes after lift-off.

The trajectory was near nominal during the first-stage powered phase with the following discrepancies noted at MCC-H during S-IB stage powered flight:

(a) The switch selector events associated with the start of the J-2 engine were not available, probably as a result of the RF blackout during staging.

(b) Loss of synchronization of the IU telemetry data stream occurred at various times during the flight.

During the S-IVB stage powered flight, the switch selector events were not available at MCC-H for launch-escape tower (LET) jettison

A or B commands. However, other measurements including Q-ball internal temperature confirmed tower jettison.

Coast phase.- The following planned events and functions were noted by the flight controller during the S-IVB/CSM coast phase to CSM separation:

(a) Pitch-down initiation to desired service propulsion subsystem (SPS) firing attitude

(b) Fuel-tank venting and liquid hydrogen (LH_2) tank ullage pressure decay

(c) Liquid oxygen (LOX) tank blowdown

(d) Separation of the CSM from the S-IVB/IU and ARS readings.

Reports from the flight controller stationed on the Rose Knot Victor (RKV) ship during the SPS firing phase included the following:

(a) About halfway through the first burn the SPS oxidizer inlet pressure dropped and reached 141 psi. The SPS chamber pressure began fluctuating at the same portion of the burn with a general downward trend to 80 psia.

(b) The SPS engine was cut off by the backup timer in the control programmer.

(c) Chamber pressure fluctuation was erratic during second SPS burn.

(d) Telemetry was very noisy during the first 3 minutes of acquisition and numerous dropouts occurred during the signal reception period. Data were usable after approximately 2 minutes of acquisition.

Some last minute program changes in the RKV low-speed program caused some minor difficulties but did not affect the mission support.

Reentry phase.- The earth landing suibsystem (ELS) activate backup command was sent by the RKV, as planned, upon completion of the 180° roll maneuver of the command module at T+1515.1 seconds. No other ground commands were transmitted during the mission.

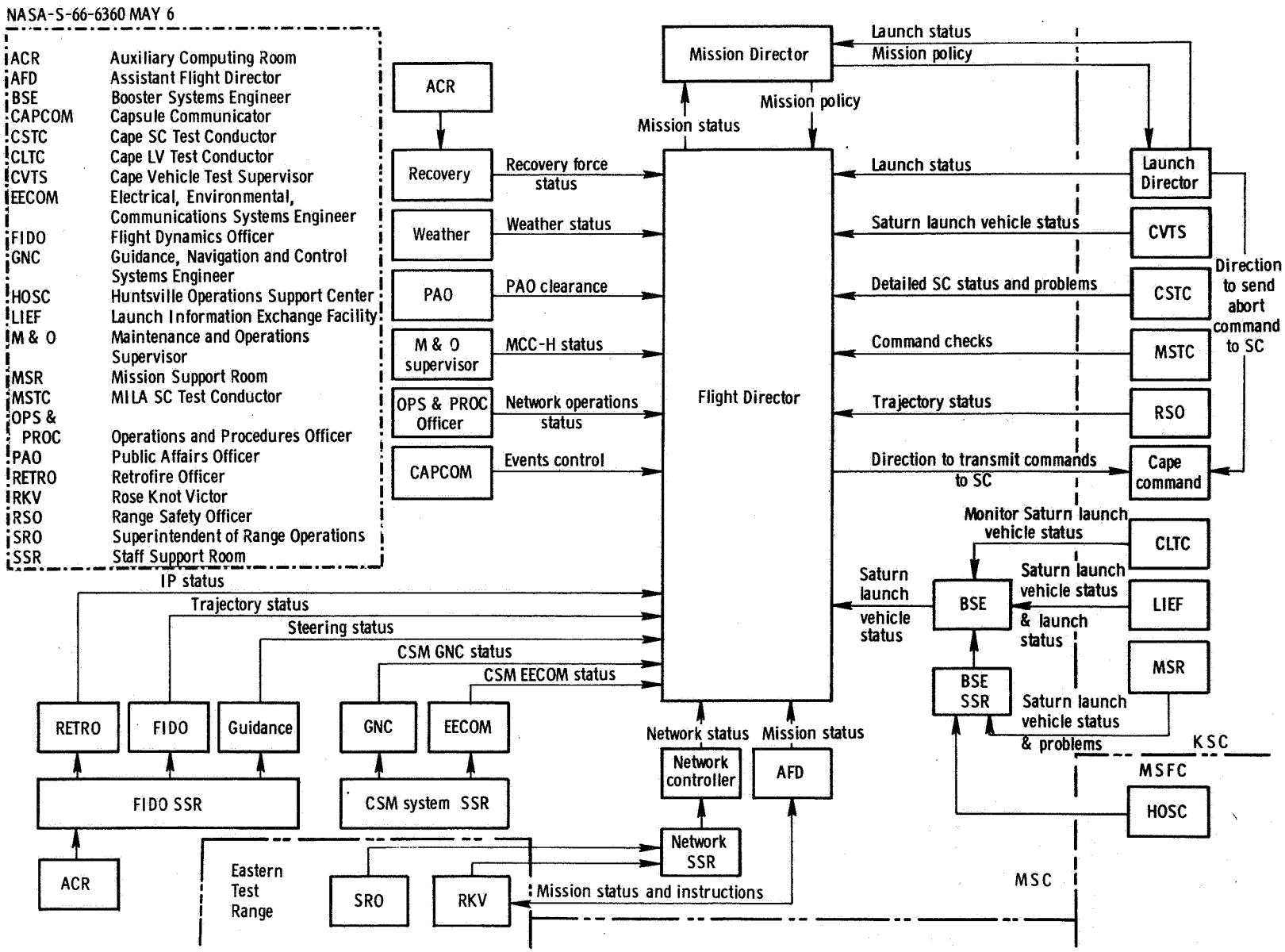


Figure 9.1-1.- Mission AS-201 operation and support plan.

9.2 Network Instrumentation and Communication

The network was put on mission status for Mission AS-201 at 2234 G.m.t. on February 14, 1966. Overall operation was satisfactory, with very few major problems being encountered.

The *only* major communications problem involved the break of the Air Force Eastern Test Range (AFETR) submarine cable to Antigua near Jupiter, Florida, at 0200 G.m.t. on February 23, 1966. A different route for data and voice was established, using leased circuits, and was used for the mission. The only significant radar problem resulted from the fact that the type of radar beacon/antenna system used aboard the CSM allowed only one antenna of the four to transmit to the ground at any one time. This prevented the other radars from effectively acquiring the spacecraft and will require close scheduling of radar site procedures for future flights.

No radar data were available at KC-H from T-0 to approximtely T+280 seconds because of the power failure at Cape Kennedy resulting in the loss of impact predictor (IP) computers. Radar and telemetry times for the mission are indicated in table 9.2-I.

The command subsystem configuration originally consisted of a tone remoting subsystem between MCC-H and ETR. The tone remoting subsystem was basically a system whereby a combination of specified tones was sent from a flight control console located at KC-H to key the ETR transmitter. During simulated confidence tests, it was found that the long-line system from MCC-H to Cape Kennedy was susceptible to noise bits which could generate spurious commands. As a result, a command system was established which made use of the ETR Satellite Operations Control Center (SOC) command capability. Commands were generated directly through the SOC by the MCC-H flight controller, on voice cue from the KC-H Flight Director, eliminating the use of the noisy long line. For succeeding missions it is planned to use a digital command system similar to the one used on Gemini missions.

The real-time computer complex (RTCC) at KC-H had no significant problems during the prelaunch period. The RTCC received no impact predictor data until approximately T+270 seconds. Bermuda data were received beginning at approximately T+360 seconds. The IU data were received throughout the launch phase. During reentry the RTCC received law-speed data from Grand Turk Island, Bermuda, Antigua, and Ascension Islands.

During the prelaunch count, the ETR real-time computer facility (RTCF) provided high-speed trajectory data support at T-270 minutes and T-160 minutes to MCC-H and Goddard Space Flight Center (GSFC). The RTCF experienced a power failure at lift-off resulting in the loss of

both computers until approximately T+280 seconds. The power failure was caused by a fuse holder being loosened by the launch vehicle blast and vibration. During reentry phase, present position data were computed and transmitted to MCC-K, and passed by voice direct to the recovery carrier.

The Goddard Real-Time Subsystem (GRTS) was used for the computation and data fluw integrated subsystem testing (CADFISS) during the pre-launch count. The GRTS accepted IP data by way of the launch monitor subsystem after T+270 seconds and drove the displays at MCC-K. High-speed radar data were accepted from Bermuda and law-speed radar data from the *supporting* network.

The Bermuda remote site data processor (RSDP) failed to accept any S-IVB telemetry data. Frame 30 in the A3 multiplexer had been chosen for the synchronous check for the data processor. When the multiplexer was shut off at lift-off, it caused the data to change in the bit stream. For Mission 202 the multiplexer is unchanged but has been reprogrammed so as to move the synchronous check to a different place in the bit stream where it would not affect the data.

TABLE 9.2-I.- RADAR AND TELEMETRY TIMES FOR MISSION AS-201

Station	Mode	Time, g.e.t., hr:min:sec			
		Radar		Telemetry	
		Acquisition (AOS)	Loss (LOS)	Acquisition (AOS)	Loss (LOS)
MLA	(2)	16:12:01	16:19:56		
CNV	(1)	16:12:01	16:15:31		
PAT	(1)	16:12:15	16:22:58		
TEL 2				16:12:01	16:17:44
TEL 3				16:12:01	16:17:10
GBI	(1)	16:13:37	16:17:13	16:12:41	16:24:36
GBI	(2)	16:13:29	16:24:06		
GTK[a]	(2)	16:15:37	16:27:54	16:15:21	16:27:01
BDA[a]	(2)	16:17:29	16:27:41	16:16:10	16:27:33
ANT[a]	(2)	16:19:59	16:31:02	16:15:21	16:27:01
RKV				16:28:40	16:39:00
ASC[a]	(2),(3)	16:34:61	16:41:07	16:33:34	16:49:36

[a]These stations used for trajectory computations.

NOTE: Radar mode

Beacon track - (1) IU/S-IVB
(2) CM/CSM
Skin track (3) CM/CSM

9.3 Recovery Operations

Recovery force deployment.- The planned landing areas for Mission AS-201 included: (a) hunch site landing area, (b) launch abort landing area, and (c) primary landing area.

Recovery forces were positioned within these areas so that any point in a given area could be reached within a specified access time.

A total of 6 ships, 13 aircraf't, and 10 helicopters, in addition to various special vehicles, were positioned in support of the mission. Ships and aircraft in the primary landing area are indicated in figure 9.3-1. Table 9.3-I lists the type of support provided in each of the planned *landing* areas.

Ships and aircraft and associated personnel providing recovery support were assigned from operational Department of Defense (DUD) units. Special equipment, such as shipboard spacecraft retrieval cranes, airborne UHF electronic receivers (homing systems), and spacecraft flotation collars, was furnished to the DOD by NASA.

Three HC-130 rescue aircraft, located in the vicinity of the primary landing area, had an additional capability of tracking the spacecraft with direction-finding equipment. Each of these aircraft received signals prior to entry into blackout, during main parachute descent, and after spacecraft landing.

Aircraft in the primary landing area included fixed-wing command and control aircraft to act as on-scene commander until arrival of the primary recovery ship, the USS Boxer, and helicopters. The helicopters provided location support and movement of swimmer teams, flotation equipment, and photographers to the *landing* point.

Location and retrieval.- First recovery force tracking information came from the HC-130H aircraft as they acquired signals (237.8 Mc) from the spacecraft beginning approximately 1500 nautical miles uprange of the primary landing area. Timely information was supplied by the aircraft at the beginning and end of blackout. Good signals were received by location aircraft from the command module beacon as the spacecraft descended on the main parachutes. Signal bearings and radar tracking from the USS Boxer indicated the spacecraft was descending approximately 45 miles uprange northwest of the aim point. At T+1653 seconds, (about 1 minute after SC landing) Search 1 and Air Boss 1 reported visual contact from over the spacecraft.

The swimmer and photography helicopter *from* the USS Boxer arrived at 1721 G.m.t. and deployed swimmers. The flotation collar was attached and fully inflated by 1732 G.m.t. (fig. 9.3-2). The back-up

swimmer team was deployed, and recovered the forward heat shield (fig. 9.3-3) and various pieces of associated ablative material floating within 1000 yards of the spacecraft. In addition, one of the liners from a drogue mortar was recovered.

The U.S.S. Boxer was alongside the spacecraft at 1858 G.m.t. and had a line attached to the spacecraft at 1904 G.m.t. The spacecraft was lifted from the water and secured aboard the ship at 1920 G.m.t. (fig. 9.3-4). The spacecraft, while being lifted, was at a greater angle (apparently due to water taken in under the heat shield) than planned and as indicated by the boilerplate used in simulations. This change in angle required greater head clearance over the deck and the dolly, making positioning on the dolly more difficult.

During spacecraft retrieval, attempts were made to retrieve the main parachutes which were still attached to the spacecraft. However, the drag created by the parachutes on the retrieving line was too great and the main riser was cut. After cutting the riser, swimmers were able to secure the parachutes to a large life raft. By this time darkness had set in and as the ship made its approach to pick up the drifting swimmers, life raft and parachutes, the currents created around the ship, acting on the parachutes, pulled the raft under water and broke the line securing the parachutes.

At 1620 G.m.t. on the launch day, personnel aboard the U.S.S. Wilson on station I (fig. 9.3-1) observed an exceptionally large splash about 6 to 7 miles uprange of the ship. The ship arrived at the observed point of splash approximately 12 minutes after it occurred. The debris was scattered over an area of approximately 500 yards square. Splash position was determined to be 26°59.5'N, 75°01'W. Samples of the debris were forwarded to MSFC for possible identification as being from the S-IB.

Observers in the planned landing area, both airborne and aboard ship, at about 1640 G.m.t., reported sighting contrails overhead passing in a downrange direction. Lookouts on the U.S.S. Boxer further reported seeing one object break into three parts with some fire and smoke surrounding the objects. Sighting elevation angles were 60° to 70° as objects passed out of sight in a downrange direction.

Recovery aides performance.- The spacecraft recovery aid HF (10.006 Mc) antenna was found to be deployed, but no signals were received by any of the recovery forces although they were receiving strong WWV signals (10 000 Mc).

Reception of signals from the UHF transceiver (296.8 Mc) was reported only by Air Boss 1 from 1641 G.m.t. to 1652 G.m.t. at a maximum range of 20 nautical miles.

The UHF telemetry (237.8 Mc) beacon was used by the three HC-130H rescue aircraft to track the spacecraft before and after blackout and to main parachute deployment with the DF equipment (ARD-17). The range at initial acquisition was approximately 1500 nautical miles.

The flashing light performed nominally with reported aircraft ranges up to 9 nautical miles. The recovery ship reported a range of 3 nautical. miles.

The dye marker was still active at spacecraft pickup time (1910 G.m.t.). Recovery aircraft reported ranges up to 8 nautical miles and the recovery ship reported a range of 2 nautical miles.

Postrecovery inspection.- Postrecovery procedures were performed in accordance with the Apollo Recovery Operations Manual:

(a) The Flight Qualification and Data Storage recorders were removed and returned direct to MSC.

(b) Visual inspection showed no excessive heating effects except between the RCS A ring roll thrusters.

Other observations included:

(c) Slight warping of crew compartment heat shield near hot areas.

(d) Active scimitar antenna in good condition with slight charring of ablator,

(e) VHF antennas and recovery light erected normally.

(f) HF antenna erected normally but was bent during retrieval and later cut off.

(g) Main parachute release on +Y side did not fire.

(h) *Aft* heat shield showed uniform burning. Gouges on heat shield were caused when the spacecraft was lifted aboard the handling dolly with insufficient hoisting clearance.

(i) Spacecraft windows had a slight film residue. The windows appeared to be in good condition with no cracks.

(j) Outer hatch appeared normal. It required 400 in-lb to unlatch.

(k) Inner hatch required slightly over 600 in-lb to unlatch, 300 in-lb to relatch, and 300 in-lb to re-open,

(l) Approximately 1 and 1/2 quarts of water were in the bottom of the spacecraft.

(m) A burnt odor was noticed inside the spacecraft.

(n) Laboratory type mercury thermometer (scale 0 to 230° F) was found lying loose on the spacecraft floor.

(o) Two screws were missing from the cover of the Data Storage Equipment recorder.

(p) Condensation on various surfaces was noticed.

The spacecraft was off-loaded at Norfolk, Virginia on March 6, 1966, and RCS deactivation procedures were initiated.

Deactivation was completed March 10, 1966, and the spacecraft was loaded aboard a C-133B aircraft which departed Norfolk the evening of March 10, 1966, and arrived at Long Beach Municipal Airport on March 11, 1966. The spacecraft was then moved to the contractor's Dmey facility for postflight testing and analysis.

TABLE 9.3-I.- RECOVERY SUPPORT FOR MISSION AS-201

Landing area	Access time		Support
	Ships	Aircraft	
Launch site	-	15 min	4 HH-3C helicopters 4 LARC 2 LVTR 1 MSO 1 Range boat 1 LCU 1 Bulldozer 1 Crane 1 Truck
Launch abort	24 hr	3 hr	4 Destroyers 1 Oiler 7 HC-97 aircraft
Primary	7 hr	2 hr	1 LPH 6 SH-3A helicopters (1 photo, 2 swimmers, 3 search) 3 HC-130H aircraft (search and rescue) 3 P-3A aircraft (Air boss)
		Total	6 Ships 13 Aircraft 10 Helicopters

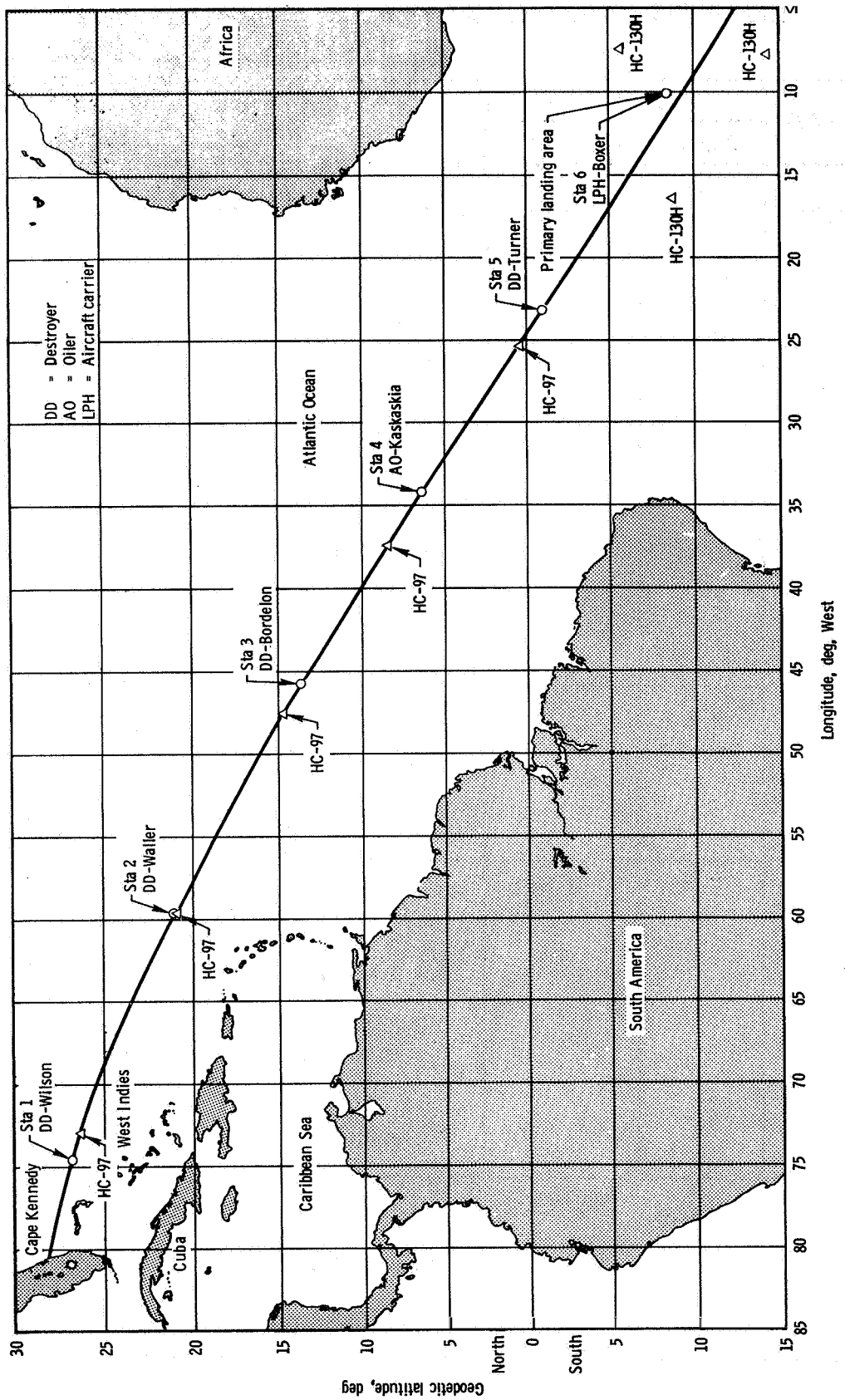


Figure 9.3-1.- Recovery force deployment, Mission AS-201.

NASA-S-66-3362 MAY 6



Figure 9.3-2.- Spacecraft in water, collar attached, Mission AS-201.

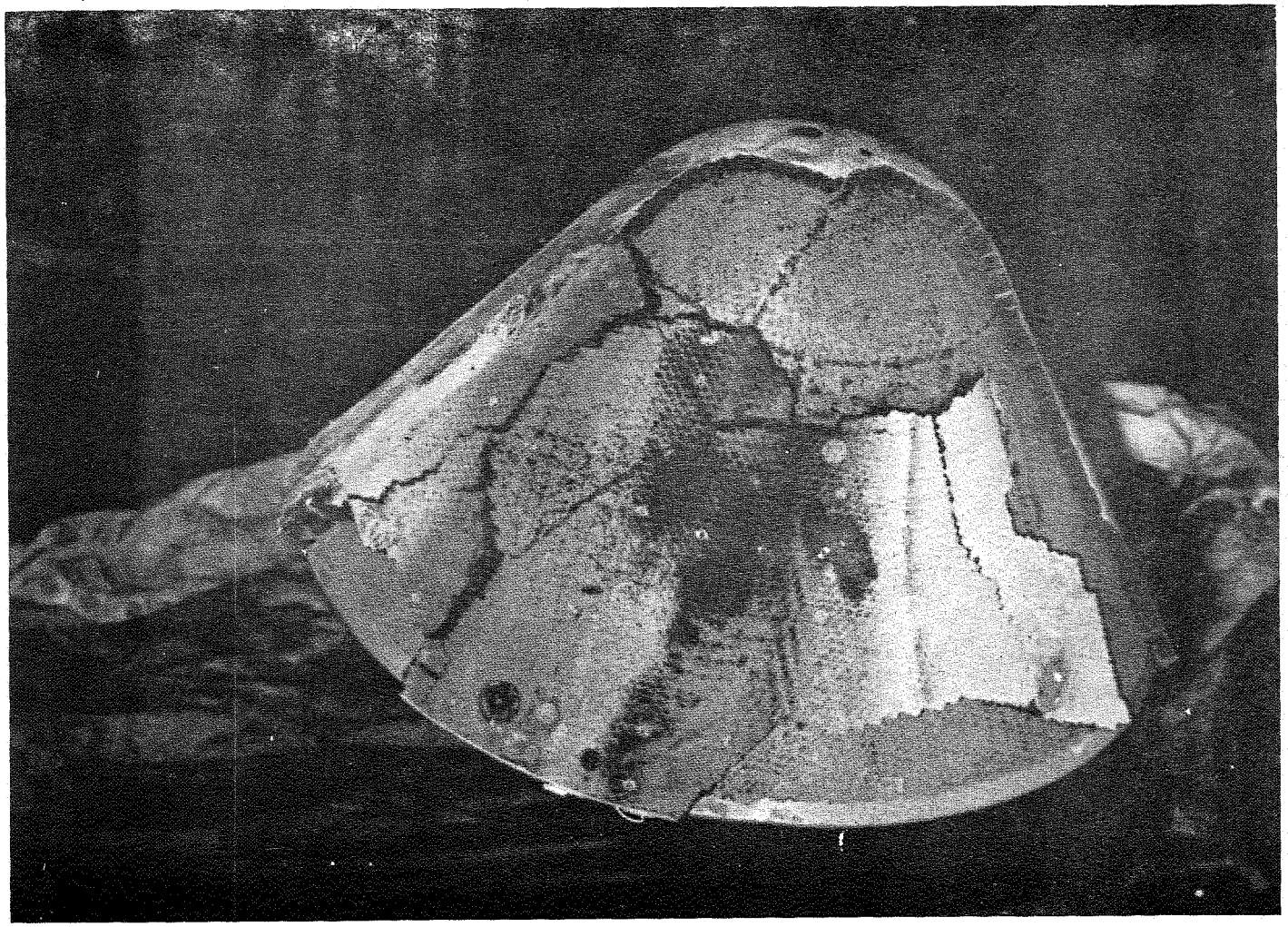


Figure 9.3-3.- Forward heat shield, Mission AS-201.

NASA-S-66-6364 MAY 6

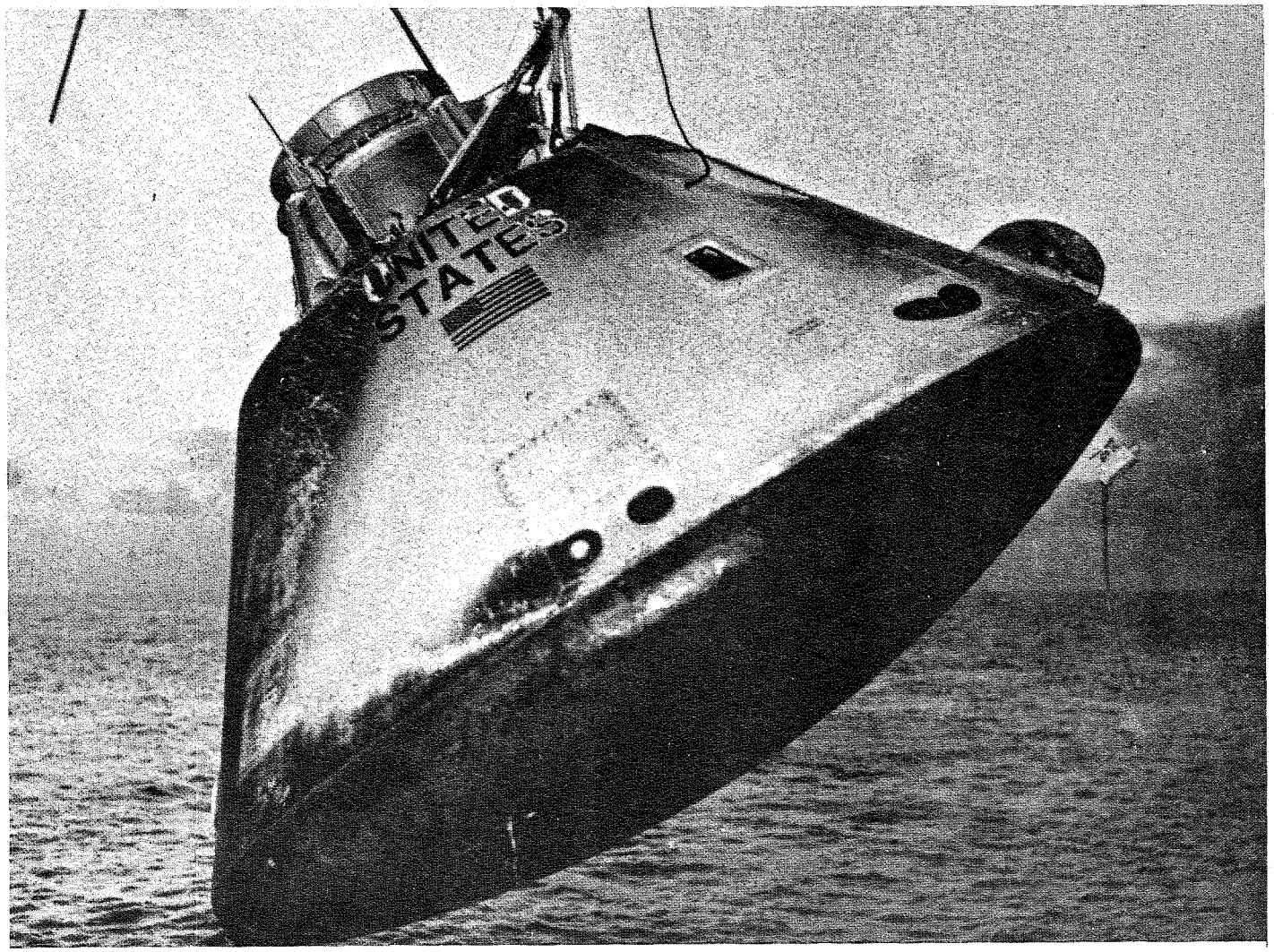


Figure 9.3-4.- Spacecraft being hoisted aboard U.S.S. Boxer Mission AS-201.

10.0 POSTFLIGHT TESTING AND ANOMALY SUMMARY

10.1 Postflight Testing

Planned postflight testing for analysis of suibsystem performance and the resolution of anomalies occurring during the flight of Mission AS-201 were conducted at the contractor's facility and at MSC. Each of the following items, which are discussed in further detail elsewhere in this report, is noted in the section referenced in parenthesis.

(a) Radioactive sensors in the aft heat shield - The radioactive sensors were removed from the aft heat shield. During reentry the sensors had failed, allowing approximately 1.5 mCi of cobalt 60 to evaporate and be redeposited on the aft heat shield, resulting in low-level radioactivity readings on the heat shield. This type sensor will not be utilized on subsequent spacecraft (not discussed elsewhere in this report since no radioactivity data were collected as a result of the sensor failure).

(b) Electrical power subsystem - Electrical continuity checks and analysis of the main buses A and B, pyro buses A and B, reaction control suibsystem (RCS), stabilization and control subsystem (SCS), instrumentation, circuit breakers, relays, batteries, inverters, controls, et cetera, were conducted in the spacecraft with the mission programer and sequencers in place. Bench tests were performed on the sequencer, and vibrational environmental tests were performed *on* the control panel for evaluation of circuit breaker 18 (section 7.12).

(c) Command module leak tests - Pressure tests were performed *on* the command module (CM) to a pressure level of 6.5 psig to check the cabin leak rates, (section 7.17).

(d) Cabin pressure relief valve tests - Pressurization and vacuum tests were conducted on the cabin pressure relief valve while it was still installed in the spacecraft. The valve was removed and further pressure, vacuum, and environmental vibration tests were conducted (section 7.17).

(e) Crew window tests - The crew windows were removed for chemical analysis, transmissibility tests and emission spectrographic analysis, and stress studies (section 7.19).

(f) Instrumentation measurement tests - Postflight electrical continuity tests were conducted on all questionable instrumentation measurements prior to removal of equipment from the vehicle. Calibrations were completed on those measurements requiring such action (section 7.13).

(g) HF beacon - Transceiver continuity, signal radiations, frequency output, and salt water spray and immersion tests were performed on the beacon and HF antenna as installed in the spacecraft with nod flight circuits and mission programmer (section 7.16).

(h) Waste water, water-glycol and cabin air tests - Samples of gases from the spacecraft cabin, waste water from the water management subsystem, and water-glycol from the environmental control subsystem were subjected to laboratory analysis (section 7.17).

(i) Acoustic transducer calibration - Cabin acoustic transducers were removed from the cabin and sent to the vendor for examination and calibration (section 7.18).

(j) Heat shield - Cores were cut from preselected areas of the crew compartment and aft heat shield for study of char and reentry heating effects. Core samples were split and sent to the vendor and to MSC for study and evaluation (section 7.4).

(k) Environmental control unit - The environmental control unit was removed at the contractor's Downey plant and shipped to the vendor for temperature control, evaporator rate, sensor calibration, and inspection. Sensor calibration testing is incomplete (section 7.17).

(l) VHF/AM transmitter - The transmitter was removed from the spacecraft and subjected to bench checks (section 7.16).

(m) Reaction control subsystem tests - Postflight testing was conducted on the propellant isolation valves, oxidizer and fuel tank bladders, engine solenoid valves and relief valve burst diaphragms. The propellant tanks were removed to investigate contamination levels and two engines were removed and sent to the vendor for sectioning (section 7.9).

(n) A 1/5-scale model of the SPS zero g can was built at MSC and used to simulate the helium ingestion condition experienced on this flight. Similar testing was done at contractor's facility and full-scale tests were conducted at the White Sands Test Facility with spacecraft 003. (section 7.7).

10.2 Summary of Failures, Malfunctions, and Deviations

Definitions.- In this report, the terms failure, malfunction, and deviation are defined as follows:

(a) A failure is the inability of a system, subsystem, component, or part to perform its required function within specified limits, under specified conditions, for specified duration. A catastrophic failure is a failure resulting in the immediate loss of the mission.

(b) A malfunction is an extremely faulty operation of an individual component, subsystem, or system.

(c) A deviation is a significant difference between precalculated, or expected, parameters and actual parameters. The value of the actual deviation parameter may indicate either superior or inferior conditions to those precalculated or expected, and may or may not be within mission specifications.

The failures, malfunctions, and deviations for Mission AS-201 are summarized for documentary purposes as follows. The report section numbers indicate where the items are discussed.

Failures.-

(a) No signals were received from the HF transceiver (section 7.16).

(b) The radiation capsules in the aft heat shield failed structurally during reentry heating, allowing the vaporized contents to enter the surrounding ablator, precluding the acquisition of radiation data from this mission (section 10.1).

(c) Four thermocouples in the aft heat shield failed below the thermocouple specification maximum temperature, and nine thermocouples and five calorimeters produced no data (sections 7.4 and 7.15).

(d) Mechanical failure in the two acoustic sensors resulted in only partial data being received (sections 7.15 and 7.18).

(e) The service module reaction control subsystem quad A engines did not fire (section 7.9).

Malfunctions.-

(a) The service propulsion subsystem performance was below nominal (section 7.7).

(b) The equivalent of one negative yaw engine in either quad B or quad D, of the service module reaction control subsystem, was inoperative (section 7.9).

(c) Fuel and oxidizer were found on the helium side of the reaction control subsystem (section 7.9).

(d) Leaking oxidizer isolation valves were found in the command module reaction control subsystem (section 7.9).

(e) Nondeadfaced 28 volt wires shorted after CM/SM umbilical disconnect (section 7.12).

Deviations. -

(a) There were high lateral acceleration readings on the tower accelerometers prior to, and at lift-off (section 7.2).

(b) Spacecraft - LEM adapter skin panel vibration levels at S-IB ignition exceeded lift-off criteria (section 7.2).

(c) Sealant material around the CM/SM tension ties insulation was omitted, allowing hot gas entry (section 7.4).

(d) The side ablative hatch latch required excessive torque to release during the recovery operation (sections 7.5 and 9.3).

(e) The existence of an invariant 40-bit word and the nominal wow and flutter of the onboard recorder resulted in ground station data processing difficulties (section 7.15).

(f) Two screws were missing and one screw was found loose in the data storage equipment onboard tape recorder cover (section 7.15).

(g) A low water-glycol evaporator outlet temperature occurred during the flight (section 7.17).

(h) The cabin pressure was regulated slightly above specification limits (section 7.17).

(i) A small quantity of water was found in the crew compartment after the flight (section 7.17).

11.0 CONCLUDING REMARKS

Mission AS-201 demonstrated the structural integrity of a Block I type ApoUo spacecraft, for a nominal Saturn IB hunch trajectory and the compatibility of the spacecraft with the S-IB Launch vehicle. The structural loads imposed during launch fell within acceptable limits.

Satisfactory separation of the S-IVB from the S-IB, the launch escape subsystem and boost protective cover from the command and service module, the command and service module fromthe spacecraft, = LEM adapter, and the command module from the service module occurred as planned Without excessive spacecraft loads.

Launch vehicle propulsion, guidance and control, and electrical subsystems performed adequately throughout the boost phase, with no abort signals generated by the spacecraft emergency detection subsystem.

The service propulsion subsystem started in a space environment and operated satisfactorily for 80 seconds. The chamber pressure then deteriorated about 30 percent because of helium ingestion. As a result of the helium ingestion, restart and second burn were erratic.

Satisfactory performance of the partial environmental control subsystem installed on spacecraft 009 was obtained with the exception of low water-glycol evaporator outlet temperature.

Operation of the electrical power subsystem was as planned until after initiation of reentry when some 28-volt non-deadfaced power wires shorted in the umbilical stub causing seven circuit breakers to open, thus affecting several subsystems.

Loss of attitude control due to the electrical power subsystem malfunction resulted in a rolling reentry, instead of the planned lifting reentry, which was damped-out following drogue deployment.

The service module reaction control subsystem satisfactorily provided attitude and rate control, and +X translation (less than nominal) with quad A inactive and one of the negative yaw engines inoperative.

Operation of the command module reaction control subsystem was as planned until the electrical power subsystem malfunction. The stabilization and control subsystem operated as planned throughout the mission.

The command module heat shield performed satisfactorily and demonstrated the capability of protecting the command module for a manned low earth orbital reentry.

The earth landing subsystem and the recovery aids performed satisfactorily with the exception that no signals were received from the HF transceiver, and, due to the electrical power subsystem malfunction, one leg of the main parachute harness was not disconnected.

In general, the desired flight measurements were obtained, except during the period of maximum reentry heating.

Satisfactory operation of the mission support facilities required for launch, mission operations, and recovery was demonstrated.

12.0 APPENDIX A

12.1 Spacecraft History

The Apollo spacecraft 009 command module (CM), service module (SM), and the launch-escape subsystem (LES) structure were initially assembled and checked out at the contractor's facility at Downey, California (fig. 12.1-1). After an integrated systems test and Customer Acceptance Readiness Review (CARR) were completed October 20, 1965, the CM, SM, and LES structures were shipped from Downey, California, to the John F. Kennedy Space Center (KSC), Florida.

At KSC, the U S motors, pyrotechnics, and earth-landing subsystem (ELS) were installed and the CSM and spacecraft - U M adapter (SLA) were mated. (A list of significant KSC milestones is shown in fig. 12.1-2.) The CM, SM, SLA, and U S were stacked on top of the Saturn IB launch vehicle at KSC launch complex 34.

The preflight checkout of spacecraft assemblies, subsystems, and integrated systems at Downey and at KSC, was performed in accordance with operational checkout procedures (OCP) for spacecraft 009.

The countdown at launch complex 34 was started at 7:00 p.m. e.s.t. on February 20, 1966, and proceeded on schedule to T-13 hours. At 6:17 p.m. e.s.t. on February 22, the launch was delayed 24 hours due to adverse weather in the launch area. A resumption of the countdown was rescheduled for 5:15 p.m. e.s.t. on February 23; however, after re-evaluating the weather on February 23 and February 24, two additional 24-hour delays were required and countdown was resumed at 5:15 p.m. e.s.t. on February 25 at T-13 hours. After several unscheduled holds in the count (section 12.3), lift-off occurred approximately 18 hours later, at 11:12 a.m. e.s.t.

After landing in the primary landing area, the command module was located and retrieved by the recovery forces (see section 9.3), and transported to Norfolk, Virginia, aboard the recovery ship, U.S.S. Boxer. After decontamination at Norfolk, the CM was shipped by air to the contractor's Downey facility for inspection and postflight testing (section 10.1).

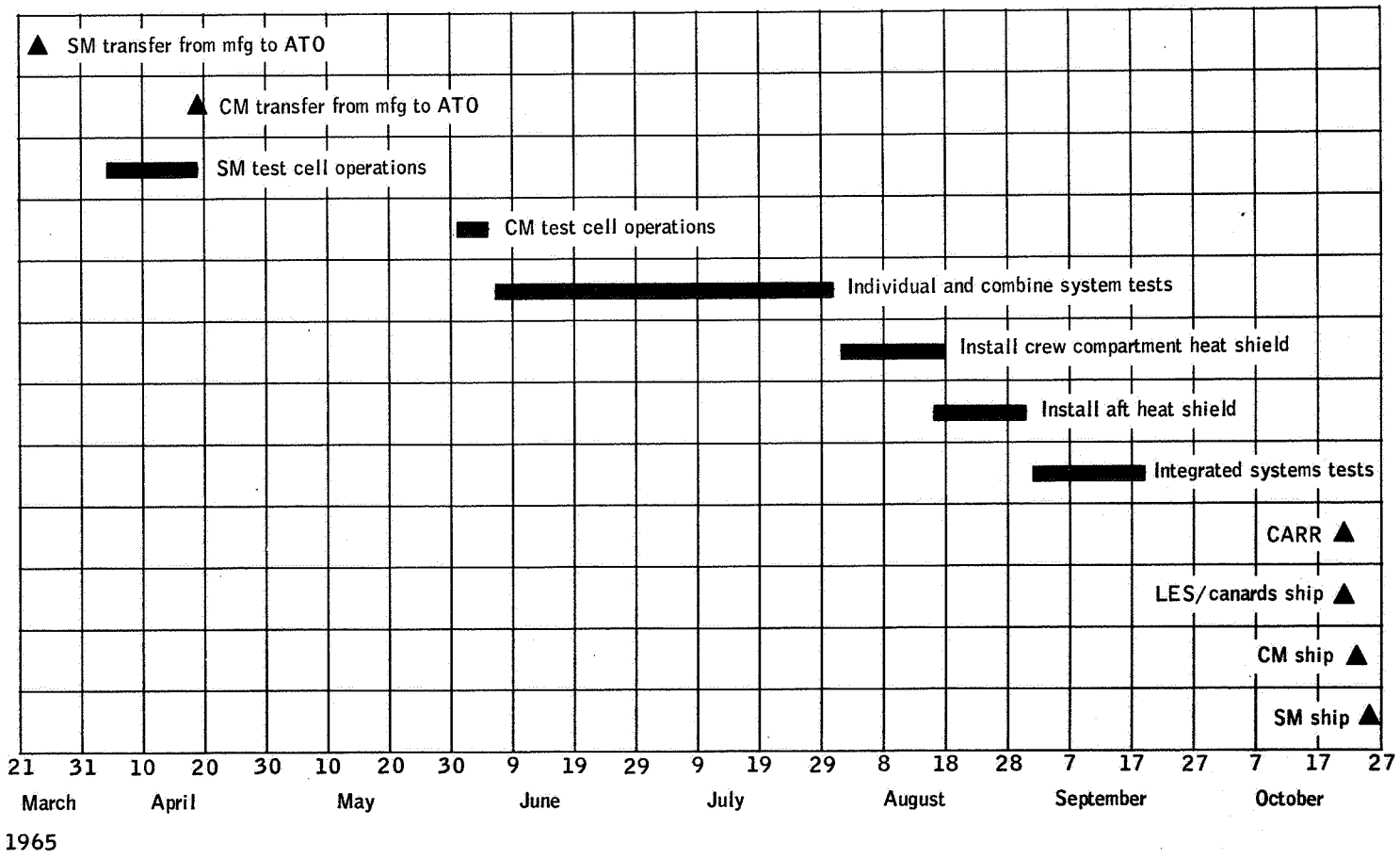


Figure 12.1-1.- Apollo spacecraft 009 at Downey, preflight.

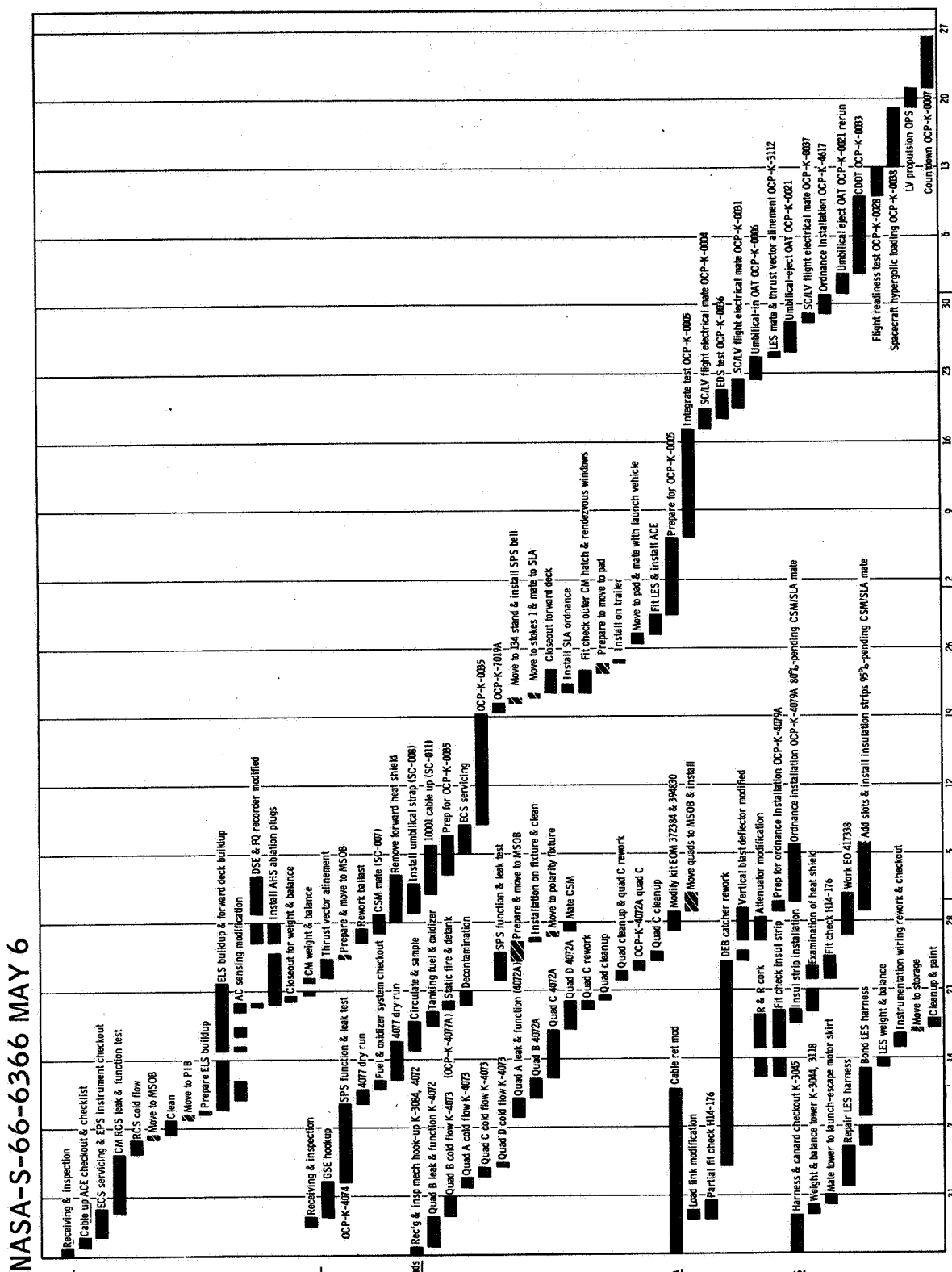


Figure 12.1-2.- Apollo spacecraft 009 at Cape Kennedy, preflight.

12.2 Launch Operations

The launch precount and countdown operations for Mission AS-201 were accomplished during the period from February 20 to 26, 1966, as indicated in figure 12.2-1. The precount operation on spacecraft 009 was picked up at T-52 hr 30 min at midnight on February 20, 1966. Ground support equipment (GSE) and spacecraft power-up had been performed prior to the start of the precount. The precount was scheduled to take 3 hours 30 minutes, but was not completed until T-47 hr 11 min (approximately 1 hr 49 min late) because of ACE ground station problems (section 12.2) involving both computers and timing anomalies to the computers. The only spacecraft anomaly encountered in the precount was an open telemetry measurement for the service propulsion system (SPS) helium tank temperature (measurement SP0002T). This was corrected prior to helium servicing.

Pyrotechnic power-off stray voltage checks and hook-up were started at 5:30 a.m. e.s.t. on February 21 (T-47 hr) and were completed at 11:30 a.m. e.s.t. (T-41 hr). Local and remote resistance checks of the pyro circuits were then initiated and finally completed at 2:40 p.m. e.s.t. on February 21 (T-37 hr 50 min), approximately 3 hours 10 minutes behind the scheduled operation. Problems with the pyro test equipment and procedural clarifications were the main reasons for the delay encountered in the pyro work.

Preparations for helium servicing, including disconnection of ACE carry-on equipment and installation of access doors, were started at 3:00 p.m. e.s.t. on February 21 (T-37 hr 30 min) and completed at 3:30 a.m. e.s.t. on February 22. At that time GSE and spacecraft power-up was initiated in preparation for helium servicing. At 5:30 a.m. e.s.t. on February 22 the countdown clock was held at T-23 hours for a scheduled built-in hold of 1 hour 45 minutes.

At 6:00 a.m. e.s.t. on February 22 spacecraft helium servicing was initiated approximately 1 hour 15 minutes ahead of schedule. The overall helium servicing operation was scheduled to take 5 hours 30 minutes, but was not completed until approximately 3:00 p.m. e.s.t. The additional 3 hours 30 minutes was due to numerous problems with the helium servicing GSE and procedural problems with the service module reaction control subsystem (SM RCS) vacuum bleed operation. Countdown time at the completion of helium servicing was T-15 hr 15 min. Disconnection of the spacecraft facility hypergolic lines had been worked in parallel with the disconnect of spacecraft to GSE lines; as a result the scheduled 4 hours of pad clear time were not required for that task.

Close-out of spacecraft access panels and installation of the boost protective cover proceeded from 3:00 p.m. e.s.t. on February 22 until 5:15 p.m. e.s.t. when the countdown was held at T-13 hours for an

estimated 24-hour weather delay. The hold for weather continued for 72 hours until 5:15 p.m. e.s.t. on February 25. During the hold period, power continued to be applied to the spacecraft, and all system parameters were monitored for variation. At 10:00 p.m. e.s.t. on February 24, a check was made of the command module and service module flight qualification instrument systems and the pyro battery voltages were checked.

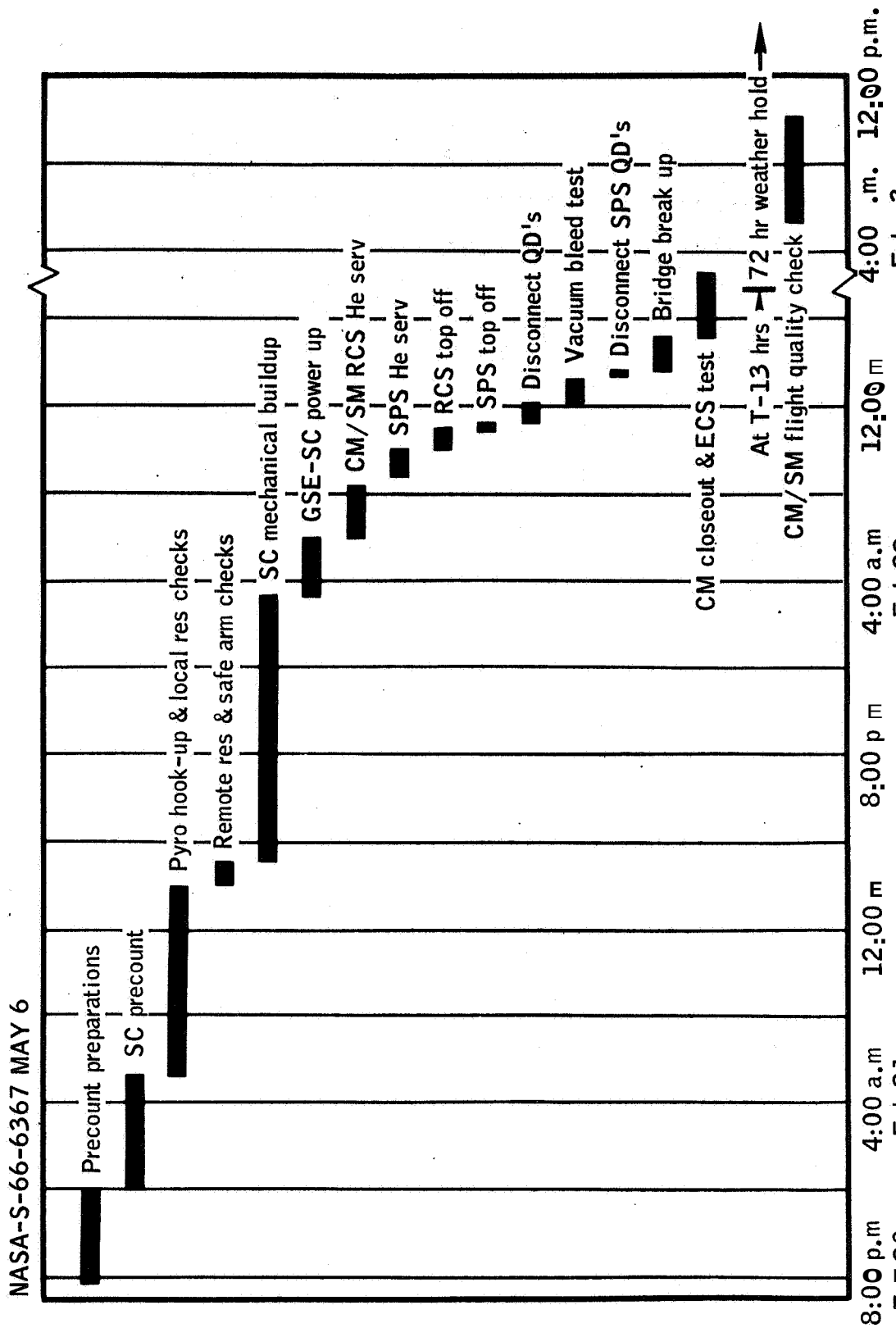
The countdown was resumed at T-13 hr at 5:15 p.m. e.s.t. on February 25. All spacecraft functions were accomplished according to the count and the countdown continued to T-9 hr 20 min at 8:55 p.m. e.s.t. At this time the count was held for the planned 30-minute built-in hold period. The count was resumed at T-9 hr 20 min (9:25 p.m. e.s.t.). A problem was encountered during the white room latch up and troubleshooting activity delayed moving the service structure for approximately 1 hour 35 minutes.

The spacecraft RE checks were completed at 2:34 a.m. e.s.t. on February 26 while the count was being held at T-4 hr 26 min to complete liquid oxygen (LOX) loading. The count was resumed at 2:49 a.m. e.s.t. and LOX loading was completed at 3:00 a.m. e.s.t. Liquid hydrogen (LH_2) loading was delayed while a helium regulator problem was corrected.

At 3:30 a.m. e.s.t. (T-3 hr 45 min), while the helium regulator problem was being corrected, the hatch closeout period was moved forward and the crew was on station on the access arm at T-3 hr 15 min. During performance of final switch checklist the spacecraft operations office (SCO) was unable to verify the pre-set position of the stabilization and control subsystem (SCS) thumbwheels. At 4:55 a.m. e.s.t. spacecraft personnel cleared the access arm and at 5:17 a.m. e.s.t. (T-1 hr 58 min) the launch vehicle LH_2 loading was started. At 5:45 a.m. e.s.t. (T-1 hr 30 min) the count was held for 30 minutes to complete LH_2 loading. The count was resumed at 6:15 a.m. e.s.t.

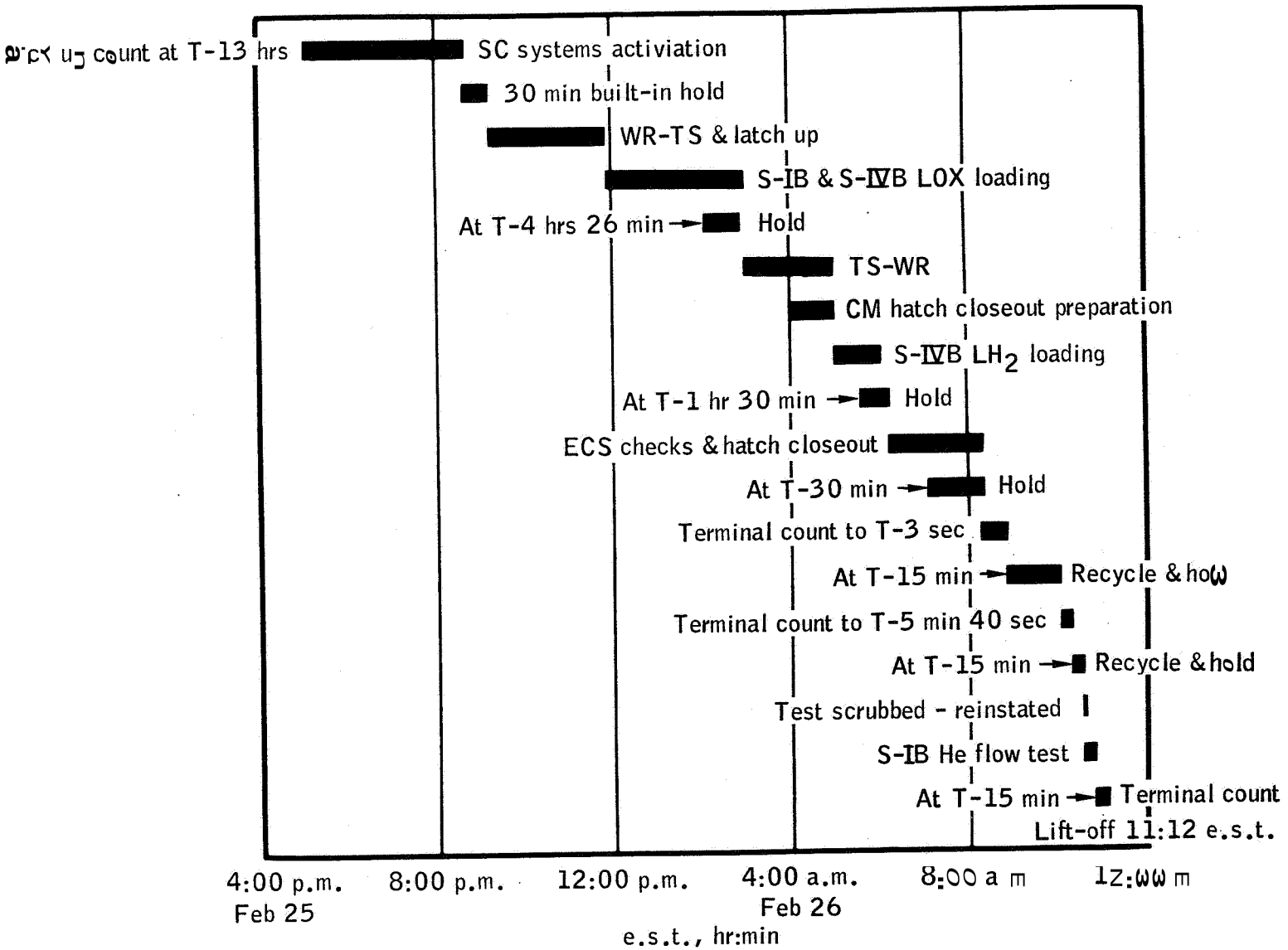
The spacecraft closeout crew was back on the access arm at 6:17 a.m. e.s.t. (T-1 hr 28 min). The SCS thumbwheel settings were reverified, the installation of the inner hatch was completed at 6:51 a.m. e.s.t., and environmental control subsystem (ECS) checks were started. The count was held again at T-30 min (7:15 a.m. e.s.t.). The cabin leak check was completed at 7:25 a.m. e.s.t. with an acceptable leak rate of 3 pounds/hour. All remaining ECS functions were complete by 7:35 a.m. e.s.t. The outer hatch installation was complete at 7:53 a.m. e.s.t. and the boost protective cover (BPC) installation was started. Two BPC fasteners were broken off during installation causing a 1/8-inch protrusion of the upper edge for a distance of approximately 4 inches. The gap was taped and the BPC installation was completed at 8:30 a.m. e.s.t. The access arm was swung back and the count was resumed at T-30 min at 8:33 a.m. e.s.t.

The count continued until T-3 sec when a cutoff was received because of a failure of a 3000-psi helium pressure switch in the Saturn IB ready circuit. At 9:11 a.m. e.s.t. the count was recycled to T-15 min and holding, The count was picked up at T-15 min at 10:17 a.m. e.s.t. At T-5 min 40 sec the count was held and then recycled to T-15 min because of additional information from Marshall Space Flight Center analysts in regard to the 3000-psi helium problem. The test was canceled at 10:45 a.m. e.s.t. and then reinstated again at 10:57 a.m. e.s.t. The count was picked up at T-15 min at 10:57 a.m. e.s.t. At T-4 min 20 sec the spacecraft battery relay bus voltage was reported at 0.3 V below the acceptable limit. The out-of-tolerance condition was accepted for flight and the count continued to lift-off (11:12 a.m. e.s.t.) with no further anomalies.



(a) February 20th through 23rd.

Figure 12.2-1.- Countdown, Mission AS-201.



(b) February 25th through 26th.

Figure 12.2-1.- Concluded.

13.0 APPENDIX B

13.1 Photographic Coverage

Photographic coverage required for the analysis of spacecraft 009 for Mission AS-201 included both motion and still photography, and consisted of engineering sequential launch film, tracking film, recovery film, and preflight and postflight views of components, assemblies, and systems which confirmed their configuration and visual condition.

The locations of the cameras used in covering the launch phase of the mission in relation to the launch pad and the ground track are shown in figures 13.1-1 and 13.1-2.

Of the 10 requests by MSC in the Program Support Requirements Document (PSRD) for engineering sequential film and tracking film coverage, only five could be fulfilled. The remainder of the requests could not be met for lack of available equipment or facilities at the time of launch, and because the cameras ran out of film when eight automatic-start, fixed, high-speed cameras started at the time the countdown was recycled at T-5 seconds.

Table 13.1-I presents an evaluation of the content coverage of the films available for analysis of the spacecraft performance.

TABLE 13.1-I.- ACTUAL PHOTOGRAPHIC COVERAGE, MISSION AS-201

Identification (a)	Camera location	Tracking film: Film (all color) Size,	Tracking film: Film (all color) Frame rate, fps	Tracking film: Lens	Remarks
Item 1.2-18	Melbourne Beach, Fla.	5	3	500 in.	First acquisition starts just after S-IB ignition and lift-off. Vehicle is out of focus during first part of lift-off; however, this is not objectionable. Following scenes are good: S-IB burn inboard and outboard engine cutoff, retrofire, S-IB separation, S-IVB ignition, tower-jettison motor fire, launch-escape tower separation and tumble. Camera is at a near right angle to flight path and covers right side of vehicle.
Item 1.2-19	Vero Beach, Fla.	5	3	500 in.	First acquisition starts just after S-IB ignition and lift-off. Vehicle is out of focus during first part of lift-off; however, this is not objectionable. Following scenes are good: S-IB burn inboard and outboard engine cutoff, retrofire, S-IB separation, S-IVB ignition, tower-jettison motor fire, launch-escape tower separation and tumble. Camera is at a near right angle to flight path and covers right side of vehicle.
Item 1.2-15	Kennedy Space Center, Fla.	70	3	360 in.	First acquisition starts just after S-IB ignition and lift-off. Film is slightly underexposed. Following scenes are fair: S-IB ignition, inboard and outboard engine cutoff, retrofire, S-IB separation, S-IVB ignition, tower-jettison motor fire, launch-escape tower separation. Camera is just behind vehicle focused at exhaust nozzles after pitchover.
Item 1.2-6	Kennedy Space Center, Fla.	5	96	80 in.	First acquisition starts at T-5 sec. S-IB ignition and lift-off obscured by heavy smoke. Film shows a close-up of vehicle on launch pad prior to ignition and picks it up again just after lift-off as smoke thins out. Entire vehicle is shown as it gradually pitches over. Most of film presents a view looking into the S-IB nozzles.
Item 1.2-13	Kennedy Space Center, Fla.	16	64	40 in.	First acquisition starts at lift-off. Film is underexposed and too dark for engineering value.
Item 1.2-14	Kennedy Space Center, Fla.	16	64	40 in.	First acquisition starts at T-125 sec on launch pad. Camera is centered on the CM and LES tower at lift-off. Lift-off and pitchover are good. Most of film shows S-IB burn looking at exhaust nozzles. Film ends with S-IB still burning.
S 6-129	Kennedy Space Center, Fla.				First acquisition starts after lift-off and following scenes are fair: S-IB burn, pitchover, inboard and outboard engine cutoff, retrofire, S-IB separation, S-IVB ignition. Entire film is slightly overexposed.
Item 1.2-5	Kennedy Space Center, Fla.	35	96	80 in.	First acquisition starts at T-5 sec. Camera is centered on S-IB. Following scenes are fair: S-IB ignition, lift-off, inboard and outboard cutoff, retrofire, separation, S-IVB ignition. Film is slightly underexposed and out of focus.
	Aircraft				First acquisition starts just after lift-off. Vehicle is a very small image; however, length of S-IB plume in relation to vehicle length is shown very well.

[a] Item i DOD identification; E & T technical engineering specification; S-66 & MSC identification.

TABLE 13.1-I.- ACTUAL PHOTOGRAPHIC COVERAGE, MISSION AS-201 - Concluded

Identification [a]	Camera location	Film (all color) Size,	Film (all color) Frame rate,	Lens	Remarks
Engineering film (fixed camera)					
E-79	34-3	1	200	50	First acquisition starts at T-5 sec. Fixed camera is centered on CSM area and shows SC umbilical disconnect at ignition; however, heavy smoke covers vehicle during lift-off. This camera is located almost directly behind vehicle (800 ft).
E-80	34-4	1	200	70	First acquisition starts at T-5 sec. Fixed camera is centered on CSM area and shows SC umbilical disconnect and swing away. Camera is located at right angles to vehicle and covers left side of vehicle.
Recovery film					
S-66-92	Recovery ship, U.S.S. Boxer	16	24		Acquisition from 5:15 p.m. G.m.t. until sunset. Film is a little underexposed. Following scenes are fair: CM alongside of recovery ship, swimmers getting line from ship and attaching it to CM, close up of CM upper deck, CM being lifted from flotation collar and placed on dolly onboard ship, water draining from main heat shield, damage to main heat shield, dye marker container, scimitar antenna, RCS nozzles, removal of main hatch, inside CM showing onboard recorder.
S-66-93	Two helicopters	16	32 to 48		Acquisition from 5:15 p.m. G.m.t. until sunset. Two films of same recovery operation. Following scenes are good: swimmers jumping out of helicopter, swimmers attaching flotation collar to CM, dye marker pattern removing aids, blinking light, one main parachute riser still connected to CM. A great deal of film is of little engineering value in that it just shows local scenery.
S-66-94	Recovery ship, U.S.S. Boxer	16	24		Acquisition from 5:15 p.m. G.m.t. until sunset. Following scenes taken from recovery ship are good: CM in flotation collar next to carrier, close up of CM upper deck and recovery aids, close-up of drogue parachute mortar cans and RCS motors, CM being lifted onto carrier and placed in dolly, main heat shield, main hatch window.

[a] Item is DOD identification; E is technicolor identification; S-66 is MSC identification.

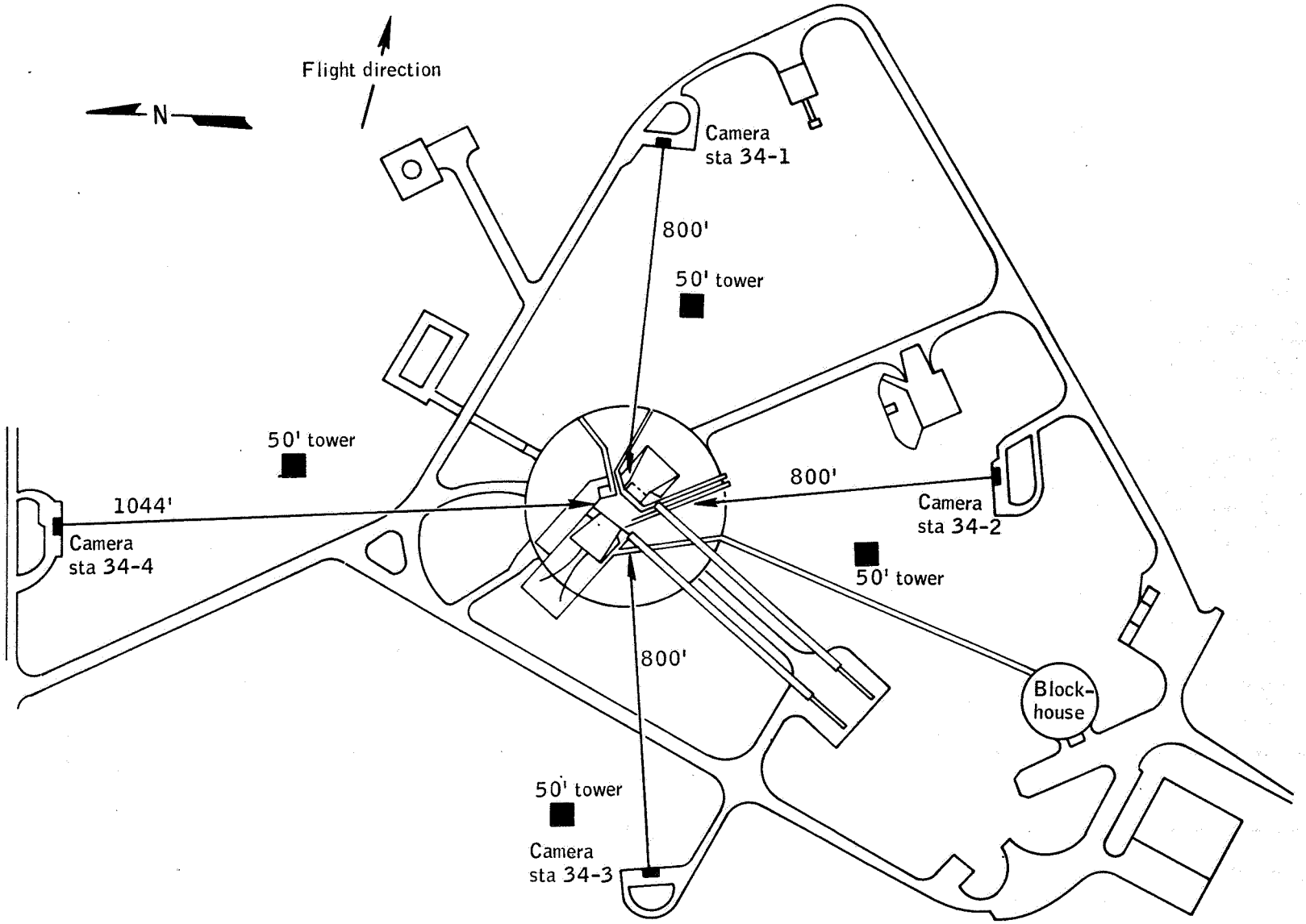


Figure 13.1-1.- Camera locations, Mission AS-201.

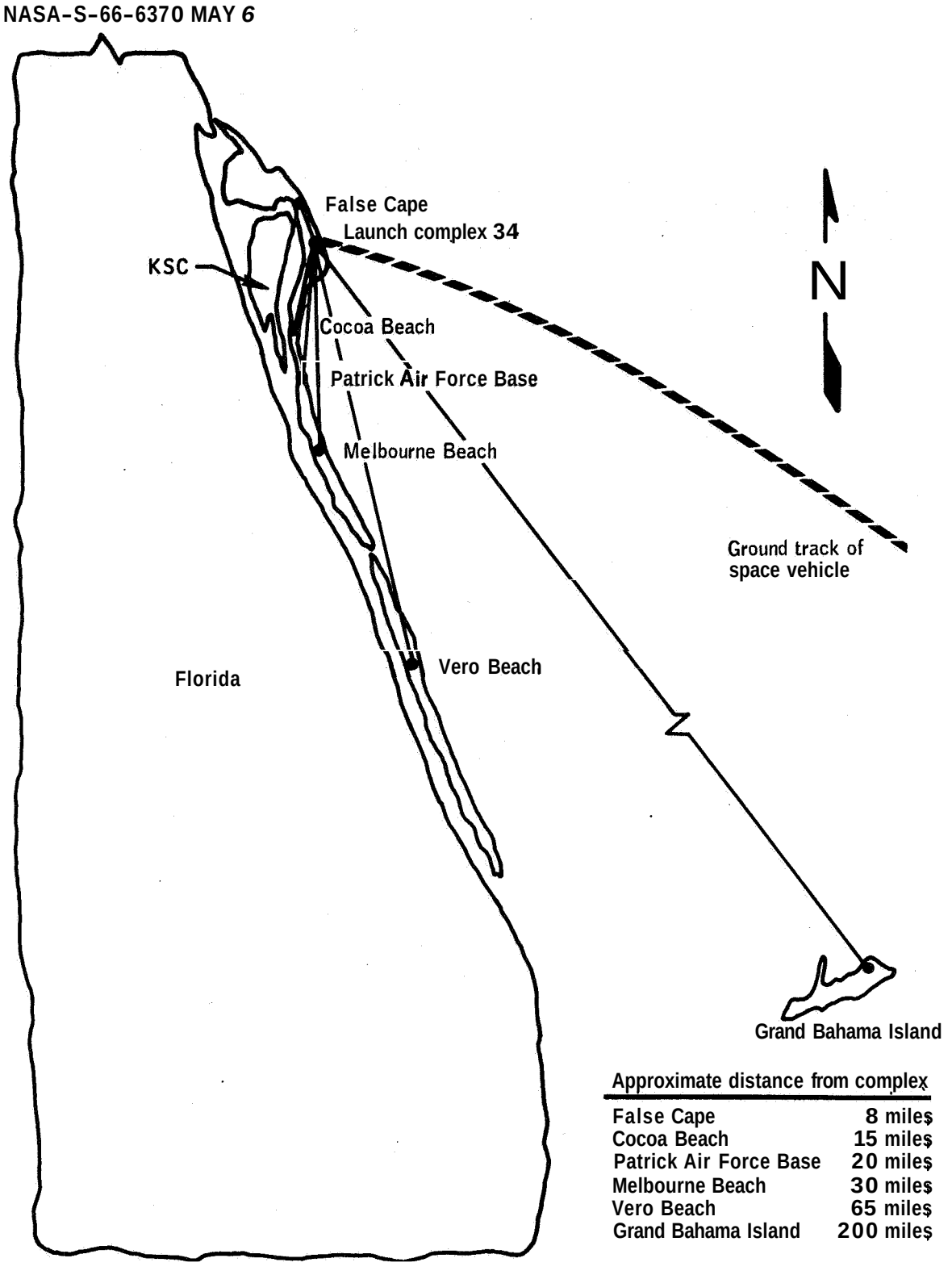


Figure 13.1-2.- Long range camera locations, Mission AS-201.

13.2 Metric Data Review

Description.- Mission analysis data included those which were recorded onboard the spacecraft and those which were transmitted to the telemetry receiving sites.

The data which were recorded onboard only consisted of the output of: three 90 x 10 commutators recorded in differentiated pulse duration modulated (DPDM) format, two acoustic sensors recorded in direct analog mode, and eight vibration and acceleration sensors recorded in wide-band frequency modulated (FM) mode.

The data which were only transmitted by telemetry consisted of the output of: one 90 x 10 commutator and 12 vibration and acceleration sensors.

The data which were both recorded onboard and transmitted by telemetry to the ground consisted of the output of one 90 × 10 commutator and those recorded as a 51.2 kilobit/sec pulse code modulated (PCM) wavetrain. These were recorded onboard on four parallel digital tracks and were transmitted by telemetry as a serial bit stream.

Performance.- Magnetic tapes, pen recorder strip charts, and oscillograph records were delivered to MSC, Houston, for use in evaluating the mission. Raw data processing was completed on a schedule as indicated in table 13.2-I.

In processing the commutated data, the data are fed into a decommutator and then into an analog-to-digital converter where they are converted to a digital format acceptable to the computer which provides scaling, plotting, and other data-processing functions. In order for the decommutator to function properly it must lock-on to a synchronization pulse which occurs at the beginning of each frame of data. During that period of the mission in which the spacecraft bus voltage was law, the synchronization pulses from the two law-level commutators disappeared; therefore, decommutation of those channels during that period was impossible (T+1650 sec to T+2121 sec). Mission time covered by recovered data is indicated in figure 13.2-1.

The recovery of data from the recorded PCM is somewhat more complex in that the serial bit stream is divided into four-bit characters for recording onto four digital tracks of the data storage equipment (DSE). A clock signal is also recorded on track 5. Recovery of these data requires a conversion back to serial PCM which can be performed by the flight recorder. The flight recorder was brought back to MSC and used as a part of the data reduction equipment. The reconstructed serial PCM wavetrain generated during this initial playback was re-recorded successfully onto a working tape. When this tape was played into the

decommutation equipment, however, synchronization could not be maintained by the automatic phase-lock equipment usually employed. Only after considerable analysis was it possible to recover any data. In order to accomplish this, synchronization was established using the clock signal recorded on track 5.

The event times used in this report were taken from flight data as indicated in table 13.2-II.

An Arcasonde at Ascension Island at 1850 G.m.t. on February 26, 1966, provided density, pressure, temperature, and speed of sound data to 190 000 feet m.s.l. These data were extrapolated to 400 000 feet using the hydrostatic equation and a temperature structure constructed around the 15° N atmosphere from the "Air Force Interim Supplemental Atmosphere to 90 km" and preliminary data from the "U.S. Standard Atmosphere Supplements, 1966." These data were used in lieu of Nike Apache Pitot tube data.

TABLE 13.2-I.- DATA PROCESSING

Source	Raw data tapes received, days	Processing completed days		
		Tabulated data	Plots	special requests, (a)
CC-K	T+0			T+30
PAM		T+2	T+2	
PCM		T+12	T+14	
Antigua	T+2			T+21
PAM		T+5	T+5	
PCM		T+10	T+11	
Ascension Island	T+4			T+21
PAM		T+8	T+8	
		T+8	T+10	
Rose Knot Victor	T+10			T+30
PAM		T+15	T+15	
PCM		T+16	T+19	
Aircraft	T+12			T+21
PAM		T+16	T+16	
Onboard tape	T+2			T+45
PCM		T+20	T+20	
1 - low level		T+15	T+17	
2 - low level		T+15	T+17	
1 - high level		T+16	T+16	
2 - high level[b]		T+16	T+16	

Source	Raw data tapes received, days	Processing completed, days		
		Digital PSD	Analog rms time histories	Special requests, (a)
MCC-K				
telemetry	T+0	T+2	T+6	
Onboard recording	T+2	T+9	T+9	T+65
Rose Knot Victor				
telemetry	T+10	T+16	T+17	

[a]Special request processing of flight data is continuing at the time of publication of this report and will continue as required.

[b]2 - high level was also processed from real-time tapes.

TABLE 13.2-II.- SOURCES OF MISSION AS-201 EVENT TIME USED IN EVALUATION

Event	Source	Time, sec
Start control programmer	CH8031X	663.1
Tape recorder off	CT0012X (DSE) CT0013X (R and D)	665.4 665.2
Direct ullage on	CD0140X, CD0141X	843.7
S-IVB/CSM separation	CD0127X, CD0128X	844.9
Direct ullage off	CD0140X, CD0141X	846.7
RCS +X translation on, control programmer	CH8074X	846.7
RCS +X translation off, control programmer	CH8074X	846.6
RCS +X translation on, control programmer	CH8074X	1181.2
First SPS gimbal position signal	CH8074X	1181.2
SPS thrust on	CH8071X	1211.2
RCS +X translation off, automatic	CH1087X, CH0088X, CH1088X, CH0087X	Intermittent data
Tape recorder on	CT0012X, CT0013X	1321.9
RCS +X translation on, automatic	CH1087X, CH0088X, CH1088X, CH0087X	Intermittent data
RCS +X translation off, control programer	CH8074X	1395.2
SPS thrust off	CH8072X, CH8071X	1395.2
Second SPS gimbal position signal	CH8074X	1395.7
RCS +X translation signal on, control programmer	CH8074X	1395.7
SPS thrust on	CH8071X	1410.7
RCS +X translation signal off, automatic	CH1087X, CH0088X, CH1088X, CH0087X	Intermittent date
RCS +X translation signal off, control programmer	CH8074X	1420.7
SPS thrust off	CH8071X	1420.7
Initiate 5 deg/sec pitch rate	CH8010V	1424.2
Terminate 5 deg/sec pitch rate	CH8010V	1442.1
CM/SM separation command	CD0023X CD0024X	1454.7
CM/SM physical separation	CS0100X	1455.0
Initiate CM 5 deg/sec pitch rate	CH8010V	1462.6
Terminate CM 5 deg/sec pitch rate	CH8010V	1479.1

TABLE 13.2-II.- SOURCES OF MISSION AS-201 EVENT TIME USED IN EVALUATION

- Concluded

Event	Source	Time, sec
Initiate CM 5 deg/sec roll rate	CH8011V	1479.2
Terminate CM 5 deg/sec roll rate	CH8011V	1515.1
0.05g	CH3184V	1580.7
Drogue parachute deployment	CK0061A, CK0062A	1855.4
Main parachute deployment	CK0061A, CK0062A	1908.4
Touchdown	CK0061A, CK0062A	2239.7
S-IB ignition command	MSFC	-3.038
S-IB ignition	MSFC	-2.45
Range zero	KSC	16:12:01 G.m.t.
First motion	MSFC	0.11
Lift-off	MSFC	.37
Start pitch and roll	MSFC	11.2
Roll disable	MSFC	20.5
Tilt arrest	MSFC	134.4
IECO	MSFC	141.5
OECO	MSFC	146.9
S-IB/S-IVB separation	MSFC	147.7
S-IVB engine start	MSFC	149.3
LET jettison	MSFC	172.6
Initiate active guidance	MSFC	176.1
S-IVB cutoff	MSFC	602.9
Start pitchover	MSFC	613.9
Start spacecraft separation sequence	MSFC	663.1
Achieve separation attitude	MSFC	728.3

NASA-S-66-6371 MAY 6

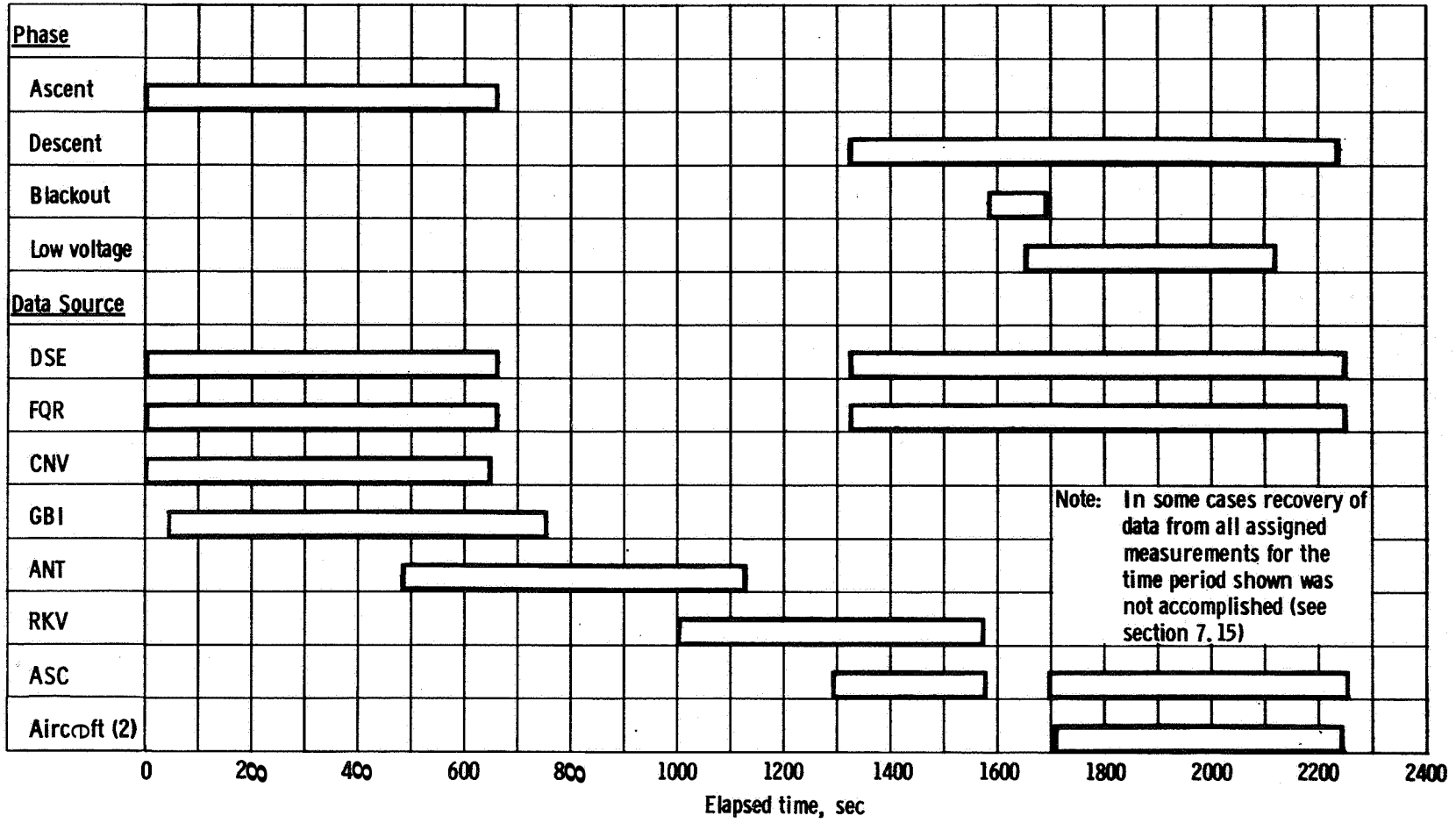


Figure 13.2-1.- Data coverage of flight time, Mission AS-201.

14.0 REFERENCES

1. Data Processing Planning Office: Flight Data Report for Mission AS-201 (Spacecraft 009). NASA Apollo Working Paper 1205, 1966.

2. Staff of Manned Spacecraft Center: Postlaunch Memorandum Report for Apollo Pad Abort I. Nov. 13, 1963.

3. Staff of Manned Spacecraft Center: Postlaunch Report for Apollo Mission A-001 (BP12). MSC-R-A-64-1, May 28, 1964.

4. Staff of Manned Spacecraft Center: Postlaunch Report for Apollo Mission A-101 (BP-13). MSC-R-A-64-2, June 18, 1964.

5. Staff of Manned Spacecraft Center: Postlaunch Report for Apollo Mission A-102 (BP-15). MSC-R-A-64-3, Oct. 10, 1964.

6. Staff of Manned Spacecraft Center: Postlaunch Report for Apollo Mission A-002 (BP-23). MSC-R-A-65-1, Jan. 22, 1965.

7. Staff of Manned Spacecraft Center: Postlaunch Report for Apollo Mission A-003 (BP-22). MSC-A-R-65-2, June 28, 1965.

8. Staff of Manned Spacecraft Center: Postlaunch Report for Apollo Mission PA-2 (BP-23A). MSC-A-R-65-3, July 29, 1965.

9. Staff of Manned Spacecraft Center: Postlaunch Report for Apollo Mission A-004 (Spacecraft 002). MSC-A-R-66-3, Apr. 15, 1966.

10. Staff of North American Aviation: Apollo Vehicle Model Specification - Basic Block I. SID 64-1237, North American Aviation, Inc., Feb. 22, 1965.

11. Staff of North American Aviation: CEI Detail Specification, Part I, Performance/Design Requirements, Airframe 009 Apollo Spacecraft. SID 63-701, North American Aviation, Inc., Feb. 22, 1965.

12. Staff of NASA Headquarters: Project Apollo Coordinate System Standard. OMSF Directive SC-008-001-L, June 1965.

13. Staff of George C. Marshall Space Flight Center: Results of the First Saturn IB Launch Vehicle Test Flight, AS-201. MPR-SAT-FE-66-8, May 6, 1966.

14. McAdams, Robert E.; and Kincaid, Richard E.: AS-201 (AFRM-009) Spacecraft Operational Trajectory. MSC IN 65-FM-158, vol. 1, Nov. 22, 1965.

15. Staff of North American Aviation: Apollo Technical Manuals. Structural Loads and Criteria. SID 64-183, North American Aviation, Inc., Jan. 1963.

16. Martinello, R. C.; Boeltor, L. M. K.; Taylor, T. J. M.; Thomsen, E. G.; and Marrin, E. H.: Isothermal Pressure Drop for Two-Phase Two Component Flow in a Horizontal Pipe. Transactions ASME, vol. 66, 1944, pp. 139-151.

17. TRW Systems: Preliminary Report AS-201. Propulsion Performance Analysis. TRW Systems 2261-6023-T8-000, Apr. 22, 1966.

18. Staff of North American Aviation: GFE Communication Equipment Performance and Interface Specification, Block I. SID 65-159, North American Aviation, Inc., Feb. 1965.

19. Staff of North American Aviation: An Investigation of Aerodynamic Noise Measured on a 0.055-Scale Apollo Saturn Vehicle in the NASA Ames 14-foot Transonic and 9- by 7-foot Supersonic Wind Tunnels. SID 63-1480 (NAS9-150), North American Aviation Inc., Dec. 31, 1965.

20. North, Warren, ; and Shows, James C. : Effect of Simulated hunch Vibrations on Ability of Crew to Monitor Gemini Spacecraft Displays and Controls. Gemini Working Paper 5010, Apr. 16, 1964.

21. Taub, Harvey A.: The Effects of Vibration on Dial Reading Performance. AMRC-TDR-64-70, July 1964.

DISTRIBUTION

Addressee	Number of copies
National Aeronautics and Space Administration **Washington, D.C. 20546**	
Associate Administrator Office of Manned Space Flight, M	1
Apollo Program Director, MA	1
Flight Operations Director, MAO	1
Program Control Director, MAP	1
Reliability and Quality Assurance Director, MAR	2
Systems Engineering Director, MAS	2
Test Director, MAT	8
MSF Field Center Development Director, MC	1
Deputy Director, Saturn-Apollo Applications, MLD	1
Deputy Director, Mission Operations, MO-1	1
Advanced Manned Missions Program Director, MT	2
National Aeronautics and Space Administration **Manned Spacecraft Center** **2101 Webster-Seabrook Road** **Houston, Texas 77058**	
Director, AA	1
Deputy Director, AB	1
Special Assistant to the Director, AC	1
Executive Assistant to the Director, AF	1
Chief of Center Medical Programs, AH	1
Office of Patent Counsel, AL3	1

Addressee	Number of copies
Center Medical Office, AM	1
Public Affairs Office, AP	1
Flight Safety Office, AR	2
Assistant Director for Administration, BA	1
Reproduction Services Branch, BF6	1
Forms and Publications Section, BF52	46
Field Test Branch, BH6	1
Security Branch, BM4	1
Technical Information Preparation Branch Records, BM5	4
Technical Information Dissemination Branch, BM6	6
Technical Information Dissemination Branch, BM6 Attention: M. P. McDonough	10
Assistant Director for Flight Crew Operations, CA	1
Astronaut Office, CB	3
Flight Crew Support Division, CF	5
Assistant Director for Engineering and Development, EA	3
Information Systems Division, EB	2
Crew Systems Division, EC	5
Computation and Analysis Division, ED	3
Instrumentation and Electronic Systems Division, EE	7
Guidance and Control Division, EG	6
Propulsion and Power Division, EP	7
Structures and Mechanics Division, ES	10
Advanced Spacecraft Technology Division, ET	5

Addressee	Number of copies
Experiments Program Office, EX	1
Assistant Director for Flight Operations, FA	2
Flight Control Division, FC	4
Landing and Recovery Division, FL	2
Mission Planning and Analysis Division, FM	3
Flight Support Division, FS	2
Gemini - Office of Program Manager, GA	1
Test Operations Manager, GT	1
Apollo - Office of Manager, PA	3
NASA-RASPO, PB Grumman Aircraft Engineering Corporation Bethpage, L.I., New Pork 11714	3
NASA-RASPO, PC 12214 Lakewood Blvd. Downey, California 90240	4
Systems Engineering Division, PD	7
C and SM Project Engineering and Checkout Division, PF	4
Mission Operations Division, PM	3
Program Control Division, PP	2
Reliability, Quality, and Test Division, PR	1
ApoUo Analysis and Reporting Team, PM4	25
Resident Liaison Offices	
Goddard Space Flight Center Liaison Office, GSF-L	1
Kennedy Space Center Liaison Office, HA113	1
Marshall Space Flight Center Resident Liaison Office, RL	1

Addressee	Number of copies
Libraries	
NASA Headquarters Library, USS-10	6
Ames Research Center Library	6
Flight Research Center Library	6
Goddard Space Flight Center Library	2
John F. Kennedy Space Center Library	6
Lewis Research Center Library	6
Marshall Space Flight Center Library	6
NASA Ames Research Center Moffett Field, California 94035 Attention: Director	1
NASA Flight Research Center Post Office Box 273 Edwards, California 93523 Attention: Director	1
NASA Goddard Space Flight Center Greenbelt, Maryland 20771 Attention: Director, 100	1
NASA Langley Research Center Langley Station Hampton, Virginia 23365 Attention: Director, 0.000	1
NASA Lewis Research Center 2100 Brookpark Road Cleveland, Ohio 44135 Attention: Director, 100	1
NASA George C. Marshall Space Flight Center Huntsville, Alabama 35812 Attention: Director, M-DIR	1
NASA Electronics Research Center 565 Technology Square Cambridge, Massachusetts 02139	1

Addressee	Number of copies
NASA MSC-White Sands Test Facility Office of the Manager, RA P. O. Drawer MM Las Cruces, New Mexico 88001	1
John F. Kennedy Space Center, NASA NASA Kennedy Space Center, Florida 32899	7
NASA Marshall Space Flight Center Aero-Astrodynamics Laboratory, R-Aero-F Huntsville, Alabama 35812	4
NASA-RASPO Massachusetts Institute of Technology 75 Cambridge Parkway Cambridge, Massachusetts 02142	2
NASA-RASPO AC Spark Plug Company Milwaukee, Wisconsin 53200	2
North American Aviation, Inc., S&ID Attention: D. M. Cole Systems Engineering, Dept. 692 32214 Lakewood Blvd. Downey, California 90240	6
North American Aviation, Inc., S&ID Attention: Dale D. Myers Apollo Program Manager 12214 Lakewood Blvd. Downey, California 90240	1
North American Aviation, Inc. AT&O Florida Facilities 5505 North Atlantic Ave. Cocoa Beach, Florida 32899	4
Grumman Aircraft Engineering Corp. Bethpage, L. I., New York 11714	4
Arnold Engineering Development Center Attention: General Gossick Arnold Air Force Station, Tennessee 37389	1